A STUDY OF PRETENSIONED HIGH STRENGTH CONCRETE GIRDERS IN COMPOSITE HIGHWAY BRIDGES

by

REID WILSON CASTRODALE, B.S., M.S.

DISSERTATION

Presented to the Faculty of the Graduate School of

The University of Texas at Austin

in Partial Fulfillment

of the Requirements

for the Degree of

DOCTOR OF PHILOSOPHY

THE UNIVERSITY OF TEXAS AT AUSTIN

May 1988

D E D I C A T I O N

To my wife Jessica, our children Andrew and Laura, our parents and family, and many other friends, whose continual support encouraged me to persevere and complete this lengthy project.

And to those in the profession and academia who may profit from this research through reading this document or through the experience that I have gained through my years of research at The University of Texas at Austin.

A C K N O W L E D G E M E N T S

The research described in this dissertation was part of Research Study 3-5-84-381 administered by the Center for Transportation Research at The University of Texas at Austin. The study was sponsored by the Texas State Department of Highways and Public Transportation and the Federal Highway Administration. The research was conducted at the Phil M. Ferguson Structural Engineering Laboratory located at the Balcones Research Center at The University of Texas at Austin.

The research and writing of this dissertation were co-supervised by Drs. Ned H. Burns and Michael E. Kreger. The author would like to thank Dr. Burns and Dr. Kreger for their guidance, encouragement and patience during testing and writing. A special thanks is extended to Dr. John E. Breen for his valuable input in the early phases of the project and for his careful and thoughtful review of the completed manuscript. The direction of Dr. Ramon L. Carrasquillo in developing the high strength concrete mixes used in this study is also greatly appreciated. The author would like to thank the remaining members of the committee, Dr. David L. Fowler and Dr. Stelios Kyriakides, for their helpful comments and discussion after reviewing the manuscript.

David L. Hartmann participated in the study as part of his work toward a masters degree. His able assistance was greatly appreciated, as was his eagerness to learn and friendship, which made

the work more enjoyable and rewarding. Many other students assisted in all phases of the project, especially Ross Osborne, Tim Bradberry, Dominic Kelly and Charlie Quade.

The help of each member of the staff of the Ferguson Laboratory was also greatly appreciated, for without it the research could not have been completed. A very special thanks is extended to Sharon Cunningham and Jean Gehrke for preparing the final copy of this dissertation in my absence.

Reid W. Castrodale
November 1987
Charlotte, North Carolina

A STUDY OF PRETENSIONED HIGH STRENGTH CONCRETE GIRDERS IN COMPOSITE HIGHWAY BRIDGES

Publication No.

Reid Wilson Castrodale, Ph.D.
The University of Texas at Austin, 1987

Supervising Professors: Ned H. Burns
Michael E. Kreger

Recent developments have made concrete with strengths up to 12,000 psi commercially available for construction of pretensioned highway bridge girders. The implementation of this material has preceded the full understanding and documentation of its behavior and effect on the design of bridge structures.

Therefore, a review of codes, practice, and the literature is necessary for high strength concrete to be used safely and efficiently in pretensioned bridge girders.

Selected girder cross-sections are reviewed to determine their sensitivity to different design parameters and their effectiveness with the use of high strength concrete. A series of sections is proposed that are more efficient for use with high strength concrete than some sections currently in use. Several factors are identified that limit the design potential for some sections.

AASHTO and ACI Codes are reviewed for application to high strength concrete. Test data and analytical studies related to the

use of high strength concrete are also reviewed. Areas needing further study are identified.

A two-fold test program was conducted. The initial study provided a comparison between the transfer length of 0.5-in. diameter strand in normal and high strength concrete. In the second study, two one-third scale model long- span high strength concrete pretensioned bridge girders with normal strength concrete composite decks were statically loaded to failure in flexure and shear. One girder was typical of current designs in which the minimum reinforcement is provided to satisfy design criteria while the second girder had additional prestressed reinforcement and exceeded maximum reinforcement limits. Surface concrete strains, strand strains, stirrup strains, and deflections were monitored from construction until failure.

Based on the review of codes, literature, test data, and additional analytical studies, proposals and recommendations are made regarding the design of pretensioned high strength concrete bridge girders. The best approach to the AASHTO and ACI approximate ultimate analysis for composite members and new maximum and minimum reinforcement limits are among the proposals made. Girder stability is considered at length. Areas requiring additional testing and study are identified.

TABLE OF CONTENTS

TABLE OF CONTENTS (continued)

TABLE OF CONTENTS (continued)

TABLE OF CONTENTS (continued)

TABLE OF CONTENTS (continued)

TABLE OF CONTENTS (continued)

LIST OF TABLES

L I S T O F T A B L E S (continued)

L I S T O F T A B L E S (continued)

L I S T O F T A B L E S (continued)

LIST OF FIGURES

L I S T O F F I G U R E S (continued)

L I S T O F F I G U R E S (continued)

L I S T O F F I G U R E S (continued)

L I S T O F F I G U R E S (continued)

L I S T O F F I G U R E S (continued)

CHAPTER 1

INTRODUCTION

1.1 Background

The use of high strength concrete as a building material has been a topic of discussion for many years. In an article published in 1932, Thomas T. Towles [129] speculated on the benefits of using concrete with a design compressive strength of 7,000 psi compared with a 5,000 psi mix, which was considered to be near the maximum practical concrete strength at the time. It was clear to him that the use of higher strength concrete would lead to significant cost benefits, especially in long span construction and where many spans are required.

Since that time, it has become possible to produce concrete with a design strength much higher than even the expectations of Towles in 1932. Peterman and Carrasquillo [104] have demonstrated that concrete with a compressive strength between 9,000 and 12,000 psi can be readily obtained on a commercial basis by careful mix proportioning using standard portland cements, selected common aggregates, and chemical admixtures. The use of high range water reducers (HRWR), which are also referred to as "super-plasticizers", have made it possible to produce workable mixtures with the extremely low water/cement ratios that are required to attain high strengths.

The same observations that Towles made in 1932 are being made today, but with even greater expectations for cost benefits because of

the higher strengths that are now possible. One way in which the use of high strength concrete has been demonstrated to provide greater efficiency is illustrated by the two bridge cross sections shown in Fig. 1.1, which illustrates the results of a study performed in Sec. 2.4.1. This figure shows that, for a span length of 115 ft and a bridge width of 36 ft, the required number of AASHTO-PCI Type IV girders can be reduced from nine using 6,000 psi concrete, which is the standard concrete strength for pretensioned girders in Texas, to four when 10,000 psi concrete is used. As indicated on the figure, the use of high strength concrete also results in a reduction in the total number of strands required for the bridge, which is a result of the reduced dead load. A normal strength concrete (4,000 psi) deck was used in both cases. The deck thickness was 1 in. greater for the design using high strength concrete girders because of the increased deck span. The use of fewer girders for a given span leads to savings in material, shipping, and erection costs and also reduces the time required for fabrication and erection.

Another benefit of the use of high strength concrete in highway bridge design is illustrated in Fig. 1.2, where an increase in girder concrete strength is shown to result in significantly greater maximum spans for a given cross-section, girder spacing (GS), and deck thickness. The dashed line indicates spans which exceed a limiting span length based on stability considerations. While means are available to increase the limiting span for a section, the extent

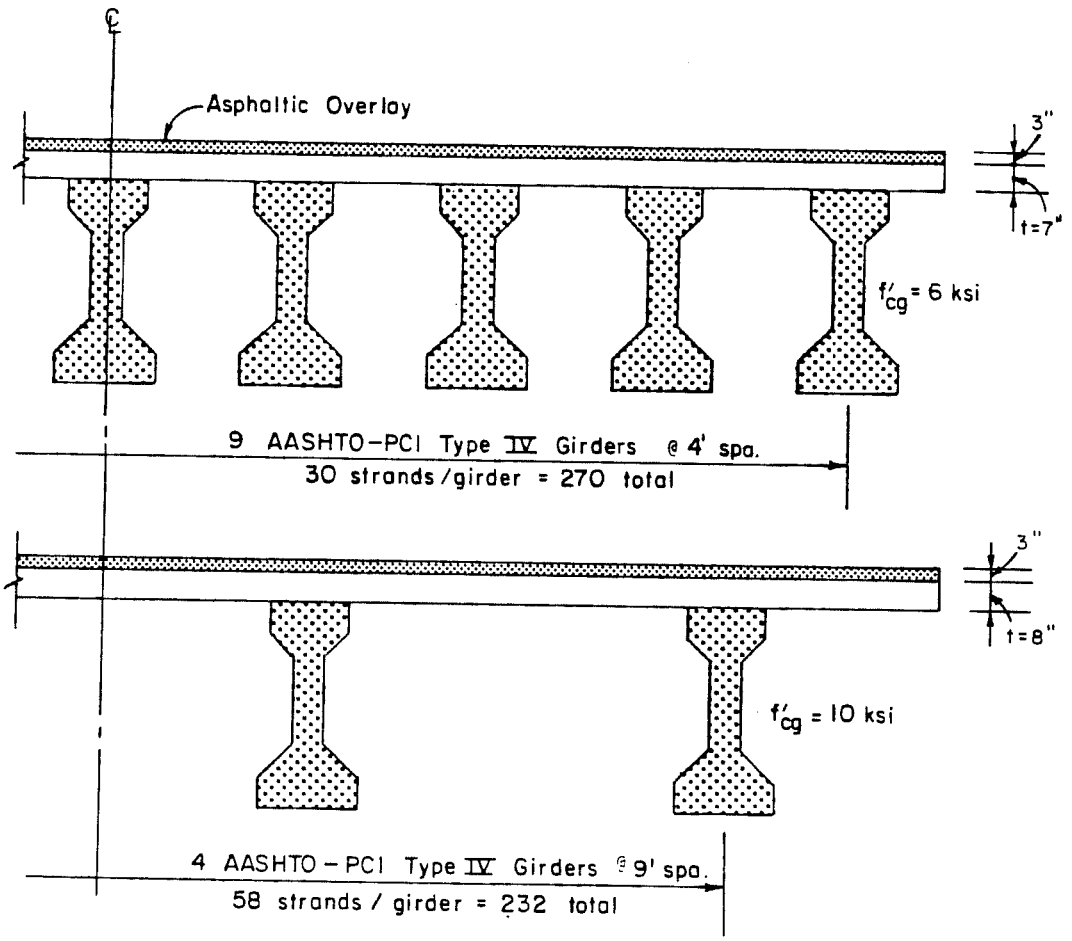

Fig. 1.1 Comparison of bridge designs for same span using normal and high strength concrete

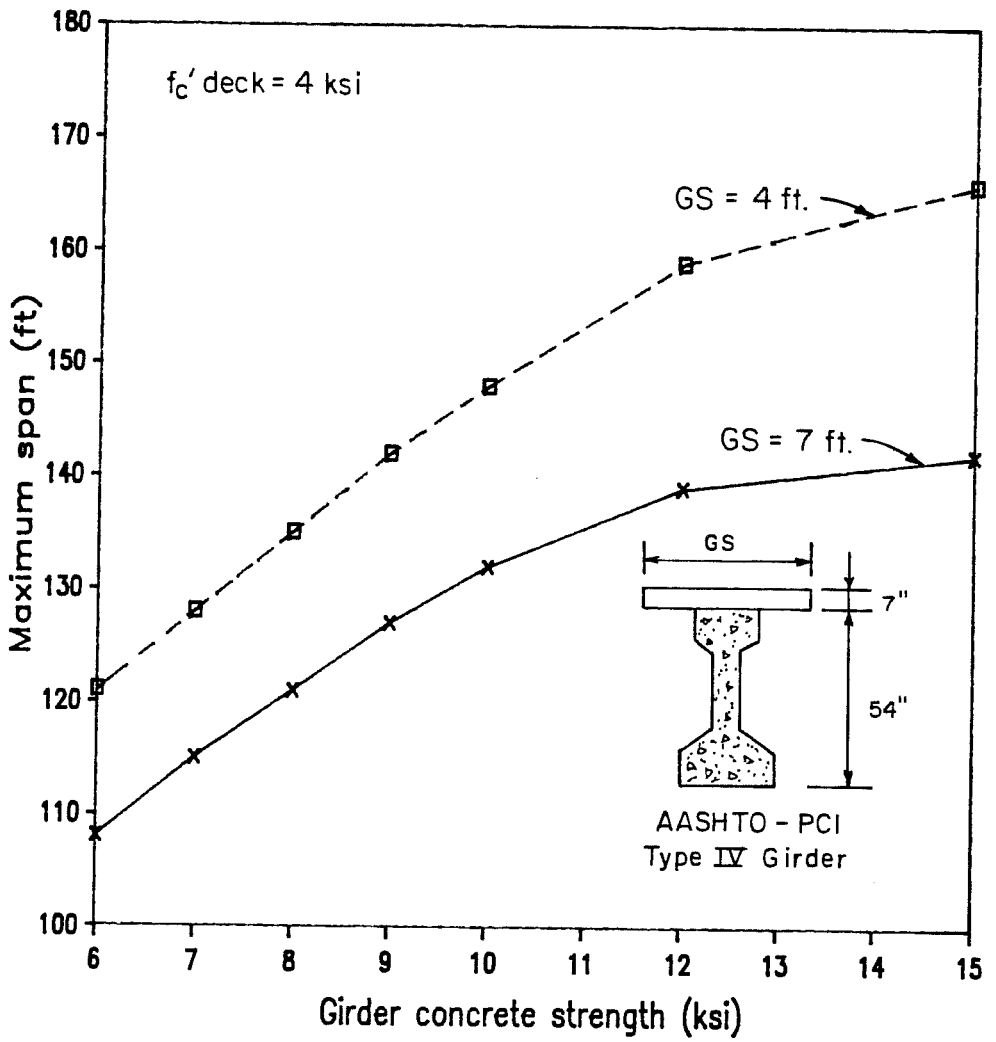

Fig. 1.2 Maximum span versus girder concrete strength

of the line emphasizes the importance of considering stability in the design of long-span girders.

Where multiple spans are required, an increase in possible span lengths leads to a reduced number of piers and lower shipping costs. Increased span lengths can also allow elimination of supports, which can improve traffic safety at highway crossings. Another possible benefit from increased maximum span lengths is the use of shallower members for the same span length, which would improve clearances or result in reduction of embankment costs.

There are uncertainties, however, regarding the adequacy of current design codes for high strength concrete. Research on material properties of high strength concrete has shown that some properties differ significantly from those of normal strength concrete. A major area of difference is in the stress-strain behavior as illustrated in Fig. 1.3 [81], where typical stress-strain curves are shown for a range of concrete strengths. High strength concrete has a greater stiffness (or modulus) than other concrete and is more brittle, which is demonstrated by the short and steep descending branch of the stress-strain curve. The more brittle nature of high strength concrete has led to concern regarding the ductility of members constructed using high strength concrete. It has also been speculated [22] that the brittle nature of high strength concrete will lead to smooth shear cracks which would reduce the contribution of aggregate interlock to the ultimate shear strength. Furthermore, many

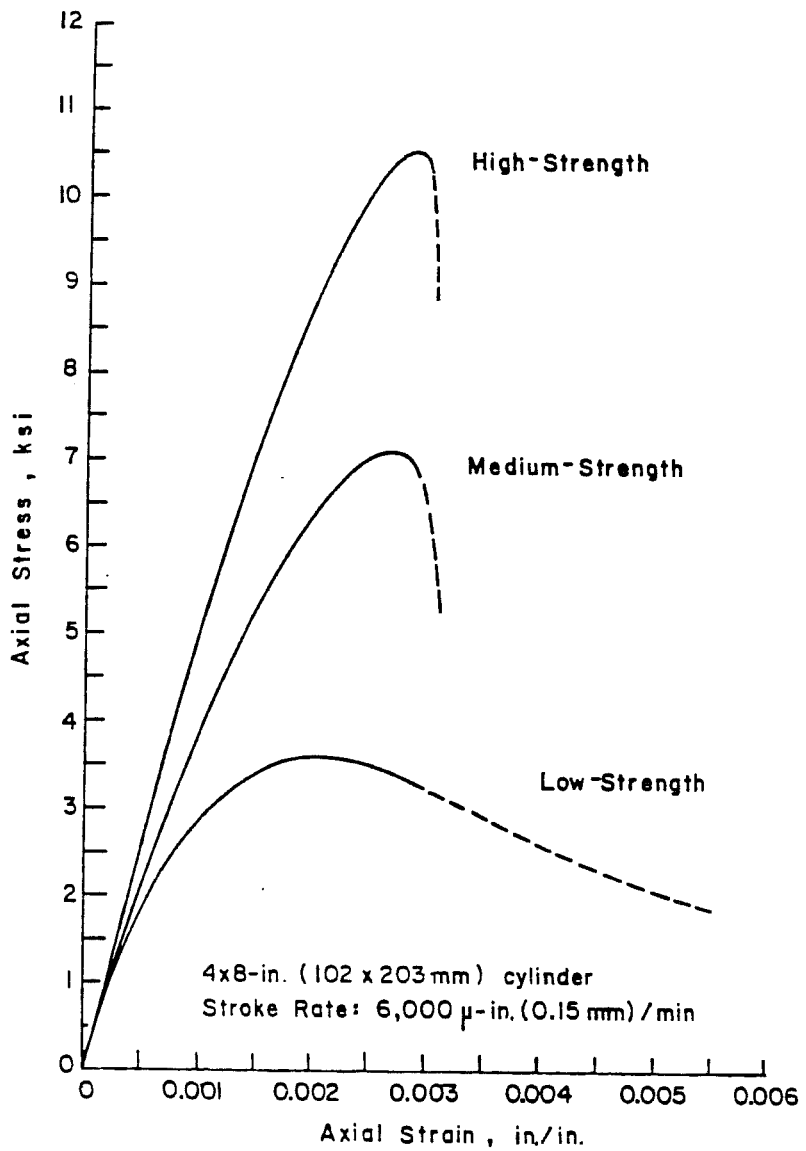

Fig. 1.3 Typical stress-strain curves

of the present code design provisions are based on test data for which the concrete strengths rarely exceed 6,000 psi. Since little data is available on the behavior of high strength concrete pretensioned bridge members, it is not possible to establish whether current codes are adequate for the design of such members.

The realization of the full potential of high strength concrete in pretensioned bridge girders may also be limited by traditional techniques and methods of design and construction which were developed for use with normal strength concrete. This may be especially true where standardization has taken place such as for pretensioned girders, where most cross sections in use today were developed in the late 1950's and early 1960's for use with normal strength concrete.

Because of these concerns regarding the use of high strength concrete and the applicability of current bridge codes to its use, it is essential that the material and structural behavior be clearly understood and incorporated into design codes before high strength concrete comes into general use. Current design and construction techniques should also be reviewed to determine where changes could be made for more efficient use of the material.

1.2 Objectives and Scope of the Study

1.2.1 General. This study was begun to investigate the feasibility and criteria for use of high strength concrete in the design of pretensioned highway bridge girders.

While the definition of high strength concrete varies for different regions of the country, for this study it is considered to be concrete with a design compressive strength between 6,000 and 12,000 psi. The lower limit corresponds to the standard concrete strength for pretensioned girders in Texas which is 6,000 psi and the upper limit represents a practical maximum strength that can be produced commercially. Since the upper limit is not intended to be restrictive, strengths higher than 12,000 psi are considered in some analyses that follow in order to better define trends. Only concrete made using common materials and admixtures will be considered.

The study is limited to the consideration of high strength concrete pretensioned bridge girders which become part of a highway bridge with a normal strength composite deck. Only simple span, non-skew bridges are considered. The deck is assumed to be applied with the girder unshored. Low relaxation strands are the only type considered in the study since this type of strand has virtually become the industry standard. Draping is used to control stresses at the ends of members.

The 13th edition of the American Association of State Highway and Transportation Officials (AASHTO) Standard Specifications

for Highway Bridges [10] is used as the main source for design practice for the girders and bridge structures considered. Where helpful, the American Concrete Institute (ACI) Building Code Requirements for Reinforced Concrete (ACI 318-83) [15] and the Commentary on Building Code Requirements for Reinforced Concrete (ACI 318-83) [17] are also consulted for design practice.

1.2.2 Test Programs. Due to the lack of data in the literature on composite bridge construction with high strength concrete pretensioned girders, two test programs were developed to provide data that would allow evaluation of the use of high strength concrete in the design of pretensioned bridge girders.

The first series was a limited comparison of transfer characteristics of 0.5-in. diameter strand in normal and high strength concrete. These tests provided data to evaluate whether current transfer length provisions found in the codes could be applied to high strength concrete members.

The second series involved testing of scale-model high strength concrete pretensioned girders with a normal strength composite deck, representative of actual long- span bridge designs. Tests of girder specimens provided data for the evaluation of current design provisions, for verification of analysis techniques, and permitted development of recommendations where revision of the codes was necessary. Both flexure and shear tests were performed on scale-model girder specimens.

Tests were conducted at the Phil M. Ferguson Structural Engineering Laboratory at the University of Texas Balcones Research Center.

1.3 Organization of the Study

Chapter Two consists of the comparison and evaluation of bridge designs using selected pretensioned girder cross-sections. Three proposed cross-sections, developed for use with high strength concrete, are included in the comparisons. Chapter Three contains a literature review of the topics of interest in the study. The fourth chapter describes and evaluates the transfer specimen tests. Chapter Five describes construction and testing procedures for the scale-model girder tests while Chapter Six provides comments on behavior, and reports the data collected during construction and testing of the specimens. Chapter Seven combines the evaluation of current practice, as determined by the literature review of Chapter Three, and test data gathered in the study with representative bridge designs to develop recommendations for design of composite bridges using high strength concrete girders. The study concludes in Chapter Eight with a summary of the investigation, and presentation of conclusions and recommendations.

Appendix A contains mix and strength design data for the high strength concrete used in the scale-model girders, and Appendix B details the history of the girder specimens. Appendix C contains

descriptions of computer programs used in this study. Appendix D details the derivation of proposed maximum and minimum reinforcement limits.

CHAPTER 2

STUDY OF BASIC PARAMETERS AFFECTING DESIGN

2.1 Introduction

The preceding chapter presented a brief outline of potential benefits of using high strength concrete in pretensioned bridge girders. In this chapter, designs using a range of concrete strengths are compared to provide a more complete understanding of the benefits and trends that accompany the use of high strength concrete. Different girder cross section shapes are considered in the study to determine which are better suited for use with high strength concrete. Conditions which may limit span lengths in some cases are also identified.

The design procedure used in this chapter conforms to the current AASHTO Specifications [10], using both allowable stress and ultimate strength design criteria and specified highway bridge loadings. The computer program BRIDGE, which is described in Appendix C, was used to perform design calculations.

The chapter begins by presenting a sample of girder cross sections which are either in current use or have been proposed for use, including a series of girder sections developed as a part of this study. Various characteristics of the cross sections are then compared. A comparison of designs for the selected cross

sections is made with specific interest in the ability of sections to utilize high strength concrete. The final section of the chapter contains conclusions regarding the cross sections studied, their use with high strength concrete, and general comments on the use of high strength concrete.

2.2 Girder Cross Sections

In a recent study performed at the Portland Cement Association (PCA), Rabbat et al. [109] reviewed many girder cross sections in use in the United States at the time and proposed a series of bulb-tee sections as the national standard. However, that study did not consider concrete strengths greater than 7,000 psi. Therefore, it is desirable to study the use of different girder cross sections with high strength concrete. This section presents a selected set of girder cross sections that will be used in comparisons to determine the effect of high strength concrete on bridge designs. A set of cross sections will also be proposed.

2.2.1 Girder Cross Sections Considered.

While many girder cross sections are in use today across the country, only a representative sampling of sections wll be considered in this study. Three section depths were chosen to provide a range of span capabilities: 40 in., 54 in., and 72 in. The 40- and 54-in. depths are the most commonly used in the state of Texas and the 72-in. depth

has been commonly used and proposed elsewhere. The sections selected for consideration in this study are shown in Fig. 2.1, grouped by depth. Section dimensions are given in Table 2.1. The notation used for section dimensions is illustrated in Fig. 2.2. Where two numbers separated by a slash are part of the section designation, the first number specifies the section depth and the second number represents the web width. Of the sections shown, the Type C, Type 54, Type 72, and AASHTO-PCI Type IV girders are currently used in Texas.

To provide a comparison of different cross section shapes free from the effects of depth, 54-in. sections were created based on the PCA bulb-tee (PCA BT) [109] and the Ministry of Transport/Cement and Concrete Association (MOT/C&CA) inverted-tee sections [113]. The MOT/C&CA sections, which are referred to as "M-sections", have been used in shallower depths for bridges in the UK. Both sections were created by using standard dimensions for the top and bottom flanges and adjusting the height of the web to produce the desired depth. A modified AASHTO-Prestressed Concrete Institute (PCI) Type IV section, which was also proposed and studied in Ref. [109], will also be included in the studies of this chapter. This cross section was used as the prototype for the scale-model girder tests reported in Chapters 5 and 6.

2.2.2 Proposed Girder Cross Sections. New proposals for girder cross sections, which are designated using a "UT" prefix, are

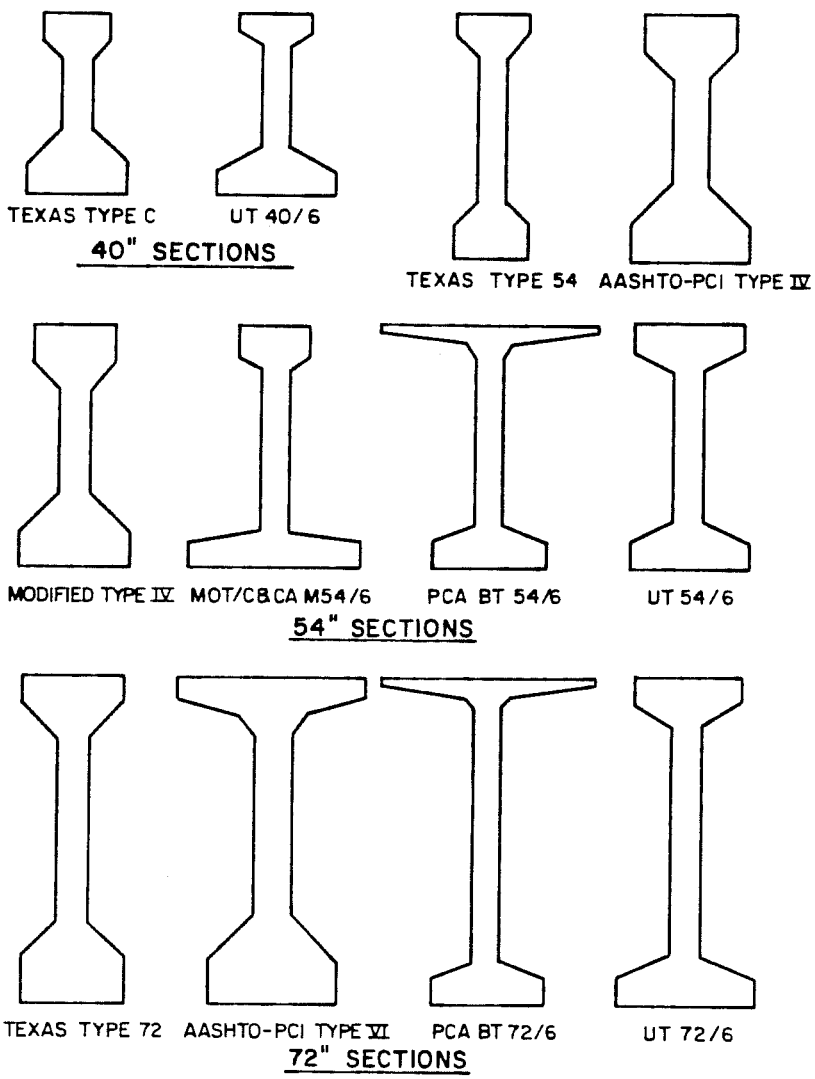

Fig. 2.1 Girder cross sections considered in this study

Table 2.1 Section dimensions

	Horizontal dimensions				Vertical dimensions					
	b1	b2	b3	b4	h1	h2	h3	h4	h5	h6
40-in. sections										
Texas Type C	14	7	7	22	6	3.5	0	16	7.5	7
UT 40/6	16	6	6	26	4.5	2.5	0	22.5	5	5.5
54-in. sections										
Texas Type 54	16	6	6	16	4	5	0	32	5	8
AASHTO-PCI Type IV	20	8	8	26	8	6	0	23	9	8
Modified Type IV	18	6	6	24	8	6	0	23	9	8
MOT/C&CA M 54/6	16	6	6	38	7	2	0	37	2	6
PCA BT 54/6	48	10	6	24	2	2	2	39	3	6
UT 54/6	24	6	6	26	5.5	4.5	0	33.5	5	5.5
72-in. sections										
Texas Type 72	22	7	7	22	5.5	7.5	0	40.5	7.5	11
AASHTO-PCI Type VI	42	16	8	28	5	3	4	42	10	8
PCA BT 72/6	48	10	6	24	2	2	2	57	3	6
UT 72/6	24	6	6	30	5.5	4.5	0	50.5	6	5.5

Dimensions in inches; See Fig. 2.2 for key to dimensions.

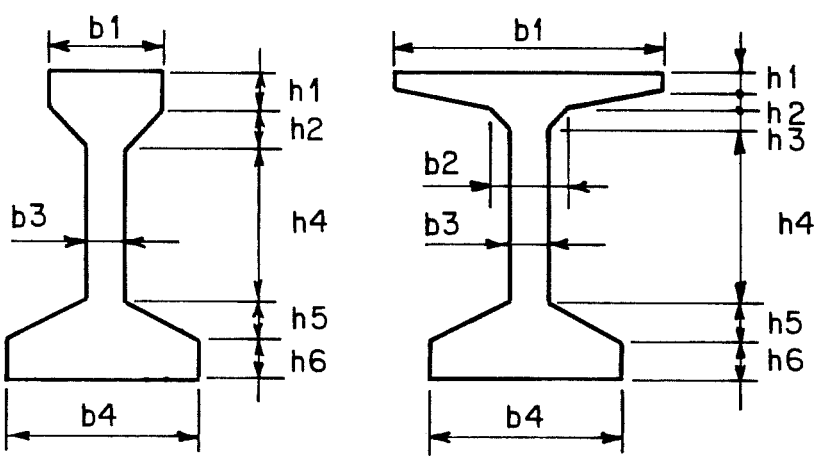

Fig. 2.2 Key to cross section dimensions given in Table 2.1

shown in Fig. 2.1 for three depths considered. Dimensions for these sections are included in Table 2.1.

The following objectives were used in the development of the proposed sections:

1. to provide span capabilities similar to those for sections in current use, but with reduced area,
2. to provide extended span capabilities with the use of high strength concrete
3. to provide a range of span capabilities that gives flexibility of section use to the designer.

Dimensions for the proposed sections were selected using the following criteria:

1. use 6-in. web to facilitate concrete placement and to provide sufficient shear capacity,
2. use a 2:1 slope on the taper of the flanges to provide a good concrete finish and permit easy form removal,
3. provide sufficient thickness of top and bottom flanges to minimize damage during handling,
4. provide sufficient bottom flange width for stability during erection,
5. size bottom flange to minimize excess concrete using a 2 x 2-in. strand grid with 2 in. from girder surface to

center of strand (cover was increased by 0.25 in. on the top surface of the bottom flange),

6. provide sufficient thickness in the top flange to minimize the need for reinforcement, yet allow room for standard ties to be placed,
7. provide sufficient top-flange width to allow use of precast deck panels.

Although not included in the designs on which the proposed sections were based, the bottom flange should be of sufficient size to permit use with continuous construction [42].

A series of designs were performed for each trial section shape to determine the maximum span capabilities for different concrete strengths and girder spacings. The maximum span lengths were then compared with maximum spans for other sections of the same depth. Dimensions were then adjusted in an attempt to increase the maximum span or reduce the area. In evaluating the trial designs, practical upper limits were recognized for span length (150 ft), which was due to transportation and lifting constraints, and number of strands (74 0.5-in. diameter strands), which corresponds to the current maximum stressing capacity of a typical prestressing plant in Texas. The final dimensions represent the best compromise between maximum span capability, cross-sectional area, and use of desired dimensions.

2.3 Comparisons of Section Properties

2.3.1 Basic Properties and Efficiency Ratios.

Section properties are given for the selected and proposed cross sections in Table 2.2. From the data in this table, it can be seen that the proposed sections have smaller cross section areas and lower weights than comparable Texas and AASHTO-PCI sections. Such comparisons are incomplete unless accompanied by results of actual designs, which will be presented in the sections which follow.

Efficiency factors proposed by Guyon and Aswad have been used to compare different sections [109]. Guyon's factor, ρ

$$\rho = r^2/y_b y_t = I_x/Ay_b y_t \qquad (2.1)$$

where ρ = radius of gyration $= \sqrt{I_x/A}$

y_b = distance from centroid to bottom of section

y_t = distance from centroid to top of section

I_x = moment of inertia of section about x axis

A = gross area of cross section

is intended to correlate with the minimum area for a given section modulus. However, it should be noted that this factor is incapable of distinguishing between orientations of the section, i.e., the factor would be the same for tee and inverted-tee sections of the same dimensions. A high value of the factor indicates a more efficient

Table 2.2 Section properties

	Area (in^2)	I_x (in^4)	y_b (in)	y_t (in)	S_b (in^3)	S_t * (in^3)	Weight ** (lb/ft)
40-in. sections							
Texas Type C	495	82602	17.09	22.91	4833	3606	516
UT 40/6	458	84961	16.60	23.40	5118	3631	477
54-in. sections							
Texas Type 54	493	164022	25.53	28.47	6425	5761	514
AASHTO-PCI Type IV	789	260741	24.73	29.27	10544	8908	822
Modified Type IV	681	233854	24.37	29.63	9596	7892	709
MOT/C&CA M 54/6	628	227192	21.55	32.45	10543	7001	654
PCA BT 54/6	593	237893	27.44	26.56	8670	8957	617
UT 54/6	624	237824	26.28	27.72	9050	8580	649
72-in. sections							
Texas Type 72	863	532060	33.73	38.27	15773	13902	899
AASHTO-PCI Type VI	1085	733320	36.38	35.62	20157	20587	1130
PCA BT 72/6	701	484993	36.36	35.64	13339	13608	730
UT 72/6	776	530295	33.45	38.55	15853	13756	808

* - Section modulus for top fiber of section.

** - Computed using concrete unit weight of 150 pcf.

section, i.e., a greater section modulus for the area used. Aswad's efficiency factor, α is similar:

$$\alpha = 3.46S_b/Ah \qquad (2.2)$$

where S_b = section modulus for bottom fiber of section

h = overall section depth.

It is reported that Aswad found that girders with the highest efficiency factor produced bridges with the lowest cost per square foot of superstructure [109].

These efficiency factors are presented for the girders used in this study in Table 2.3. The UT sections have higher values for Guyon's factor, ρ, than all other sections except the bulb-tees. Considering Aswad's factor, α, the 40-in. and 72-in. UT sections have values higher than all other sections of the same depth. For 54-in. sections, the value of α for the UT section is exceeded slightly by the bulb-tee section by a wide margin for the MOT/C&CA inverted-tee M 54/6 section.

The differences in results for the two factors reveal either inadequacies in the individual factors or in the premise that the efficiency of an entire bridge design can be accurately summarized by factors based only on section properties. Complete designs will be used to more fully assess the efficiency and capabilities of sections.

2.3.2 Strand Pattern. The number and location of strands that can be contained within a section are significant factors

Table 2.3 Efficiency factors for sections

	Guyon's Factor, ρ (Eq. 2.1)	Aswad's Factor, α (Eq. 2.2)
40-in. sections		
Texas Type C	0.4263	0.8448
UT 40/6	0.4780	0.9680
54-in. sections		
Texas Type 54	0.4579	0.8361
AASHTO-PCI Type IV	0.4565	0.8561
Modified Type IV	0.4756	0.9027
MOT/C&CA M 54/6	0.5173	1.0755
PCA BT 54/6	0.5504	0.9369
UT 54/6	0.5240	0.9300
72-in. sections		
Texas Type 72	0.4774	0.8780
AASHTO-PCI Type VI	0.5216	0.8928
PCA BT 72/6	0.5339	0.9144
UT 72/6	0.5300	0.9820

Guyon's factor, $\rho = r^2/y_b y_t = I_x/Ay_b y_t$

Aswad's factor, $\alpha = 3.46S_b/Ah = 3.46I_x/Ahy_b$

in determining the span capacity of the section. Characteristics of strand patterns for sections considered in this study are summarized in Table 2.4. Strands are placed on a 2 by 2-in. grid with two columns of strands centered in the web and a minimum of 2 in. from the center of a strand to the surface of the concrete as shown in Fig. 2.3. Strands are added in pairs to the lowest unfilled row.

Columns 1 through 3 are related to the number of strands that can be placed in the bottom flange (see Fig. 2.3). A greater number of strands in the bottom flange generally corresponds to the possibility of longer spans, especially with higher concrete strengths. However, it was found while developing the proposed sections, that an additional row of strands in the bottom flange made little difference in the maximum span until very high concrete strengths were used. Therefore, the large number of strands in the bottom flanges of some Texas sections and the AASHTO sections may not be efficient for practical designs.

The remaining columns of the table concern an effective limit on the number of strands that can be used in design. This limit is encountered if strands must be added above the centroid of the section in an attempt to satisfy stresses. Once the strand pattern is filled to the centroid of the concrete section, the addition of more strands reduces the prestress moment and increases the compression acting on the section.

Table 2.4 Strand pattern characteristics

Column number:	1	2	3	4	5	6	7
40-in. sections							
Texas Type C	10	6	48	17.09	8	52	74
UT 40/6	12	4	36	16.60	8	44	66
54-in. sections							
Texas Type 54	6	5	28	25.53	12	42	70
AASHTO-PCI Type IV	12	7	64	24.73	12	74	102
Modified Type IV	10	7	58	24.37	12	68	96
MOT/C&CA M 54/6	18	2	36	21.55	10	52	84
PCA BT 54/6	10	3	26	27.44	13	46	72
UT 54/6	12	4	36	26.28	13	54	80
72-in. sections							
Texas Type 72	10	8	68	33.73	16	84	112
AASHTO-PCI Type VI	12	8	76	36.38	18	96	120
PCA BT 72/6	10	3	26	36.36	18	56	80
UT 72/6	14	4	44	33.45	16	68	96

Column headings:

1. Number of strands in bottom row
2. Number of rows in bottom flange, i.e., with more than 2 strands in row
3. Number of strands in bottom flange
4. Distance from bottom of girder to centroids of strands, y_b
5. Number of rows below centroid of section
6. Maximum number of strands below centroid of section
7. Maximum number of strands possible in section

Assumptions:

2 x 2-in. grid
2 in. minimum from center of strands to surface of girder

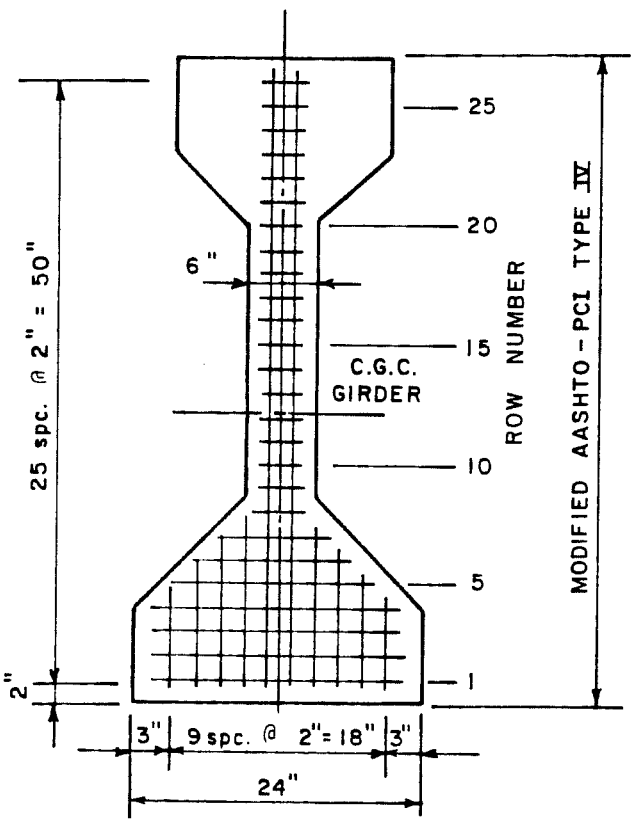

Fig. 2.3 Typical strand pattern

This effect is illustrated in Fig. 2.4 where the product of the eccentricity and the number of strands, which is an index of the prestress moment available in the section, is plotted versus the number of strands for the three section depths. Adding strands above the centroid results in the descending branch of the curves. The point of zero slope corresponds to the number of strands given in column 6 in Table 2.4. The cause for this effect is illustrated by the plots of eccentricity versus number of strands presented in Fig. 2.5. Here the slope of the plots, which begins by descending only slightly, increases as the limiting number of strands is approached and exceeded. The product of the decreasing function (Fig. 2.5) and the linearly increasing number of strands leads to the curves found in Fig. 2.4.

There are few situations in which the addition of strands above the centroid will be beneficial or desirable in design. Therefore, the numbers in column 6 of Table 2.4 provide a practical estimate of the maximum number of strands that can be effectively used in a section.

A further consideration in determining the maximum number of strands that can be used for a design is the stressing capacity of available prestress plants. According to information obtained from the Texas State Department of Highways and Public Transportation (TSDHPT), a single 2.5 million lb stressing bed exists in the state,

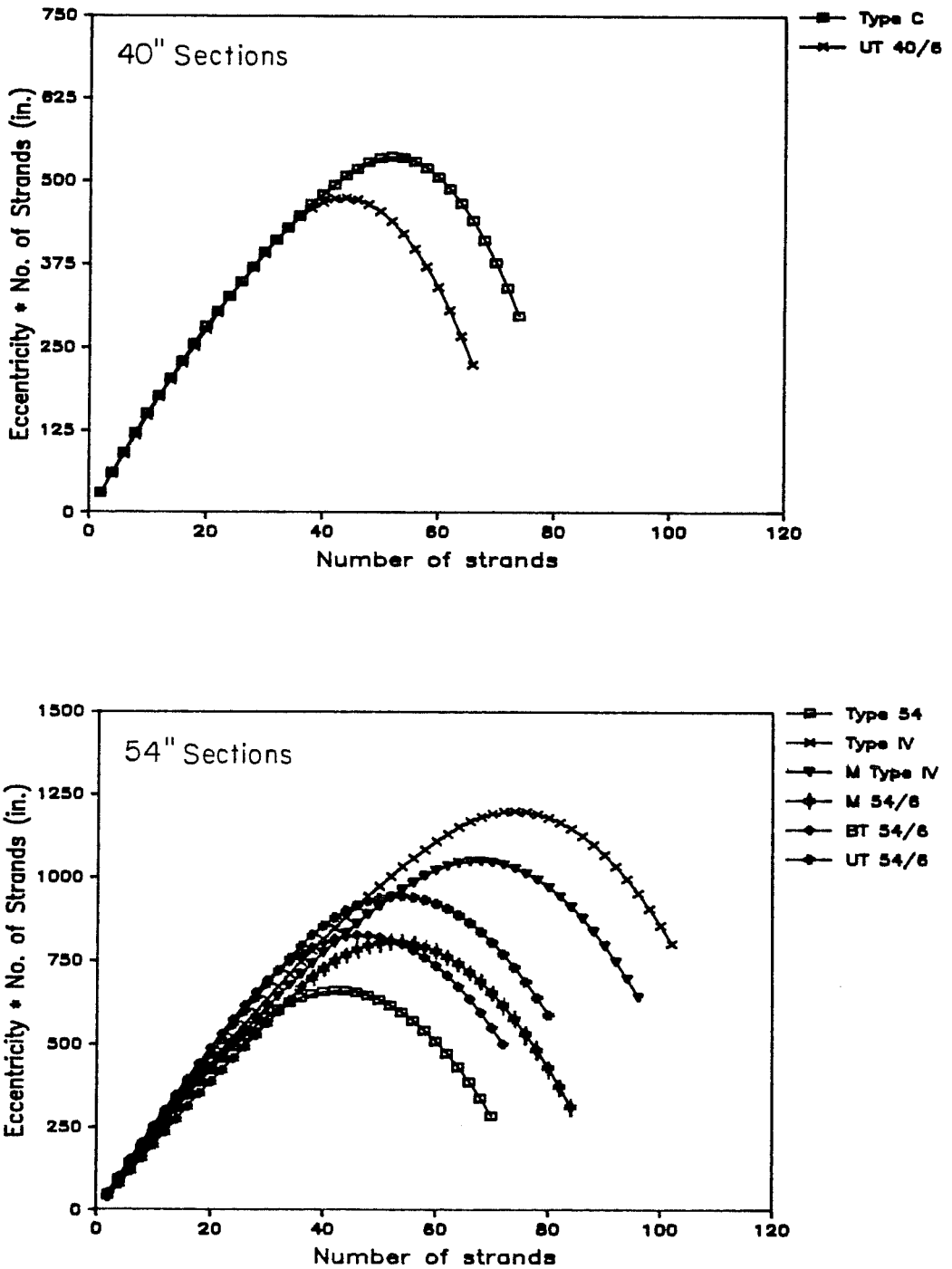

Fig. 2.4 Product of eccentricity and number of strands versus number of strands.

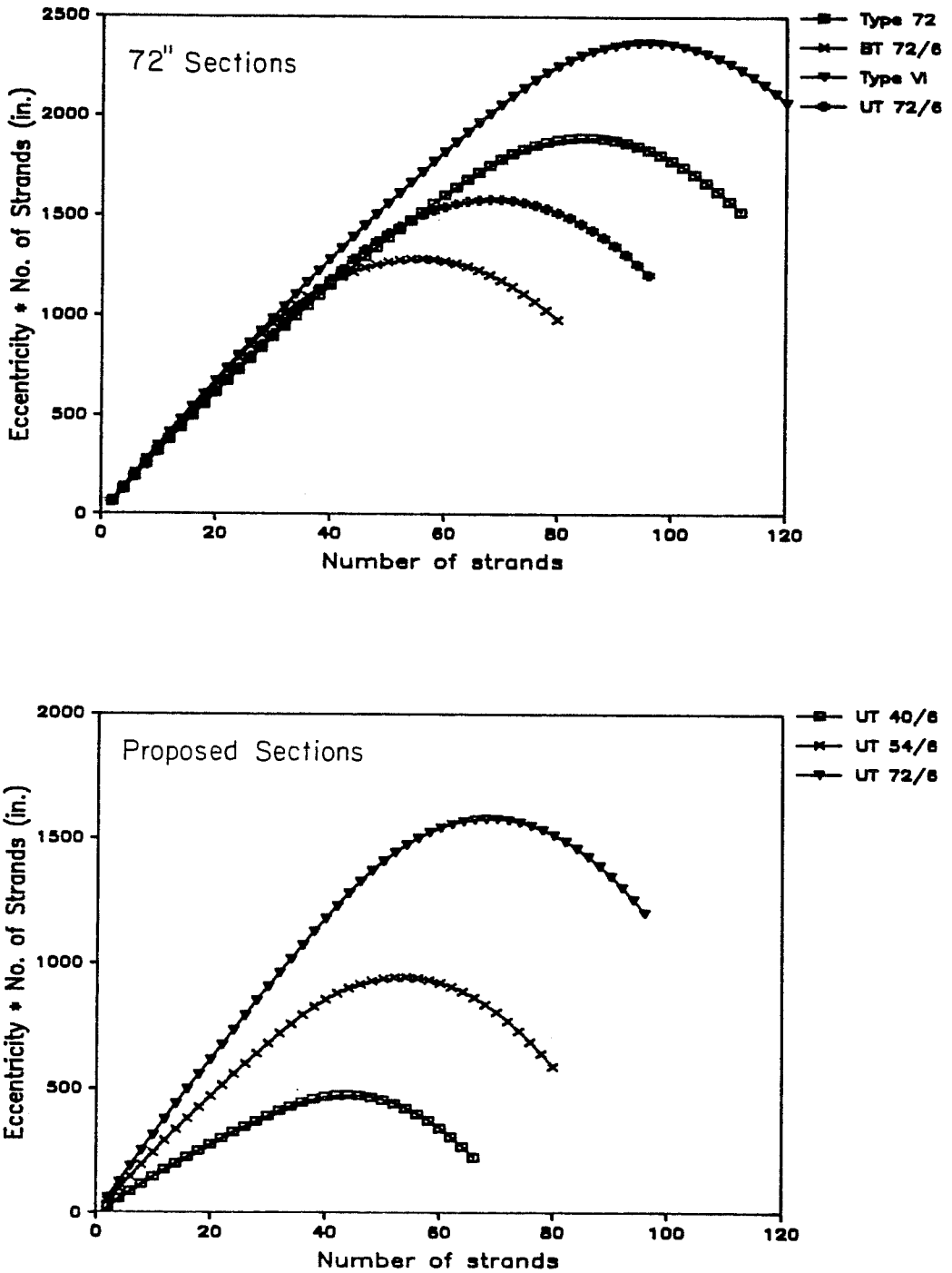

Fig. 2.4 Product of eccentricity and number of strands versus number of strands (continued).

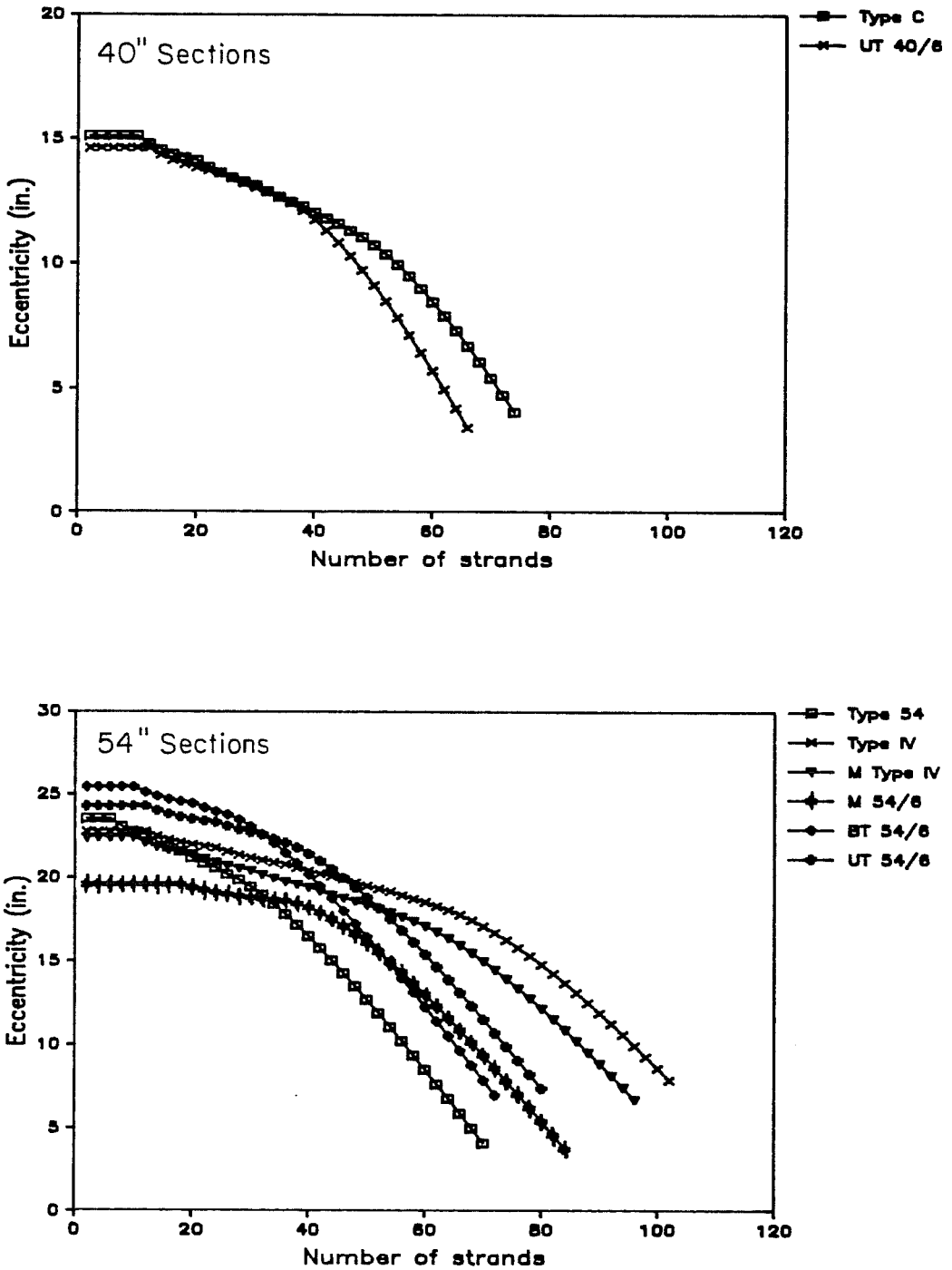

Fig. 2.5 Eccentricity versus number of strands.

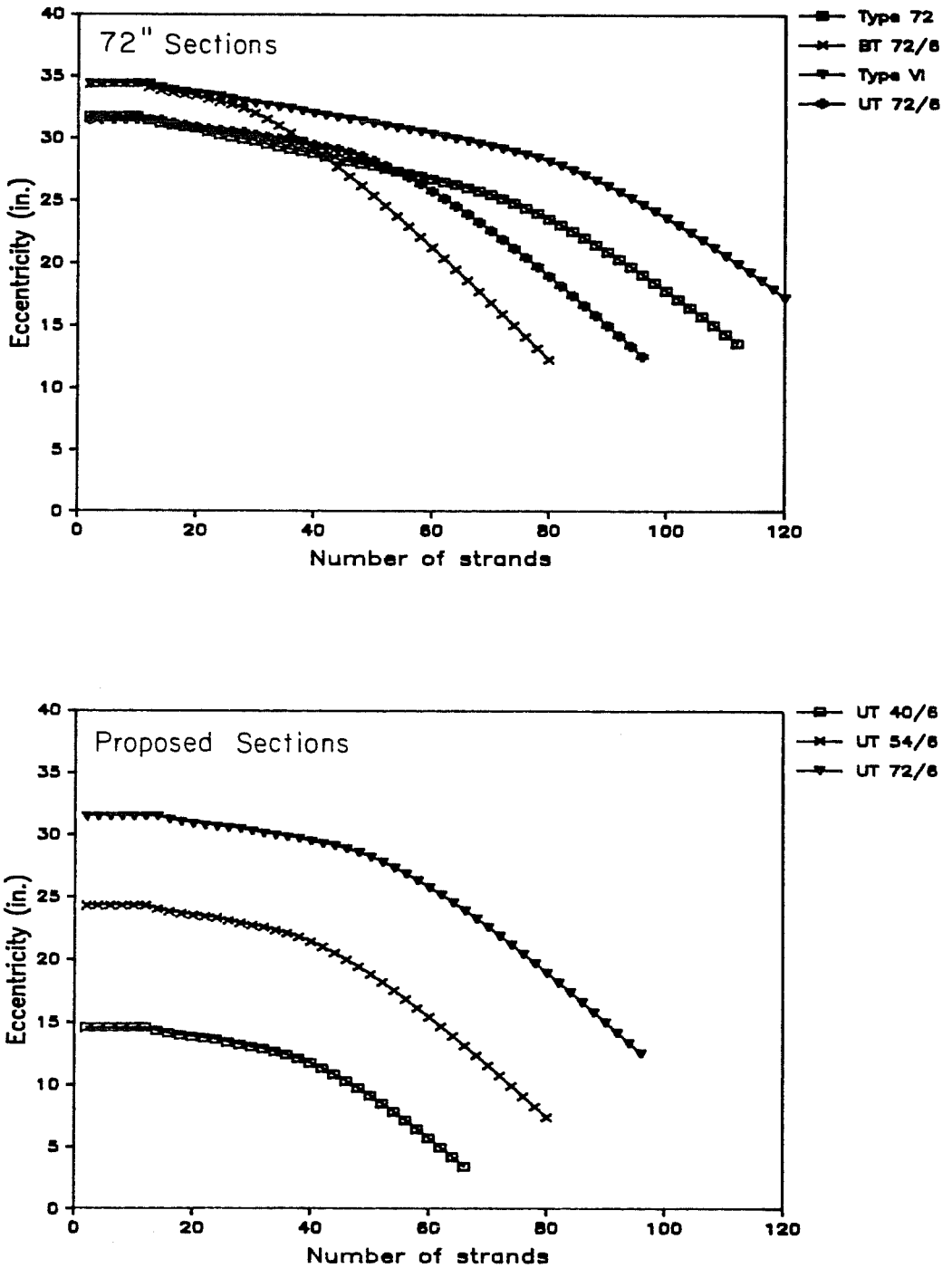

Fig. 2.5 Eccentricity versus number of strands (continued).

while other large beds have a capacity of 2 million lb. Using 0.5-in. diameter strands stressed to the maximum stress limit allowed by AASHTO ($0.8f_{pu}$, where f_{pu} is the specified ultimate stress of the strand), these beds would be limited to sections with no more than 74 and 60 strands, respectively. Using 74 strands as the limit for prestress bed capacity and the number of strands below the centroid from Table 2.4 as a general indication of the maximum number of strands used in a section, all designs with 40 and 54-in. sections could be constructed in Texas. Using the same basis for 72-in. sections, all designs utilizing the PCA BT and UT sections could be constructed, but some designs could not be built for the Texas and AASHTO sections due to excessive numbers of strands. However, larger capacity beds could be constructed or a combination of pretensioned and post-tensioned construction could be used to utilize designs with a large number of strands.

2.3.3 Girder Stability. Two aspects of girder stability will be considered here: the width of the bottom flange with respect to overturning, and the lateral stability of the girder. Both conditions are critical during handling and erection of the girder when it is unbraced and subjected to lifting loads. Section properties related to both conditions are given in Table 2.5 and are discussed below.

Table 2.5 Lateral stability factors for sections.

	I_y (in.^{4})	Maximum lifting span * (ft)	Tilt angle ** (deg)	Tilt ratio **
40-in. sections				
Texas Type C	13,020	106	32.8	1.55
UT 40/6	18,486	118	35.6	1.40
54-in. sections				
Texas Type 54	6,927	95	17.4	3.19
AASHTO-PCI Type IV	29,513	123	27.7	1.90
Modified Type IV	22,550	119	26.2	2.03
MOT/C&CA M 54/6	37,410	141	41.4	1.13
PCA BT 54/6	41,310	140	23.6	2.29
UT 54/6	23,578	121	26.3	2.02
72-in. sections				
Texas Type 72	24,707	123	18.1	3.07
AASHTO-PCI Type VI	72,776	149	21.1	2.60
PCA BT 72/6	41,634	145	18.3	3.03
UT 72/6	32,560	135	24.2	2.23

* - Spans were computed using the approach given in Ref. [6] and modified in Ref. [7,122], assuming:

Lifting points located at 5 percent of the span from ends of the girder, factor of safety against buckling (FS) = 2.0, E_c = 4,000 ksi, and $y_T = y_t$.

** - These values represent the angle or slope from the bottom corner of the bottom flange to the centroid of the girder (see Fig. 2.6).

From a conversation with a manufacturer of girders, it was learned that the Texas Type 72 girders tend to be unstable and may blow over in the wind if not adequately braced. The problem also exists with the Texas Type 54 girders, but to a lesser degree. This problem of overturning is related to the width of the base relative to the height of the member, and can be considered mathematically by computing a "tilt ratio" or "tilt angle" which is the slope or angle of the line connecting the outer edge of the bottom flange and the centroid of the section (see Fig. 2.6). This gives a quantitative indication of whether the section is top heavy with a tendency to turn over. As shown in Table 2.5, the two Texas sections mentioned above have the highest tilt ratios which appears to confirm the applicability of this measure for predicting overturning problems. The 72-in. PCA bulb-tee has a ratio very near those of the Texas sections, which indicates that overturning may be a problem for this section as well. The lower tilt ratios computed for other sections agree with experience in the field for these sections. The UT sections have ratios comparable or less than those associated with sections which generally exhibit no overturning problems. Therefore, it is unlikely that the proposed sections will experience problems associated with overturning.

An important factor in assessing the lateral stability of a section is the weak axis moment of inertia, I_y, which is given

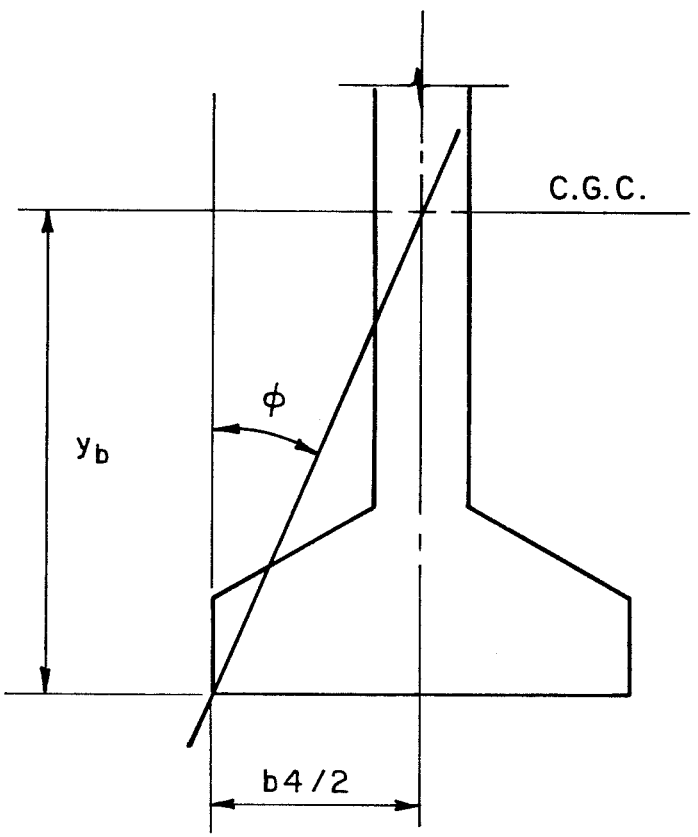

$$\text{TILT RATIO} = \frac{y_b}{b4/2}$$

$$\text{TILT ANGLE} = \phi$$

$$= \tan^{-1}\left(\frac{1}{\text{TILT RATIO}}\right)$$

Fig. 2.6 Definition of tilt ratio and tilt angles

for each section in Table 2.5. There is considerable variation, especially for the 54-in. sections. The UT sections have lower weak axis moments of inertia than bulb-tee and AASHTO sections but have greater values than the Texas sections.

Lateral stability of a member is generally most critical during lifting. This problem has been addressed in a number of papers [6,7,92,122,123]. Using a modified form [7,122] of a method given by Anderson [6], the maximum span permitted for lifting a girder can be determined, as shown in Table 2.5 (see Sec. 7.7.1, Eq. 7.13). The analysis is based on a factor of safety against buckling of 2. For the values in the table, the concrete modulus of elasticity, E_c, was assumed to be 4,000 ksi and lifting loops were assumed to be positioned at a distance equal to 5 percent of the span from each end of the girder. The dimension, y_T, was assumed to be the distance from the top face to the centroid of the girder. The analyses are presented and discussed in greater detail in Sec. 3.7 and 7.7.

The UT sections compare favorably with the Texas standard sections and the two forms of the AASHTO-PCI Type IV girder. However, sections with wide top or bottom flanges showed marked increases in maximum span length. This trend was quite evident for the 54-in. sections but less pronounced for the 72-in. sections. This analysis shows that UT sections have maximum spans as long or longer than other

I-shaped sections but shorter than sections with very wide top or bottom flanges.

It should be noted that the maximum lifting spans which appear in Table 2.5 are not absolute limits and that spans exceeding these limits can be used if appropriate measures are taken. Spans may be increased by moving lifting loops farther into the span, although stresses must be checked at critical locations. Moving the lifting loops to a distance of 10 percent of the span from the ends results in a 12.5 percent increase in the span lengths given in Table 2.5 for all sections. The use of rigidly attached lifting yokes at the ends of the girder will also improve the maximum lifting span by increasing y_T. Raising the lifting point 12 in. above the top of the girder increases the maximum spans given in Table 2.5 by 7 to 11 percent. Changing the modulus of elasticity of concrete from 4,000 to 5,400 ksi, which corresponds to an increase in concrete strength from 4 to 9 ksi, results in an increase in the maximum span of 7.8 percent for all sections.

Because the maximum span capability of many sections is limited by the maximum lifting span, spans in excess of the lifting limit will be indicated, where appropriate, by a broken line on the figures that follow. The maximum lifting span, however, does not remain constant in these figures, but increases with increasing concrete strength. The modulus corresponding to the concrete strength

at release, which is defined below for these designs, is used to determine the maximum lifting span.

The maximum lifting span limit will be compared with field experience in Texas in Sec. 3.7.2 and with behavior observed during fabrication and testing of long-span scale-model girder specimens in Sec. 7.7.2.

2.4 Comparison of Designs

A series of designs was performed using the sections presented earlier in this chapter. Girder spacings (GS) of 4, 7 and 10 ft were used with concrete design strengths varying from 6 to 15 ksi. Unless indicated otherwise, the concrete at release was 75 percent of the design strength, except for 6 ksi designs where the release strength was 5 ksi (83 percent). All designs used low relaxation seven wire strand of 0.5-in. diameter except for a limited series which used 0.6-in. diameter low relaxation strands and is noted as such. Strand patterns described in the preceding sections were used.

Designs conformed to the AASHTO Specifications [10], using allowable stress and ultimate strength design criteria and specified highway bridge loadings including impact. The criteria used in these designs were found, in Chapter 7, to be acceptable for use with high strength concrete. These design computations were performed using the computer program BRIDGE which is described in Appendix C.

2.4.1 Maximum Spans. The maximum span for which the allowable stress and ultimate strength design criteria could be satisfied was determined for combinations of girder spacing and concrete strength for each section. The results of these maximum span designs are summarized in the plots of Fig. 2.7 through 2.10. The figures show the increase in maximum span with increasing concrete strength for the sections and girder spacings considered. In order to more clearly show the increase in maximum span length with increasing concrete strength, ratios of the maximum span length to the maximum span for the 6 ksi design are plotted versus concrete strength in Fig. 2.11 through 2.14. For both series of figures, a separate figure is provided for each section depth, and the final figure shows the plots for the three proposed sections. Sub-figures are used to show the plots for the three girder spacings as required for clarity. Where spans exceed the maximum lifting spans computed using the modulus corresponding to the concrete strength at release, broken lines are used to define the curves. Maximum lifting spans for designs with a design strength of 15 ksi are 10.7 percent greater than those for 6 ksi designs. The values found in Table 2.5 are very close to the maximum lifting spans actually used for some 6 ksi designs. Results for each section depth will be reviewed, then overall trends observed in these figures will be discussed.

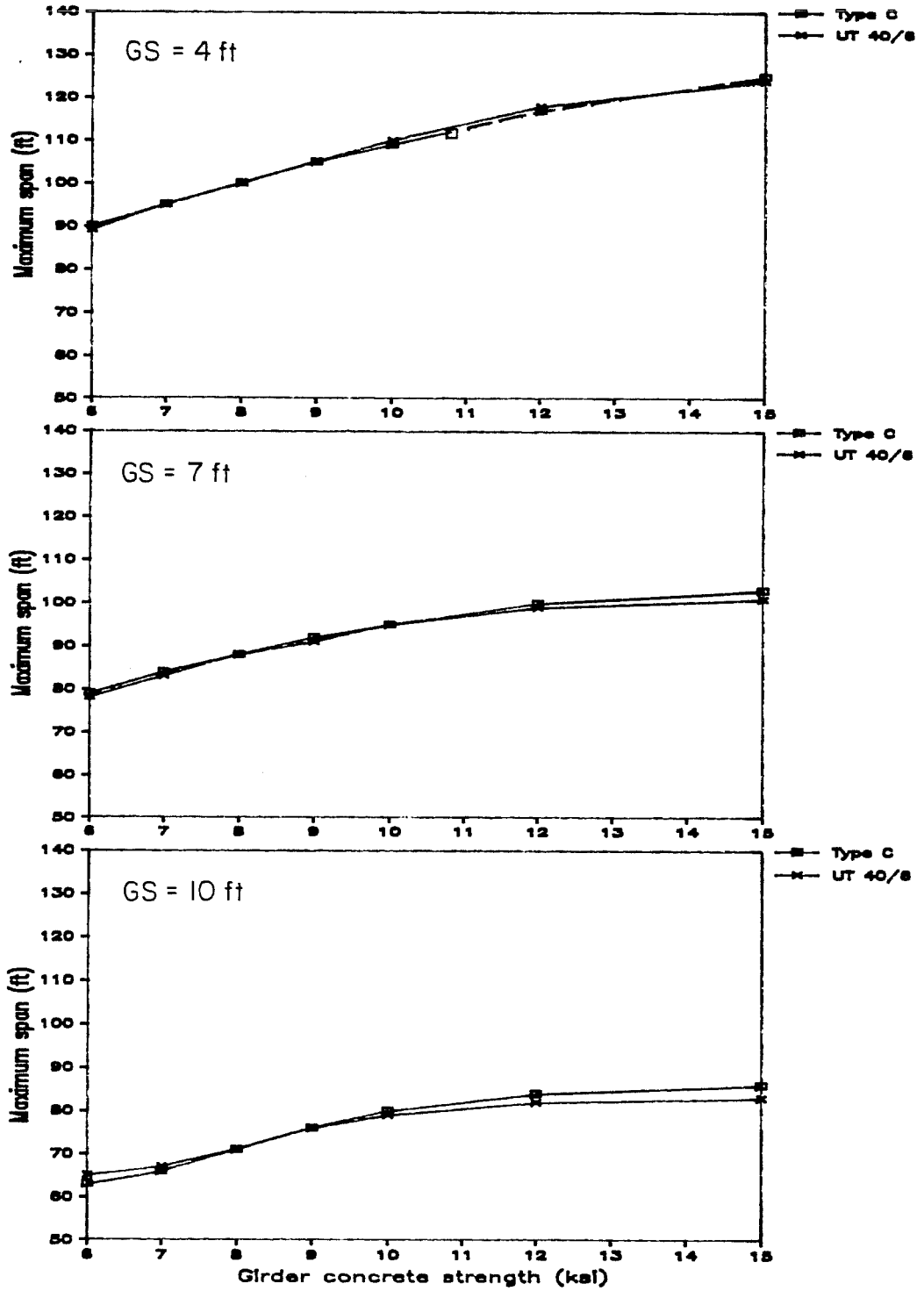

Fig. 2.7 Maximum span versus concrete strength - 40" sections.

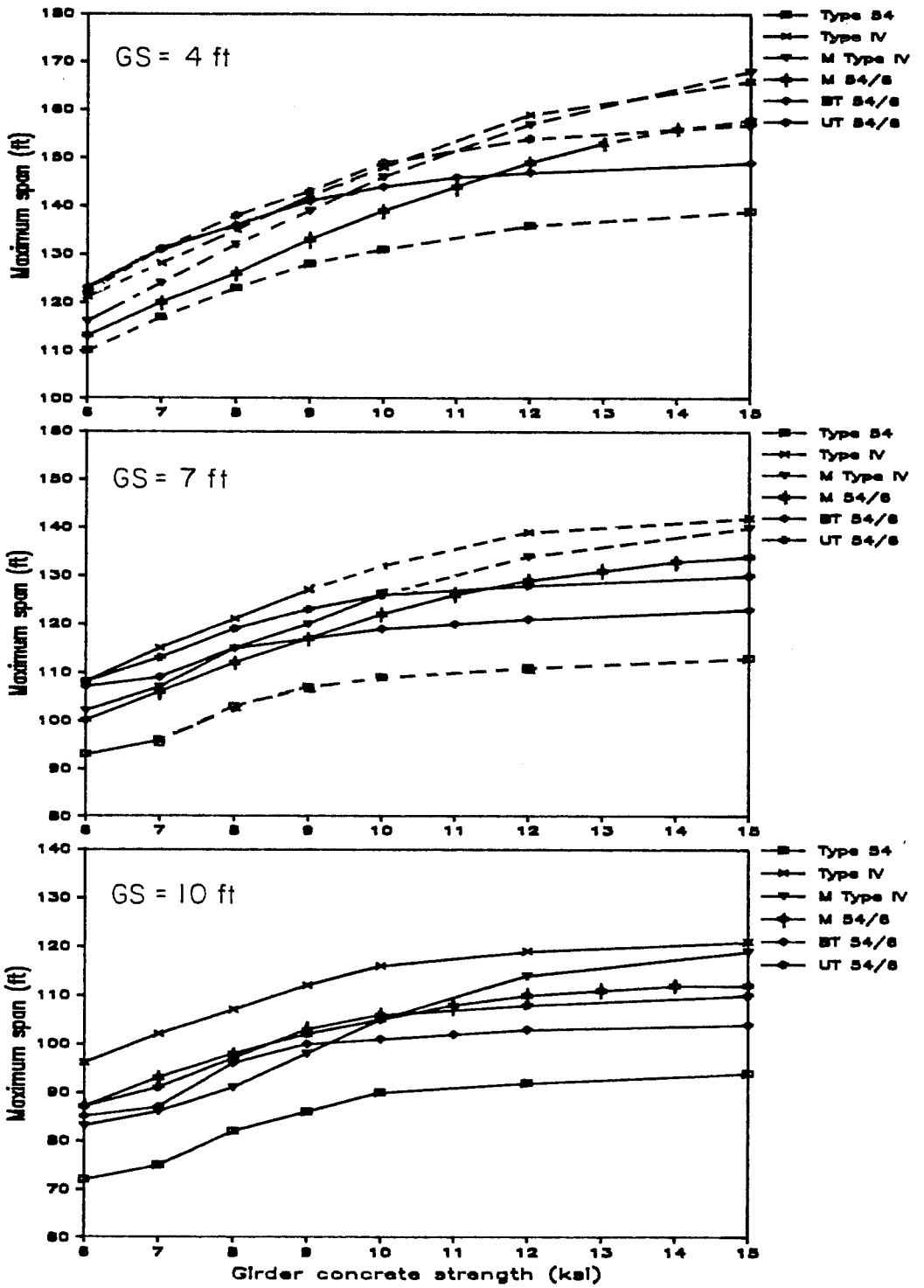

Fig. 2.8 Maximum span versus concrete strength - 54" sections.

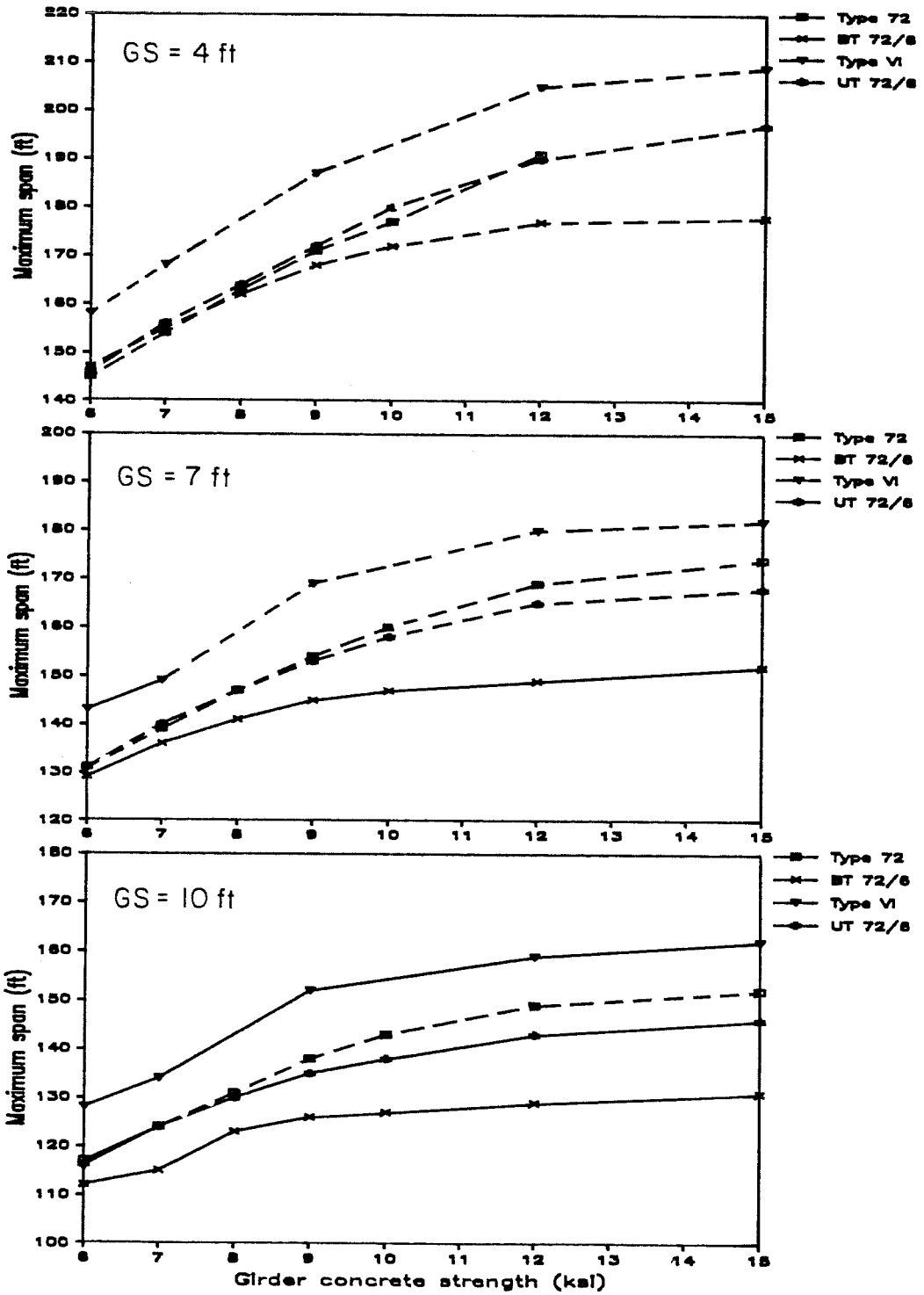

Fig. 2.9 Maximum span versus concrete strength - 72" sections.

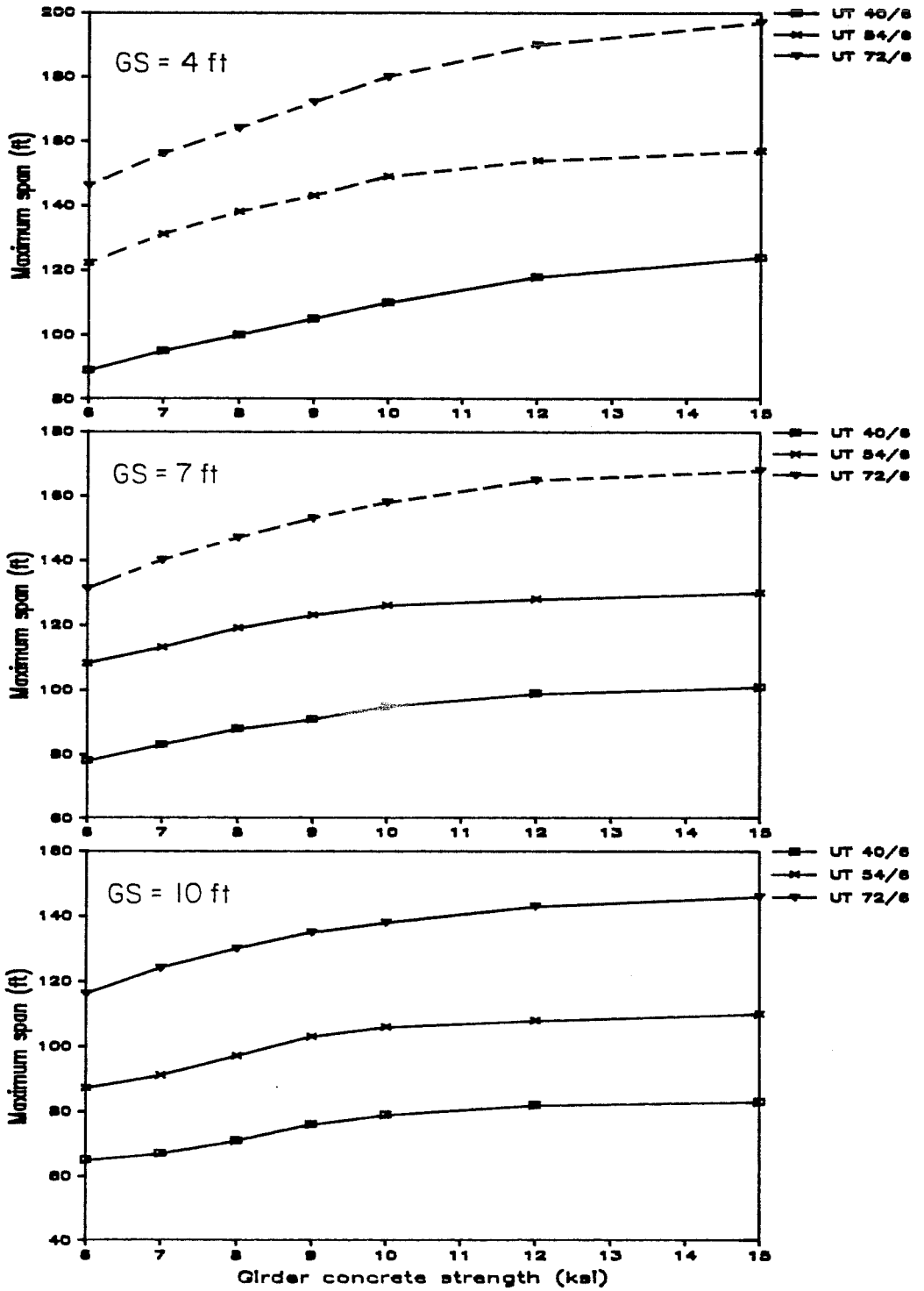

Fig. 2.10 Maximum spans versus concrete strength - proposed sections.

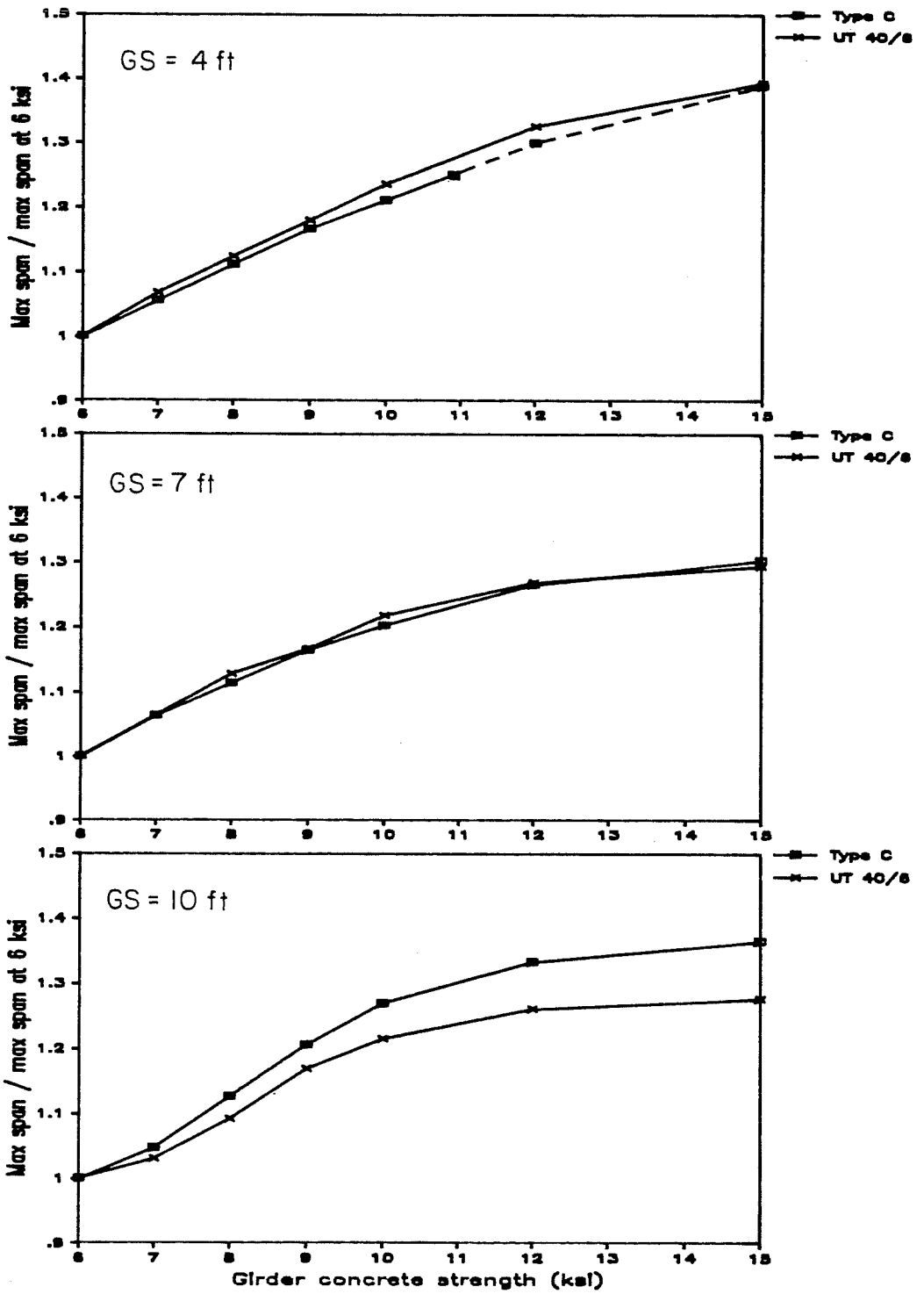

Fig. 2.11 Ratio of increase in maximum span versus concrete strength for 40" sections.

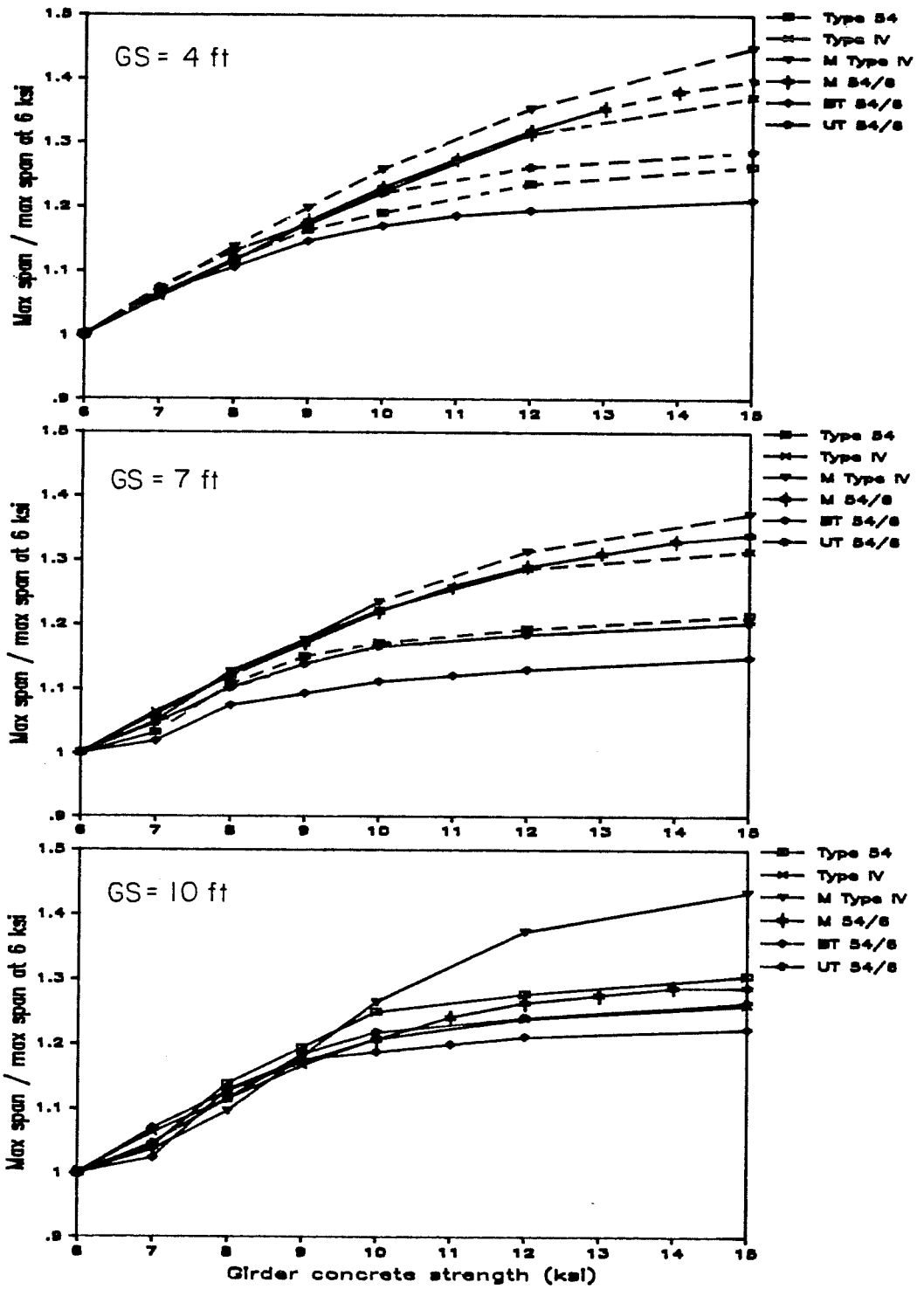

Fig. 2.12 Ratio of increase in maximum span versus concrete strength for 54" sections.

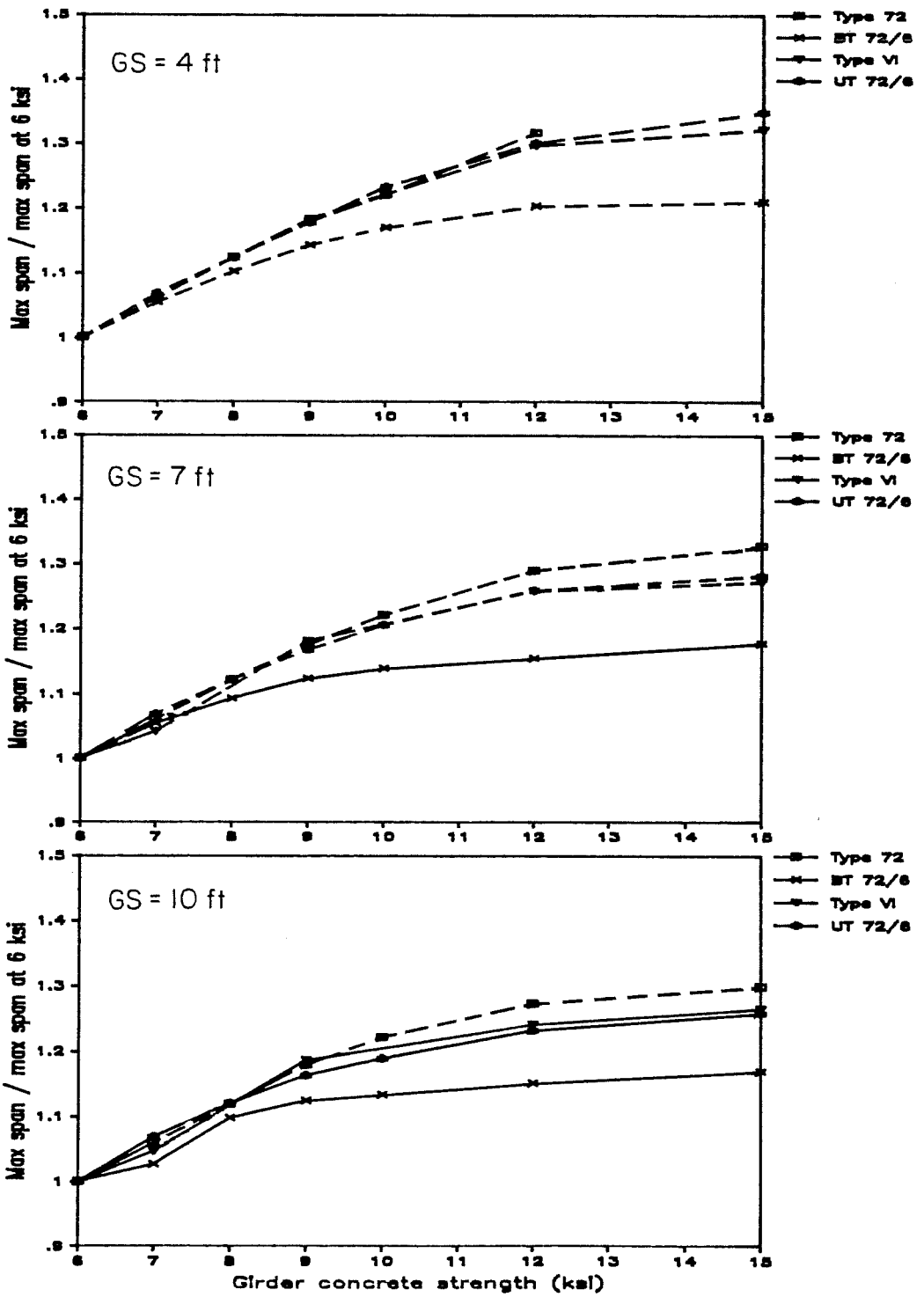

Fig. 2.13 Ratio of increase in maximum span versus concrete strength for 72" sections.

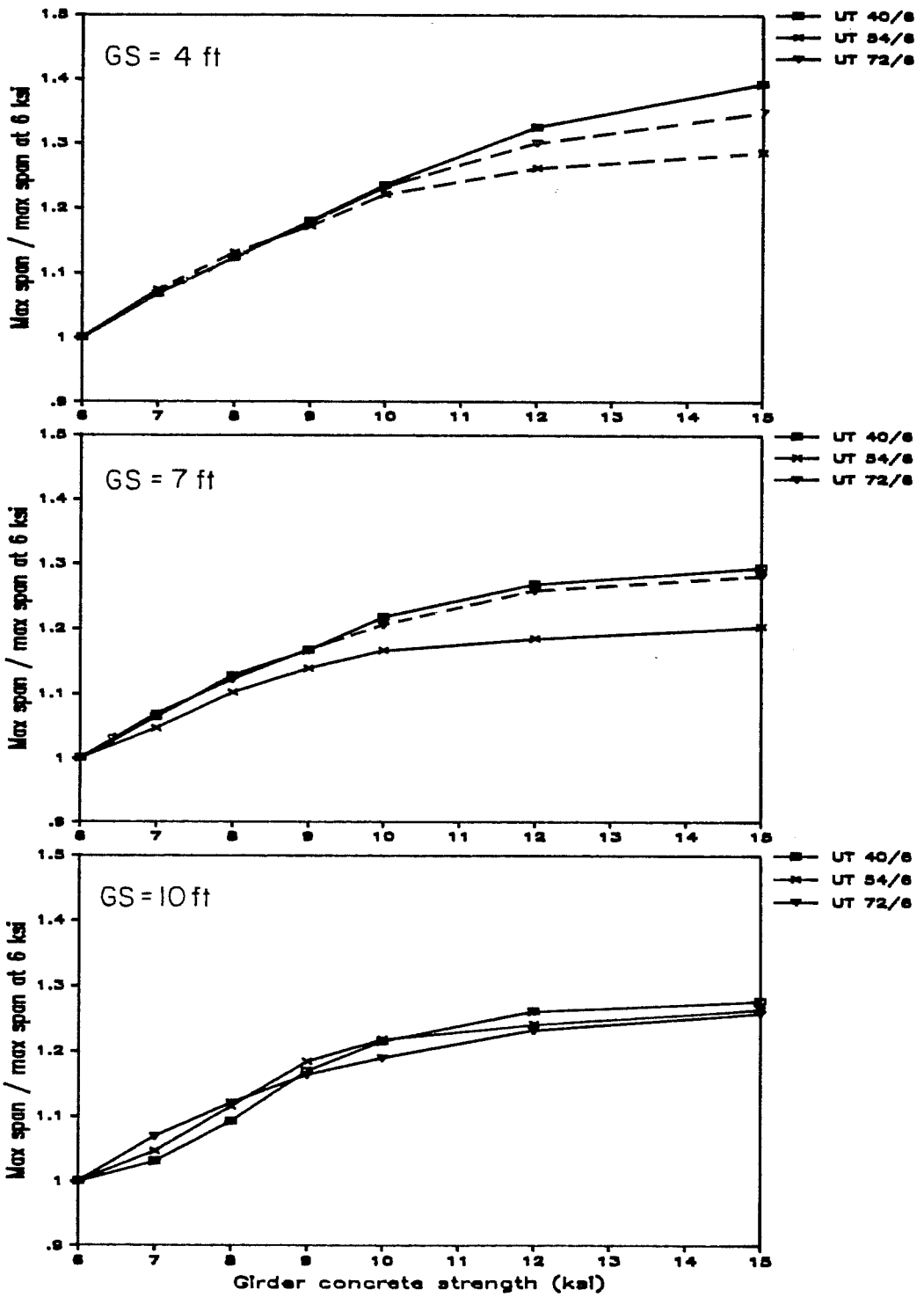

Fig. 2.14 Ratio of increase in maximum span versus concrete strength for proposed sections.

Maximum spans for the two 40-in. sections were similar for all concrete strengths and girder spacings, with the difference in spans never exceeding 3 ft. The figures indicate that spans in excess of 110 ft can be obtained using these sections with high strength concrete. The increase in span from normal strength (6 ksi) concrete to 12 ksi concrete ranged from approximately 30 to 40 percent with an increase of approximately 15 to 20 percent for 9 ksi concrete. The plots indicate that spans continue to increase even with very high strength concrete. Designs for the Type C section with GS = 4 ft and f_c' greater than 11 ksi are the only designs to exceed maximum lifting spans. Therefore, stability does not appear to be a large concern for maximum span designs using 40-in. sections.

The maximum spans for the 54-in. sections show great variability due to the variety of sections examined. The very light Texas Type 54 produced the shortest spans and the heaviest section, the AASHTO-PCI Type IV, gave the longest spans for all but a few cases. All sections except the Texas Type 54 and the bulb-tee reached spans in excess of 150 ft for GS = 4 ft. The proposed section had spans that were very close to the spans for the Type IV section for lower concrete strengths at GS = 4 and 7 ft while, for GS = 10 ft and concrete strengths in excess of 9 ksi, the proposed section gave spans of approximately 10 ft less than the Type IV. Some sections showed continuing increases in span with increasing concrete strength

while the increase in maximum span length for most sections decreased or stopped for concrete strengths greater than 10 ksi. The Type IV, modified Type IV, and M54/6 (or inverted-tee) girders showed the most consistent span gain with increasing concrete strength, especially for girder spacings of 4 and 7 ft. Span lengths for the bulb-tee increased only 15 to 20 percent for high strength concretes. The proposed section provides an increase in maximum span length of about 5 percent over the bulb-tee for high strength concrete, but this increase is less than most other sections provide.

The lateral stability of 54-in. sections at maximum spans is a significant concern for the closer girder spacings. Only the bulb-tee and inverted-tee (M 54/6) sections had maximum span designs less than the maximum lifting span for concrete strengths of 7 ksi or greater for GS = 4 ft. This means that the increase in span length with higher strength concrete cannot be realized for most sections due to stability considerations. For GS = 7 ft, maximum span designs for bulb- and inverted-tee sections and the proposed (UT) section were unaffected by maximum lifting span limitations. A significant increase in maximum spans for the Type IV and Modified Type IV sections occurred before the maximum lifting span was exceeded at concrete strengths of 9 and 10 ksi, respectively. The Type 54 was still severely limited by stability considerations at this girder spacing. For GS = 10 ft, maximum span designs remained below the

maximum lifting spans for all sections. Therefore, stability is a major concern where high strength concrete is used to obtain longer spans for closely spaced 54-in. girders and may restrict the use of span lengths that would otherwise be acceptable. In general, sections with the largest weak axis moment of inertia are affected least by stability limitations.

The maximum spans were similar for the proposed 72-in. section and Texas Type 72 section for all concrete strengths and girder spacings. The AASHTO Type VI had significantly greater spans and the bulb-tee had shorter spans. The Type VI could be used to reach spans of over 200 ft with high strength concrete, while the proposed and Texas Type 72 sections reached spans in excess of 180 ft. These spans are too long to be practical for general use and therefore are not of great significance. For the proposed section, the increase in span from normal strength concrete to 12 ksi concrete ranged from about 25 to 30 percent with an increase of approximately 15 to 20 percent for 9 ksi concrete. Spans did not increase significantly for concrete strengths greater than 12 ksi.

These plots indicate that maximum span designs for the 72-in. sections are limited even more severely by stability considerations than the 54-in. sections. For GS = 4 ft, all designs shown exceed the maximum lifting spans. For GS = 7 ft, only small increases in the maximum spans are possible before the maximum lifting span is

exceeded, except for the bulb-tee designs which did not exceed the maximum lifting span limit. At GS = 10 ft, designs for the Texas Type 72 were still severely limited while designs for all other sections were unaffected by the lifting span limit. As for the 54-in. sections, stability considerations are very significant in the design of long spans using 72-in. sections and will restrict, in many cases, the possible span lengths resulting from increased concrete strength.

The plots for the proposed sections (Fig. 2.10) indicate that a wide range of spans can be obtained using the three sections. The sections also exhibit similar behavior in that increasing concrete strengths result in increased maximum spans for concrete strengths up to at least 10 ksi. This is also evident in Fig. 2.14, where spans for the 40 and 72 in. sections increase approximately 25 to 40 percent with increasing concrete strength, while the 54-in. section gives roughly a 20 to 25 percent increase and exhibits a reduction in the rate of span increase at a lower concrete strength.

Figure 2.10 also indicates that for these sections stability limitations are more restrictive as the section depth increases. Maximum span designs for the 72-in. section are significantly restricted for GS = 4 and 7 ft while maximum span designs for the 40-in. section are unaffected by the lifting span limit. Maximum span designs for the UT 54/6 are limited by stability only for GS = 4 ft.

All of these figures indicate a general trend that, as girder spacing increases, the benefit from use of the higher concrete strengths is reduced. This means that for GS = 10 ft, the maximum useful concrete strength is about 9 ksi, but for GS = 4 ft, the use of concrete with strengths in excess of 12 ksi continues to provide noticeable increases in span length. Sections with greater area also appear to provide greater spans which is most evident for the AASHTO-PCI Type IV and VI sections.

A plateau is apparent in a number of the curves at lower concrete strengths. This is attributed to the use of a 5 ksi release strength for 6 ksi designs which is a higher proportion of the design strength than was used for other designs.

Maximum span data can also be presented as a plot showing the maximum girder spacing permitted for a given span and concrete strength. This type of plot is shown for the AASHTO-PCI Type IV section in Fig. 2.15 for spans of 100, 120, and 140 ft. As noted the figure, the 140 ft span exceeds the maximum lifting spans for the section for all concrete strengths considered.

These data indicate that a significant increase in girder spacing is possible when increased concrete strengths are used. However, strengths in excess of about 11 ksi provide little additional benefit. This plot shows that for a 120-ft span, half the number of girders will be required if a concrete strength of approximately 8.5

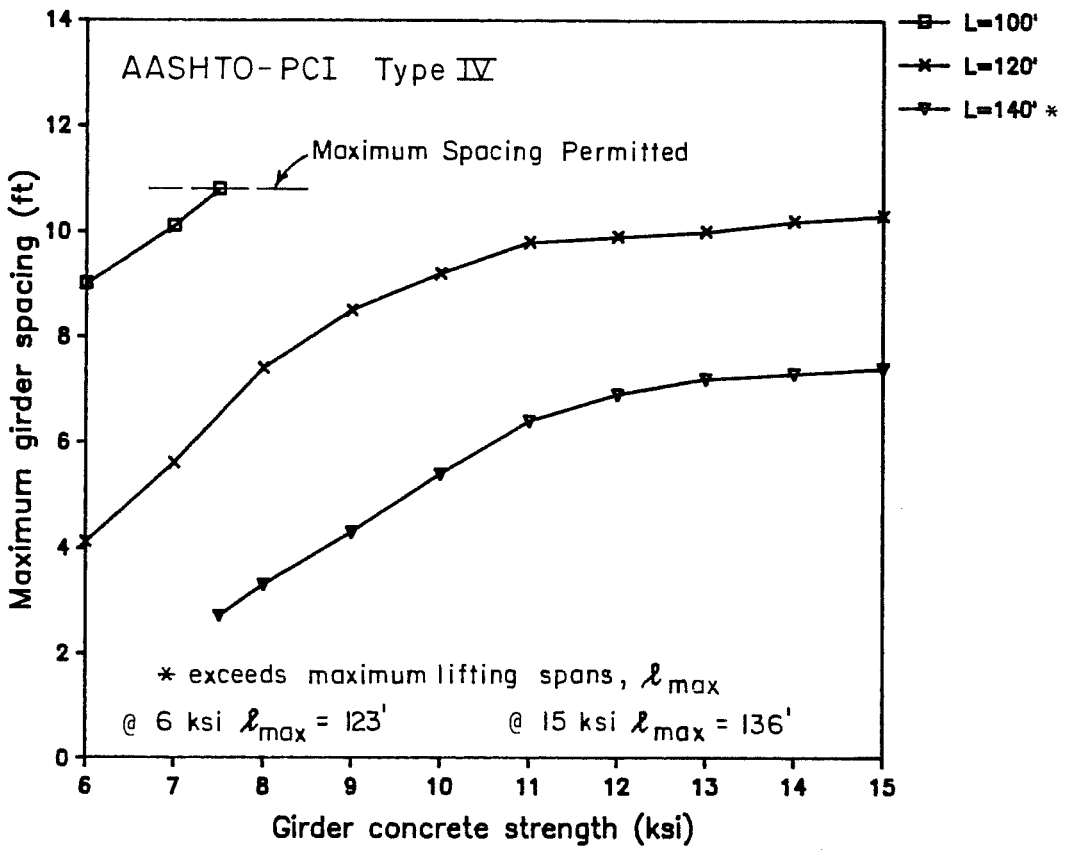

Fig. 2.15 Variation in girder spacing with concrete strength.

ksi is used instead of 6 ksi, which is the normal concrete strength for pretensioned girders in Texas. This is a significant reduction for only a moderate increase in concrete strength. It should be noted that this benefit only occurs for longer spans and that for shorter spans, the effect of increasing concrete strength is limited by maximum allowable spacing requirements.

2.4.2 Strand Usage. Strand usage for two types of designs will be discussed in this section. The number of strands required to produce the maximum spans examined above will be considered first. Then, the effect of concrete strength on the number of strands required for a given span will be investigated. The minimum number of strands required for the maximum spans are plotted versus the concrete strength in Fig. 2.16 through 2.19, for each section depth and for the proposed sections, respectively. In most cases, strand usage parallels the maximum span plots with sections demonstrating the greater maximum spans requiring more strands to achieve the greater span. This is an expected observation and reveals little about section efficiency. Some designs using the AASHTO-PCI Type IV and Type VI sections and the Texas Type 72 section may require a number of strands greater than the capacity of current prestress beds in Texas, which is indicated on the figures. This indicates that the large maximum spans shown in preceding plots may not only be impractical from the perspective of handling and transportation, but

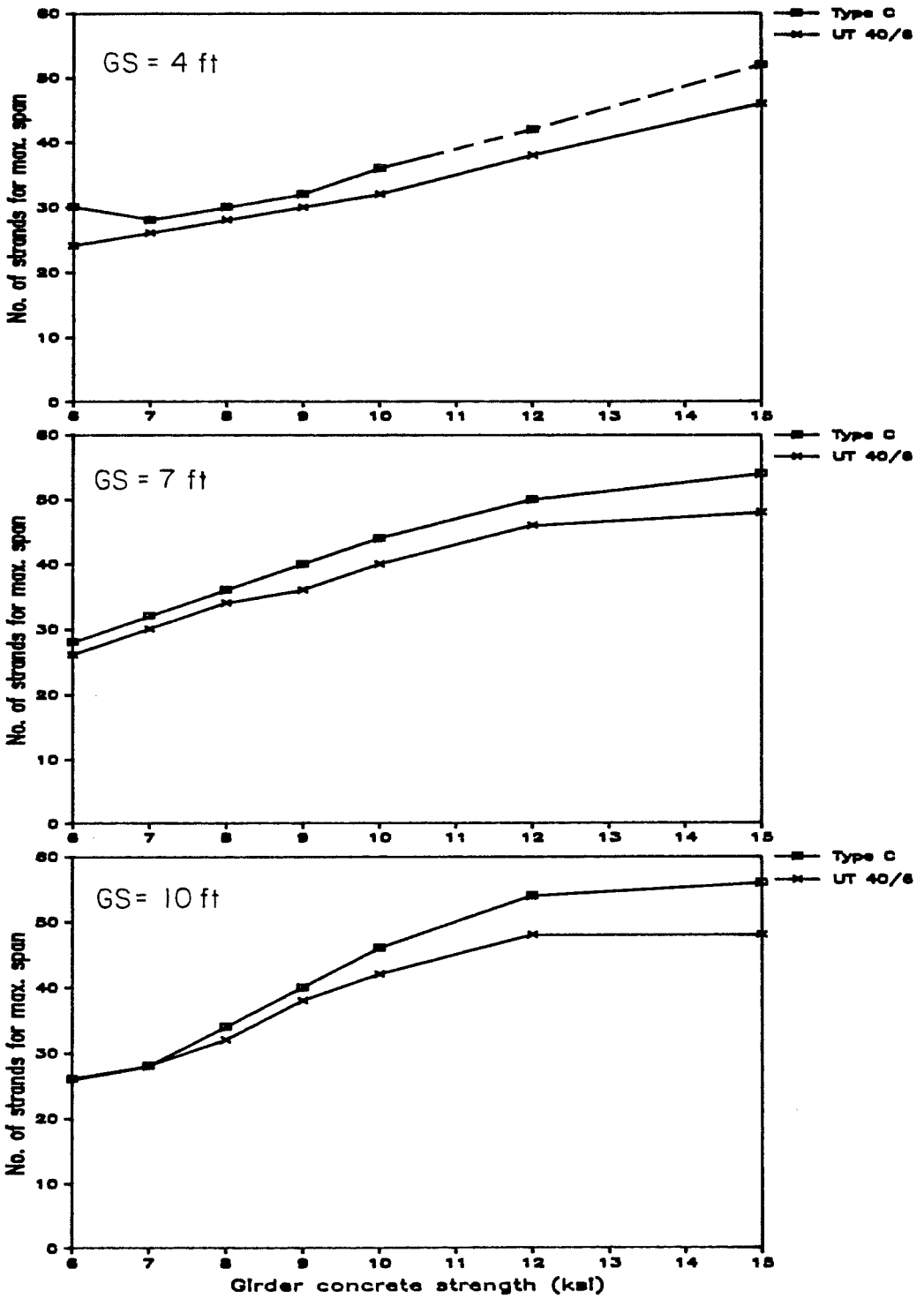

Fig. 2.16 Numbers of strands for maximum span versus concrete strength - 40" sections.

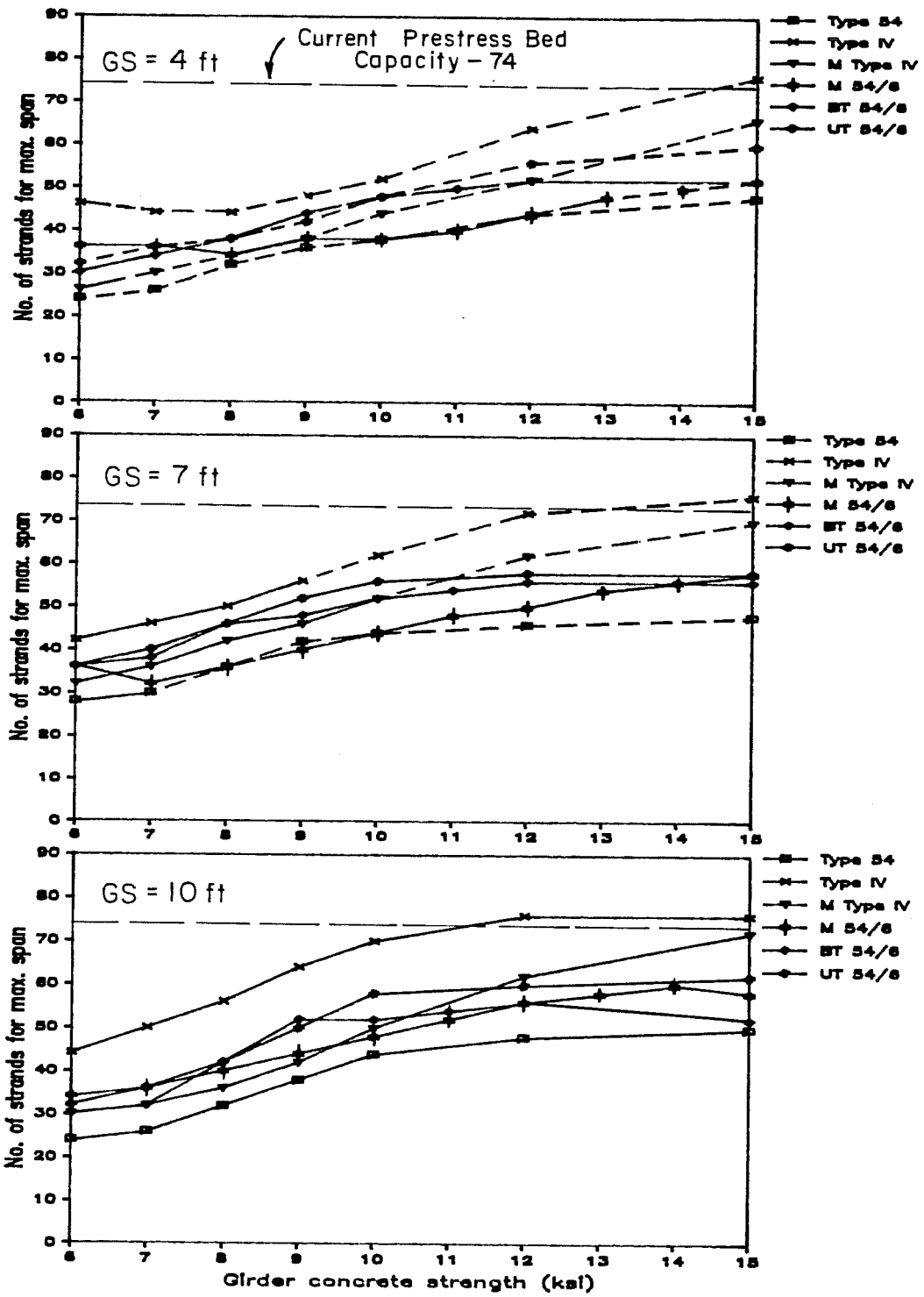

Fig. 2.17 Numbers of strands for maximum span versus concrete strength - 54" sections

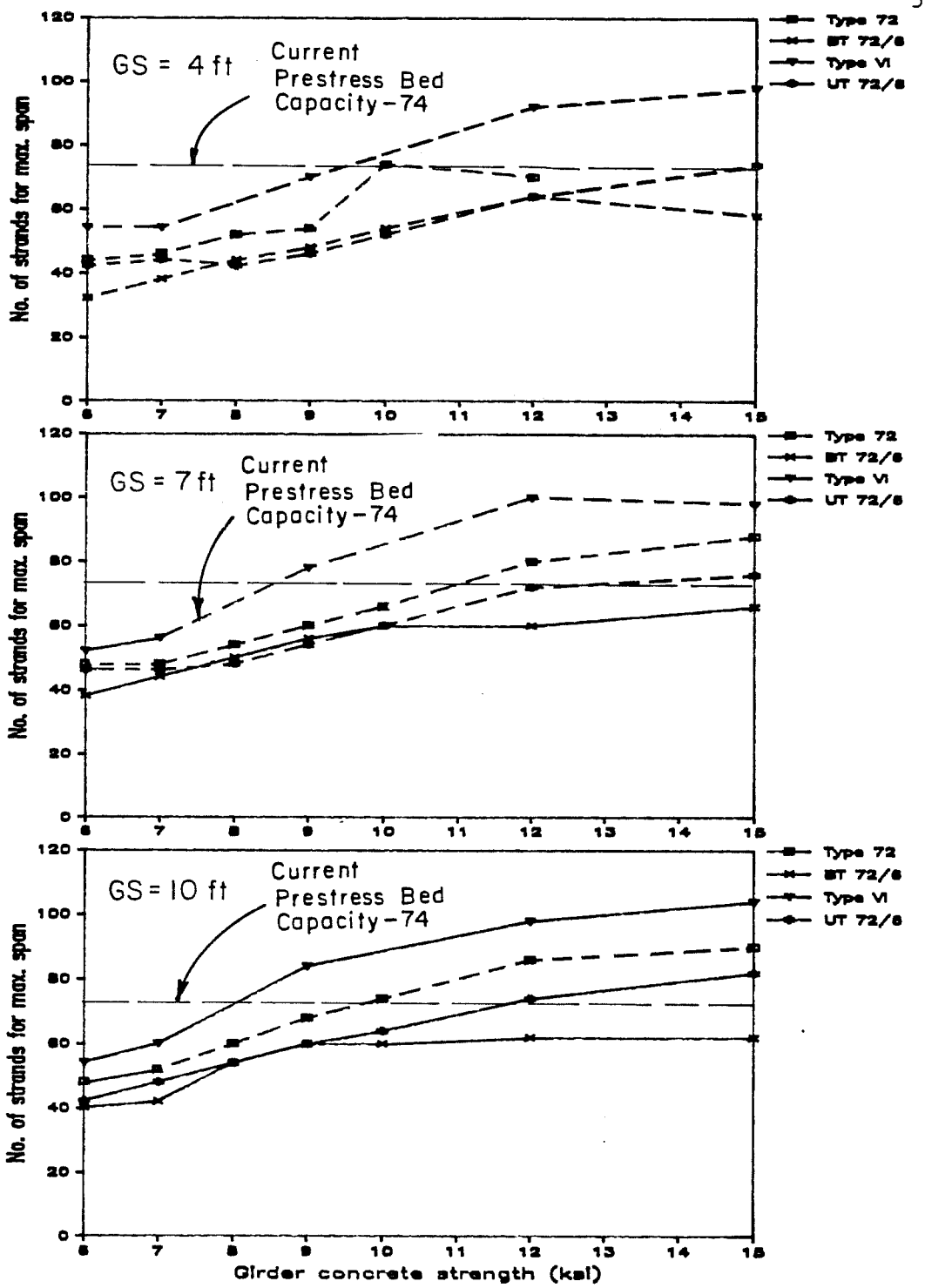

Fig. 2.18 Numbers of strands for maximum span versus concrete strength - 72" sections

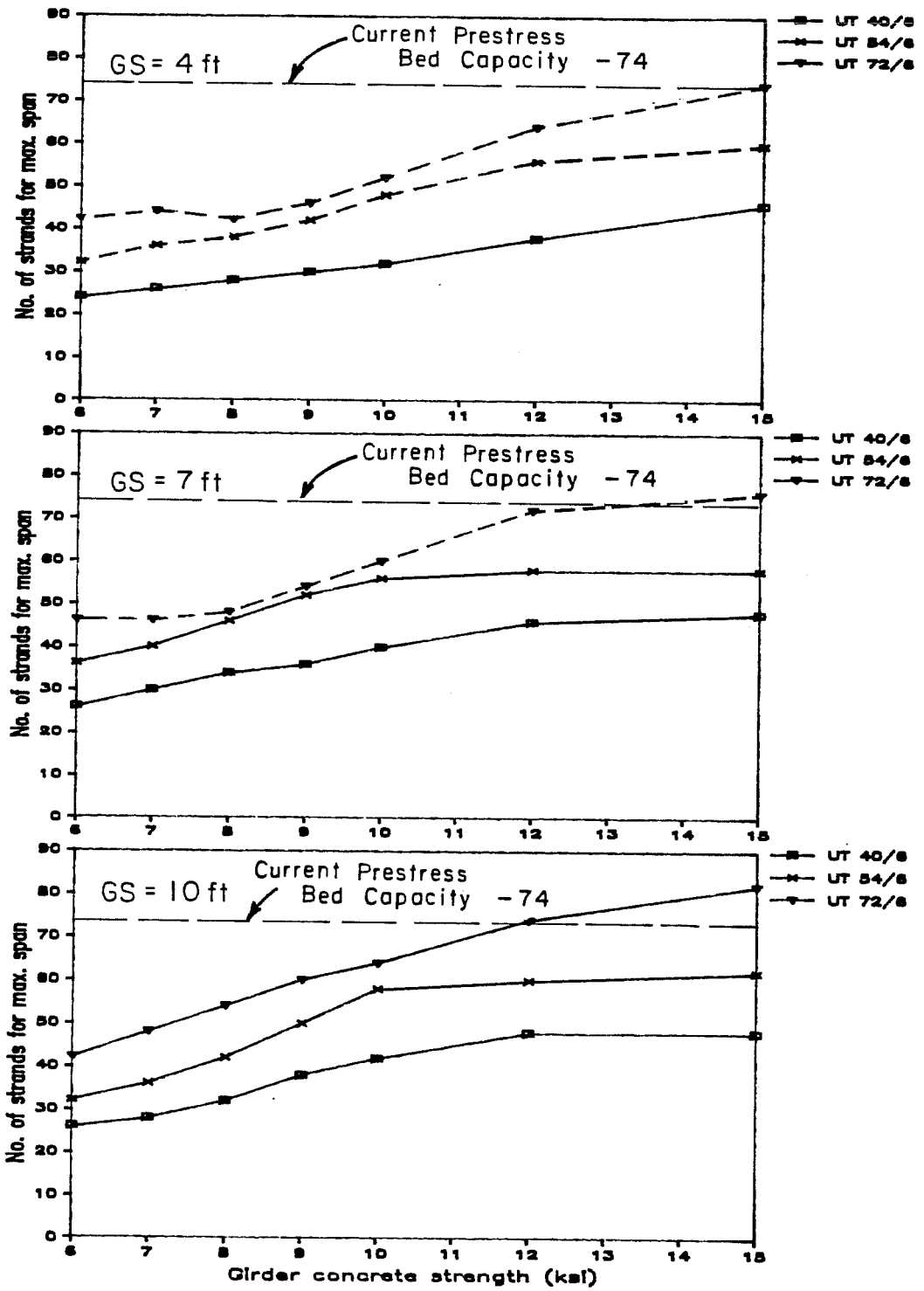

Fig. 2.19 Number of strands for maximum span versus concrete strength - proposed sections

also with respect to construction, since such large prestress forces are required. The proposed 72-in. UT section requires up to 80 strands, but only for very high concrete strengths.

For maximum span designs, the number of strands indicated on the figures generally represents both the minimum and maximum number of strands that can be used for the maximum span. This is because a maximum span is usually defined by the convergence of more than one limiting stress as illustrated in Fig. 2.20 for an AASHTO-PCI Type IV girder. For different combinations of section, girder spacing, span, and concrete strength, different combinations of stress limits define the maximum span. In some cases, a single condition may control the design in cases where strands are being added above the centroid of the section (Fig. 2.20, GS = 4 ft). Designs may also be controlled because draping strainds at the ends of the girder is not sufficient to keep stresses within allowable limits at release.

The minimum number of strands required for spans up to the maximum span are shown in Fig. 2.21 for AASHTO-PCI Type IV and 54 in. bulb-tee sections. Data are presented for two girder spacings and the figure for both sections. Data are presented for two girder spacings and four concrete strengths. The data indicate that the number of strands required for the maximum span increases rapidly for longer spans, which are possible through the use of higher concrete strengths. Approximately the same number of strands is required for

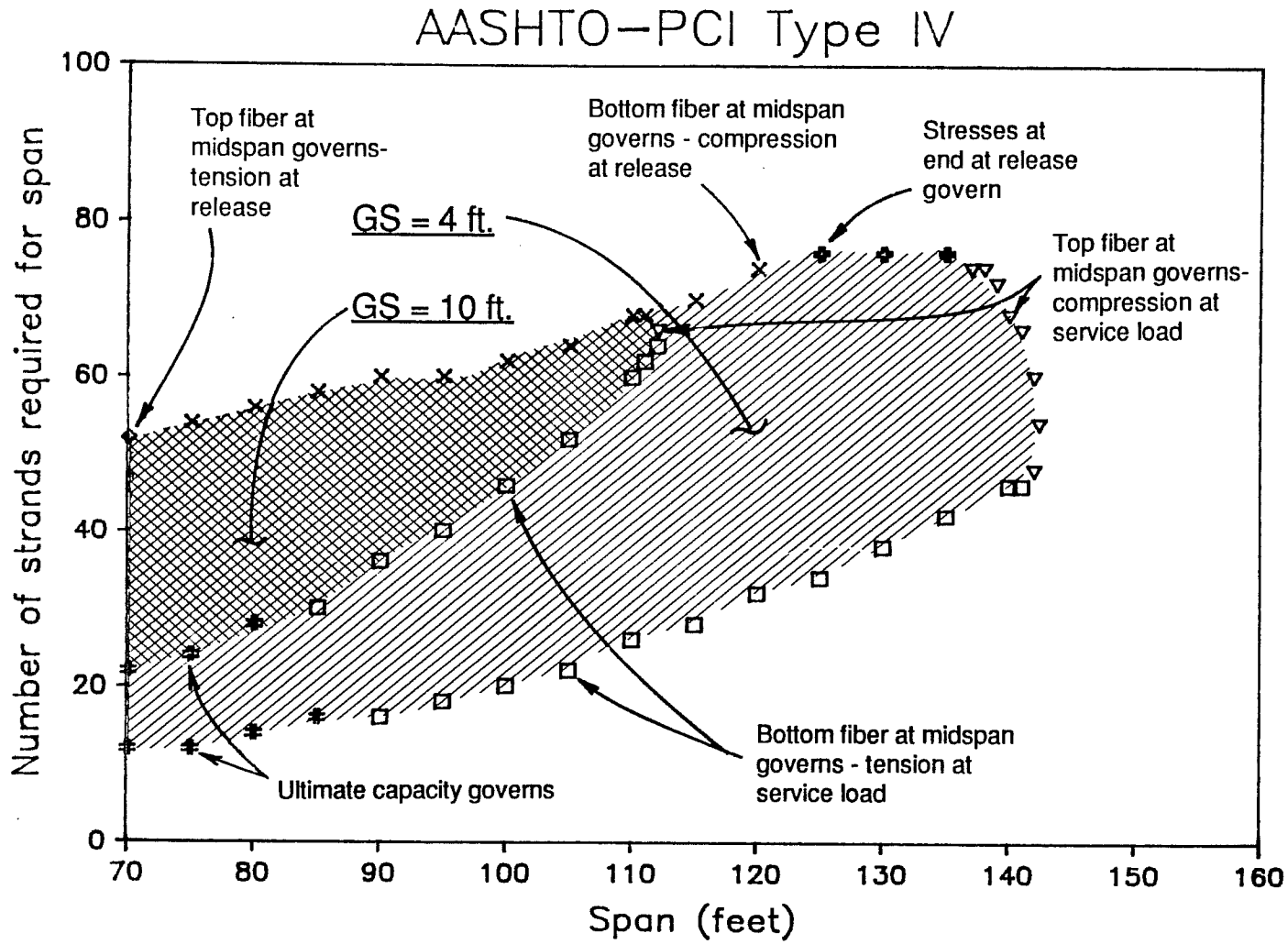

Fig. 2.20 Conditions controlling number of strands with increasing spans

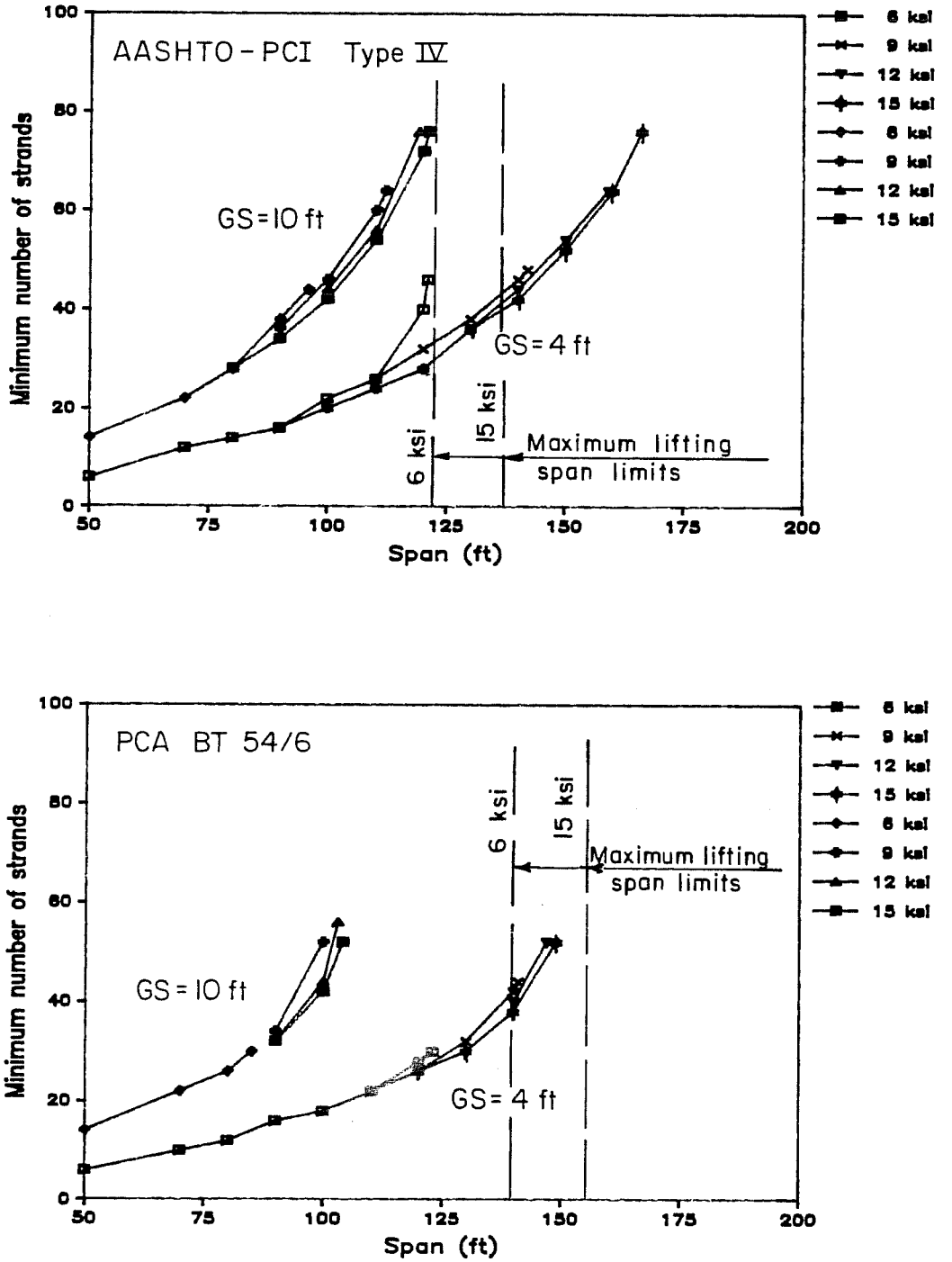

Fig. 2.21 Variation in number of strands required for maximum spans.

a maximum span design at the two girder spacings. The range of maximum lifting spans for the concrete strengths considered is indicated on the figure for both sections.

The minimum number of strands required to obtain a given span versus concrete strength is shown in Fig. 2.22 for an AASHTO-PCI Type IV section. The data show that the number of strands used in spans less than the maximum span are not significantly affected by the concrete strength. Therefore, there is no significant benefit with respect to strand usage when replacing normal strength concrete with high strength concrete in an otherwise identical bridge design. The ultimate capacity of the section is found to control the designs of many of the short span girders.

2.4.3 Section Efficiency. An indication of the efficiency of the different sections was obtained by dividing maximum spans (determined by allowable stress and ultimate strength criteria) by the girder area and by the number of strands required for the span. The resulting values represent the span per unit of cross-sectional area and the span per strand and therefore, larger values indicate a more efficient use of girder area or strands. The maximum span to area ratios are plotted in Fig. 2.23 through 2.26 and the maximum span to number of strand ratios are plotted in Fig. 2.27 through 2.30. For each ratio, a figure is provided for each section depth and the proposed sections. Spans exceeding maximum lifting spans are

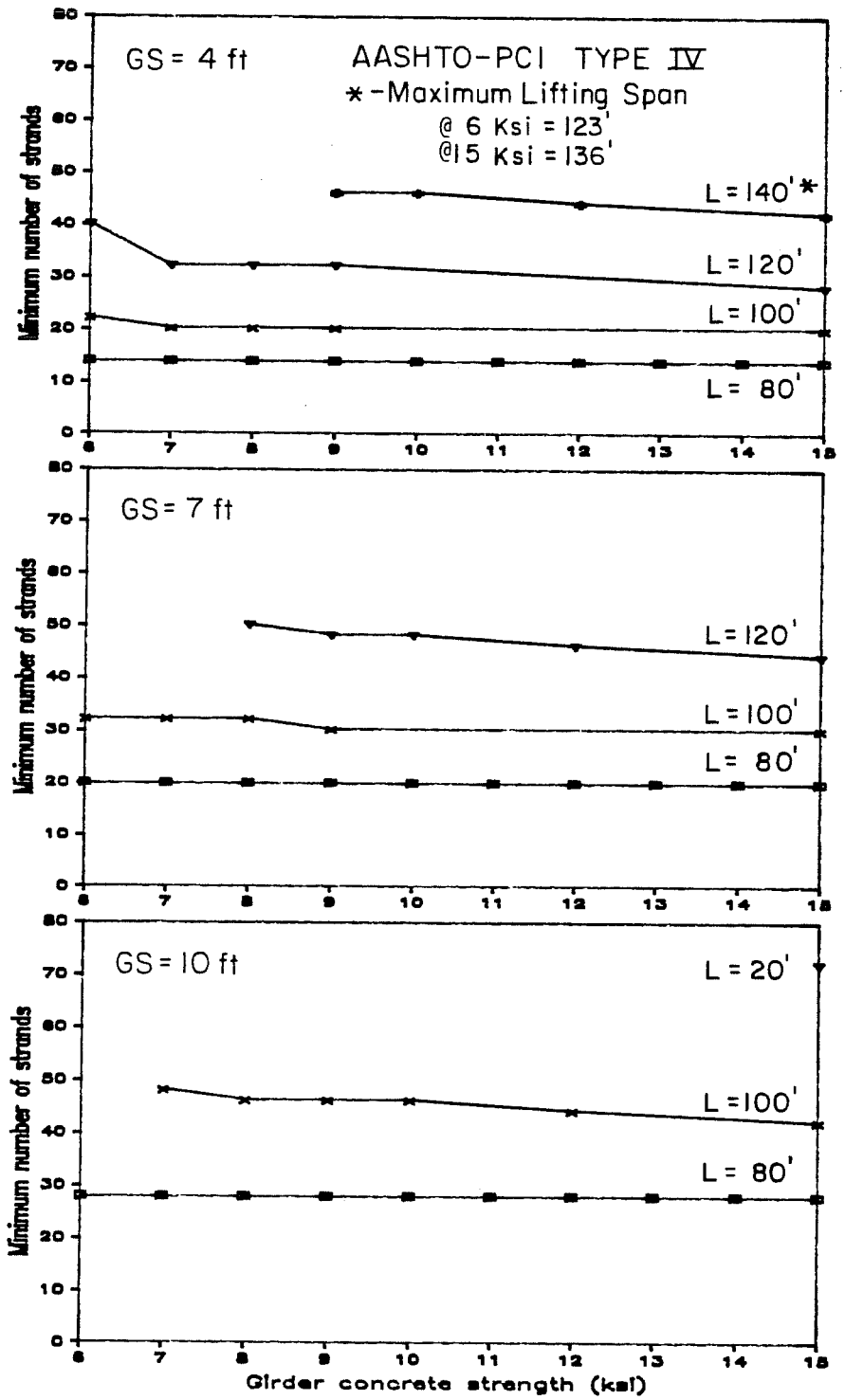

Fig. 2.22 Variation in minimum number of strands with girder concrete strengths.

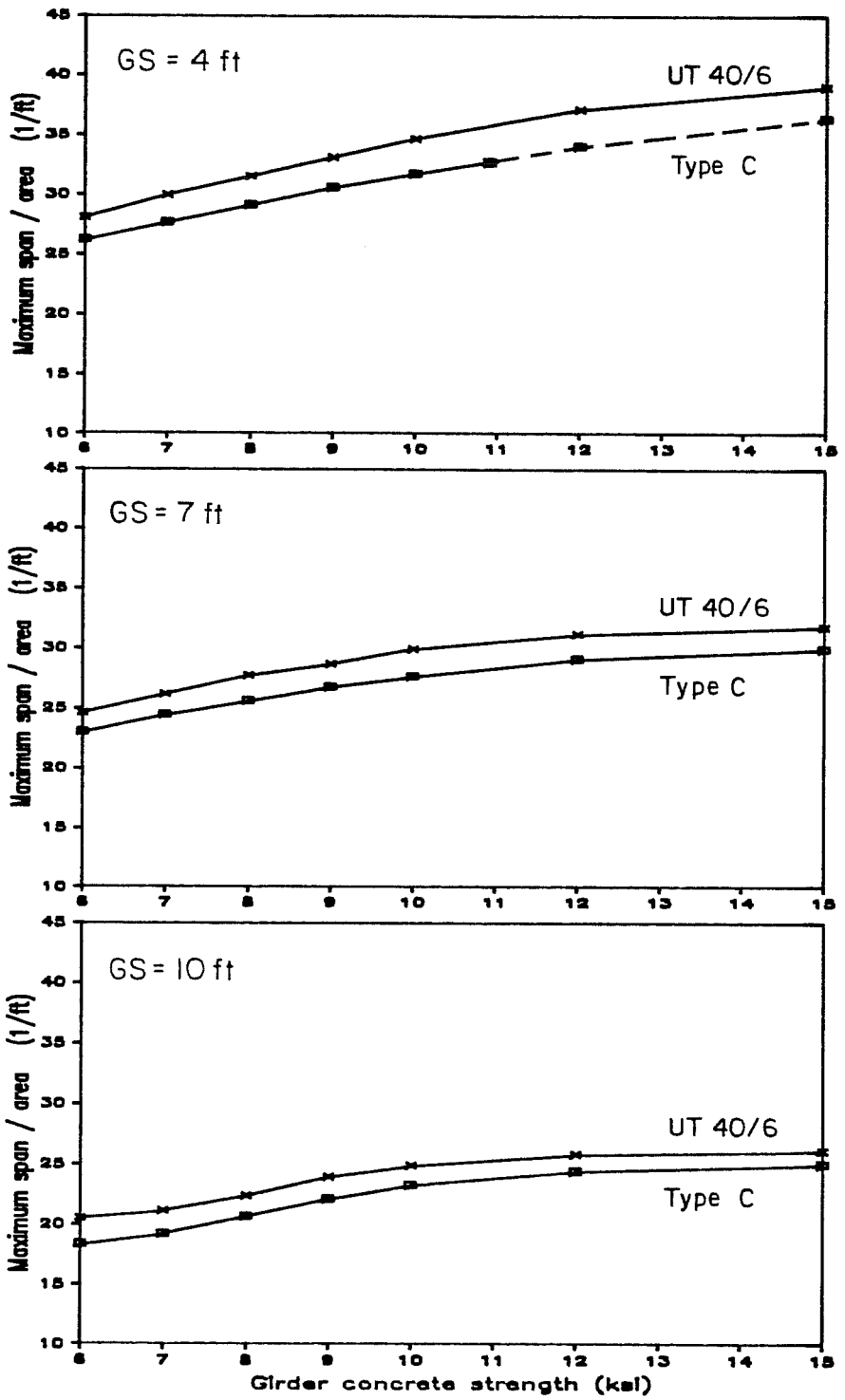

Fig. 2.23 Ratio of maximum span to area of girder versus concrete strength - 40" sections.

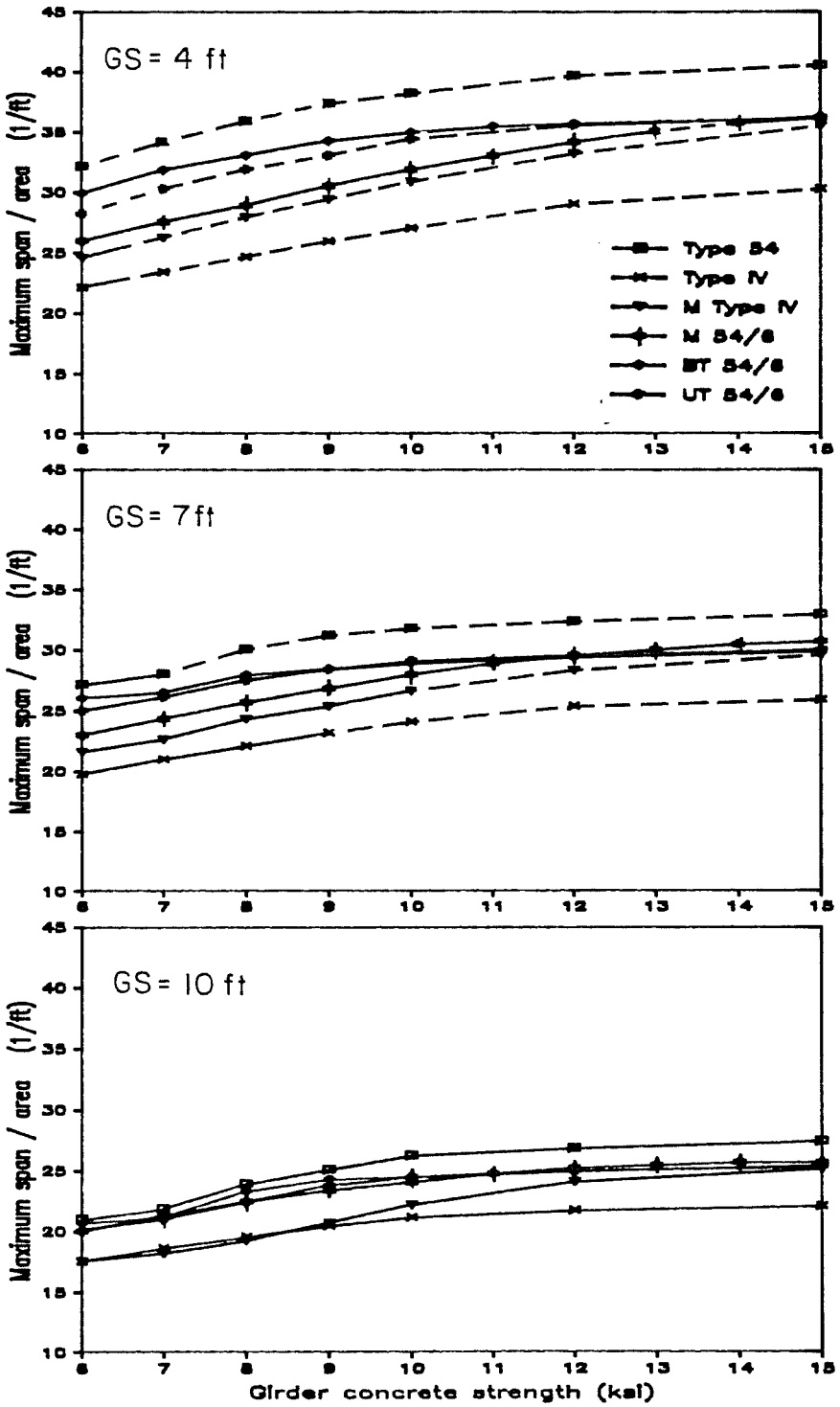

Fig. 2.24 Ratio of maximum span to area of girder versus concrete strength - 54" sections.

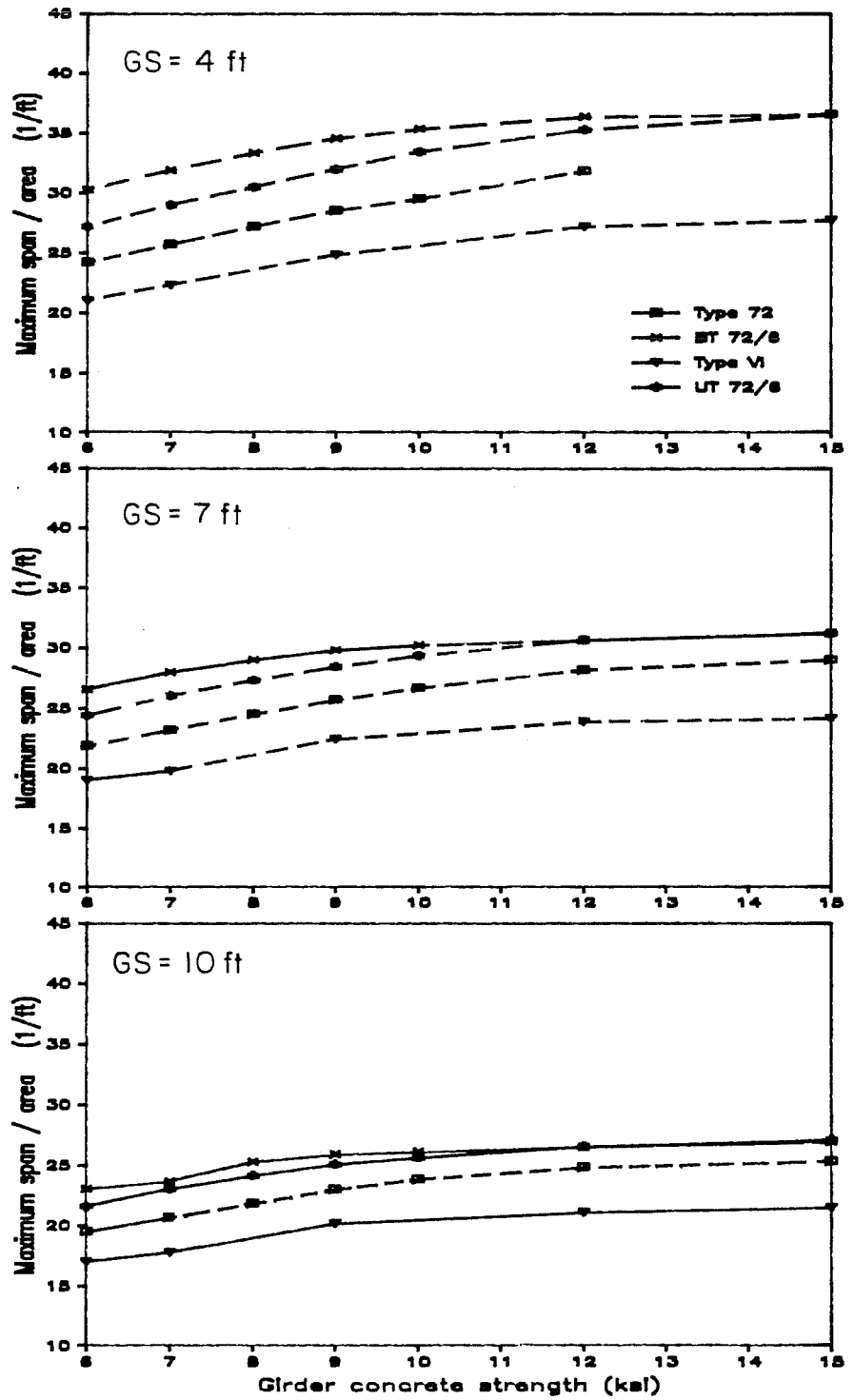

Fig. 2.25 Ratio of maximum span to area of girder versus concrete strength - 72" sections

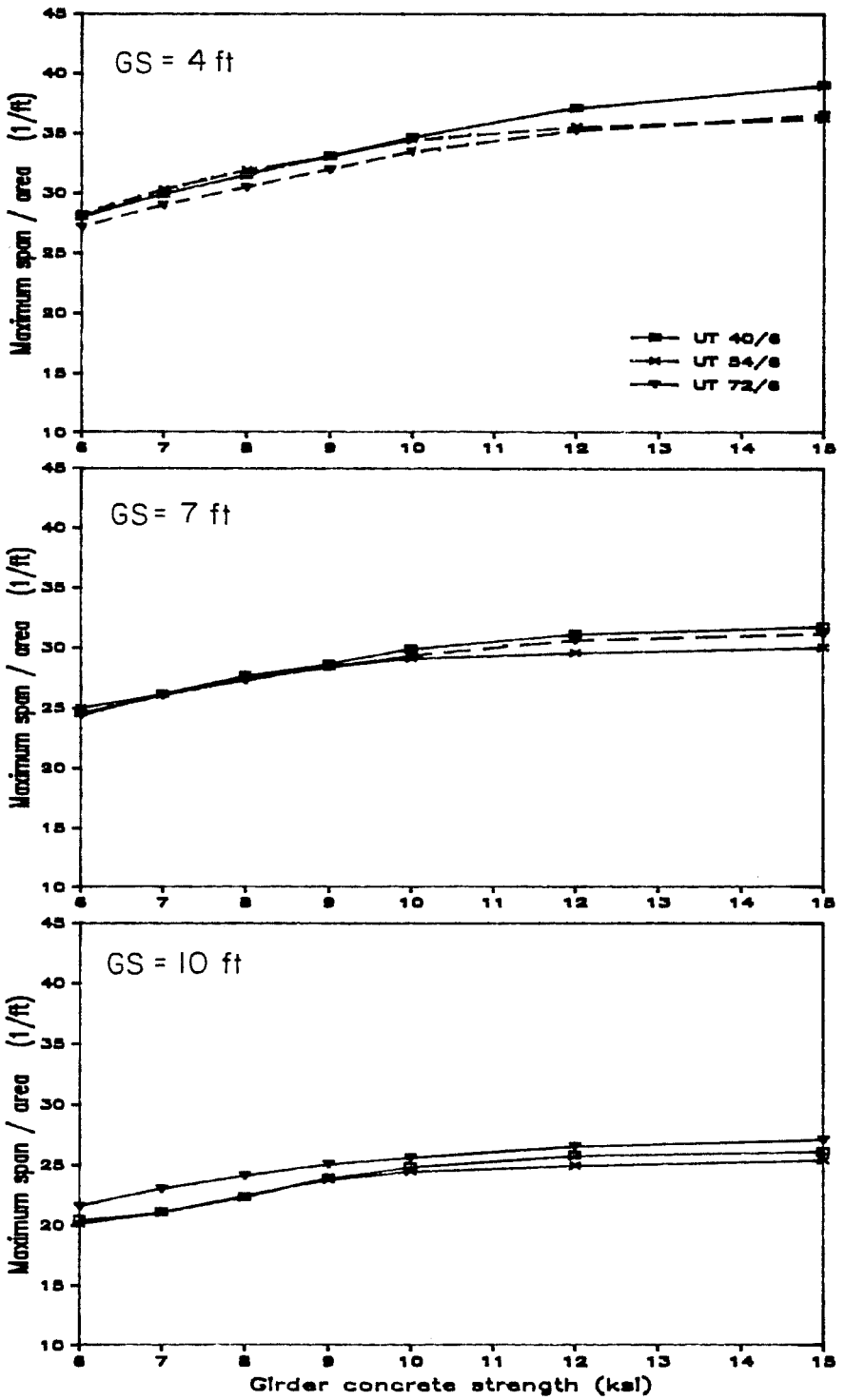

Fig. 2.26 Ratio of maximum span to area of girder versus concrete strength - proposed sections.

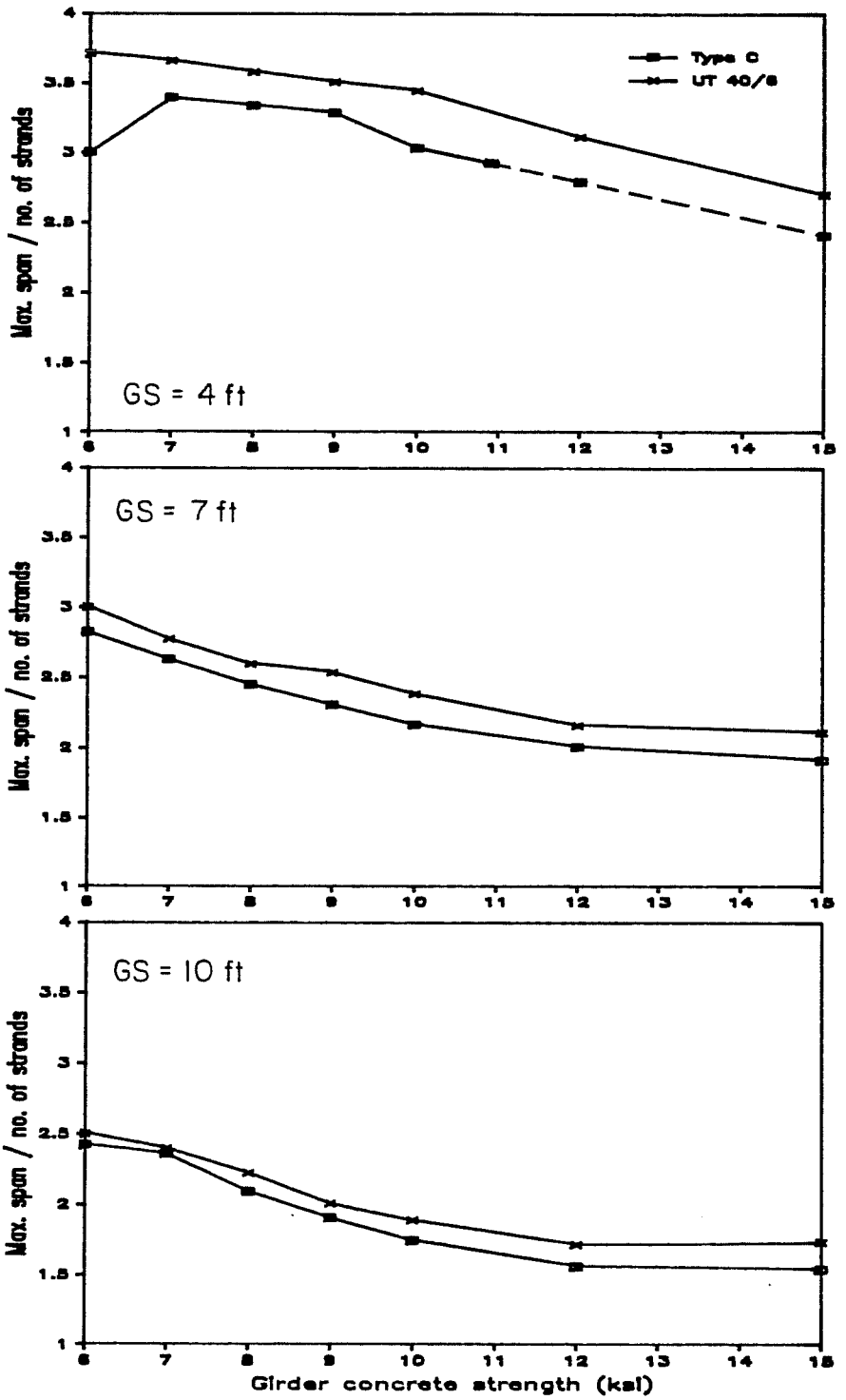

Fig. 2.27 Ratio of maximum span to number of strands versus concrete strength - 40" sections.

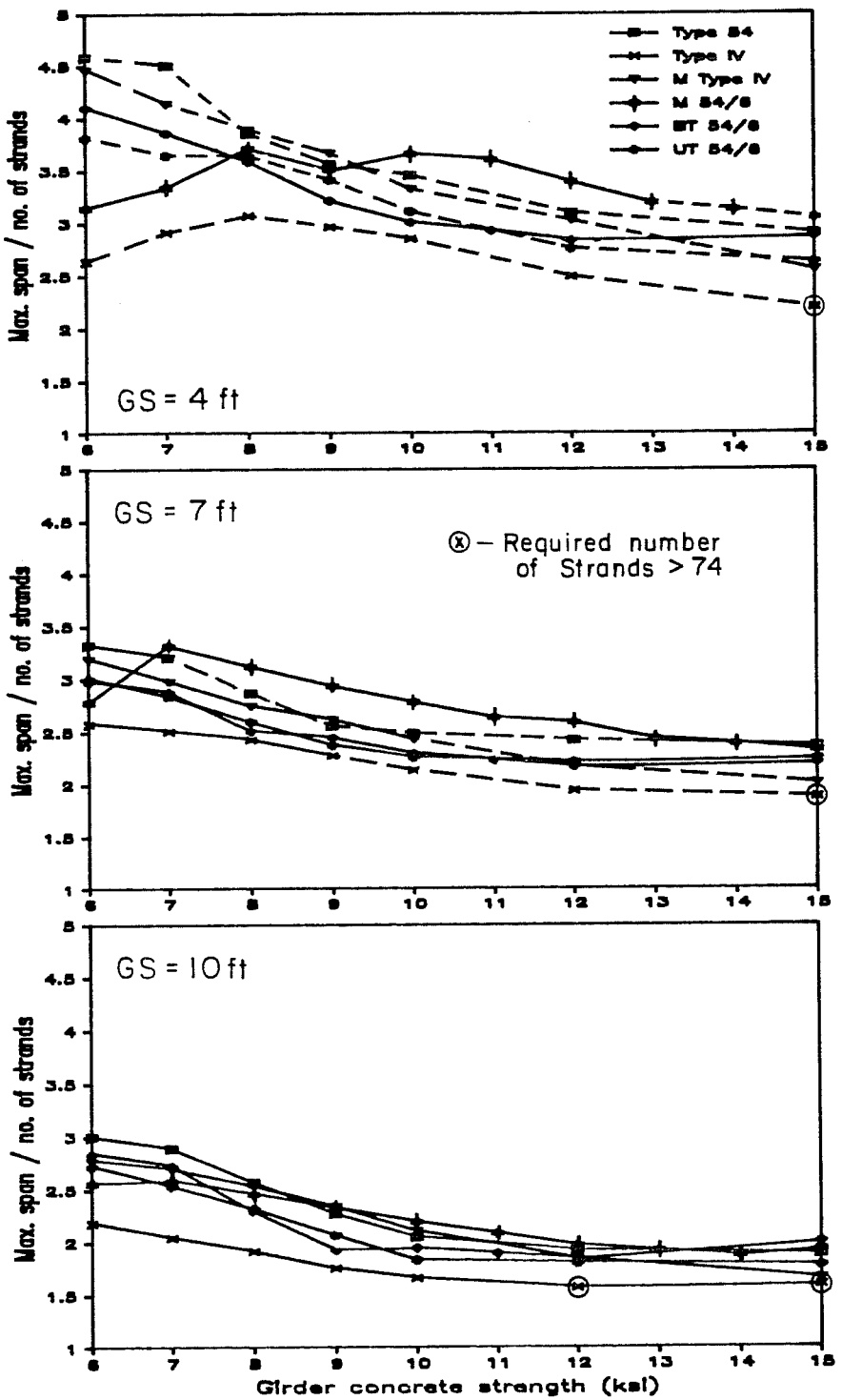

Fig. 2.28 Ratio of span to number of strands versus concrete strength - 54" sections.

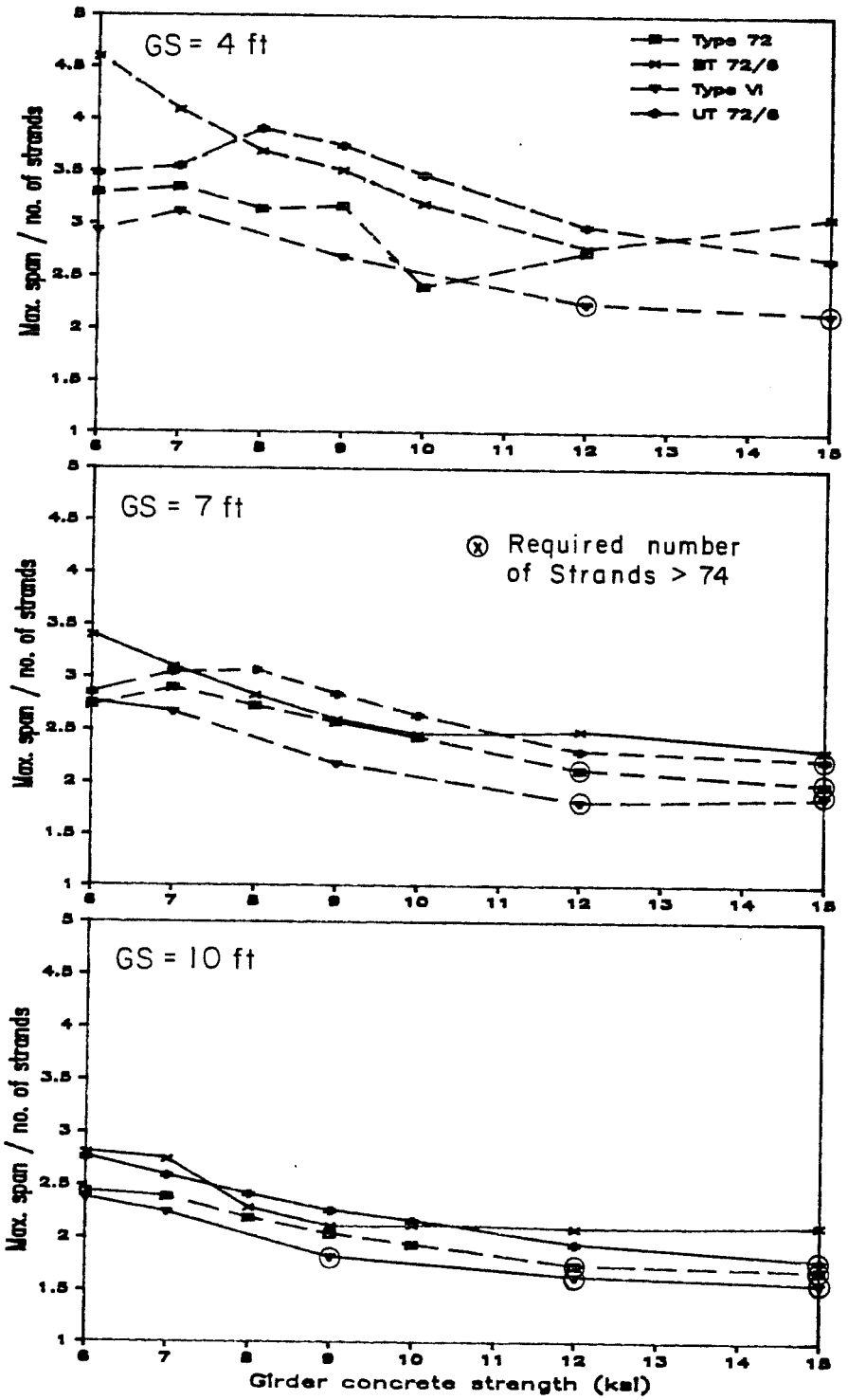

Fig. 2.29 Ratio of maximum span to number of strands versus concrete strength - 72" sections.

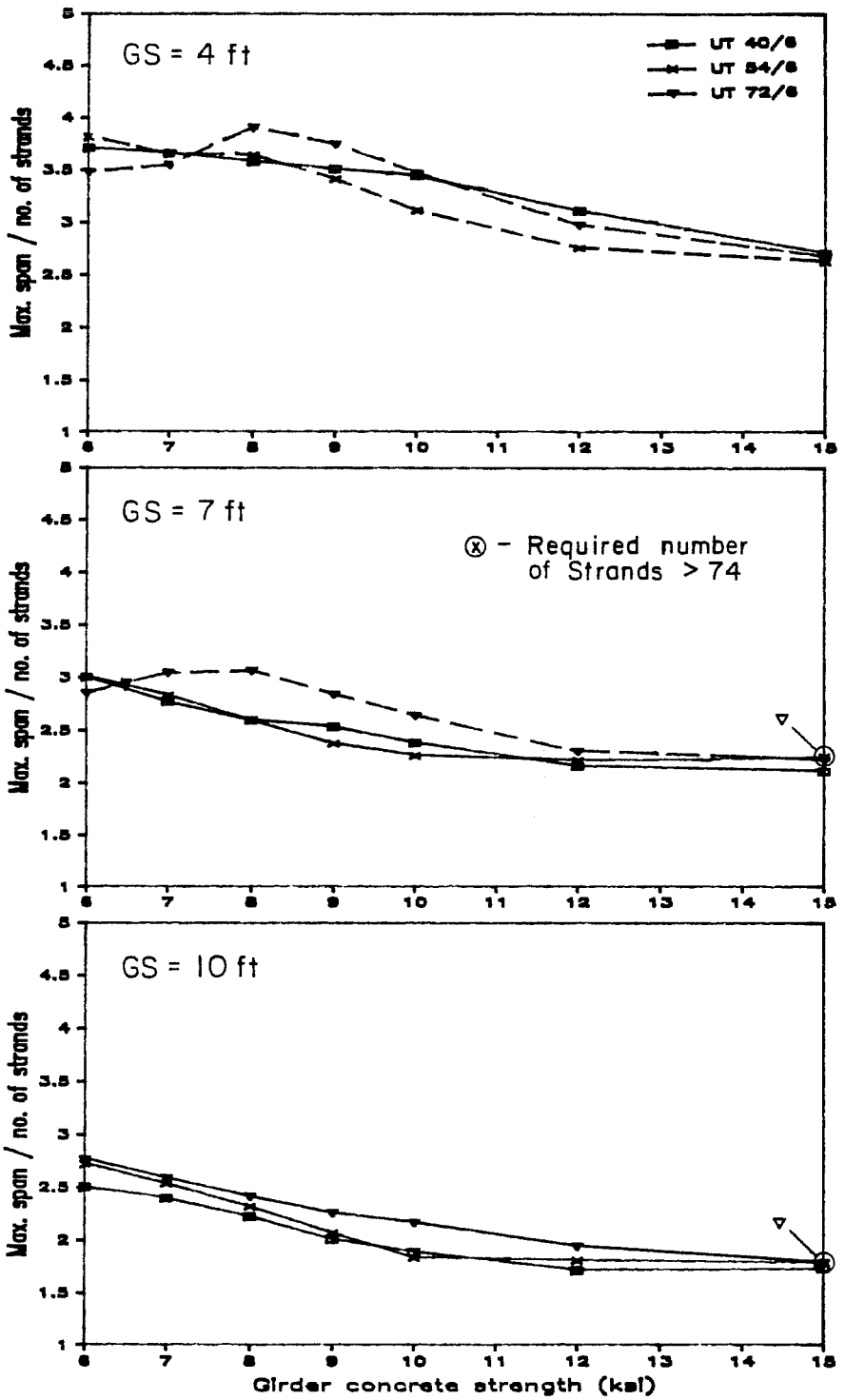

Fig. 2.30 Ratio of maximum span to number of strands versus concrete strength - proposed sections.

indicated by dashed lines on the plots. Designs where the current maximum prestress bed capacity is exceeded are indicated by placing a circle around the point.

For the 40-in. sections, the proposed section proves to be more efficient in both comparisons. For both comparisons with 54-in. sections, the proposed section is very close to the bulb-tee and is a significant improvement over the Type IV girder. For the comparison with respect to area, the proposed section and the bulb-tee are exceeded by only the Type 54 girder which is limited in span. However, for the strand comparison, other sections proved to be more efficient in most cases, although trends are difficult to identify due to the erratic nature of the plots. The situation is similar for the 72-in. sections where in the area comparisons the bulb-tee is best, with the proposed section slightly less or equally efficient. In the comparison involving number of strands, the proposed section proved superior in some cases to the other sections. An examination of the figures showing plots for the proposed sections reveals that the efficiency of the sections is similar.

While these comparisons give an indication of the relative efficiency of the sections, the results of the comparisons are not conclusive and do not consider all aspects of design. However, they do indicate that the proposed sections have efficiencies similar to

the bulb-tees, and are generally superior to the AASHTO-PCI and Texas standard sections.

2.4.4 Sensitivity to Strength at Release. Sensitivity of the maximum span designs to concrete strength at release is indicated in Fig. 2.31 through 2.34 by the ratio of maximum span computed using a release strength of 50 percent of the design strength to the span computed using a release strength of 75 percent of the design strength, except for 6 ksi, where 83 percent is used. The data shown indicate that the effect of the reduction in release strength is lessened as the concrete strength is increased and as the girder spacing is decreased. The proposed sections tended to be about average in sensitivity when compared with other sections. Of the proposed sections, the 54-in. section was the most sensitive to reduction of the concrete strength at release. The section at release - proposed sections with the largest bottom flange area showed the least sensitivity for all concrete strengths and girder spacings. Therefore, if the use of lower release strengths is perceived as a major concern or advantage for using high strength concrete, a larger bottom flange could be added to the proposed sections to improve this aspect of behavior without greatly affecting other aspects. The use of closer girder spacings would also reduce the impact of lower release strengths. It should be noted that the reduced concrete

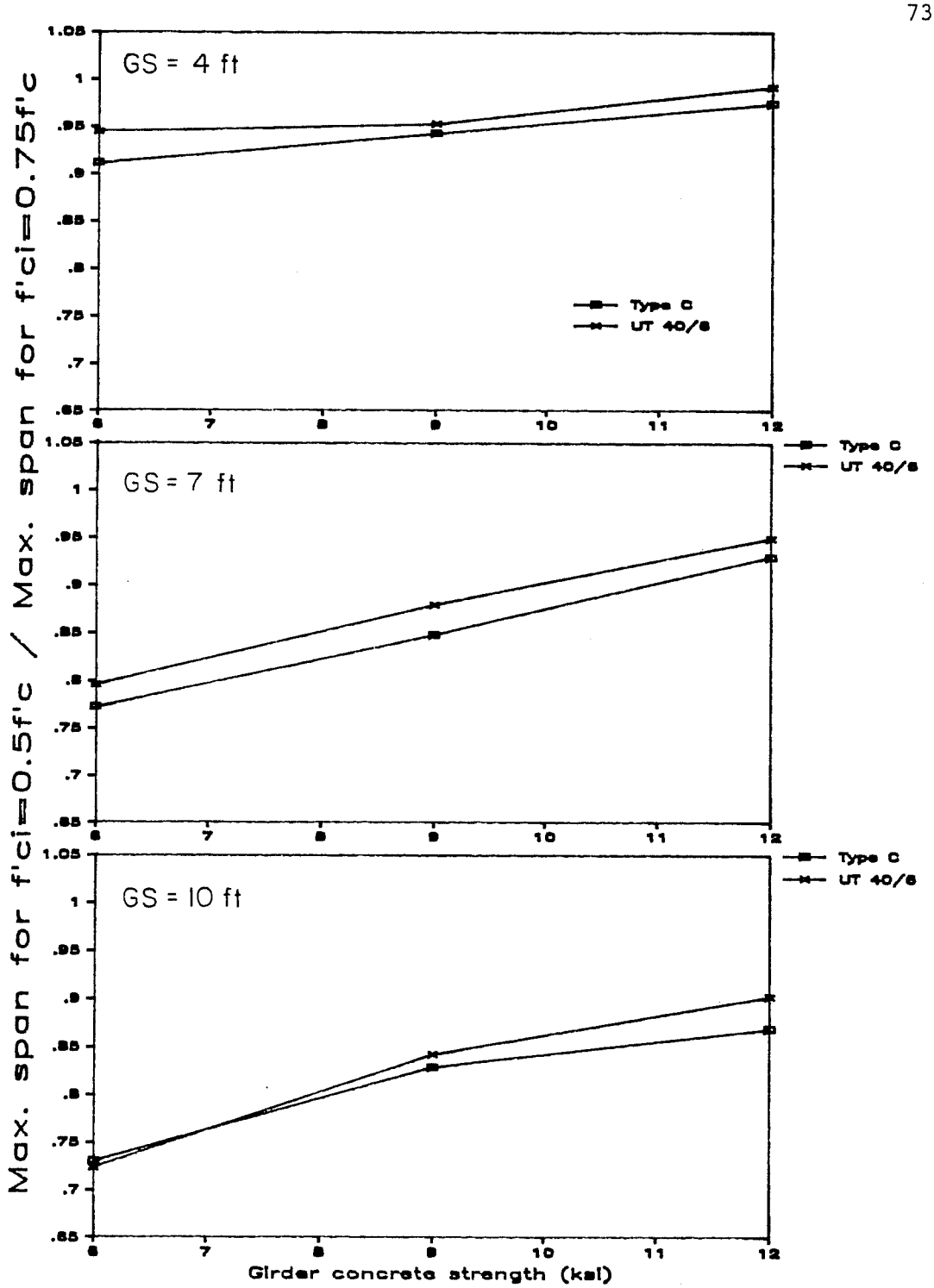

Fig. 2.31 Reduction in maximum spans due to lower concrete strength at release - 40" sections.

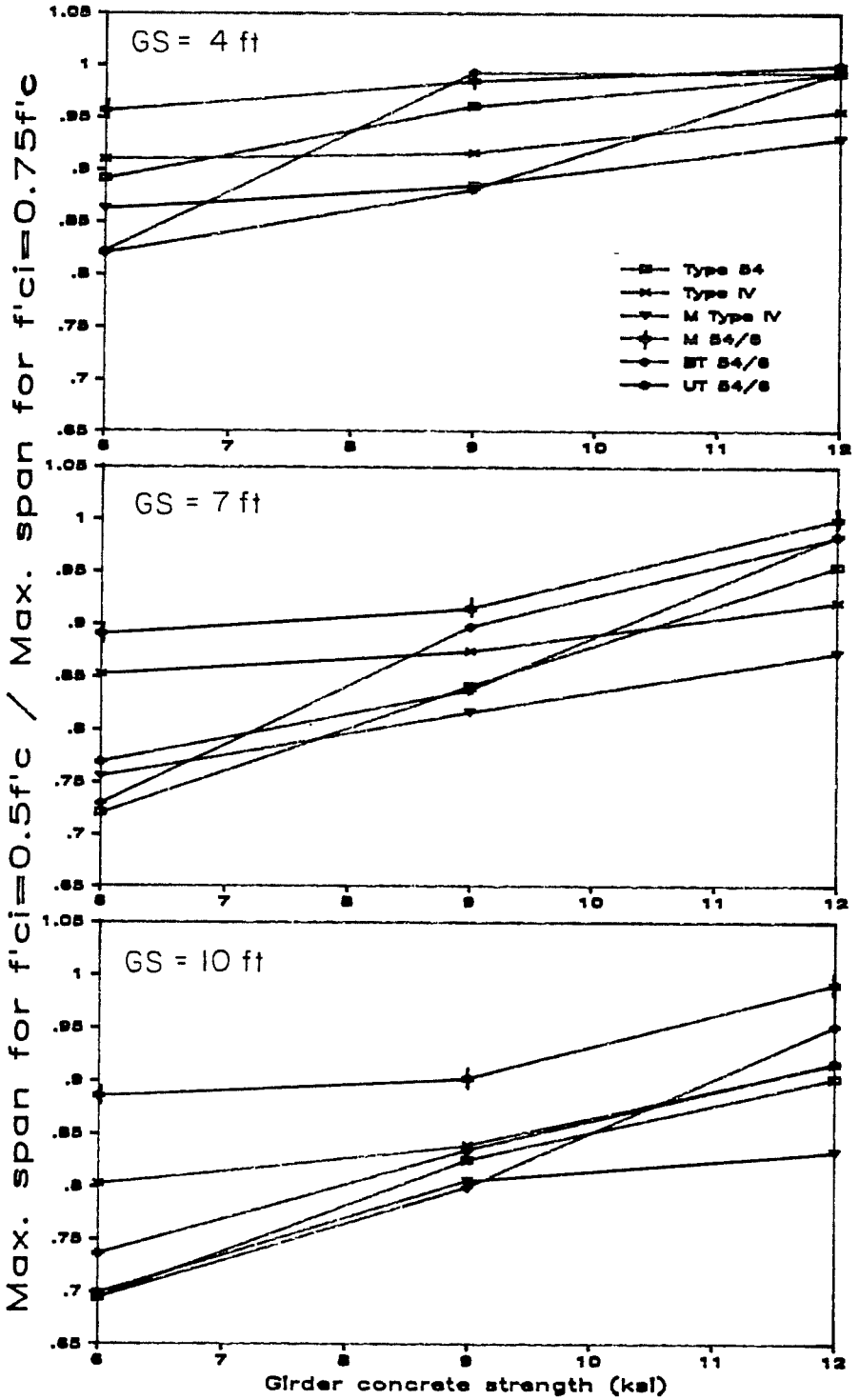

Fig. 2.32 Reduction in maximum spans due to lower concrete strength at release - 54" sections.

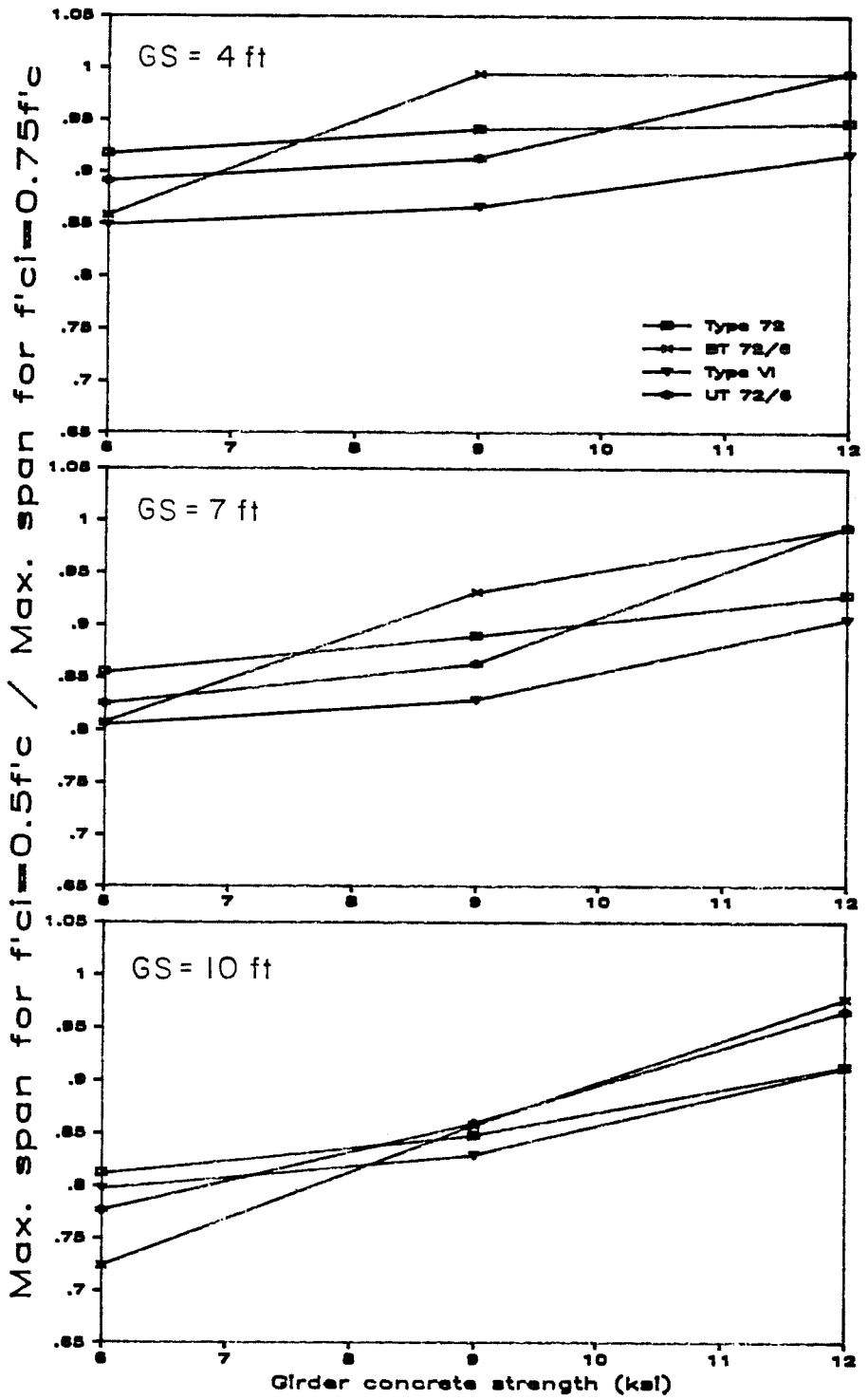

Fig. 2.33 Reduction in maximum spans due to lower concrete strength at release - 72" sections.

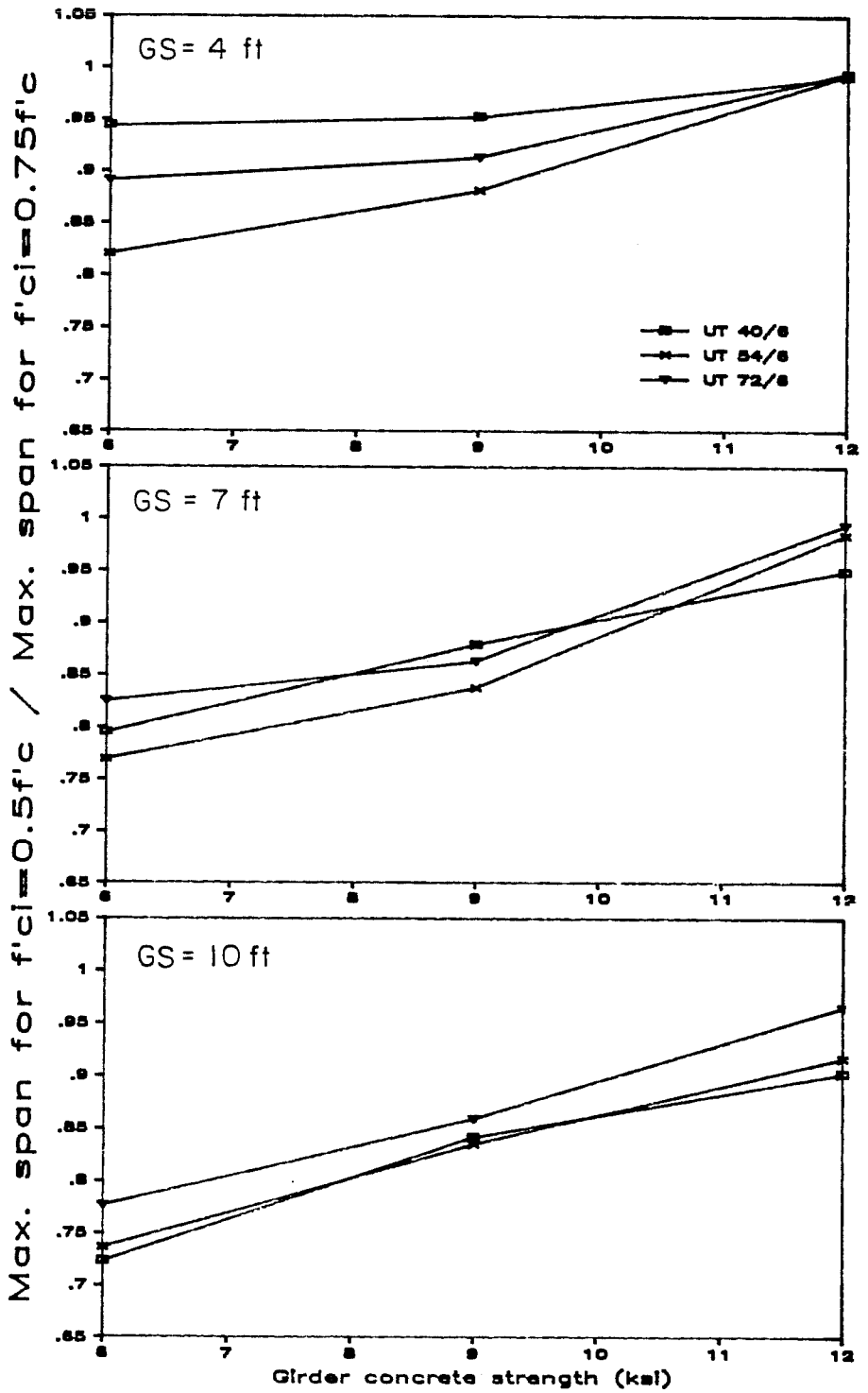

Fig. 2.34 Reduction in maximum spans due to lower concrete strength at release - proposed sections.

strength at release would also result in a 5.8 percent reduction in the maximum lifting span.

2.4.5 Effect of Strand Size. Designs using 0.6-in. diameter strand are compared with those for 0.5-in. diameter strands in Fig. 2.35, 2.36, and 2.37 for the AASHTO-PCI Type IV girder. The maximum spans are shown in Fig. 2.35, the ratio of spans is plotted in Fig. 2.36, and the difference in spans is plotted in Fig. 2.37, with all quantities shown versus concrete strength. Spans in excess of the maximum lifting span are shown as dashed lines in Fig. 2.35. The effect of using the larger strand is minimal for lower concrete strengths but increases as the concrete strength increases. The effect also increases as girder spacing is widened. Because of the increased span lengths possible, especially for GS = 10 ft, stability would be a greater problem when 0.6-in. diameter strands are used.

For this study, the use of larger diameter strand appears beneficial only when high strength concrete is used and only about a 10 percent (which corresponds to about 10 ft) increase in span results. The use of larger strand may also increase the required prestressing force to a level that exceeds the capacity of many prestressing beds. To illustrate, in order to obtain the 10 percent increase in span at GS = 10 ft and f'c = 12 ksi, 62 strands are needed with a maximum initial prestress force of approximately 2.9 million

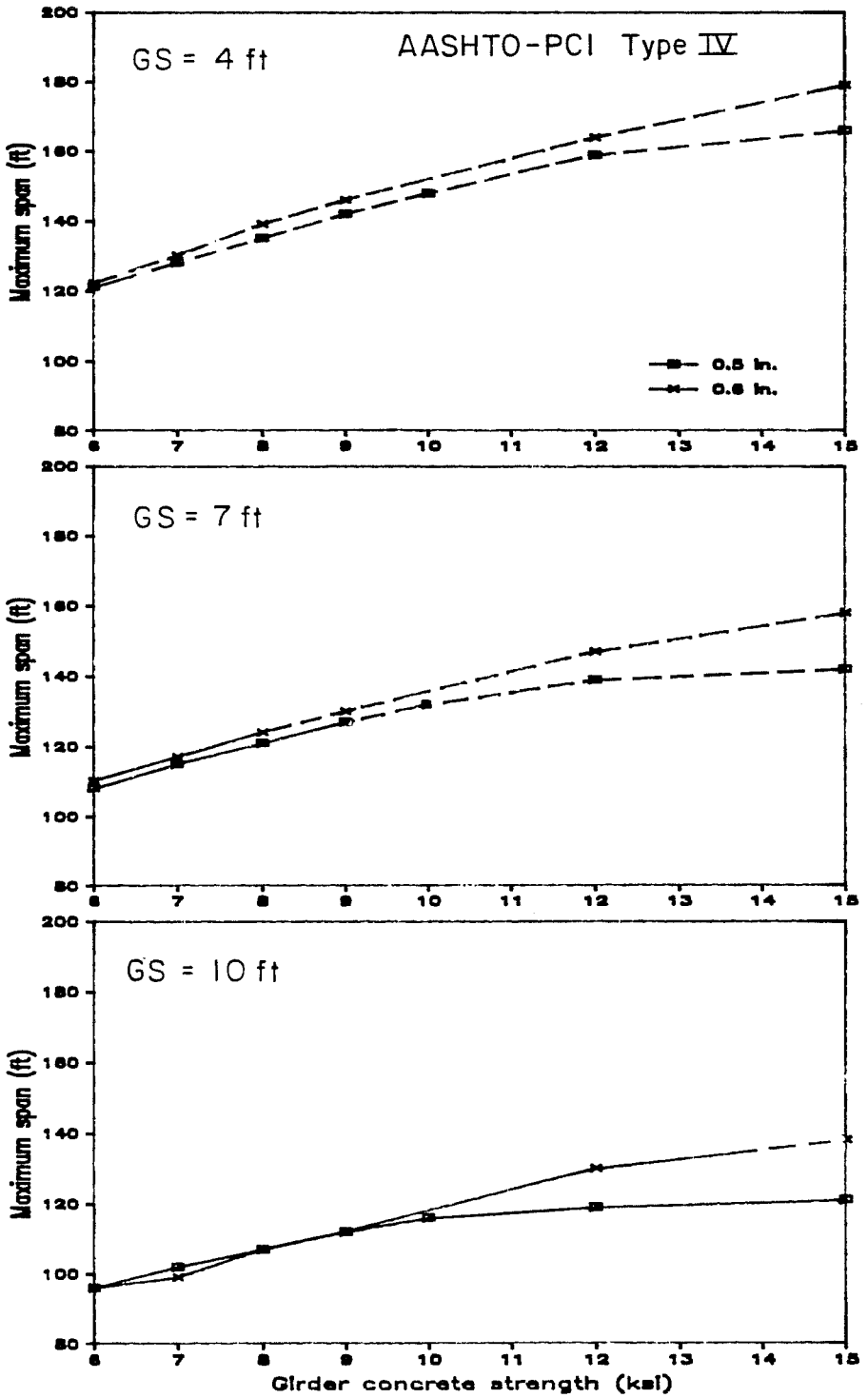

Fig. 2.35 Maximum span versus concrete strength for AASHTO-PCI Type IV with 0.5-in. and 0.6-in. diameter strand.

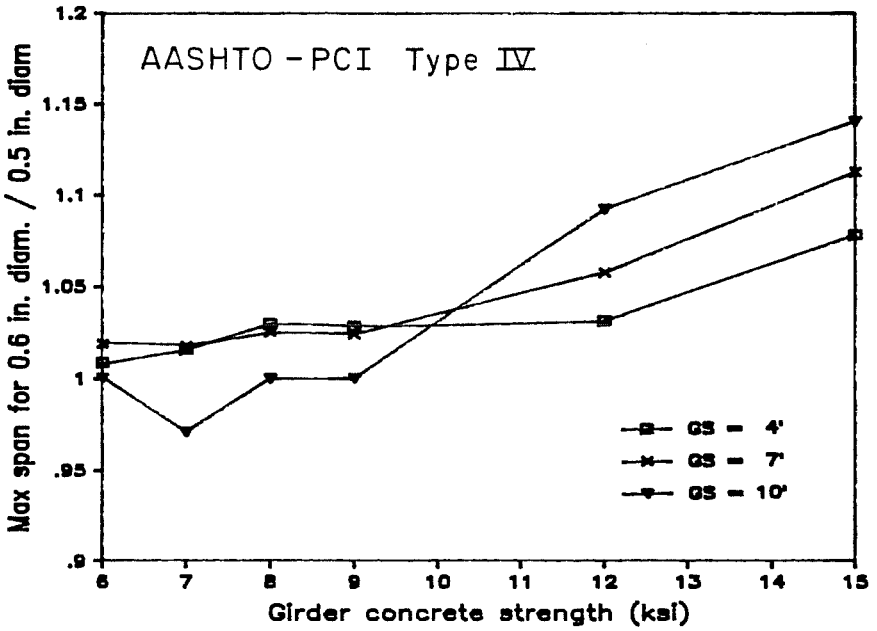

Fig. 2.36 Ratio of increase in maximum span with use of 0.6-in. diameter strand.

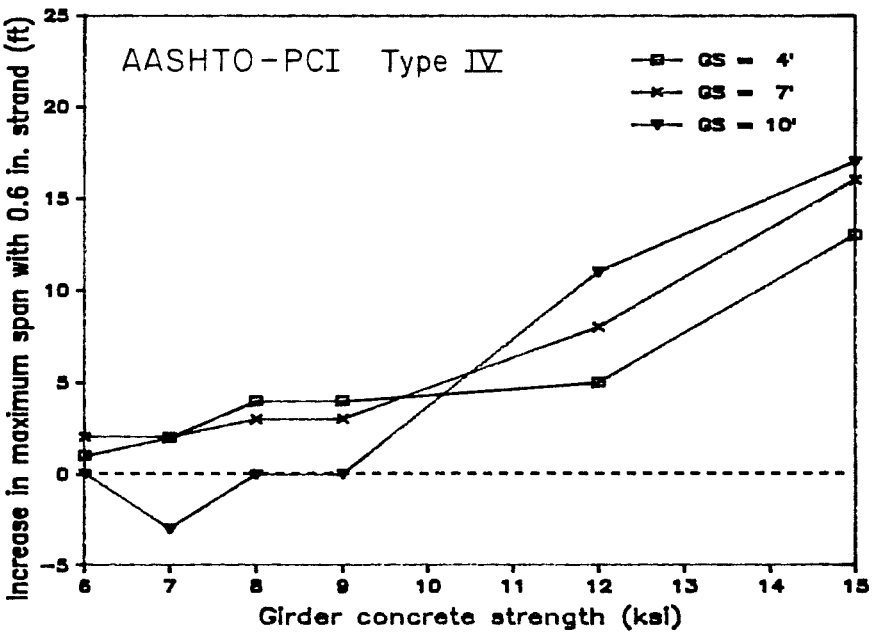

Fig. 2.37 Increase in maximum span with use of 0.6-in. diameter strand.

million pounds. This force is greater than the capacity of any prestressing bed in Texas.

2.5 Summary and Conclusions

The following conclusions can be drawn from the study presented in this chapter:

1. The three proposed sections provide good alternatives to currently used sections. The proposed sections have similar span capabilities yet reduced section sizes when compared with sections of the same depth that are in current use in Texas. The proposed sections are slightly larger than bulb-tee sections of the same depth and have similar or improved span capabilities.
2. An increase in concrete strength allows an increase in maximum span for a given section of 10 to 40 percent, depending on section and girder spacing. However, certain practical limits must be considered, such as capacity of the prestressing bed, maximum lifting spans, and transportation of the member.
3. The maximum lifting span, which is intended to prevent lateral buckling of members when they are lifted, may severely limit the maximum span capacity of some sections. This limit is especially restrictive for 54-

and 72-in. sections. In general, sections with greater weak axis moments of inertia were affected the least by these stability limitations. (The reader is referred to Sec. 7.7 for a more complete assessment of the lateral stability of these sections. This section indicates that further considerations may be required to determine the safety of a member with respect to lateral stability.)

4. Where increases in maximum spans mentioned above are limited by the maximum lifting span, special considerations may be available in the design or handling of the member to make possible the use of longer spans.
5. An increase in concrete strength can allow a significant increase in girder spacing for a given span, thus requiring fewer girders for a given structure. In some cases, the spacing can be more than doubled when high strength concrete is used.
6. Increasing concrete strength does not significantly reduce the number of strands required for a given span and girder spacing.
7. No simple measure of section efficiency appears to reflect the effect of all significant aspects of design. The comparison of actual designs is the best way to determine relative performance of different sections.

8. Some sections show marked reductions in maximum span capacity when the concrete strength at release is lowered. The section with a large bottom flange, however, showed the least span reduction when a reduced release strength was used.

9. The use of larger strands permits increased maximum spans if high strength concrete is used. Otherwise, no benefit is realized other than a reduction in the number of strands required for a design.

Therefore, high strength concrete can be best used in pretensioned bridge girders to provide a significant increase in span capacity (unless limited by stability considerations) or to reduce the required number of girders for a given span.

CHAPTER 3

REVIEW OF LITERATURE AND CURRENT DESIGN PRACTICE

3.1 Introduction

Since some basic properties of high strength concrete differ from normal strength concrete in significant ways [22], it is imperative that current design practice be reviewed to identify and correct any problems in the use of high strength concrete with current design provisions. Material properties and design techniques that would allow the designer to make more efficient use of high strength concrete should also be identified. This, then, is the purpose of the current chapter, with emphasis on the design and behavior of highway bridges with pretensioned girders.

The chapter begins with a review of overall design concepts that apply to pretensioned girder bridges. Material properties of high strength concrete are then presented. Topics are then considered where the different properties of high strength concrete may affect the design and performance of these bridge structures. As topics are considered, current code provisions are discussed, along with analytical studies and methods, proposals for code revisions, and the results of tests related to the topic. The background of code provisions will be considered when it is beneficial for understanding the intent of the code.

Production of high strength concrete is not considered in this chapter since it is outside the scope of this study. However, it should be noted that a study by Peterman and Carrasquillo [104] and ongoing research at the University of Texas at Austin have shown that high strength concrete as defined in this study can be commercially mixed and placed in pretensioning plants in Texas.

The AASHTO Standard Specifications for Highway Bridges [10] is the model code for the design of highway bridges in the United States and serves as a standard or guide for the preparation of State specifications. The AASHTO specifications will therefore be used as the primary reference to establish current or past practice in bridge design. Provisions of the specification related to the design of pretensioned girder bridges are similar to those for pretensioned and composite members found in the current ACI Building Code Requirements for Reinforced Concrete (ACI 318-83) [15]. While the ACI document is intended for use with buildings rather than bridges, it and its Commentary [17] give an indication of the direction and intent of general design practice and will therefore be used as secondary code references.

Notation used in this chapter is generally consistent with the information source. In a number of cases, this leads to the use of different notation for the same quantity when discussing information

from different sources. A proposal for a consistent set of notation is presented in Sec. 7.11.

3.2 Design Approach

The design of prestressed members by either AASHTO or ACI requirements is based on satisfaction of both ultimate and service load criteria. The service load criteria are satisfied when concrete and steel stresses, computed at all critical load stages during the life of the structure, do not exceed allowable values specified in the codes. Design for service conditions using these criteria is therefore referred to as "allowable stress design" [10]. Section 9.13.1.2 of the AASHTO Specification [10] implies that the intent of allowable stress design is to ensure satisfactory behavior of a member under service conditions throughout its life. The ACI Code Commentary [17] states that "permissible stresses are given to control servicability." The design of an overwhelming majority of pretensioned girder bridges is controlled by allowable stress design and ultimate analysis is usually performed only as a check.

The allowable stresses that affect behavior most significantly are the concrete tensile stresses at service conditions which are intended to prevent or limit cracking. The AASHTO Specification allows three levels of tensile stress in the precompressed tensile zone of a member. The maximum tensile stress in this zone is

$6\sqrt{f_c'}$ which may be used when bonded reinforcement is provided. One half that stress, or $3\sqrt{f_c'}$, is permitted where corrosive environments are encountered and bonded reinforcement is provided. No tensile stress is allowed if bonded reinforcement is not present. The basic limit of the ACI Code [15] permits a stress of $6\sqrt{f_c'}$ and allows a stress of up to $12\sqrt{f_c'}$ if deflections are within limits and cover is increased. The stress limits may be waived entirely if tests or analysis demonstrate that performance will not be impaired. In this way the ACI Code recognizes that a low allowable tensile stress may not provide good servicability if, for example, the live load is large and transient, which could lead to large camber growth [17]. A method for determining allowable stresses appropriate for a given structure is given in Ref. [105]. The ACI Code Commentary [17] also recognizes that the use of stressed or unstressed bonded tendons as well as reinforcing bars will serve to control cracking.

Major steps in the design of highway bridges using this approach are outlined in the top half of Fig. 3.1. Parameters given in the first step are largely determined by geometry of the structure and local construction practice. Girders are designed in the second

CURRENT DESIGN APPROACH

I. Set Certain Parameters

1. Bridge geometry
2. Girder cross section
3. Strand size and general pattern
4. Girder spacing and deck dimensions
5. Concrete strength of girder and deck

II. Determine number of strands to be used

1. Estimate prestressing losses
2. Check stresses at critical stages of construction
3. Adjust concrete strength of girder as required

III. Check other quantities

1. Ultimate flexural capacity
2. Ultimate shear capacity
3. Deflections

LIMIT STATES

I. Ultimate behavior

1. Capacity in flexure and shear
2. Ductility

II. Serviceability

1. Cracking
2. Deflections
3. Durability
4. Economy
5. Constructability
6. Esthetics

III. Effects of fatigue

Fig. 3.1 Current design approach and limit states

step using trial designs to obtain a strand pattern which satisfies allowable stresses. After a pattern has been determined, the ultimate capacity of the structure is computed to demonstrate sufficient capacity to resist ultimate loads. Deflections should be checked, but AASHTO provides no limits.

A second approach to the design of bridge members has been suggested [95,105] in which the various aspects of the behavior of a structure are considered directly rather than indirectly as done in allowable stress design. This can be done by investigating the "limit states" appropriate for a highway bridge structure, as shown in the bottom half of Fig. 3.1. A limit state is some characteristic or aspect of behavior of a structure that must satisfy some standard in order for a structure to have acceptably fulfilled its intended purpose. Conversely, a limit state may be considered as a possible way in which the structure may fail to fulfill its intended purpose. All of the limit states shown must be addressed in some way if a code is to be complete, with the exception of the last three entries under servicability which are outside the scope of a code. The 1983 Ontario Highway Bridge Design Code is an excellent example of a limit state design code.

Only a few of these limit states are directly addressed by the current code design approach for prestressed concrete, such as estimating the ultimate capacity of a structure. Cracking is

addressed by limiting tensile stresses and durability is ensured by specifying minimum concrete quality and cover over reinforcement, and by limiting cracking. The remaining limit states are treated indirectly by current codes, such as providing ductility by limiting reinforcement. Loads and effects are specified for computing instantaneous and long-term deflections, but no procedures or limits are given. Effects of fatigue are included by limiting concrete stresses.

It is not clear whether current design procedures, including allowable stress design, will be safe for high strength concrete, especially where code provisions are indirect as mentioned above. This question will be considered throughout the remainder of this study to determine whether current provisions remain applicable and acceptable or need revision for use with high strength concrete.

3.3 Basic Properties of Strength Concrete

3.3.1 Compressive Strength.

Typically, concrete strength is determined using the 28-day compressive strength of 6 x 12-in. cylinders. A revision of these criteria for use with high strength concrete has been suggested.

The use 4 x 8-in. cylinders has been proposed for high strength concrete to reduce the required crushing force. A number of investigators have determined relationships between 6 x 12-in. and 4 x

8-in. cylinder data for high strength concrete. Results conflict among investigators, with some suggesting that 4 x 8-in. cylinders are approximately 10 percent stronger than 6 x 12-in. cylinders [104,36], while others found that the smaller cylinders had strengths approximately seven percent less than the larger cylinders [35]. Malhotra [78], in a study of cylinders with strengths up to about 8,000 psi, found that the smaller cylinders were stronger and that the margin of difference increased with increasing concrete strength. He also found that the increased variability of compressive strength of the smaller cylinders resulted in the need to test more than twice as many 4 x 8-in. cylinders to obtain the same level of confidence.

Since high strength concrete often continues to gain strength after 28 days, a later age has been used for the standard test age in several cases [4,39,43]. Data on strength gain with age has been reported by several investigators [104,35,36] and summarized in the Committee 363 Report [22]. Data presented in Fig. 3.2 show that high strength concrete gains strength more rapidly at early ages, but after 28 days the gain is not significantly different from normal strength concrete.

High strength concrete is more sensitive to curing conditions than normal strength concrete [36,104], although strength reductions were not greater than 10 percent. This conclusion was based on comparisons of compressive strength tests at 28 days for moist cured

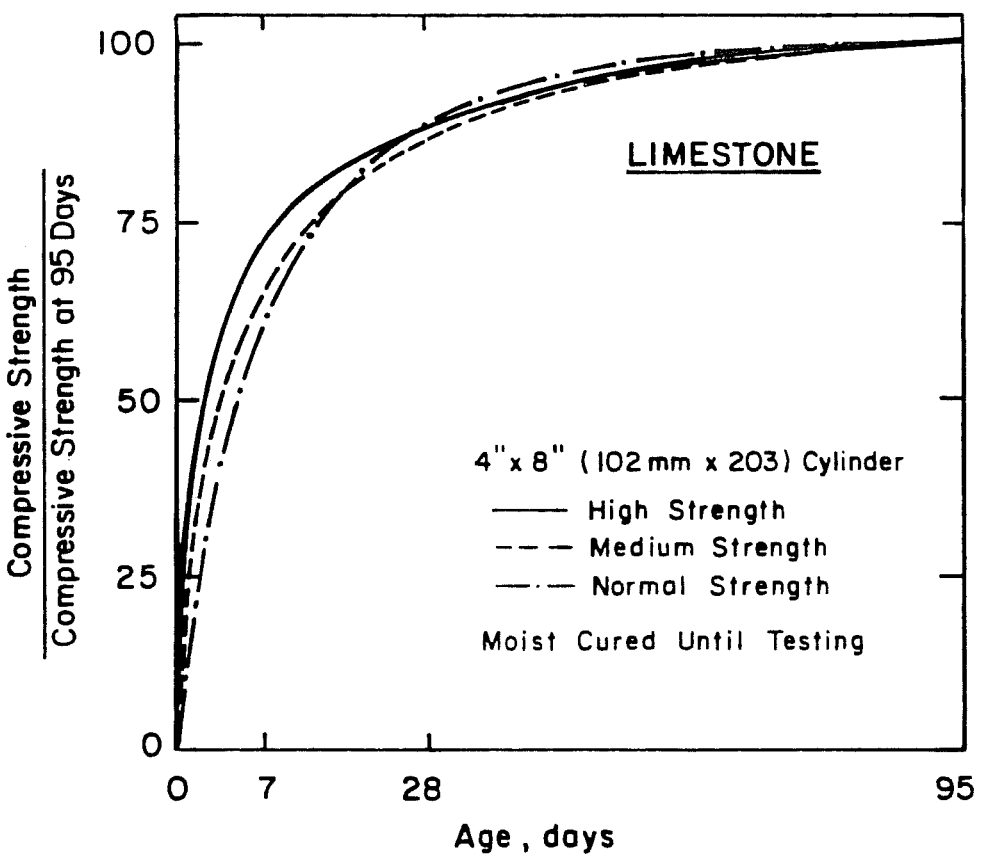

Fig. 3.2 Normalized strength gain with age [35]

cylinders and cylinders which were moist cured for 7 days, then allowed to dry until testing. Adequate curing is difficult due to self-dessication that is aggravated by the impermeability of high strength concrete which prevents externally applied water from participating in hydration [104].

3.3.2 Stress-Strain Curve and Modulus of Elasticity.

It is widely recognized that high strength concrete behaves differently than normal strength concrete in compression [22,99,135]. The behavior is illustrated by the typical stress-strain curves in Fig. 3.3 [36]. Stress-strain curves for high strength concrete remain approximately linear to a higher fraction of the maximum stress, which occurs at slightly greater strains than for normal strength concrete, and the descending branch is much steeper. Behavior is sensitive to materials used, as evidenced by the two sets of curves in Fig. 3.3.

There is considerable discussion about the characteristics of the descending branch since results are highly dependent upon testing equipment and techniques. While special methods have been used to obtain strains as high as 0.01 in./in., the special test conditions required are seldom found in real structures [99]. Behavior for strengths above approximately 9,000 psi may be described as approximately linear elastic and brittle [99].

Much attention has been given to the determination of the modulus of elasticity of high strength concrete. Modulus data

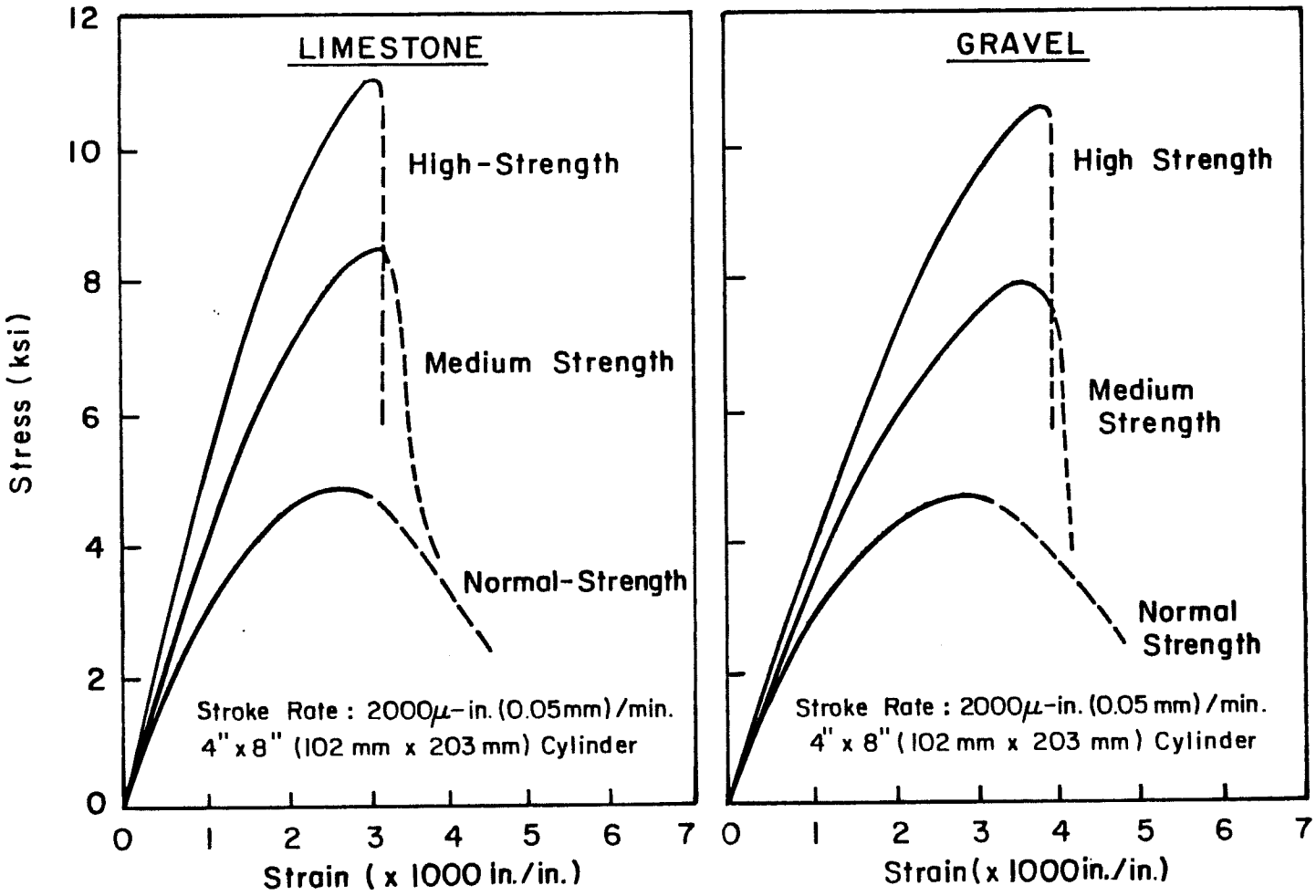

Fig. 3.3 Typical stress-strain curves for different concrete strength [36]

presented in Fig. 3.4 [81,124] show that wide scatter exists for high strength concrete. Because the expression currently used by both AASHTO and ACI to relate concrete strength to the modulus of elasticity is unconservative for much of the high strength data (Fig. 3.4), an alternate equation has been proposed by investigators at Cornell [82]. Modulus measurements are strongly affected by the type of aggregate used [36,126].

Measured strains at maximum stress for a range of concrete strengths are shown for flexure and axial compression tests separately in Fig. 3.5 and combined in Fig. 3.6. The strains tend to increase slightly with increasing strength. Data from flexure tests show good agreement with axial compression tests, with compression test data exhibiting slightly higher results.

Measured ultimate strains for a range of concrete strengths are shown for C-shaped specimens (flexure specimens, see Ref. [71, 103, 124]), beams, and cylinders in Fig. 3.7. All flexure data considered here are for rectangular sections, with the exception of the normal strength concrete test data reported by Mattock and Kriz [86], which had triangular compression zones. Data from all types of specimens, combined in Fig. 3.8, indicate that strains generally tend to decrease with increasing concrete strength and that cylinder data is noticably lower than flexure specimen data. This second fact is illustrated by Fig. 3.9 which shows that the percentage of data

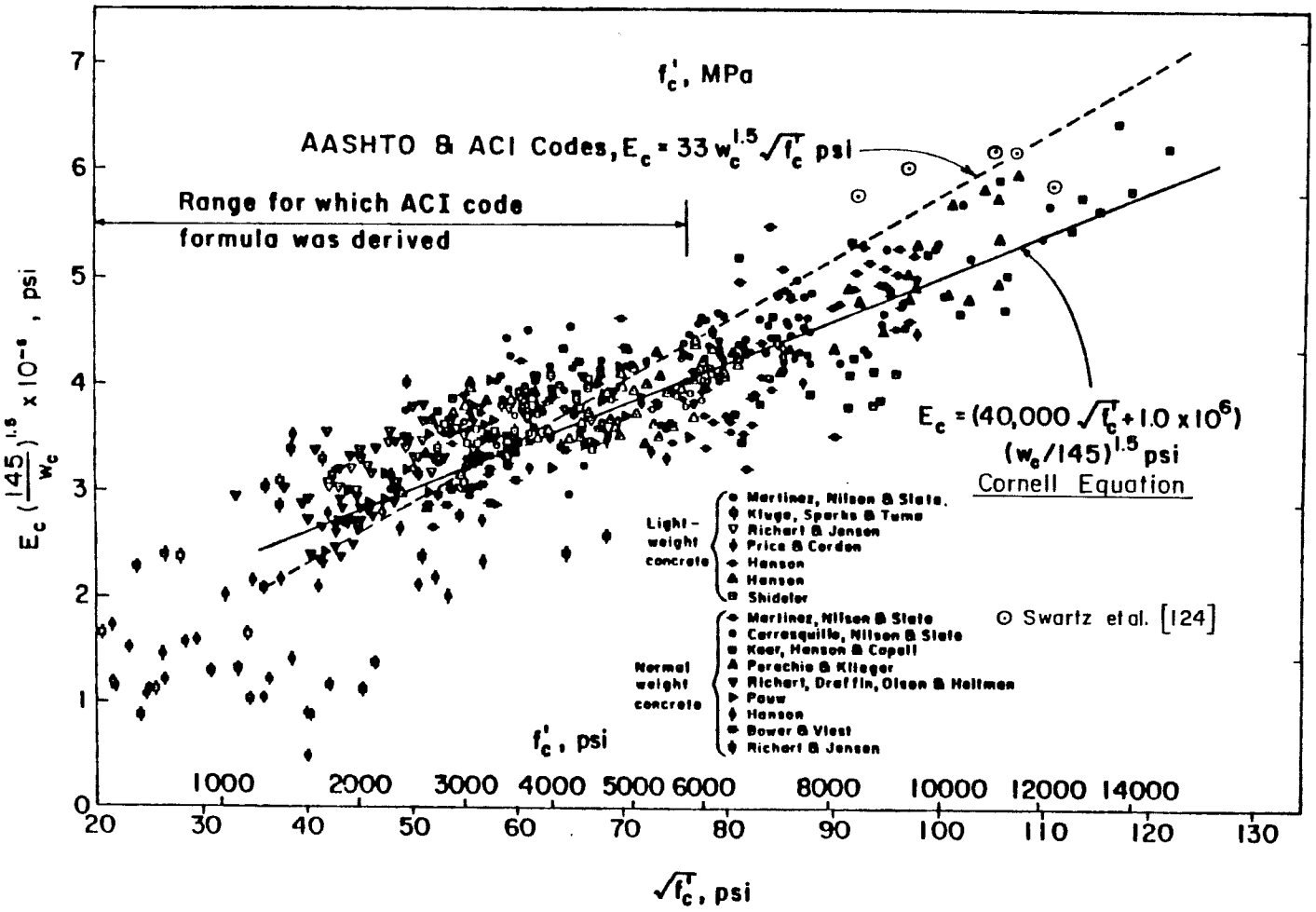

Fig. 3.4 Modulus of elasticity versus concrete strength [81 124].

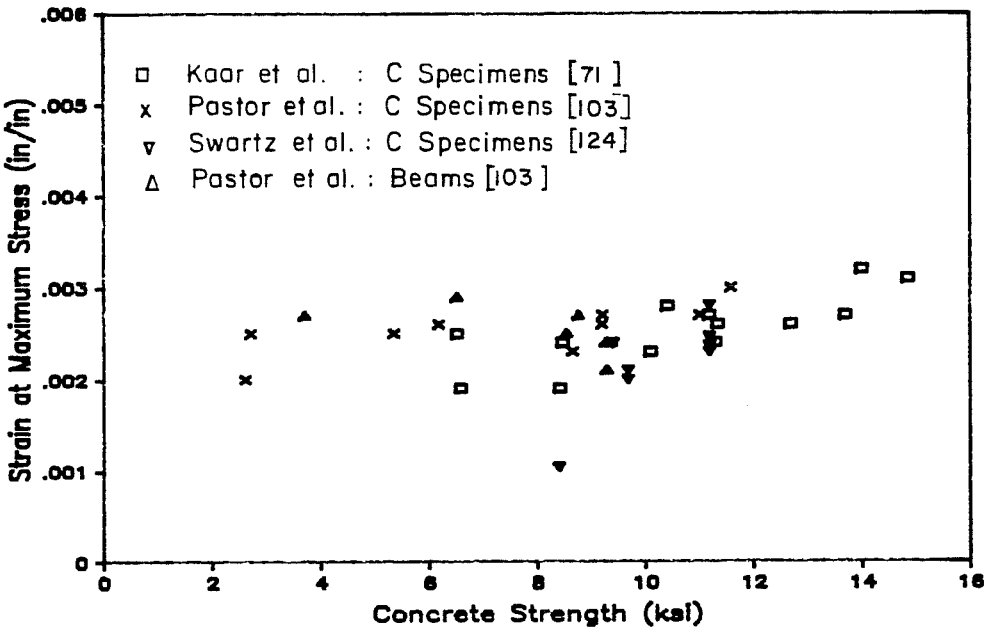

a) C Specimen and Beam Data

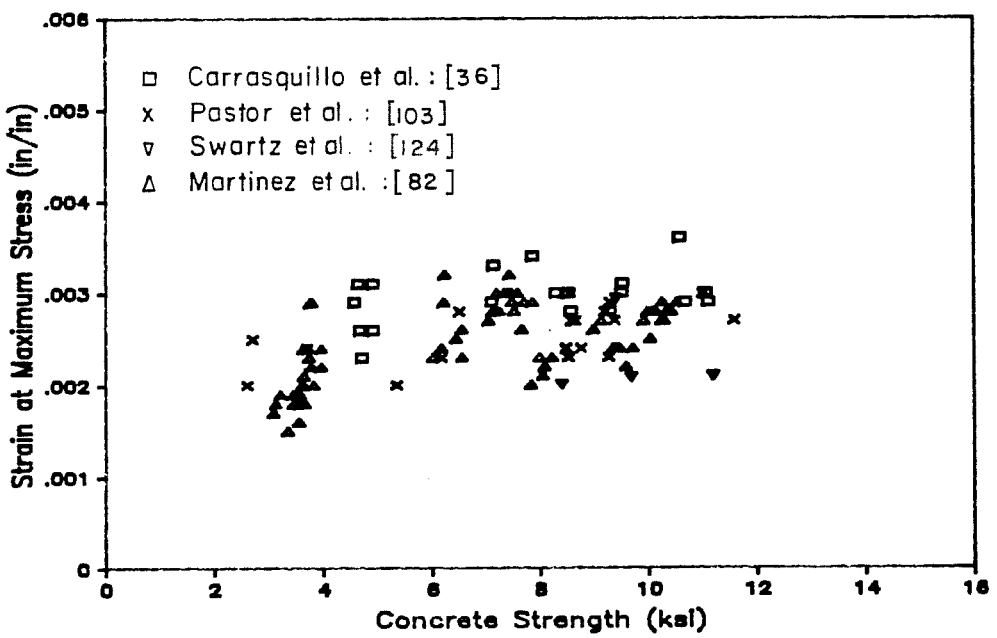

b) Cylinder Data

Fig. 3.5 Strains at maximum stress from flexure and axial tests.

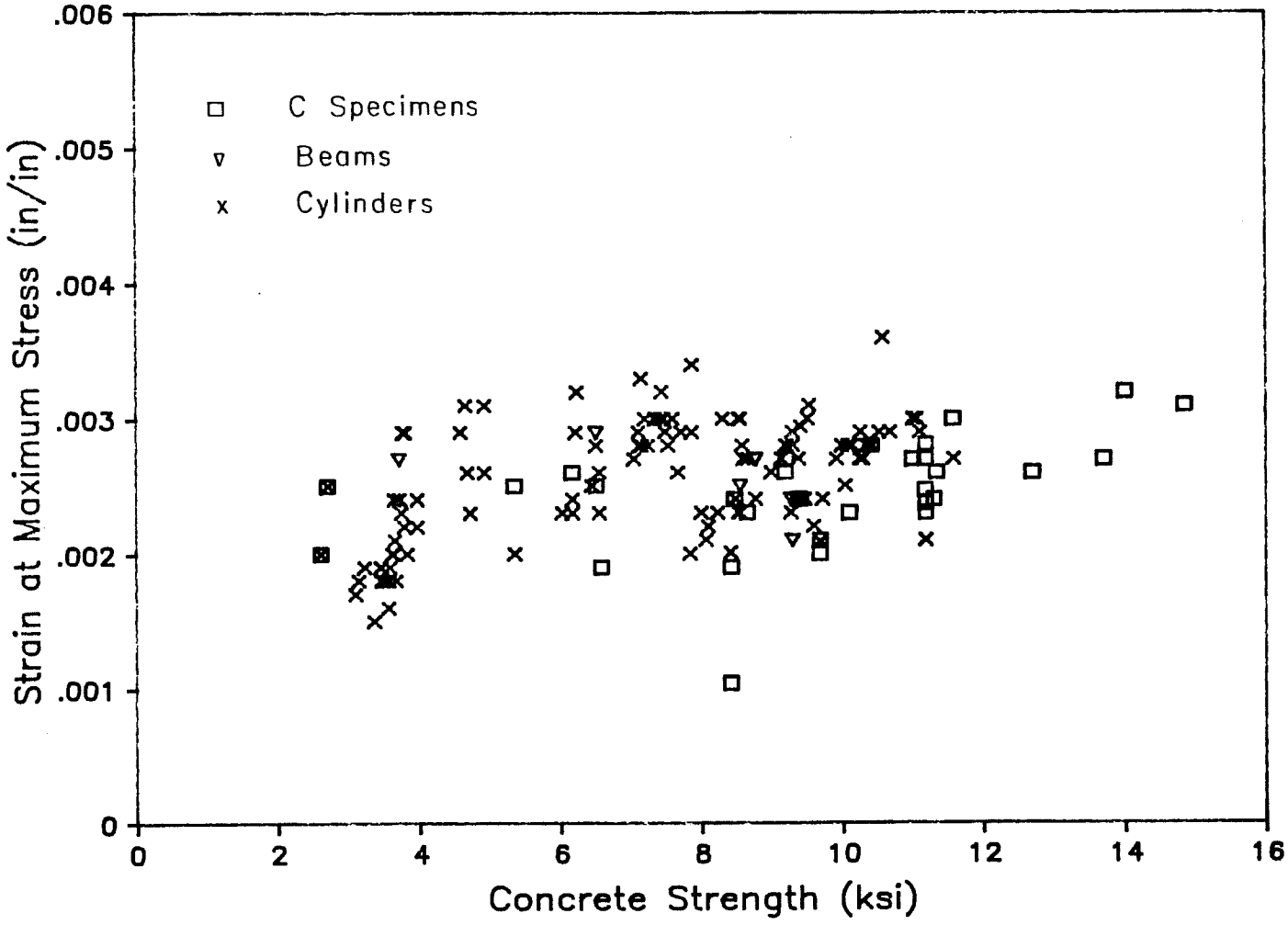

Fig. 3.6 Summary of strains at maximum stress

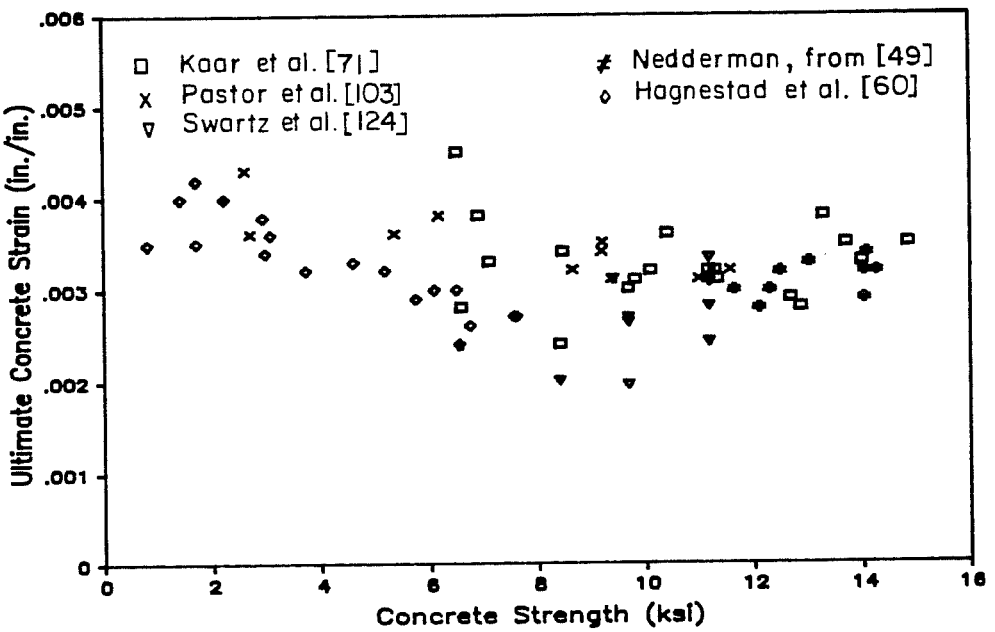

a) C Specimen Data

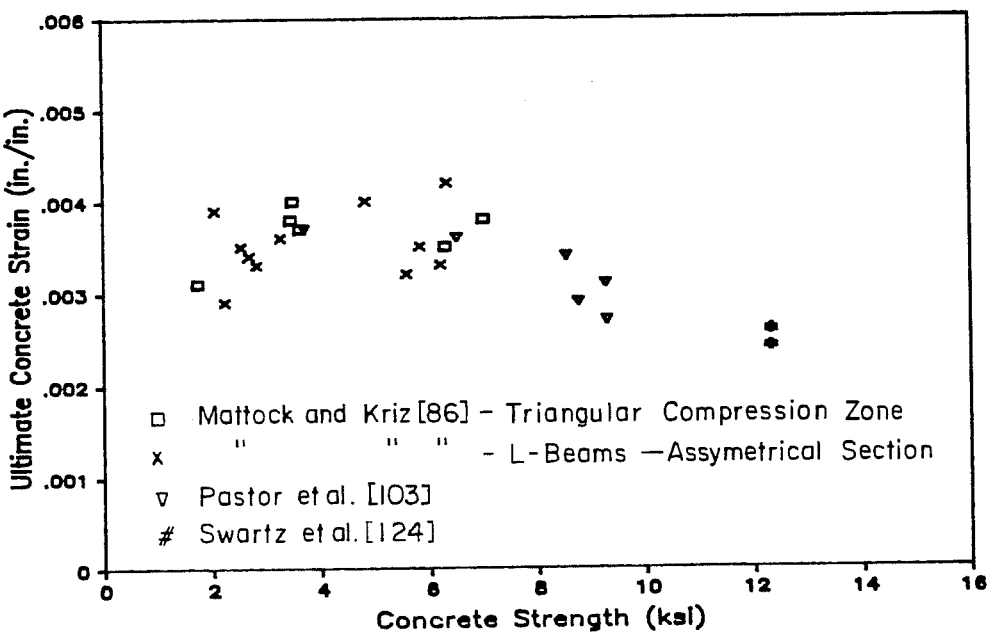

b) Beam Data

Fig. 3.7 Ultimate strains in concrete

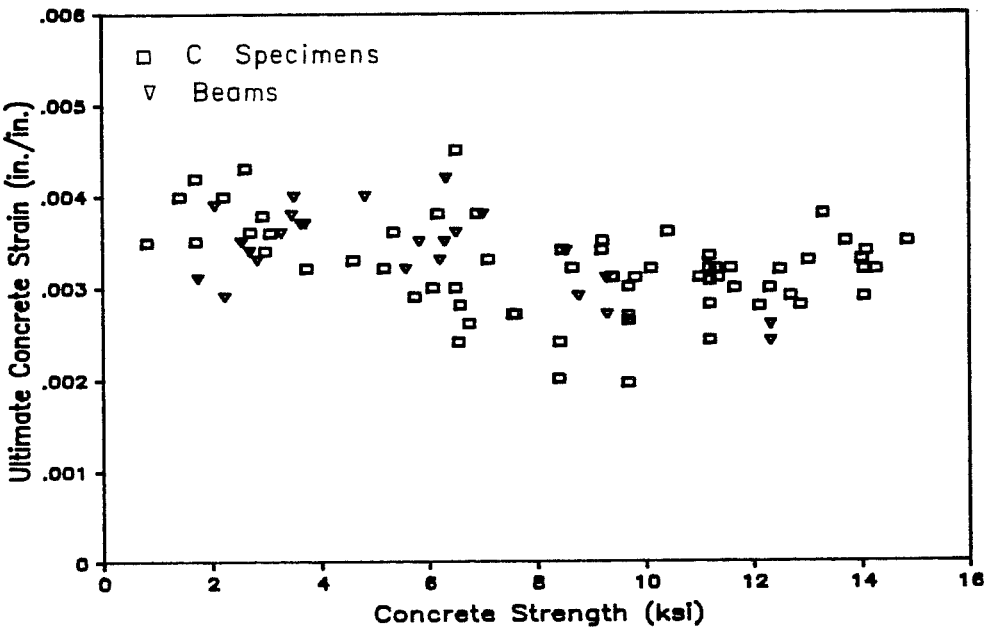

c) Combined C Specimen and Beam Data

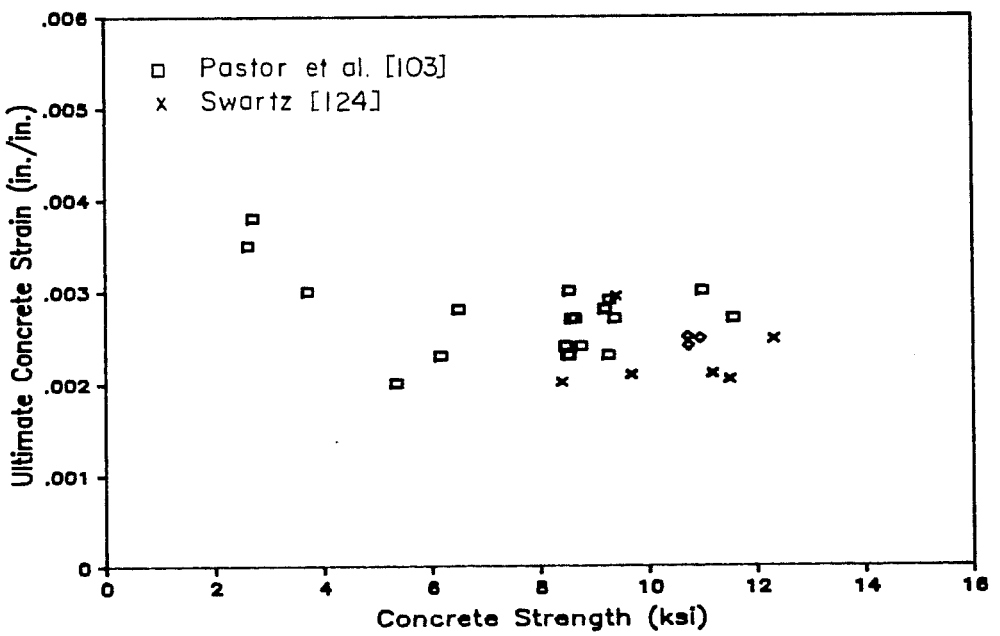

d) Cylinder Data

Fig. 3.7 Ultimate strains in concrete (continued)

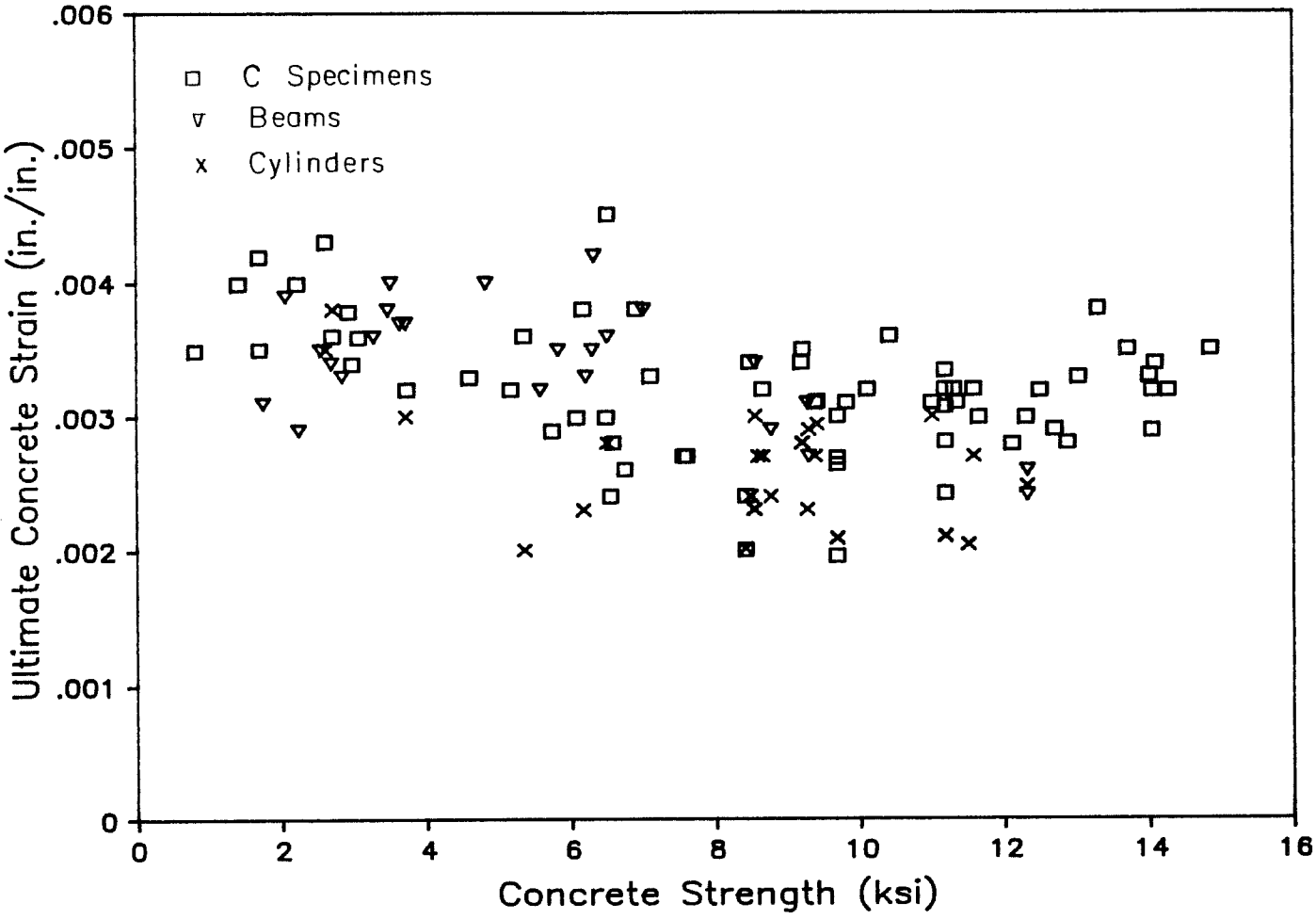

Fig. 3.8 Summary of ultimate strain data

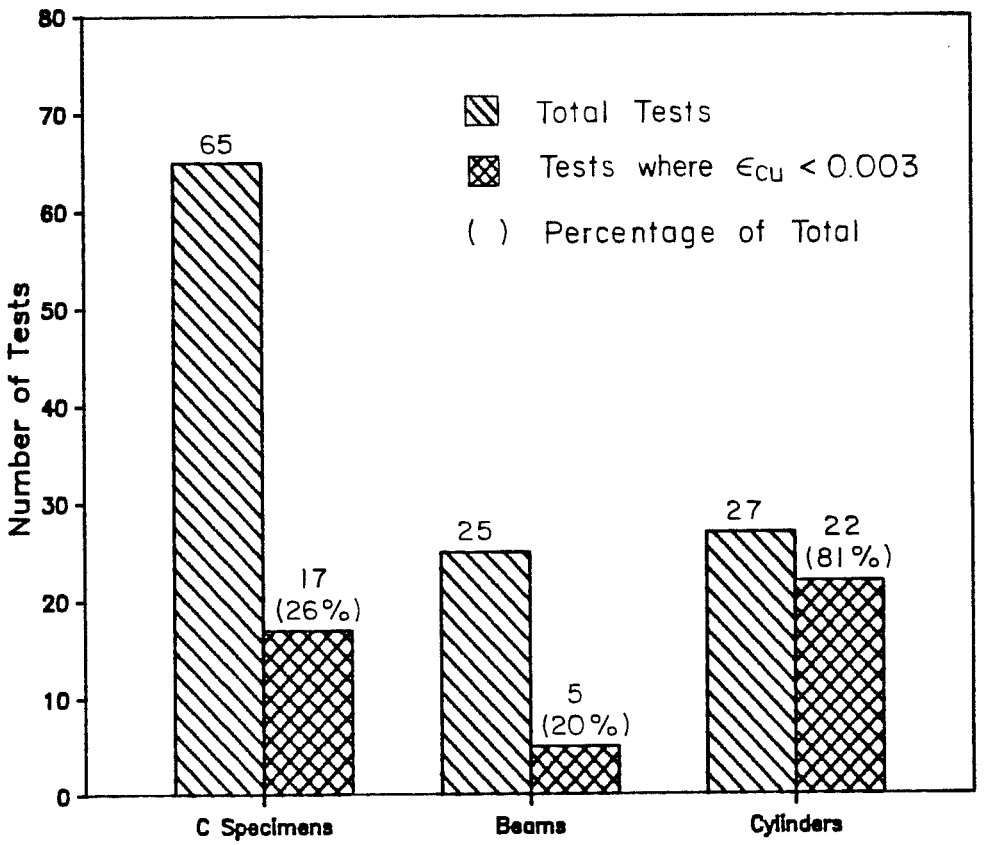

Fig. 3.9 Comparison of number of tests of different types of specimens for ultimate strain.

falling below the code specified ultimate strain of 0.003 is much larger for cylinder data than for flexure specimen data. The data of Fig. 3.8 indicate that the current limit of 0.003 is not as conservative for high strength concrete as normal strength concrete ($f_c' < 6000$ psi) and also show that the use of a limiting strain of 0.004, as considered by some [31,135], would be unconservative. Data reported by Tognon et al. [128] for very high strength concrete (f_c' of about 19 ksi) indicate linear behavior to a strain of approximately 0.003 with failure occurring at a strain of about 0.004. Therefore, for very high strength concrete, the current limit may become overconservative.

Strains at maximum stress and ultimate are compared in Fig. 3.10 for flexure and cylinder data. For the cylinder data, no trend is evident as the two strains are nearly equal for the range of concrete strengths shown. For the flexure tests, the two strains tend to converge as concrete strength increases with the ultimate strains being greater than the strains at maximum stress. This indicates that the descending branch of the stress-strain curve is more readily detectable in flexure tests.

Strain and modulus data from flexure and compression tests of the same concrete are compared in Figs. 3.11 and 3.12. Values for the modulus and strain at maximum stress agree well between flexure and cylinder tests as indicated by the clustering of data about the line

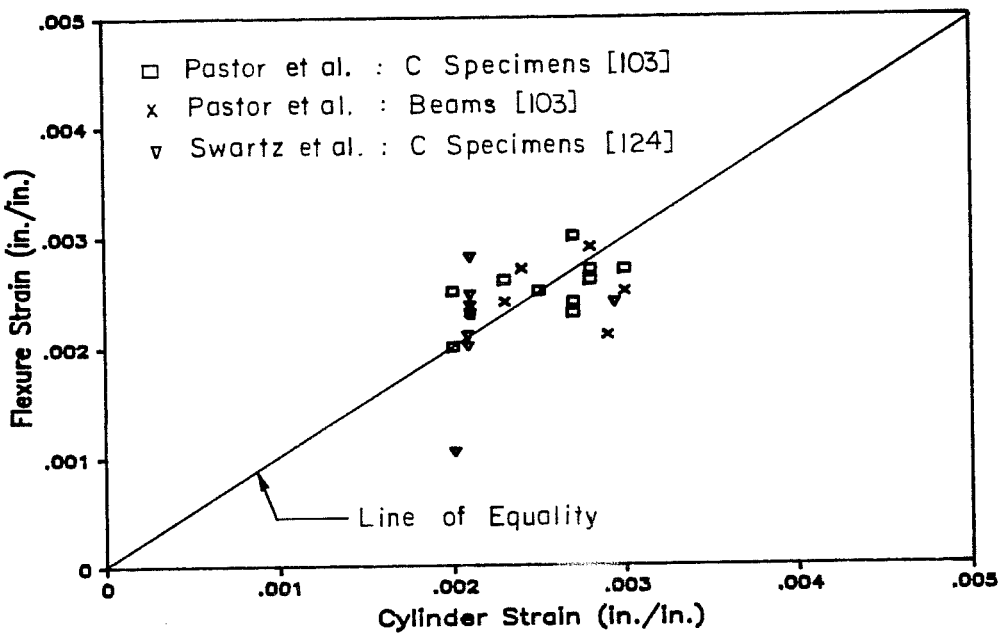

a) Strain at Maximum Stress

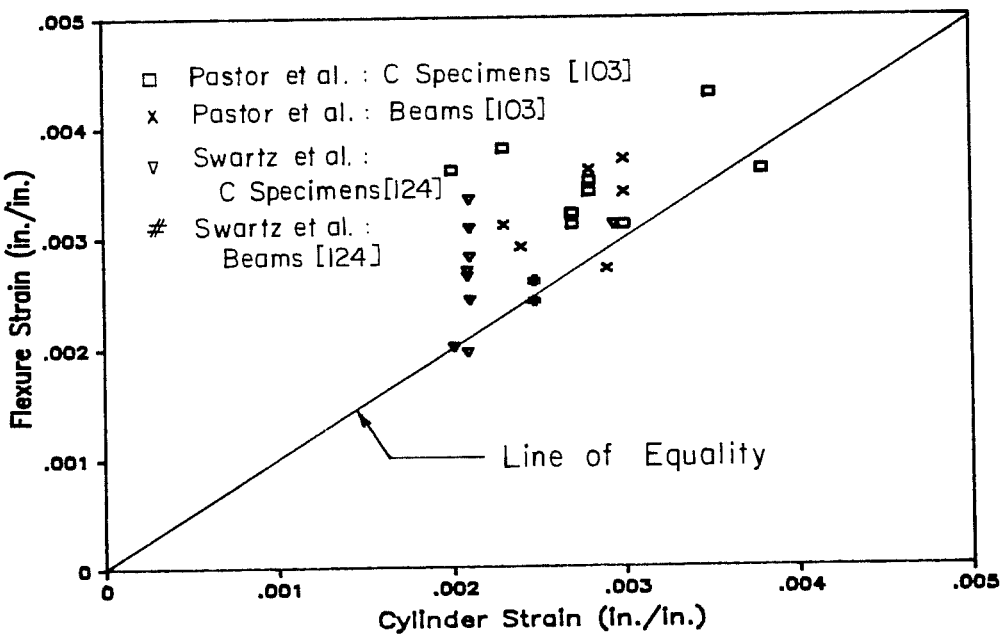

b) Ultimate Strain

Fig. 3.10 Comparison of ultimate strains and strains at maximum stress

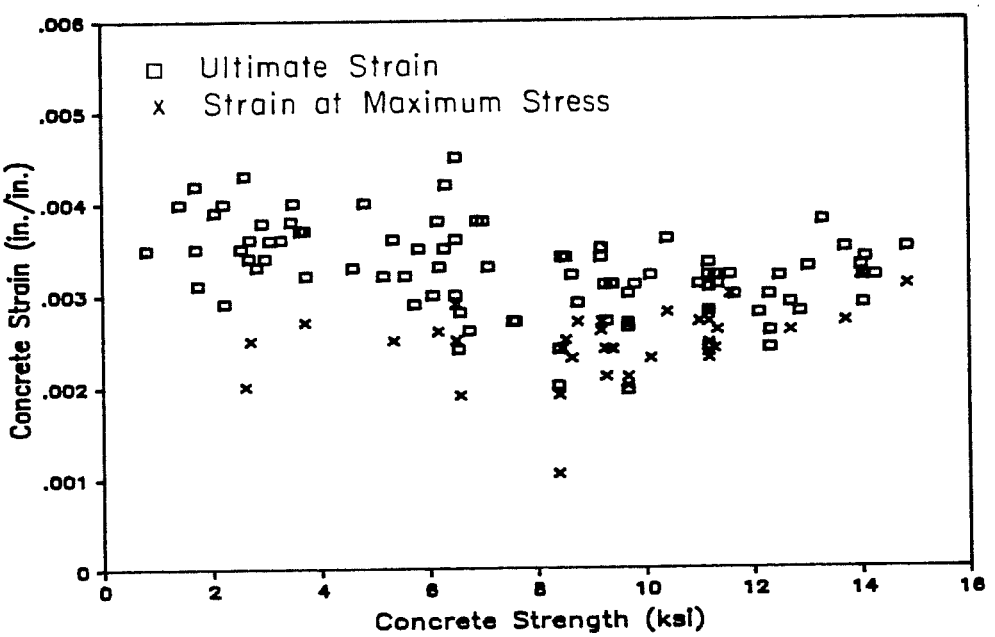

a) Combined C Specimen and Beam Data

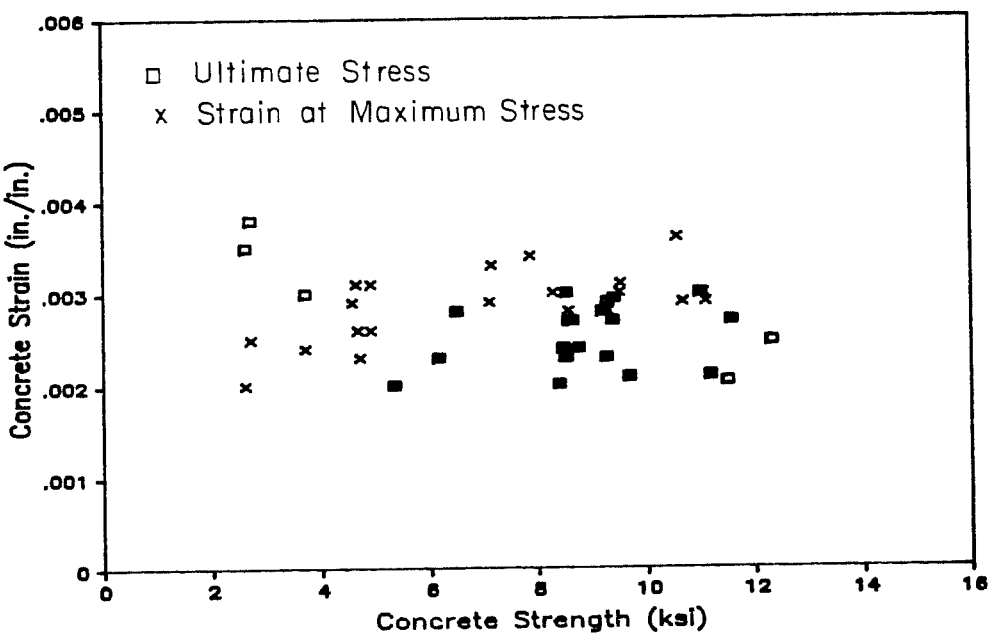

b) Cylinder Data

Fig. 3.11 Comparison of strains measured in flexure and cylinder tests

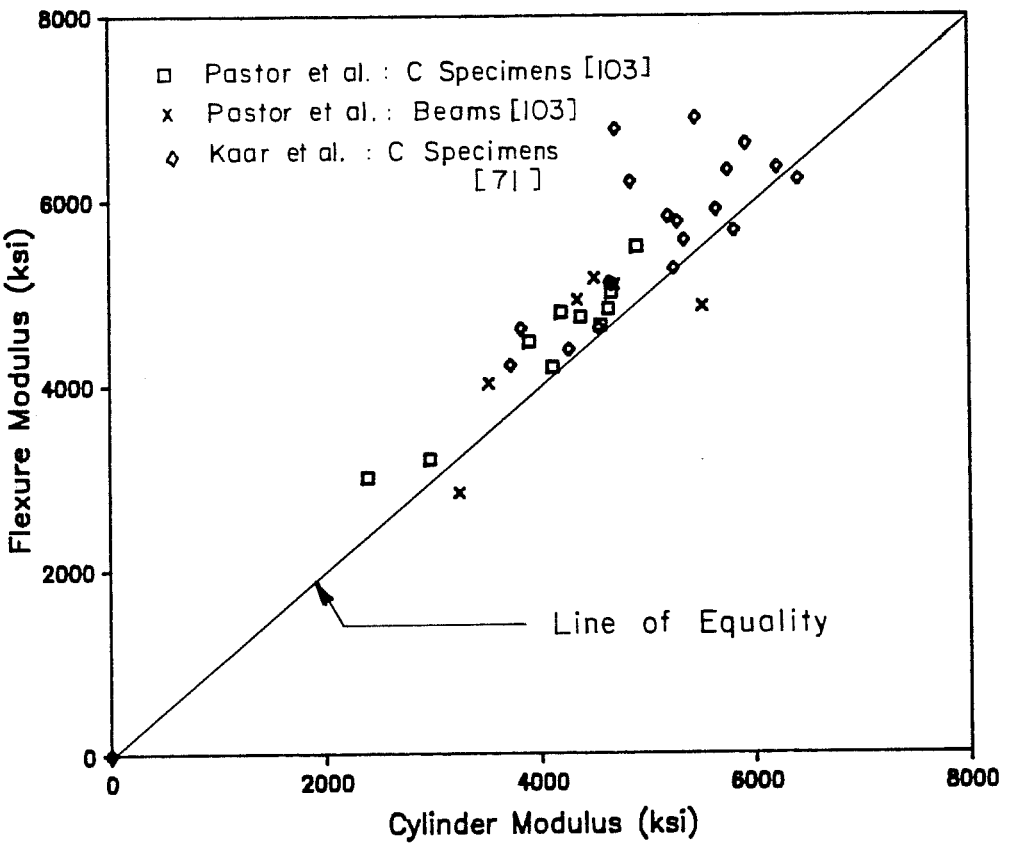

Fig. 3.12 Comparison of moduli measured in flexure and cylinder tests

of equality. Kaar et al. [71] report that moduli from cylinder tests are higher than for flexure tests. For ultimate strains, cylinder test data underestimate strains obtained in flexure tests. Therefore, it appears that cylinder data can be used for predicting flexural behavior up to the peak stress but that the cylinder data tends to underestimate the extent of the descending branch of the stress-strain curve [103].

3.3.3 Tensile Strength. The tensile strength of concrete measured by split cylinder and modulus of rupture tests for high strength concrete tend to exceed values computed using ACI expressions [36,104]. New formulas have been proposed for predicting both types of tensile strength from compressive strength [36]. However, Nilson [99] suggests that because both measures of tensile strength are sensitive to curing conditions and because significant differences exist between curing conditions in the field and the laboratory, current expressions should remain unchanged. The modulus of rupture for high strength concrete under drying conditions was up to 26 percent less than values for moist cured concrete. This reduction is greater than observed for normal strength concrete [36].

It should be noted that as concrete strength increases aggregate fracture across the failure plane also increases, leading to a smoother failure surface [36].

Overman et al. [101] observed that, for full scale tests where beams are deep, cracking occurred at stresses less than the AASHTO specified $7.5\sqrt{f_c'}$. A value of 6.7 to $7.0\sqrt{f_c'}$ is recommended for bridge girders.

3.3.4 Creep, Shrinkage, and Thermal Effects. Studies at Cornell [99] have shown that creep coefficients for high strength concrete are lower than for normal and low strength concrete, as summarized in Table 3.1. However, because stresses applied to high strength concrete will generally be higher, total creep is expected to be similar to that of other concrete [22]. Ngab et al. [98] found the relation between applied stress and creep to be linear to about 70 percent of f_c' for high strength concrete rather than 30 to 50 percent for normal strength concrete. In the same study, the ratio of sustained-load strength to short-term strength for high strength concrete ranged from 0.85 to 0.95 while values for normal strength concrete varied from 0.70 to 0.75. Smadi et al. [117], after finding less variation in this ratio with concrete strength than reported by Ngab [98], suggest that 0.8 be used as the sustained strength ratio for all normal weight concrete. Ngab et al. [98] found that the sensitivity of creep to curing conditions often resulted in lower creep factors for dry cured concrete.

Table 3.1 Creep coefficients [99]

Material	f'_c (psi)	C_{cu}	$C_{cu}/C_{cu,LSC}$
Low strength concrete	3,000	3.1	1.00
Medium strength concrete	4,000	2.9	0.94
" " "	6,000	2.4	0.77
High strength concrete	8,000	2.0	0.65
" " "	10,000	1.6	0.52

LSC = Low strength concrete

= 3,000 psi

C_{cu} = Creep coefficient

= Creep strain / initial elastic strain

While available data is limited, total shrinkage for high strength concrete appears to be similar to normal strength concrete, although high strength concrete may shrink at a higher initial rate [4, 22]. Ngab et al. [98] indicate that total drying shrinkage of high strength concrete may be approximately 500 microstrains for concrete moist cured until 28 days, although there was much variation in the data.

Thermal properties of high strength concrete are similar to those for normal strength concrete [22].

3.3.5 Cover and Durability. To prevent corrosion, AASHTO [10] specifies a minimum cover of 1.5 in. for prestressing steel and principal reinforcement and 1 in. for stirrups and ties. Additional cover should be provided where direct exposure to salt water, salt spray, or chemical vapor cannot be avoided. ACI Committee 343 [21] recommends that cover for reinforcement, where concrete is exposed to weather, should be 2 in. for principal reinforcement and 1.5 in. for stirrups and ties. If concrete is not exposed to weather, only 1.5 in. is required for principal reinforcement and 1 in. for stirrups and ties. If the environment is corrosive, increased cover and concrete quality should be considered. The ACI Code [15] requires cover of 1.5 in. for prestressed beam reinforcement whether exposed or not, but, when allowable tensile stresses are exceeded, the

cover shall be increased by 50 percent. The ACI Commentary [17] recommends a cover of 2 in. where the environment is corrosive.

While ACI Committee 363 [22] recommends the use of entrained air where high strength concrete will be exposed to freezing while wet, the limited data available is not conclusive. Use of entrained air causes a significant reduction in strength and should be avoided if the highest possible strength is desired. A loss of from 2 to 5 percent of strength for each one percent void space in concrete has been reported [4,22].

3.3.6 Unit Weight. The unit weight of high strength concrete is slightly higher than for normal strength concrete. Carrasquillo et al. [36] found that average unit weights for normal strength (f_c' = 3,000 to 6,000 psi), medium strength (f_c' = 6,000 to 9,000 psi), and high strength (f_c' > 9,000 psi) mixes containing limestone aggregates were 144, 146 and 152 lb/cu ft, respectively.

3.4 Analysis and Ultimate Capacity in Flexure

This section begins with a review of the historical background and derivations of the basic AASHTO and ACI provisions which are based on simplifying assumptions regarding the concrete stress block and strand stress. Tests intended to verify the applicability of the simplified approaches for use with high strength concrete are reviewed. The more rigorous and general strain compatibility or

moment-curvature approaches, which use either simplified or more realistic estimates for concrete and steel stress-strain relationships, will then be discussed. The strain compatibility approach may also be used to compute member behavior throughout its load history. The section concludes with a consideration of the application of the simplified and strain compatibility approaches to composite members.

Each analysis method provides an estimate of the stress in the reinforcement at ultimate, determines the location of the resultants of the resisting compression force in the concrete and compression reinforcement, and computes the moment capacity from these forces and locations using basic principles of analysis. The discussion in this section is limited to the consideration of the assumptions used in the analysis methods and the accuracy of ultimate capacity predictions using these methods.

3.4.1 Simplified Methods.

3.4.1.1 AASHO and AASHTO Specifications. Equations for computing ultimate moments for prestressed members first appeared in the 1961 edition of the AASHO Specifications [9] after being a part of tentative specifications for two years. For rectangular or flanged sections where the neutral axis lies within the flange, the ultimate moment was computed using

$$M_u = A^*_s f^*_{su} d(1-0.6p^* f^*_{su}/f'_c \quad (3.1)$$

and, for flanged sections in which the neutral axis falls outside the flange, which usually occurs if the flange thickness is less than $1.4dp^* f^*_{su}/f'_c$, the ultimate moment, M_u, was computed using

$$M_u = A_{sr} f_{su} d(1-0.6A_{sr} f^*_{su}/b'df'_c) + 0.85f'_c(b-b')t(d-0.5t) \quad (3.2)$$

where

A^*_s = area of prestressing steel

$A_{sr} = A^*_s - A_{sf}$
= area of steel required to develop ultimate compressive strength of the web of a flanged section

$A_{sf} = 0.85f'_c(b-b')t/f^*_{su}$
= the steel area required to develop the ultimate compressive strength of the overhanging portions of the flange

d = effective depth of prestressing steel

b = width of compression flange for flanged member or width of rectangular member

b' = width of a web for a flanged member

t = average thickness of the flange of a flanged member

$p^* = A^*_s/bd$
= reinforcing ratio for prestressing steel

f^*_{su} = average stress in prestressing steel at ultimate load

f'_c = compressive strength of concrete at 28 days.

These equations, which are shown using current notation, are unchanged from the 1961 Specifications.

The above equations are the only provisions given in the AASHTO Specifications for ultimate flexural design of prestressed members. In contrast, ultimate flexural design in the ACI Code is based on general assumptions, which can be applied to a wide variety of situations and section geometries. Equations similar to Eq. 3.1 and 3.2 are provided in the ACI Commentary. A set of general assumptions similar to those in the ACI Code appear in the chapter of the AASHTO Specifications on reinforced concrete design and are used for prestressed concrete design, although the Specifications state that provisions for reinforced and prestressed concrete are independent of each other.

These equations first appeared in the "Tentative Recommendations for Prestressed Concrete" [19] which were made in 1958 by ACI-ASCE Joint Committee 323 (now 423) on Prestressed Concrete. A report by Warwaruk, Sozen, and Siess in 1962 [133] summarized much of the testing and analysis from which the Committee recommendations were developed. The equations given above were developed by assuming the following: (1) a linear variation of strain across the section, (2) concrete resists no tension, (3) failure occurs when the strain in the extreme compression fiber reaches a useful limit, and (4) that the compression stress block may be characterized by factors k_2, k_u, and f_{cu} as shown in Fig. 3.13 (which also contains the equations

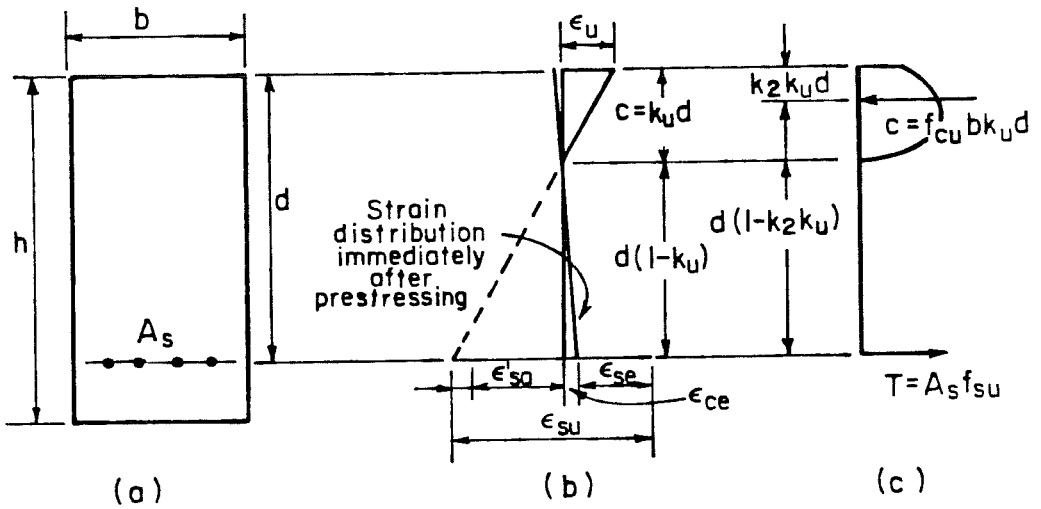

$$M_f = A_s f_{su} d(1-k_2 k_u)$$

where

k_u = pf_{su}/f_{cu}
= ratio of neutral axis depth at failure to effective depth

k_2 = ratio of the depth of the compressive force to depth of the neutral axis

f_{cu} = $0.7f'_c$ (from test data)
= effective strength of the concrete in the compression zone at failure.

ϵ_{su} = $\epsilon_{se} + \epsilon_{ce} + \epsilon'_{sa}$
= reinforcement strain at failure

ϵ_{se} = effective prestrain corresponding to effective prestress

ϵ_{ce} = concrete strain at the level of the reinforcement due to effective prestress.

ϵ'_{sa} = increase in strain in the prestressed reinforcement between prestress and failure.

ϵ_u = useful limit of strain in compressed concrete

Fig. 3.13 Stress and strain conditions at failure for prestressed beams reinforced in tension only - Warwaruk, et al. (Ref. [133])

and definitions of these quantities). Warwaruk et al. [133] reason that the factor k_2, which can vary from 0.5 for a rectangular stress distribution to 0.333 for a triangular distribution should be taken as 0.42 which is an average of the two extremes. The relation between f_{cu}, the effective concrete strength in the compression zone, and f'_c was determined experimentally for two ranges of concrete strength. These factors were combined, using the relation for f_{cu} for the lower strength range, to obtain the equation used in the AASHTO Specification for rectangular sections.

Warwaruk et al. [133] point out that the equation for flanged sections, which was developed by Committee 323, is inconsistent in that it assumes the flange to be stressed at $0.85f'_c$ while the web, treated as a rectangular section, is stressed to $0.72f'_c$. The equation is sufficiently accurate in spite of the discrepancy.

The current AASHTO Specifications provide an equation to estimate stress in bonded prestressed reinforcement at ultimate:

$$f^*_{cu} = f'_s (1 - 0.5p^*f'_s/f'_c) \tag{3.3}$$

where f'_s = ultimate strength of prestressing steel.
This equation may be used when the stress-strain properties of the prestressing steel are similar to standard properties and the effective prestress after losses, f_{se}, is not less than $0.5f'_s$. The Specifications allow use of a detailed analysis to

better determine f^*_{su}, but no guidance is given on how the analysis should be performed.

This equation also originated in Committee 323. Warwaruk et al. [133] discuss the expression and indicate that it is based on a comparison of the available test results with the parameter $p^*f'_s/f'_c$ which varies approximately in proportion to the depth of the neutral axis at ultimate for rectangular sections with prestressing steel only [84]. The report contains data for rectangular beams with compressive strengths of about 5,000 psi prestressed with materials with ultimate strengths close to 250 ksi. According to Khachaturian and Gurfinkel [74], the equation is unconservative for flanged sections, giving steel stresses higher than actually exist. The equation may also underestimate the capacity of beams with high percentages of steel [17]. Warwaruk et al. [133] note the shortcomings of the equation but acknowledge that the simplicity of the equation more than offsets the small inaccuracies in its application.

Committee 323 [19] refers to the Warwaruk report [133] for detailed analyses that may be used in lieu of Eq. 3.3. Two alternate methods are given: the first is a series of equations that are used to develop a single equation which is very accurate for a given ratio

of f_{sy}/f_{su}; and the second involves iterations or graphical solutions in which the stress-strain curve of the prestressing steel is used with equations developed from strain compatibility to determine the stress at ultimate.

3.4.1.2 ACI Building Code. The current ACI Code (318-83) [15] provisions for analysis of prestressed sections at ultimate consist of general assumptions regarding strain conditions at ultimate and parameters that define a simplified concrete stress block. Use of other ultimate stress blocks is allowed if they provide "predictions of strength in substantial agreement with results of comprehensive tests." No equations are given in the body of the Code, but equations are provided in the Commentary [17] as examples of the application of the assumptions. Design for prestressed flexural members is the same as for conventionally reinforced concrete members with the substitution of strand stress at nominal strength, f_{ps}, for the yield stress of conventional reinforcement, f_y. The nominal moment capacity, M_n, for rectangular sections or flanged sections where the depth of the equivalent rectangular compression block, a, is equal to or less than the thickness of the compression flange, can be written for sections with only bonded prestressed tension reinforcement as:

$$\phi M_n = \phi[A_{ps} f_{ps} d_p (a - 0.5\rho_p f_{ps}/f'_c)] \quad (3.4a)$$

$$= \phi[a_{ps} f_{ps} (d_p - a/2)] \quad (3.4b)$$

where $a = A_{ps} f_{ps}/(0.85 f'_c b)$ (3.5)

a = depth of equivalent rectangular stress block

A_{ps} = area of prestressed reinforcement in tension zone

f_{ps} = stress in prestressed reinforcement at nominal strength (see Eq. 3.12)

d_p = distance from extreme compression fiber to centroid of prestressed reinforcement

ρ_p = reinforcement ratio for prestressed reinforcement $= A_{ps}/bd_p$

ϕ = strength reduction factor.

Where the compression flange thickness is less than a, the design moment strength for members with only prestressed tension reinforcement can be computed using:

$$\phi M_n = \phi[A_{pw} f_{ps} (d_p - a/2) + 0.85 f'_c (b - b_w) h_f (d_p - h_f/2)] \quad (3.6)$$

where

$$A_{pw} f_{ps} = A_{ps} f_{ps} - 0.85 f'_c (b - b_w) h_f \quad (3.7)$$

$$a = A_{pw} f_{ps}/(0.85 f'_c b) \quad (3.8)$$

A_{pw} = that part of the tension reinforcement required to develop the web

b_w = web width

h_f = overall thickness of flange.

The ultimate design provisions from which these equations were developed are based on stress-strain relationships for ultimate flexural design proposed by Whitney [134], Jensen [68], and others [58]. A modified form of the Stussi stress block and Whitney's

equivalent rectangular stress block (ERSB), shown in Fig. 3.14 for reinforced concrete members reinforced in tension only, were used to model the compression stress block at failure [61,87]. The Stussi parameters k_1, k_2, and k_3 define the magnitude and location of internal compressive force in the concrete at failure. Using these factors and assuming linear distribution of strain across the section, the ultimate moment capacity and depth of compression zone, $k_u d$, for failure initiated by yielding of the tension steel was shown to be:

$$M_u/(bd^2f'_c) = q(1-(k_2/(k_1k_3))q) \tag{3.9}$$

$$k_u = \epsilon_u/(\epsilon_{su} + \epsilon_u) = c/d \tag{3.10}$$

where M_u = factored moment at a section $\leq \phi M_n$

q = reinforcement index $= A_s f_y/(bdf'_c) = \rho f_y/f'_c$

ϵ_u = strain in extreme fiber of concrete in compression at ultimate load

ϵ_{su} = strain in reinforcement at ultimate load

f_y = yield point of reinforcement

c = distance from neutral axis to compression edge of member.

Data from tests of special unreinforced C-shaped specimens were used to establish the range of values for the Stussi parameters [61].

The ACI-ASCE Joint Committee 327 on Ultimate Strength Design [20] recommended use of a form of Eq. 3.9 for reinforced members in which the tension steel yields at failure:

$$M_u = A_s f_y d(1-0.59pf_y/f'_c) \tag{3.11}$$

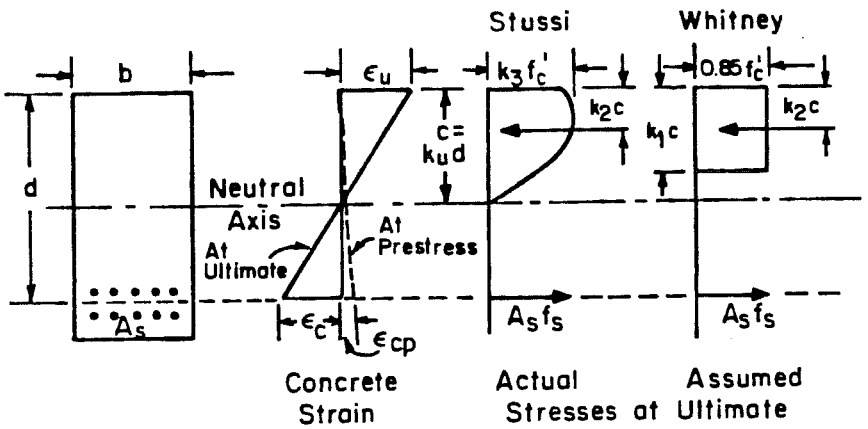

$$M_{ult} = A_s f_s (d - k_2 c) = 0.85 k_1 f'_c bc(d - k_2 c)$$

where

f_s = stress in tensile reinforcement at ultimate strength

k_u = c/d
= $\epsilon_u/(\epsilon_c + \epsilon_u)$

k_1 = ratio of average stress to maximum stress

k_2 = $k_1/2$
= ratio of depth to resultant of concrete compressive force, to depth of neutral axis

k_3 = 0.85
= ratio of maximum stress to 6 x 12-in. cylinder strength, f'_c

ϵ_s = $\epsilon_u[0.85 k_1 f'_c/(pf_s) - 1] + \epsilon_{cp} + \epsilon_{se}$
= tensile steel strain at ultimate beam strength

ϵ_{se} = effective steel prestrain

ϵ_{cp} = concrete precompression strain at level of steel in a prestressed beam

ϵ_c = concrete tensile strain at ultimate at level of steel in prestressed beam

ϵ_u = maximum concrete compression strain at ultimate beam strength

Fig. 3.14 Stress and strain conditions at failure for prestressed beams reinforced in tension only - Matlock, et al. (Ref. [87])

which assumes the Stussi parameters to be

$$k_3 = 0.85$$

$$k_2/k_1 = 0.5.$$

Similar equations are provided for use with other types of reinforced concrete sections. An abstract of the Committee report appeared as an appendix to the 1956 edition of the ACI Code [11] to introduce ultimate strength design. Prestressed concrete was not addressed in this edition.

In 1957, Hognestad [59] presented further analyses of test data to verify the validity of the 0.59 coefficient in Eq. 3.11 and demonstrated this coefficient could be obtained using the assumptions of Whitney's ERSB. Although the assumptions used to develop these equations are not accurate for non-rectangular sections and rectangular sections subjected to asymmetrical bending, the error is small if failure is initiated by yielding of the reinforcement. Later tests and analysis confirmed this [86]. Ultimate design methods were also shown to be sufficiently accurate for prestressed members [66].

Mattock, Kriz, and Hognestad [87] proposed the general statement of the ultimate design assumptions including the ERSB in 1961. Prestressed members were discussed and an iterative approach was suggested to determine the steel stress at ultimate.

The ACI Building Code (318-63) [12] adopted this general statement of ultimate strength design with only a few revisions and

extensions for both reinforced and prestressed concrete. Capacity reduction factors were also introduced. Strand stress at ultimate was estimated using the same equation and limitations as appear in the AASHTO Specifications.

Other than changes in notation, only a few substantial changes in the Code provisions have occurred since 1963. In 1971 [13], equations for computing ultimate moment were removed from the body of the Code. In the 1983 edition of the ACI Code, the equation used to provide an estimate of strand stress at ultimate was revised to better reflect current practice, including use of low relaxation strand, high strength concrete, compression steel, and nonprestressed reinforcement [84]. The equation now appears as

$$f_{ps} = f_{pu}\left(1 - \frac{\gamma_p}{\beta_1}\left[\rho_p \frac{f_{pu}}{f'_c} + \frac{d}{d_p}(\omega - \omega')\right]\right) \qquad (3.12)$$

where f_{pu} = specified tensile strength of prestressed reinforcement

γ_p = factor for type of prestressing tendon
= 0.40 for f_{py}/f_{pu} not less than 0.85 (stress-relieved strand)
= 0.28 for f_{py}/f_{pu} not less than 0.90 (low relaxation strand)

β_1 = a factor used in the definition of the ERSB which relates the depth of the compression block, a, to the depth to the neutral axis, c. For $f'_c \leq 4{,}000$ psi, $\beta_1 = 0.85$. For $f'_c > 4{,}000$ psi, β_1 is reduced continuously at a rate of 0.05 for each 1,000 psi of strength in excess of 4,000 psi, but β_1 shall not be less than 0.65.

ω = reinforcement index for nonprestressed tension reinforcement

$= A_s f_y / bdf'_c$

ω' = reinforcement index for nonprestressed compression reinforcement
$= A'_s f_y / bd'f'_c$

d = distance from extreme compression fiber to centroid of nonprestressed tension reinforcement, in.

d' = distance from extreme compression fiber to centroid of nonprestressed compression reinforcement, in.

3.4.1.3 Results of Tests. The first research on high strength concrete in flexure was conducted by Nedderman in 1973 at the University of Texas at Arlington (see [76,49]). Concrete strengths in the range of approximately 11.6 to 14.25 ksi were used in the study. Kaar, Hanson, and Capell reported additional work in 1978 [71] in which concrete strengths up to 14.85 ksi were used. Both investigations used C-shaped specimens similar to those used in the tests by Hognestad et al. [60] to determine the validity of the ERSB for high strength concrete. On the basis of their findings, a lower limit was placed on the factor β_1 (formerly k_1) in the 1977 edition of the ACI Code [14], but otherwise, the ERSB was found to be appropriate for use with high strength concrete.

Leslie, Rajagopalan, and Everard [76] published results from tests of high strength concrete beams in 1976 and recommended a smaller value for the ultimate strain and a triangular stress block instead of the ERSB. However, in the discussion of this paper, Ghosh and Chandrasekhar [49] and Wang, Shah, and Naaman [130] demonstrate

that a triangular stress block would produce a negligible improvement over the current ERSB and question the need for a reduced ultimate strain.

An analytical study by Wang, Shah and Naaman [131] in 1978 gave further indication that the current ERSB could be used with high strength concrete to provide reasonable estimates of ultimate capacity in flexure. They maintain that ultimate strains in excess of the current limit of 0.003 could be attained even for high strength concrete. This assertion was supported by a later paper by the same authors [132] which reported data for concrete cylinders tested in parallel with a hardened steel tube where strains of 0.006 were consistently obtained for concrete strengths up to 11,000 psi.

Tests of C-shaped specimens and reinforced beams made with high strength concrete conducted at Cornell University by Pastor, Nilson and Slate [103] were reported in 1984. Again, the data show that current ERSB parameters give a reasonable and conservative representation of high strength concrete at ultimate. The use of more sophisticated stress blocks was recommended only if very accurate results were desired. Nilson [99] commented later that, on the basis of test data, existing ultimate design provisions were satisfactory for all concrete strengths if the tensile steel yielded.

The State-of-the-Art Report on the use of high strength concrete presented by ACI Committee 363 in 1984 [22] echoed the above

findings by stating that present ACI provisions could be used without change for under-reinforced members with concrete strengths up to 12,000 psi.

A recent report additional tests of C-shaped specimens and reinforced beams by Swartz et al. [124] showed that the factor $k_2/(k_1k_3)$ was close to the ACI value but that β_1 was closer to 0.83 which is higher than the 0.65 given by the Code.

The background of the original equation for estimating f_{ps} and the effect of the revision was presented by Mattock [84]. The paper included a study of the accuracy of Eq. 3.12 when applied to T-beams, which demonstrated that the equation had sufficient accuracy.

3.4.2 Strain Compatibility Methods. The compatibility or moment-curvature analysis method for determining the ultimate moment capacity of prestressed members is a more general form of the basic approaches that have been discussed above. The method can be used with the assumptions of the ERSB to obtain ultimate moment capacities without the use of an equation to estimate the strand stress. It can also be used to predict the complete load-deformation behavior of a member if a complete representation of the stress-strain relationship for the concrete is used.

The basic requirement of the method is the establishment of strain compatibility and force equilibrium across the section. A top

fiber strain (or some other quantity) is assumed and height of the neutral axis is adjusted until a strand strain is obtained that produces a force equal to the compression force in the concrete. The ultimate moment can be either the moment when the top fiber strain is a certain value, such as 0.003 for ACI, or, more accurately, the maximum moment resisted by the section as top fiber strain is increased. Compression reinforcement or nonprestressed tension reinforcement can be accomodated in the analysis, the details of which can be found elsewhere [34,93,133].

While many analytical expressions have been proposed for the concrete stress-strain curve, only a sampling of those which are simple and do not require stress-strain data for calibration of coefficients are presented here. Equations and parameters for five stress-strain relationships are presented in Fig. 3.15 and the curves are compared for 5,000 and 10,000 psi concrete in Fig. 3.16.

Naaman [95], after reviewing a number of expressions for the stress-strain characteristics of prestressing strand, recommended the expression by Menegotto and Pinto as most suitable. Figure 3.17 illustrates the relationship and Table 3.2 gives coefficients derived for use in the relationship.

The stress-strain behavior of nonprestressed steel can be approximated by assuming elastic-plastic behavior, which is conservative. If strain hardening is to be considered, Wang, Shah,

Investigator			Equations and Parameters	
Jensen [68]	f_c	=	$\epsilon_c E_c$	for $\epsilon \le \epsilon_0$
	f_c	=	f'_c	for $\epsilon > \epsilon_0$
	ϵ_0	=	f'_c/E_c	
	ϵ_{cu}	=	$f'_c/E_c/(1-\beta)$	
	β	=	$1/(1+(f'_c/4000)^2)$	

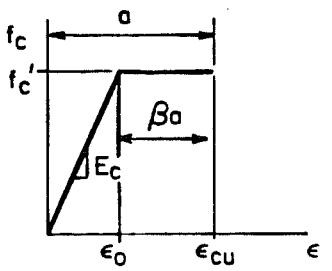

Hognestad [58]	f_c	=	$f''_c(2\epsilon/\epsilon_0-(\epsilon/\epsilon_0)^2)$
	ϵ_0	=	$2f''_c/E_c$
	f''_c	=	$0.85f'_c$
	ϵ_{cu}	=	0.0038

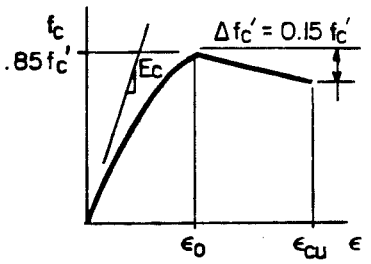

Burns [34]	f_c	=	$f'_c(2\epsilon/\epsilon_0-(\epsilon/\epsilon_0)^2)$
	ϵ_0	=	$2f'_c/E_c$
	ϵ_{cu}	=	0.0035

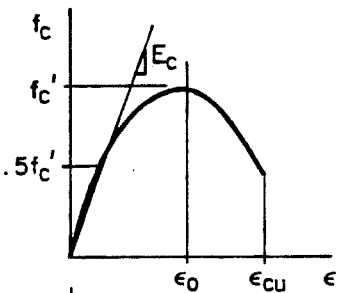

Kent and Park [73]	f_c	=	$f'_c(2\epsilon/\epsilon_0-(\epsilon/\epsilon_0)^2)$
	ϵ_0	=	0.002
	ϵ_{50u}	=	$\dfrac{3 + 0.002f'_c}{f'_c - 1000}$

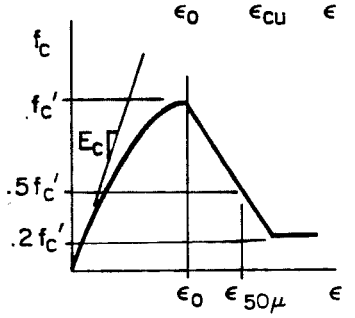

Carreira and Chu [37]	f_c	=	$f'_c(\beta(\epsilon/\epsilon_0)/(\beta- 1+(\epsilon/\epsilon_0)^\beta)$
	ϵ_0	=	$(4.88f'_c+168)\times10^{-5}$
		=	0.002 (approx.)
	β	=	$1/(1-(f'_c/E_{it}\epsilon_0))$
	E_{it}	=	E_c (approx.)

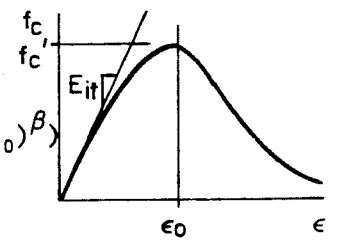

Fig. 3.15 Analytical stress-strain curves for concrete

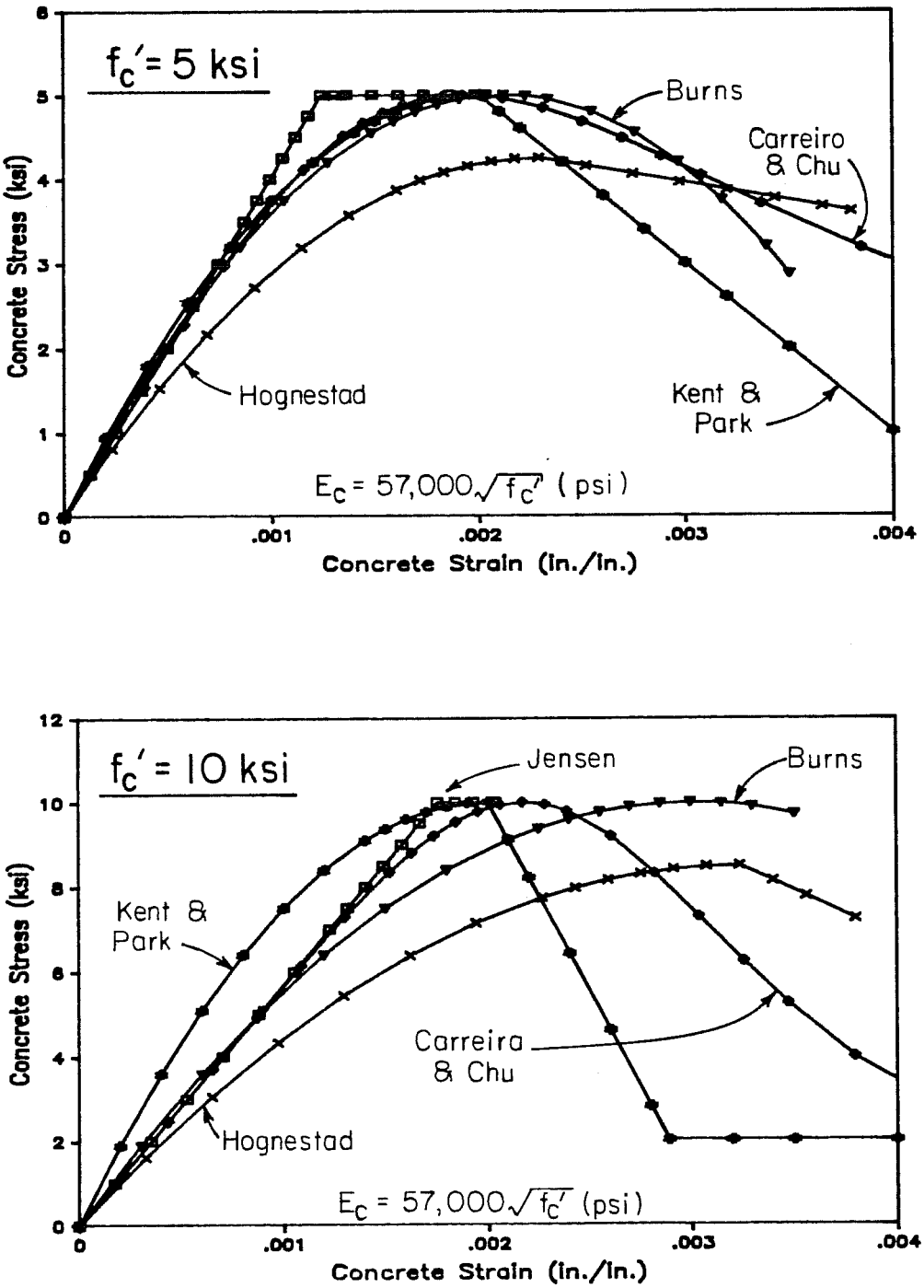

Fig. 3.16 Comparison of analytical stress-strain curves for concrete.

$$f = E\epsilon \left[Q + \frac{1 - Q}{\left[1 + \left(\frac{E\epsilon}{Kf_y} \right)^N \right]^{1/N}} \right]$$

$$Q = \frac{f_u - Kf_y}{E\epsilon_u - Kf_y}$$

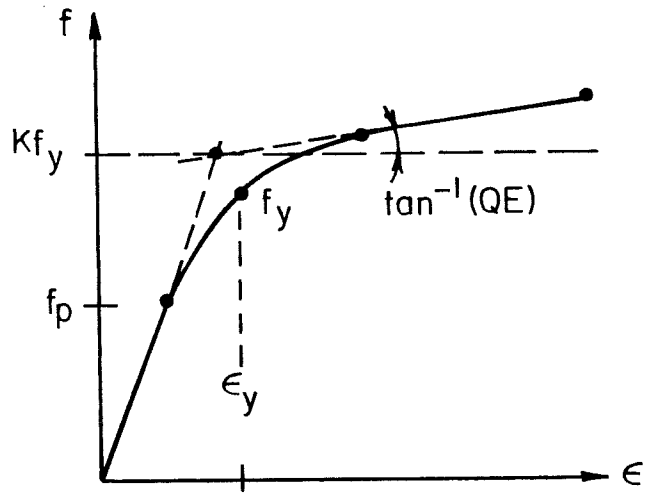

Menegotto and Pinto (1973)

Notation applies to reinforcing or prestressing steel:

Subscript y for yield, u for ultimate,
p for proportional limit, E for elastic modulus.

Fig. 3.17 Analytical stress-strain curve for prestressing steel [95]

Table 3.2 Coefficients for the stress-strain relationships of typical prestressing steels [95]

Fitting Constraints	Stress-Strain Relationship	Bars 160 ksi (1104 N/mm^2)	Wires 235 ksi (1620 N/mm^2)	Strands 270 ksi (1863 N/mm^2)
To satisfy Minimum Specified ASTM Standards*	Goldberg and Richard	N = 2.773	N = 2.743	N = 4.265
	Menegotto and Pinto	N = 4.24 K = 1.04728 Q = 0.01797	N = 2.91 K = 1.1470 Q = 0.00625	N = 4.77 K = 1.1341 Q = 0.01185
Typical Actual Behavior	Menegotto and Pinto	N = 7.1 K = 1.0041 Q = 0.0175 for E_{ps} = 28790 f_{pv} = 141.8 f_{pu} = 160 ε_{pu} = 0.041	N = 6.06 K = 1.0325 Q = 0.00625 for E_{ps} = 29300 f_{pv} = 222.4 f_{pu} = 244 ε_{pu} = 0.087	N = 7.344 K = 1.0618 Q = 0.01174 for E_{ps} = 27890 f_{pv} = 243.5 f_{pu} = 278 ε_{pu} = 0.069

*f_{py} = 0.85 f_{pu}; ε_{pu} = 0.010 for wire and strands and 0.007 for bars, ε_{pv} = 0.040; elastic modulus = 27000 ksi for strands, 28000 ksi for bars and 29000 ksi for wires; 1 ksi = 6.9 N/mm^2.

and Naaman [131] present a method for describing the complete stress-strain curve for nonprestressed steel.

3.4.3 Composite Design. Both the AASHTO Specifications [10] and the ACI Code [15] give little guidance in the application of the ultimate design equations and concepts to composite structures. The only specific comment of help is found in the ACI Code which indicates that, where properties of the elements of a composite structure differ, "...the properties of the individual elements or the most critical values, shall be used in design."

When a strain-compatibility analysis is used, actual properties for girder and flange concrete can be used unless the ERSB is used. If the ERSB is used, the section must be assumed to be composed of a single strength of concrete or the assumptions of the ERSB can be applied to the girder and deck concrete individually. When the girder and deck concrete strengths are considered individually, the top fiber strain of both the girder and deck must be assumed incorrectly to be 0.003 in order to satisfy the assumptions of the ERSB approximation.

3.5 Ductility and Reinforcement Limits

Naaman [95] defines ductility as "a measure of the ability of a material, section, structural element or structural system to sustain inelastic deformation prior to collapse, without substantial loss in resistance." This ability is essential for structures if

sufficient warning of impending collapse is to be given to permit evacuation, removal of load, repair, or other action before collapse of the structure. Another general way of expressing this concept is that brittle failures are to be avoided [102]. In practice, limits are placed on the quantity of reinforcement to ensure ductility [77].

In this section, the ductility of pretensioned sections or members and related reinforcement limits will be considered.

3.5.1 Development of Code Provisions. The development of code provisions began with the ACI-ASCE Joint Committee 327 Report on Ultimate Strength Design [20] that appeared in 1955 and 1956. This Report contained the following limit on the reinforcement ratio, p, for reinforced concrete:

$$p \leq 0.40f'_c/f_y \tag{3.13}$$

where the coefficient 0.40 was to be reduced by 0.025 for each 1,000 psi in excess of 5,000 psi. This limited the reinforcement ratio to about "...0.9 of that required to develop the full compressive strength of the section." A different method was used for columns in which behavior was categorized with respect to the load producing balanced failure, i.e., the load at which concrete reaches the ultimate strain and the tension steel yields. No provision for minimum reinforcement was given. The report was intended to apply to reinforced concrete members.

The Appendix to the 1956 ACI Code [11], which dealt with the ultimate strength design of reinforced concrete members, contained Eq.

3.13 with the related variation in the coefficient for different concrete strengths. No minimum reinforcement limit or provisions for prestressed concrete were given.

The "Tentative Recommendations for Prestressed Concrete" prepared by ACI-ASCE Joint Committee 323 [19] in 1958 included the following maximum reinforcement limits:

$$pf_{su}/f'_c \leq 0.30 \quad \text{(rectangular)} \tag{3.14}$$

$$A_{sr}f_{su}/b'df'_c \leq 0.30 \quad \text{(flanged)} \tag{3.15}$$

These limits on prestressed reinforcement were intended to "avoid approaching the condition of over-reinforced beams for which the ultimate flexural strength becomes dependent on the concrete strength...." Members with reinforcement ratios which exceeded these limits were permitted, although the ultimate capacity was limited. A mix of prestressed and nonprestressed steel was permitted and the maximum reinforcement limit for this case was

$$pf_{su}/f'_c + p'f'_y/f'_c \leq 0.30 \tag{3.16}$$

where p'and f'_y are the reinforcement ratio and yield stress, respectively, for the nonprestressed reinforcement. No requirements for mimimum reinforcement were given.

The requirements of the 1961 edition of the AASHO Specifications [9] were the same as those of the Committee 323 Report [19] with an additional expression similar to Eq. 3.16 given that applied to flanged sections with nonprestressed reinforcement.

Minimum steel percentage was mentioned in the heading of a section, but no limit was provided.

Mattock, Kriz, and Hognestad [87] suggested that "if it is considered desirable for design purposes to establish a limiting value of q, the reinforcement index, less than q_b..., then ... this limiting value [should] be expressed as a fraction of q_b and not in the form in current use." The tension reinforcement index for the balanced condition, q_b, was given for reinforced concrete as

$$q_b = p_b f_y f_c' = 0.85 k_1 \epsilon_u / (\epsilon_y + \epsilon_u) \qquad (3.17)$$

where p_b = the reinforcement ratio corresponding to the balanced condition
ϵ_u = maximum concrete compression strain in flexure
ϵ_y = yield strain in the conventional reinforcement.

A simple, approximate formula was given to determine an alternative limit, q_{lim}, for the reinforcement index, q:

$$q_{lim} = 80/\sqrt{f_y}, \qquad (f_c' < 4{,}000 \text{ psi}) \qquad (3.18)$$

where, for concrete strengths in excess of 4,000 psi, q_lim is reduced by 0.02 for each 1,000 psi. This formula ensures that q would be from 70 to 80 percent of q_b for a wide range of concrete and steel strengths.

An examination of the report on prestressed concrete by Warwaruk, Sozen, and Siess [133] of 1962 is very instructive. The introduction to the section "Limits on Longitudinal Reinforcement" is extracted below:

> Ideally, there need be no limits on the amount of longitudinal reinforcement that is provided in a prestressed concrete beam. Whatever the amount of reinforcement, the flexural strength can be calculated.... However,... in certain ranges the flexural strength is very sensitive to variations in the beam properties and it would be undesirable to proportion a beam in such a range, not only because the theory may not be accurate, but also because errors made in the field may prove catastrophic. Consequently, limits must be placed on amount of longitudinal reinforcement in relation to the concrete strength, the properties of the reinforcement, and the dimensions of the section. To insure that the strength of the beam is insensitive to possible variations in the material and geometrical variables, the reinforcement strain at ultimate must be well in the inelastic range of the stress-strain curve.... Thus, a reasonable lower limit to the computed reinforcement strain at ultimate ϵ_{su} is 0.01.

For prestressing steel in use at the time, a strain of 0.01, which is used in ASTM A416 [25] to define yield, was near the end of the knee in the stress-strain curve. Therefore, variations in the steel strain caused by variations in other properties of the section would produce only minor changes in the stress in the steel, and the effect on the ultimate capacity would be minimal. This is illustrated graphically in Fig. 3.18 where a slight variation in $\rho f_c'$ for Case 2 will lead to a large variation in stress in the prestressing steel, resulting in a significant fluctuation in moment capacity.

Warwaruk et al. [133] used the strain compatibility relationship

$$k_u = F\epsilon_u/(F\epsilon_u + \epsilon_{su} - \epsilon_{se} - \epsilon_{ce}) \tag{3.19}$$

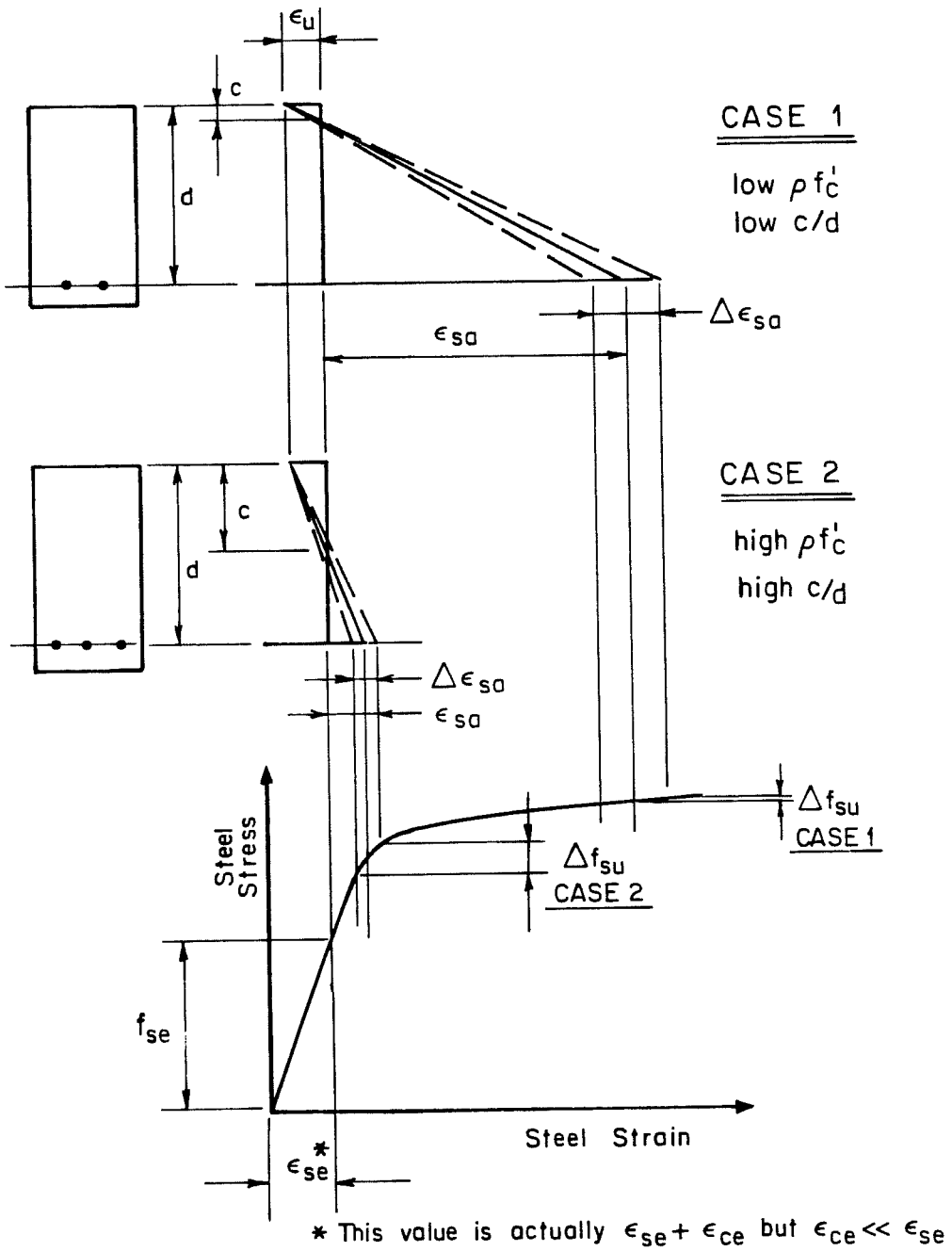

Fig. 3.18 Effects of variation in ρ and f'_c on f_{su}

(see Appendix D for explanation of terms) to derive the maximum limit on the reinforcement index. It was assumed that $F\epsilon_u = 0.003$ for bonded beams, $\epsilon_{se} = 0.0045$ which is an average for the typical range of 0.004 to 0.005, and $\epsilon_{ce} \approx 0$ since it is small compared with other strains. The minimum value of ϵ_{su}, which corresponded to the maximum value of k_u, was set at 0.01. The resulting equation was:

$$k_u = \rho f_{su}/f_{cu} \leq 0.35 \tag{3.20}$$

where f_{cu} = average compressive stress in concrete.

Using the relationship $f_{cu} = 0.7f_c'$, Eq. 3.18 becomes

$$\rho f_{su}/f_c' \leq 0.25 \tag{3.21}$$

The limit in Eq. 3.21 differs from the limit of 0.30 used in the Committee 323 Report [19] because there, $F\epsilon_u$ was assumed to be 0.004. These equations apply to rectangular beams with no supplementary reinforcement. Warwaruk et al. [133] indicated that the use of beams with values of k_u near the limit was not advisable except "under controlled conditions of manufacture" and that lower values of k_u indicate increased ductility.

Warwaruk et al. [133] introduced a minimum reinforcement limit by requiring the ultimate moment, M_u, to exceed the moment causing

cracking, M_{cr}, i.e.,

$$M_u \geq M_{cr} \tag{3.22}$$

to prevent sudden failure immediately after cracking.

The 1963 edition of the ACI Code [12] contained the maximum reinforcing limit given by Committee 323 [19] for prestressed members and also introduced a minimum requirement of

$$M_u \geq 1.2M_{cr} \tag{3.23}$$

The maximum reinforcement limit for non-prestressed reinforced concrete members was changed to

$$p \leq 0.75p_{bal} \tag{3.24}$$

as suggested by Mattock, Kriz, and Hognestad [87].

In the Bureau of Public Roads document [33] of 1966 on ultimate design of conventionally reinforced concrete bridge structures, the maximum reinforcement concept of Eq. 3.24 was used but the coefficient was reduced to 0.5.

The Codes have changed little in the intervening years. ACI Committee 343 [21] has endorsed use of ACI and AASHTO limits without change. The current AASHTO Specifications [10] indicate that the maximum reinforcement limit is intended to ensure yielding of the steel as ultimate capacity is approached. In the 1983 edition of the ACI Code [15], the value of the maximum reinforcement limit was changed from 0.30 to $0.36\beta_1$ in order to account for the use of high strength concrete.

3.5.2 Analytical Studies and Recent Proposals. Since the approaches to limiting the maximum reinforcement of non-prestressed and prestressed members differ and neither directly address the ductility of members, much analytical work has been done to (1) try to relate the different limits to ductility indices and to determine the usefulness and accuracy of current methods, or (2) propose alternate methods. Recent analytical studies are summarized below.

Ductility is most often defined in terms of the ratio of deformation at ultimate to the deformation at yield. The deformation considered can be curvature, which is related to the ductility of the section, or deflection, which gives an indication of the ductility of the member. The current limits provide curvature ductilities of at least 2 for reinforced sections [77] and from 1.5 to 3 for prestressed sections [57]. MacGregor [77], after reviewing levels of ductility suggested by others, recommends a minimum curvature ductility of 3 for structures requiring limited ductility and 4 for structures in seismic regions. The use of the definition of ductility as a ratio of deformations is complicated for prestressed members by the stress-strain response of prestressing strand which lacks a well defined yield point. This results in poorly defined yield curvatures or deflections that must be arbitrarily determined [55,57].

The effect of the use of high strength concrete on the applicability of code provisions has been studied for reinforced

members [2,131] and for prestressed members [57,94]. Studies of reinforced members indicate that sections or members made from high strength concrete have ductilities comparable to normal strength concrete and that the method of computing the balanced reinforcement ratio is conservative when compared with results of analytical studies [135,131]. Harajli et al. [57] found that a significant reduction in ductility could occur for both prestressed and reinforced members at low levels of the reinforcement index ω. The evaluation and comparison of results of the studies is complicated by the use of different parameters as the basis for comparisons.

A number of changes to the current provisions have been proposed as simplifications or clarifications. Naaman [94] recommends that the current maximum reinforcement limit (ω) for prestressed members remain at 0.30 but that the definition of the effective depth be changed slightly. Naaman, Harajli, and Wight [57] show that

$$\omega = 0.85\beta_1 c/d \tag{3.25}$$

which could apply to both prestressed and partially prestressed members with a slight modification of current definitions. Using this concept, Naaman [95] proposes a new form of the maximum reinforcement limit that applies to all sections and combinations of types of reinforcement

$$c/d \leq 0.42 \tag{3.26}$$

which is equivalent to the current limit. A similar proposal was made by Thompson and Park [127]

$$a/h \leq 0.2 \tag{3.27}$$

as a result of a series of analytical studies related to seismic design. A second recommendation was to reduce the current maximum reinforcement ratio limit (ω) to 0.2.

Tadros and Peterson [125] report a proposal by Dilger to replace ϵ_y in the balanced reinforcement equations for reinforced concrete in the ACI Code [15] by $(f_{py} - f_{se})/E_{ps}$ for use with prestressed members. However, they find a number of difficulties with this approach.

Khachaturian and Gurfinkel [74] recognize the intent of Code requirements and recommend use of a limiting strain in the prestressing steel, i.e.,

$$\epsilon_{su} \geq \epsilon_{sl} \tag{3.28}$$

where ϵ_{su} = strain in prestressing steel at ultimate

ϵ_{sl} = limiting strain in prestressing steel

= 0.01 for low (minimum) ductility

= 0.02 for high ductility.

The lower limit corresponds to current Code limits.

3.5.3 Results of Tests. Data from flexural tests of prestressed beams with high strength concrete appear to be nonexistant. However, high strength concrete beams with conventional

reinforcement have been tested. These tests programs are summarized below and results are compared later in the section.

Leslie, Rajagopalan, and Everard [76] reported tests of 12 singly reinforced beams with four reinforcement ratios and three cement contents. Concrete strengths ranged from 9,300 to 11,800 psi. The beams were loaded monotonically to failure at third points with a shear span-to-effective depth ratio of 2.67. Deflection data from the tests were used to determine the ductility index for each beam.

Tognon, Ursella, and Coppetti [128] tested four beams with a concrete strength of approximately 18,800 psi and three beams with a concrete strength of about 4,600 psi. Concrete strengths were converted from cube strengths using a multiplier of 0.8 [41]. Pairs of high and normal strength beams with equal reinforcement ratios were tested. Beams were singly reinforced and loaded approximately at third points with shear span-to-effective depth ratios of approximately 3.8 to 4. Deflection was measured and plotted for each test.

Swartz, Nikaeen, Narayan Babu, Periyakaruppan, and Refai [124] tested four high strength concrete beams with different reinforcement ratios and stirrup spacings in the shear spans. The beams were singly reinforced and loaded at third points with shear span to effective depth ratios of 2.6 and 3 for the two beams that failed in flexure. The other beams failed in shear. Deflection at midspan was measured and plotted for all four beams.

Pastor, Nilson, and Slate [103] tested a series of four high strength concrete rectangular beams with various tension reinforcement ratios and two beams with lower strengths for comparison. A second series of six high strength concrete beams were tested to study the effect of compression steel and transverse reinforcement on member and section ductility. Beams were loaded at third points to failure with a shear span-to-effective depth ratio varying between 4.4 and 4.9. Deflections and curvatures were determined throughout the test, and ductility indices were computed for each beam. Beams B-4, B-5, and B-6 failed prematurely due to rupture of longitudinal steel at locations where stirrups were welded to the bars.

The curvature and deflection ductility data from the above tests are plotted versus the reinforcement ratio, the fraction of the balanced reinforcement ratio (computed by ACI), and the reinforcement index in Fig. 3.19, 3.20, and 3.21. Where ductility ratios were not given, an estimate was made from available data. There is considerable scatter in the data, but Fig. 3.20 shows a rather clear trend in the plot of the ratio of the reinforcement ratio to the balanced reinforcement ratio and the curvature ductility. The high strength concrete data from Tognon et al. [128] include one point which fell below most of the other data in the figure. For this beam a brittle failure occurred (i.e., the ductility ratio was approximately 1) at a reinforcement ratio of about two thirds of balanced. This indicates that current practice, which assumes that a

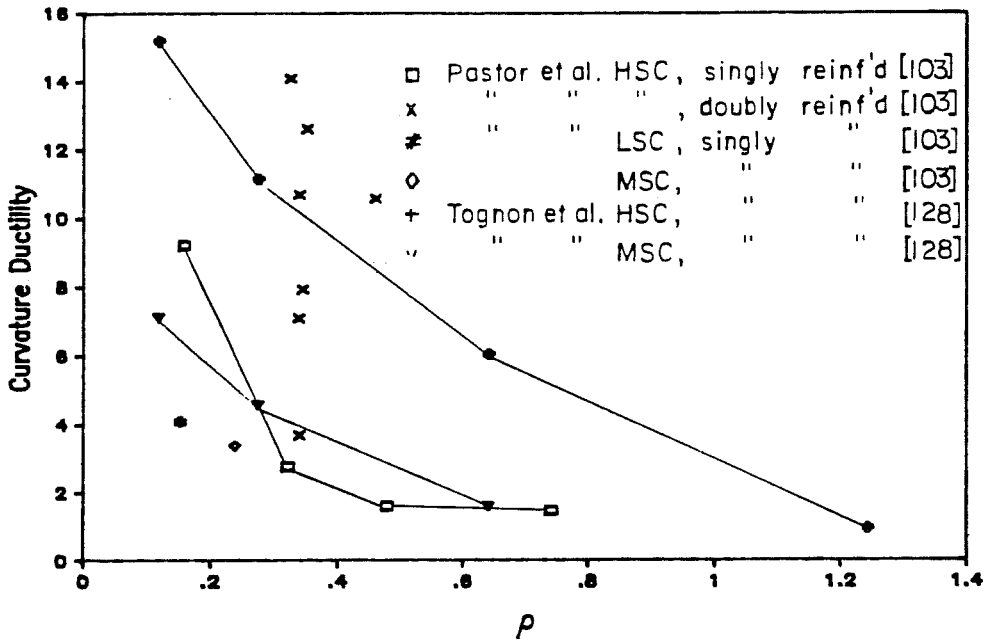

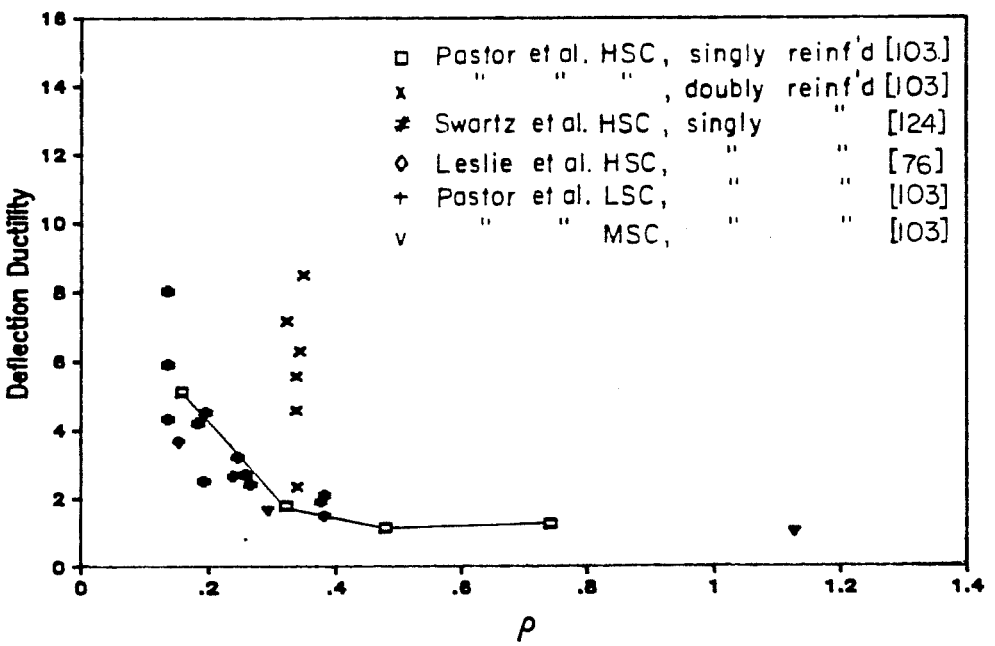

Fig. 3.19 Ductility indices versus reinforcement ratio

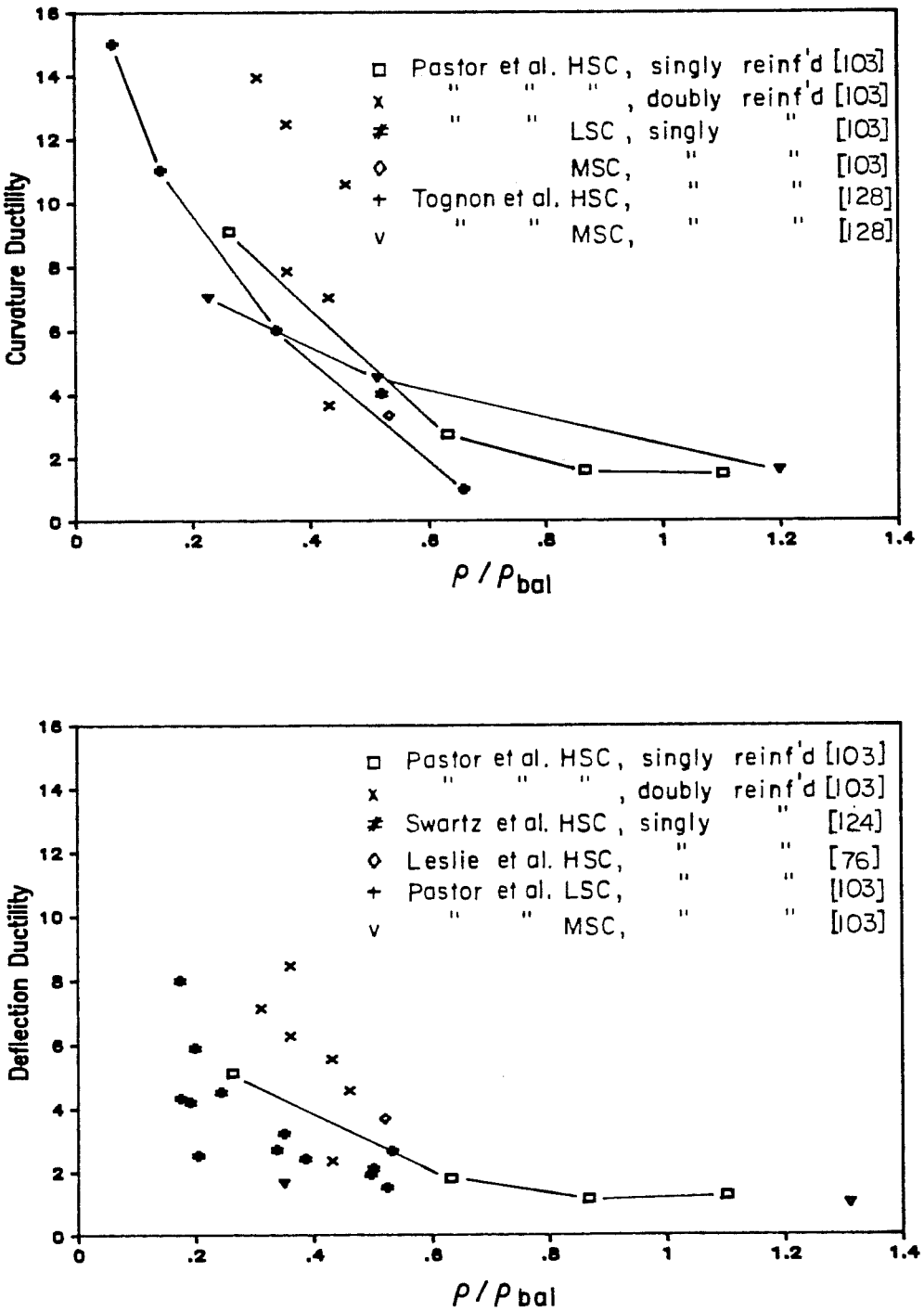

Fig. 3.20 Ductility indices versus fraction of balanced reinforcement ratio

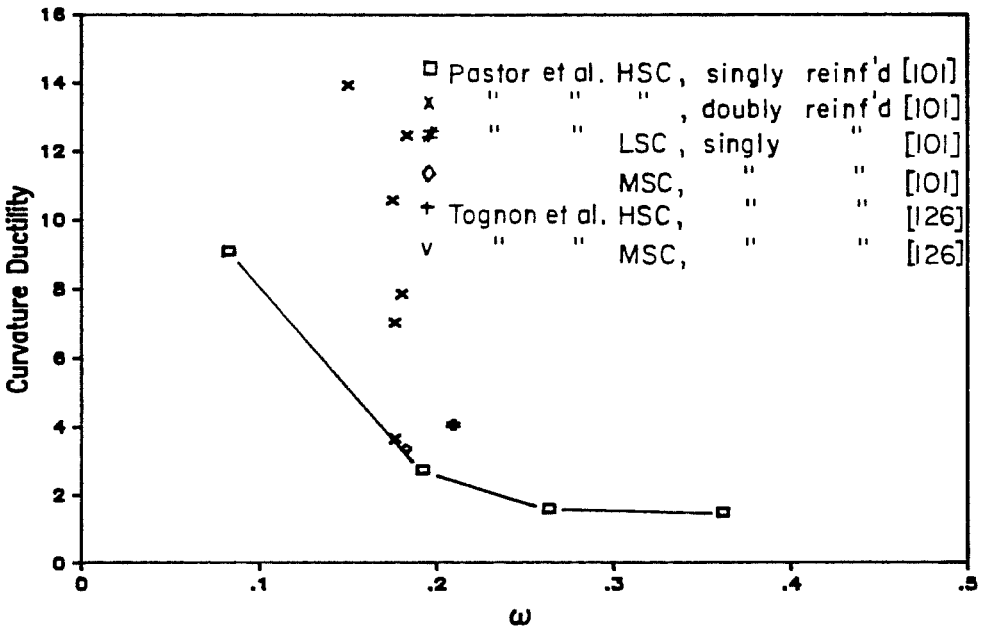

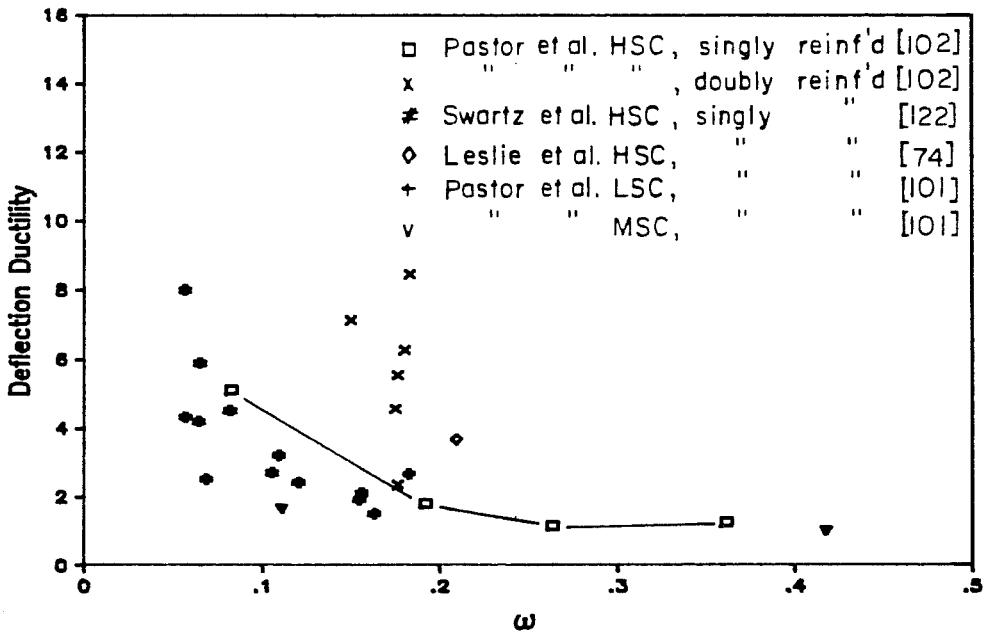

Fig. 3.21 Ductility indices versus reinforcement index

brittle failure occurs when the reinforcement ratio equals the balanced ratio and limits the reinforcement ratio to 75 percent of the balanced ratio, would have allowed this design which resulted in a brittle failure. A similar figure was not possible for the reinforcment index because values at balanced conditions were not available for the data.

Figure 3.22 shows the relation between curvature and deflection ductilities measured for the same test specimens. Agreement is not good which demonstrates that the two measures of ductility are not uniquely related and therefore cannot be used interchangeably.

Results of analytical studies by Ahmad and Shah [2] for deflection ductility of singly reinforced beams (Fig. 3.23) and by Wang et al. [131] for curvature ductility of singly and doubly reinforced beams (Fig. 3.24) show that both ductility ratios are nearly independent of concrete strength for a given fraction of the balanced reinforcement ratio. The second study also shows that ductility increases with increasing concrete strength for a constant reinforcement ratio.

Pastor et al. [103] conducted a series of tests studying the effect of compression reinforcement and ties. Compression steel was found to be more effective in increasing ductility than ties. It was proposed that an area of compression steel equal to at least one half

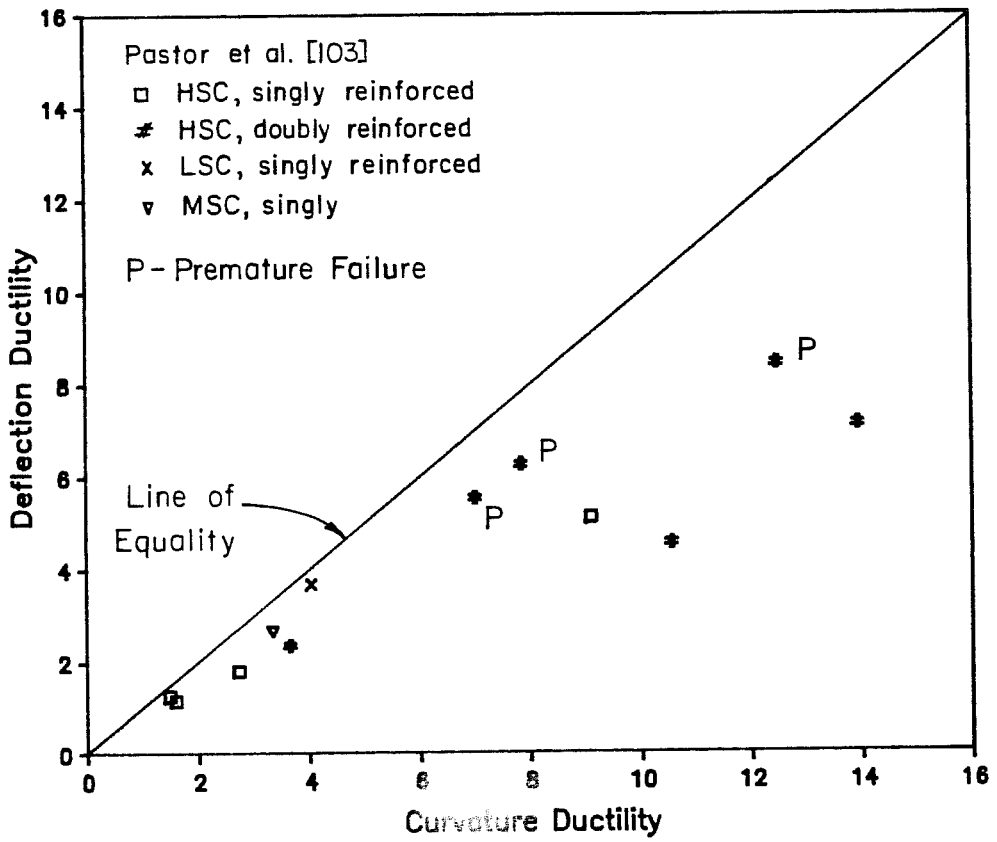

Fig. 3.22 Comparison of curvature and deflection ductility for same specimens

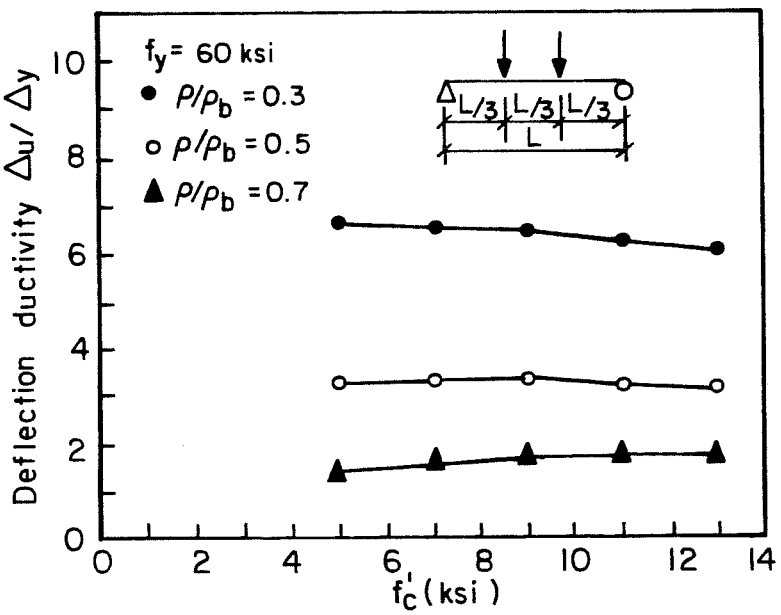

Fig. 3.23 Effect of concrete strength on the deflection ductility of a singly reinforced beam [2]

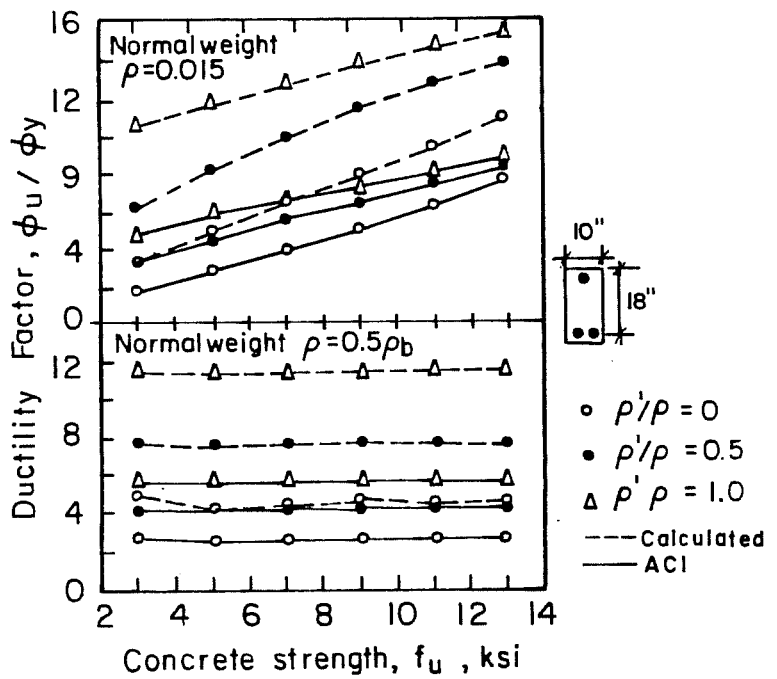

Fig. 3.24 Comparison of ductility ratios for beams (Ref. [131])

the tension steel area be used to improve ductility. Ties should be provided to restrain buckling of the compression steel.

Tests and analytical studies by Martinez et al. [82] and Ahmad and Shah [1] on columns indicate that confinement of high strength concrete was effective in increasing the ultimate strain and stress. However, as noted by Pastor et al. [103], confinement is not as effective in beams because of the presence of a strain gradient that leads to non-uniform expansion of the concrete.

Harajli and Naaman [55,56] observed some loss of ductility in normal-strength-concrete partially and fully prestressed beams that survived 5 million cycles of fatigue loads.

3.6 Deflections

3.6.1 Code Provisions and Limits. The AASHTO Specification [10] and ACI Code [15] do not provide methods for computation of short- or long-term deflections of prestressed members. The AASHTO Specifications only mention that all effects must be considered in the calculation of deflections. The ACI Code states that computation of immediate deflections shall be based on elastic analysis and that the gross section modulus may be used for uncracked sections. For long-term deflections, all effects must be considered. The Commentary to the ACI Code [17] provides a list of references that give specific recommendations regarding the computation of deflections.

AASHTO gives a table of recommended minimum depths for reinforced sections unless computed deflections show that shallower depths can be used with no adverse effects. No such table is given for prestressed members. The same table appears in the ACI Committee 343 Report [21] for general use. The fact that the values in the table are intended for continuous members and should be increased for simple spans is not acknowledged. In the ACI Code, immediate and long-term live load deflections of prestressed members must meet limits intended for buildings. The Bureau of Public Roads booklet [33] provides limits on live load deflections for reinforced concrete bridges with simple spans less than 70 ft. These limits are based on the ratio of live load to full service load. The 1983 Ontario Highway Bridge Design Code contains a deflection limit based on the maximum deflection due to a factored highway live load and the fundamental flexural frequency of the bridge.

In the chapter related to design of steel structures, the AASHTO Specification limits the live load deflection to the span length divided by 800 for bridges without pedestrian traffic, and the span length divided by 1000 for bridges with pedestrian traffic. These limits, which have apparently been suitable when applied to steel structures, have often been used in the absence of other limits for prestressed concrete bridges in the absense of other limits.

3.6.2 Analytical Methods. Estimating deflection for prestressed members under short-term service loads is straight-forward

because the section is generally uncracked and elastic analysis with gross section properties can be used as recognized by the codes [10, 15]. If a member is cracked and the concrete is still behaving elastically, a cracked section analysis must be used. The ACI Commentary [17] suggests other references. Moment-curvature techniques also provide a general approach to estimating deflections at any level of load. Warwaruk et al. [133] describe this procedure and demonstrate its accuracy by comparing calculated deflections with test results for normal strength concrete beams.

The determination of long-term deflections is much more complex and has been the subject of much investigation. As mentioned previously, the Commentary to the ACI Code [17] provides a list of references that include methods for computing long-term deflections. Martin [80] proposed a simplified method which extends the long-term deflection multiplier approach used for reinforced concrete in the ACI Code by making many assumptions about time effects. Naaman [95] reviews several methods of computing both long- and short-term deflections. Suttikan [119] developed a computer program PBEAM that included time effects in the analysis of prestressed members and showed good agreement with test data. Kelly [72] reviewed a number of methods including those by Martin [80] and Suttikan [119], and proposed an approach similar to Martin's but with more detail in the analysis. The method was programmed for use on a microcomputer and gave excellent results for a set of full-scale bridge girders.

3.6.3 Expected Effect of High Strength Concrete. Little work has been done on measuring the long-term deflection behavior of high strength members. The ACI Committee 363 Report [22] mentions that some work is underway at Cornell University and that preliminary results indicate deflections of high strength concrete members are significantly lower than those for similar normal strength members. This leads the investigators to believe that concrete strength should be included in formulas used to determine long-term deflection multipliers. However, the Committee feels that the expected long-term behavior of prestressed high strength concrete members may not be much different from normal strength concrete members because, while creep would be lower, stresses would be higher.

The members studied in Kelly's work [72] and related work by Bradberry [32], while designed as normal strength members, were actually high strength members with low stresses. Deflections of the girders were measured from fabrication to completion of the bridge structure. Kelly conducted a sensitivity study comparing the long-term behavior of low, typical, and high strength concrete and found that, for the single bridge studied and a typical construction schedule, the girders and bridge using high strength concrete exhibited the least cambers at erection, the smallest time dependent response, and the greatest final camber. The differences in behavior were attributed to the increased modulus of elasticity for high strength concrete.

3.7 Girder Stability

In this section, the analysis used to examine the lateral stability of girders is discussed as presented in the literature. The basic analysis used in Chapter 2 to compute the maximum lifting span is presented.

3.7.1 Analytical Methods. As mentioned in Chapter 2, a number of papers have been written regarding the analysis of the lateral stability of slender concrete members when lifted. Papers by Swann and Godden [123] and Muller [92] consider the problem in detail with the former study also reporting data from tests of model girders. However, the approach presented by Anderson in Ref. [6] is simple and clear. This approach was corroborated and amplified by Swann [122], the coauthor of Ref. [123], and also by Anderson [7] in response to the comments by Swann. The fact that Swann supports use of this simple analysis is significant since he had earlier published the more detailed analytical and experimental investigation of the problem. The modified form of Anderson's analysis is presented below.

In the analysis, the factor of safety against lateral buckling, FS, is expressed as

$$FS = y_T/0.64\Delta_y \tag{3.29}$$

where y_T = distance from the center of rotation to the centroid of the member and is generally taken as the distance from the top face of the beam to the centroid of the section

Δ_y = midspan deflection of the beam under its own weight with the beam simply supported so that bending occurs about the y axis.

For a beam with constant section properties along its length, the deflection Δ_y can be computed using the equation

$$\Delta_y = \frac{5\ w_g l^4}{384\ E_c I_y} \tag{3.30}$$

where w_g = self weight of the beam

l = span length

E_c = modulus of elasticity for concrete

I_y = weak axis moment of inertia for section.

A factor of safety aganist buckling of at least 2 is recommended which means that y_T should be greater than $1.28\Delta_y$. Swann [122] recommends that y_T be taken as the vertical distance between a line through the lifting points and the center of gravity of the whole beam, since camber of the beam may significantly reduce this quantity in some cases.

Anderson [6] suggests that resistance to lateral buckling can be improved in a number of ways. One method is to move the lifting points further from the ends of the girder. This is effective, but stresses must be checked at the lifting points and at critical points near midspan. Calculation of Δ_y would then be based on the beam supported on its side at the lifting points, which can be computed as the difference between the deflection computed using Eq. 3.30 with l equal to the distance between lifting points and the deflection

caused by the moment at the lifting point due to the overhanging portion of the member, Δ_0, which can be computed using the equation

$$\Delta_0 = \frac{M_0(l-2a)^2}{8E_cI_y}$$

where M_0 = moment at lifting point due to overhang

$= \omega_g a^2/2$

l = full length of beam

a = distance from lifting point to end of beam

Other methods for improving resistance to lateral buckling are to use or develop sections with greater weak axis moment of inertia, to use high strength concrete which increases E_c, to keep the self weight of the beam low, and to attach temporary bracing to the member during handling.

Swann [122] introduced an additional analysis in which the lateral bending moment, M_y, which is the potential cause of failure, can be determined using the equation

$$M_y = M_x\theta$$

$$= M_x\theta_o(1/(1-1/FS)) \qquad (3.31)$$

where M_x = bending moment about the x-axis due to self weight

θ = angle of tilt (in radians) of the member about a line through the lifting points

θ_o = angle of tilt (in radians) due to imperfections if the beam were completely stiff

This analysis reveals that use of a reasonable factor of safety against buckling may not prevent failure if imperfections are large. The value of θ_o can be estimated using the equation

$$\theta_o = (d_o + 0.67b_o)/y_T$$

where d_o = transverse distance from the minor axis of the section to where the lifting points have been inadvertently fixed

b_o = lateral bow or sweep of the beam at midspan

Swann adds that the factor of safety can be increased by use of a lifting yoke which is rigidly attached to the beam. Such a device places the center of rotation above the top of the beam which increases y_T and therefore reduces θ_o. This method of improving lateral buckling behavior may be more economical than the use of external bracing.

3.7.2 Practice and Experience in Texas. This section contains information obtained from the Texas State Department of Highways and Public Transportation (TSDHPT) related to the lateral stability of bridge members during fabrication, transportation and erection.

The section that has experienced the most problems in use is the Texas Type 54 (see Fig. 2.1). In a number of cases, members have been damaged prior to placement in bridges. As a result, spans for this section have been limited to 96 ft. Limits have also been set for other Texas sections including the Type 72, which is restricted to spans less than 122 ft. "Hog-rods" are specified for use as temporary lateral bracing where spans exceed these limits. No such limit is imposed on the AASHTO-PCI Type IV, which is the only AASHTO-PCI

section in use in Texas. Type 72 girders have been used for spans up to 136 ft and AASHTO-PCI Type IV girders have been used for spans of 130 to 135 ft.

State standards recommend that lifting loops be placed at the maximum practical distance from ends of girders and that vertical lines be used for lifting. The State, however, exercises no control over the location of lifting loops or the means of handling or transport. It is estimated that lifting loops could be placed as far as 1 in. away from the minor axis. Sweep of beams may be as much as 4 in. and may be aggravated by transportation and exposure to unbalanced solar heating. Pairs of lifting loops, which are often used for long beams, were estimated to be located 3 and 14 ft from ends of girders for a specific case. Rigidly attached lifting yokes have been used in some cases to improve lateral stability of girders during handling.

3.8 Fatigue

The AASHTO and ACI code documents treat the issue of fatigue in pretensioned members by setting allowable stresses. A thorough review of previous tests and the development of fatigue related provisions in the AASHTO Specifications, ACI Code, and other pertinent documents are given by Overman, Breen, and Frank [101]. On the basis of this review and results of tests of full-scale pretensioned girders, the use of strand stress range as the basis for design of pretensioned bridges for fatigue is recommended and a proposed

procedure and limits are given. No special consideration is given to high strength concrete in this report.

ACI Committee 363 [22] reports that very little data is available on the behavior of high strength concrete subjected to repeated loads, but expects that "the fatigue strength of high strength concrete is the same as that for concretes of lower strengths."

No known studies have been conducted on how the stress range in strands will be affected by the use of high strength concrete in pretensioned bridge girders.

3.9 Loss of Prestress

The AASHTO Specification [10] provides a basic method for estimating prestress losses that accounts for the factors involved. A lump sum estimate for losses is also given, but the concrete strengths considered are 4,000 and 5,000 psi.

The 1983 edition of the ACI Code [15] gives no procedure for computing losses. The Commentary [17] recommends references [19, 23, 106, 137] for use in computing losses. Lump sum losses that appeared in earlier editions of the Commentary were considered obsolete and were therefore omitted.

The references mentioned above may not be sufficient if a very detailed analysis is required because the total loss occurs at an unspecified time [63]. Many of the detailed analytical methods for determining long-term deflections compute prestress losses as part of

the analysis and may therefore be used if necessary. The procedure by Suttikan [119] is an example of such a procedure.

Kelly [72] compares several procedures for computing prestress losses, including those found in AASHTO [10] and the Texas SDHPT computer program PSTRS10. He concludes that the AASHTO approach is the best, although some modifications were recommended.

There are no known detailed studies of the effect of high strength concrete on losses in pretensioned members.

3.10 Bond and Development of Reinforcement

3.10.1 Prestressing Steel. Bond and development of prestressing strand in pretensioned members must be examined for two conditions. The first is the transfer or transmission length which is the distance required to transfer the force in the tendon to the concrete through bond, usually at release. The second is the anchorage or development length which is the bonded length of strand required to develop the ultimate stress in the tendon. The same equation is given in AASHTO and ACI for computing the development length, L_d, and included in it is the equation for transfer length, L_t:

$$L_t = (f_{se}/3)D \tag{3.32}$$

$$L_d = (f_{se}/3)D + (f^*_{su} - f_{se})D$$

$$= (f^*_{su} - 2/3\ f_{se})D \tag{3.33}$$

where D = nominal diameter of bar, wire, or prestressing strand, in.

f_{se} = effective stress in prestressed reinforcement after allowance for all prestress losses, ksi

f^*_{su} = average stress in prestressing steel at ultimate load, ksi

Figure 3.25 shows how the development length is composed of the transfer length and an additional length. The derivation of these equations cannot be found in the literature but is based on data from a series of tests conducted at PCA in the late 50's and early 60's [54,70]. These equations have not changed since their introduction in the codes of the early 60's. Committee 343 [21] includes the same provisions in its report.

There is little data available for transfer length determination and less for development length. Kaar, LaFraugh, and Mass [70] studied the effect of the variation of concrete strength at release on the transfer length. A total of 43 test prisms were constructed to study the behavior of five sizes of strand, as many as five concrete strengths, and the effect of gradual or sudden release. The authors concluded that concrete strength had little effect on the transfer length for strand diameters up to 0.5 in. They also found that the transfer length changed very little with time, increasing generally less than 10 percent over a year.

Average transfer length data from the study by Kaar et al. [70] are presented in Fig. 3.26 for the larger sizes of strand. This figure presents data from pairs of specimens where each increment on the horizontal scale represents a different concrete strength within the range shown on the figure. Mean data for the cut end and dead

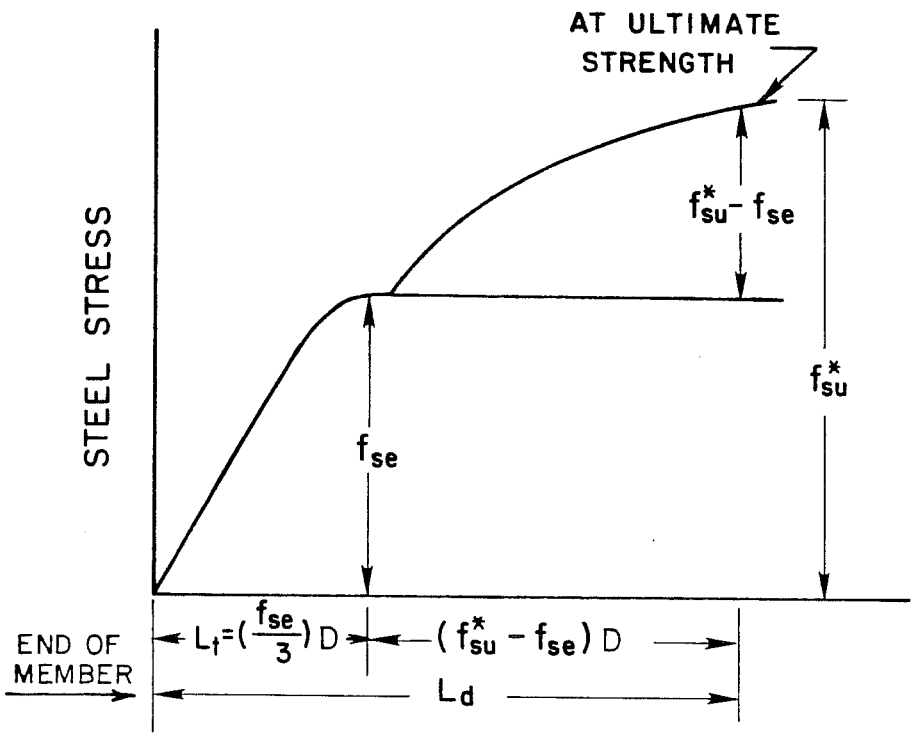

Fig. 3.25 Variation of steel stress with distance from free end of strand (Ref. [17])

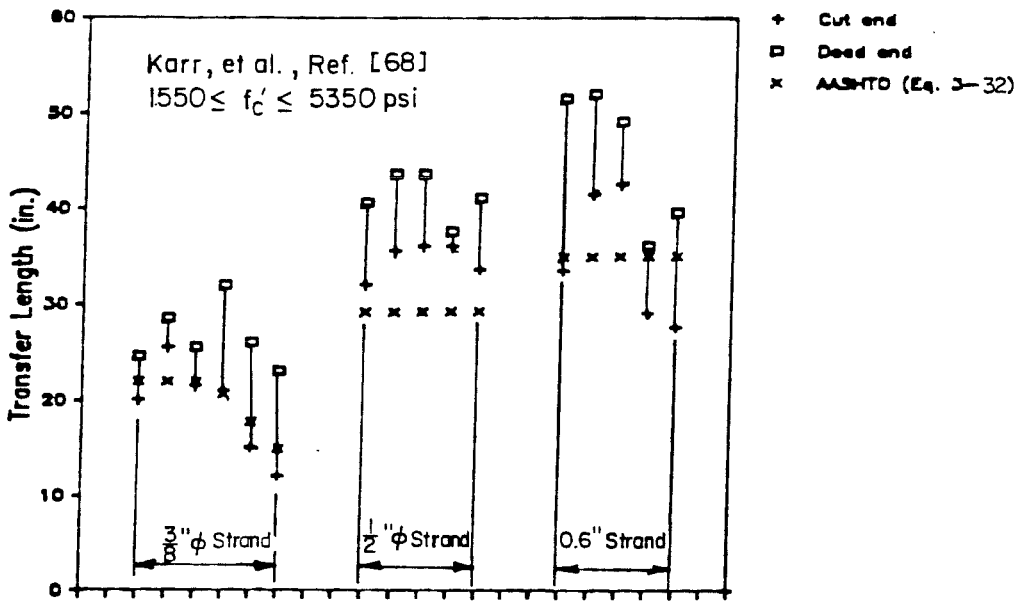

Fig. 3.26 Transfer lengths for different sizes of strand and concrete strengths [68]

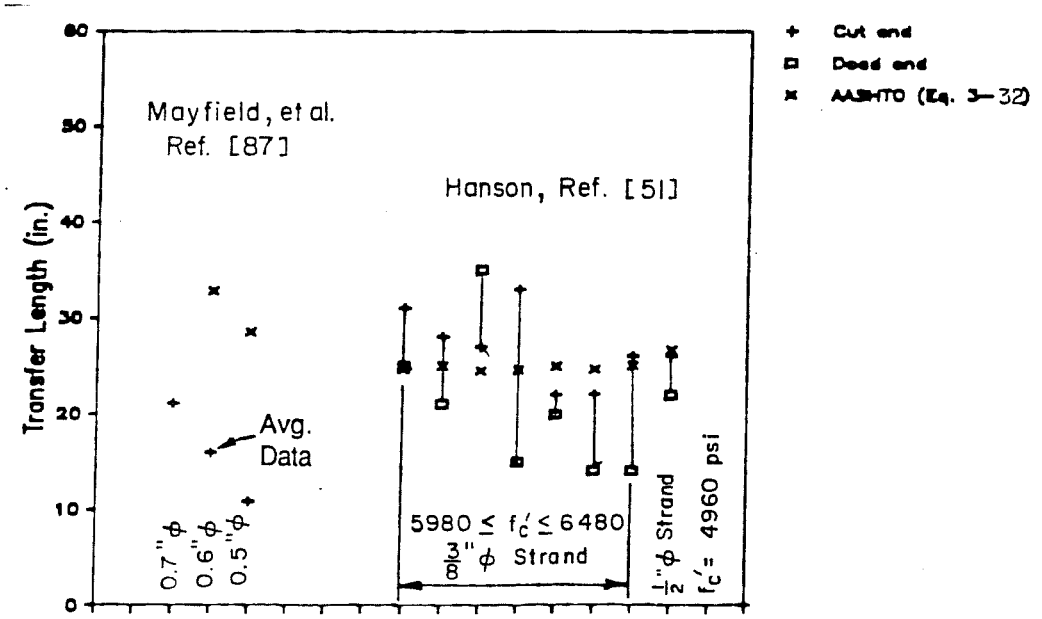

Fig. 3.27 Transfer lengths for different sizes of strand and concrete strengths [51, 87]

end are connected by a vertical line for each pair of specimens. A value for the transfer length for each pair of specimens was computed using Eq. 3.32 and is also shown on the figure. A comparison of the computed values with the test data indicate that Eq. 3.32 generally predicts a shorter transfer length than was measured and is therefore unconservative for much of this data.

Hanson and Kaar [54] studied the development length of three sizes of strand using 47 beam specimens, 34 of which failed in bond or had bond failure simultaneously with flexural failure. The condition of the strand was a minor variable and an external anchor was provided on three specimens. Seventeen of the specimens were constructed using 0.5-in. diameter strand. An analytical method for determining the development length of strand was presented which demonstrated reasonable agreement with the data. On the basis of the analytical model, minimum embedment lengths for the sizes of strand tested were given: 70 in. for 1/4-in. strand; 106 in. for 3/8-in. strand; and 134 in. for 1/2-in. strand. It was also found that the strand size and length of embedment had a significant effect on the average bond stress that led to general bond slip. It was noted that an appreciable capacity existed in the strand after initial slip had been observed.

Other data on transfer and development length have been reported [27,28,29,53,65,89,100,121]. It is difficult to make direct comparisons due to differences in testing procedure or reporting and

the use of different materials, such as Dyform strand and plain wire. However, a number of investigators [53,62,79,136] have used this and other data to attempt to develop a better expression for both transfer and development lengths. From their work a number of expressions have been proposed, but none has achieved widespread acceptance.

Committee 363 [22] states that there is insufficient data on bond of strand in high strength concrete to make any recommendations. No references are given. Transfer data from Mayfield et al. [89] and Hanson [53] and corresponding transfer lengths computed using Eq. 3.32 are presented in Fig. 3.27 using the same format as Fig. 3.26. Only data on standard strands and moderate to high strength concrete are shown. The AASHTO equation is quite conservative for Mayfield's data but appears to be more of an average for the data reported by Hanson. Other data is available for high strength concrete transfer and development lengths [120,121], but the information regarding the tests is incomplete.

3.10.2 Nonprestressed Steel. The Committee 363 [22] statement regarding lack of data for making recommendations holds for nonprestressed reinforcement as well.

3.11 Ultimate Capacity in Shear

3.11.1 Vertical Shear. Ramirez and Breen [111] have traced the development of AASHTO and ACI provisions for the ultimate shear design of prestressed concrete members. The current provisions assume that the shear capacity is composed of a component provided by

the concrete (concrete contribution) and a second component that is provided by reinforcing steel. The concrete contribution is assumed to be equal to the shear that causes cracking in one of two modes: web cracking or inclined flexural cracking. After cracking, the concrete contribution is attributed to a number of mechanisms including aggregate interlock across the crack. The steel contribution is computed assuming that cracking occurs at 45 degrees and that the steel is yielding at ultimate. The design provisions are empirical and can be difficult to apply in certain cases.

Due to the restrictive and complex nature of provisions based on equations and the fact that the rationale behind the provisions is not an accurate representation of the conditions at ultimate, alternate procedures have been proposed. Many of these have been based on a general form of the truss model [38,40,110]. These approaches allow the crack inclination to vary from 45 degrees and may or may not include some form of concrete contribution.

Because the ultimate capacity in shear includes a concrete contribution which depends in part on aggregate interlock, concern has been expressed regarding the shear capacity of high strength members because cracking planes in high strength concrete have been observed to be much smoother than for normal strength concrete [22]. As a result, a number of investigators have studied the shear behavior of reinforced [3,44,45,90,91,124] and prestressed [44,46] high strength concrete beams. The limited results of the one study in

which prestressed beams were examined indicate that the shear capacity of beams with and without stirrups can be adequately and conservatively predicted by the current procedures, even though cracks were smoother than those in normal strength concrete beams and were inclined at 20 to 35 degrees.

Data for reinforced concrete beams tested by Frantz and Mphonde [90] (without stirrups) and Elzanaty, Nilson, and Slate [45] (15 of 18 specimens were without stirrups) indicate that the V_c equations based on $\sqrt{f_c'}$ become less conservative as f_c' increases. Therefore, it was proposed [17] that the 1983 edition of the ACI Code be revised to limit values of $\sqrt{f_c'}$ used in Chapter 11 to 90 psi. This limit was changed to 100 psi by ACI Committee 318 vote at the Spring 1987 ACI Convention. This would apply to both reinforced and prestressed members.

The ACI Committee 363 Report [22] indicates that no information is available regarding the minimum shear reinforcement required to prevent brittle failure immediately following the formation of diagonal cracks in high strength members.

3.11.2 Horizontal Shear. The AASHTO Specifications [10] assume that full horizontal shear will be transfered between a cast-in-place deck and precast girder when the top of the girder is intentionally roughened, all web reinforcement is extended into the

deck (provided a minimum quantity is present), and the web element is designed to resist the full ultimate shear. Where these requirements are not satisfied, a specified stress is allowed on the interface which depends upon the condition of the surface and the quantity of reinforcement crossing the joint. The ultimate horizontal shear stress, v, which is compared to the allowable limits, is computed using a mixture of elastic and ultimate analysis by the equation

$$v = V_u Q/Ib \tag{3.34}$$

where V_u = factored shear force at section
Q = statical moment of cross sectional area, above or below the level being investigated for shear, about the centroid
I = moment of inertia about the centroid of the cross section
b = width of contact surface between precast girder and cast-in-place deck.

The ACI Code [15] provisions are similar, although the ultimate force allowed for different surface and reinforcement conditions is based on slightly different stresses. If the allowable ultimate forces at the interface are exceeded, design shall be performed using the shear friction approach. The ACI Commentary [17] gives references [50,52,83,85,115] which report test data or present design approaches, for further guidance in providing steel to cross the interface.

A reading of the above references reveals that there is considerable divergence of opinion on test methods and design approaches for horizontal shear. Saemann and Washa [115] feel that the current approach is acceptable, but that it should be modified to

include the effect of variation in the shear span. Grossfield and Birnstiel [51] note that the quantity of steel in the girder affects the horizontal shear behavior by limiting the size of the shear cracks that propagate to the interface. For structures subjected to moving loads, Mattock and Kaar [85] propose that horizontal shear stresses be investigated only within the region located a distance equal to the effective depth from the end of the girder.

Mast [83] proposes the use of shear friction concepts instead of the current provisions because stresses determined by elastic analysis may not accurately estimate the conditions at ultimate, since uncracked concrete behavior is assumed. The use of the shear friction approach is shown to be conservative for the reported data. He further asserts that it is necessary to develop rational methods based on physical models, such as the shear friction approach, rather than creating an approach based on fitting curves to data.

No known study or tests exist for horizontal shear with high strength concrete. However, Saemann and Washa [115] observed a minor improvement in shear capacity when f_c' was increased where the web and flange concrete strengths were approximately equal. In a later study, Mattock and Hawkins [88] note a similar increase in shear capacity with an increase in strength from 2,500 to 4,000 psi and conclude that concrete strength appears to limit the effectiveness of additional reinforcement above a certain level.

that propagate to the interface. For structures subjected to moving loads, Mattock and Kaar [85] propose that horizontal shear stresses be investigated only within the region located a distance equal to the effective depth from the end of the girder.

Mast [83] proposes the use of shear friction concepts instead of the current provisions because stresses determined by elastic analysis may not accurately estimate the conditions at ultimate, since uncracked concrete behavior is assumed. The use of the shear friction approach is shown to be conservative for the reported data. He further asserts that it is necessary to develop rational methods based on physical models, such as the shear friction approach, rather than creating an approach based on fitting curves to data.

No known study or tests exist for horizontal shear with high strength concrete. However, Saemann and Washa [115] observed a minor improvement in shear capacity when f_c' was increased where the web and flange concrete strengths were approximately equal. In a later study, Mattock and Hawkins [88] note a similar increase in shear capacity with an increase in strength from 2,500 to 4,000 psi and conclude that concrete strength appears to limit the effectiveness of additional reinforcement above a certain level.

3.12 Summary

This literature review indicates that numerous aspects of behavior and design using high strength concrete remain to be investigated. Material properties of high strength concrete have been studied extensively and general trends have been identified but general expressions which include behavior of high strength concrete must still be developed. A limited number of tests have demonstrated that the simplified strength design methods used in current codes are satisfactory for predicting the capacity of high strength concrete members. However, no test data exist for composite, pretensioned members that use high strength concrete. It was noted that no procedures are given in current codes for designing composite members composed of different concrete strengths.

Current code provisions concerning ductility were found to be based on assumptions inconsistent with certain aspects of current practice and codes. A simple, understandable, meaningful, and general approach for determining the relative ductility of prestressed structures does not appear to be available. Good methods have been developed for estimating both long and short-term deflections of members, although they have not been confirmed for members designed with high strength concrete. No limits on deflections of prestressed members are given in the AASHTO Specifications. An approach was presented for the analysis of the lateral stability of members and the experience and practice of the TSDHPT regarding the handling of

girders were given. No studies of prestress losses, fatigue, or bond of conventional reinforcement are available for high strength concrete. However, a limited amount of data is available for the transfer length of prestressing strand in concrete, although the concrete strengths are in the middle and lower part of the range considered in this study. Very few tests of prestressed concrete members in shear have been conducted and no composite members have been tested.

The test programs reported in the following chapters are intended to provide data in a number of the areas identified above where additional work is needed. The topics of strand bond (transfer length) and member behavior were isolated as areas in which tests would be conducted as a part of this study. Tests of composite members were specifically directed toward the study of capacity and ductility of such members. The tests also allowed study of the behavior of composite structures at levels of load near service conditions. While properties were determined for materials used in the tests, providing additional high-strength material data for analysis of material properties was not intended.

The current state of knowledge and design practice regarding high strength concrete will be considered again in Chapter 7, where the findings of this literature review and the results of the test programs are combined to form the basis for further evaluation, analysis and development of design procedures for use with high

strength concrete. The additional studies will include development of a strength design approach for composite members, revision of current ductility provisions (maximum and minimum reinforcement limits), and analytical examinations of other aspects of design including lateral stability, strand stress ranges with respect to fatigue, prestress losses, and deflections. Comment will also be made on a number of areas in which information became available during the tests, including placement of concrete and the lateral stability of members.

CHAPTER 4

TRANSFER LENGTH TEST PROGRAM AND RESULTS

4.1 Introduction

"Transfer length" is the distance required to transfer prestressing force from a strand to concrete at release. The concept is illustrated by the two plots of Fig. 4.1 which show the variation in strand and concrete stresses after release. Prior to release the strand is at a constant stress along its entire length (f_{so}). The transfer length is important because it defines the location at which the full effect of the prestress is available which is especially critical for shear design. Both the ACI and AASHTO codes provide an expression to estimate the transfer length.

A limited series of transfer tests was performed to determine how the transfer length for strand in high strength concrete compares to that for normal strength concrete, because data for high strength concrete is very limited. The goal of the test program was to determine whether the current code expression for computing transfer lengths may be applied to high strength concrete. It was not the intent of the program to provide sufficient data to permit development of a new expression for estimating transfer length.

The primary variable considered in the study was the strength of the concrete, with secondary variables being the effect of gradual or sudden release of the prestress force and the level of concrete stress after release. Specimens had a square cross section with a

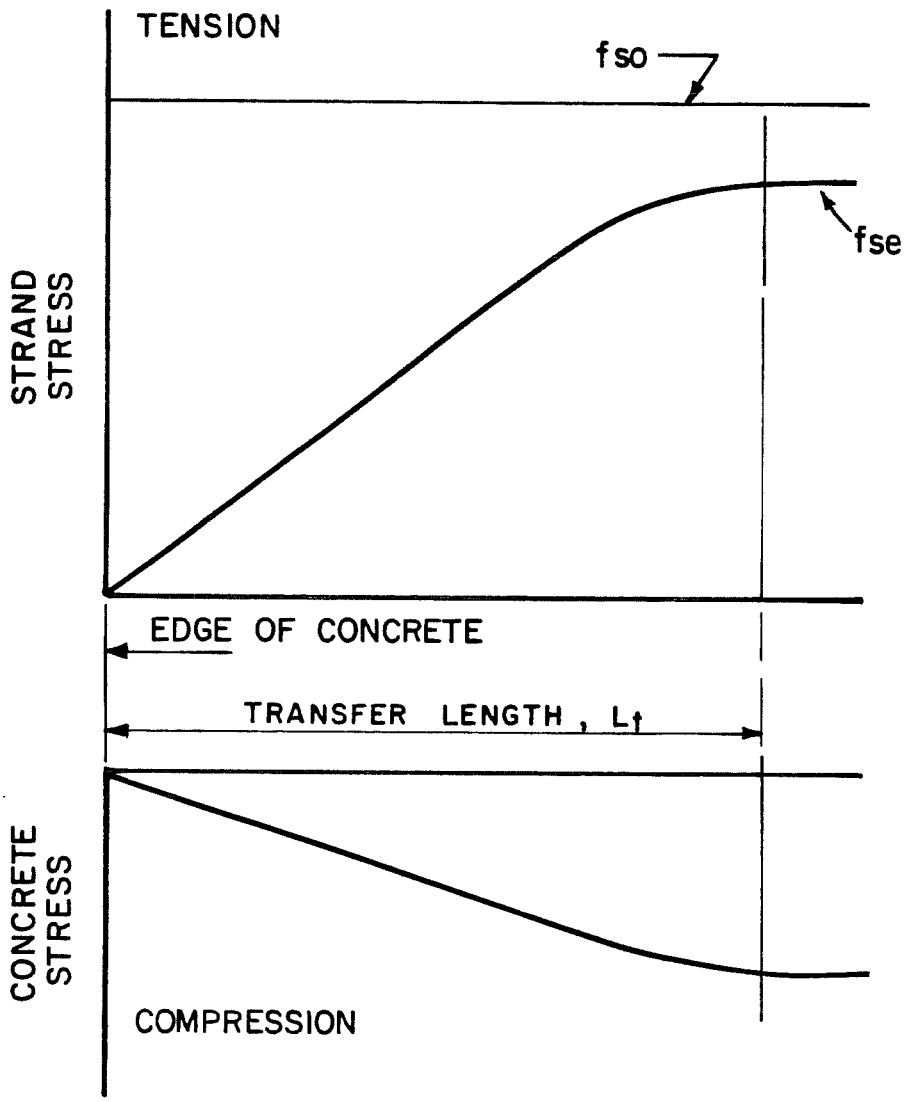

Fig. 4.1 Conceptual sketch of conditions defining the transfer length

0.5-in. diameter strand placed in the center of the section. The specimens were otherwise unreinforced. Twelve specimens were cast, eight from a normal strength mix and four from a high strength mix, providing measurements for determining the transfer length at 24 locations, since data was taken at both ends of each specimen. The transfer lengths were determined by concrete strain measurements taken by mechanical means.

4.2 Specimen Description

Previous studies on transfer length [64,65,67,70,100,112] were consulted to determine the specimen type and dimensions. The two square cross-sections shown in Fig. 4.2 were selected to approximate the concrete stresses present in the transfer regions of a pretensioned girder and to provide a comparison of transfer lengths for concrete stressed to different levels. Specimens were 10 ft long with 8 in. of strand debonded at each end. The concrete surrounding the debonded strand remained unstressed after release. Therefore, the measured change in strain following release in the first gage length contained only the change in strain occurring between the end of the debond and the first gage point. In this way, the strain from the end of the bonded strand could be determined for each 2-in. interval along the specimen using an 8-in. long mechanical strain measuring device (demec gage). A steel extension has been provided by other investigators for the same purpose [70].

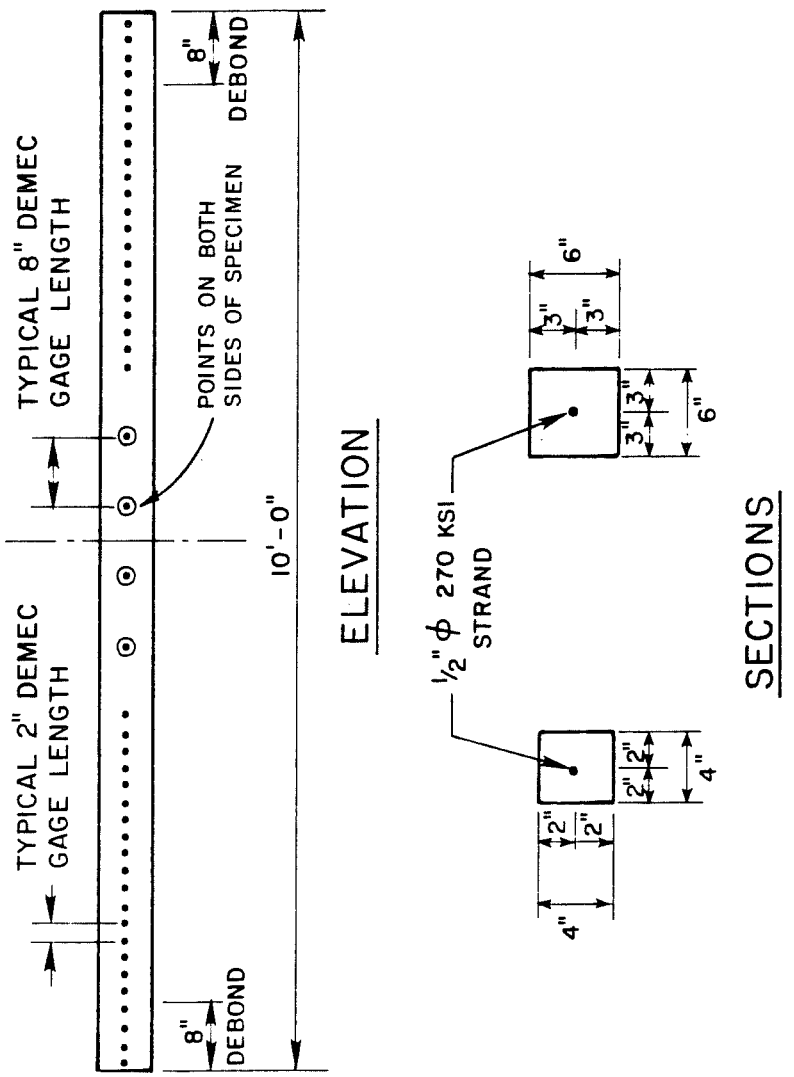

Fig. 4.2 Transfer length specimens

Two concrete mixes, with design strengths of 5,000 psi and 10,000 psi, were used in the specimens. Layout of the specimens in the prestressing bed for each cast is shown in Fig. 4.3. The use of two lines of specimens permitted the investigation of both sudden and gradual release of the prestress force.

In Fig. 4.3 each specimen is given a unique label. The number and letter appearing first indicate the nominal concrete strength and whether release of the prestress force was sudden (S) or gradual (G). The second number indicates the size of the cross section (4 or 6 in.), and the final number distinguishes between pairs of otherwise identical specimens. Ends of the specimens will be distinguished by reference to the north or south end as shown on the figure. The figure also indicates the location where the strand was flame cut to produce the sudden release.

The normal strength specimens were cast first and included specimens of both size cross sections, while only the smaller cross section was used for the high strength specimens. The larger section specimens were omitted from the high strength series due to the difficulty in taking the large number of strain readings associated with eight specimens.

4.3 Materials

4.3.1 Concrete. As mentioned earlier, two strengths of concrete were used. The first cast used a mix with a design strength

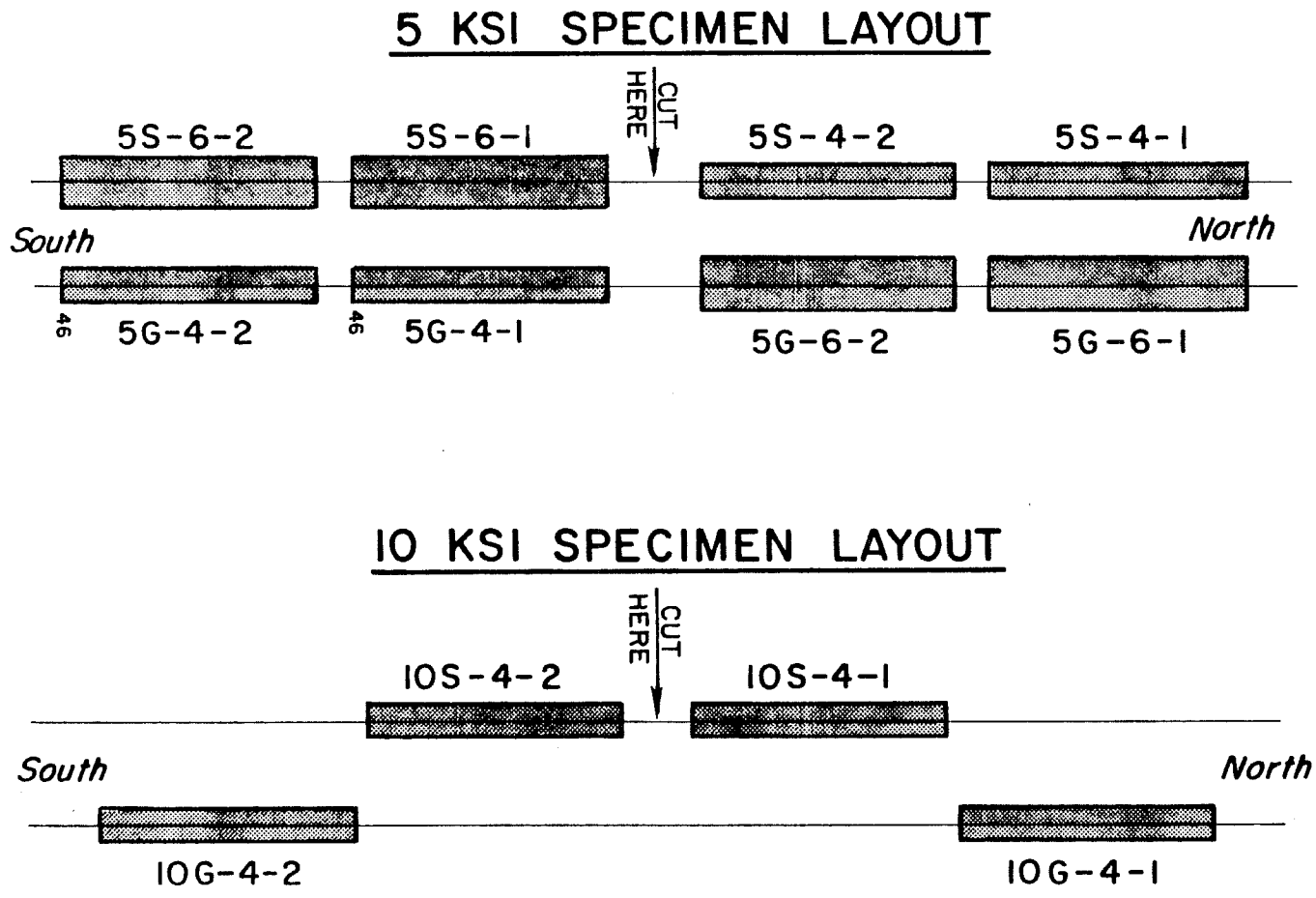

Fig. 4.3 Layout of transfer specimens in prestressing bed

of 5,000 psi at 28 days and the second was designed for a strength of 10,000 psi at 28 days. Mix proportions for the two batches are given in Table 4.1. Cylinder strengths were determined the day of release or the following day and at 28 days. The results of the cylinders tests are given in Table 4.2.

4.3.2 Prestressing Strand. The prestressing strand used met the specifications for 0.5-in. diameter seven wire stress-relieved Grade 270 ksi strand. The elastic modulus was taken to be 27,500 ksi. The surface condition of the strand was good with only very light rust (no pitting). The strand was wiped clean before use to remove accumulated dust.

4.4 Fabrication

Strands were tensioned in the pretensioning bed at the laboratory the day before the specimens were cast. An initial load of 1,000 lb was applied to each strand using a system of pulleys and dead weights. The remainder of the force required to tension the strand to approximately 189 ksi was applied by a 200 ton hydraulic ram that tensioned both strands simultaneously. Load was monitored by pressure in the ram, strand elongation, and load in each strand as measured by a load cell. The elongation was locked off using retaining nuts then the ram was depressurized.

Formwork consisted of a base section to which side forms were attached. Each specimen was cast in an independent form. Forms were lacquered and oiled before each use.

Table 4.1 Mix designs and properties

	Normal Strength	High Strength
Design Strength (psi)	5,000	10,000
Mix Design (Quantities in lbs. per cu. yard)		
Type I Cement	564	814
Sand	1,340	1,279
3/8 in. Crushed Limestone	2,000	1,740
Water (gallons)	25	31.5
Water Reducing Admixture (Note 1)	---	16 oz.
Super-plasticizer (Note 2)	---	48 oz.
Quantity Delivered (c.y.)	1.5	4
Cost per Yard Delivered	$47	$56
Mix Properties		
Slump (in.)	5	1 and 10 (Note 3)
Water / Cement Ratio	0.59	0.29
Cement Content (sacks/cy)	6	10.5

Note 1 - 300 R - Master Builders
Note 2 - 400 N - Master Builders - 32 oz. at plant after batching was complete, 16 oz. upon arrival of truck at laboratory.
Note 3 - 1 in. slump at batch plant prior to addition of super-plasticizer; 10 in. slump at laboratory after second dose.

Table 4.2 Concrete strength data

		Normal Strength	High Strength
Concrete Strength Data			
Age	(days)	7	8
Mean Strength	(ksi)	5.1	9.5
No. of Cylinders		3	3
Age	(days)	28	28
Mean Strength	(ksi)	5.9	10.2
No. of Cylinders		4	4

At ends of each specimen, the strand was debonded by covering the strand with an 8-in. piece of vinyl tubing that had been slit and filled with grease. The tubing was then wrapped with duct tape as shown in Fig. 4.4.

Concrete was batched in a commercial plant and brought to the laboratory in a mixer truck. The batching process was monitored by laboratory personnel. Concrete was placed in the forms and vibrated using internal vibrators. Figure 4.5 shows the forms after casting and prior to covering with plastic sheeting for curing. Side forms on Specimen 5S-6-1 deflected outward during casting. The specimen was not used because of the varying cross section. Cylinders were cast and cured with the specimens at ambient conditions for use in determining concrete strength of the specimens.

After the concrete had cured for four days, the plastic and side forms were removed. Demec gage measurement points were applied at midheight of one side of each specimen as shown in Figs. 4.2 and 4.6 using "5 minute" industrial type epoxy. Measurement points for three additional gage lengths were placed on the other side to allow determination of bending effects. A total of 50 points were applied to each specimen. Demec measurement points were placed on a cylinder from the high strength batch to provide a temperature correction for the readings.

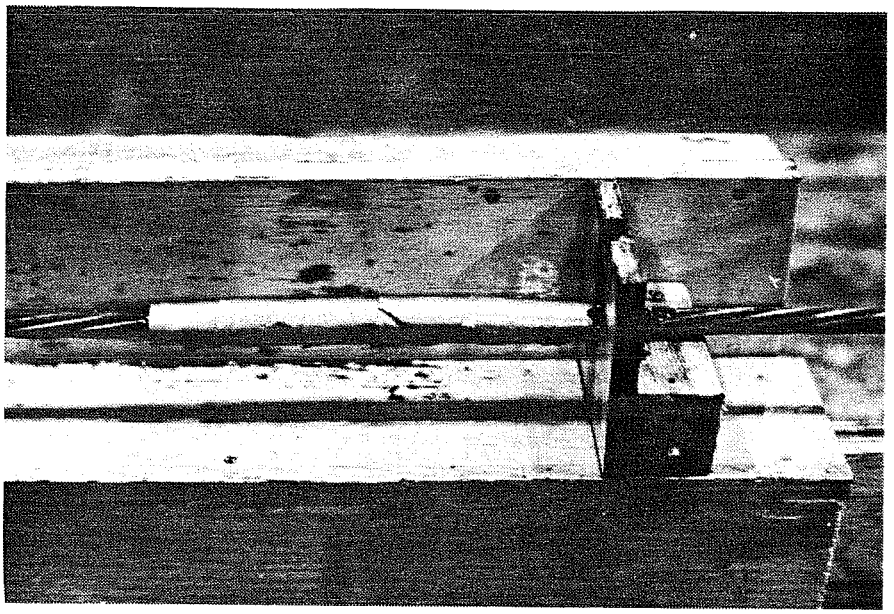

Fig. 4.4 Photograph of stand debond

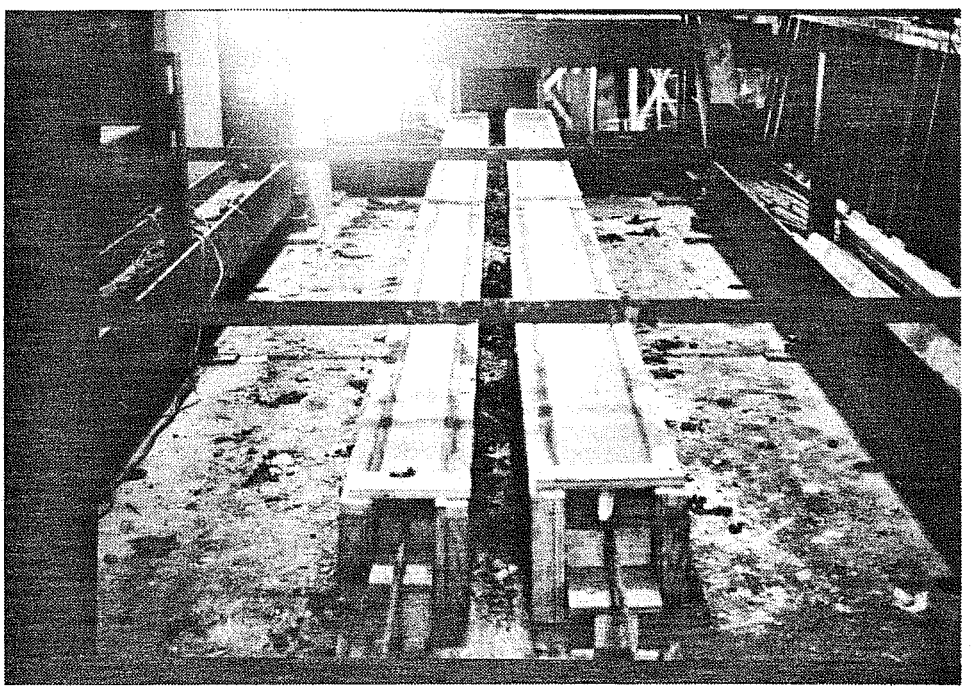

Fig. 4.5 Photograph of specimens in prestressing bed after placement of concrete.

4.5 Test Procedure

Release occurred seven days after the specimens were cast. An initial set of demec readings was taken for each interval. The first three gage lengths at the ends of each specimen were taken using a 2-in. demec gage while all others were taken using an 8-in. gage. Shortly after completion of the initial readings, one of the strands was flame cut to create a sudden release of the prestress force. Then the tensioning ram was repressurized, the retaining nuts loosened, and the pressure allowed to bleed off slowly to produce a gradual release of the prestress force in the other strand. A second set of readings was then taken. Readings were taken on the instrumented cylinder before and after taking readings for each specimen.

4.6 Test Results

The change in concrete strains at release was determined from initial and final demec gage readings. A plot was made for each specimen showing the variation of strains along the length of the specimen, excluding the debond length. The transfer length was then determined as the distance from the end of the bonded strand to the point at which the strain in the concrete becomes constant, as shown in Fig. 4.7 for a typical specimen from each concrete batch.

Distances from the end of the bonded strand to the point where the full prestress and 80 percent of the prestress have been developed are shown for both ends of each specimen in Table 4.3. The distance required for transfer of 80 percent of the prestress is included

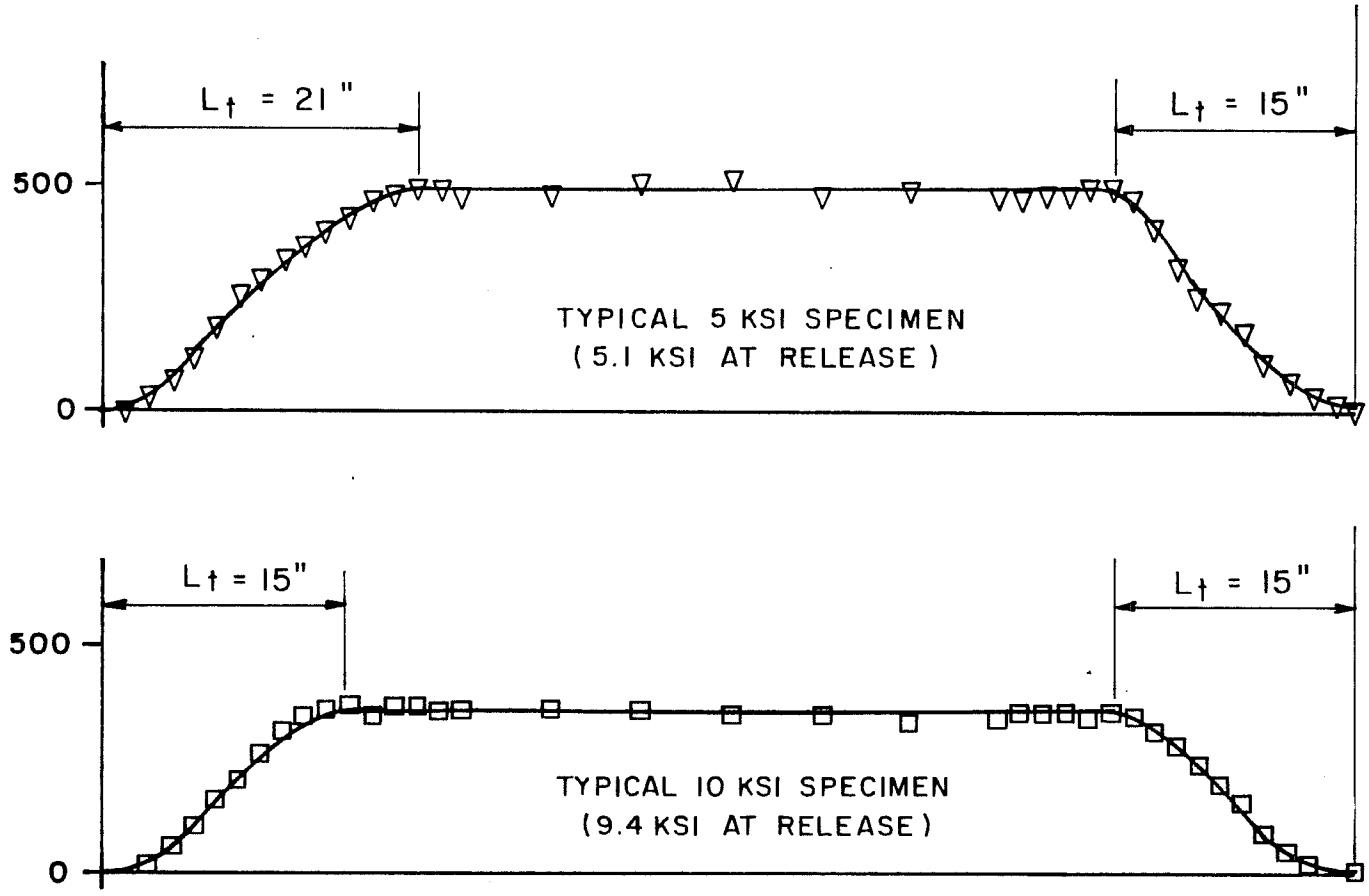

Fig. 4.7 Typical variation of strain with distance along specimens

Table 4.3 Results of transfer tests

Specimen Designation	Measured Transfer Lengths* (in.) Full Transfer North	Full Transfer South	80% Transfer North	80% Transfer South	
5G-4-1	41	25	15	17	
5G-4-2	21	15	13	11	
5S-4-1	23	13	15	9	
5S-4-2	15	23	11	17	
10G-4-1	13	17	7	9	
10G-4-2	15	15	9	9	
10S-4-1	13	17	7	13	
10S-4-2	19	11	17	9	
5G-6-1	21	33	19	25	
5G-6-2	25	33	19	27	(Estim.)
5S-6-2	23	19	17	11	

* - Values shown for transfer lengths are distances (in inches) from end of bonded strand to point at which full prestress or 80 percent of the prestress was developed.

Note: Because 8-in. gage lengths in the center region of the specimens did not overlap, transfer lengths > 25 in. could only be determined in 8-in. increments.

Table 4.4 Summary of transfer test results

Specimen Type (in. x in.)	Concrete Strength (ksi)	Measured Mean (in.)	Measured Maximum (in.)	AASHTO Value (in.)
4 x 4	5.1	22	41	30
4 x 4	9.4	15	19	29
6 x 6	5.1	26	33	31

AASHTO Value: $Lt = fse/3\ D$ (from Ref. [10], Sec. 9.27.1)

because it is viewed by some investigators as a more reliable measure of the transfer length. It should be noted that, because the 8-in. demec gage lengths did not overlap in the center of the specimens, transfer lengths could only be determined to the nearest 8-in. increment when greater than 25 in. A statistical summary of the full transfer data and comparison with transfer lengths computed by the AASHTO expression appear in Table 4.4. Frequency plots of distances required for transfer of the full prestress force are shown in Fig. 4.8 for the three categories of specimens.

Concrete strains measured in the central portions of the specimens after release and effective strand stresses before and after release appear in Table 4.5. Strand stresses after release were determined by deducting the change in strand stress corresponding to the average concrete strain in the center of the specimen from the effective stress prior to release.

4.7 Observations and Conclusions

The following observations can be made from data obtained from this limited test series:

1. Transfer lengths for 0.5-in. diameter strand in high strength concrete were approximately 30 percent shorter than in normal strength concrete.
2. The gradual or sudden release of the prestress force had no significant effect on the transfer lengths measured in these tests.

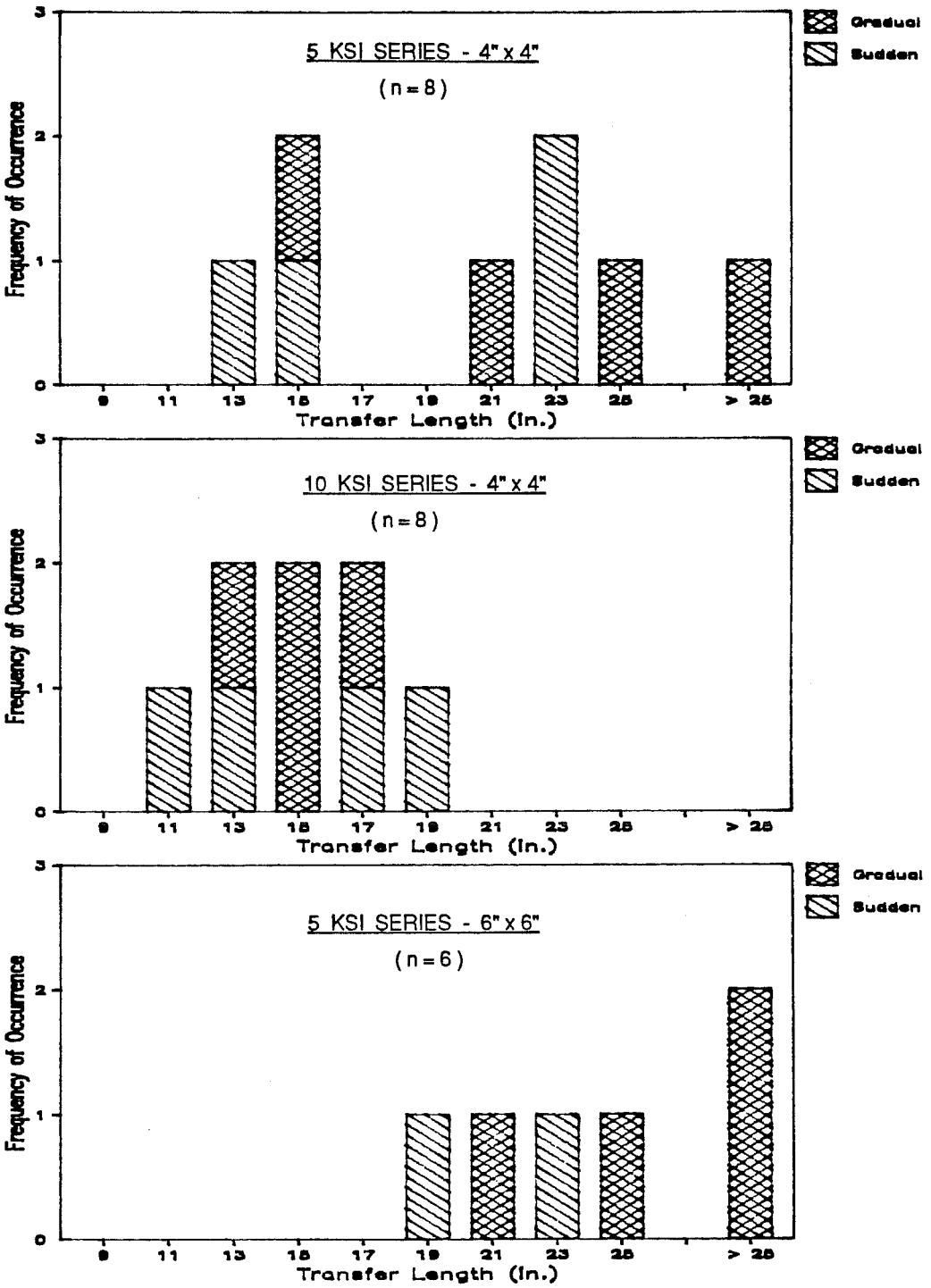

Fig. 4.8 Frequency plots of transfer length data

Table 4.5 Concrete strain and effective strand stress data

	Normal Strength	High Strength
Concrete Strains after Release (microstrain)		
4 in. specimens		
Gradual	483	341
Sudden	449	355
6 in. specimens		
Gradual	204	
Sudden	210	
Effective Strand Stress Data (ksi)		
Before Release - 4 and 6 in. specimens		
Gradual	182.6	188.0
Sudden	185.3	191.2
After Release - 4 in. specimens		
Gradual	169.3	178.6
Sudden	172.9	181.4
After Release - 6 in. specimens		
Gradual	177.0	
Sudden	179.5	

Notes: Concrete strains are for central portion of specimen where strain is constant. Values shown represent an average for the type of specimen indicated.

Effective strand strains are determined by subtracting change in strand stress corresponding to concrete strains from effective strand stress before release.

Strand modulus = 27,500 ksi; area = 0.153 in^2).

3. An increase in cross section size resulted in increased mean values for measured transfer lengths.
4. Measured transfer lengths for both high and normal strength concrete specimens were less than values computed using the AASHTO expression.

While this was a limited series of tests, the following conclusions may be drawn from the above observations:

1. Transfer lengths for high strength concrete are shorter than for normal strength concrete.
2. The current AASHTO expression provides a conservative yet reasonable estimate for the transfer length of strand in high strength concrete.

CHAPTER 5

ONE-THIRD SCALE GIRDER TEST PROGRAM

5.1 Introduction

The purpose of this series of tests was to observe the behavior of pretensioned bridges constructed using high strength concrete girders and a normal strength concrete deck. Testing of such a structure was necessary because data on behavior of high strength concrete members is very limited and also because data related to composite bridge structures are not available in the literature. Analytical models used to predict service load and ultimate behavior have not been confirmed for use with high strength concrete because of this lack of data. There is also little data to demonstrate that structures employing high strength concrete, which is a brittle material, will have sufficient ductility.

Therefore, the purpose of this testing program was to gather data on the service-load and ultimate behavior of a composite bridge structure with a high strength concrete girder and low strength deck. Tests included specimens with both moderate and heavy reinforcement so that ductility of the structure could be studied.

Aspects of behavior that were of particular interest included ultimate capacity in flexure, load-deflection behavior (which gives an indication of member ductility), strains in the concrete and

prestressing steel under load and at failure, and long-term deflections. Ultimate shear capacity was also of interest as preliminary data for a more complete series of shear tests that followed.

Test specimens were one-third scale models of a long-span modified AASHTO-PCI standard pretensioned bridge girder with a composite deck that was placed with the girder unshored. Specimens had identical external dimensions, and all strands were tensioned to the same force. Nominal concrete strength for the specimens was 12,000 psi in girders and 3,600 psi in slabs.

The principal variable in the investigation was the quantity of prestressing steel. Specimen 1 contained 13 3/8-in. diameter strands while nine strands were used for Specimen 2.

The second variable was the quantity of shear reinforcement. Stirrups in Specimen 1 provided the maximum stirrup contribution to shear strength permitted by the codes ($V_s = 8\sqrt{f_c'}\, b_w d$). Specimen 2 had half the number of stirrups of Specimen 1, or ($V_s = 4\sqrt{f_c'}\, b_w d$). The effect of stirrup details on shear capacity was investigated in Specimen 1 by using standard and modified stirrup details for the two ends of the girder. In Specimen 2, the effect of strand bond on shear capacity was studied by providing an overhang at one end of the girder but using standard details at the other end.

5.2 Specimen Description and Design

5.2.1 Flexural Design. Specimens were intended to be representative of members that are in wide use, yet make efficient use of high strength concrete. Therefore, a modified AASHTO-PCI Type IV girder was used for the prototype. The section was modified by reducing the distance between side forms by 2 in., as suggested in Ref. [109]. The nominal girder concrete strength of 12,000 psi is near the practical upper limit of field-produced concrete at this time. A concrete strength at release of 9,000 psi was assumed, although this did not control designs. A 3,600 psi composite cast-in-place deck was added to the unshored girder to complete the structure. Girders were pretensioned with 0.5-in. diameter Grade 270 low relaxation seven wire strands placed on a 2 by 2 in. grid. Rows were filled from the bottom and strands were draped to produce stresses within the allowable limits at the ends of the girder at release. A single typical interior girder and deck were used in the design. The presence of diaphragms was neglected. Composite section dimensions and properties are shown in Fig. 5.1.

The goal of the design of Specimen 1 was to obtain crushing of either the deck or girder concrete near the load at which strands yield (produce the balanced reinforcement condition). A series of preliminary designs were conducted for the prototype using AASHTO loadings and allowable stresses, with losses computed using the

	PROTOTYPE
GIRDER	
I ($in.^4$)	233,854
A ($in.^2$)	681
y_t (in.)	29.63
y_b (in.)	24.37
STRAND PATTERN	
SPECIMEN 1	
No. of Strands	64
g at Midspan	8.063"
g at End	18.063"
SPECIMEN 2	
No. of Strands	44
g at Midspan	5.455"
g at End	8.636"

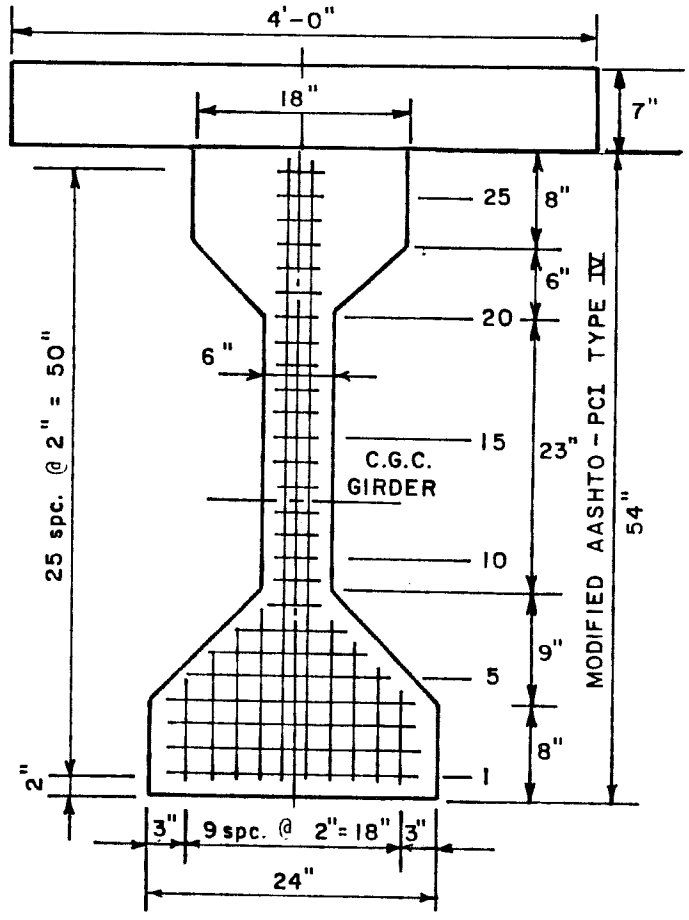

Fig. 5.1 Prototype dimensions and section properties

procedure given in Ref. [137]. This was supplemented by moment-curvature analyses to give an improved prediction of strand and concrete stresses at failure. The thickness of the slab was obtained from information found in Ref. [109] (see Table C.1).

It was found that a long span with close girder spacing would produce the desired balanced failure if strands were provided in addition to the minimum required for allowable stress design. A span of 146 ft with girders spaced 4 ft apart was selected. This span is close to the maximum span for the section at this spacing. The prototype design required 64 strands to obtain a failure near the balanced reinforcement condition. While allowable stress design criteria could be satisfied with as few as 40 strands, it was felt that the additional strands could possibly be required to control long-term deflections.

In order to permit testing of a specimen in the laboratory, the prototype was reduced to a scale model. A scale factor of one-third was selected which reduced the span to 48 ft 8 in. with a girder spacing of 16 in. Dimensions and loads were scaled so that the same stresses would be present in the scale-model specimen as in the prototype. Because stresses were the same but the depth was reduced by one-third in the test specimens, the strain gradient across the depth of the section was not the same for specimen and prototype, with the strain gradient in the specimen being three times greater.

Because strands could not be scaled directly, 3/8-in. diameter Grade 270 low relaxation seven-wire strand was used. Thirteen strands were required in the model, positioned on a 1 1/4 by 1 1/4 in. grid which provided a strand layout that closely resembled the prototype layout. However, the 3/8-in. strand could not properly model the bond of the 1/2-in. strands used in the prototype. This was unavoidable, but had a significant effect only in the shear tests. Dimensions and properties for the scale-model are shown in Fig. 5.2. Strand patterns at midspan and at ends of the girders are shown for both specimens in Fig. 5.3.

Design of Specimen 2 was postponed until testing of Specimen 1 was completed. Since a near-balanced flexure failure was obtained with Specimen 1, Specimen 2 was designed to produce a more ductile failure. It was also desired that both the girder and deck concrete be near crushing at ultimate, with the girder still making a significant contribution to the compression zone. A moment-curvature analysis was again used to determine the expected strains in concrete and steel at failure and the load- deflection response of the structure. These criteria were best satisfied for the model by a 9 strand pattern which corresponds to approximately 44 strands in the prototype. This design, which uses the fewest strands possible to satisy allowable stresses for the given span and spacing, is typical of current highway bridge designs.

	SCALE MODEL
GIRDER	
I ($in.^4$)	2876
A ($in.^2$)	75.25
y_t (in.)	9.876
y_b (in.)	8.124
STRAND PATTERN	
SPECIMEN 1	
No. of Strands	13
g at Midspan	2.788"
g at End	5.865"
SPECIMEN 2	
No. of Strands	9
g at Midspan	1.944"
g at End	3.083"

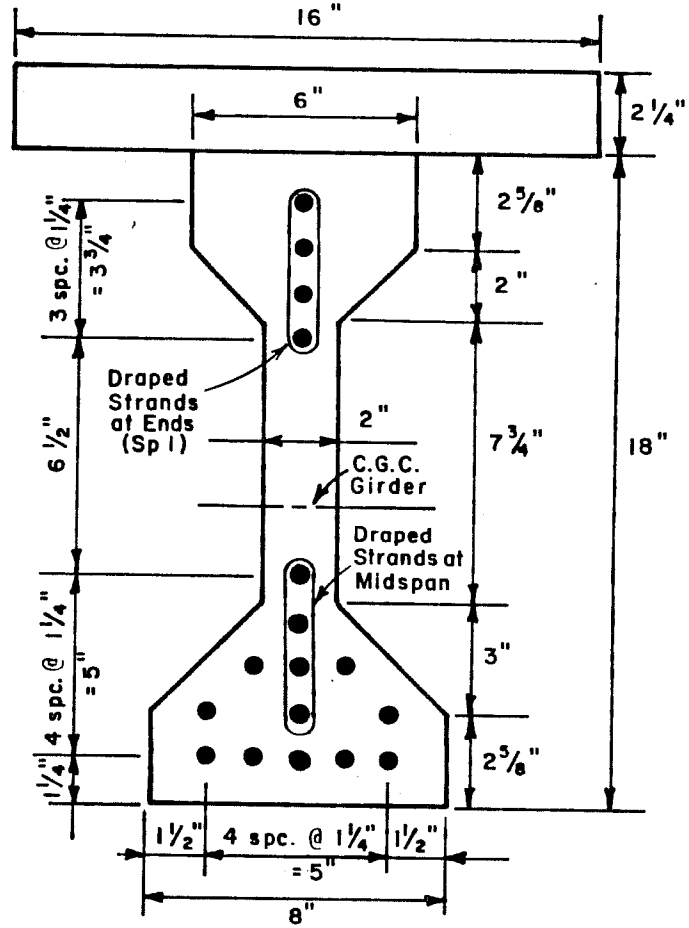

Fig. 5.2 Scale model dimensions and section properties

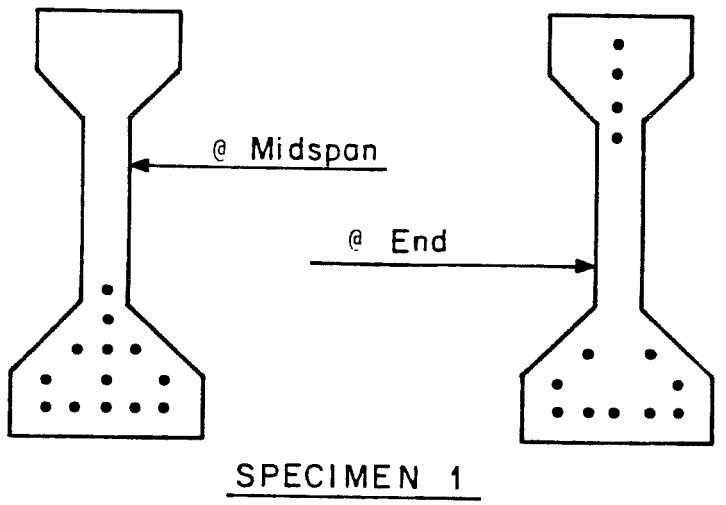

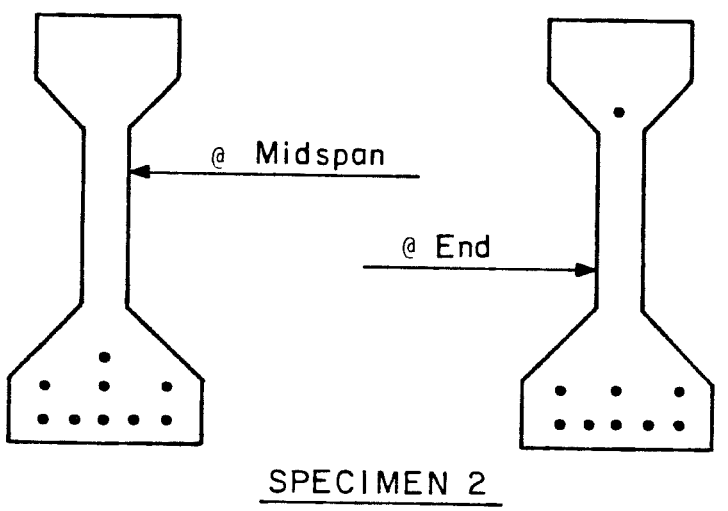

Fig. 5.3 Strand patterns for specimens

used at the south end, and a stirrup which crossed beneath the center column of strands and hooked up at the edges of the section was used at the north end (Fig. 5.5). The second stirrup detail was expected to provide more confinement for the strands. For Specimen 2, the standard Texas stirrup detail was used in the shear span at both ends, but a 6-in. overhang was provided for the shear test of the north end in order to study the effect of strand bond on the shear capacity of the section.

End reinforcement details used in the specimens, which are shown in Fig. 5.6 and 5.7, were based on the standard Texas detail for a Type IV girder, which appears in Fig. 5.8. For Specimen 2, an extension of the standard detail was provided for the overhang. At locations where interior supports were to be located for shear tests, additional stirrups and mild steel longitudinal reinforcement was provided to limit cracking during the flexure test. Stirrup spacing was reduced in the central region of the specimens, as shown in Fig. 5.4.

5.3 Materials

5.3.1 Concrete. A high strength concrete with a design strength of 12,000 psi at 28 days was used for the girders. To determine the mix design for this concrete, 22 trial batches were produced and tested. Data from these trial batches are reported in

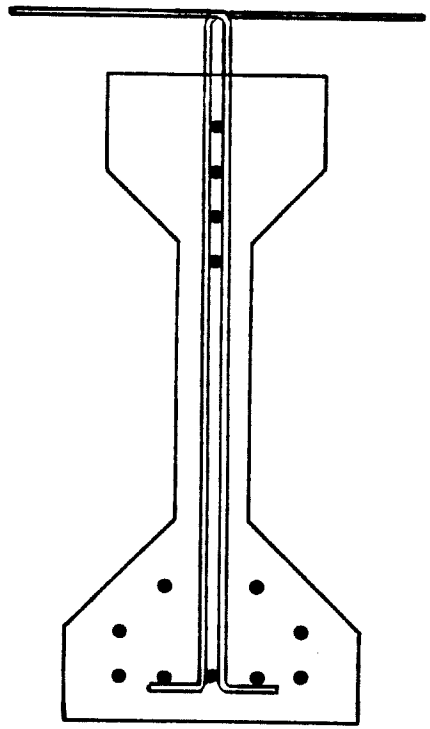

STANDARD
SPECIMEN 1, SOUTH END
SPECIMEN 2

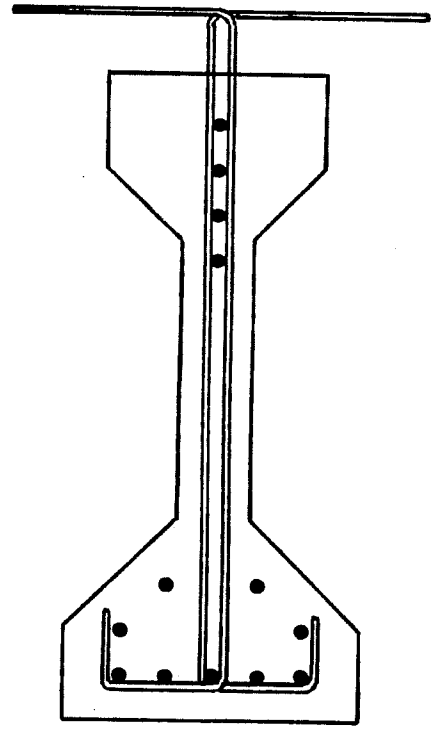

MODIFIED
SPECIMEN 1, NORTH END

Fig. 5.5 Stirrup details

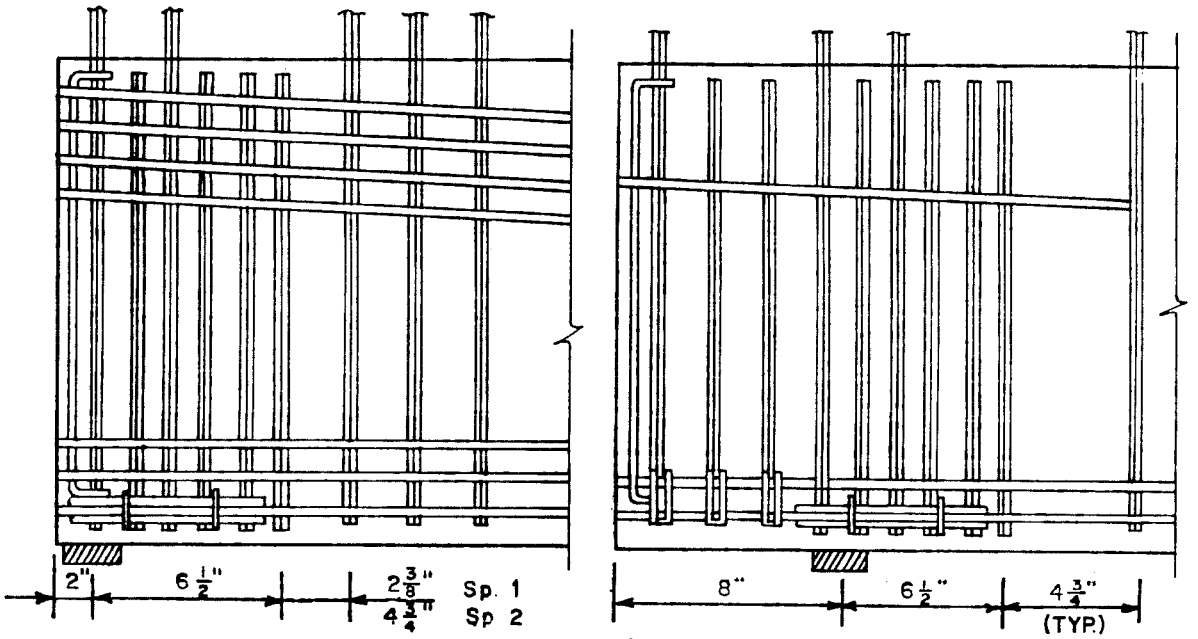

SPECIMEN 1

SOUTH END-SPECIMEN 2

NORTH END-SPECIMEN 2

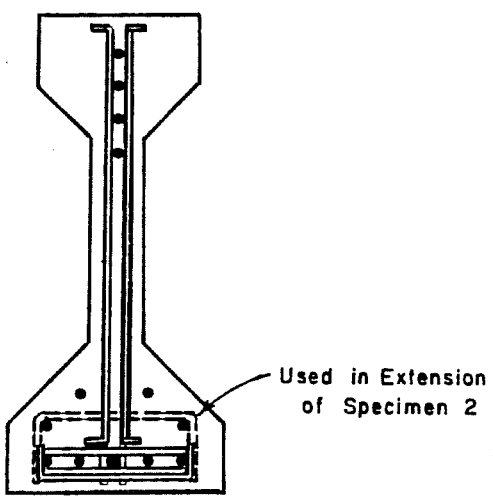

END VIEW

All Reinforcing Bars are No. 2
Prestressing Strands are $\frac{3}{8}$" diam.

Fig. 5.6 Scale model end reinforcement details

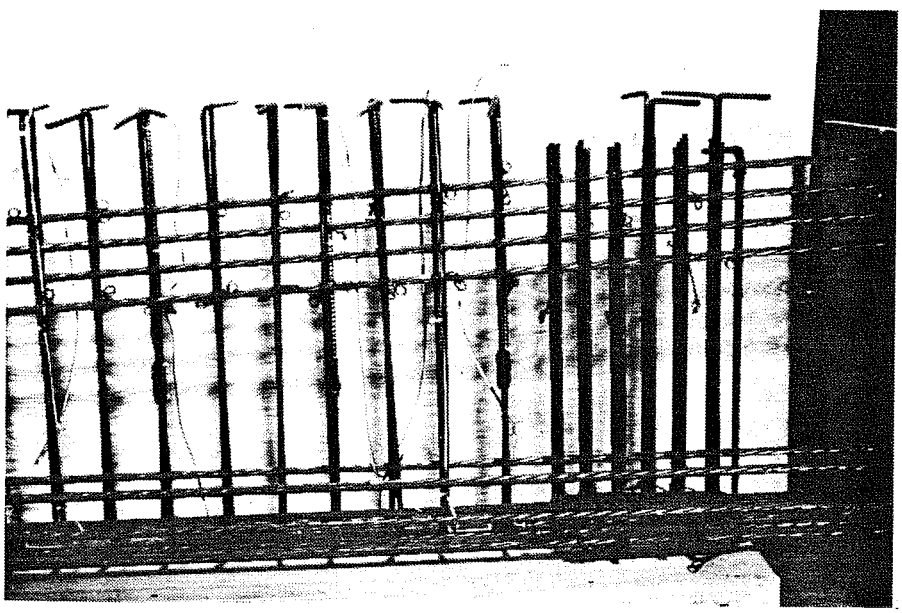

Fig. 5.7 Photograph of end reinforcement detail - south end, Specimen 1.

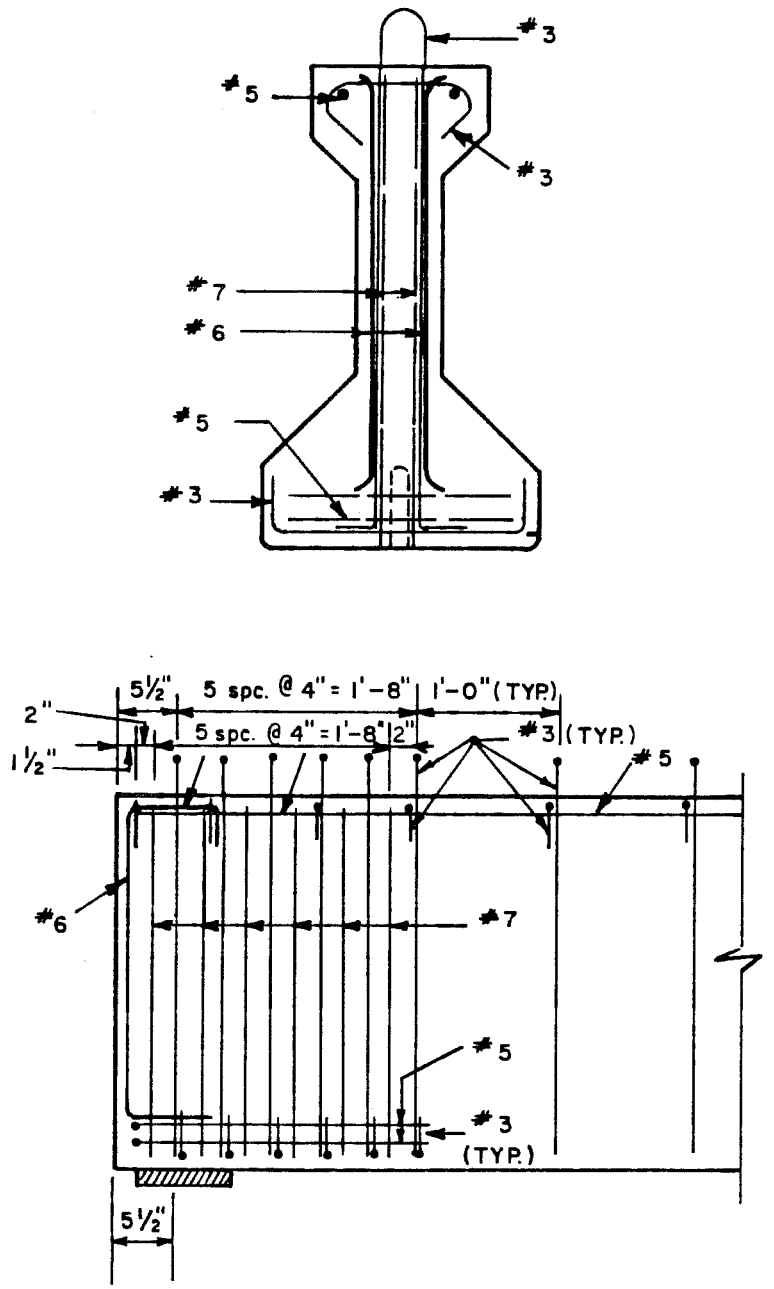

Fig. 5.8 Texas SDHPT standard end reinforcement detail for Type IV girder

Ref. [35]. Strength data for the girder and deck concrete at critical events during fabrication and testing for Specimen 1 and 2 in Table 6.1 and 6.7, respectively. Complete strength data and information regarding the mix design for the high strength concrete used in the specimens appear in Appendix A. The normal strength concrete mixes used for the deck, which were designed to have a strength of 3,600 to 4,000 psi at the time of the flexure test, were standard mixes and contained entrained air. Different mixes were used for the two specimens to satisfy testing schedule requirements. All mixes were batched at a ready mix plant and were transported to the laboratory in a mixer truck.

Properties of the concrete were determined by testing 6 by 12-in. cylinders under axial compression and 6 by 6 by 21 in. beams loaded at third points. Steel and plastic molds were used for the cylinders. Some cylinders were cured in a lime bath, while most were air cured with the specimens after receiving a coat of curing compound after removal from the molds. The modulus of elasticity for the concrete was determined using a compressometer or strain gages applied to the cylinders.

5.3.2 Prestressing Strand. The prestressing strand was 3/8-in. Grade 270 ksi seven wire low-relaxation strand donated by Florida Wire and Cable Company. The strand was lightly rusted with some light pitting.

Load-strain characteristics of the strand were given in the mill test report supplied with the strand, and were supplemented by tests conducted in the laboratory with electronic strain gages attached to single wires of the strand. The load- strain curve and other test data provided with the mill report appear in Fig. 5.9, along with the average apparent modulus determined from strand tests using strain gages. The average cross sectional area of the strand was 0.0845 in^2, which was determined by weighing and measuring lengths of strand and then computing the area by assuming the unit weight of steel to be 490 pcf.

5.3.3 Nonprestressed Reinforcement. The small size of deformed reinforcement required for model construction is not produced domestically. However, it was discovered that a mill in Mexico was producing small sizes of deformed reinforcement. The name and address of the mill was:

Alta Resistencia, S.A.
Sucursal Monterrey
Abraham Lincoln 4016
Fraccionamiento Lincoln
Monterrey, N.L.
Telephone: 70-32-23

Quantities of this steel were obtained in sizes corresponding to No. 2, No. 1.5, and No. 1.25, although only No. 2 bars were used in the specimens. As received, this steel had a high yield strength and limited ductility. Heat treatment at a local commercial

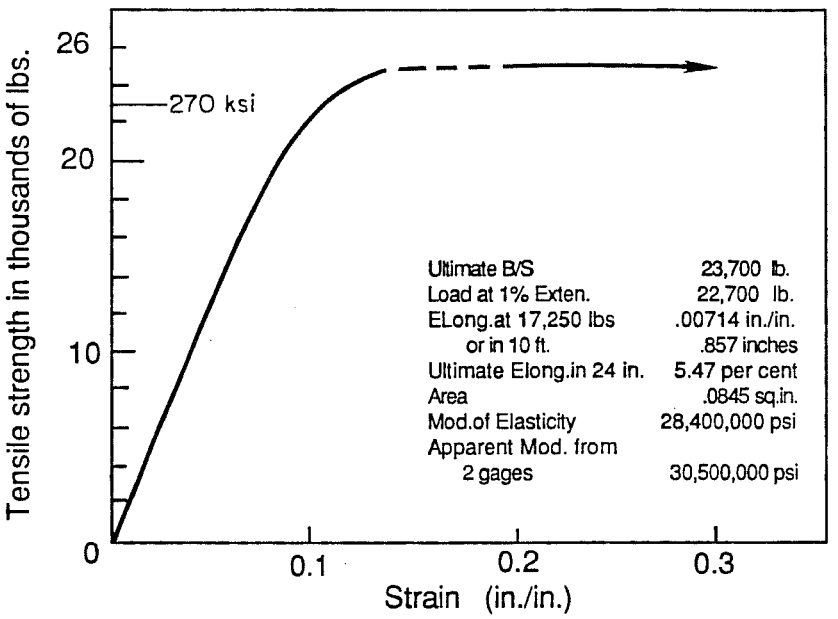

Fig. 5.9 Load-strain curve and associated data for prestressing strand

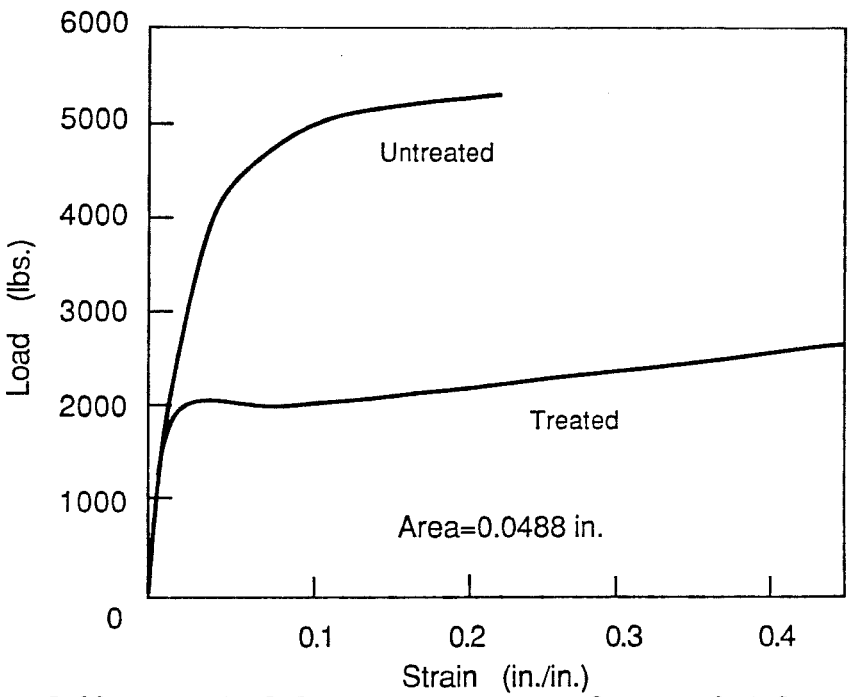

Fig. 5.10 Typical load-strain curves for No. 2 deformed bars

heat treatment facility was used to produce a steel with characteristics typical of domestic reinforcement. After treatment, the steel yielded at an average stress of 44 ksi and had a significant yield plateau. Typical load-strain curves for the untreated and treated No. 2 reinforcing bars are shown in Fig. 5.10, which also gives the average area for these bars. The area was determined using the weighing method described in the preceding section.

5.4 Fabrication

5.4.1 Prestressing Operation.

Strands were tensioned in the prestressing bed at the laboratory. A post-tensioning ram, loaned to the laboratory by the VSL Corporation, was used to apply an initial tension to each strand. This ensured a uniform stress in the strands. Chucks and wedges were donated by the Great Southwest Marketing Company.

Initial tensioning was achieved in stages. First, a strand was tensioned to the full prestressing force of 17 kips to set the wedges in the chucks at the far end of the bed. The force was then released and a chuck and wedges were placed on the strand at the tensioning end. The strand was then stressed to a partial load of 10 kips, which provided a greater margin of safety while tying stirrups to the strands. Finally, the wedges were power-seated by releasing the pressure in the ram.

To remove slack and provide a repeatable reference for elongation measurements, an initial force corresponding to 500 psi in the ram was applied to each strand before tensioning to both the 17 and 10 kip level. Pressure in the ram and movement of both ends of each strand were monitored and checked for agreement during the stressing operation. Strain gages on the two instrumented strands, which were the first strands to be tensioned, were read at each stage of their tensioning and at intervals during the remainder of the tensioning procedure.

Hold-down points for draped strands were located 5 ft each side of midspan. Drape hardware was fabricated at the laboratory and supported the strands on rollers (Fig. 5.11). The hold-down hardware bolted to an anchor block attached to the strong testing floor. At one end of the prestressing bed, the same hardware was used to hold up draped strands to obtain the desired strand profile.

After stirrups and detail reinforcement were tied to the strands, a 200-ton ram pulled all strands simultaneously to a final stress of approximately 200 ksi, which corresponded to a force of 17 kips per strand. This tensioning was controlled by strand elongation and change in strain in the strands. Friction in the tensioning system precluded use of the ram pressure for load control. After full stress was achieved, elongation was maintained by tightening restraining nuts. Pressure in the ram was then released.

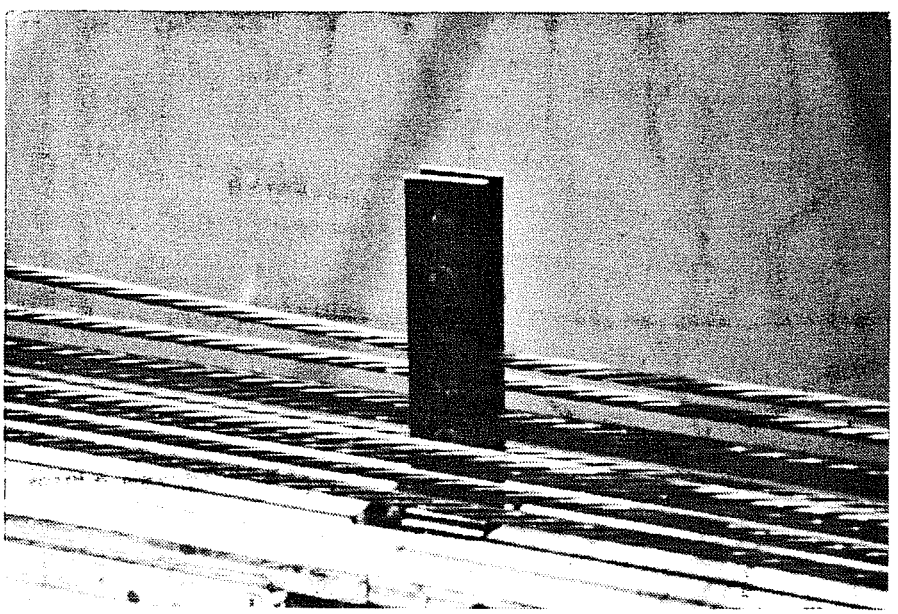

Fig. 5.11 Photograph of hold-down hardware

Transfer of the prestress force to the girder was begun by releasing the hold-down hardware near midspan. This applied an upward force on the section, which had no precompression. In Specimen 1, which had four draped strands, this force was sufficient to cause cracking over the first hold-down to be released. Dead load blocks were placed on Specimen 2 at release although the force was much less because only one strand was draped. Following release of the draping hardware, the large stressing ram was repressurized, restraining nuts were loosened, and the ram was slowly depressurized to transfer the prestress force gradually. Strands were then cut with a torch at each end to free the girder. Later, the strands were ground off flush with the end of the girder.

5.4.2 Girder Fabrication. Girder forms were constructed in three parts. The soffit form, which was bolted to the base, ran the full length of the girder, with cut-outs for the drape hardware. Side forms were built up from layers of plywood to obtain the desired contour. Each side form was built in two sections to facilitate handling. Side forms were held in place by threaded rods passing through the soffit and through angles bolted to the top of the side forms. Plywood end forms were bolted to ends of the side forms. The forms received several coats of lacquer before each use.

Stirrups and detail reinforcement were cut and bent in the laboratory. Strain gages were attached to stirrups and strands where

desired. After initial tensioning of the strands was completed, stirrups and detail reinforcement was tied to the strands. After full tension was applied to the strands, girder forms were lightly oiled and then secured in place.

Concrete was placed in three lifts using a small concrete bucket or shovels. Internal vibrators were used to consolidate the concrete, although the tight clearances between strands, stirrups and forms made them difficult to use. However, consolidation was very good and damage to the forms was limited. The concrete was struck off level with the top of the forms, then roughened to ensure proper composite action.

Forms were covered with wet burlap and plastic for curing. Specimen 1 was cast in January when the ambient temperature in the laboratory was maintained between 50 and 70°F. Specimen 2 was cast in July with a temperature range of 75 to 100°F. Forms were removed in three to five days, and the burlap and plastic were replaced for a few more days.

Electrical resistance strain gages and mechanical strain gage (demec) points were applied to the surface of the girder each side of midspan and near the ends. After release, the girder was moved to the location where the slab was cast and the completed specimen was tested.

5.3.3 Slab Fabrication. Slab forms were constructed in sections that connected together and were supported by the girder. Support was provided by coil rod hangers that crossed over the girder, and by knee braces that propped the forms against the bottom flange of the girder. Dead load blocks required to compensate for the lack of dead load in both the slab and girder were placed on the forms until the slab was cast and cured.

Concrete was placed in the deck forms using an overhead crane and a small concrete bucket. Internal vibrators and a vibrating screed were used to consolidate the concrete. The surface was trowelled then covered with wet burlap and plastic to cure for three to five days. Temperature ranges during deck curing were similar to those for the corresponding girders.

When initial curing was complete, dead load blocks were removed while the forms were stripped. Dead load blocks were immediately reapplied by hanging them beneath the specimen (Fig. 5.12). Dead load blocks were uniformly distributed until they were rearranged for placement of the loading system.

While coil rod form hangers protruded slightly from the slab in some locations and voids were present where coil rods had been removed, it did not appear that the ultimate behavior of the specimens was significantly affected.

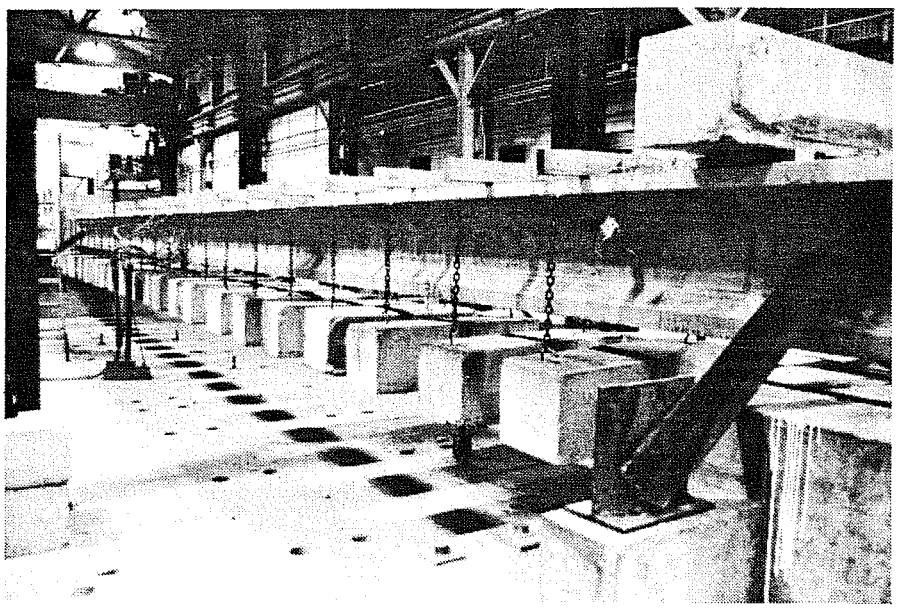

Fig. 5.12 Photograph of specimen with dead load blocks in place

5.5 Test Setup and Testing Procedures

5.5.1 Long-Term Deflections. Girder deflections at midspan were monitored from release until flexure tests were completed. Movement was measured using dial gages. This worked well except when the girder was moved from the prestressing bed to the test location.

5.5.2 Flexure Tests. Load for the flexure tests was applied by two equal concentrated loads placed symmetrically about midspan as shown schematically in Fig. 5.13, creating a constant moment region between load points. Spacing between loads was representative of a simplified AASHTO truck loading. Dead load blocks were removed from the constant moment region and concentrated just outside the load points to maintain the moment at midspan. The weight of the loading system was considered part of the dead load compensation. The distribution of dead load compensation during the flexure tests is also shown in Fig. 5.13.

Load was applied through the system of cross heads, threaded rods, and hydraulic rams shown in Fig. 5.14. At each load point, threaded rods, which were anchored to the load floor, restrained upper crossheads. A ram and load cell were suspended from the crossheads. The two lower cross heads were tied together by a beam to form a frame to prevent the cross heads from overturning. The lower cross heads, which rested on neoprene pads placed at each load point, were used to

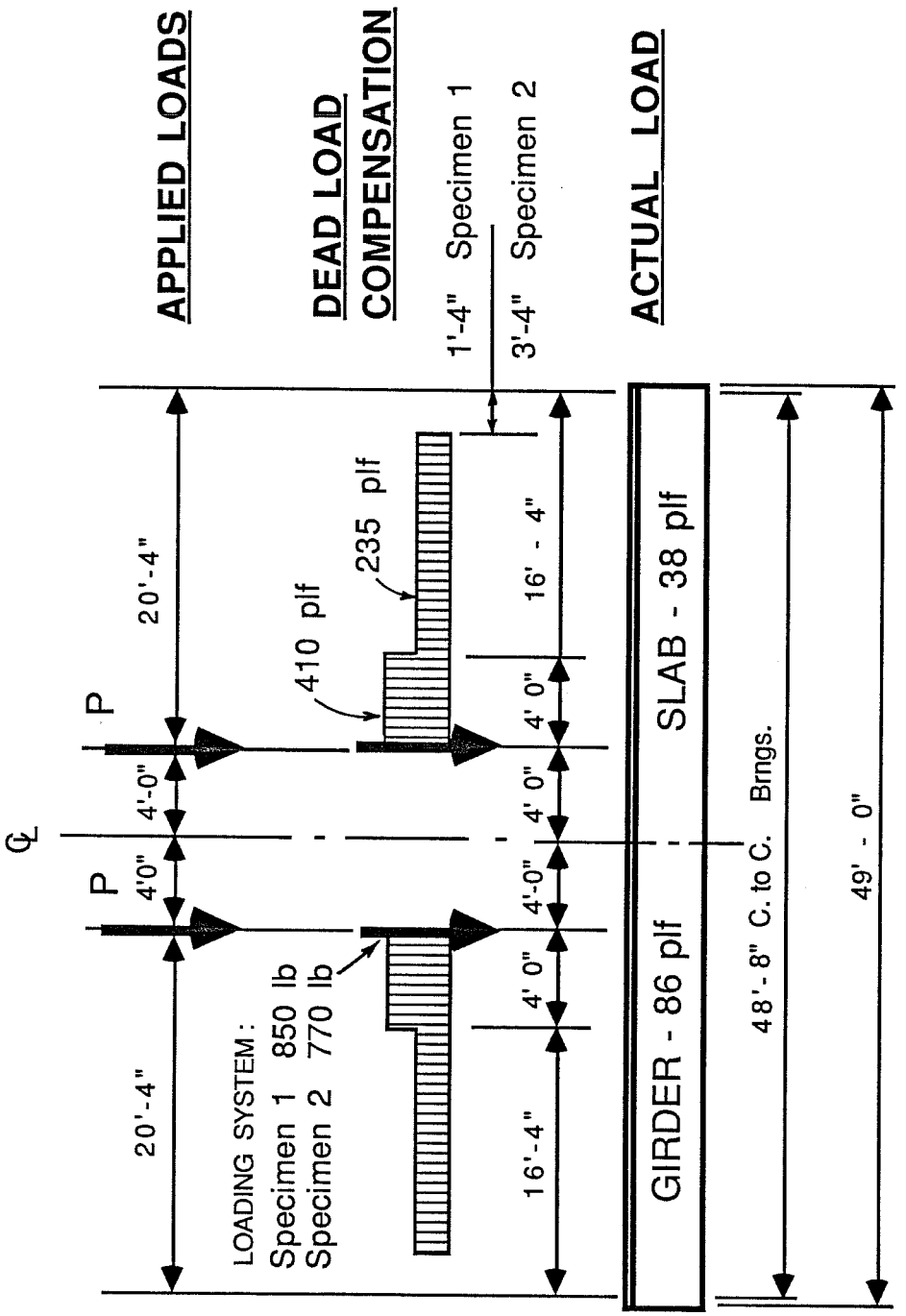

Fig. 5.13 Loads present during flexure tests

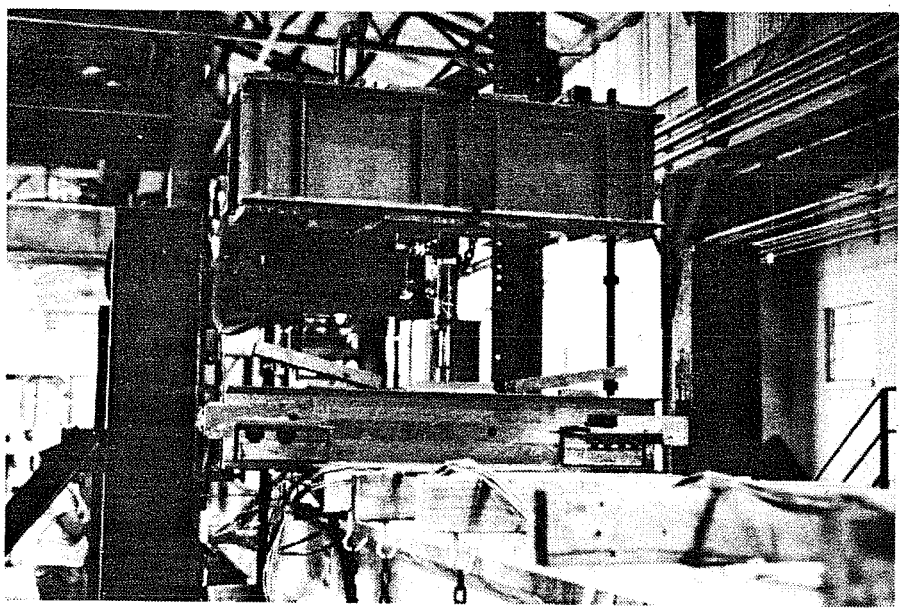

Fig. 5.14 Photograph of loading system for flexure tests

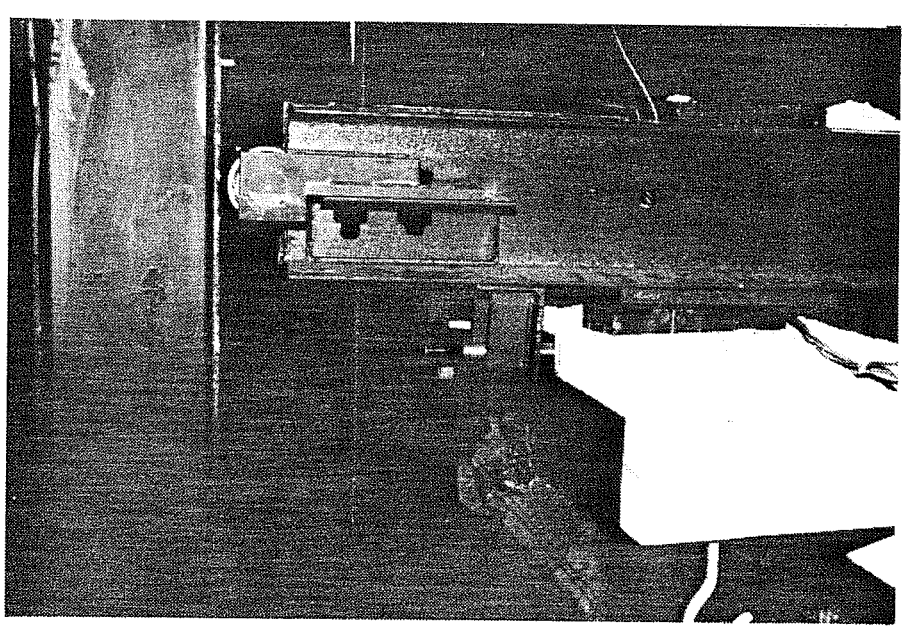

Fig. 5.15 Photograph of roller, crosshead, and braced column for lateral restraint

maintain the deflection of the specimen while the upper cross heads were lowered when rams reached the limit of their stroke. Rollers were attached to ends of the lower cross heads in such a way that lateral movement was restrained by a pair of braced columns, but vertical movement was unrestricted (Fig. 5.15).

The girder was supported by neoprene bearing pads that measured 3 by 7 by 2-in. thick. The pad footprint was scaled from the prototype. These pads, and those under the load points which were 3 by 11 by 2-in. thick, were designed by the manufacturer, Oil States Rubber Co., for the expected loads and rotations and contained nine steel shim plates.

Loading was controlled by monitoring pressure in the rams, which were connected to a common manifold. Load cells were also used during the test of Specimen 1. When a desired level of load was reached, pressure was maintained for approximately 10 seconds, then valves in the hydraulic loading system were closed and readings were taken.

Specimen 1 was loaded initially to a level above the cracking load and then completely unloaded, so that when the specimen was reloaded to failure, cracked section behavior could be observed. The initial cracking test was omitted for Specimen 2 because of the extensive shrinkage cracking that occurred prior to release. Cracks were marked at each load level.

5.5.3 Shear Tests. After the flexure test was completed, the strands were cut at the failure location, separating the specimen into two pieces. Each end was tested independently by placing a single concentrated load at the quarter point of the span as shown schematically in Fig. 5.16. High shear was therefore applied to the end of the girder which was not cracked during the flexure test and a smaller shear was present in the remainder of the span which had been cracked during the flexure test.

For the two pieces of Specimen 1, load was applied through a system consisting of a braced cross head, dywidag thread bars, and a hydraulic ram as shown in Fig. 5.17. The dywidag bars were anchored in the load floor and restrained the crosshead at the load point. A ram and load cell were suspended from the crosshead. A spherical head was placed between the specimen and ram.

The pieces of Specimen 2 were tested in a 600-kip screw-type testing machine (Fig. 5.18). Load was applied to the through a fixed head and neoprene pad.

The shear specimens were supported by a neoprene bearing pad under the end near the load point. A steel "trapped roller bearing" was used at the other end of the specimen. Bracing was provided at the ends to prevent overturning of the specimen.

The loading procedure was the same as used for the flexure tests. An initial cracking test was performed for tests of Specimen 1

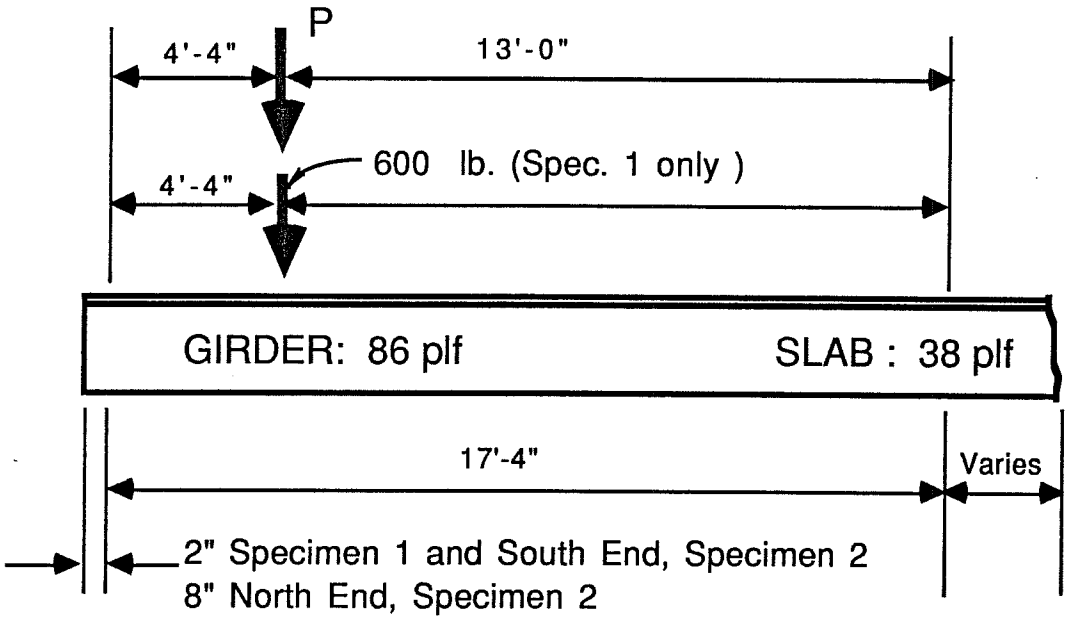

See Tables 6.2 and 6.8

Fig. 5.16 Loads present during shear tests

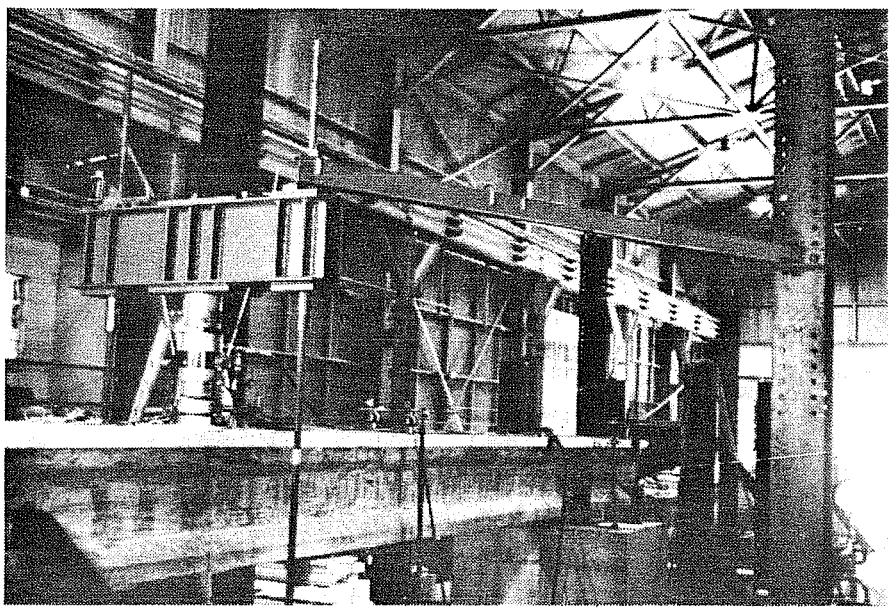

Fig. 5.17 Photograph of loading system for shear tests of Specimen 1

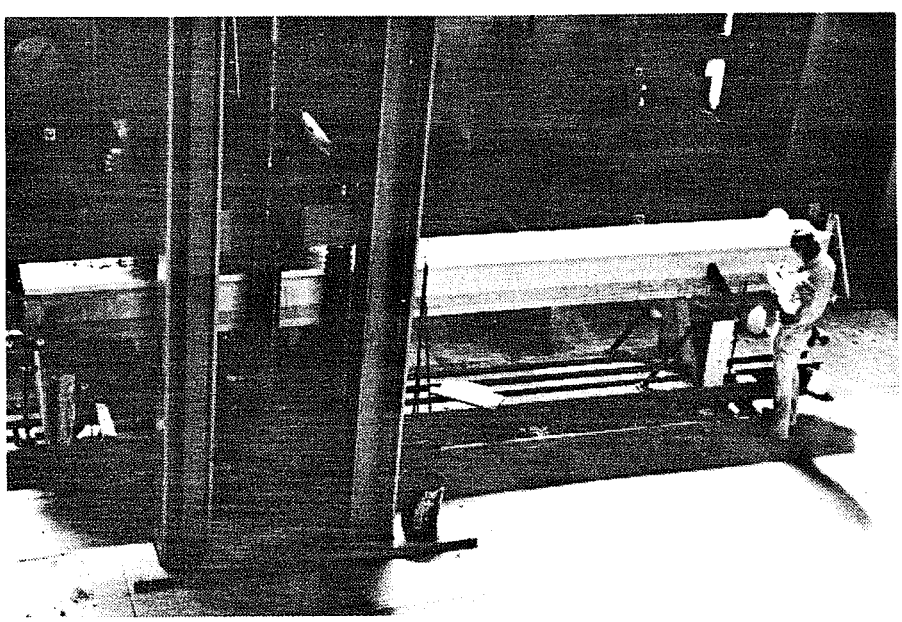

Fig. 5.18 Photograph of loading system for shear tests of Specimen 2

but was omitted for Specimen 2 due to the precracked condition of the girder.

5.6 Specimen and Test Setup Instrumentation

5.6.1 Reinforcement. Electrical resistance strain gages were attached to strands and stirrups at locations near midspan and each end as shown in Fig. 5.19 and 5.20. Foil backed temperature compensating gages with a gage length of 6 mm were used. Gages were applied to prepared surfaces on the steel using standard strain gaging procedures. Strand gages were placed on a single wire of the strand. Readings were taken using switch and balance boxes and strain indicator boxes, and were adjusted by readings taken on precision resistors connected to a channel in each switch and balance box.

Some strand gages were connected and read during stressing operations and more were connected before release. One or two stirrups at each end were connected and read beginning at release. These gages were monitored through the conclusion of the flexure test. For each shear test, strand and stirrup gages for the end being tested were connected and read.

5.6.2 Concrete Strains. Concrete strains were measured using a mechanical strain measuring device (demec gage) and electrical resistance strain gages mounted on the surface of the concrete at locations shown in Fig. 5.19, 5.20, and 5.21. Electrical resistance

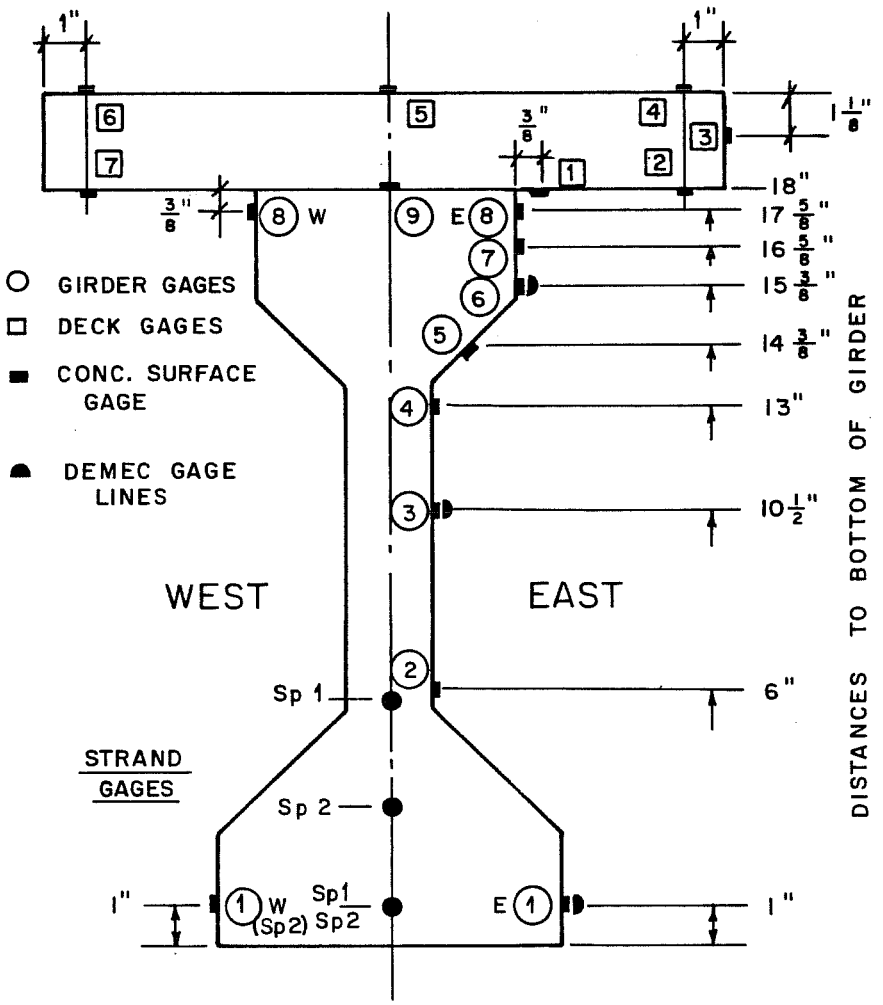

Electrical Resistance Gages are placed in locations shown 9" each side of midspan.

Concrete Gages : PL-60-11
Strand Gages : MM EA-06-062AP-120 L

Fig. 5.19 Strain gage locations near midspan

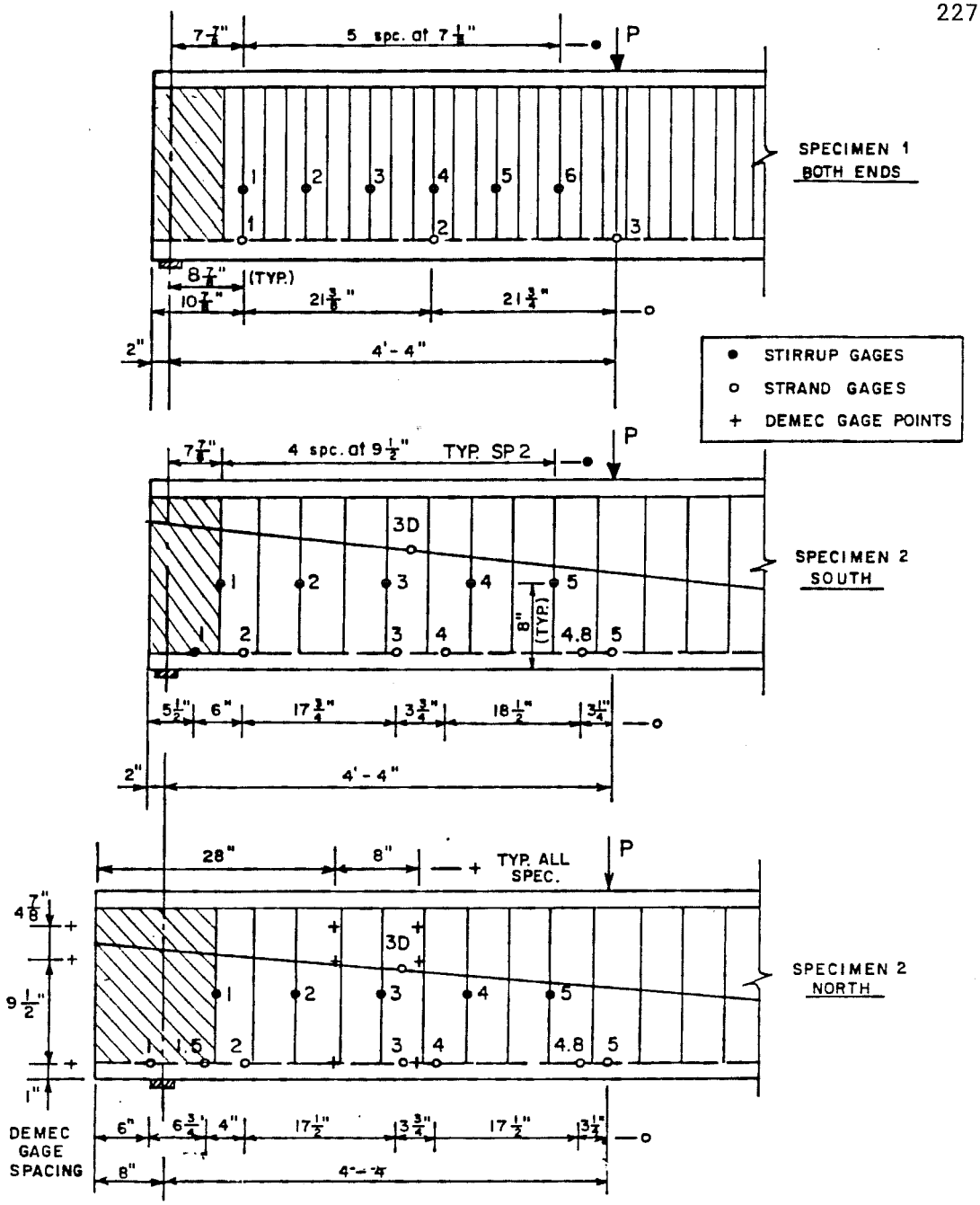

Fig. 5.20 Instrumentation near ends of girder

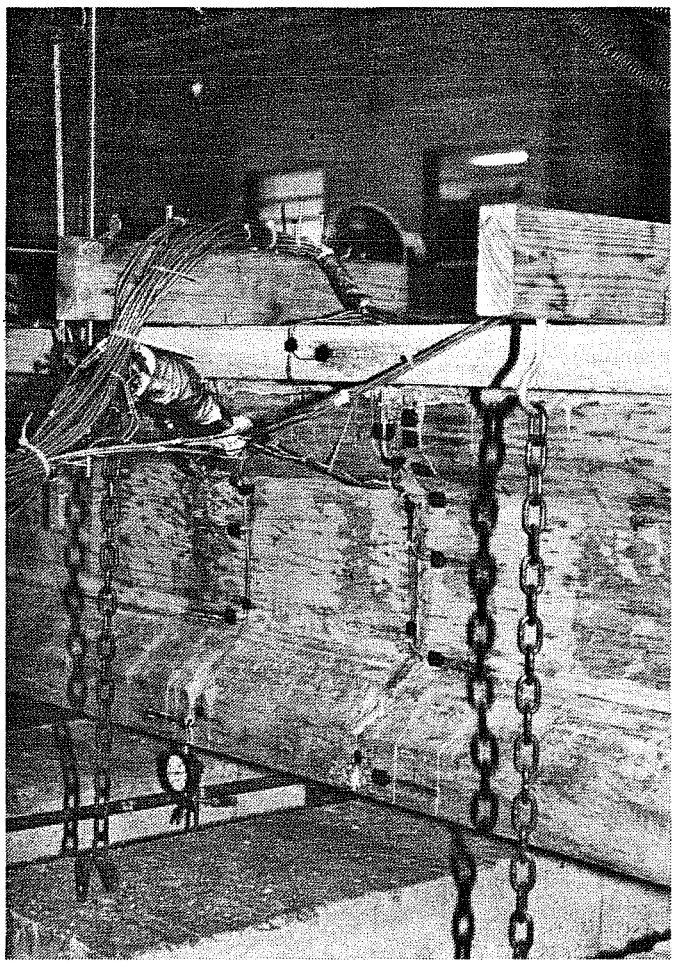

Fig. 5.21 Photograph of concrete surface gages at midspan

gages were paper backed with a gage length of 60 mm. Mechanical strain measurements were made using a 200 mm (8 in.) demec gage with a sensitivity of approximately 8 microstrains. Both types of gages were attached to specimens using model cement or epoxy. For electrical resistance gages, the surface was ground smooth and a layer of cement or epoxy was applied to seal the surface. After this coat was allowed to dry, the gage was applied using another layer of cement or epoxy. Electrical gages were connected to switch and balance boxes and strain indicators.

Prior to release, demec and electrical resistance gages were attached to the girder and initial readings were taken. The remaining electrical gages were applied after the slab was cast. All electrical gages were read through completion of the flexure test, while demec gages were read occasionally up to the time of the flexure and shear tests, but not during the tests.

5.6.3 Test Setup.

5.6.3.1 Deflections. A number of types of deflection measurements were taken during flexure tests. At midspan, dial gages were used to measure vertical deflection, sidesway, and roll. At ends of the girder, dial gages were used to measure bearing pad compression and roll. A surveying level was used to remotely monitor pad compression and midspan deflection during flexural tests to failure. A string line was stretched between ends of the specimen for

photographs and to make rough deflection measurements at midspan. A line was drawn on the girder beneath the string line with no load applied so that deflection of the specimen could be observed as the two lines diverged. String lines were also used to detect lateral deflections (sweep). Sections of steel tape were attached to the threaded loading rods mentioned earlier to monitor travel of the lower cross heads. Readings were taken for all deflection measuring devices at all load stages.

During shear tests, deflections were measured at the load point and midspan using dial gages. Lateral and roll motions were detected with dial gages at each end and at midspan. For Specimen 1, additional measurements were taken using a plumb bob at the load point to detect longitudinal or transverse movement of the specimen, and using a string line for approximate deflection measurements and photographic purposes. All deflection measuring devices were read at each increment of load.

5.6.3.2 Strand and Slab Slip. Frames were epoxied to ends of the girder to support dial gages that were used to measure both strand and slab slip (Fig. 5.22). The dial gages were capable of reading to within 0.001 in. These gages were read after each increment of load.

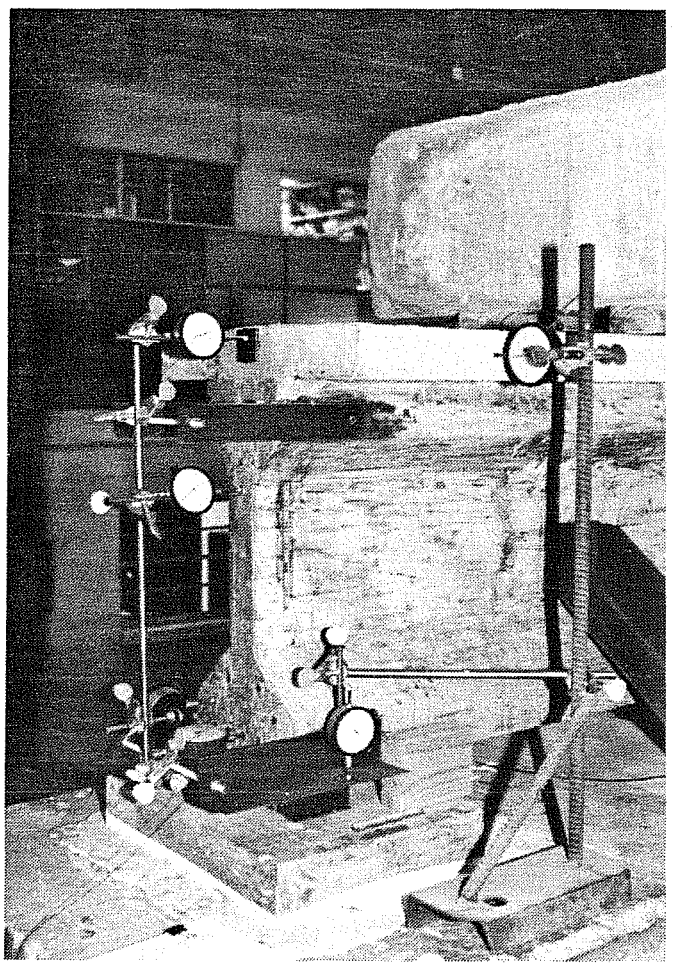

Fig. 5.22 Photograph of instrumentation at end of girder

5.7 Data Reduction

All data was recorded manually during the tests and was then processed by hand or entered into a microcomputer for manipulation and plotting. When data from more than one source was available to obtain a specific quantity, such as the prestress force or deflection at midspan, an attempt was made to reconcile any differences in readings in order to obtain the best estimate for the quantity.

CHAPTER 6

PRESENTATION OF LONG-SPAN GIRDER TEST RESULTS

6.1 Introduction

In this chapter, results of the long-span girder test series are presented. Each test is presented separately and in chronological order of testing. Where information or analysis procedures apply to more than one test, they will be described fully for the first use and the reader will be referred to that description for subsequent applications. Figures will contain an identifier in a box in one corner of the figure with "Sp 1" or "Sp 2" to represent Specimen 1 or 2, respectively. A suffix of "-N" or "-S" attached to the identifier indicates the end of the specimen being considered for shear test results.

The pretensioned, high strength concrete portion of each specimen is referred to as the "girder" throughout the fabrication and testing of the specimen. The completed composite section is composed of the pretensioned girder and the composite deck, and the extreme fiber of the composite section is the top of the deck.

A detailed chronology of the construction and testing of both specimens is given in Appendix B.

Following the presentation of test data, results of the tests will be compared. Examination of these data with respect to the topics considered in Chapter 3 is reserved for Chapter 7.

6.2 Specimen 1 (13 Strands)

In this section, behavior and properties of Specimen 1 prior to and during flexure and shear tests will be discussed. While the span of time from casting the girder to the flexure test was only approximately two months, a discussion of specimen behavior during that time period is included because of its significance in establishing effective stresses and strains at the time of the flexure test and in understanding the long-term behavior of the structure.

Specimen 1 was designed to fail near the balanced condition and therefore required more strands than the minimum needed to satisfy allowable stress design criteria. Four of the 13 strands were draped to control stresses at the ends of the section.

The first attempted flexure test, which will be referred to as the "initial flexure test" in the following discussion, was halted because of excessive lateral movement of the specimen and instability in the loading system. After this test, the loading system was redesigned so that the specimen could be pushed and then restrained laterally at the load points to maintain the reduced sweep (lateral deflection) and prevent lateral motion during the subsequent flexure test. The second flexure test, which will be referred to as the "flexure test", was conducted in two stages: the first was the loading to the cracking load, after which the specimen was completely unloaded; and the second stage, in which the specimen was loaded to failure.

Shear tests of the two ends of the flexure specimen also included cracking and failure tests. The tests are referred to by the location (south or north) of the end during the flexure test. At both ends, stirrups were provided at a spacing that corresponded to approximately $V_s = 8\sqrt{f_c'}\, b_w d$, which is the maximum quantity allowed by the codes. Standard open stirrups were used in the south end and stirrups which crossed under the center column of strands and were bent up at the corners of the section were used at the north end (see Fig. 5.5).

6.2.1 Prior to Flexure Test. This section presents material properties and reports observed behavior of the specimen prior to the flexure test.

6.2.1.1 Concrete Material Properties. Properties of girder and deck concrete were measured at intervals throughout the life of the specimen. Measured and estimated data at significant events are given in Table 6.1. Values were estimated when data was not available for the date on which an event occurred. Estimates were based on data presented in Appendix A. Strength gain with age curves are shown for both types of concrete in Fig. 6.1. Average stress-strain curves for the concrete at the time of the flexure test are shown in Fig. 6.2. Data for the curves were obtained from electrical resistance strain gages mounted on the surface of 6 by 12-in. cylinders. More data on the mix design and material properties are given in Appendix A.

Table 6.1 Concrete properties at significant events - Specimen 1

Event	Age	f_c'	E_c	f_r'
	(days)	(psi)	(ksi)	(psi)
Release				
Girder	7	10,200	(5,750)	
Deck Cast				
Girder	16	(12,000)	(6,250)	
Flexure Test				
Girder	64	12,500		
		12,900 S	6,400	(1,000)
Deck	48	3,260		
		3,490 S	3,800	
Shear Test of South End				
Girder	93	13,000		
Deck	77	(3,300)		
Shear Test of North End				
Girder	113	13,160		
Deck	97	3,300		

() - Estimated values, based on additional data presented in Appendix A.

S - Steel cylinder molds; otherwise plastic molds were used.

Note: All data are for cylinders cured with the Specimen 1 under ambient conditions.

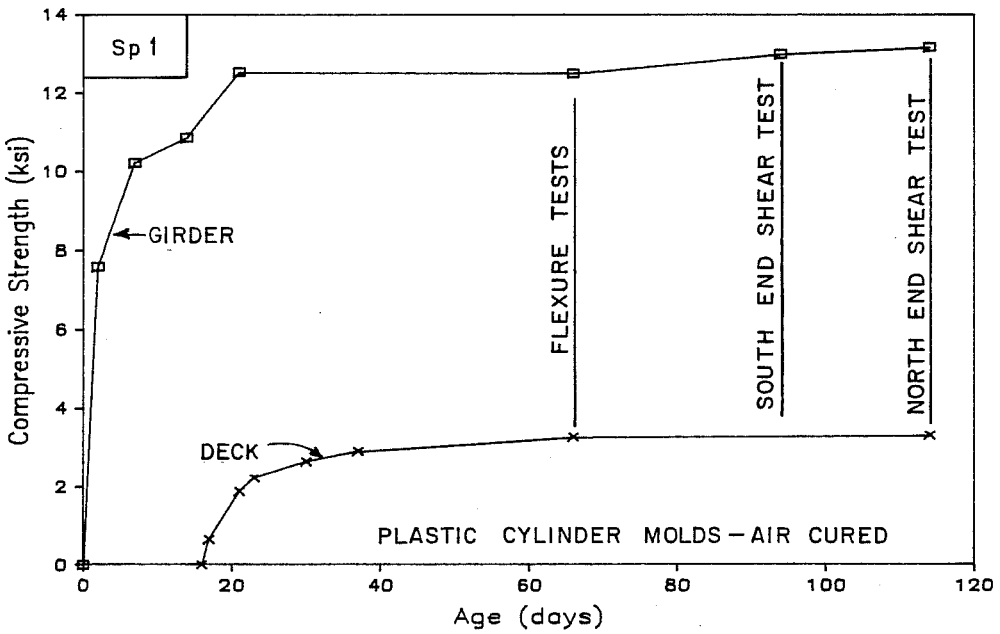

Fig. 6.1 Girder and deck concrete strength gain with age - Specimen 1

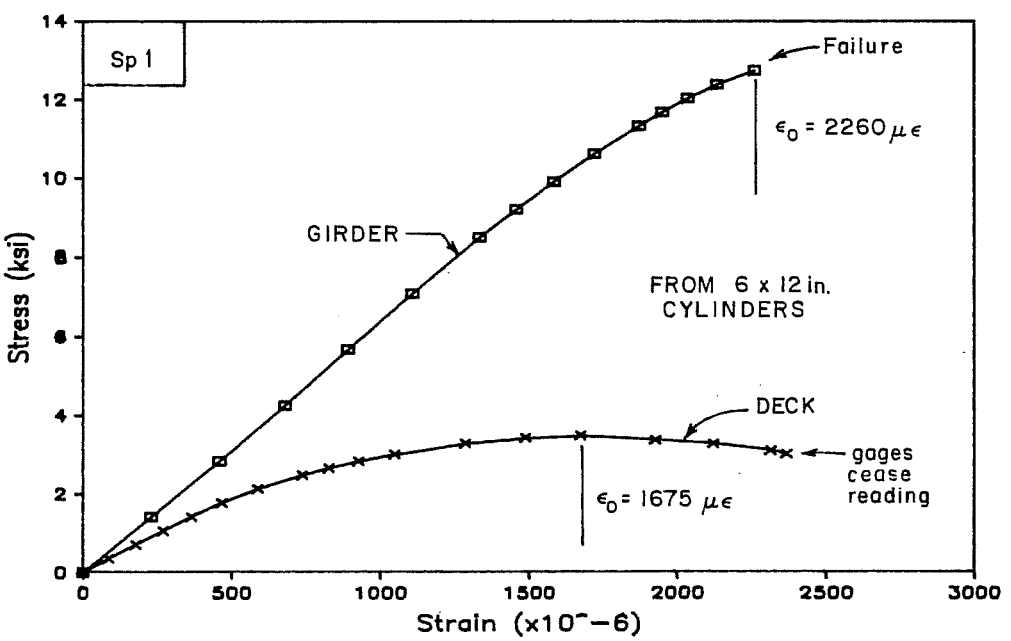

Fig. 6.2 Girder and deck concrete stress-strain curves at flexure test - Specimen 1

6.2.1.2 General Description of Behavior. A summary of specimen history, including times at which dead load compensation and deck formwork was added or removed, is given in Appendix B.

During initial stages of the transfer of prestress to the girder, a large crack and several smaller cracks formed at the south strand hold-down device, which was the first to be released (Fig. 6.3). Dead load compensation had not been placed on the girder prior to release because it had been determined that stresses after complete release were not sufficient to cause cracking of the girder. The crack formed because there was no precompression and insufficient dead load moment to resist the uplift force caused when the hold-down was released. Since there was no reinforcement in the top of the girder to limit its growth, the crack passed completely through the thickness of the girder and extended from the top of the girder into the taper of the bottom flange. No cracking was observed at the second hold-down because a longer span was available to produce dead load moment. The cracks closed when the prestress was fully released. Because the cracks closed and were located at a drape point outside the constant moment region of the flexure test, the cracks were expected to have no adverse effect on test results. Girder dead load compensation was added when deck forms were put in place three days after release.

The specimen was very flexible laterally. This, coupled with a significant sweep in the girder, caused excessive lateral movement in the specimen during the initial flexure test. The loading system

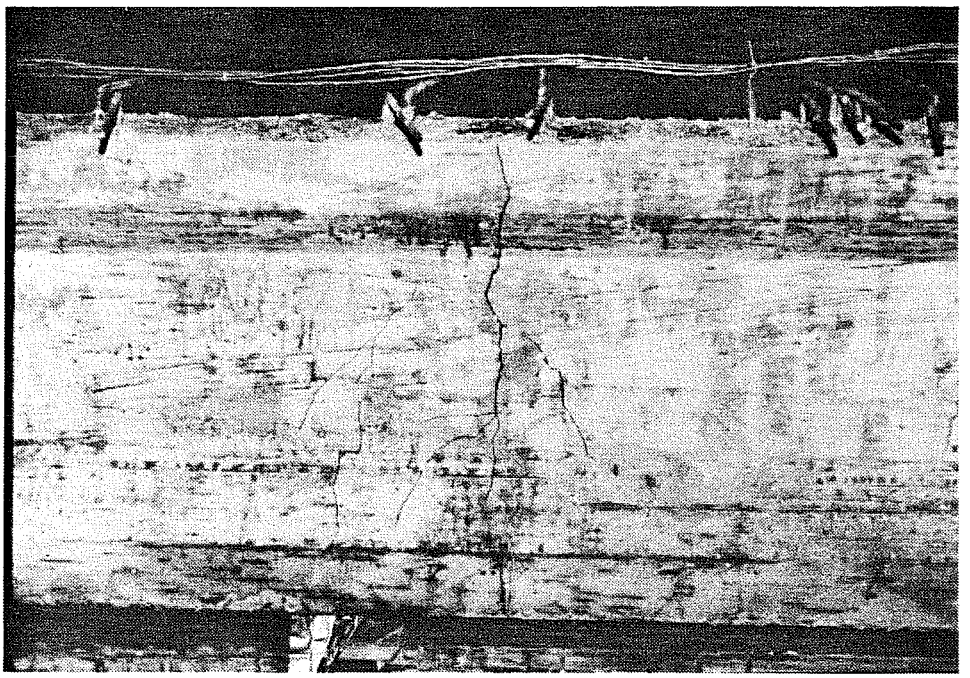

Fig. 6.3 Photograph of cracking at strand hold-down device at release

was modified to restrain lateral movement during testing and to allow reduction of the sweep, which was accomplished by pushing the specimen laterally at the level of the deck and maintaining the new position with the loading system.

Actual specimen are summarized in Table 6.2.

6.2.1.3 Deflections. Midspan girder deflections from time of release until the flexure test are shown in Fig. 6.4. Significant events are indicated on the figure. A deflection measurement using an optical level, which is also shown on the figure, agreed well with the data shown.

The effect of creep was evident as deflections increased significantly with time for the bare girder. After the deck was added deflections stabilized.

At release, a sweep of approximately 0.5 in. to the west was observed at midspan. While no measurement was made prior to the initial flexure test, at the maximum load of the initial flexure test, a sweep of 1.375 in. was measured. This reading decreased to 1.19 in. when the load was removed. After forcing the specimen laterally (to the east) at the load points, the sweep was decreased to about 0.375 in.

6.2.1.4 Effective Stresses and Strains. Strain readings for strands, girder concrete and deck concrete were corrected for time effects and discontinuities to obtain an "effective" strain for each

Table 6.2 Actual section dimensions - Specimen 1

Girder

Use Nominal Dimensions

Strand Placement

Distance from strands to bottom of girder, g

	Straight	Draped	Total
No. of Strands	9	4	13
North End	2.10"	14.71"	5.98"
Midspan	2.07"	4.58"	2.84"
South End	2.19"	14.91"	6.11"

Drape locations are 19.5' from ends of girder.

Deck

Width	16 5/8"
Thickness	2 5/16"
Offset *	5/16"

Overhang at Interior End during Shear Tests

North End	7'-7"
South End	5'-0"

Distance measured from center of support at interior end.

---

* - Offset is the distance from top of girder to bottom of deck. This area is filled with deck concrete and is as wide as the girder top flange.

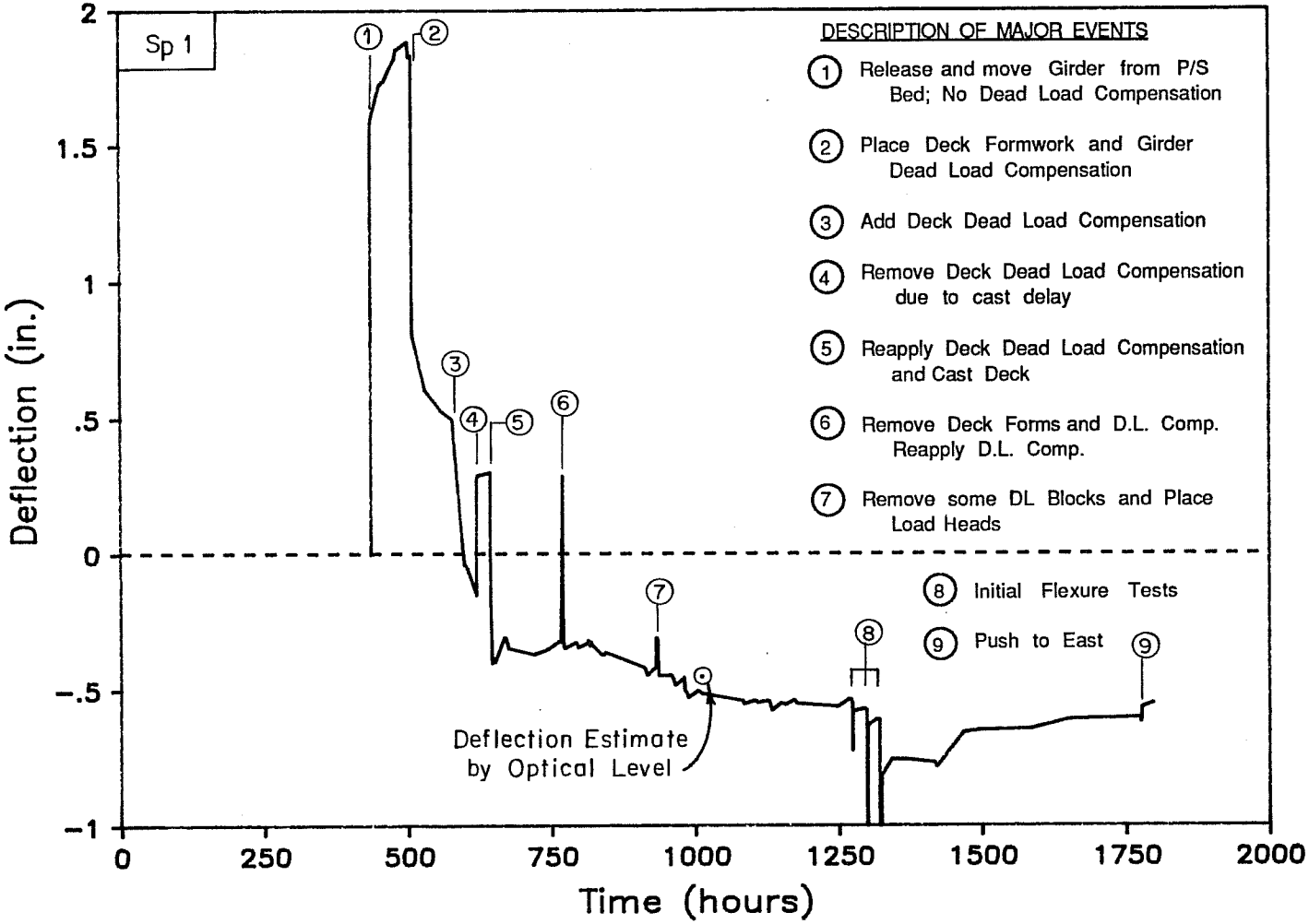

Fig. 6.4 Midspan deflection with time

gage. Corrected strains therefore represent an estimate of the elastic strain at a specific time.

For the strands, an effective strain was determined following full tensioning using elongation and strain data and considering the order of prestressing. Readings were adjusted to compensate for erratic losses in strain observed following placement of the girder concrete. Corrected strains were multiplied by the ratio of the "apparent" strand modulus (determined using strain gages attached to a single wire) to the "true" strand modulus (provided by the strand manufacturer) to obtain "true" strains. These true strains were used to determine strand stresses from the load-strain curve provided by the manufacturer and were compared with strains measured elsewhere in the specimen. Corrected strand strains at midspan for a typical straight and draped strand are shown in Fig. 6.5. The corrected strains and corresponding stresses were not adjusted for strand relaxation.

The strain at each row of strands was determined by interpolating between measured changes in strain for the two instrumented strands. These strains were used to determine an "average" strain at the centroid of all strands. Effective strand stresses and forces computed from the "average" strand strains are summarized in Table 6.3. Effective strand stresses at release were also computed using an elastic analysis and the effective strand stresses prior to release. Measured losses in strand stress were

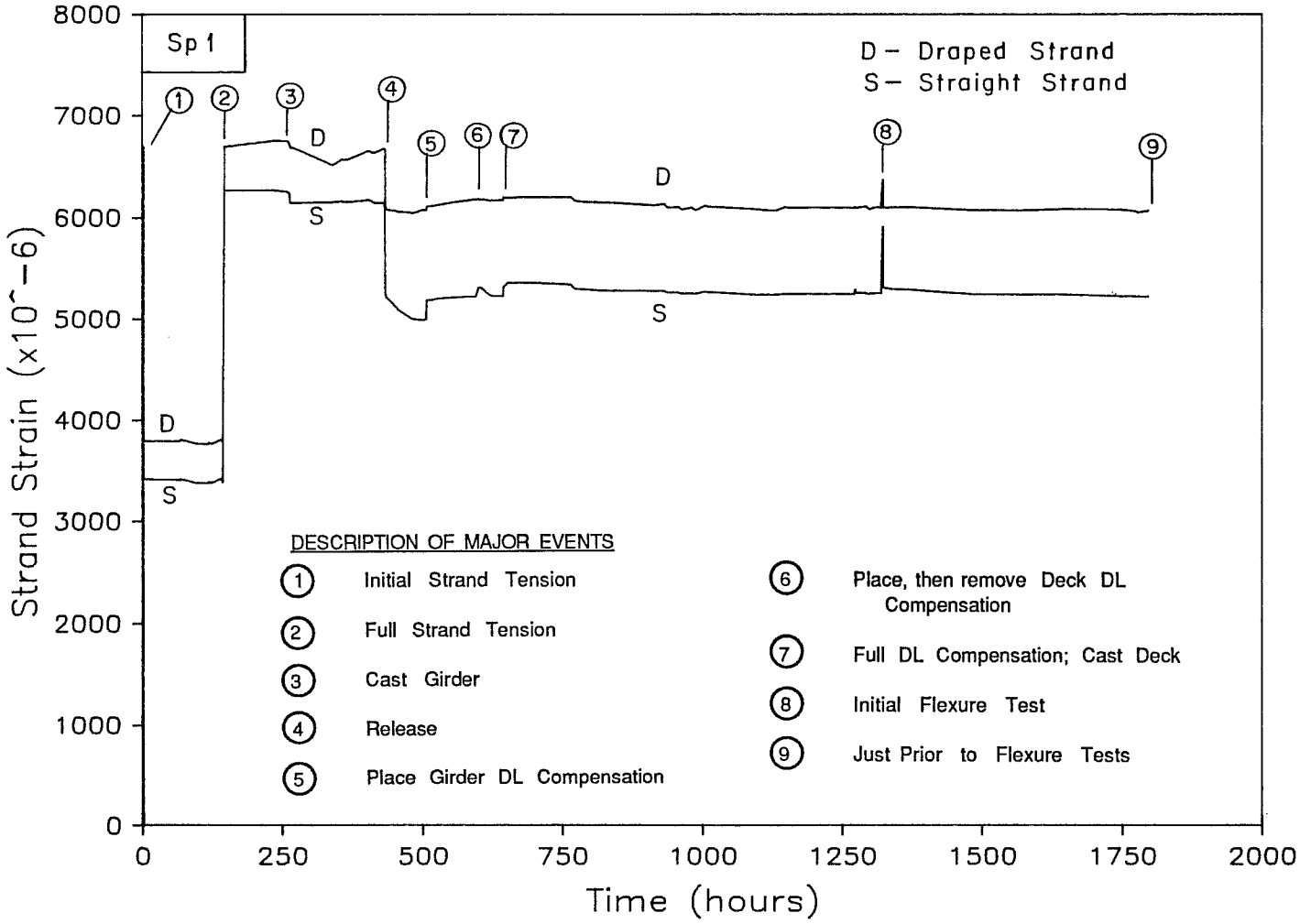

Fig. 6.5 Typical corrected midspan strand strains with time

Table 6.3 Effective strand stresses and forces - Specimen 1

	Stress (ksi)	Force (kips)
Full Tensioning		
All Locations	187.6	206.1
Prior to Release		
All Locations	181.7	199.6
After Release		
Midspan	159.6	175.3
Midspan *	159.6	175
North End *	164.2	180
South End *	164	180.6
Flexure Test		
Midspan	152.5	167.5
North End	147.5	162.0
South End	143.6	157.7
Shear Tests		
North End	143.1	157.2
South End	140.5	154.3

* - These values represent computed instantaneous elastic prestress losses plus 25%. The computed loss was increased by 25% to provide better agreement with the limited measured strain data. The elastic losses were calculated using the "Prior to Release" prestress force and gross section properties.

Area of prestressing steel = $13(0.0845 \text{ in.}^2) = 1.0985 \text{ in.}^2$

closely approximated when computed losses were increased by 25 percent. Therefore, this additional loss was added to obtain the computed stresses at both midspan and end to account for creep losses that occurred before readings were taken, and to provide a consistent basis for determining the effective strand stress.

Changes in strand strain at release near ends of the girder indicate a transfer length of less than 10 in. Combined data for active gages at both ends of the girder is shown in Fig. 6.6. Agreement between gages is quite good.

Girder concrete strains required correction for effects of creep which can be seen in the typical girder strain data shown in Fig. 6.7. Correction was complicated by a strong sensitivity of many gages to temperature which caused readings to fluctuate as much as 100 microstrains during a day. Initial creep corrections were made by subtracting changes in strain over periods where there was no change in load. When changes in load occurred, corrections were made by subtracting the difference between measured and computed changes in strain. Computed strains generally showed good agreement with measured data.

Measured and computed girder concrete strains at release are shown in Fig. 6.8a as they vary with the depth of the girder. Agreement between lines of gages at different locations is good. Agreement is also reasonable between measured strands and computed strains. Strain readings were taken shortly after release and may

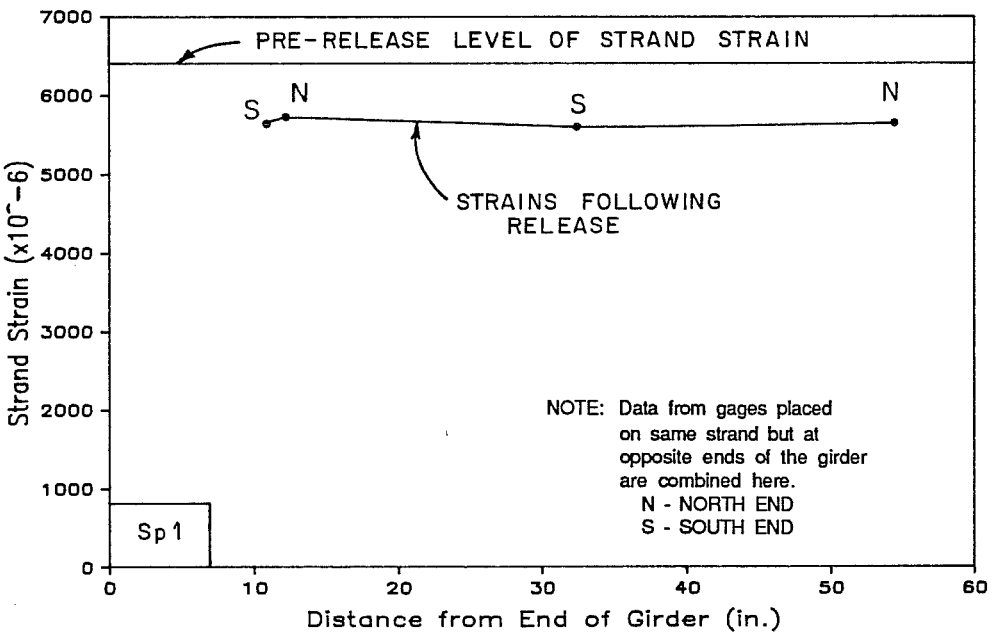

Fig. 6.6 Strand strains near ends of girder before and after release

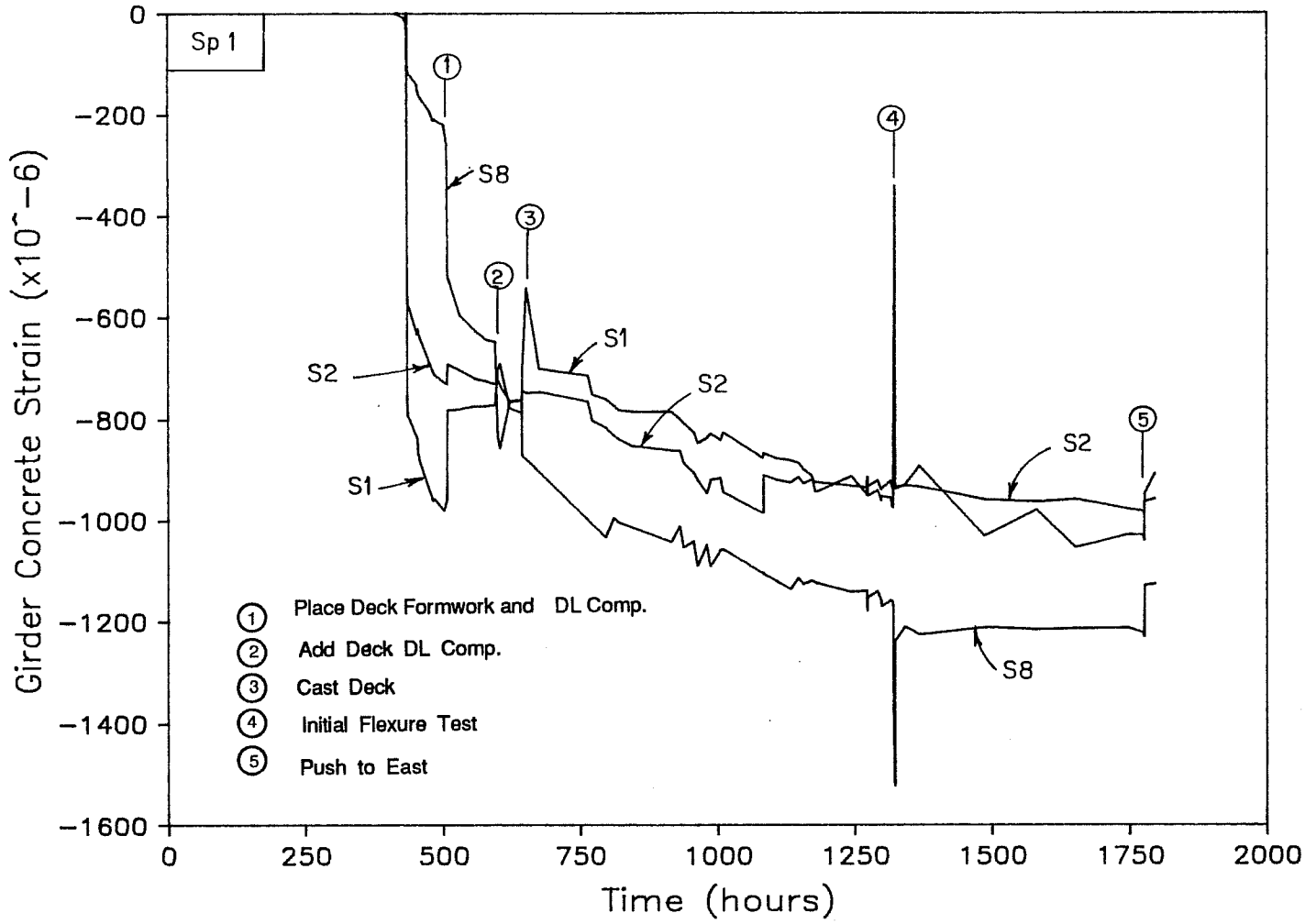

Fig. 6.7 Girder concrete strains with time for typical gages

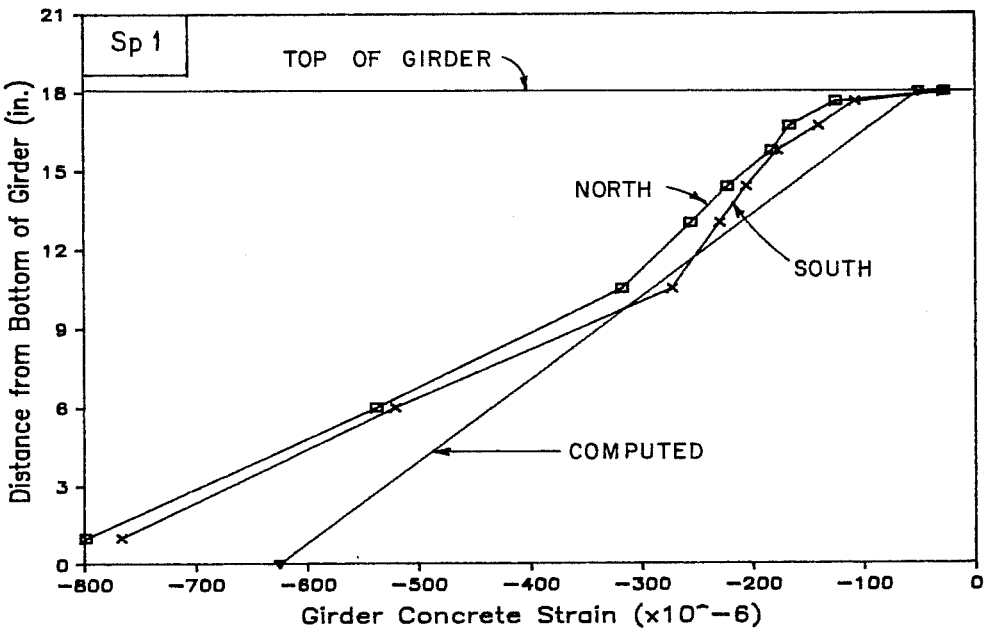

(a)

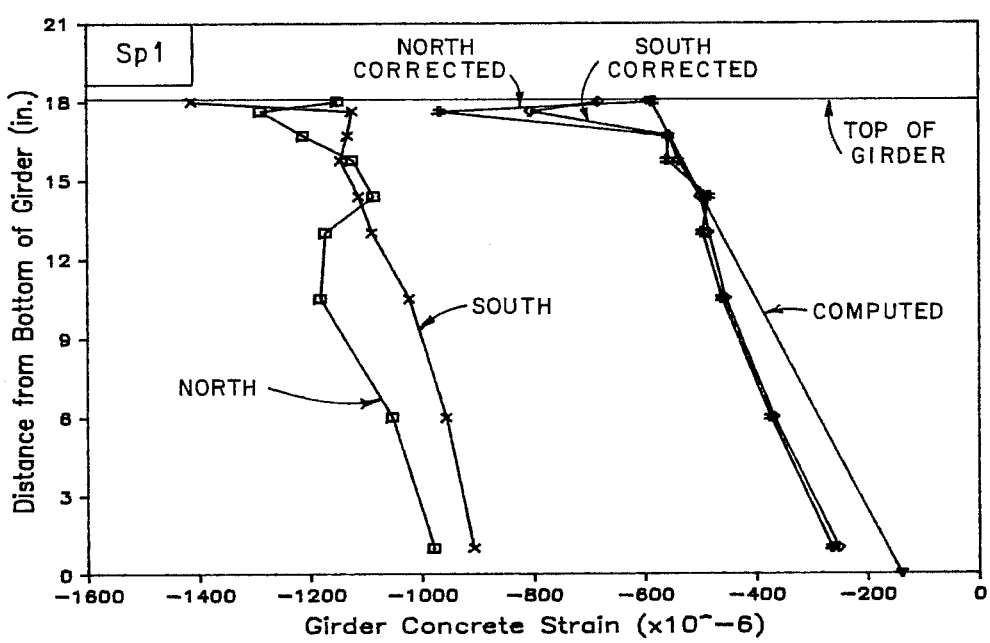

(b)

Fig. 6.8 Computed and measured girder concrete strains at release and prior to flexure tests: a) At release; b) Prior to ultimate flexure test

contain some creep. In the second plot (Fig.6.8b), corrected and uncorrected strains for both sets of gages prior to the flexure test are compared with computed strains. Agreement of the corrected strains is good between the two lines of gages and reasonable for computed strains. The variation between measured and computed strains at release and between corrected and computed strains at test are similar.

Most of the creep in the girder concrete had occurred by the time of the flexure test as indicated by Fig. 6.7. The magnitude of creep during this period was approximately 600 microstrains and was fairly uniform across the section (Fig. 6.8b).

The deck concrete was instrumented after removal of the deck forms and replacement of the dead load compensation. Typical top and bottom deck strain data prior to the flexure test are shown in Fig. 6.9. Strains and changes in strain are shown for all deck gages at three times in Fig. 6.10. Measured strains were caused mostly by creep because the only sustained elastic change in load that the deck experienced while gages were active was due to forcing the specimen to the east to reduce the sweep. Effective strains at the beginning of the flexure test were therefore considered to be the strains caused by the lateral push (Fig. 6.10), and the elastic strains caused by removal of the deck forms were neglected because calculations showed that the strains were insignificant.

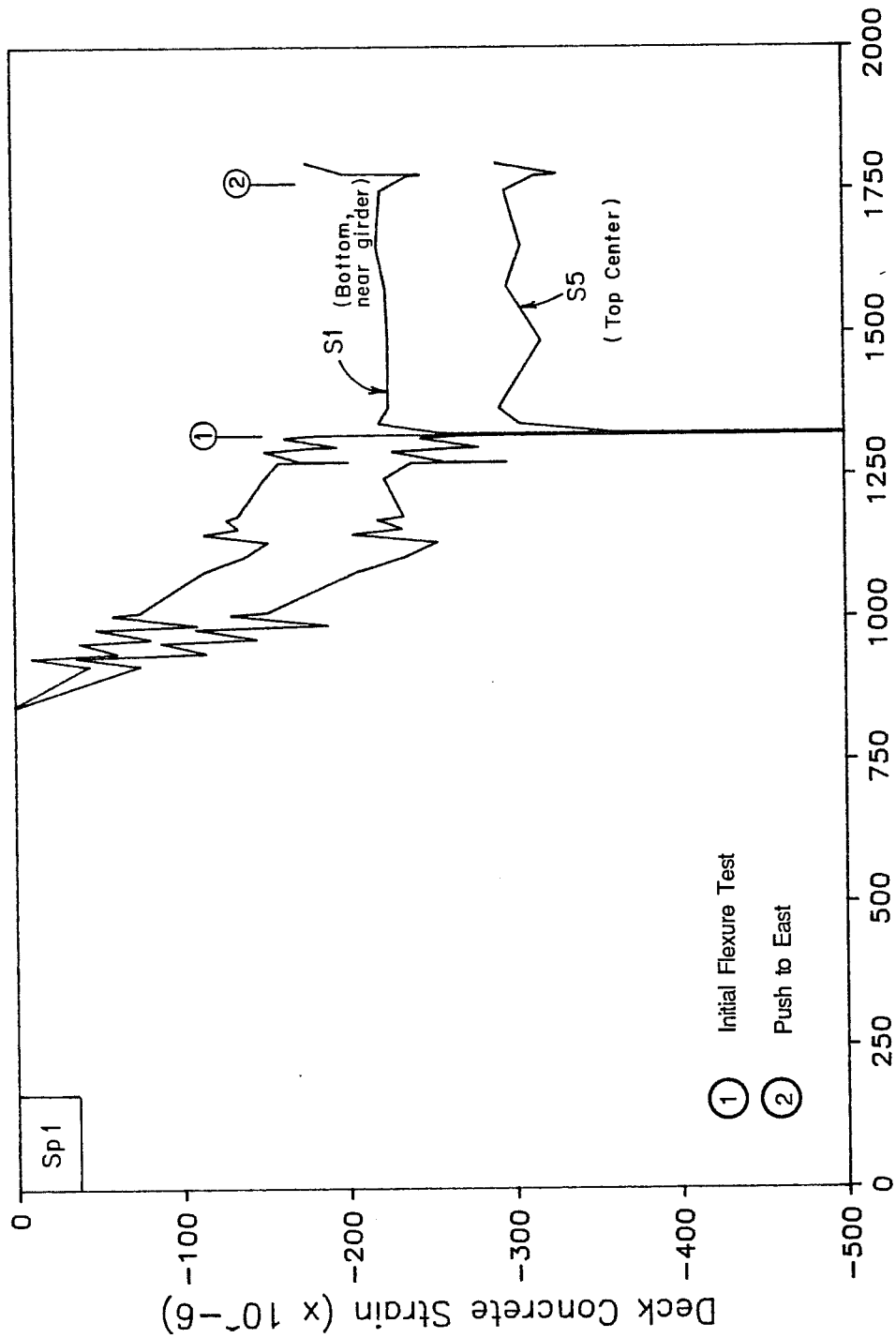

Fig. 6.9 Deck concrete strains with time for typical gages

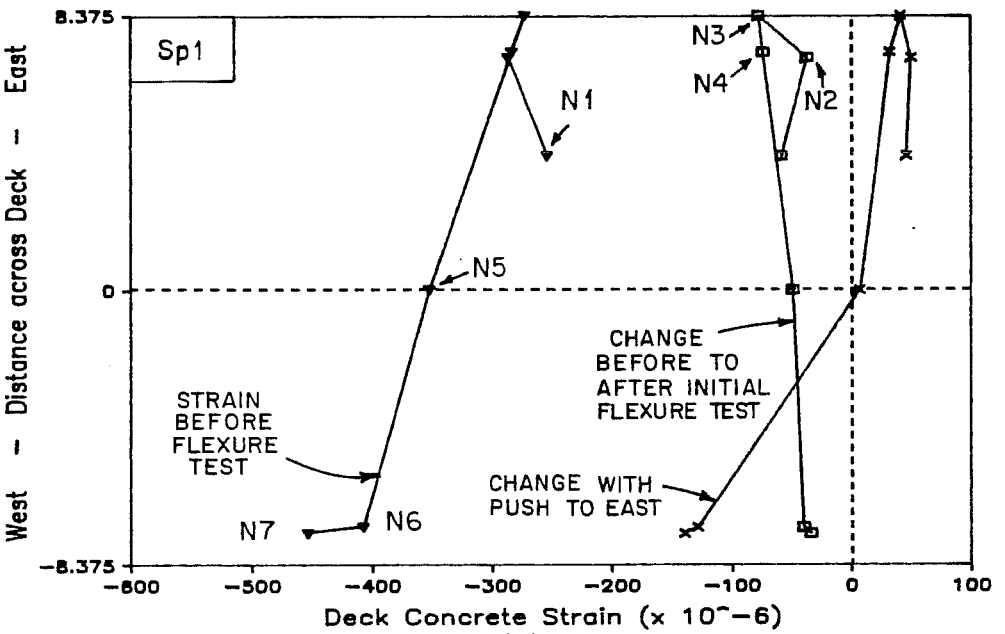

(a)

See Fig. 5.19 for Gage Location

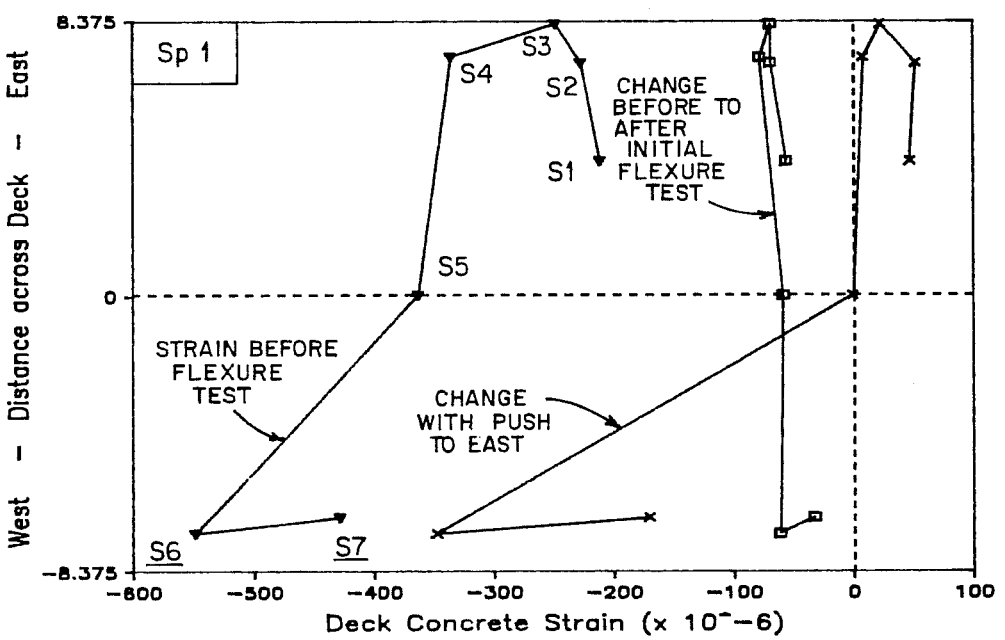

(b)

Fig. 6.10 Deck concrete strains at selected time: a) north gages; b) south gages

Deck strains were not as well behaved as the girder strain data. Some gages were erratic and some trends in the data could not be explained. Data indicate that the deck was either previously cracked or cracked when pushed to the east, because compression strains measured on the west side of the deck were significantly larger than the tensile strains measured on the east side. No deck cracking was detected before or after the lateral push. Any deck cracking would affect behavior and strains measured during early stages of the flexure test because cracks would have to close before the east side could develop additional strain.

Creep strains before the flexure test amounted to nearly 400 microstrains at the top of the deck and 250 microstrains at the bottom of the deck. By the time of the test, creep had slowed significantly, which agreed with similar behavior observed in the the girder. Nearly 100 microstrains of the creep occurred during the initial flexure test.

Stirrup strains from just prior to release until the time of the shear tests are shown in Fig. 6.11 for active gages at each end. No corrections to the readings were necessary. Gage N3 appeared unreliable and was disregarded. At release, small tensile strains were recorded in the stirrups, but no cracking in the web of the girder was detected. By the time of the flexure test, stirrup strains had changed approximately 200 microstrains in compression which indicates continuing shrinkage in the concrete. These strains do not

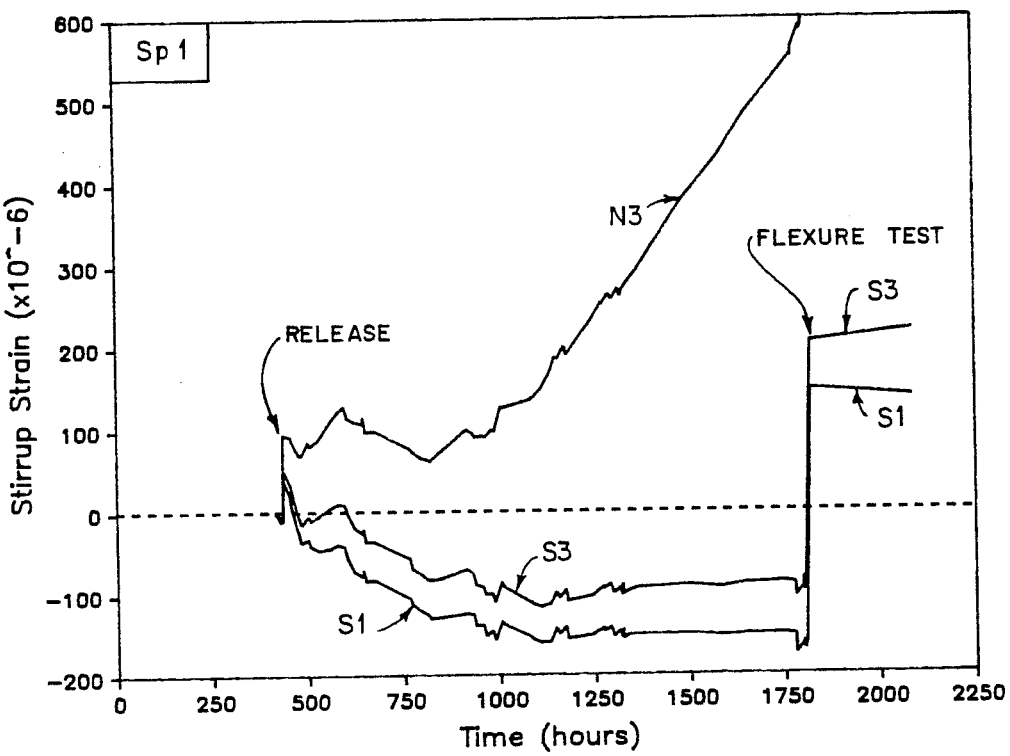

Fig. 6.11 Stirrup strains with time

include shrinkage strains that occurred prior to release. A large increase in strain occurred at the end of the flexure test and is discussed later in this chapter.

6.2.2 Flexure Test.

6.2.2.1 General Description of Behavior. The initial flexure test was halted due to excessive lateral movement of the specimen and rolling of the cross heads. After modification of the load system, the flexure test was performed in two stages: cracking and ultimate (failure). Load stages and corresponding times are given for both stages of the flexure test in Appendix B. Deflection readings were taken at all load stages while strain readings were taken at selected loads. Load stage designations represent the applied load at each load point. Load stages used in marking cracks are slightly higher than actual loads because of a later calibration of the load system.

The initial flexure test was conducted in the same manner as the later tests. At a load of 5.66 kips, a single crack appeared on the west side of the girder under the south load point and extended to the bottom of the web. The next cracks were found three load stages later at 6.40 kips, and an additional crack was observed at 6.89 kips. These cracks were also located near the load points, appeared only on the west side, and were limited to the bottom flange. Two of the cracks were extensions of the cracking which occurred at release. After a load of 7.14 kips was reached, the load was removed.

An altered load system was then constructed. Prior to the flexure test, the specimen was pushed laterally to remove some of the sweep. The modified load system provided restraint to maintain the reduced sweep.

A separate cracking test was performed in order to make possible the observation of cracked section behavior in the subsequent ultimate test. The limited cracking which occurred during the initial flexure test had a minor effect on the results of the cracking test. The loading system and procedure were identical to those used in the ultimate test.

Loading for the cracking test commenced by placing the weight of the upper cross heads on the specimen. Because this weight completed the full dead load compensation, this condition was considered to be zero applied load. Cracking of concrete was heard at 5.41 kips but no cracks were observed. At the next load stage, 5.66 kips, cracks present from the initial flexure test began to open. At 6.15 kips, cracking was observed on the east side which was uncracked during the initial flexure test. These cracks extended across the bottom of the girder and were limited to the bottom flange. After a maximum load of 7.38 kips was reached, the specimen was unloaded.

The second stage of the flexure test, the ultimate test, was then begun. The first new crack observed during the ultimate test occurred at 6.89 kips. Cracks extended into the web at 7.87 kips. At 9.35 kips, cracks reached midheight of the web (Fig. 6.12), and the

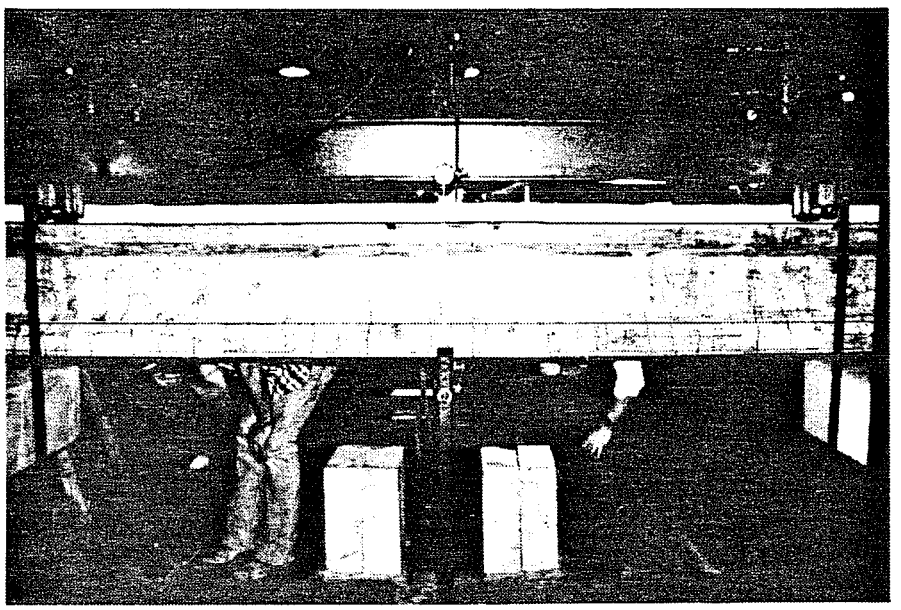

Fig. 6.12 Photograph of crack pattern at load of 9.35 kips during ultimate flexure test - Specimen 1

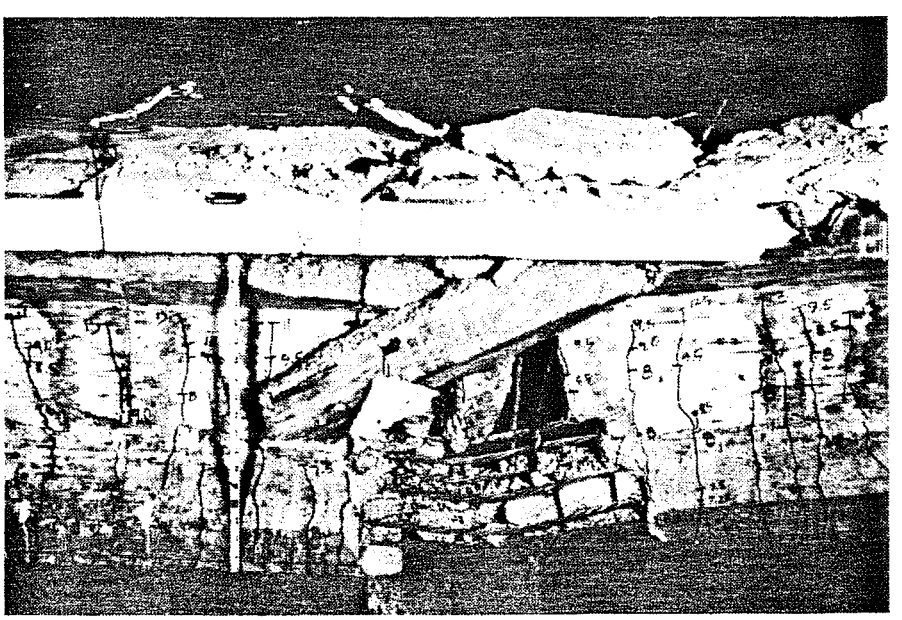

Fig. 6.13 Photograph after flexural failure - Specimen 1

deflection was held by the lower cross head while the rams were retracted and the upper cross head was reset. Cross heads and rams were reset again at 12.30 kips. At 12.79 kips a few cracks extended to the bottom of the taper of the top flange, while most ended approximately one in. below the taper (see Fig. 6.13). Cracks were well distributed but were not wide even though the deflection had increased noticeably in reaching this load stage. Inclined flexure cracks outside the constant moment region also increased in length during this load stage. As a load of 13.29 kips was reached, the specimen failed explosively in compression less than one foot south of midspan. The only warning of collapse was a small quantity of concrete dropping to the floor seconds before crushing. It was not clear whether the falling concrete was from the deck or girder.

The failed specimen is shown in Fig. 6.13. Although the specimen fell only aproximately one in. to the cribbing placed beneath it, the force of impact was sufficient to straighten steel hooks from which the dead load blocks were hung. Secondary failure cracks formed along the junction of the web and bottom flange, and branched upward into the web. The ends of the girder were thrown up into the air and drawn inward causing the bearing pads to roll off the concrete support pedestals. The sudden increase in stirrup strain after failure, which was mentioned earlier (Fig. 6.11), suggests that the ends of the girder may have cracked sufficiently at failure to leave permanent strains in the stirrups. However, no shear cracks were found in the web after failure. A dead load block that had been

resting on the deck at the north end was thrown off, landing on the edge of the deck and knocking out a v-shaped piece of the deck. This was later patched and did not affect the shear test.

The failure surface was typical of a compression failure. The surface was an inclined plane originating in the top of the girder and continuing through the deck (Fig. 6.14a). When viewed from above, the failure surface was wedge-shaped with its point over the girder (Fig. 6.14b). The appearance of the failure surface did not provide conclusive evidence for determining whether the girder or deck concrete crushed first.

Flexure cracks were well distributed during the test and remained narrow at all levels of load. At the conclusion of the cracking test, cracks near midspan were spaced at approximately 7.5 in. Prior to failure, cracks formed in the bottom flange between load points at a uniform spacing of approximately 3 in.

The loading system was successful in preventing excessive sway during the test.

Significant events during the flexure test are summarized in Table 6.4, which also includes computed and design loads of interest. The computed and design loads were based on the effective prestress force and material and section properties given earlier in this chapter. Live load plus impact was the applied load at which bottom fiber stress was computed to be $6\sqrt{f_c'}$ The impact factor was computed using the prototype span of 146 ft. AASHTO load factors were used to determine the factored load. Nominal capacity was computed

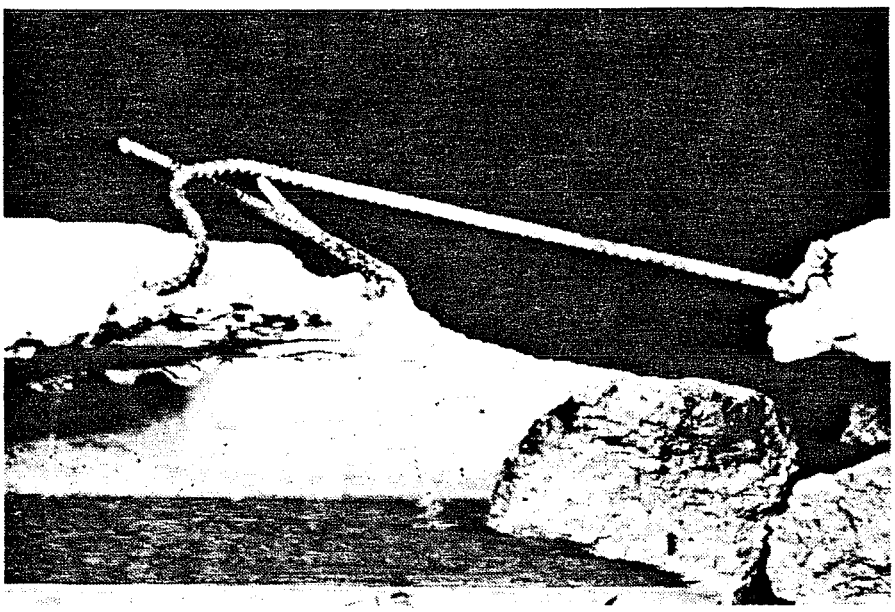

(a)

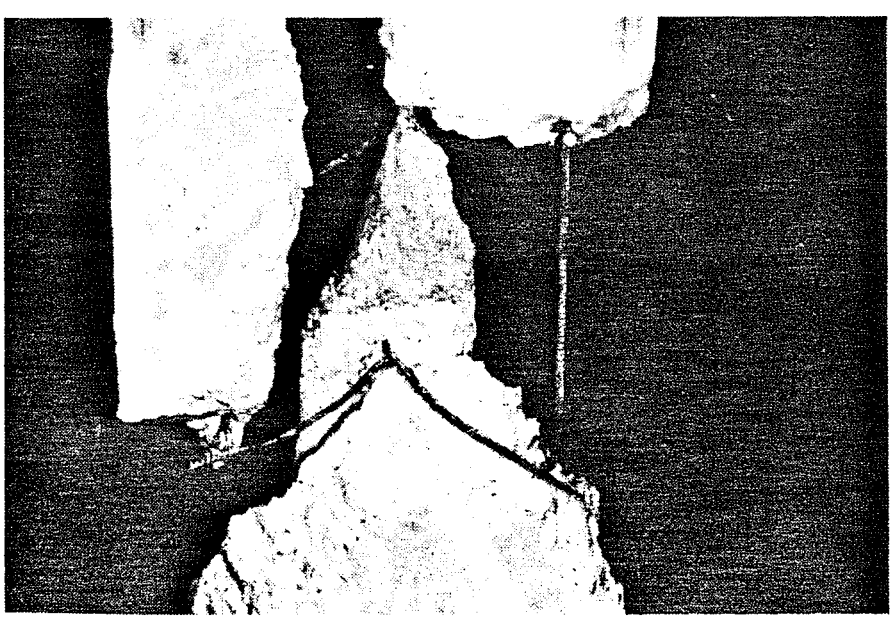

(b)

Fig. 6.14 Photographs of concrete failure surface after flexural failure - Specimen 1: a) side view; b) top view

Table 6.4 Load stages of interest during flexure tests - Specimen 12

Key (Fig. 6.15)	Description of Load Stage		Load (kips)
Computed and Observed Behavior			
CD	Computed Decompression	$0\sqrt{f_c'}$	1.89
CC	Computed Cracking	$(7.5\sqrt{f_c'})$	3.69
O	Observed Crack Opening		5.66
C	Observed Cracking	$(17.8\sqrt{f_c'})$	6.15
R	Reset Loading System		9.35
R	Reset Loading System		12.30
U	Ultimate (Maximum) and Failure Load		13.29
CW	Computed Web Cracking at h/2		25.16
Design Loads			
	Service Loads:		
LL	Live Load		2.81
LI	Live Load + Impact	$(6\sqrt{f_c'})$	3.33
FL	Factored Load (AASHTO)		8.79
NC	Computed Nominal Capacity (ϕ = 1.0)		11.14
Total Reaction at Ultimate Load			21.85

* - Impact factor computed using prototype span of 146 ft.

Note: "Load" is the force applied at each load point.
"Computed Nominal Capacity" is the difference between the nominal moment capacity computed using AASHTO procedures and the actual dead load moment divided by the shear span during the flexure test.

using AASHTO and ACI procedures because application of AASHTO equations was not clear in this case. Test results are compared with computed and design loads later in this chapter and in the next chapter.

6.2.2.2 Deflections. Net deflection at midspan is shown in Fig. 6.15 for both cracking and ultimate flexure tests with loads from Table 6.4 indicated on the figure. Readings were corrected for compression of the bearing pads. Cracking apparently occurred prior to visual detection because the curves deviate from initial linear behavior at 3.5 to 4 kips. Agreement between the cracking and ultimate test data is good with the ultimate test data showing slightly greater flexibility. Some difference in the plots is caused by a lack of readings at low loads, which may obscure actual behavior.

Resetting the load system clearly affected specimen behavior as evidenced by the offsets in the curve. These offsets indicate that, while the deflection was held constant, time effects allowed the stresses, and therefore the load, to drop. This required additional deflection to regain the load that had been on the structure, thus producing the observed offset. Readings were not taken during reloading after resetting the loading system.

The shape of the curve near failure indicates that yielding did not occur. This is corroborated by the observation that crack openings were not wide prior to failure. However, the deflection at failure was large, indicating a substantial capacity for energy

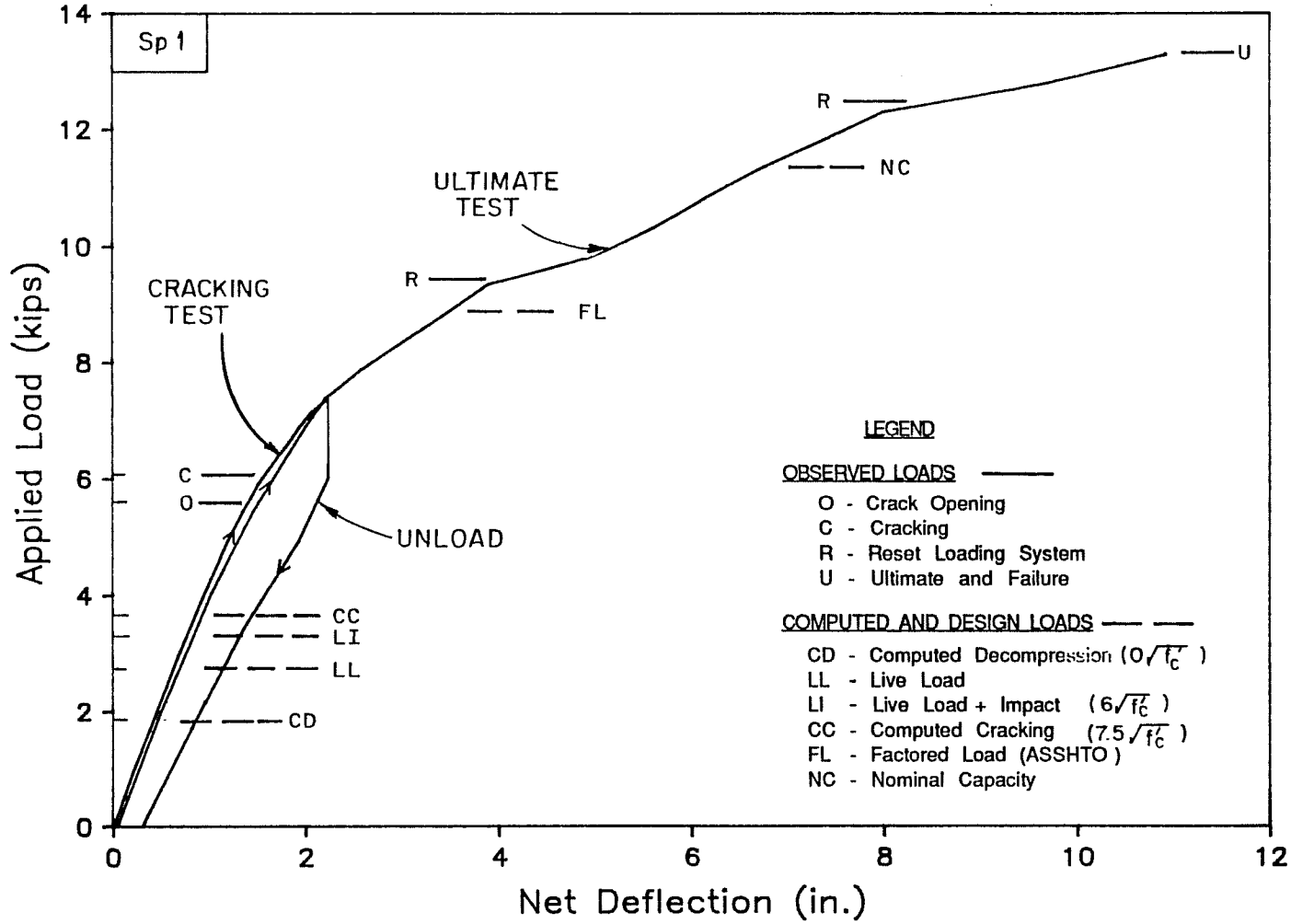

Fig. 6.15 Net deflection at midspan during flexure test

absorption, and providing ample warning of impending collapse in a structure in service.

6.2.2.3 Strand and Concrete Strains. Corrected strand strains for the instrumented strands are shown in Fig. 6.16 with the average strain which represents the strain at the centroid of the strands. Because strain data at failure were not available but the deflection was known, strains at failure were estimated by applying the ratio of the increase in deflection during the final load increment to the increase in deflection during the preceding load increment to the strain readings from the preceding load stage. Points or groups of points corresponding to these estimated values are enclosed in parentheses. Average strand stresses are shown in Fig. 6.17.

At failure, the average strand strain exceeded 1 percent, which is the strain used to define yield in ASTM A416 [25]. However, both the bottom strand strain and the average strand strain failed to reach a strain corresponding to the 0.2 percent offset.

Corrected girder concrete strains during the flexure test appear in Fig. 6.18. Strains at failure are estimated from load-deflection data as previously mentioned. Strains for the upper gages are presented with respect to gage location for selected loads in Fig. 6.19. The gages behaved well throughout the test as demonstrated by the net strain plots of Fig. 6.20 and 6.21 which correspond to plots of corrected strains in Fig. 6.18 and 6.19. Strains from both sides of the girder near the top are shown in Fig. 6.22 and indicate that

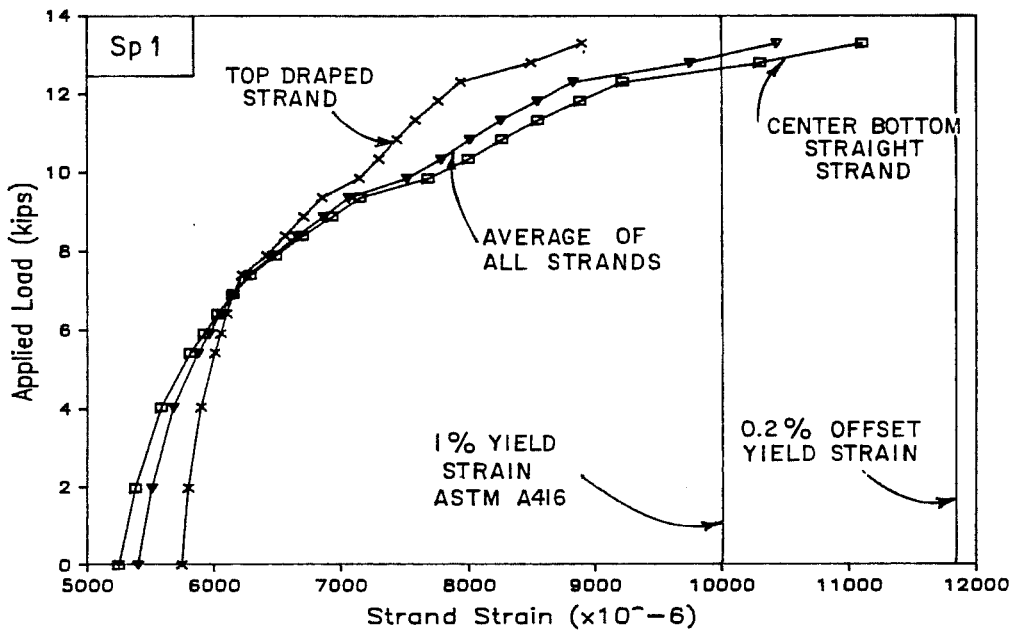

Fig. 6.16 Corrected and average strand strains during ultimate flexure test

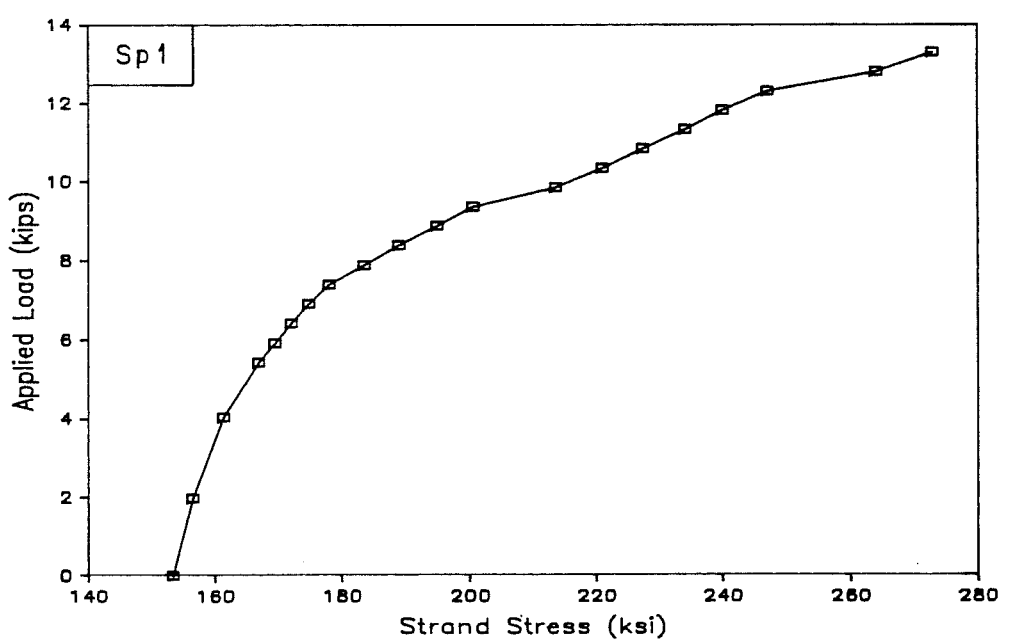

Fig. 6.17 Average strand stress during ultimate flexure test

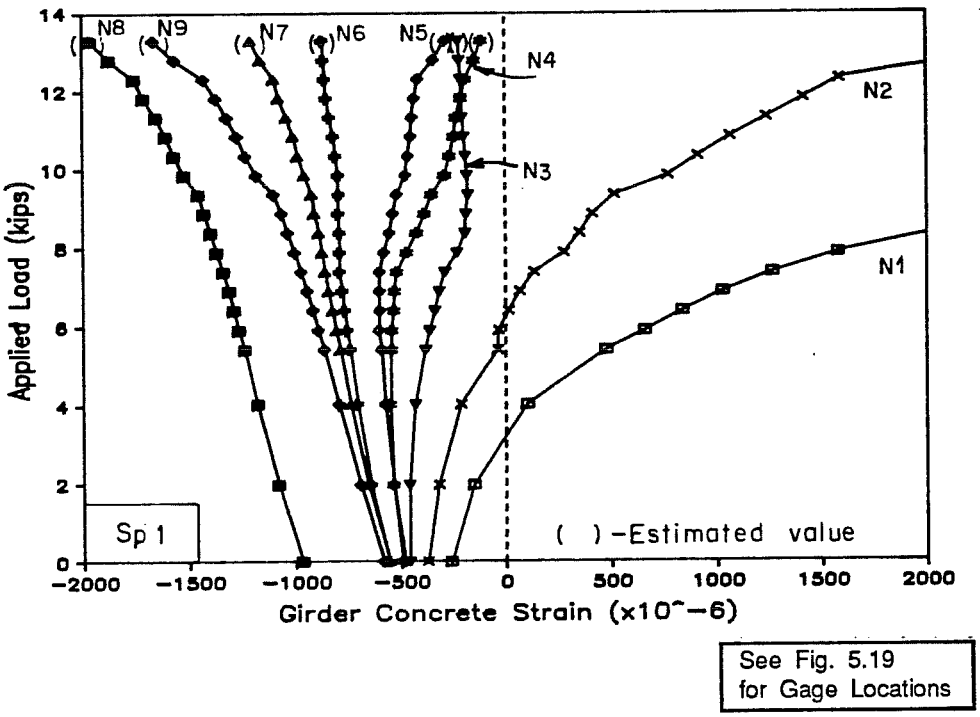

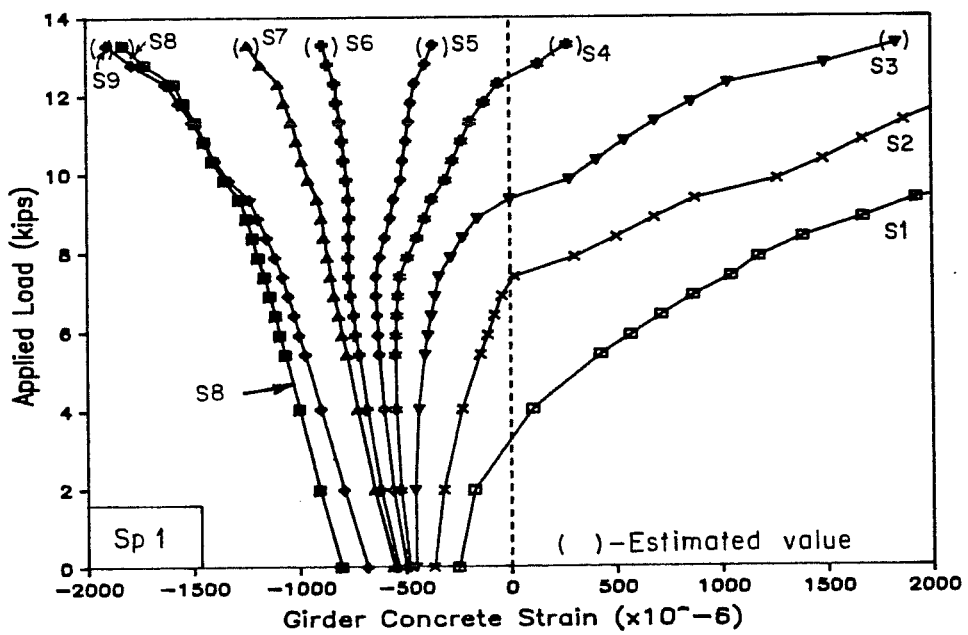

Fig. 6.18 Corrected girder concrete strains during ultimate flexure tests: a) north gages; b) south gages

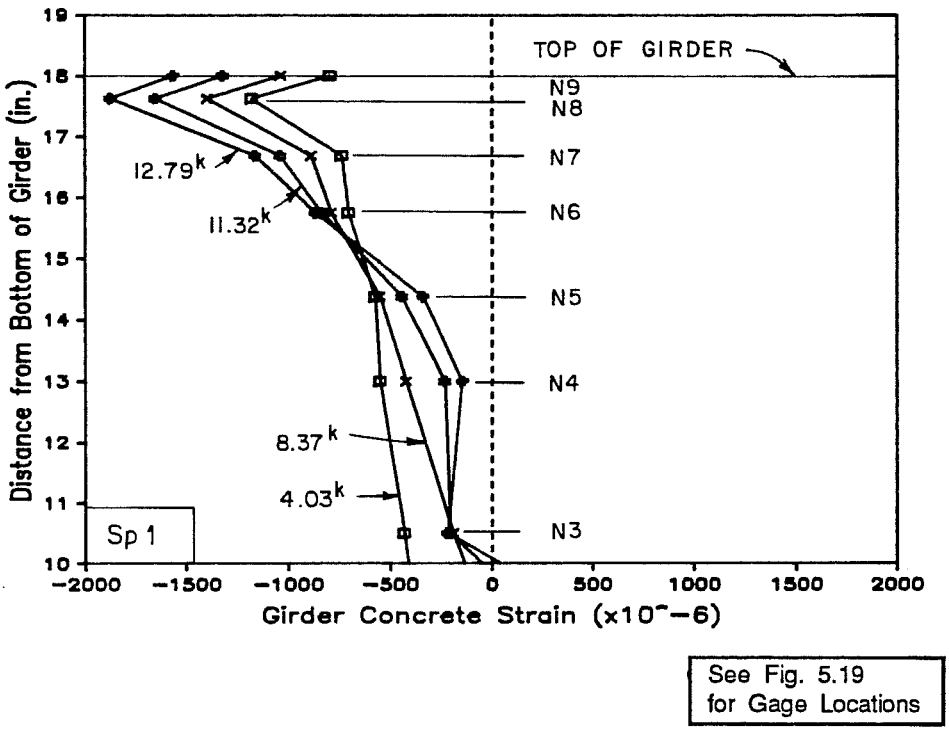

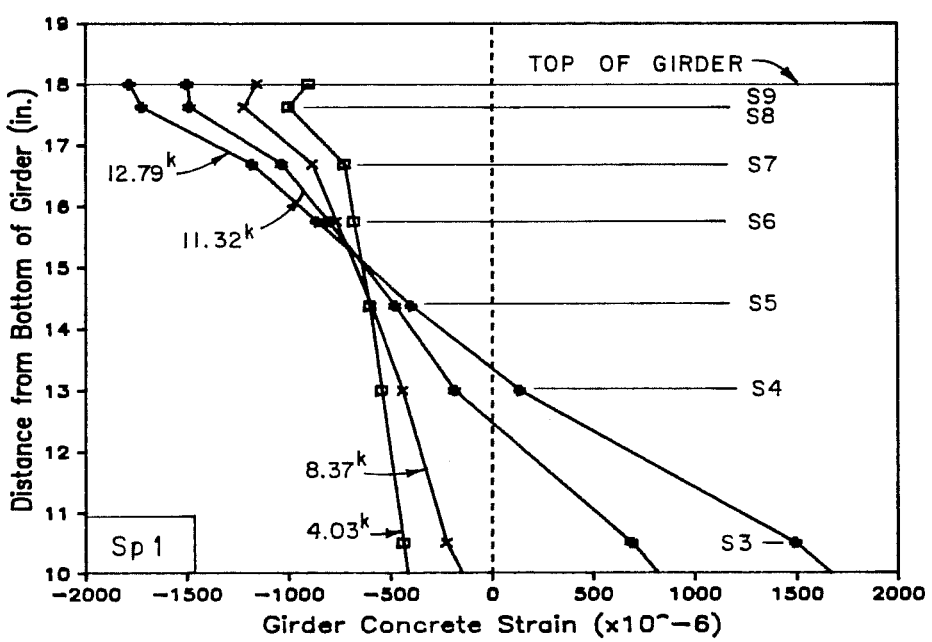

Fig. 6.19 Corrected girder concrete strains at selected loads during flexure test: a) north gages; b) south gages

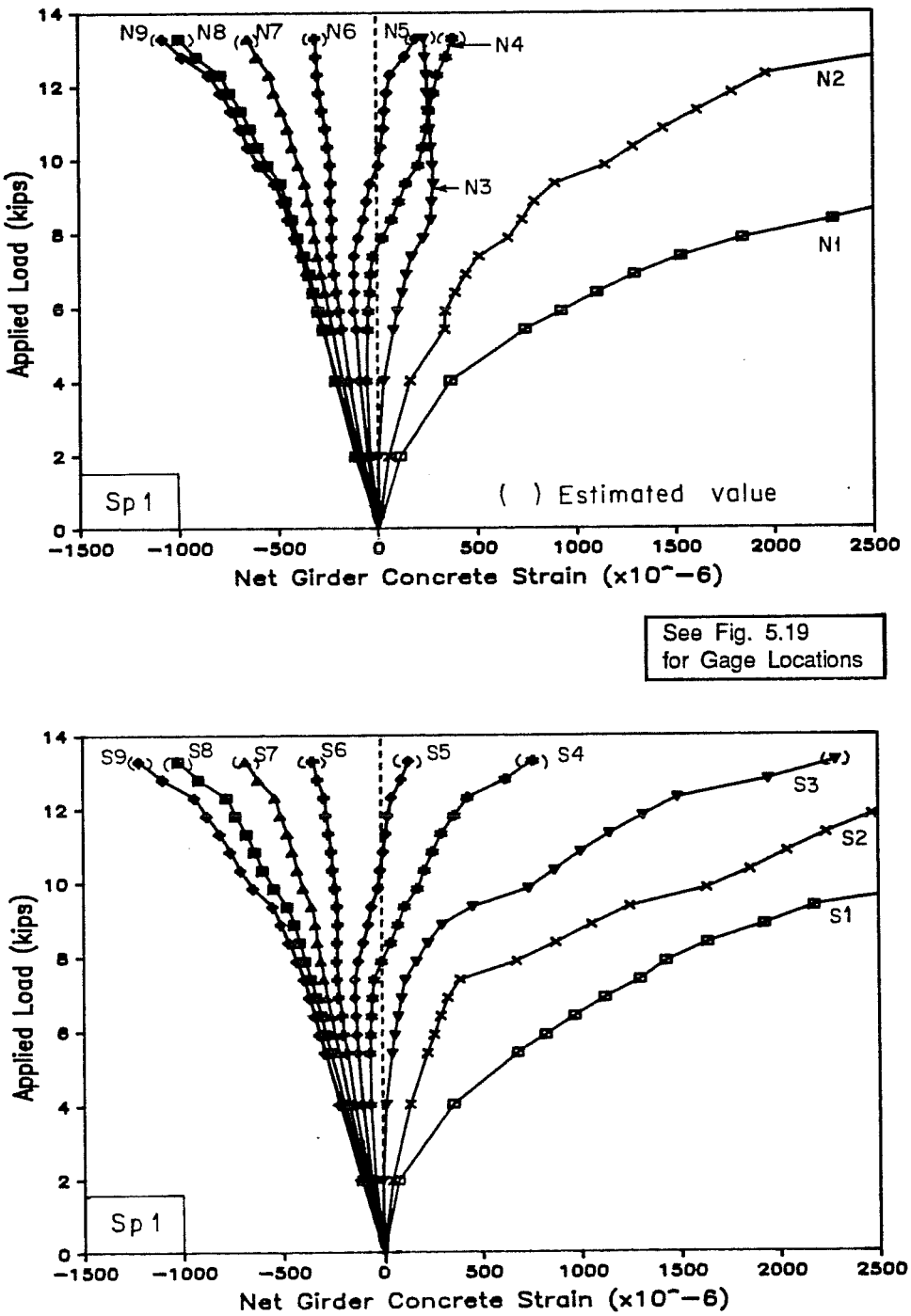

Fig. 6.20 Net girder concrete strains during ultimate flexure test: a) north gages; b) south gages

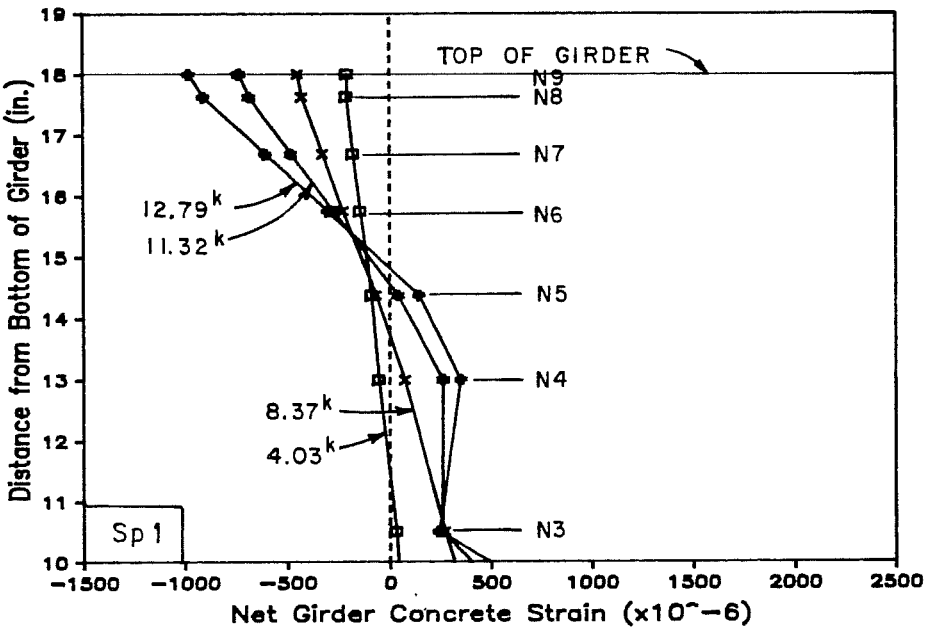

See Fig. 5.19 for Gage Locations

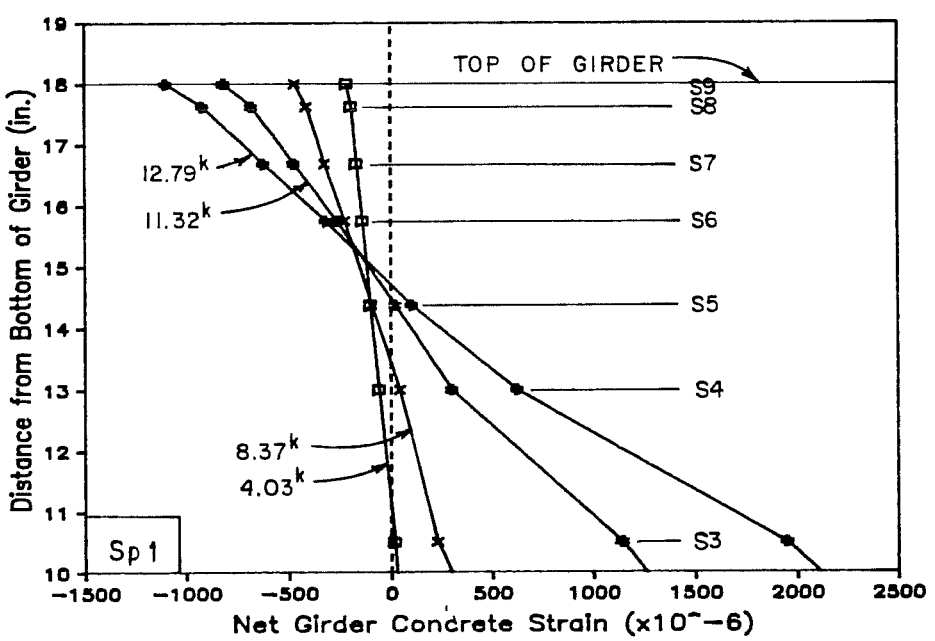

Fig. 6.21 Net girder concrete strains at selected loads during ultimate flexure test: a) north gages; b) south gages

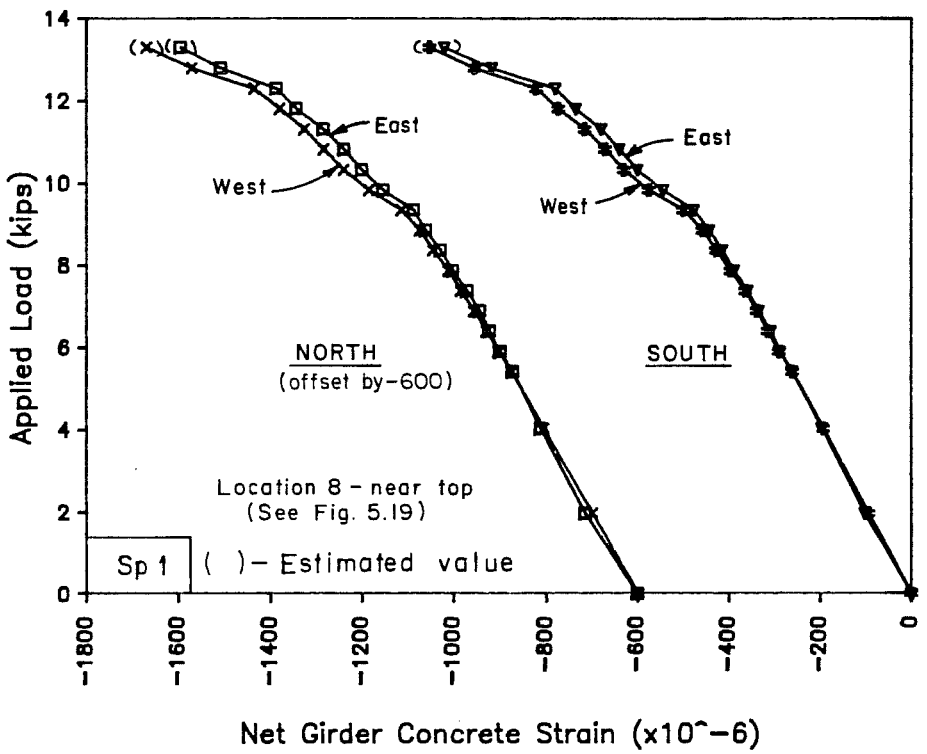

Fig. 6.22 Net concrete strains on opposite sides of girder during ultimate flexure test

the girder was not experiencing significant lateral movement during the flexure test.

At failure the strain at the top of the girder was nearly 2000 microstrains, which is close to the strain at maximum stress and failure for cylinder tests of girder concrete. Strains at the top of girder are consistent with nearby gages as demonstrated by comparing them with strains computed for the top of the girder using net strain data from two lower gages shown in Fig. 6.23.

The crack height computed using corrected girder strains is shown in Fig. 6.24. The computed crack height was approxi- mately 13.5 in. at failure, which is at the bottom of the taper of the top flange and agrees with visual observations.

Corrected deck concrete strains are shown for typical top and bottom gages in Fig. 6.25. Data from all deck strain gages are presented in Fig. 6.26 with respect to the gage location for selected loads. The increasing and pronounced strain gradient across the deck indicates asymmetrical behavior. Some of the gradient was caused by the lateral push of the specimen, but this would be a small, constant value. Lateral movement during the test did not appear sufficient to produce a strain gradient of this magnitude and no other explanation was found.

At failure, strain at the top of the deck was estimated to be between 1600 and 2400 microstrains. These strains equalled or exceeded the strain at maximum stress and approached the maximum strains which were measured during cylinder tests (see Table 7.3).

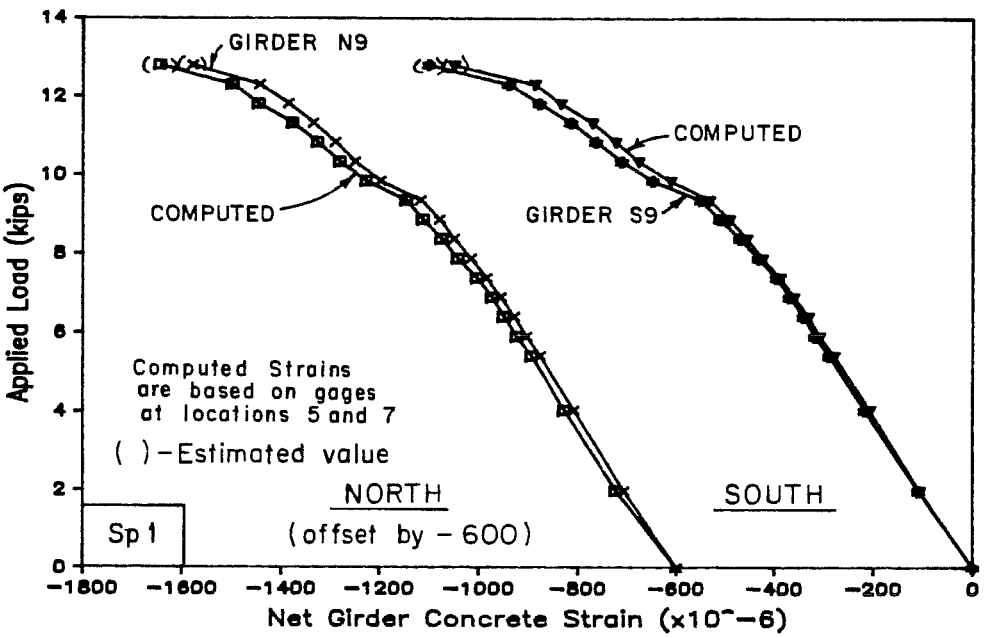

Fig. 6.23 Measured and computed top of girder concrete strains

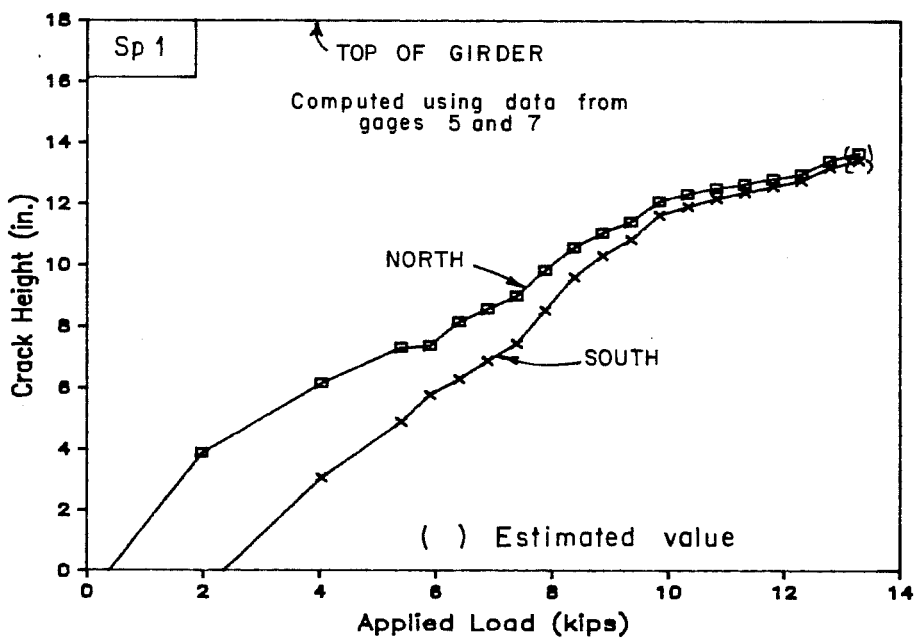

Fig. 6.24 Computed crack height

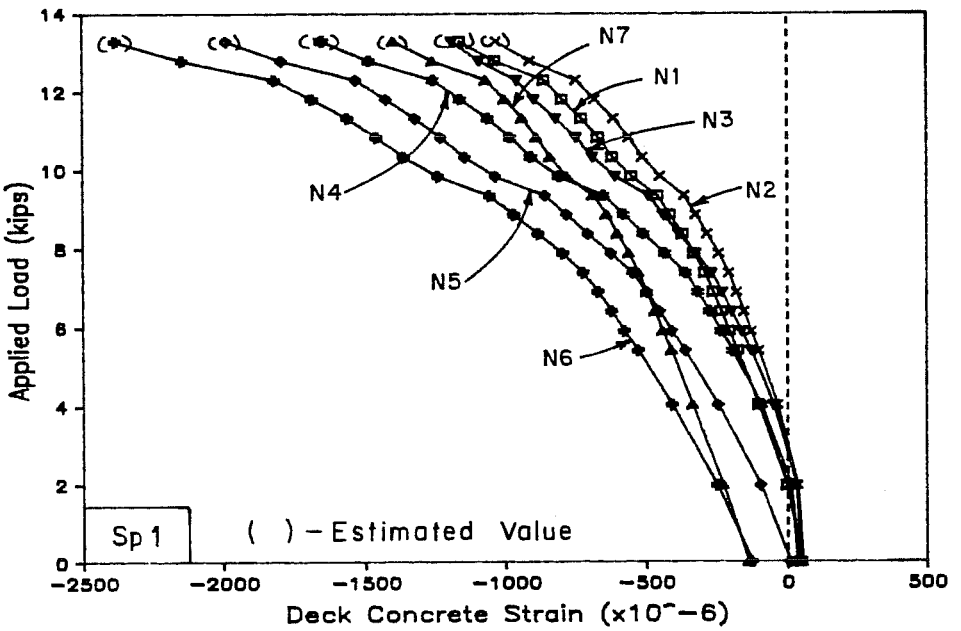

Fig. 6.25 Corrected deck concrete strains during ultimate flexure test: a) north gages; b) south gages

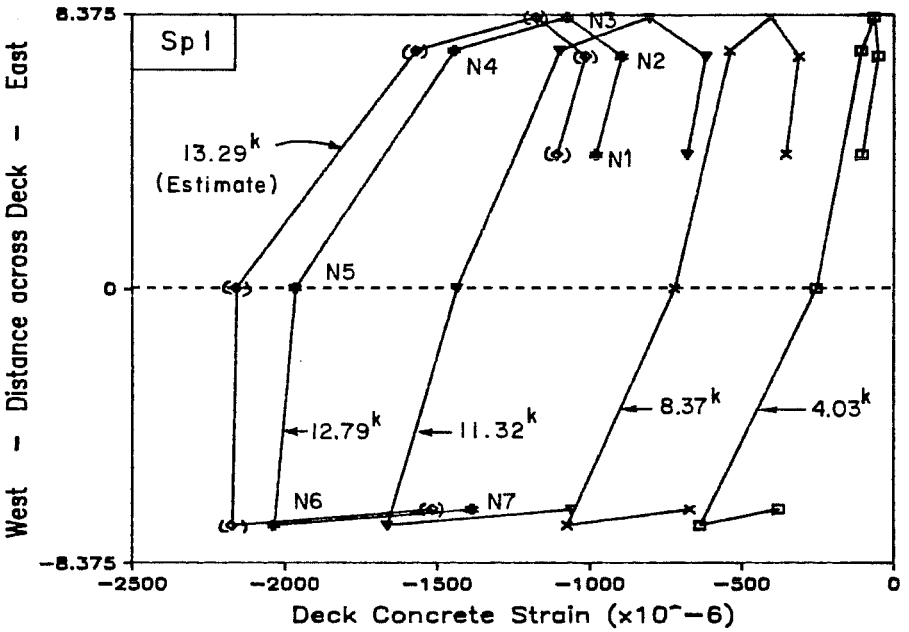

(a)

See Fig. 5.19 for Gage Locations

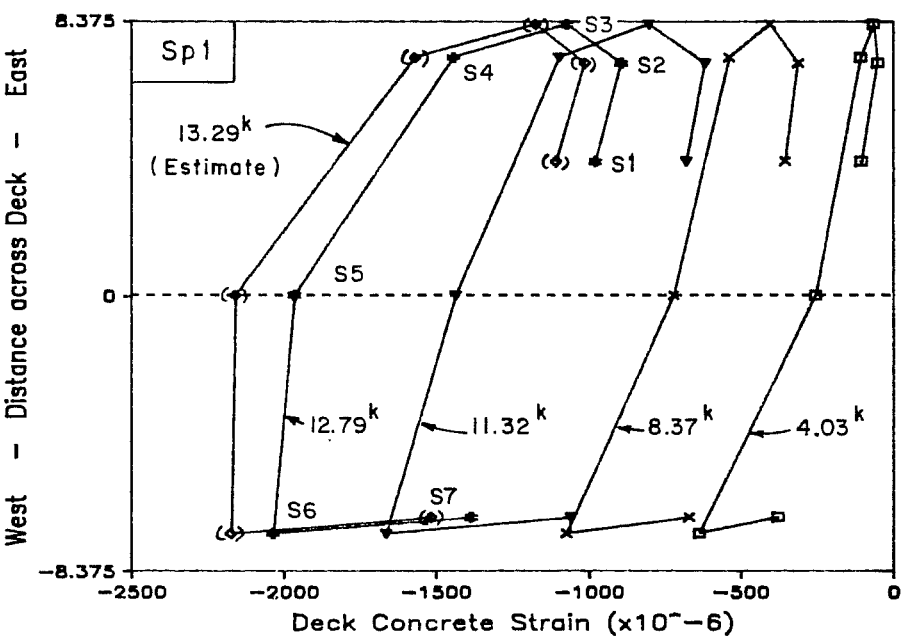

(b)

Fig. 6.26 Corrected deck concrete strains at selected loads during ultimate flexure test: a) north gages; b) south gages

However, maximum strains measured during cylinder tests were limited by failure of the strain gages rather than failure of the cylinder (see Sec. 7.3.2) and were therefore significantly less than expected. Similar concrete for Specimen 2 achieved strains in excess of 0.003.

Estimates of corrected strains at the top of the girder and deck were similar at failure. Strains measured at crushing of cylinders for the two concretes were also similar. Therefore, on the basis of these strains, it is not possible to determine which concrete initiated crushing.

Top of girder and bottom of deck net strains are shown in Fig. 6.27 with respect to their location across the deck for selected loads. Net strains for girder gages and the center top deck gage at different levels of load are plotted in Fig. 6.28. The data in the two figures demonstrate that agreement between the deck and girder strains at the level of the bottom of the deck was good and that the strain gradient through the full depth of the section for different stages of applied load remained approximately linear up to failure. This verifies that full composite action was present up to failure.

Curvature of the section was computed using strains from a pair of girder gages and three pairs of deck gages. The average of the three bottom deck gages was used with the top center deck gage because no deck gage was available directly below it. The resulting net curvatures are presented with increasing load in Fig. 6.29 and the total curvatures are shown versus total moment in Fig. 6.30. Total

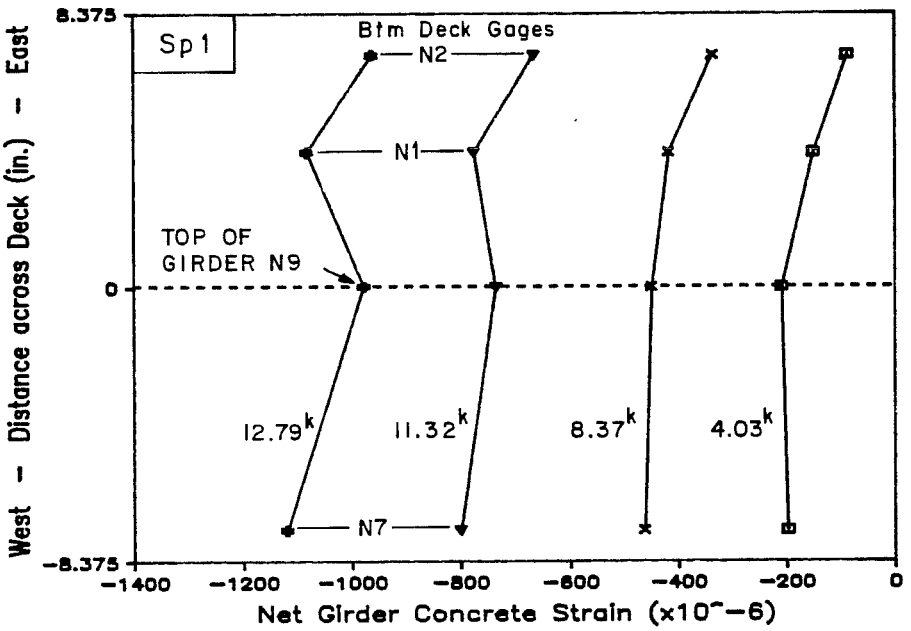

(a)

See Fig. 5.19
for Gage Locations

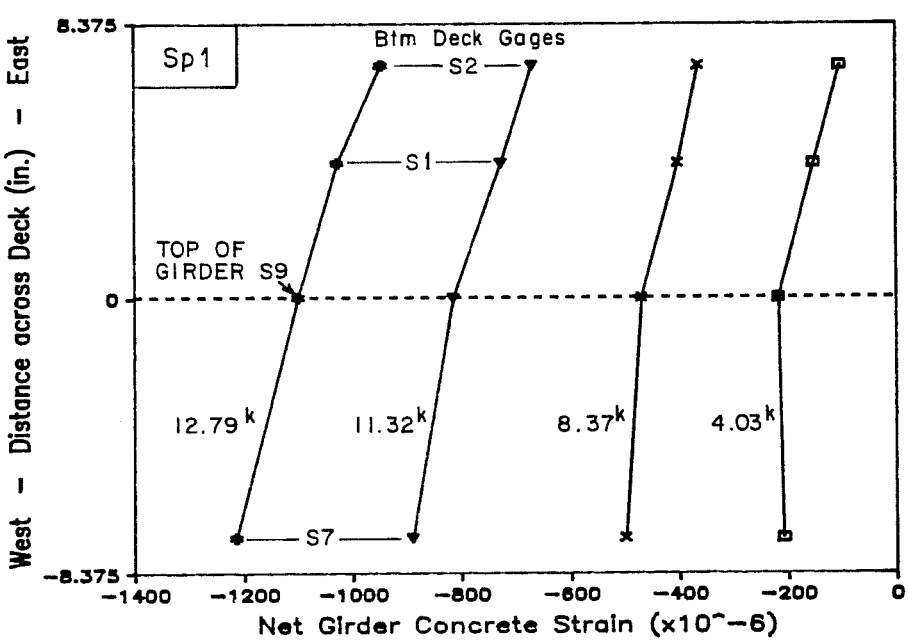

(b)

Fig. 6.27 Net concrete strains at top of girder and bottom of deck at selected loads during ultimate flexure test: a) north gages; b) south gages

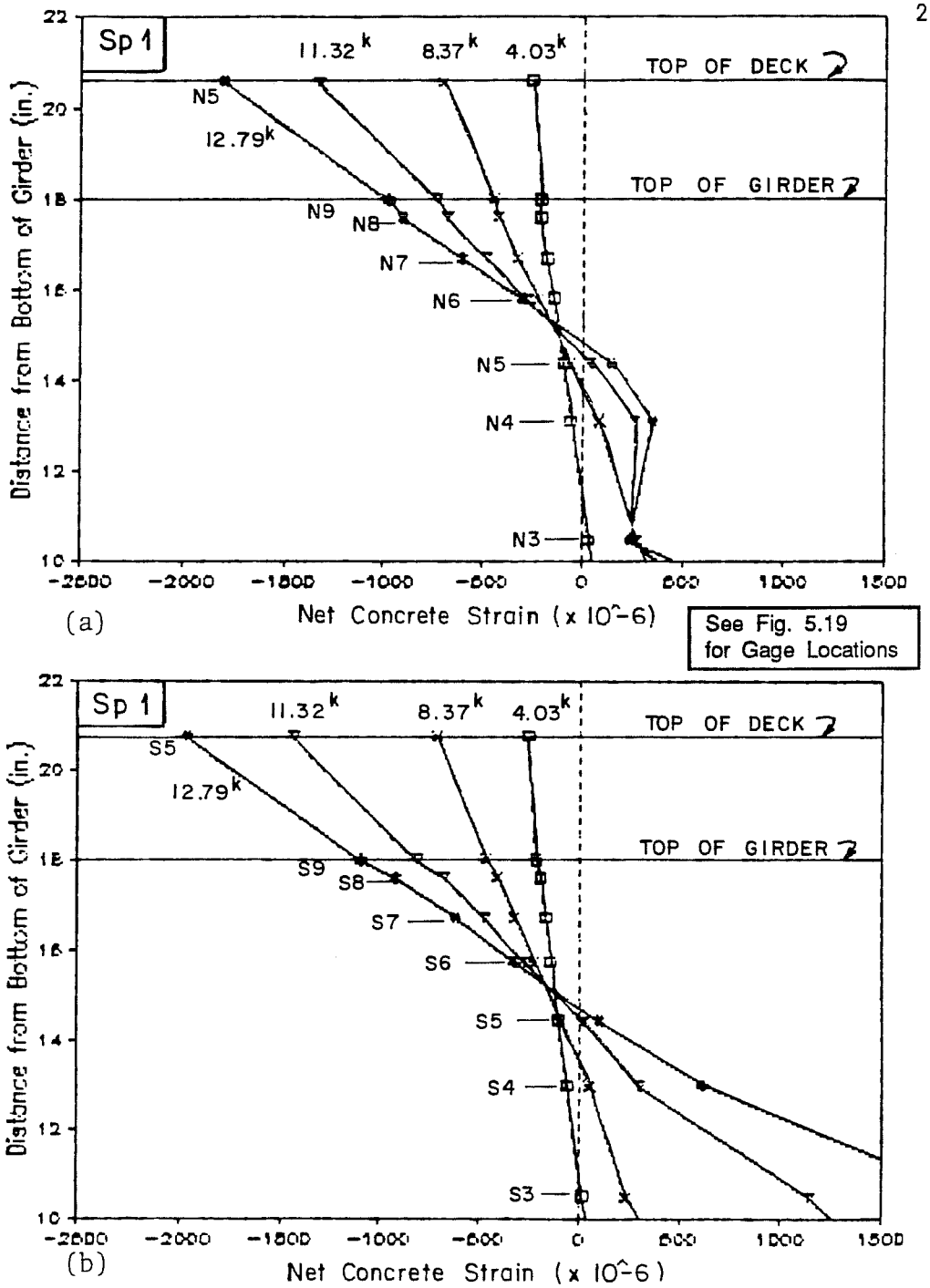

Fig. 6.28 Net girder and deck concrete strains at selected loads during ultimate flexure test: a) north gages; b) south gages

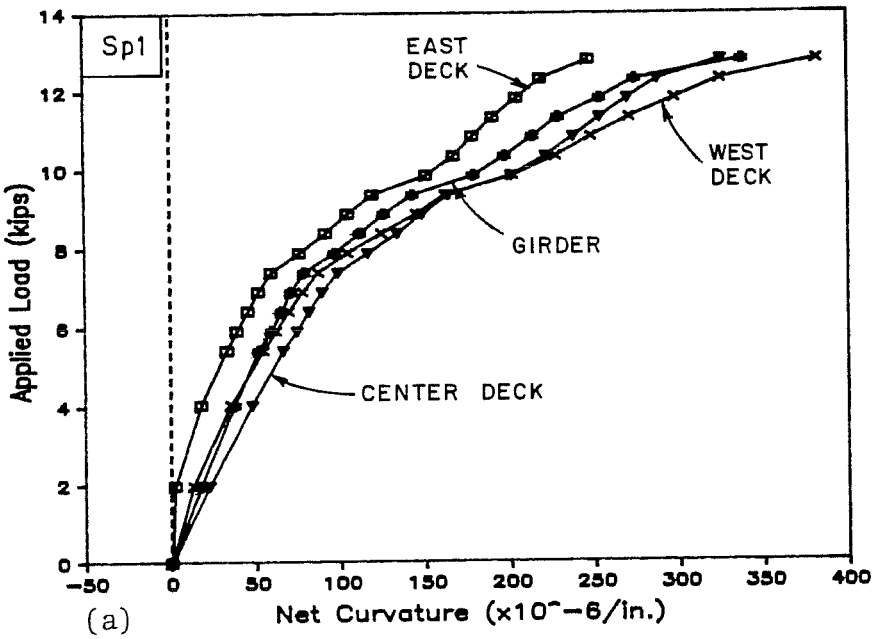

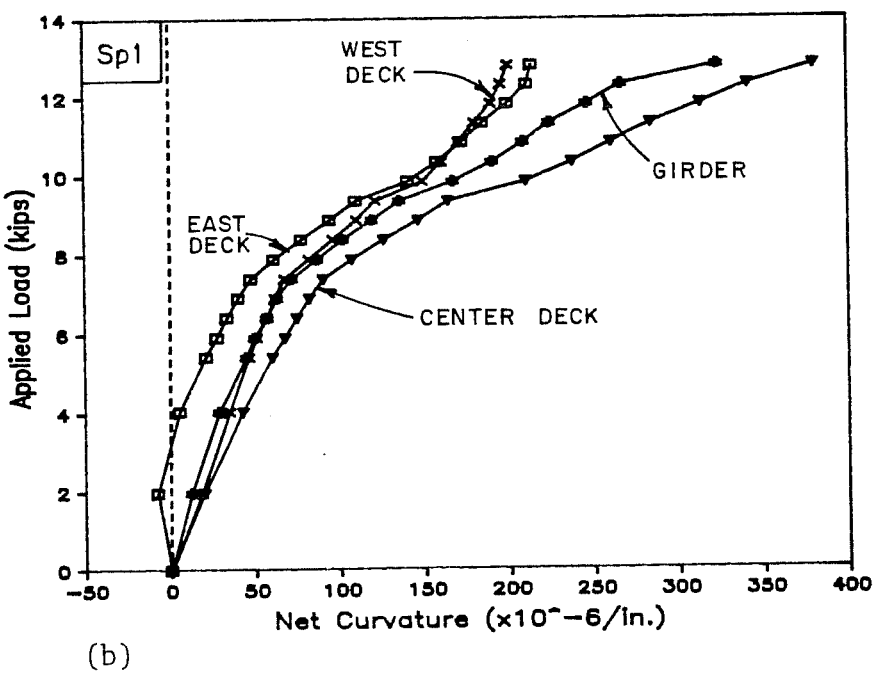

Fig. 6.29 Load-net curvature curves during ultimate flexure test: a) north gages; b) south gages

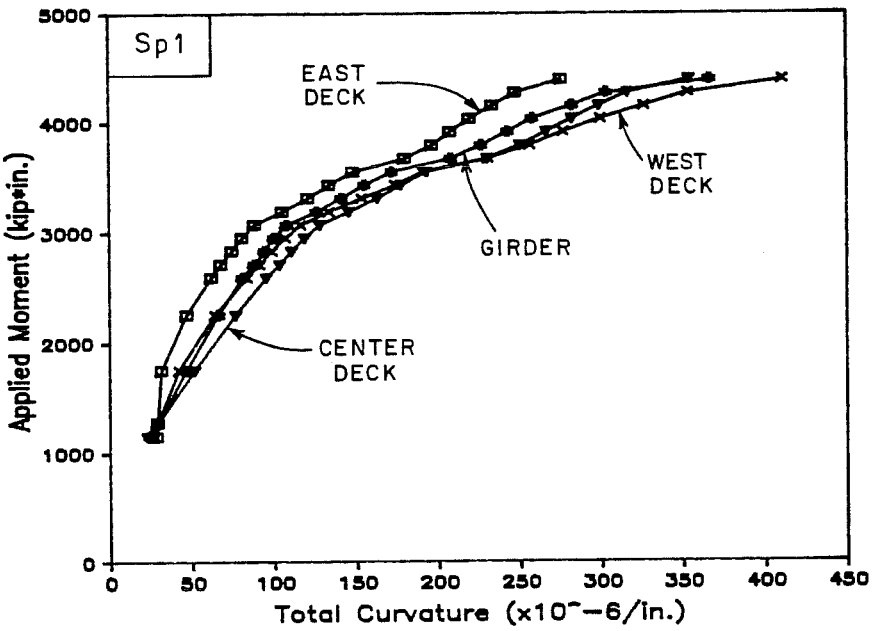

(a)

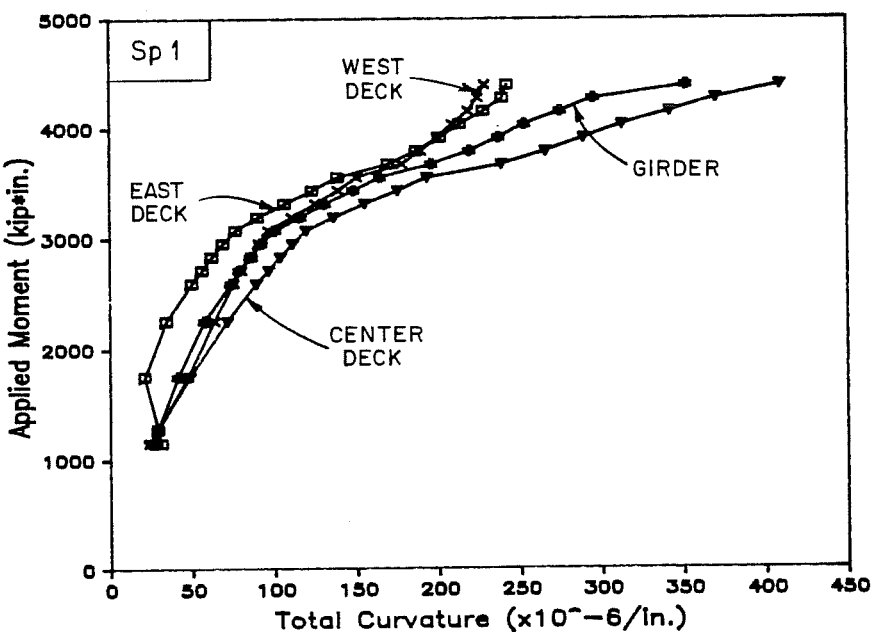

(b)

Fig. 6.30 Moment curvature curves during ultimate flexure test: a) north gages; b) south gages

curvatures were computed by adding net curvatures to a computed curvature at the beginning of the flexure test. The girder data is a reasonable average of the curves and will be used to represent specimen curvature during the flexure test.

Measured strand strains are compared with strand strains computed using girder curvature data in Fig. 6.31. Data for both lines of gages are shown on the same plot by adding an increment to the south data. These plots show that measured strand strains are consistent with the overall behavior of the specimen and that no debonding of the strands occurred during the test.

Strand strains, girder concrete strains, deck concrete strains, girder curvature, and midspan deflections are combined in Fig. 6.32. The data is normalized with respect to readings at the load stage prior to failure because data was not available for quantities other than deflection at failure.

6.2.2.4 Stirrup Strains and Strand Slip at Ends. Strains in the stirrups were negligible, indicating that no significant shear cracking occurred (Fig. 6.33). However, the large increase in strains measured at the south end after failure indicates that cracking may have occurred due to the violent flexural failure. Data was not available after failure for the north end because the gage lead was severed during failure.

No slip was measured in the strands at ends of the girder.

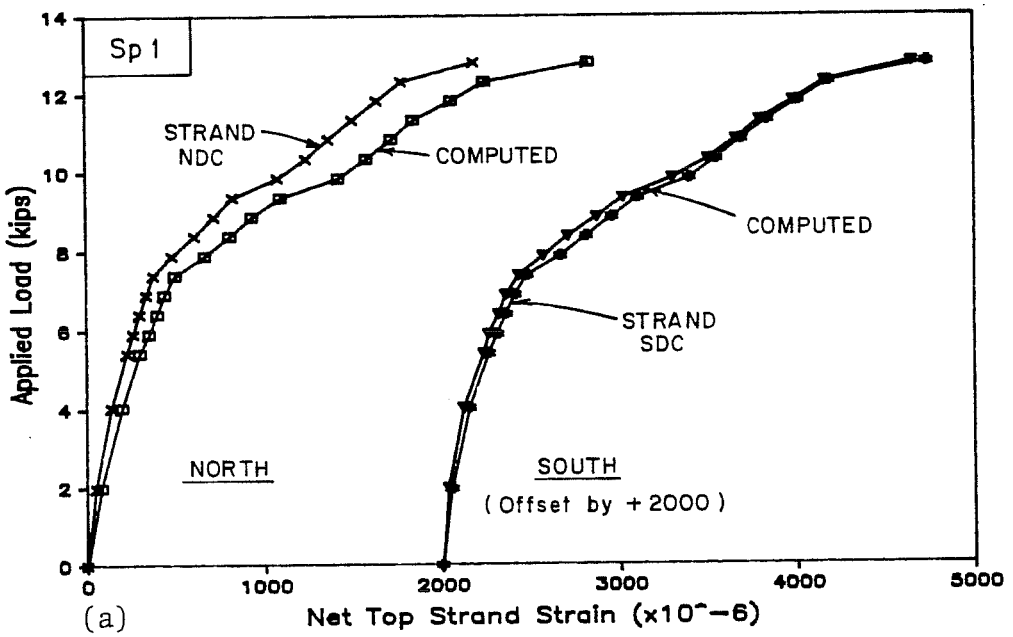

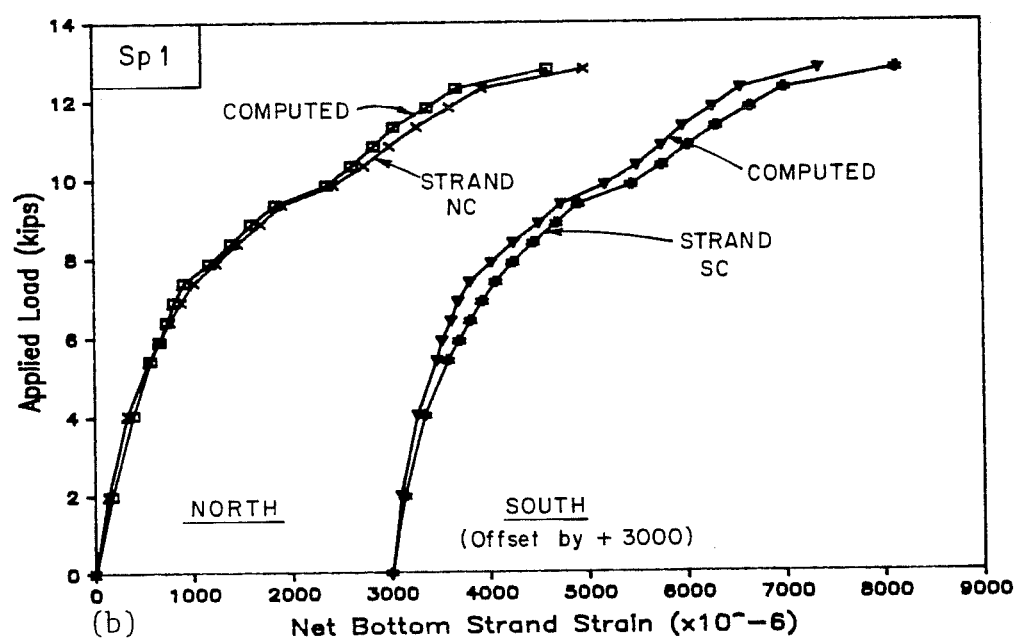

Fig. 6.31 Measured and computed strand strains during ultimate flexure test: a) measured and computed top strand strain; b) measured and computed bottom strand strain

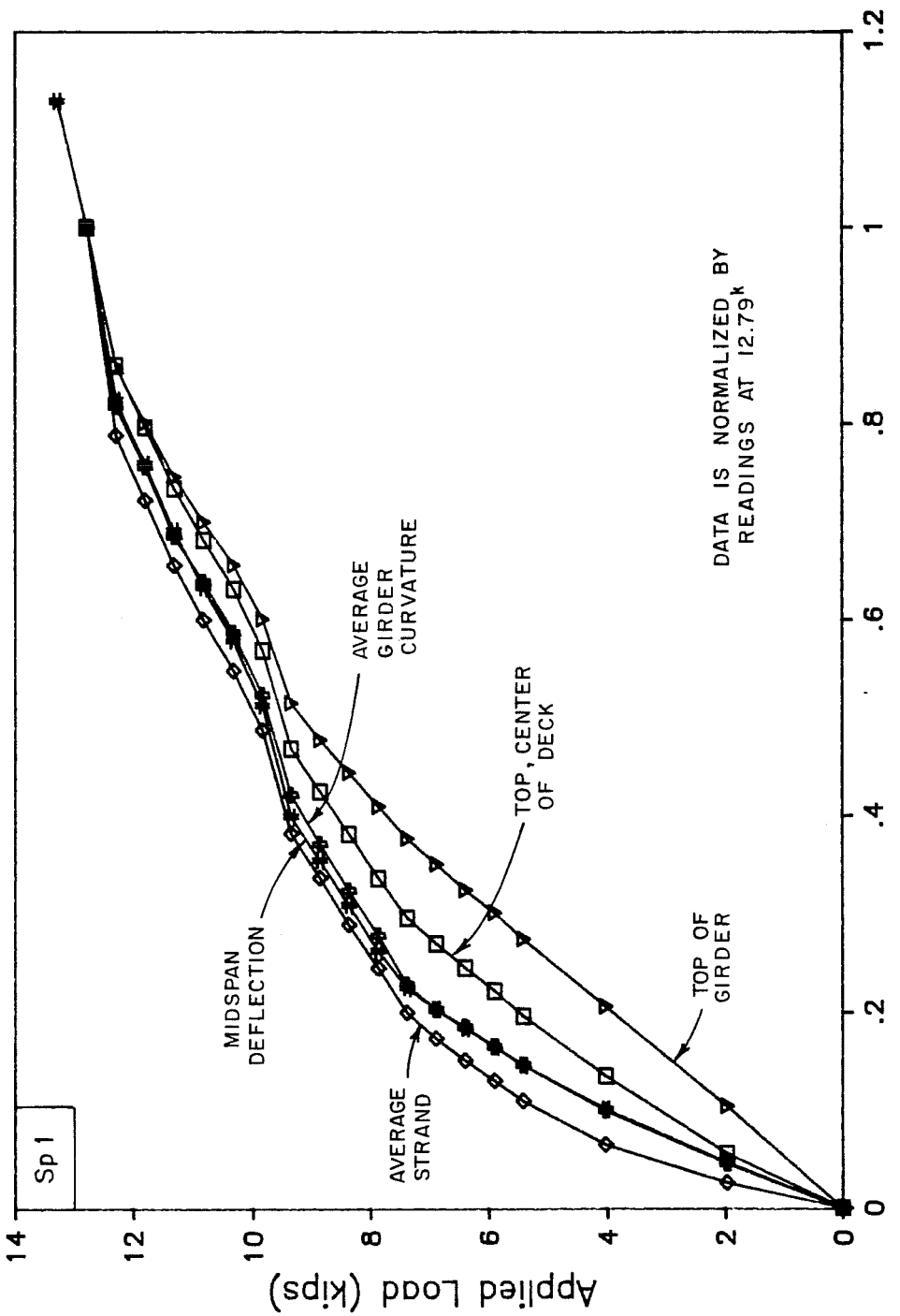

Fig. 6.32 Comparison of different types of data during ultimate flexure test

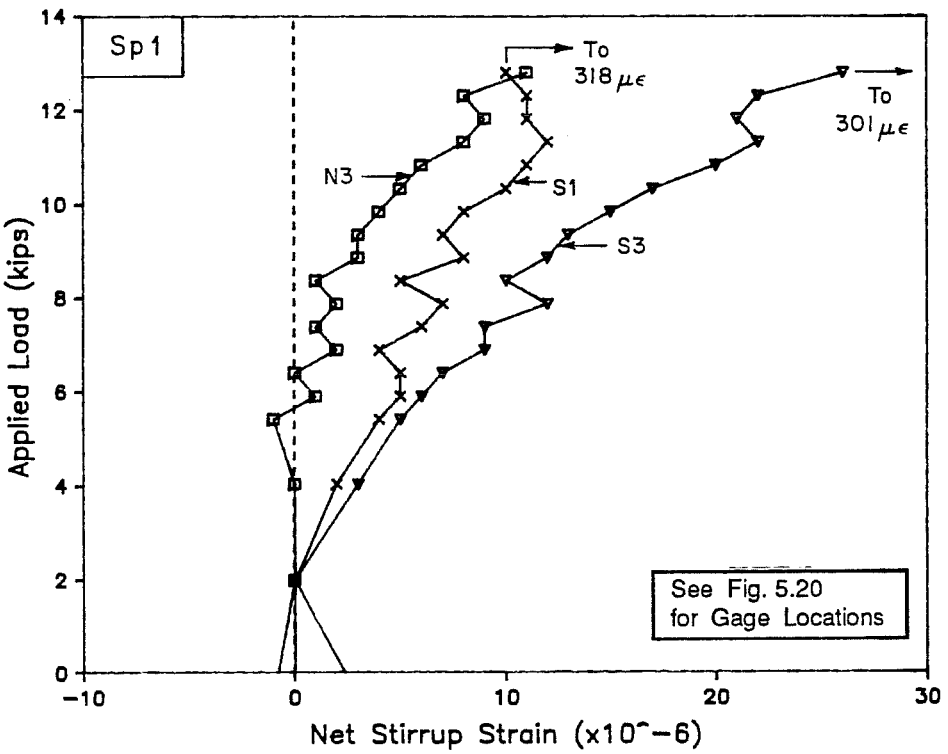

Fig. 6.33 Net stirrups strains during ultimate flexure test

6.2.3 Shear Test of South End - Standard Stirrup Detail.

6.2.3.1 General Description of Behavior. The shear test of the south end of Specimen 1 consisted of cracking and ultimate tests, in which loading was conducted in the same manner and using a similar system as the flexure test. However, on two occasions prior to actual testing, loads were applied to the specimen that were equal to or greater than those found to produce cracking during the test. This happened because the observed cracking load was well below the anticipated level. It is not known whether the specimen was cracked during the violent flexural failure, from loadings prior to the test, or whether the concrete actually cracked at the low shears as observed. Cracking may also have been present at loads lower than those reported because a close examination of the girder was not made at lower loads. Therefore, cracking data for this test is of questionable value.

No dead load compensation was used for the shear tests. This combined with a reduced span produced a state of stress in the web much different from that during the flexure test. Therefore, shear test results cannot be directly applied to the specimen as tested in flexure.

The deck was cracked through the full depth at many locations outside the shear span due to the effects of the flexural failure and

the lack of dead load with the shortening of the span. These cracks had no apparent effect on the shear capacity of the specimen.

Deflection and slip readings were taken at all load stages and strain readings were taken at all but a few load stages. The applied shear in the span of interest was used to designate load stages.

Cracks were first detected during the cracking test when very fine shear cracks extending across the full height of the web were observed at 19.53 kips. A close examination of the web was not made at the previous load stage. Loading continued with little change in cracking to 34.83 kips. There were four or five major shear cracks in the web at this load. The specimen was then unloaded.

The first event of note during the ultimate test occurred at a shear of 38.61 kips, when the specimen was unloaded to replace a pressure gage. The load was reapplied to the same level without any additional readings taken. At 44.47 kips a flexure crack was found in the shear span near the load point. At 49.41 kips, a web shear crack extended into the taper of the bottom flange near the end of the girder. Flexure cracks became inclined at 57.31 kips. The maximum load was reached at 63.24 kips when strands pulled in at the end and a crack opened across the bottom flange 8 in. from the end of the girder (Fig. 6.34). Failure was not catastrophic, but gradual, as increasing strand slip (Fig. 6.35) permitted the failure crack to open. The loading system prevented a sudden and complete failure by

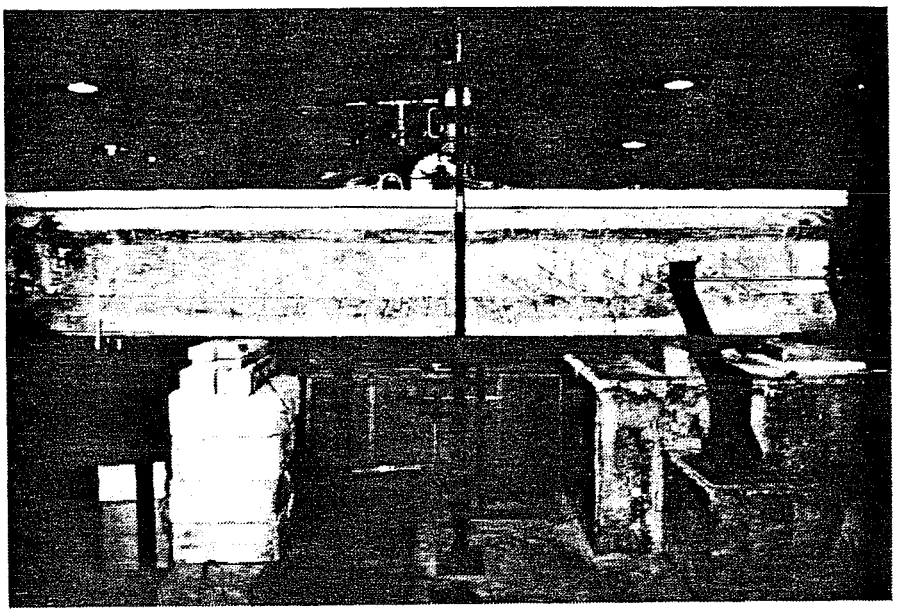

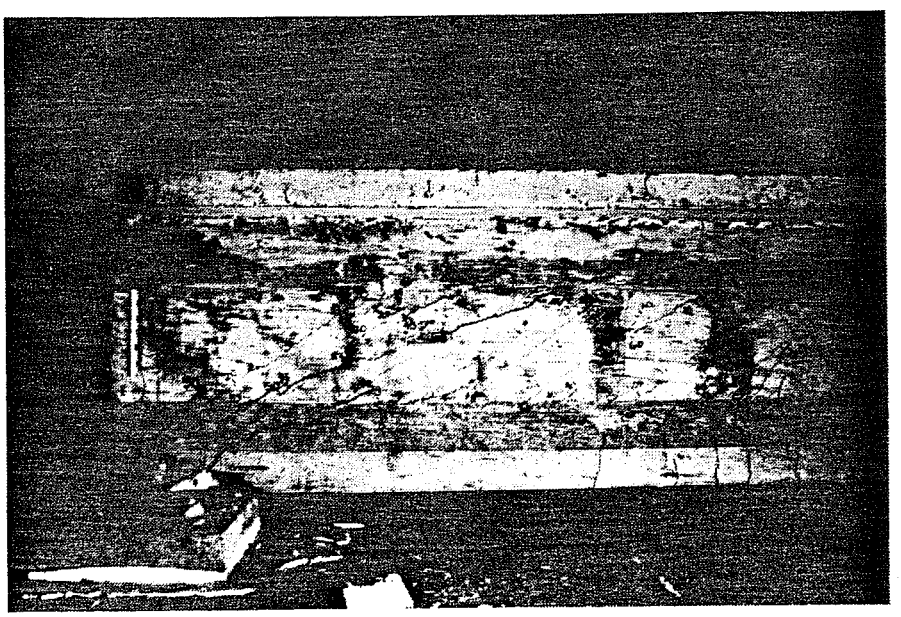

Fig. 6.34 Photographs after shear failure - south end, Specimen 1: a) west side, general view; b) east side, near support

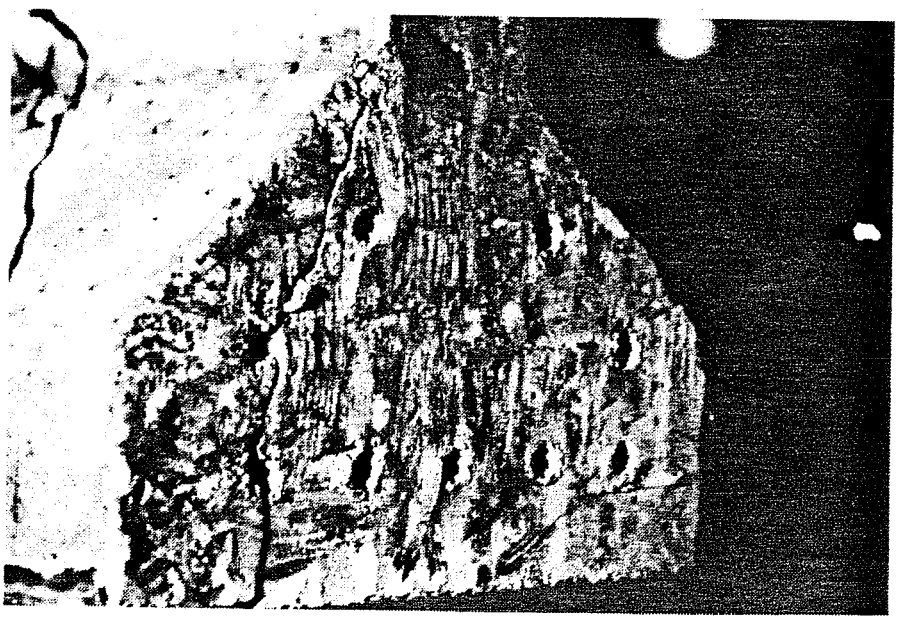

Fig. 6.35 Photograph of strand slip after shear failure - south end, Specimen 1

allowing load to be relieved as the member softened. Although a reduced load carrying capacity remained, loading was discontinued.

The failure crack spread into a number of web cracks. However, the web crack over the support which penetrated the bottom flange was not involved. A small area of spalling was noticed after failure at the junction of the web and bottom flange among the extensions of the failure crack. A longitudinal splitting crack nearly 2 ft long developed from the failure crack down the center of the bottom of the girder. A splitting crack formed across the end of the girder (Fig. 6.35) and some spalling occurred near the failure crack. No other splitting cracks were observed. Slipping of strands appeared to be the cause of failure.

Prior to failure, shear cracks were not wide. These cracks extended the full depth of the web but did not extend into either of the flanges, except for the single crack near the end which penetrated the bottom flange. Web crack inclinations were generally about 35x except for one major crack that formed at 44.47 kips during the ultimate test at an inclination of 21°. Extensions of the failure crack into the web were also inclined at about 35°.

Flexure cracks were spaced at approximately 3.5 in. up to 31 in. from the support. When load was removed after failure, flexure cracks closed so tightly that they could not be found, indicating that prestress remained in the strands.

Significant events during the shear test are summarized in Table 6.5 which also includes computed and design loads. These loads

Table 6.5 Load stages of interest during shear test of south end - Specimen 1

Key (Fig. 6.36)	Description of Load Stage		Load (kips)
Computed and Observed Behavior			
W	Observed Web Cracking		19.53
CD	Computed Decompression at Load Point	$(0\sqrt{f_c'})$	26.44
CW	Computed Web Cracking at h/2		31.95
CF	Computed Flexural Cracking at Load Point	$(7.5\sqrt{f_c'})$	34.37
R	Unload and Reload for Equipment		38.61
CI	Computed Inclined Flexural Cracking at h/2 from Load point		42.80
F	Observed Flexural Cracking	$(17.1\sqrt{f_c'})$	44.47
E	Web Cracking extends into Btm Flg. at end		49.41
I	Observed Inclined Flexural Cracking		57.31
U	Ultimate Load		63.24
Computed Shear Capacity			
	Web Cracking (Controls):		
NW	Computed Nominal Capacity (ϕ = 1.0)		58.51
	Inclined Flexural Cracking:		
NI	Computed Nominal Capacity (ϕ = 1.0)		70.15

Note: "Shear" is the applied shear in the shear span of interest.

Stirrups were equivalent to $7.93\sqrt{f_c'}b_w d$.

will be compared with test results later in this chapter and in the following chapter.

6.2.3.2 Deflections. Deflections at midspan and the load point are shown in Fig. 6.36 for both shear tests. Deflections were corrected for compression of the bearing pads. Shear cracking had a negligible effect on the stiffness of the structure and reloading after shear cracking revealed no significant changes in behavior. Behavior departs from elastic only after flexural cracking. The cause of an offset between curves whenever the specimen is unloaded and reloaded is not clear, since curves are otherwise linear and parallel.

6.2.3.3 Stirrup and Strand Strains. A typical load-strain curve for a stirrup gage is given in Fig. 6.37. Strains for each instrumented stirrup at selected loads are shown in Fig. 6.38. The load-strain curve shows no significant difference between cracking and ultimate test loadings other than an offset of aproximately 65 microstrains at maximum load in the cracking test. All but one gage registered a strain at or above yield by the load stage prior to failure. This was unexpected because shear cracks were prevented from opening widely prior to failure because the bottom flange was not cracked near the support.

Corrected strand strains are presented in Fig. 6.39. Strains at selected loads are shown, with respect to their location, in Fig. 6.40. Cracking apparently occurred near the gage at the center of the shear span at 57.31 kips. While this produced a rapid increase in stain of almost 2000 microstrains, the strand did not yield. The

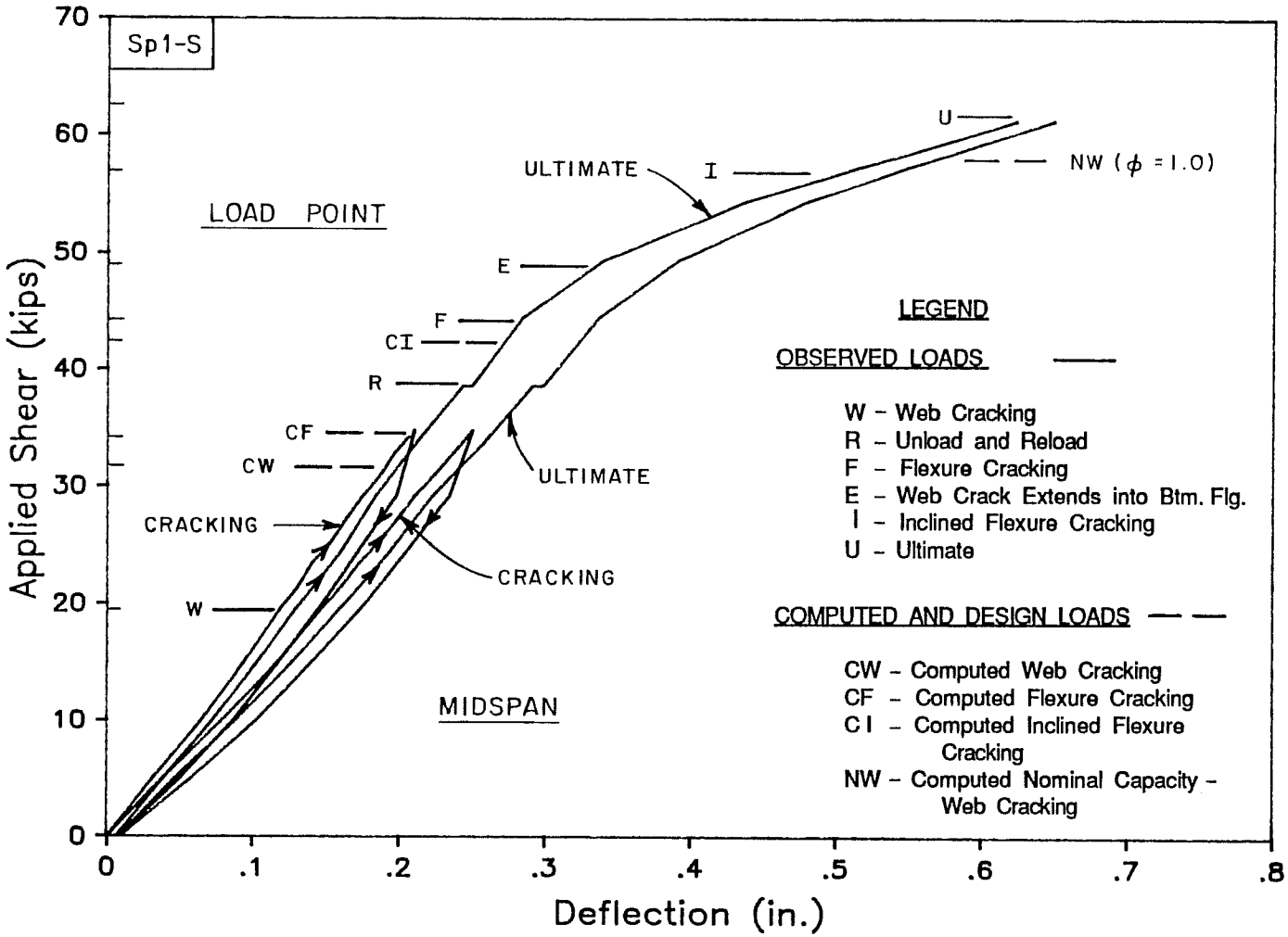

Fig. 6.36 Deflection at midspan and load point

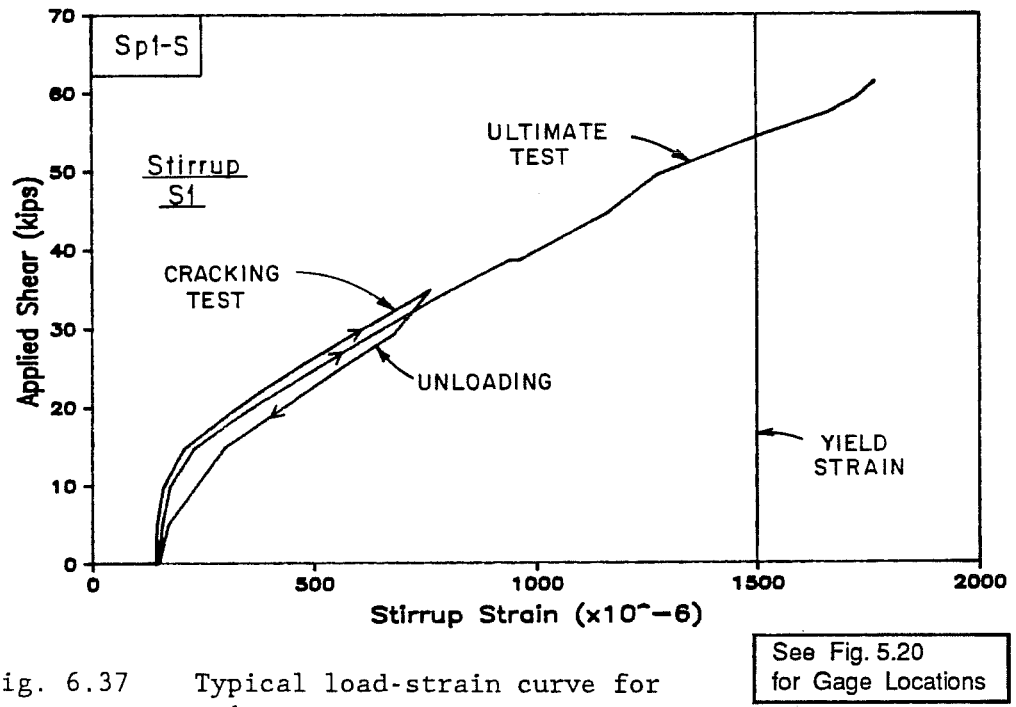

Fig. 6.37 Typical load-strain curve for stirrup

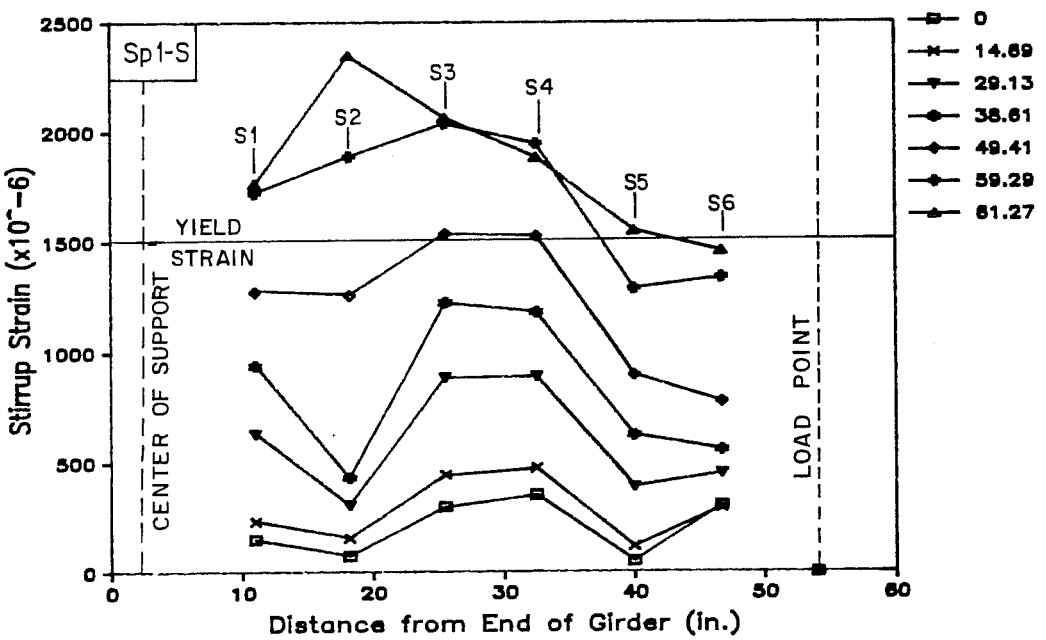

Fig. 6.38 Stirrup strains along span at selected loads

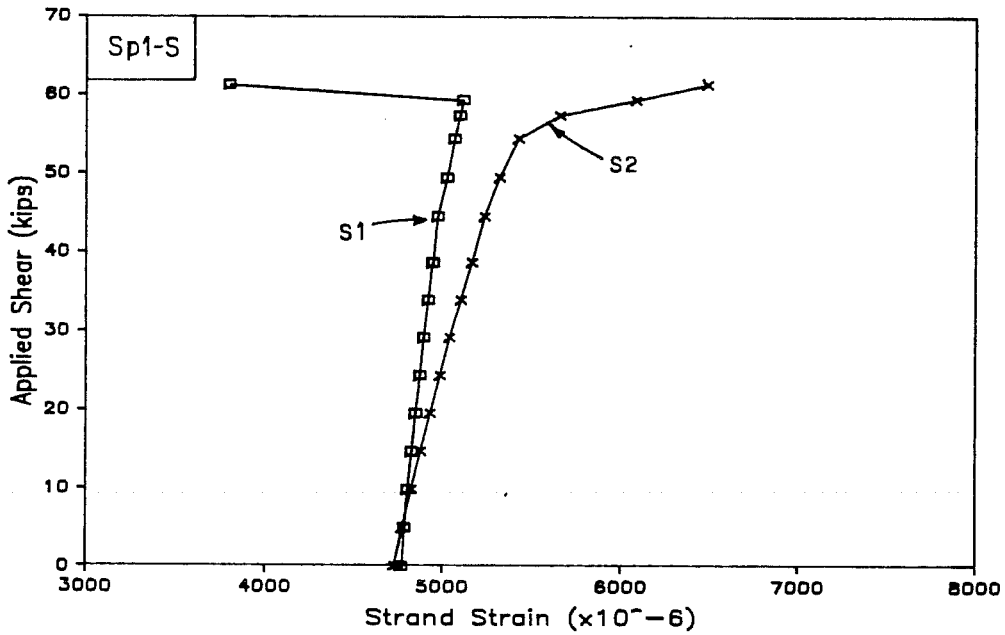

Fig. 6.39 Corrected strand strains during ultimate shear tests

See Fig. 5.20 for Gage Locations

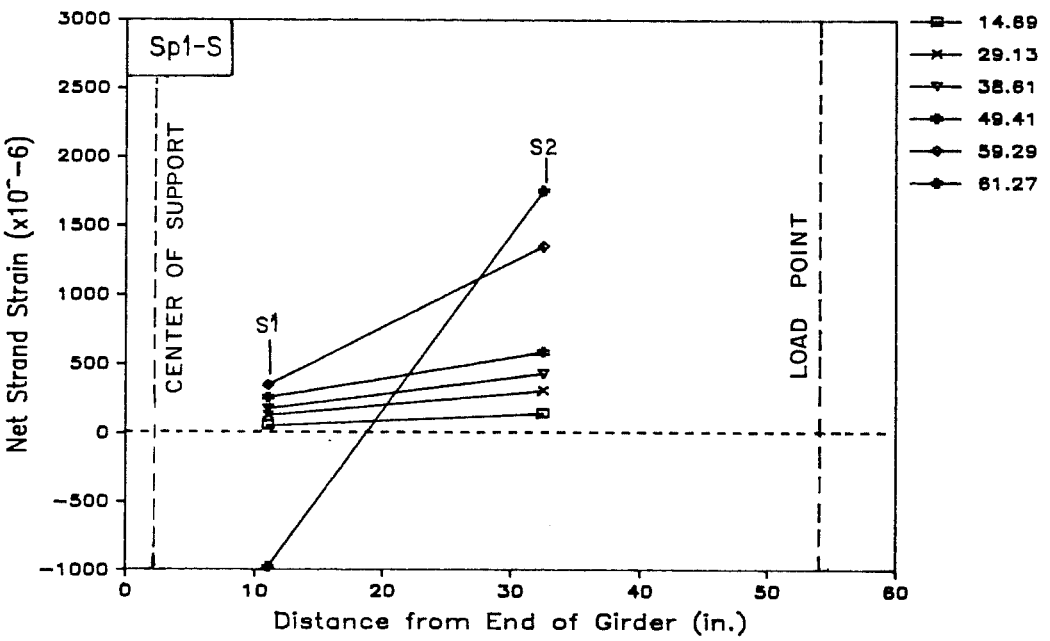

Fig. 6.40 Net strand strains along span during ultimate shear test

cracking near the gage corresponds well with the observed location of the flexure crack nearest the support. Strain near the end increased only slightly, then decreased at the final load stage when the gage either slipped from the strand or the strand slipped in the concrete.

6.2.3.4 Strand and Deck Slip. Strand and deck slip are shown in Fig. 6.41. Strand slip was gradual where it occurred and signficant capacity remained after initial slip. Both lower strands showed slip well before failure occurred and pulled in approximately 0.25 in. at failure. After failure, slip in the draped strands ranged from no visible slip at the top strand to a slip of approximately 1/32 in. on the bottom strand. Measurements of slip for the top strand and deck were negligible during the test.

6.2.4 Shear Test of North End - Modified Stirrup Detail.

6.2.4.1 General Description of Behavior. The condition of the north end prior to the shear test was similar to that of the south except that no loads were applied prior to the test that could initiate shear cracking of the section unless the specimen cracked during the flexure failure. The deck was uncracked in the shear span. Load stage designations and information are the same as for the south end.

The specimen was examined for cracks prior to the cracking test. Some very short and narrow cracks were found which later became part of early web cracking. No cracks were found at 9.82 kips. Web shear cracks appeared at the next load stage, 14.69 kips. At 24.34

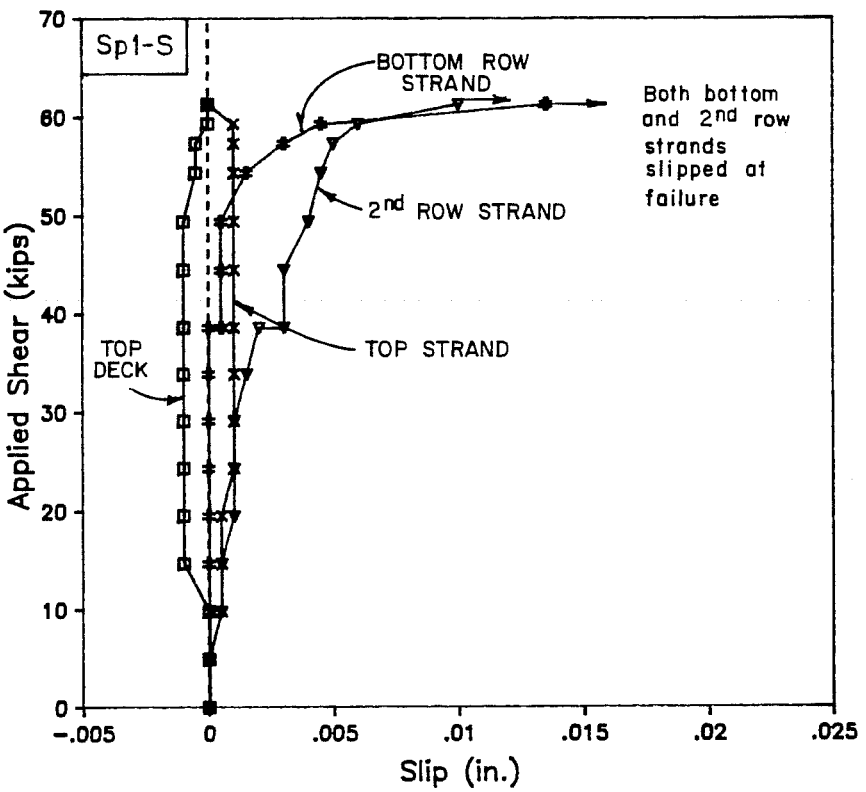

Fig. 6.41 Slip of strands and deck at end of girder during ultimate shear test

kips the web crack closest to the support penetrated into the taper of the bottom flange. At a shear of 33.88 kips, the crack near the support was opening slightly and other web cracks had fully extended across the web. Cracks were still visible after load was removed.

The first event of the ultimate test occurred at a shear of 38.61 kips when flexural cracking was detected beyond the load point. At 49.41 kips flexure cracks appeared in the shear span and new web cracks formed over the support and continued to develop as load increased. At 54.35 kips flexure cracks in the shear span became inclined. These cracks reached the top of the web at 57.31 kips and entered the taper of the top flange at 59.29 kips. The ultimate load was reached at 65.22 kips as the strands pulled in and a crack formed across the bottom flange 8.5 in. from the end of the girder (Fig.6.42). Load decreased as soon as the new crack formed. The loading system preserved the specimen from total collapse by allowing the load to be relieved as the member softened. When reloaded, the specimen supported approximately 61 kips. However, strands continued to slip (Fig. 6.43) and load could not be maintained. Loading was halted after additional deflection occurred and cracks opened further, although substantial capacity remained.

The failure crack extended into the web where it joined existing web cracks and formed new cracks (Fig. 6.42). Further cracking occurred into the bottom flange over the support. The web crack near the end of the girder that penetrated the bottom flange did

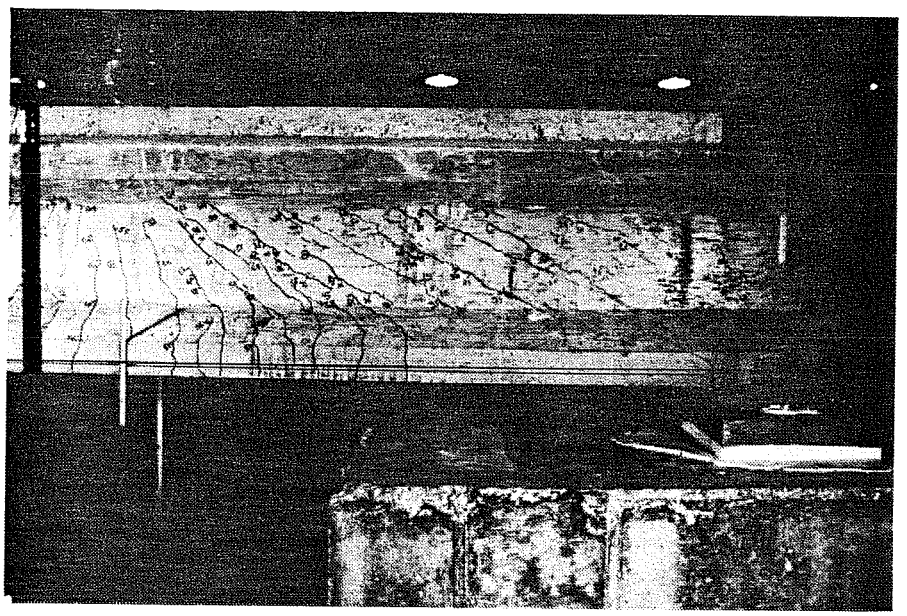

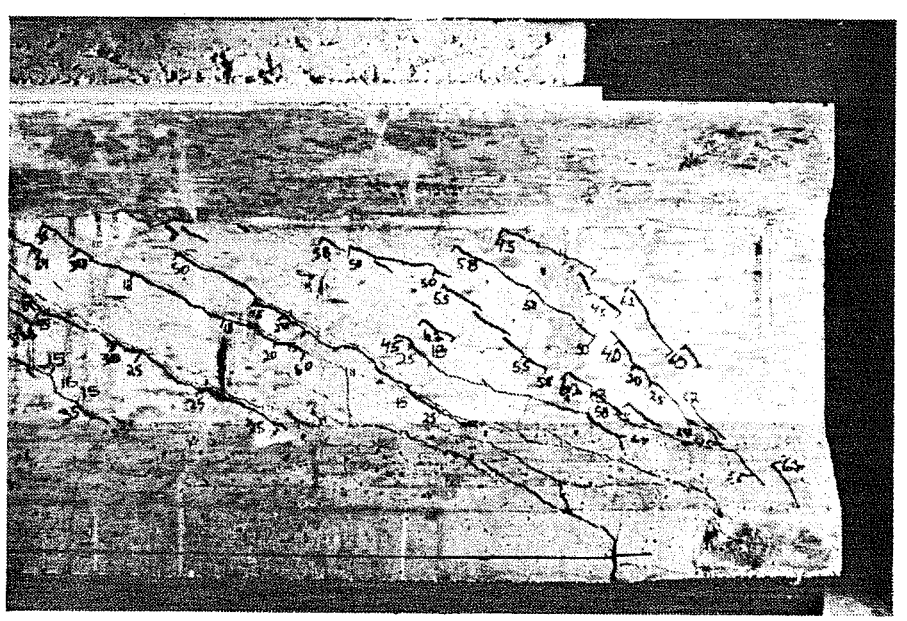

Fig. 6.42 Photographs after shear failure - north end, Specimen 1: a) west side, shear span; b) west side, near support

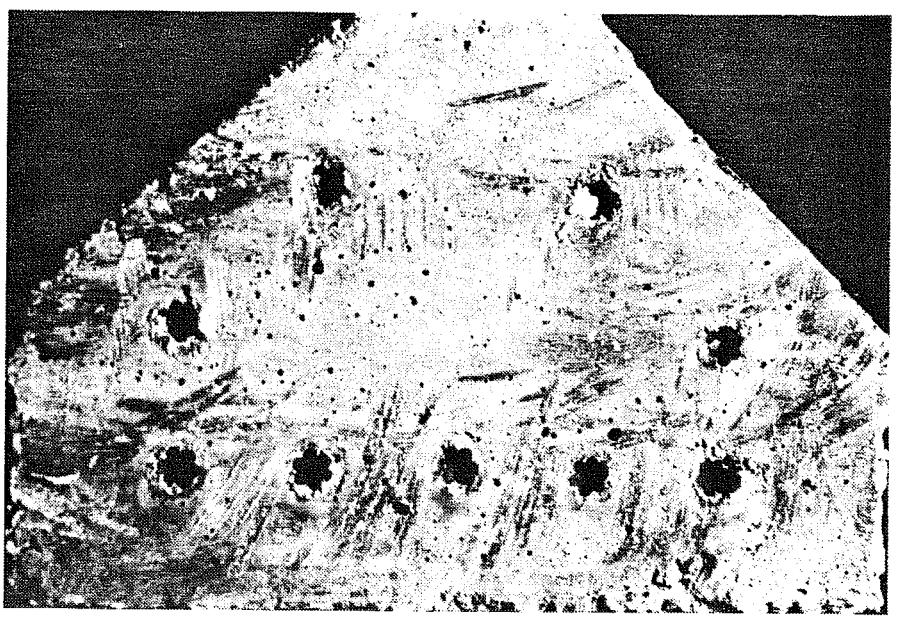

Fig. 6.43 Photograph of strand slip after shear failure - north end, Specimen 1

not appear to participate in the failure. A longitudinal crack about 8 in. long formed on the bottom of the girder extending from the main failure crack. Strand slippage appeared to be the primary cause of failure.

Shear cracks remained narrow up to failure. Typical web cracks were inclined at about 25°, but one crack was inclined at 42°. Failure cracks were parallel to the typical web cracks.

Flexural cracks, spaced about 3 in. apart, extended to approximately 30 in. from the support. These cracks closed when the load was removed.

There was no significant difference in failure load or mode to indicate that the stirrup detail employed in the north end of the specimen provided any improvement in performance over the south end.

As for the south end, Table 6.6 is provided as a summary of observed, computed and design loads.

6.2.4.2 Deflections. Deflections at midspan and load point are shown in Fig. 6.44. Behavior was linear until flexural cracking and only a small difference was recorded between cracking and ultimate test deflections. The difference between midspan and load point curves at maximum load is caused by the absence of a midspan reading at ultimate. The curves show a gradual reduction in capacity after ultimate load, but this is not accurate because load decreased immediately after ultimate load was reached and remained steady until loading was halted. The existence of any capacity following ultimate

Table 6.6 Load stages of interest during shear test of north end - Specimen 1

Key (Fig. 6.44)	Description of Load Stage	Load (kips)
Computed and Observed Behavior		
W	Observed Web Cracking	14.69
E	Web Crack Extends into Btm Flg. at End	24.34
CD	Computed Decompression ($0\sqrt{f_c'}$) at Load Point	27.53
CW	Computed Web Cracking at h/2	32.31
CF	Computed Flexural Cracking ($7.5\sqrt{f_c'}$) at Load Point	35.51
F	Observed Flexural Cracking ($10.4\sqrt{f_c'}$)	38.61
CI	Computed Inclined Flexural Cracking at h/2 from Load Point	44.19
I	Observed Inclined Flexural Cracking	54.35
U	Ultimate Load	65.22
P	Post-Ultimate Load	61.27
Computed Shear Capacity		
	Web Cracking (Controls):	
NW	Computed Nominal Capacity (ϕ = 1.0)	59.09
	Inclined Flexural Cracking:	
NI	Computed Nominal Capacity (ϕ = 1.0)	71.73

Note: "Shear" is the applied shear in the shear span of interest.

Stirrups were equivalent to $7.93\sqrt{f_c'}b_w d$.

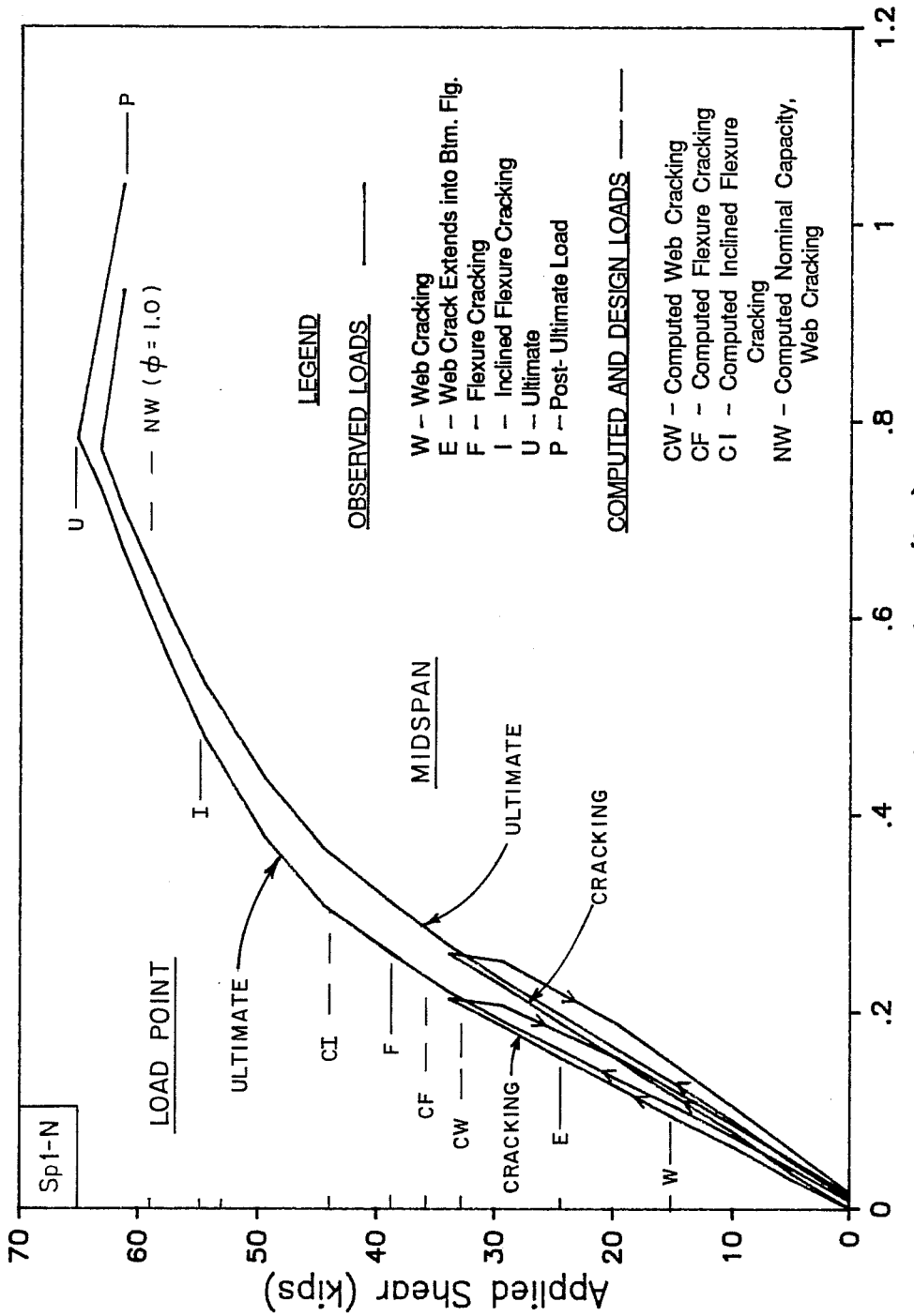

Fig. 6.44 Deflection at midspan and load point

was entirely dependent upon the ability of the load system to shed load.

6.2.4.3 Stirrup and Strand Strains. A typical load- strain curve for a stirrup gage is given in Fig. 6.45. Strains for stirrups at selected loads are shown, with respect to location, in Fig. 6.46. Strains during cracking and ultimate tests differed by a constant 130 microstrains which was twice the offset observed during the test of the south end and may indicate that cracking was more severe for this specimen. All active gages except the one nearest the load point registered strains at or above yield at failure. These high strains are unexpected for the same reasons given in the discussion of south end results.

Corrected strand strains are presented in Fig. 6.47. Strains at selected loads appear, with respect to their location, in Fig. 6.48. Cracking occurred near the load point gage at a load of 38.61 kips as indicated by the departure from linear behavior. This agrees with visual cracking observations. Strains at the load point increased more than 3000 microstrains before failure but the strand did not yield. Strains near the end increased steadily to about 250 microstrains above the reading at the beginning of the test. After the ultimate load, this gage either slipped on the strand or the strand slipped in the concrete. Strand strain data for both shear tests is combined in Fig. 6.49, demonstrating the good agreement between strand data for the two tests.

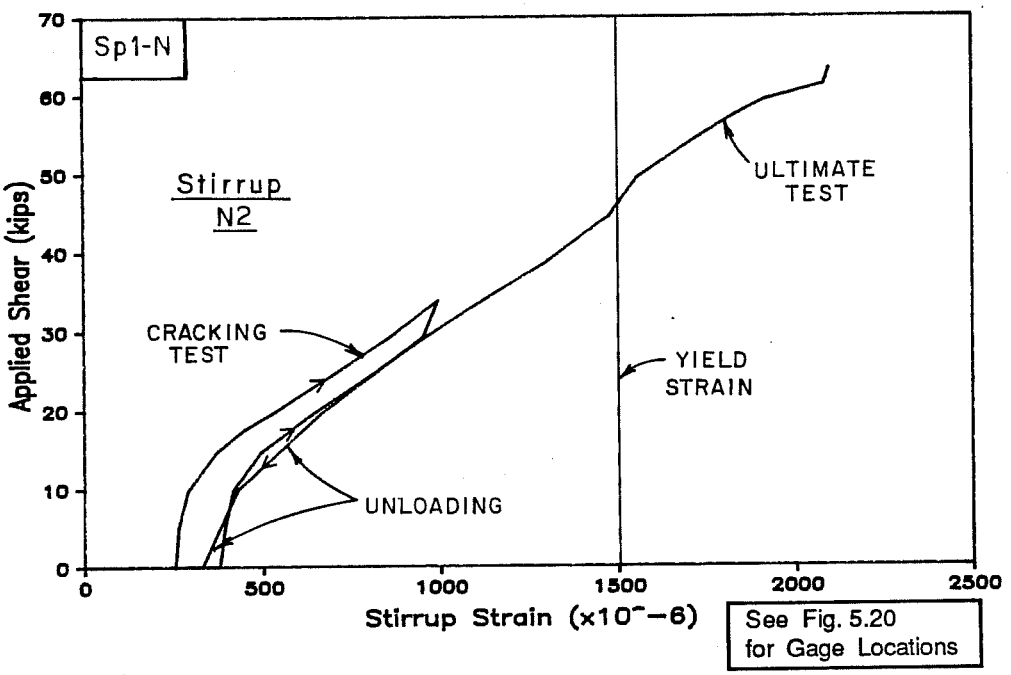

Fig. 6.45 Typical load-strain curve for stirrup

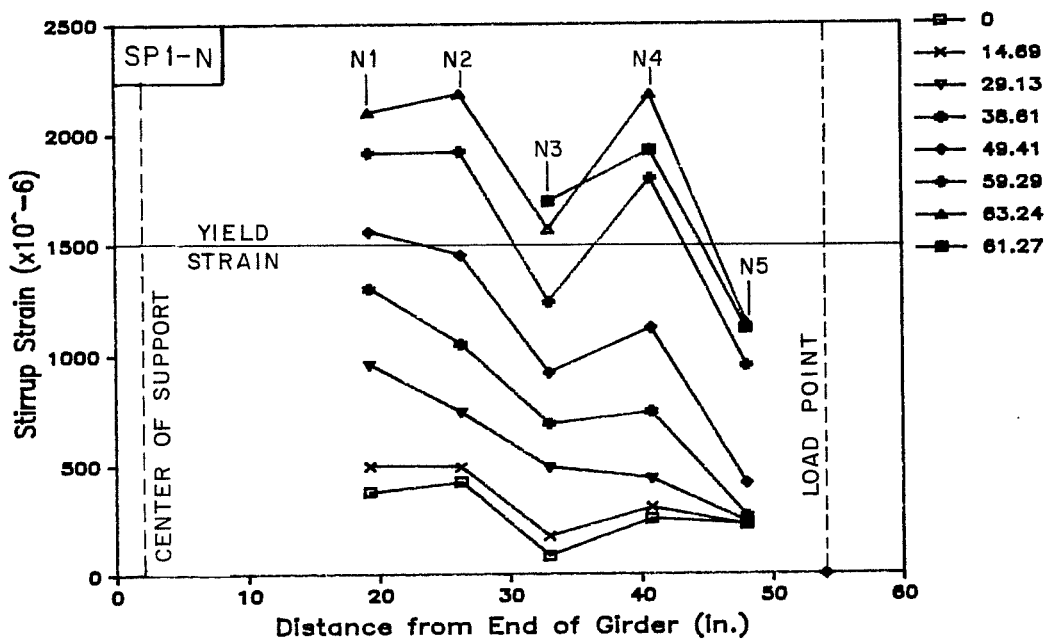

Fig. 6.46 Stirrup strains along span at selected loads

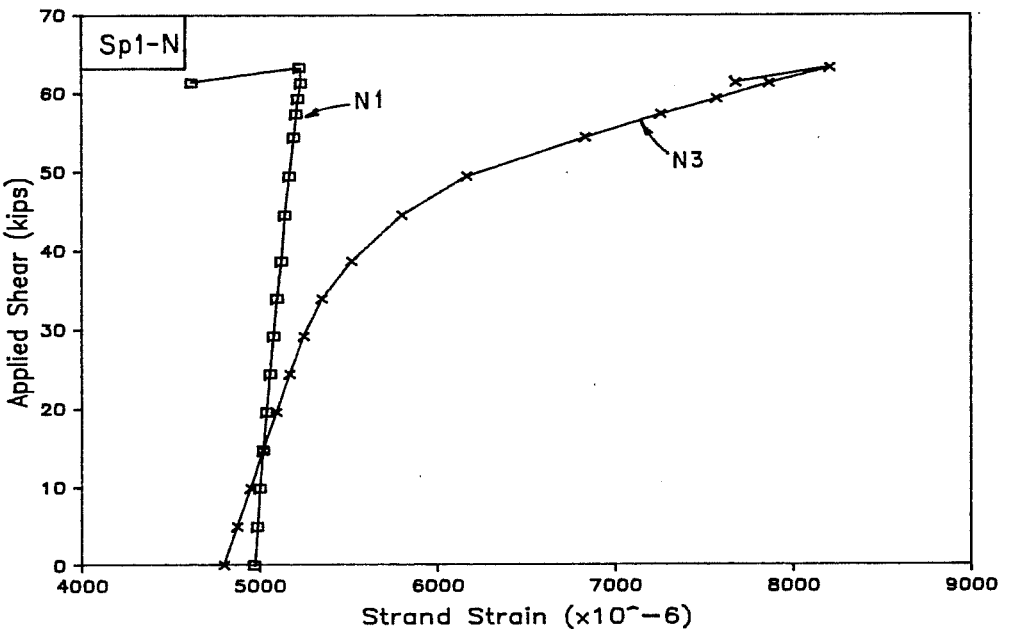

Fig. 6.47 Corrected strand strains during ultimate shear test

See Fig. 5.20 for Gage Locations

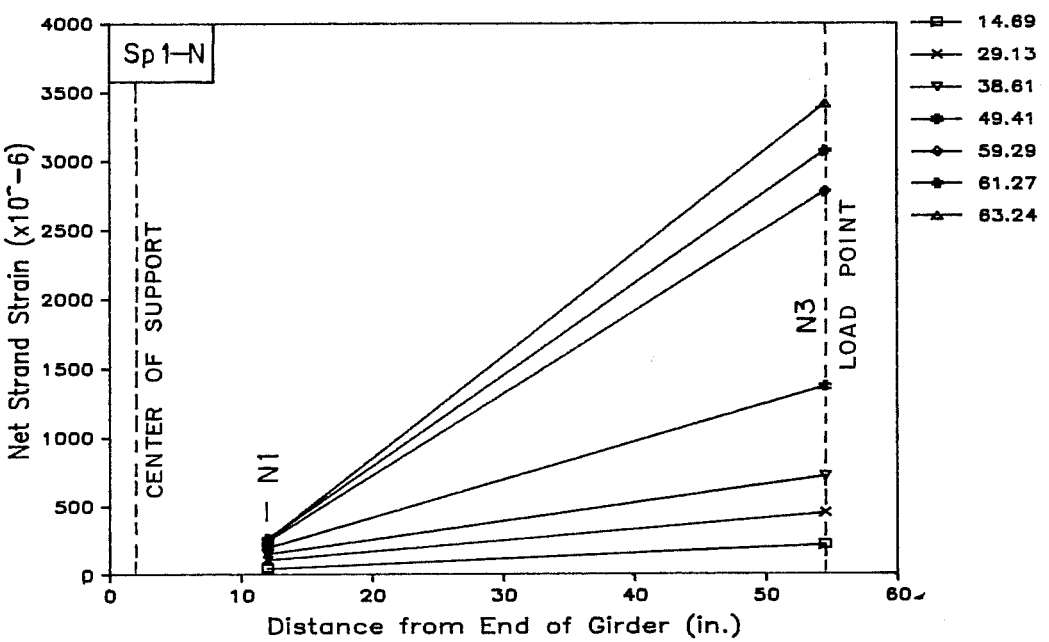

Fig. 6.48 Net strand strains along span during ultimate shear test

6.2.4.4 Strand and Deck Slip. Strand and deck slip are shown in Fig. 6.50. Strand slip did not develop gradually as observed in the south end test, but appeared suddenly at load stages just prior to ultimate. After failure all lower strands pulled into the girder about 0.2 in.8 After failure, the top strand pulled in slightly (about 1/64 in.) while the bottom draped strand slipped nearly 1/16 in. with the other draped strands exhibiting slips ranging between these amounts. Slip of the deck, while measurable, was not detected visually.

6.3 Specimen 2 (9 strands)

In this section, behavior and properties of Specimen 2 prior to and during flexure and shear tests will be discussed. While the span of time from casting the girder to the flexure test was only approximately two months, a discussion of specimen behavior during that time period is included because of its significance in establishing effective stresses and strains at the time of the flexure test and in understanding the long-term behavior of the structure.

Since the flexural failure of Specimen 1 was near the balanced condition, Specimen 2 was designed to produce a more ductile failure. The design used the minimum number of strands required to satisfy allowable stress design criteria. One of the nine strands was draped to control stresses at the ends of the section. The flexure test consisted only of an ultimate test because the girder suffered extensive cracking prior to release due to shrinkage.

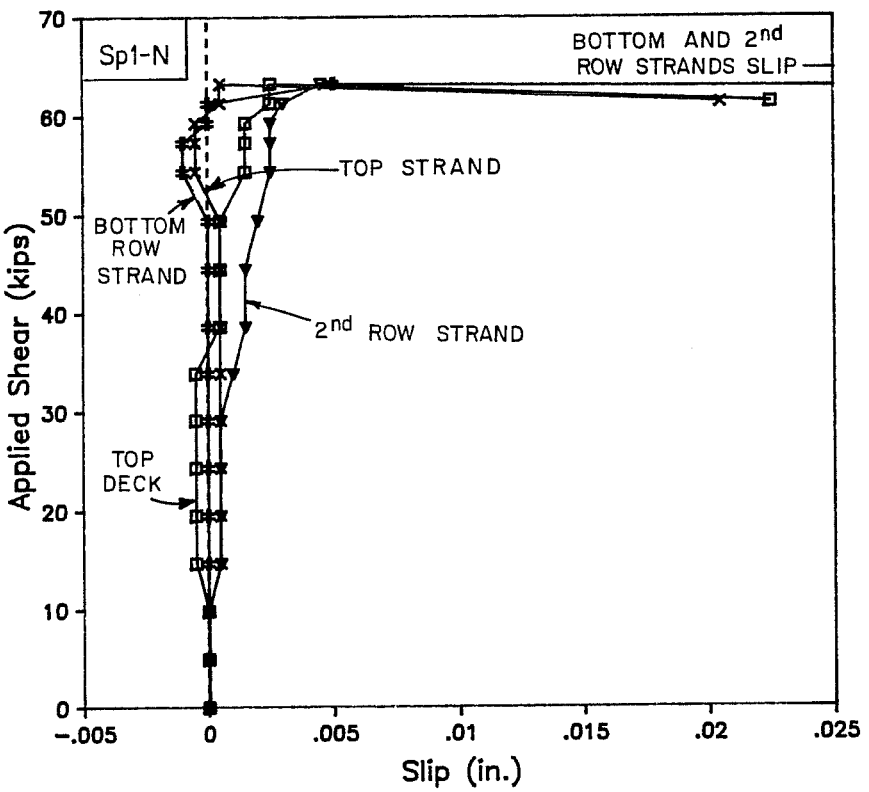

Fig. 6.50 Slip of strands and deck at end of girder during ultimate shear test

Shear tests of the two ends of the flexure specimen also included only ultimate tests because of the prior cracking of the girder. The tests are referred to by the location (south or north) of the end during the flexure test. At both ends, stirrups were provided at a spacing that corresponded to approximately $V_s = 4\sqrt{f_c'}\, b_w d$, or half the quantity of stirrups used in Specimen 1. Standard open stirrups were used for both ends, but an additional 6 in. extension beyond the support was provided at the north end in order to study the effect of bond on shear capacity.

6.3.1 Prior to Flexure Test.

6.3.1.1 Concrete Material Properties. Properties of girder and deck concrete were measured at intervals. Measured and estimated data at specific times are given in Table 6.7. Values were estimated when data were not available for the date on which an event occurred. Estimates were based on data presented in Appendix A. Strength gain with age is shown in Fig. 6.51. Average stress-strain curves at the time of the flexure test are shown in Fig. 6.52. Stress-strain curves were obtained using compressometer and head displacement data for tests of 6 by 12-in. cylinders and head to head displacement data for 3 by 6-in. and 4 by 8-in. cylinders (high strength concrete only). More information on mix design and material properties is given in Appendix A.

Table 6.7 Concrete properties at significant events - Specimen 2

Event	Age	f_c'	E_c	f_r'
	(days)	(psi)	(ksi)	(psi)
Release				
Girder	7	9,200	5,290	880
Deck Cast				
Girder	48	(10,120)	(5,500)	
Flexure Test				
Girder	56	10.800	5,675	1,100
Deck	8	4,350	4,370	
Shear Tests				
Girder	265	11,300	(5,800)	1,275
Deck	217	5,350		

() - Estimated values, based on additional data presented in Appendix A.

Note: All data are for cylinders cast in plastic molds and cured with Specimen 2 under ambient conditions.

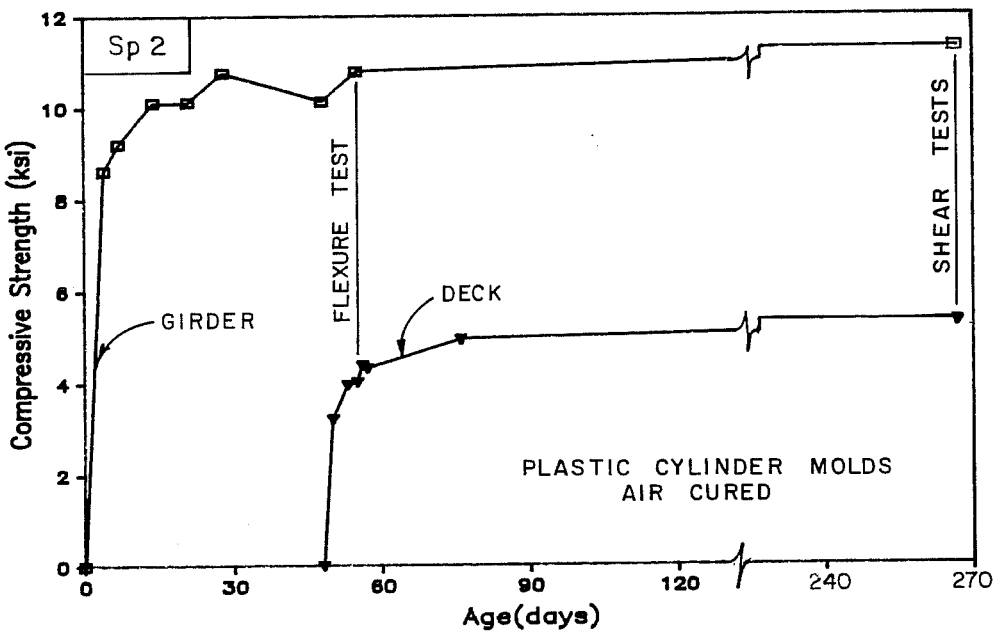

Fig. 6.51 Girder and deck concrete strength gain with age - Specimen 2

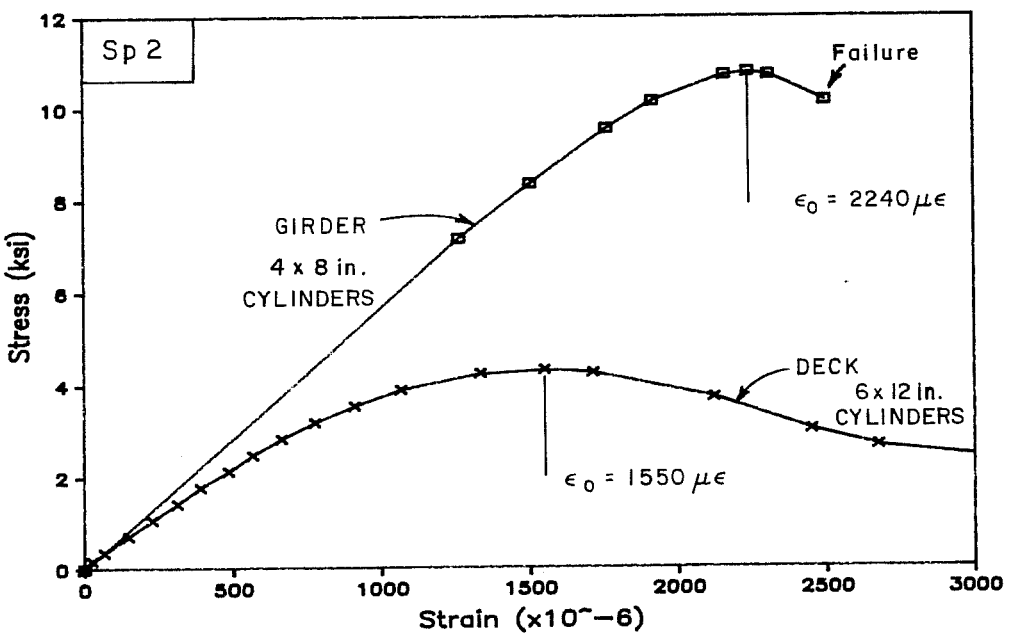

Fig. 6.52 Girder and deck concrete stress-strain curves at flexure text - Specimen 2

6.3.1.2 General Description of Behavior. A summary of the specimen history is given in Appendix B including times at which dead load compensation and deck formwork were added and removed.

When the forms were removed the girder was found to have extensive shrinkage cracking. The forms were left in place four days to improve curing. However, it appeared that the surface of the forms, which was roughened by vibrators during placement of the girder concrete, may have absorbed water instead. The forms and the unreleased prestressing strands served as the restraint required to cause cracking from shrinkage strains. The probable magnitude of shrinkage strains is considered in Sec. 6.3.1.4 with the discussion of stirrup strains prior to the flexure test.

Shrinkage cracks in the web were regularly spaced at about 7.5 in. for the full length of the specimen. Most cracks were vertical, but inclined near the ends. Horizontal cracks appeared at the junction of the web and flanges. Web cracks averaged about 0.010 in. wide with a maximum crack width of 0.035 in. A number of small cracks 0.002 in. wide or less crossed the bottom flange. The top flange cracked in few locations with cracks ranging from 0.002 in. to 0.018 in. wide. It is not known whether cracks completely penetrated the web and flanges, although some cracks did cross the top of the girder. Because the cracks were not expected to significantly affect ultimate test results, testing proceeded as planned. At release the cracks closed but the strain distribution across the section was very non-linear.

Half of the girder dead load compensation was in place at release with the remainder being put in place the following day. No additional cracking was observed at the time of release.

A second episode of unanticipated cracking occurred when deck forms were removed. Forms and dead load compensation were removed in stages with the dead load blocks replaced as soon as possible to prevent deck cracking. However, cracking was observed as blocks were removed from midspan. When the dead load was replaced, the cracks did not close fully. These cracks affected early behavior of the specimen during the flexure test but had no effect on ultimate behavior.

Prior to the flexure test, the specimen was pushed laterally to the west at the level of the deck to reduce sweep. No additional deck cracking was observed. Sweep was not large at release but increased after addition of the deck.

Actual specimen dimensions are summarized in Table 6.8.

6.3.1.3 Deflections. Midspan girder deflections from release until the flexure test are shown in Fig. 6.53. Significant events are indicated on the plot. A deflection measurement using an optical level was 0.236 in. greater than the data shown. This indicates possible movement in the dial gage stand or a change in deflection when the specimen was moved out of the prestress bed.

Camber at release was much smaller than for the first specimen because dead load compensation was present and there was a lower level of prestress. Creep caused significant increases in deflection that

Table 6.8 Actual section dimensions - Specimen 2

Girder

Use Nominal Dimensions

Strand Placement

	Distance from strands to bottom of girder, g		
	Straight	Draped	Total
No. of Strands	8	1	9
North end	1.72"	14.31"	2.84"
Midspan	1.72"	3.81"	1.95"
South end	1.80"	14.25"	2.90"

Drape locations are 19.5' from ends of girder

Deck

Width	16 3/8 "
Thickness	2 1/4 "
Offset *	3/8 "

Overhang at Interior End During Shear Tests

North end	3' 3 "
South end	9' 2 "

* - Offset is the distance from top of girder to bottom of deck. This area is filled with deck concrete and is as wide as the girder top flange.

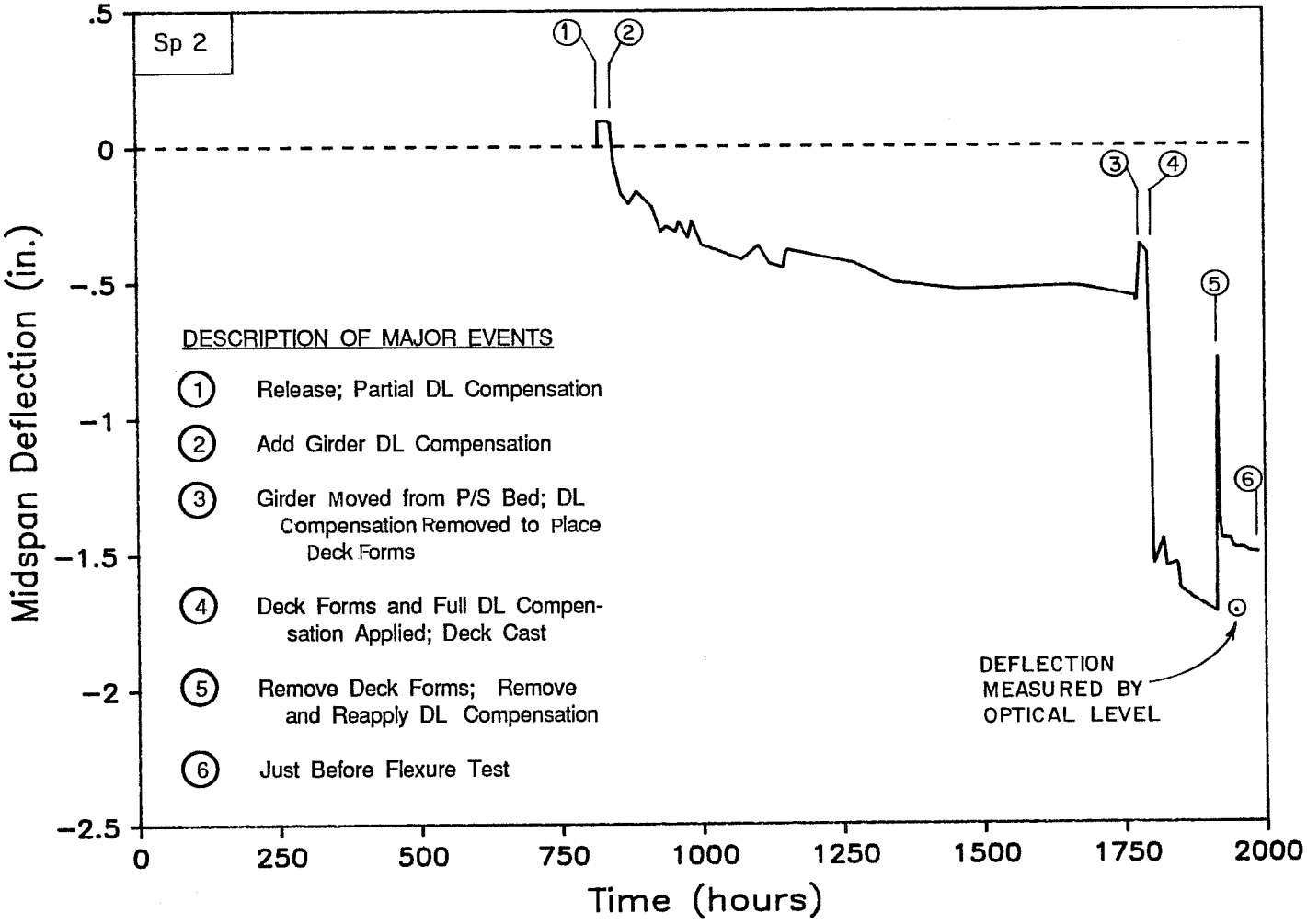

Fig. 6.53 Midspan deflection with time

continued until the time of the flexure test. The deck was not available to arrest the continuing sag because it was applied just over a week prior to the flexure test.

At release, a sweep at midspan of 0.02 in. to the east was observed. This increased to 0.03 in. during the month over which readings were taken. However, after the deck was added, the sweep was large enough to necessitate pushing the specimen approximately 3/8 in. to the west, leaving the specimen essentially straight.

6.3.1.4 Effective Stresses and Strains. Strain readings for strands, girder concrete and deck concrete were corrected for time effects and discontinuities to obtain "effective" strain for each gage. Corrected strains therefore represent an estimate of the elastic strain at a specific time. Methods described in 6.2.1.4 for Specimen 1 were also used for Specimen 2.

Typical corrected strains for straight and draped strands prior to the flexure test are shown in Fig. 6.54. A summary of the effective strand stresses and forces computed from the "average" strand strain is given in Table 6.9. Because consistent data was not available for determining the effective strand stress at the shear tests, the value used at the flexure tests was used as an estimate.

Changes in strain at release for strand gages near the ends of the girder indicate a transfer length of less than 12 in. Fig. 6.55 shows the data for active strand gages at both ends of the girder. Data for the two ends are very consistent.

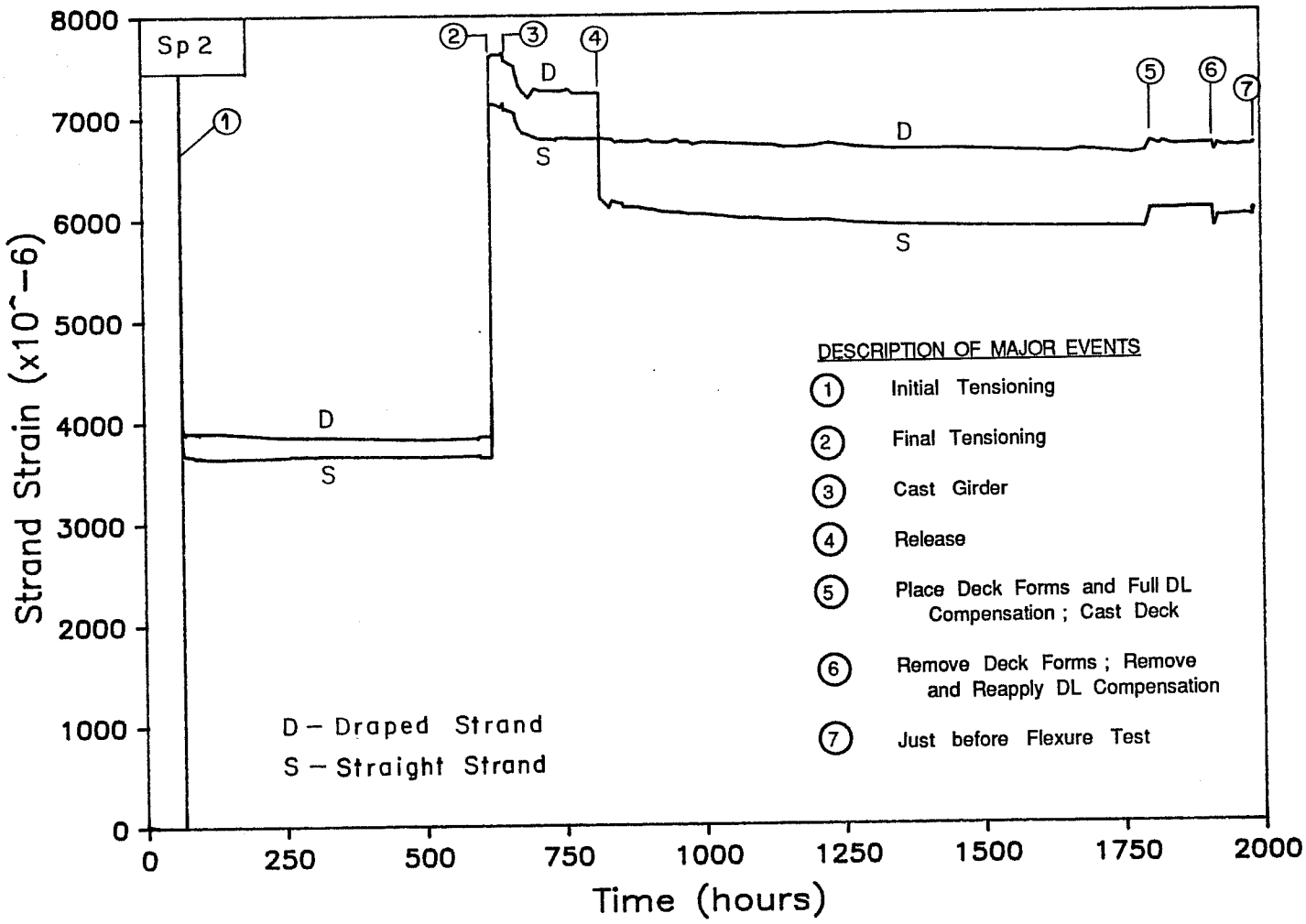

Fig. 6.54 Typical corrected midspan strand strains with time

Table 6.9 Effective strand stresses and forces - Specimen 2

	Stress (ksi)	Force (ksi)
Full Tensioning		
All locations	206.7	157.2
Prior to Release		
All locations	193.6	147.2
After Release		
Midspan	177.6	135.0
Midspan *	179.4	136.4
At both ends *	173.5	131.9
Flexure Test		
Midspan	173.1	131.7
At both ends	156.8	119.2
Shear Tests (estimated)		
At both ends	156.8	119.2

* - These values represent computed instantaneous elastic prestress losses plus 25% to provide better agreement with the limited measured strain data. The elastic losses were calculated using the "Prior to Release" prestress force and gross section properties.

Area of prestressing steel = $9(0.0845 \text{ in.}^2) = 0.76905 \text{ in.}^2$

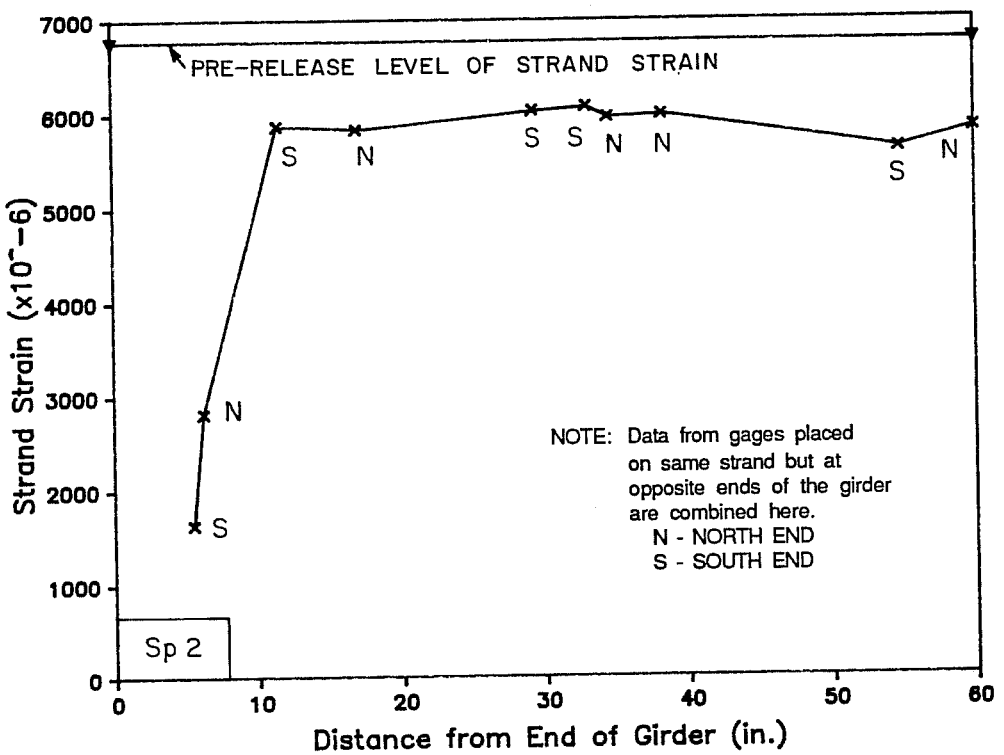

Fig. 6.55 Strand strains near ends of girder before and after release

Typical girder concrete strain data is presented in Fig. 6.56. Readings were again susceptible to large variations due to changes in temperature. Figure 6.57a shows measured and computed girder concrete strains at release as they vary with location on the girder. Agreement is fair between lines of gages, and poor when comparing measured and computed strains because of the effects of shrinkage cracking. The nonlinear strain gradient is a result of the top and bottom flanges receiving load at release while the cracks in the web were closing. Strain readings were taken shortly after release and may contain some creep. The second plot (Fig. 6.57b), compares uncorrected and corrected strains prior to the flexure test with computed strains across the depth of the girder. Agreement of corrected strains is again fair between the two lines of gages and poor for the computed strains with the effects of shrinkage still obvious. Corrected strains at the time of the flexure test are related to computed strains in much the same way as measured and computed strains at release.

Creep in the girder concrete had slowed by the time of the flexure test, as indicated by Fig. 6.56. The magnitude of creep during this period ranged from about 250 microstrains near the bottom of the girder to 450 microstrains near the top, although the data were erratic (Fig. 6.57b).

Strain gages were applied to the top of the deck prior to removal of deck forms, and the remaining deck gages were applied after form removal. Typical top and bottom deck strains prior to the

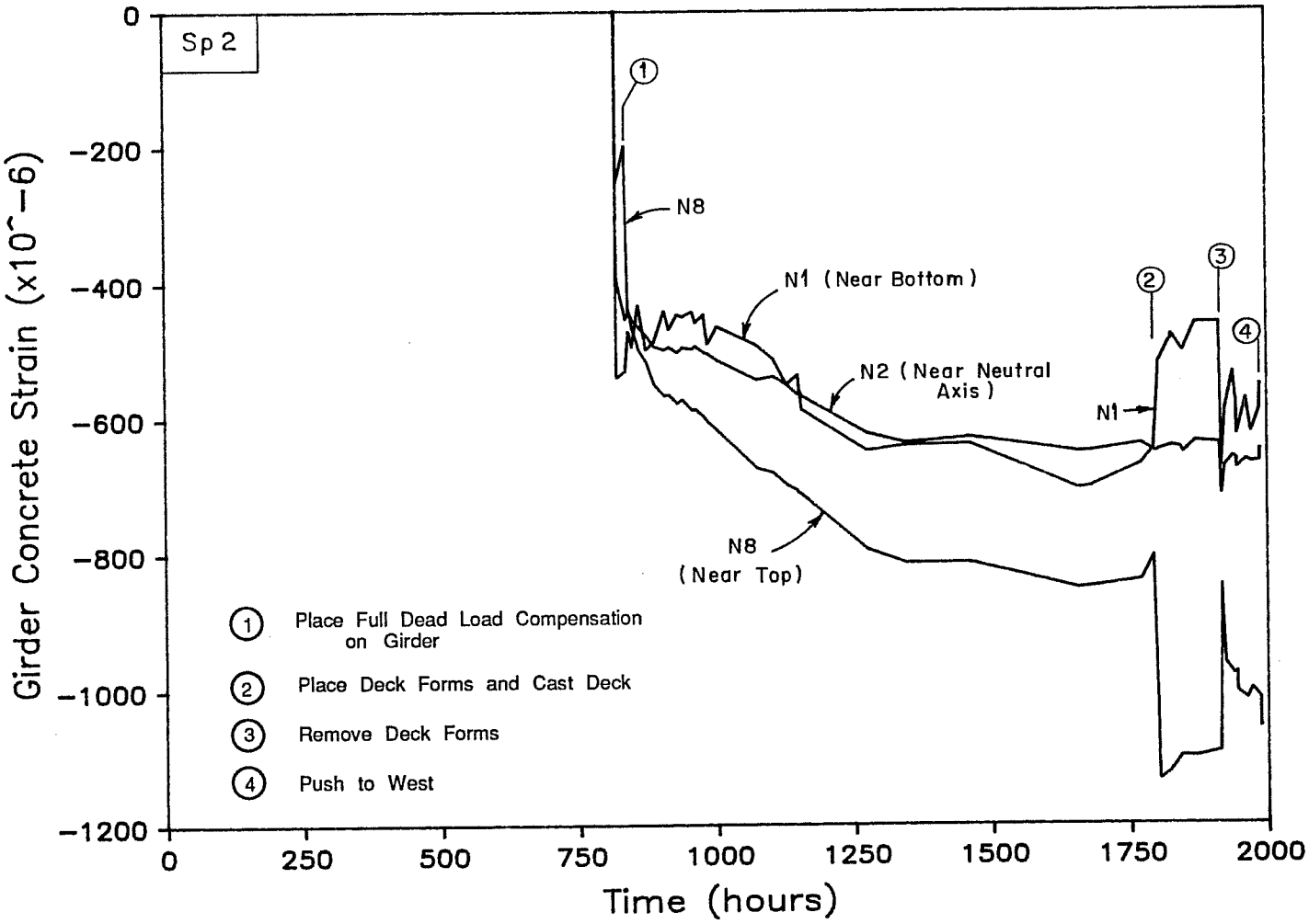

Fig. 6.56 Girder strains with time for typical gages

flexure test are shown in Fig. 6.58, and strains and changes in strain are shown for all deck gages in Fig. 6.59. While the top gages were present to measure the elastic change in strain at removal of the forms, these strains were small and were obscured by large strain variations caused by temperature (Fig. 6.58). Effective strains at the beginning of the flexure test were determined to be the strains caused by the lateral push for the same reasons given for Specimen 1.

Data indicate the presence of existing deck cracks or that additional deck cracks formed when the specimen was pushed to the west, because compression measured on the east side of the deck was significantly larger than the tensile strains measured on the west side. The difference in strains between east and west sides of the deck affected strains measured during early stages of the flexure test because cracks had to be closed before the west side could pick up additional strain.

Creep strains in the deck prior to the flexure test were about 100 microstrains at the top and negligible at the bottom. Creep was still increasing slowly at the time of the flexure test.

Stirrup strains for one stirrup at each end of the girder are shown in Fig. 6.60. The large displacement in strains shortly after placement of girder concrete appears to be caused by shrinkage in the concrete. From this data, shrinkage strains of approximately 250 microstrains occurred within a day after casting with an additional 50 microstrains occurring prior to release. Using the girder concrete

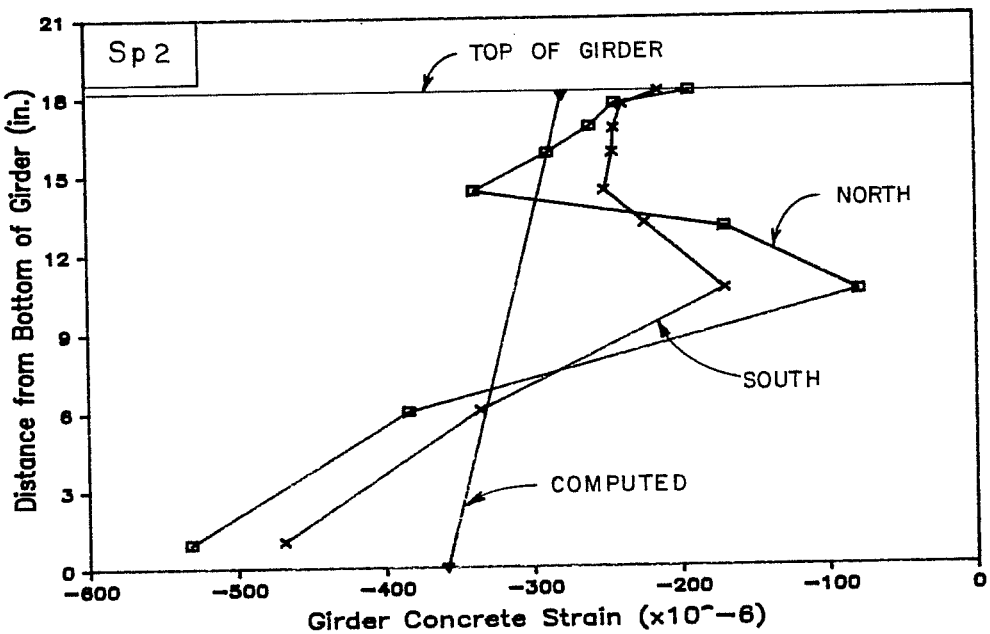

(a)

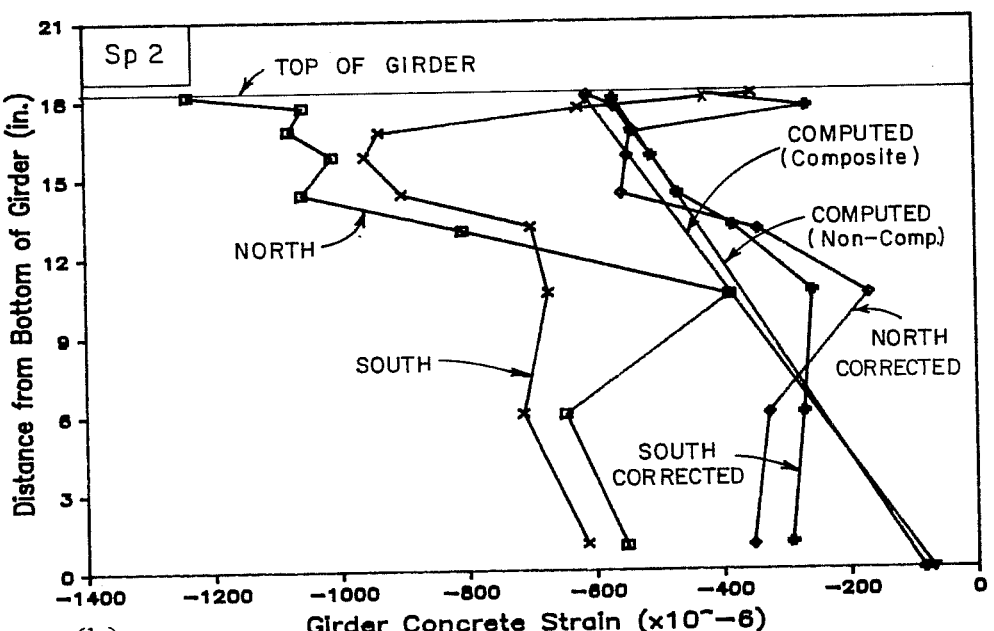

(b)

Fig. 6.57 Computed and measured girder concrete strains at release and prior to flexure test: a) at release; b) prior to ultimate flexure test

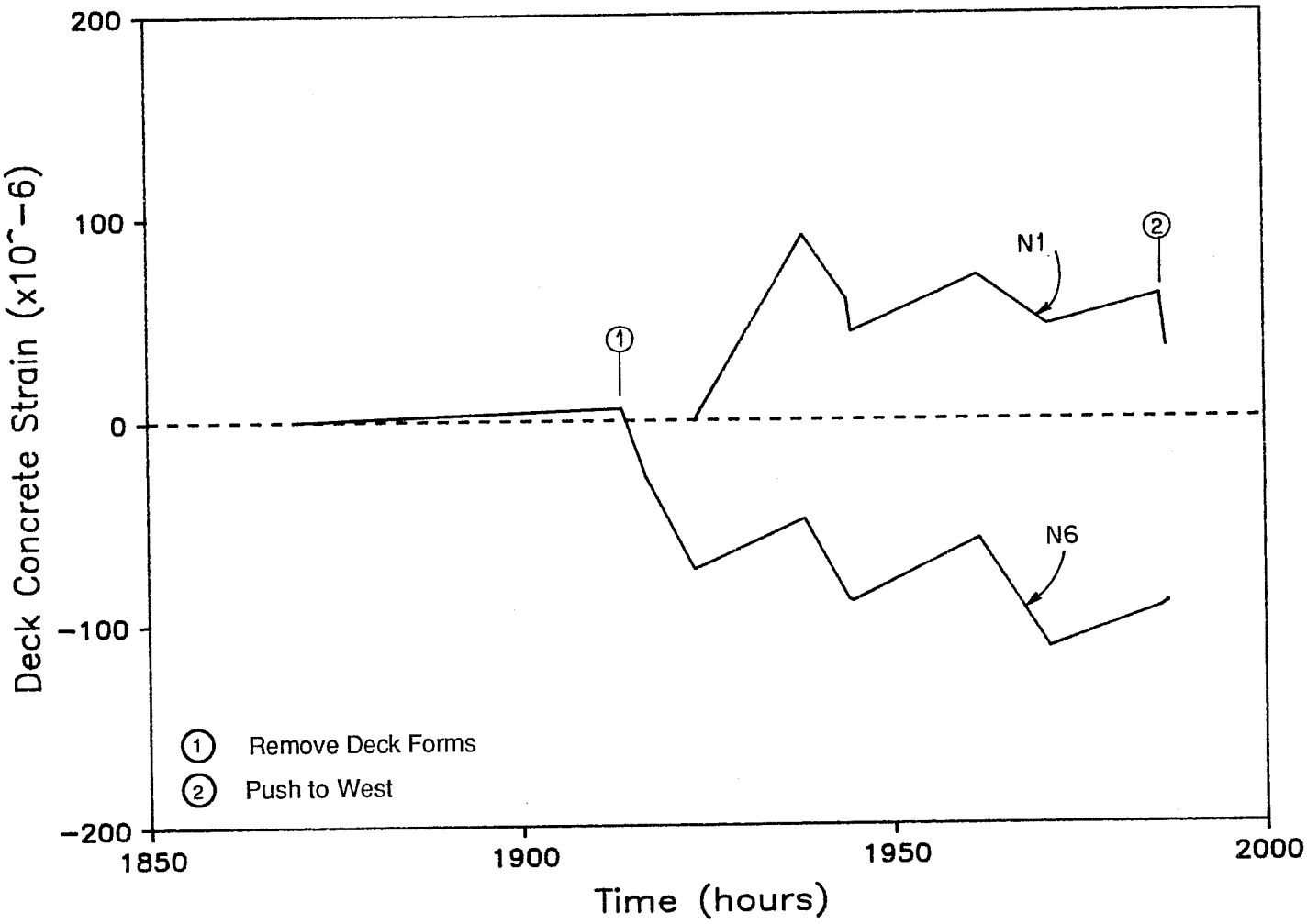

Fig. 6.58 Deck concrete strains with time for typical gages

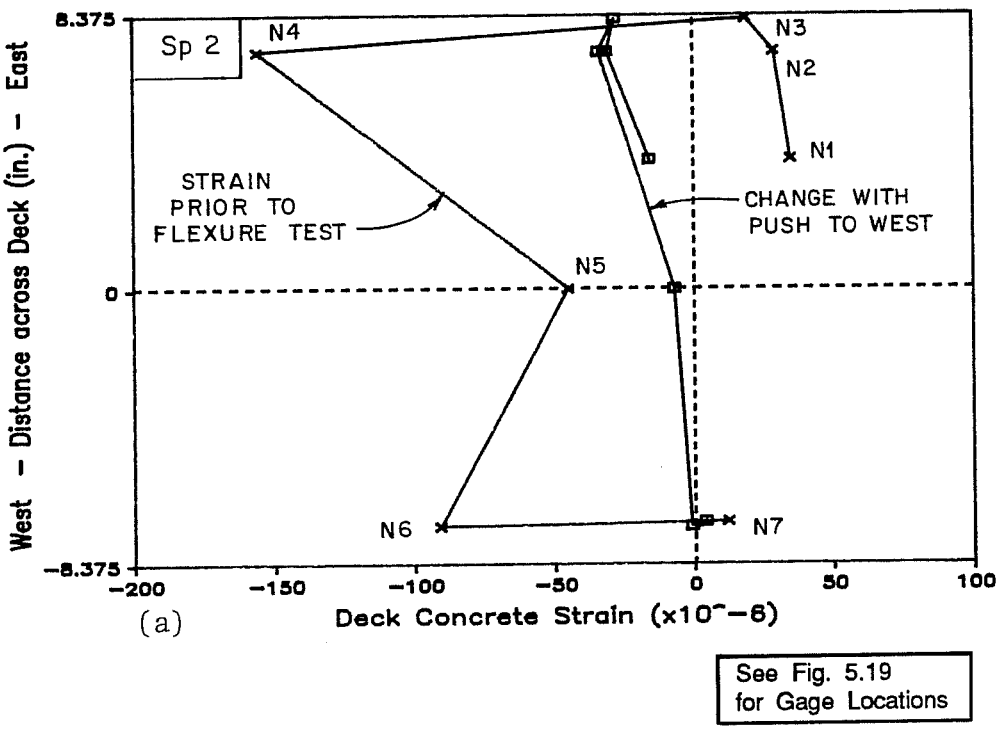

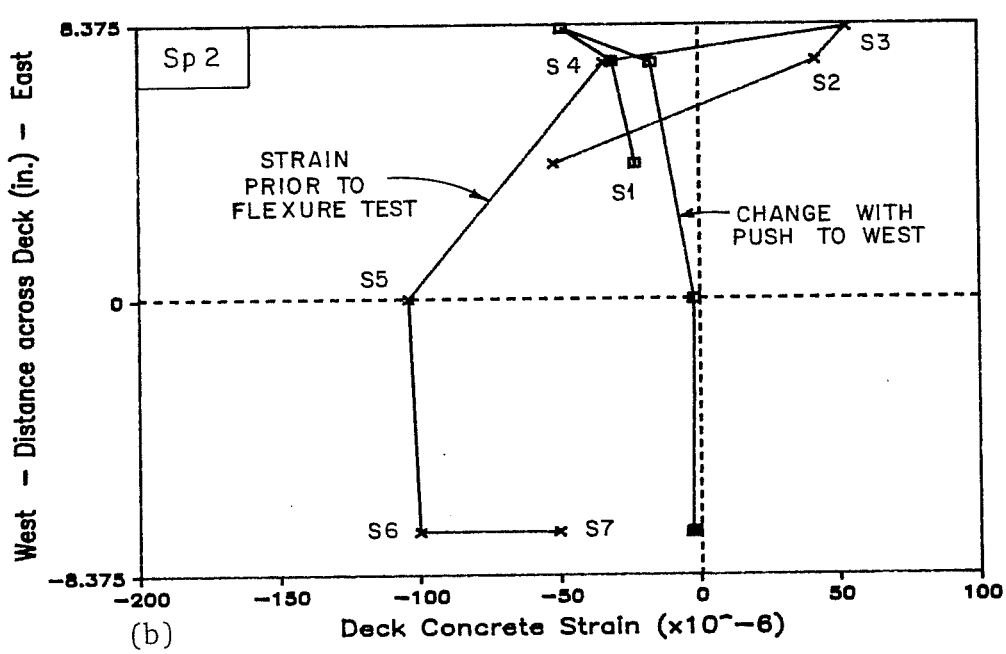

Fig. 6.59 Deck concrete strains at selected times: a) north gages; b) south gages

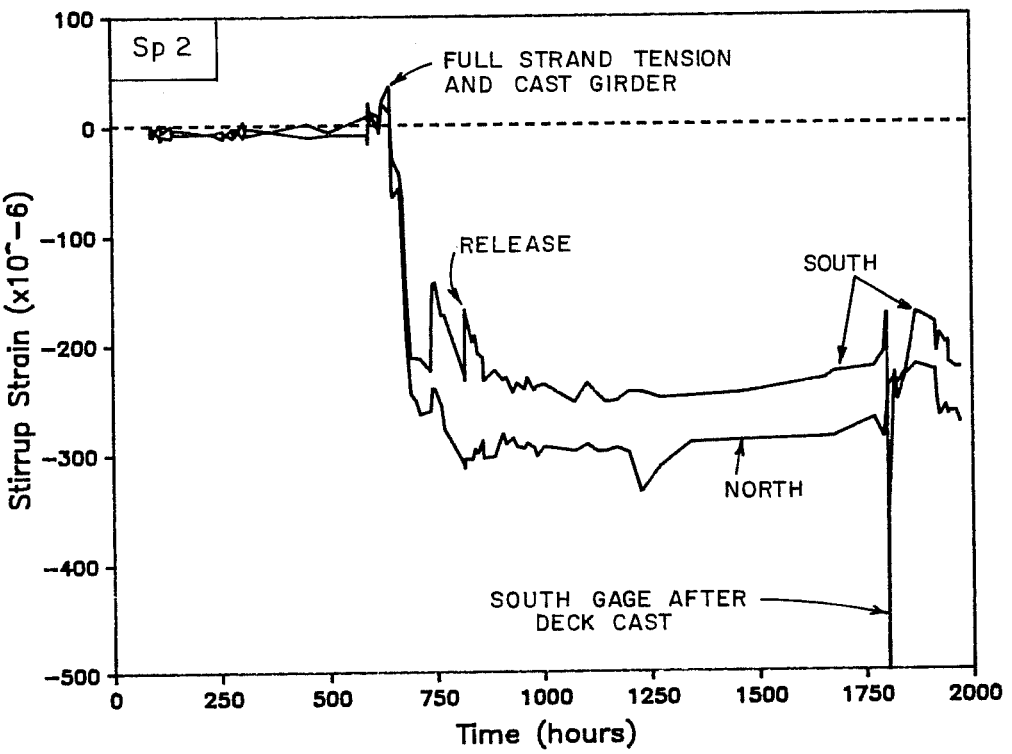

Fig. 6.60 Stirrup strains with time

modulus at release, the total shrinkage strain would correspond to a stress of 1.6 ksi which is nearly twice the measured modulus of rupture at release (see Table 6.7). This high shrinkage strain with the restraint provided by forms and unreleased strands caused the cracking. After release, strains remained fairly constant until the flexure test, except for a change when the deck was cast that was probably caused by disturbing the leads during placement of the concrete.

6.3.2 Flexure Test.

6.3.2.1 General Description of Behavior. Because of the widespread shrinkage cracks only an ultimate flexure test was conducted on Specimen 2. Load stages used during the flexure test and times at which they occurred are given in Appendix B. Frequency of readings and designation of load stages are the same as Specimen 1 except loads used during the test required no correction.

Flexure cracks were first detected in the constant moment region at 4 kips. Some cracks were directly below shrinkage cracks, but others were independent of prior cracking. Cracks extended into the web at 6 kips. At 7.5 kips load the deflection was held by the lower cross heads, rams were retracted and upper cross heads were reset. Web shear cracks about 3 in. long formed near the ends of the girder as inclined extensions of shrinkage cracks at 8 kips. Flexure cracks reached the top of the web at 8.5 kips and entered the taper of the top flange at 9.25 kips. At this load, crack widths near midspan were approximately 0.02 in. and cross heads were reset.

At the next load stage, 9.44 kips, cracks progressed through the taper and into the top flange. The deflection was maintained at this load stage while a leaking hose was replaced. Load was then brought back to 9.44 kips. At 9.67 kips cross heads were reset. Cracking in the constant moment region and the large deflection of the specimen at this load are shown in Fig. 6.61. Cracks extended nearly an inch into the top flange at this load as shown in Fig. 6.62, which was taken after failure. While attempting to bring the load back to 9.67 kips, failure occurred at a load of 9.59 kips. The specimen failed explosively in compression midway between the north load point and midspan. There was no warning of collapse other than the large deflection and many cracks.

Failure was violent and very similar to the failure observed for Specimen 1 (Fig. 6.63). Dead load blocks were again stripped from their hangers. Secondary failure cracks formed at the junction of the web and bottom flange and branched upward into the web. The ends of the girder were again thrown up into the air and drawn inward, causing the bearing pads to roll off the supports. The failure surface was typical of a compression failure. The surface was an inclined plane originating near the top of the girder and continuing through the deck (Fig. 6.64a). Viewed from above, the failure surface was wedge-shaped as shown in Fig. 6.64b. The appearance of the failure surface did not provide conclusive evidence for determining whether the girder or deck concrete crushed first.

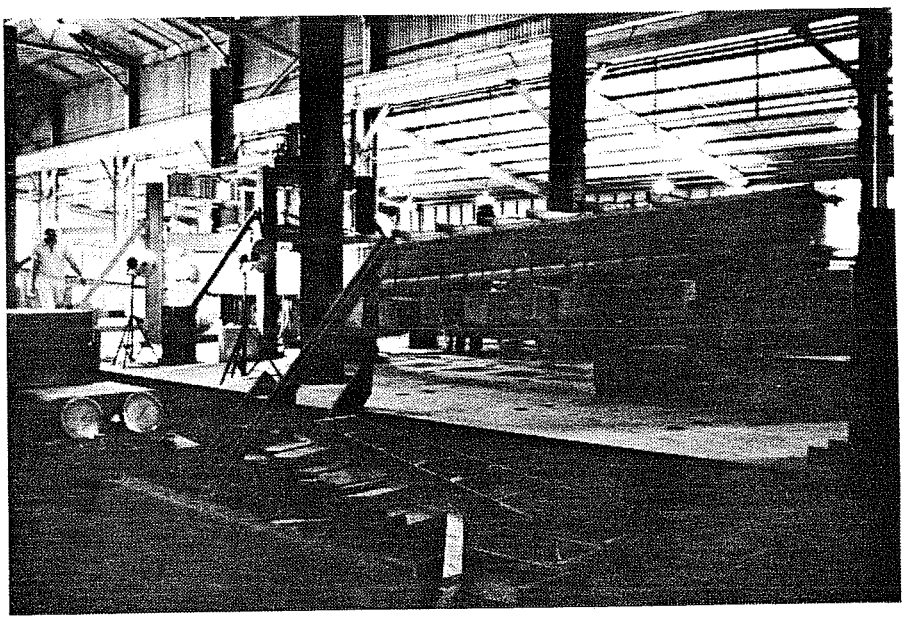

(a)

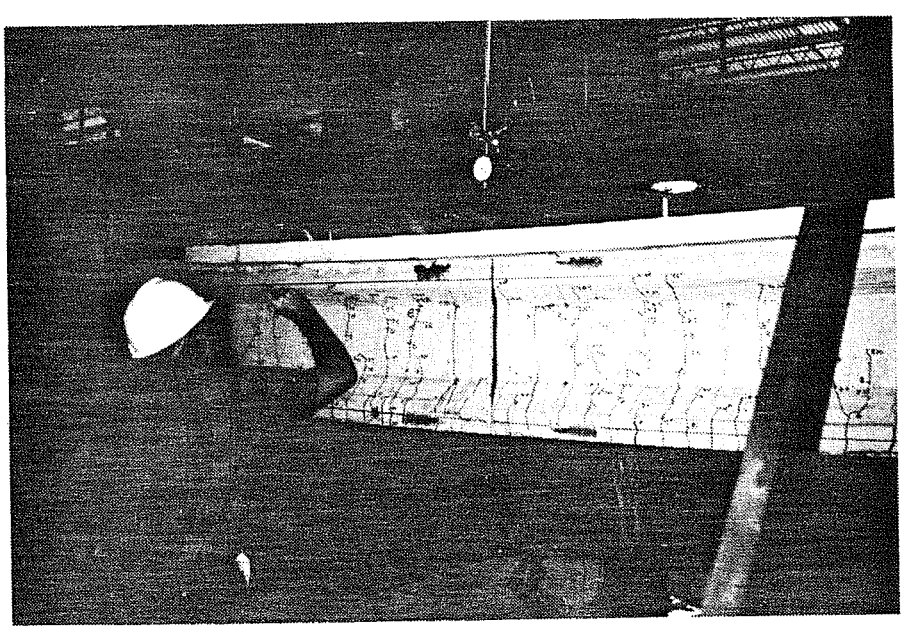

(b)

Fig. 6.61 Photographs prior to flexural failure (9.67 kips) - Specimen 2: a) entire specimen; b) midspan

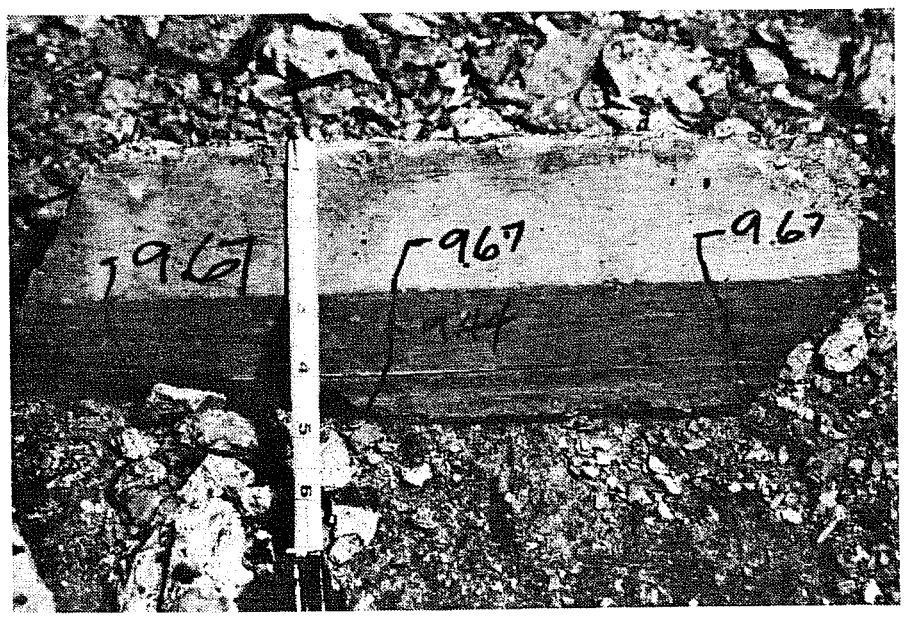

Fig. 6.62 Photograph of extent of cracking of top flange prior to flexural failure - Specimen 2

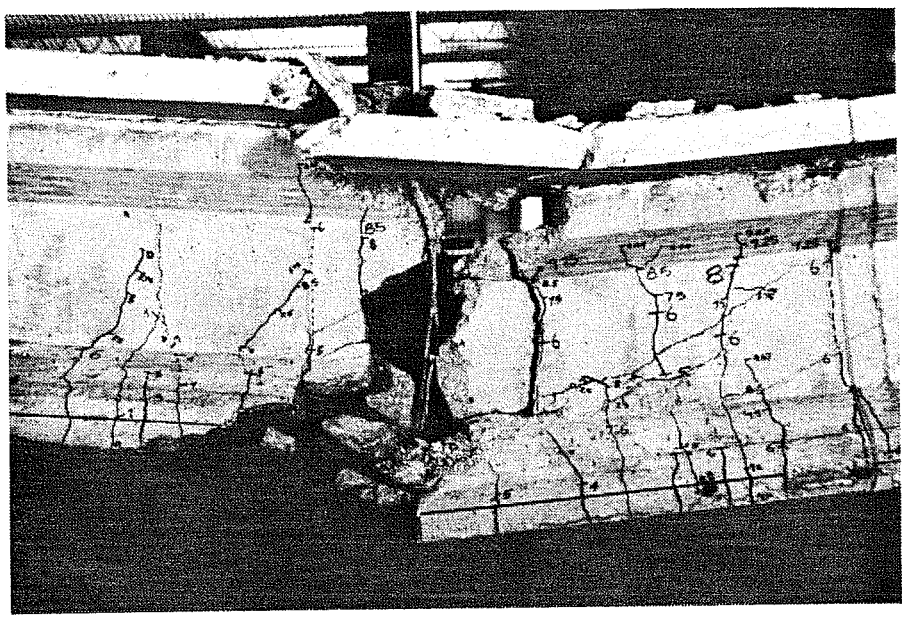

(a)

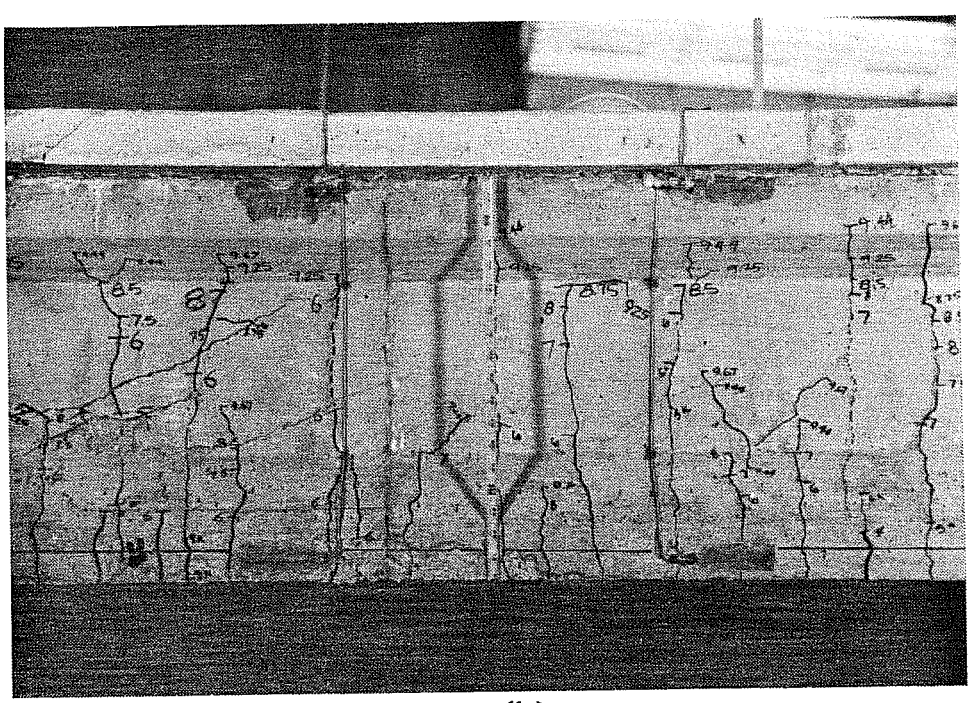

(b)

Fig. 6.63 Photographs after flexural failure - Specimen 2: a) at failure; b) at midspan

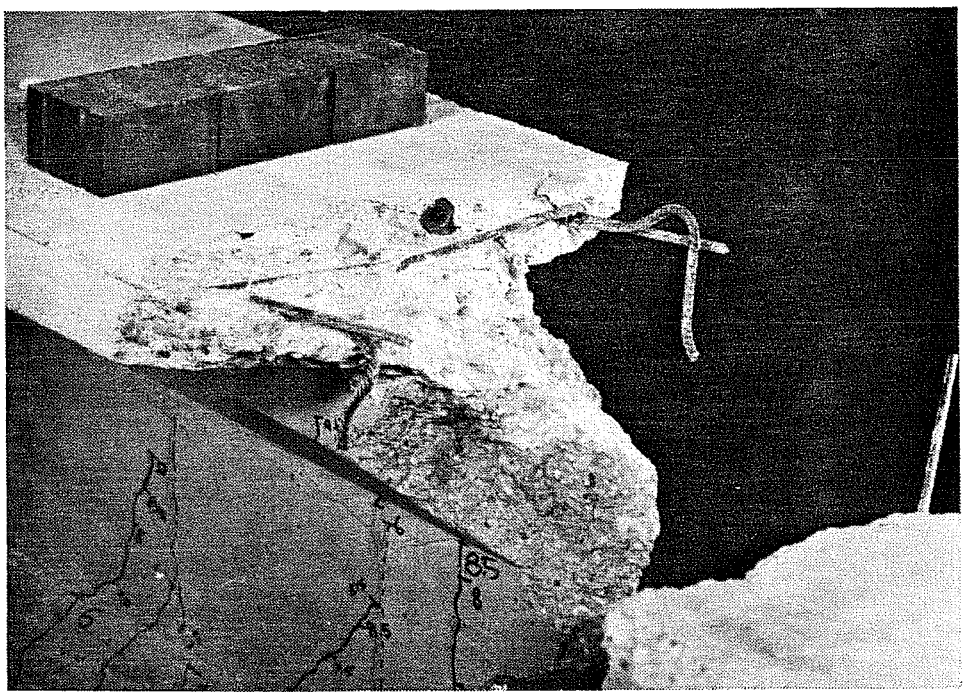

(a)

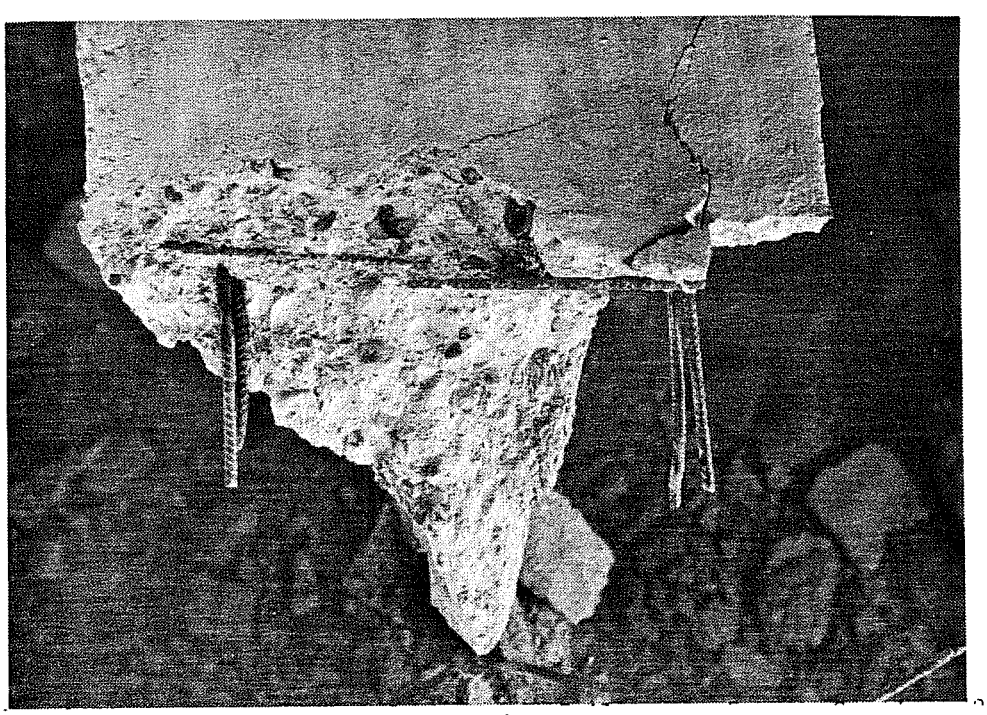

(b)

Fig. 6.64 Photographs of concrete failure surface - Specimen 2: a) side view; b) top view

At failure, spacing of flexure cracks crossing the bottom flange averaged 2.7 in. in the constant moment region. The flexure cracks nearest the supports were located 13 ft from the ends of girder and were extensions of shrinkage cracks.

Significant events during the test and design loads are summarized in Table 6.10. Loads were determined as described for Specimen 1 (Table 6.4). Test results are compared with computed and design loads later in this chapter and in the next chapter.

6.3.2.2 Deflections. Net deflection at midspan, adjusted for bearing pad compression, is shown in Fig. 6.65. Loads from Table 6.10 are indicated on the figure. Observed cracking coincided well with the onset of nonlinear behavior. The specimen exhibited a limited yield plateau and large deflections before reaching the ultimate load, which demonstrates a significant capacity for energy absorption and also indicates that such a structure in service would provide ample warning of impending collapse. While post-ultimate capacity is shown, this is illusory since the choice of load stages and the necessity of resetting the load system made this possible. If load had been applied continuously, no post-ultimate behavior would be expected, as was observed with the first specimen.

Locking the deflection to reset the loading system clearly affected the behavior of the specimen, as the presence of offsets in the load-deflection curve indicate. This phenomena was discussed during the consideration of Specimen 1 data.

Table 6.10 Load stages and interest during flexure test - Specimen 2

Key (Fig. 6.65)	Description of Load Stage		Load (kips)
Computed and Observed Behavior			
CD	Computed Decompression	$(0\sqrt{f_c'})$	0.86
CC	Computed Cracking	$(7.5\sqrt{f_c'})$	2.56
C	Observed Cracking	$(10.4\sqrt{f_c'})$	4.00
R	Reset Loading System		7.50
R	Reset Loading System		9.25
L	Lock off Loading System		9.44
U	Ultimate (Maximum) Loading		9.67
F	Failure Load		9.59
CW	Computed Web Cracking at h/2		15.86
Design Loads			
	Service Loads:		
LL	Live Load		1.87
LI	Live Load + Impact*	$(6\sqrt{f_c'})$	2.22
FL	Factored Load (AASHTO)		6.34
NC	Computed Nominal Capacity ($\phi = 1$)		8.56
Total Reaction at Ultimate Load			17.67

* - Impact factor computed using prototype span of 146 ft.

For Notes, See Table 6.4

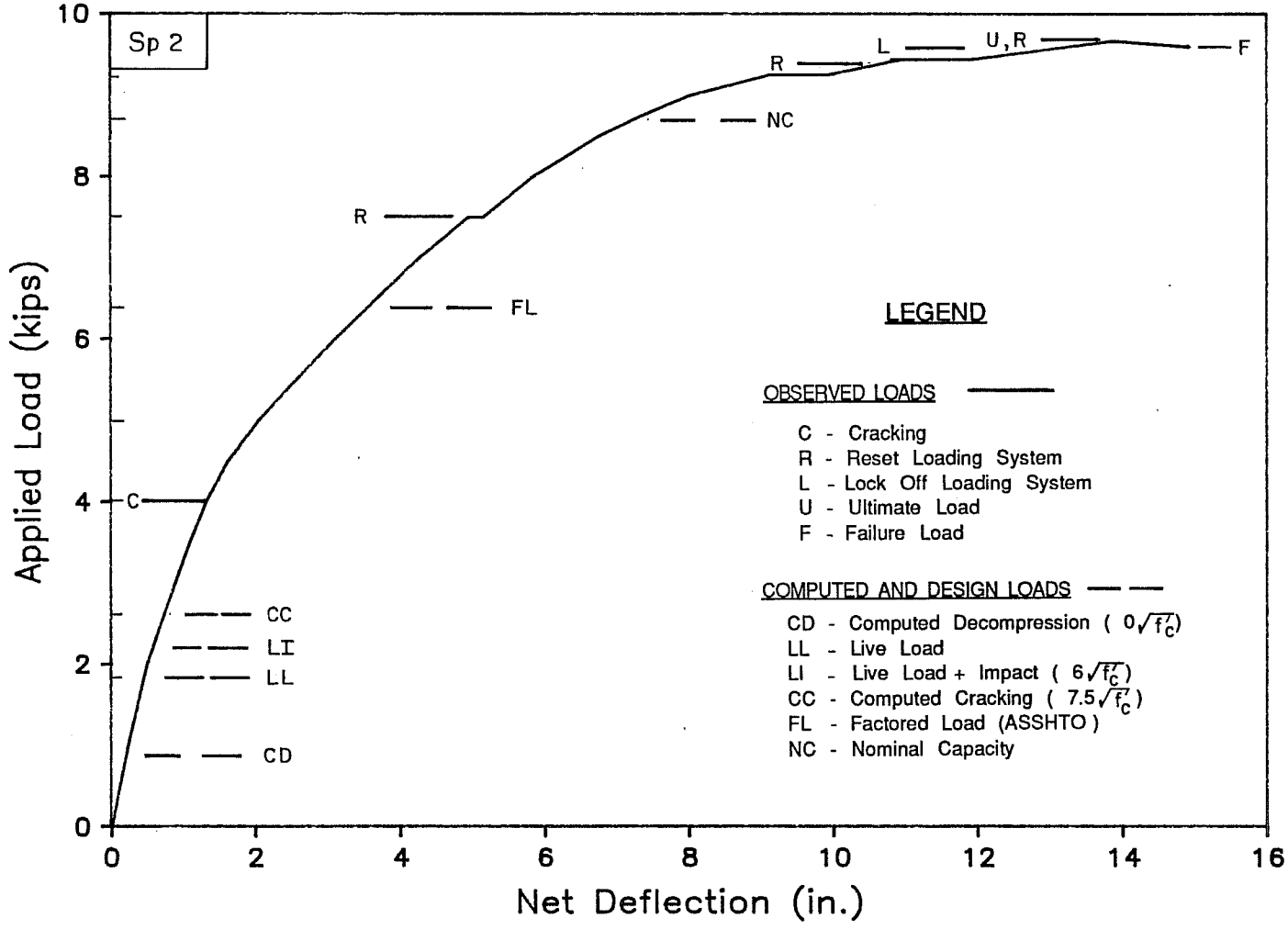

Fig. 6.65 Deflection at midspan during flexure test

6.3.2.3 Strand and Concrete Strains. Corrected strand strains for instrumented strands are shown in Fig. 6.66 with the average strain which represents the strain at the centroid of the strands. Strains for the top draped strand were estimated using bottom strand data for loads above 8.75 kips. Strains at failure were estimated using load-deflection data. Average strand stresses during the test are shown in Fig. 6.67.

Strains at ultimate and failure differed very little. At failure, the average strand strain reached 1 percent, which is the strain used to define yield in ASTM A416 [25]. However, both the bottom strand and the average strand strains failed to reach a strain corresponding to the 0.2 percent offset.

Corrected girder concrete strains are shown in Fig. 6.68. Strains at failure are estimated using load-deflection data. Strains for the upper gages are presented with respect to gage location on the girder for selected loads in Fig. 6.69. The gages behaved well during the test as shown by the net strain plots in Fig. 6.70 and 6.71, which correspond to plots of corrected strains in Fig. 6.68 and 6.69. Strains from both sides of the girder near the top and bottom (Fig. 6.72) indicated that the girder was not moving laterally during the flexure test.

At ultimate load, strain at the top of the girder was less than 1100 microstrains and perhaps as low as 700 microstrains. At failure, data were available from only one gage and this indicated a

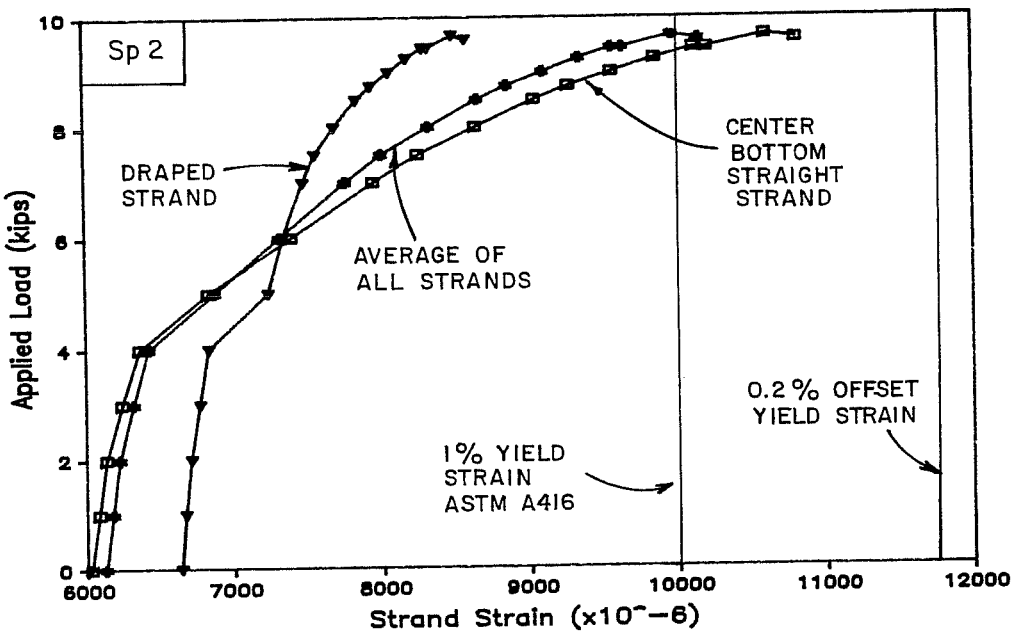

Fig. 6.66 Corrected and average strand strains during flexure test

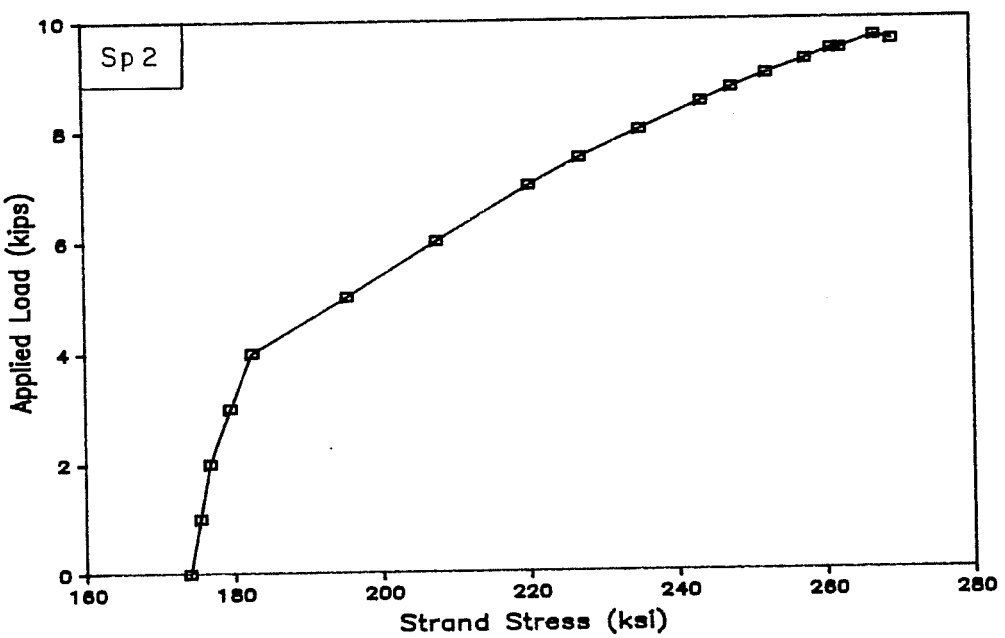

Fig. 6.67 Average strand stress during flexure test

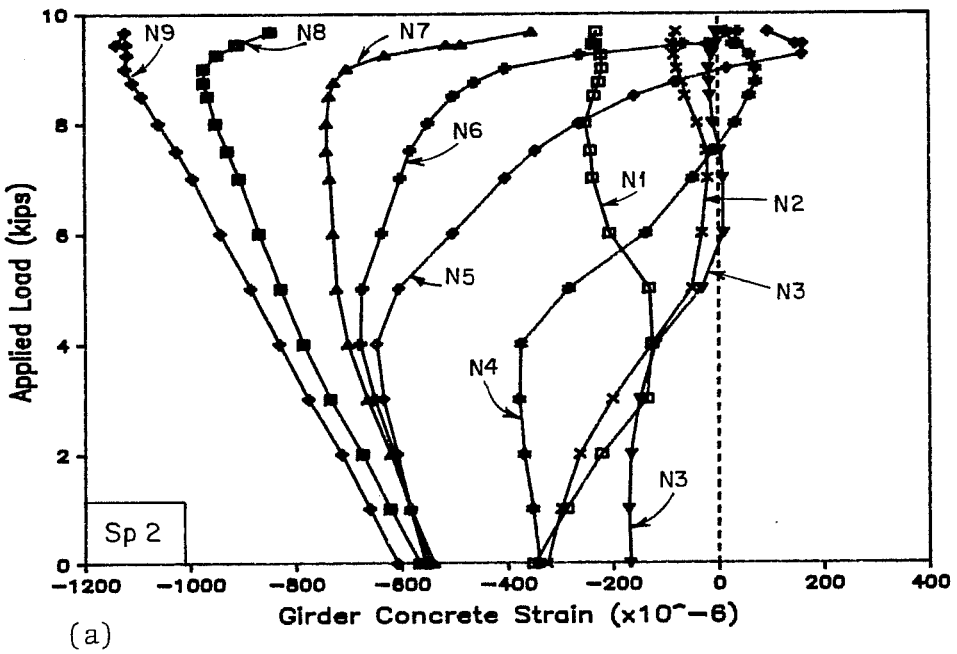

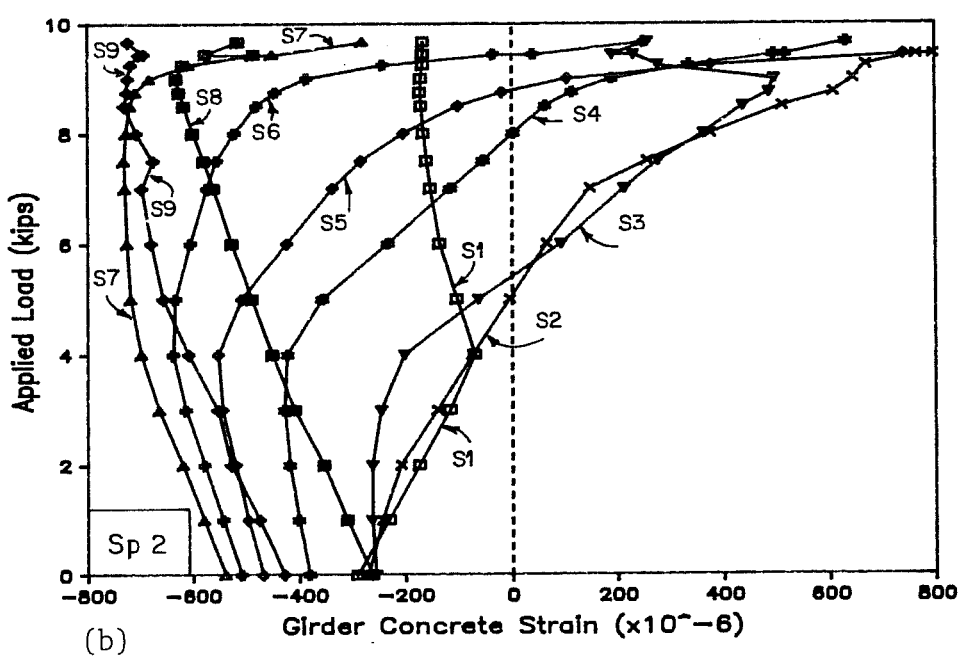

Fig. 6.68 Corrected girder concrete strains during flexure test: a) north gages; b) south gages

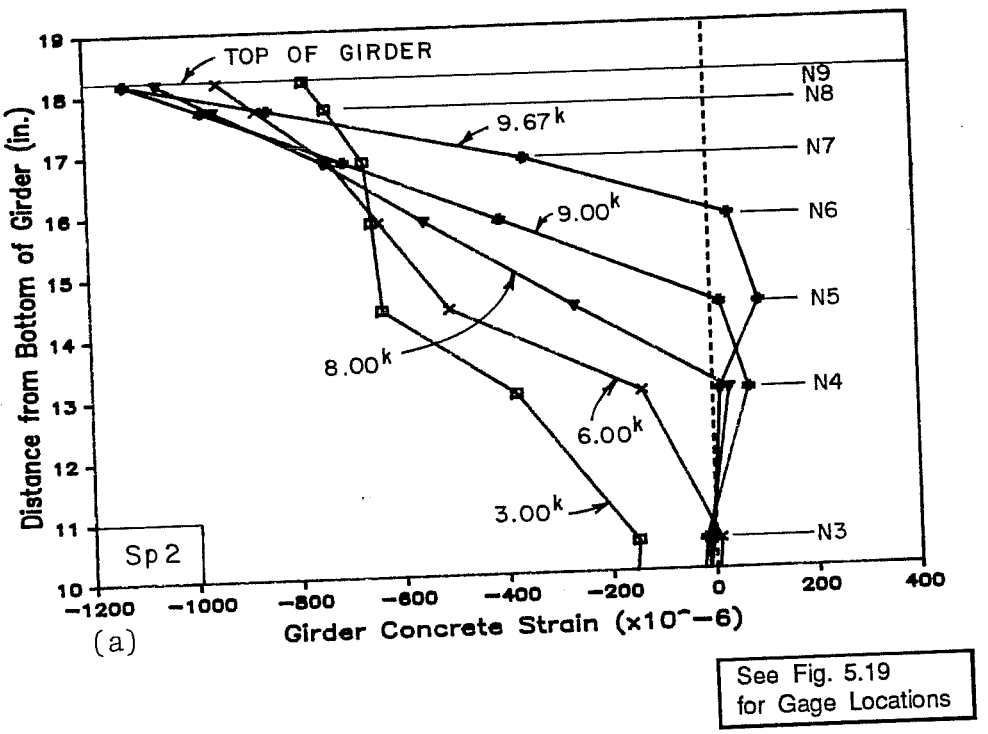

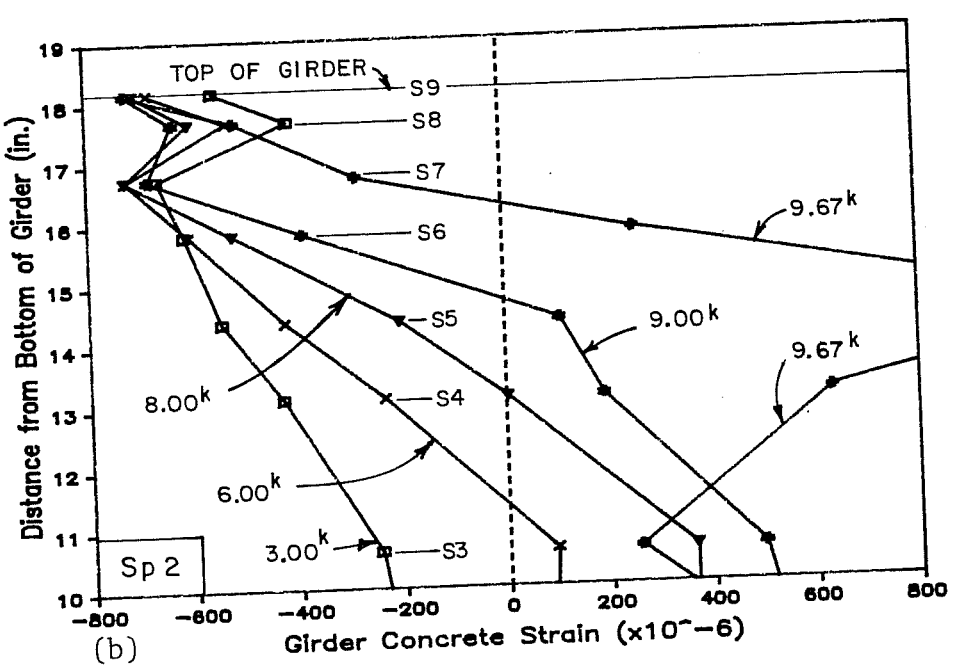

Fig. 6.69 Corrected girder concrete strains at selected loads during flexure test: a) north gages; b) south gages

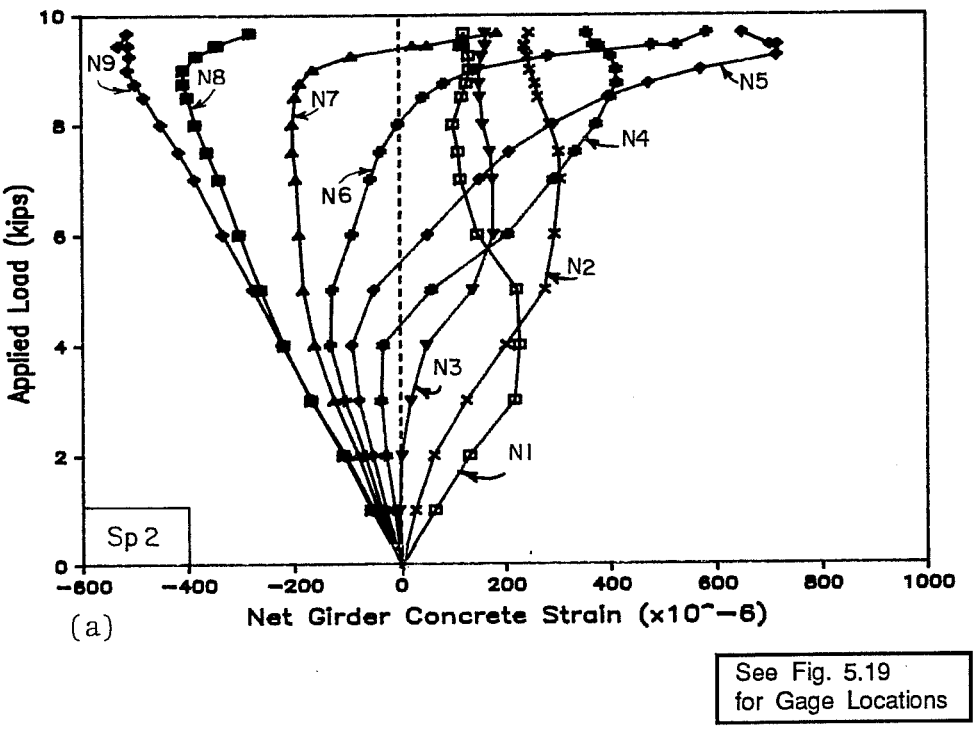

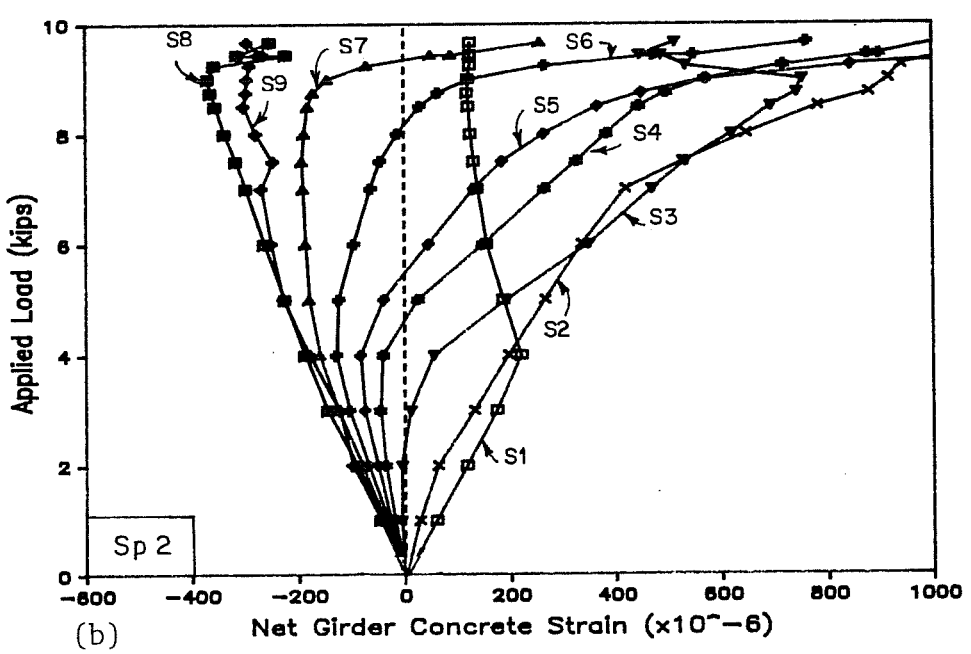

Fig. 6.70 Net girder concrete strains during flexure test: a) north gages; b) south gages

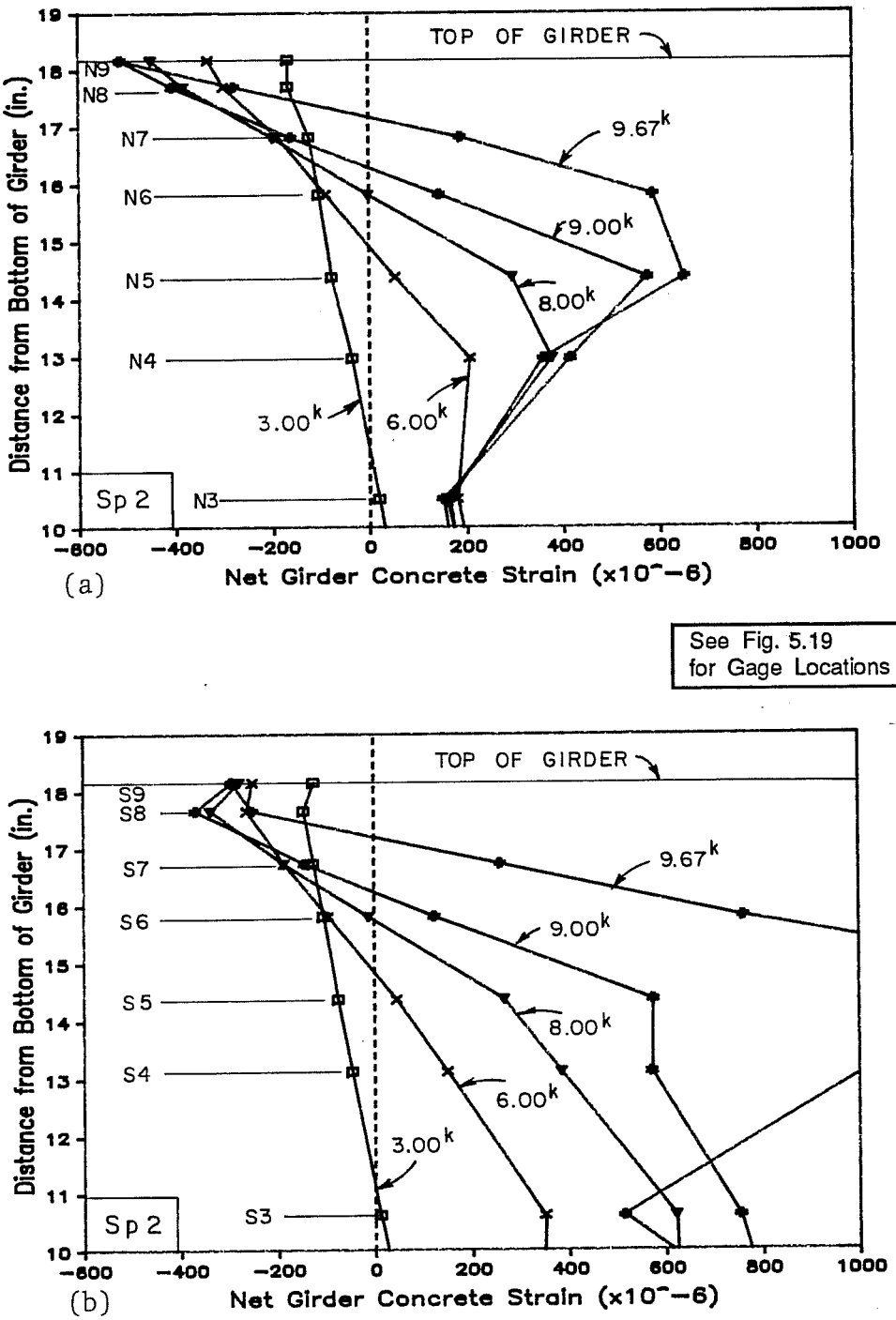

Fig. 6.71 Net girder concrete strains at selected loads during flexure test: a) north gages; b) south gages

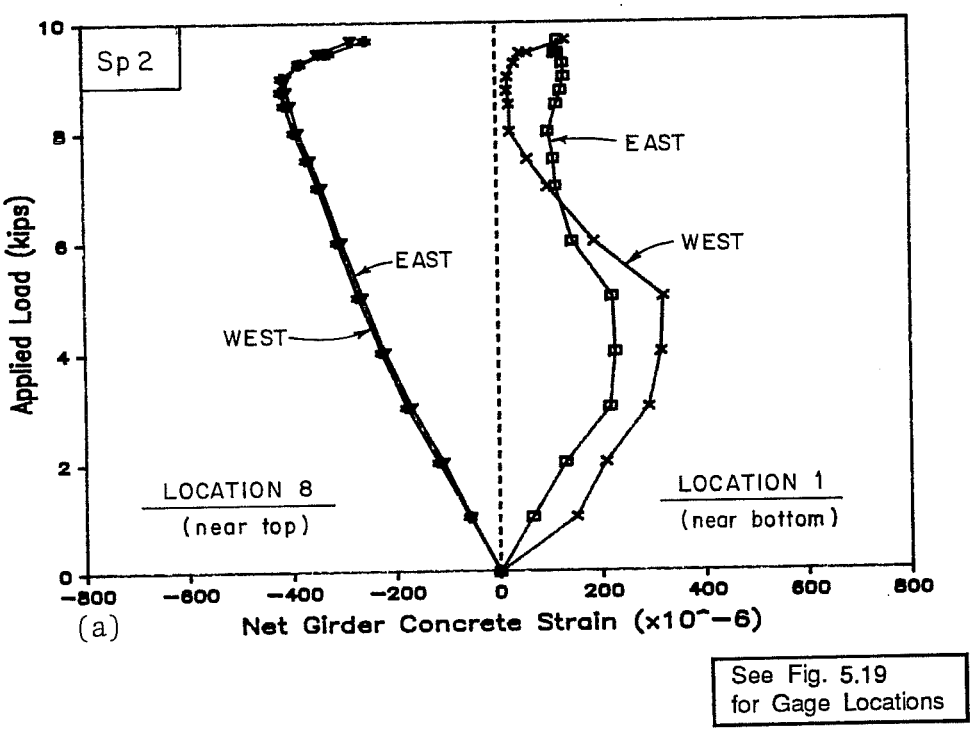

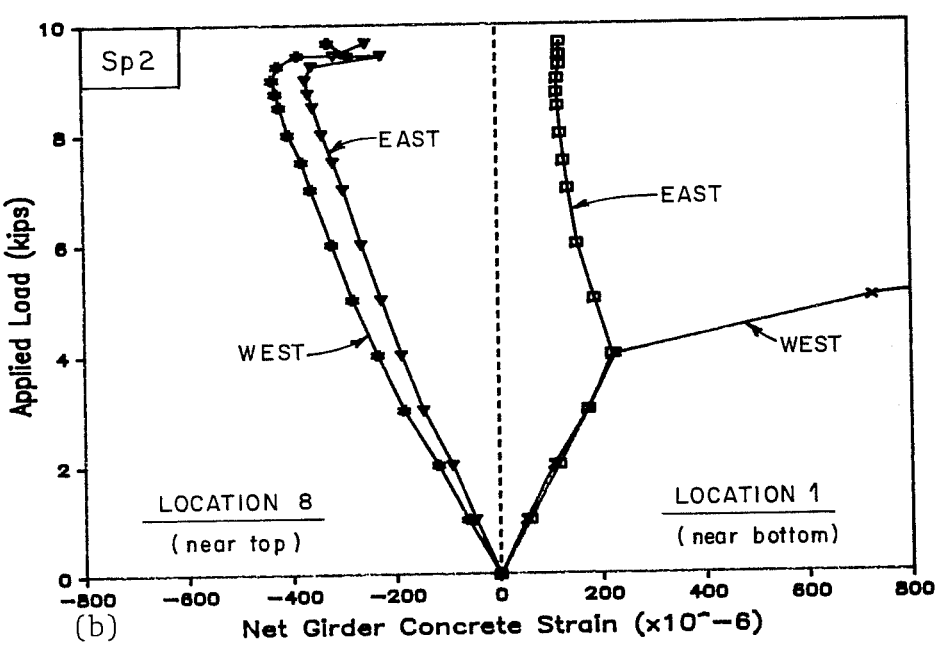

Fig. 6.72 Net concrete strains on opposite sides of girder during flexure test: a) north gages; b) south gages

decrease in strain of less than 30 microstrains from ultimate. These values are about half the strain measured at maximum stress and failure for cylinder tests of this concrete. Top of girder strains at the north location are consistent with nearby gages as demonstrated by comparing these strains with strains computed for the top of the girder using net strains from two lower gages as shown in Fig. 6.73. The top of girder gage at the south line was not functioning properly. Therefore, the top of girder strain at ultimate can be taken as 1100 microstrains based on north gage data and the computed change in strain at the south location.

The crack height computed using corrected girder strains is shown in Fig. 6.74. At failure, the computed crack height was approximately 16 in. which is 2 in. below the top of the girder and agrees well with visual observations.

Corrected deck concrete strains are shown for typical top and bottom gages in Fig. 6.75. Data for all deck strain gages are presented in Fig. 6.76 with respect to gage location for selected loads. The uniform increase in strain across the section indicated that behavior was symmetrical. The east gage at the north line on the top of the deck appears to be faulty since no reason was arrived at to explain the high strains. Both bottom gages on the west side of the deck also displayed unexplainable behavior by lagging behind the corresponding gages on the east side.

Strain at the top of the deck was 2100 microstrains at the maximum load and 2280 microstrains at failure. The strain at failure

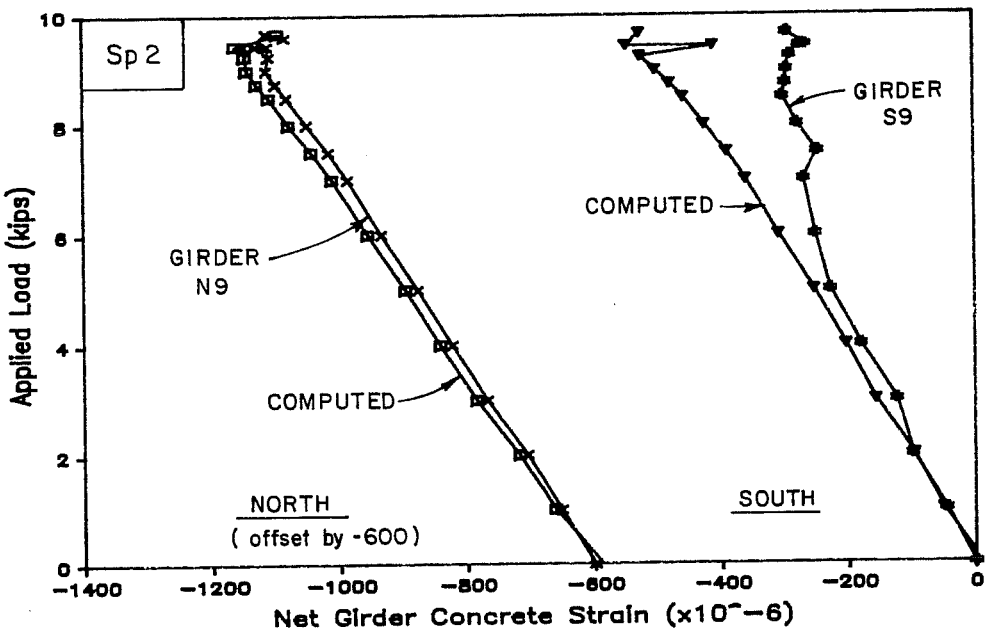

Fig. 6.73 Measured and computed top of girder concrete strains

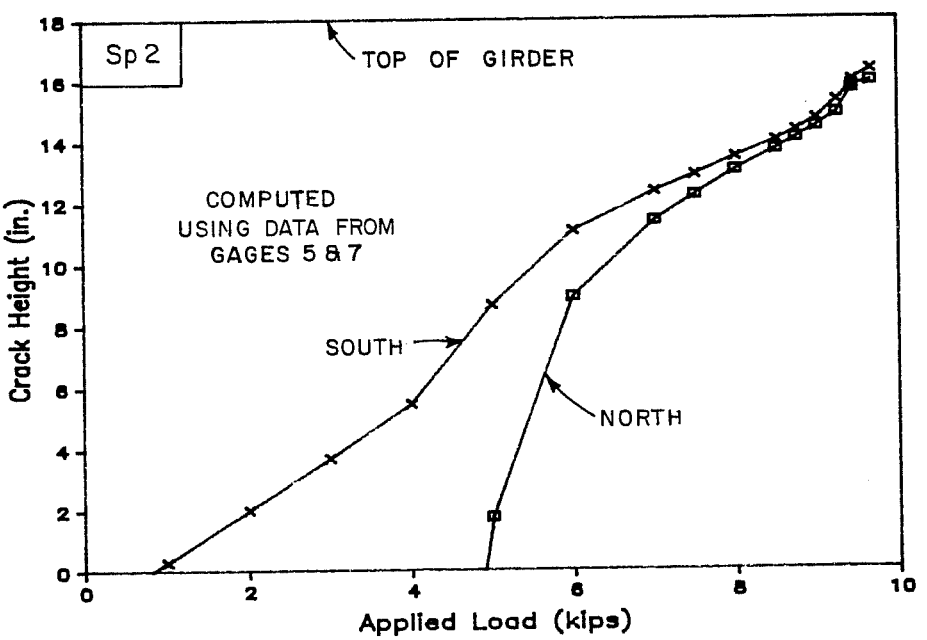

Fig. 6.74 Computed crack height

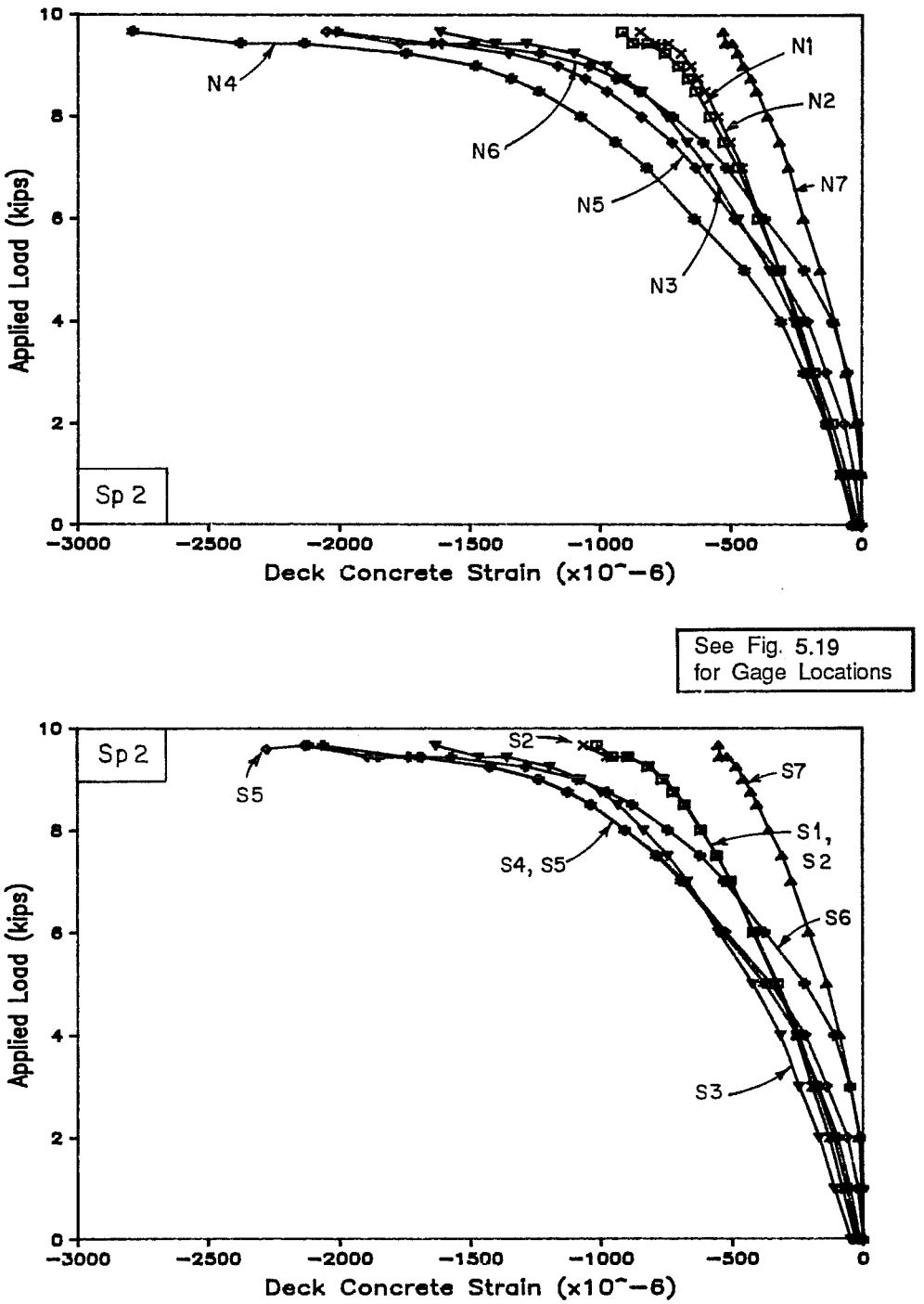

Fig. 6.75 Corrected deck concrete strains during flexure test: a) north gages; b) south gages

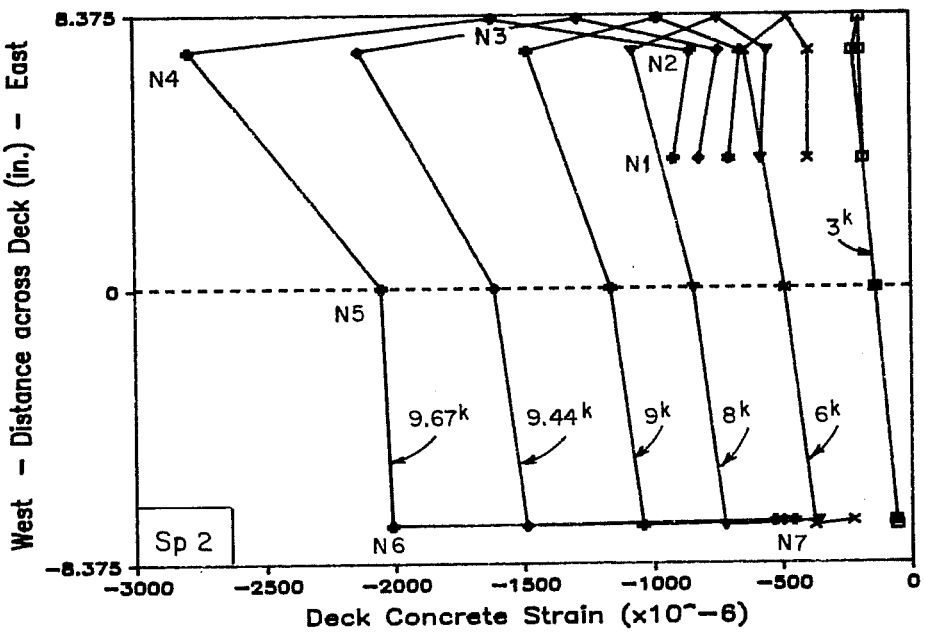

See Fig. 5.19 for Gage Locations

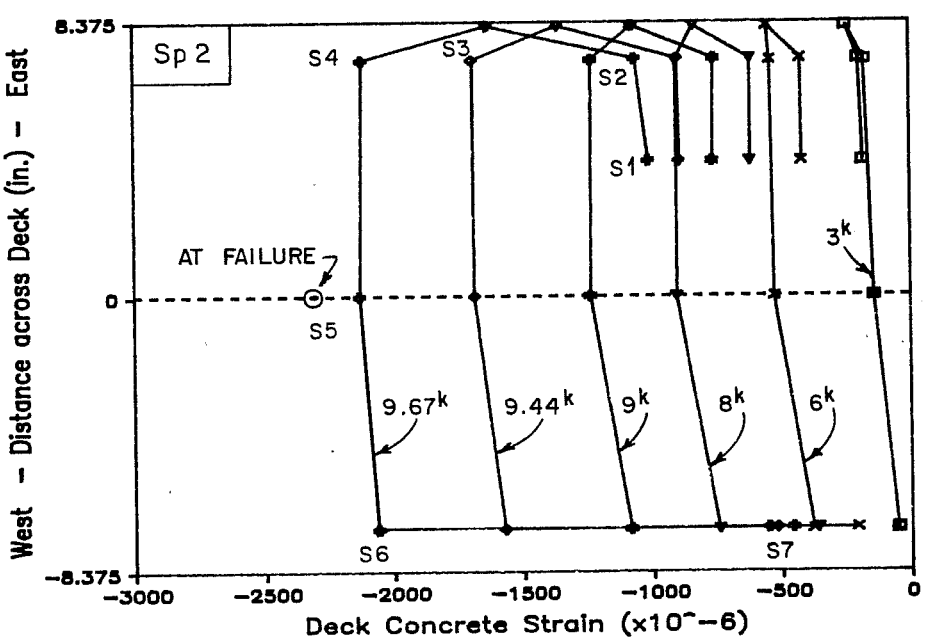

Fig. 6.76 Corrected deck concrete strains at selected loads during flexure test: a) north gages; b) south gages

was based on a reading from a single gage. The strains at the maximum and failure loads are above the strain at maximum stress measured in cylinder tests but below the maximum strain recorded in the cylinder tests.

Net strains at the top of girder and bottom of deck at selected loads are shown with respect to their location across the deck in Fig. 6.77. However, the combined plots of girder strains and the strain at the center of the top of the deck during the flexure test, which are shown in Fig. 6.78, reveal that the strain profile measured over the full depth of the specimen was nearly linear for the south set of data. This indicates that the reason for nearly constant strain at the top of the girder was due to the rising neutral axis and that full composite action was present up to failure. A reason for the strains at the bottom of the deck being significantly greater than those at the top of girder, which was especially evident at later load stages, was not identified.

The girder and deck strain data presented above do not clearly indicate which concrete initiated crushing, since neither concrete appeared to be near the limiting strains obtained during cylinder tests. The high strain gradient across the deck and girder at failure and the fact that sections were unconfined and thin in some dimensions may have affected member behavior. The fact that a high level of load was maintained on the specimen for a relatively long

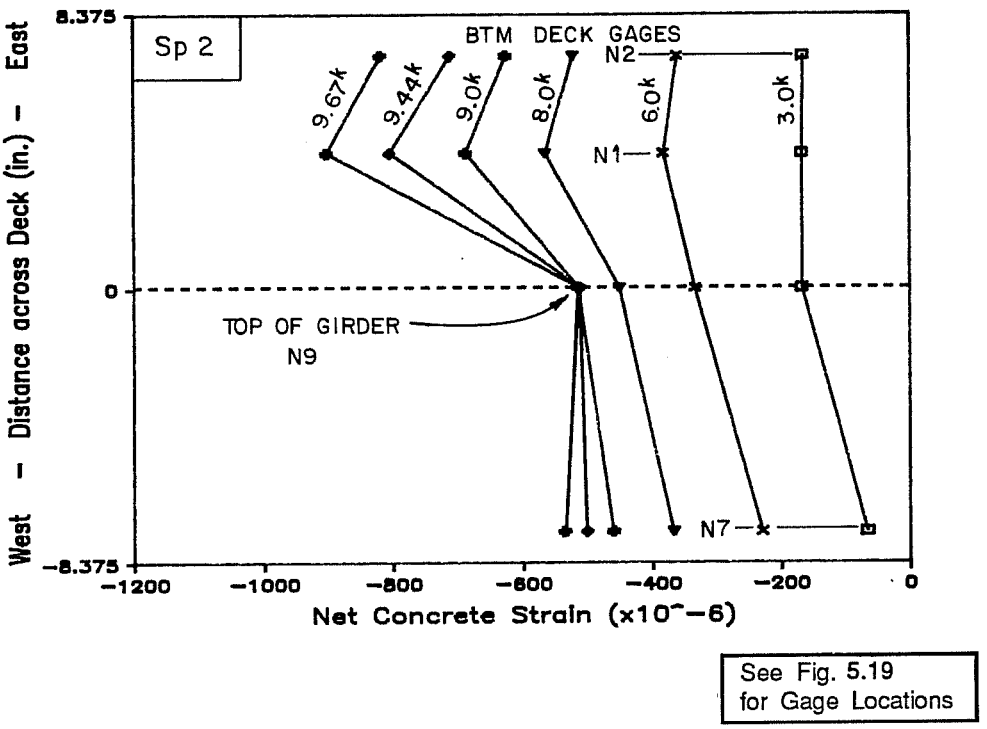

See Fig. 5.19
for Gage Locations

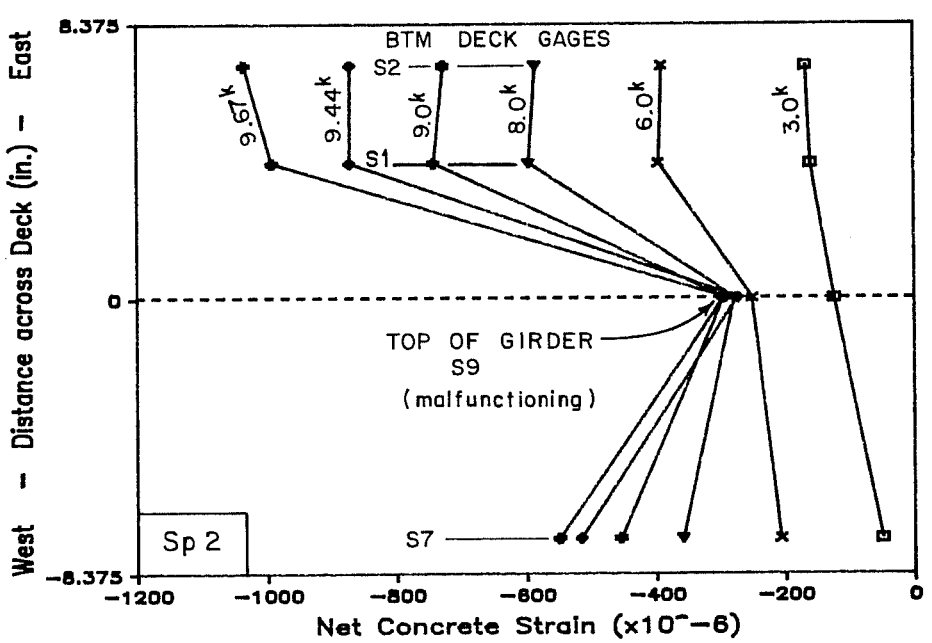

Fig. 6.77 Net concrete strains at top of girder and bottom of deck during flexure test: a) north gages; b) south gages

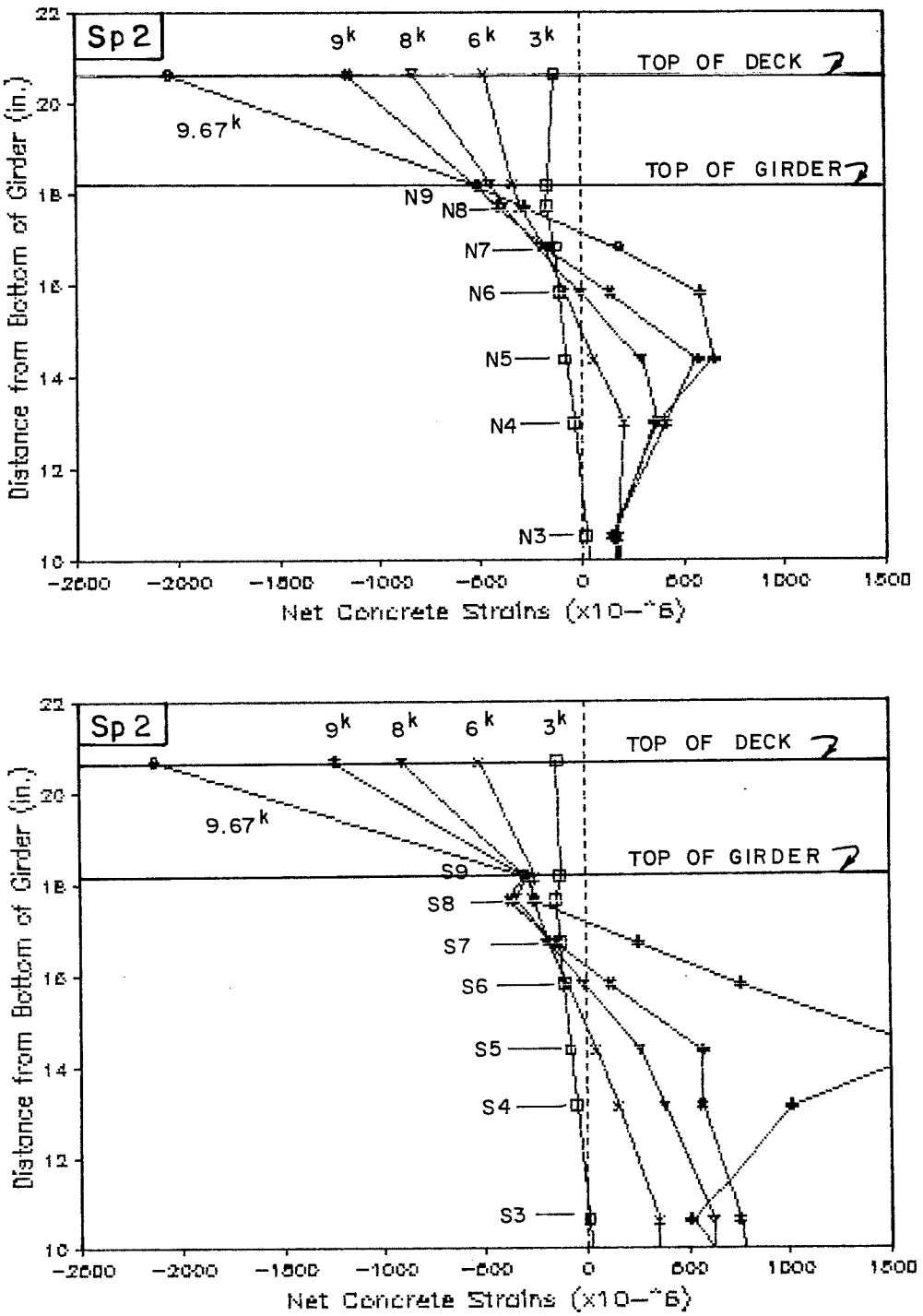

Fig. 6.78 Net girder and deck concrete strains at selected loads during flexure test: a) north gages; b) south gages

period of time may also have affected the behavior and capacity of the member.

Curvature of the section was computed using a pair of girder gages and pairs of deck gages. The average of all bottom gages was used with the top center gage because no deck gage was available directly below it. The resulting net curvatures are presented with increasing load in Fig. 6.79, and total curvatures are shown versus total moment in Fig. 6.80. Total curvatures were computed by adding net curvatures to a computed curvature at the beginning of the flexure test. Deck curvature changes very little during initial load stages while girder curvature steadily increases. This behavior probably reflects the closing of deck cracks during the early load stages. Because the plot of girder curvature shows steady change, it is the most representative of overall specimen behavior.

Measured strand strains are compared with strains computed using girder curvature data in Fig. 6.81. These plots show that the measured strand strains are consistent with the overall behavior of the specimen for the ranges of load in which gages were functioning. The top north gage does not appear to function properly at any time during the test. Both the top south and bottom north gages appear to have failed at a load near 8 kips. In addition, the bottom south gage appeared to fail just prior to ultimate as indicated by the retreat of the strain readings following gage failure.

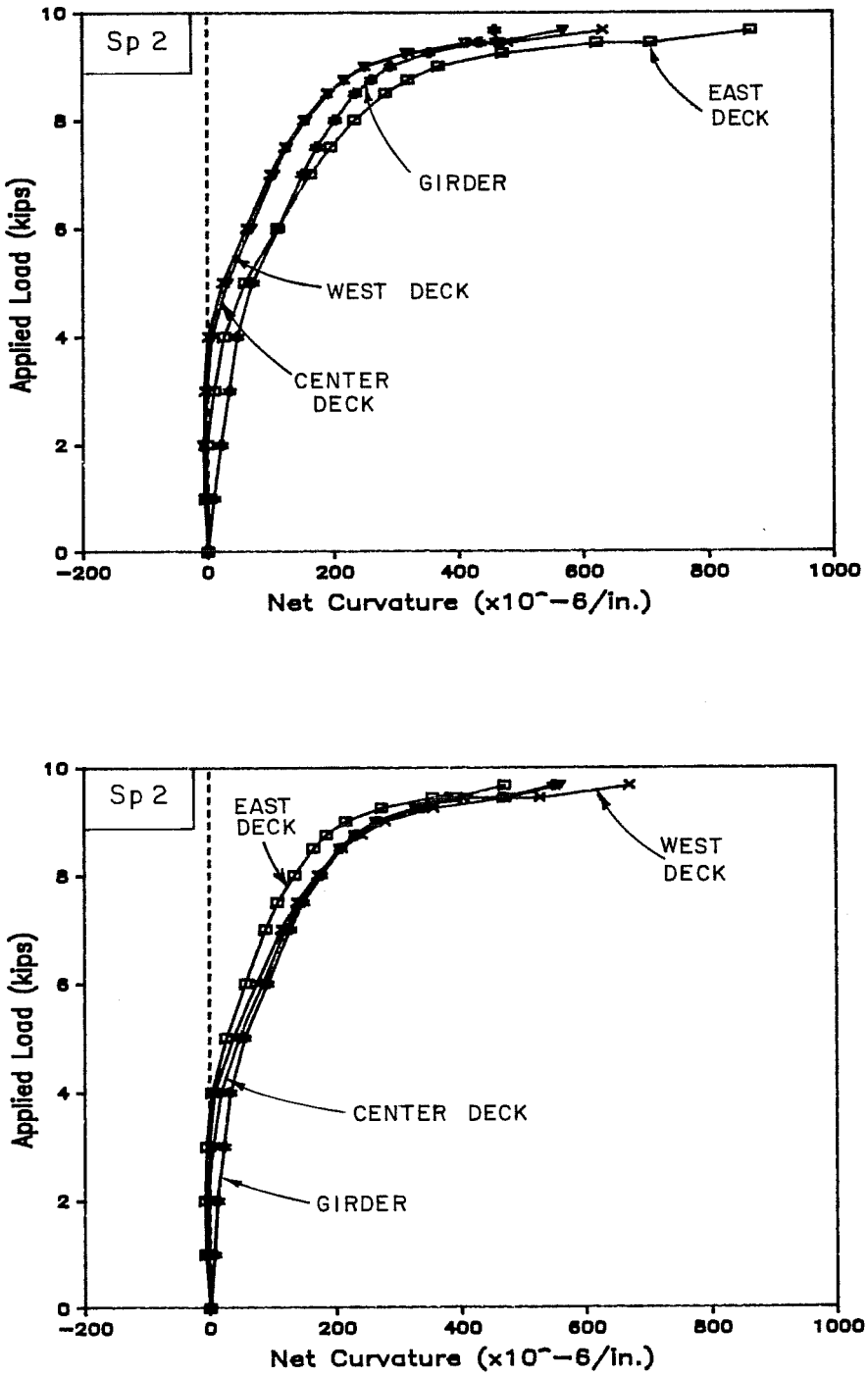

Fig. 6.79 Load-net curvature curves during flexure test: a) north gages; b) south gages

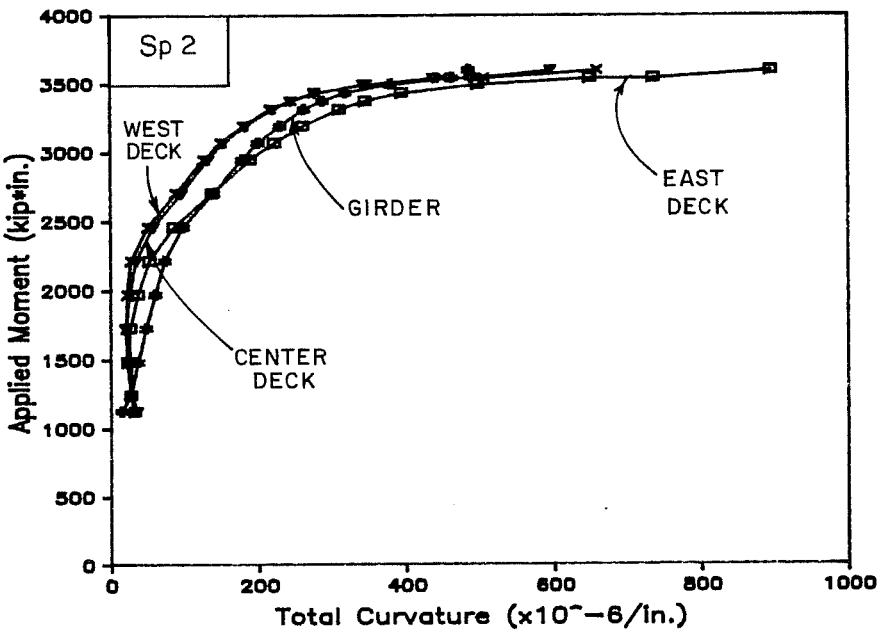

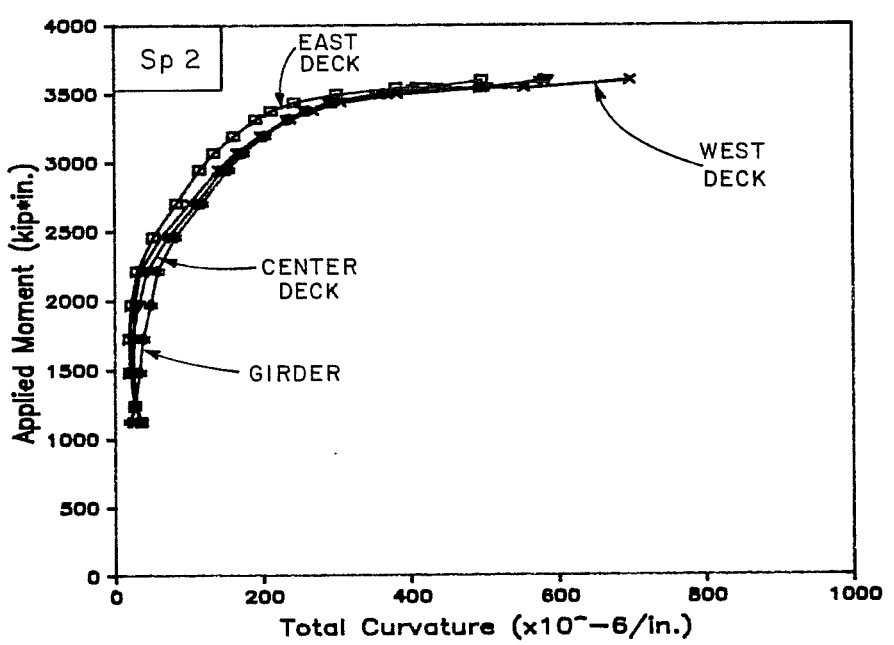

Fig. 6.80 Moment-curvature curves during flexure test: a) north gages; b) south gages

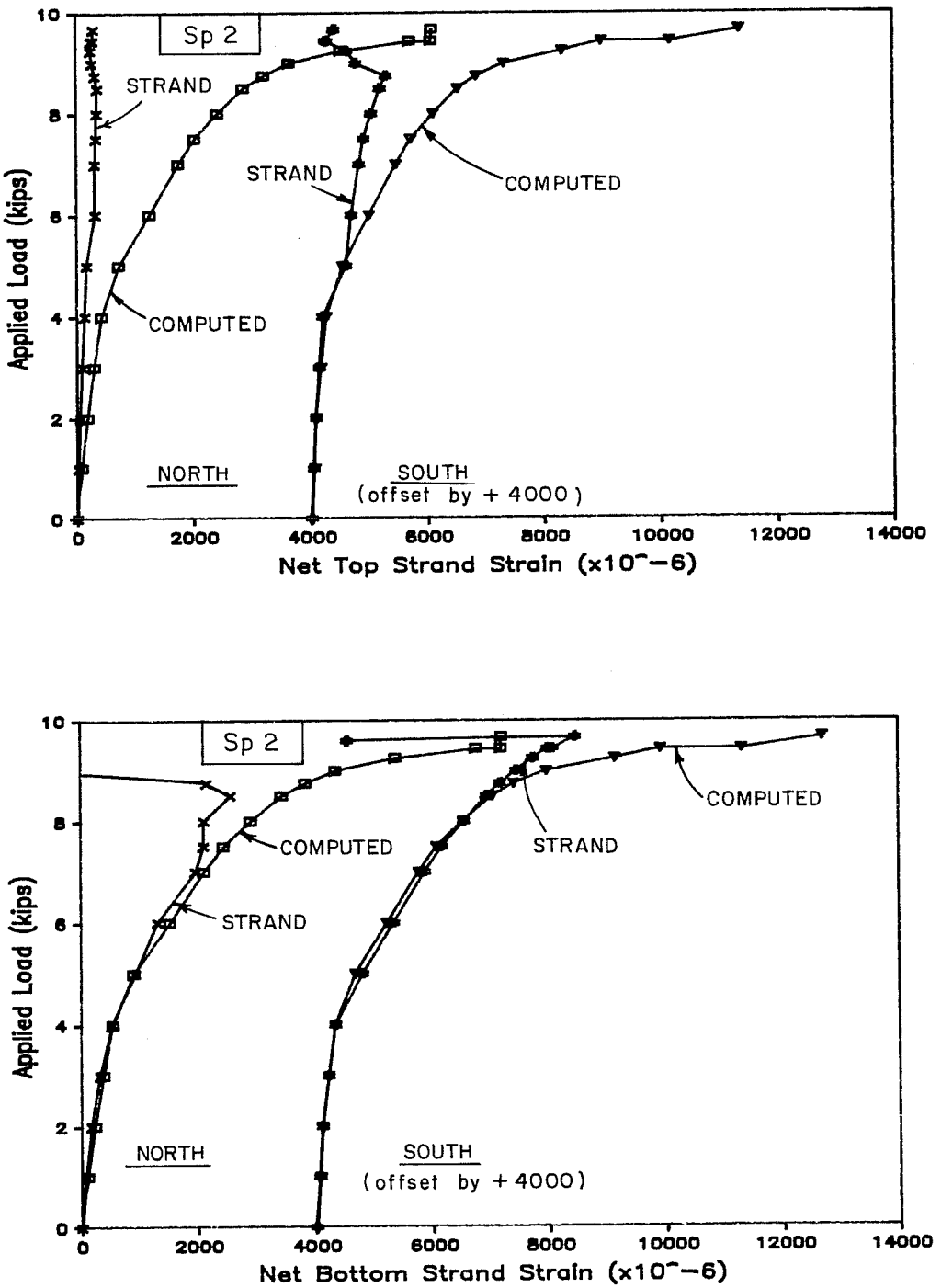

Fig. 6.81 Measured and computed strand strains during flexure test: a) top strand strains; b) bottom strand strains

The departure of the south gage data (both top and bottom) from the computed strains appears to indicate that the strands debonded in the concrete and therefore failed to experience the increase in strain consistent with the increasing section curvature. A similar trend appears in the bottom north gage data, although it is not as clear or long-lived. Slip in the top strand appears to have occurred near 5 kips while the bottom strand departs from the computed curve at 8.5 kips. This behavior was not expected but can be explained by the presence of many closely spaced flexure cracks that elevated bond stresses to a point where debonding occurred between cracks. The high shrinkage strains may have also adversely affected strand bond. The top strand may have debonded at a lower load because it was close to the more severe shrinkage cracking of the web.

Strand strains, girder concrete strains, deck concrete strains, girder curvature and midspan deflections are combined in Fig. 6.82. Data is normalized with respect to readings at the ultimate load.

6.3.2.4 Stirrup Strains and Strand Slip at Ends. Stirrup strains were significant which indicates that shear cracking occurred or that shrinkage cracks were opening under the influence of shear (Fig. 6.83). The south gage data appears to indicate cracking at 7.5 kips while the steady increase of the north gage data is evidence that a shrinkage crack was opening under the influence of shear.

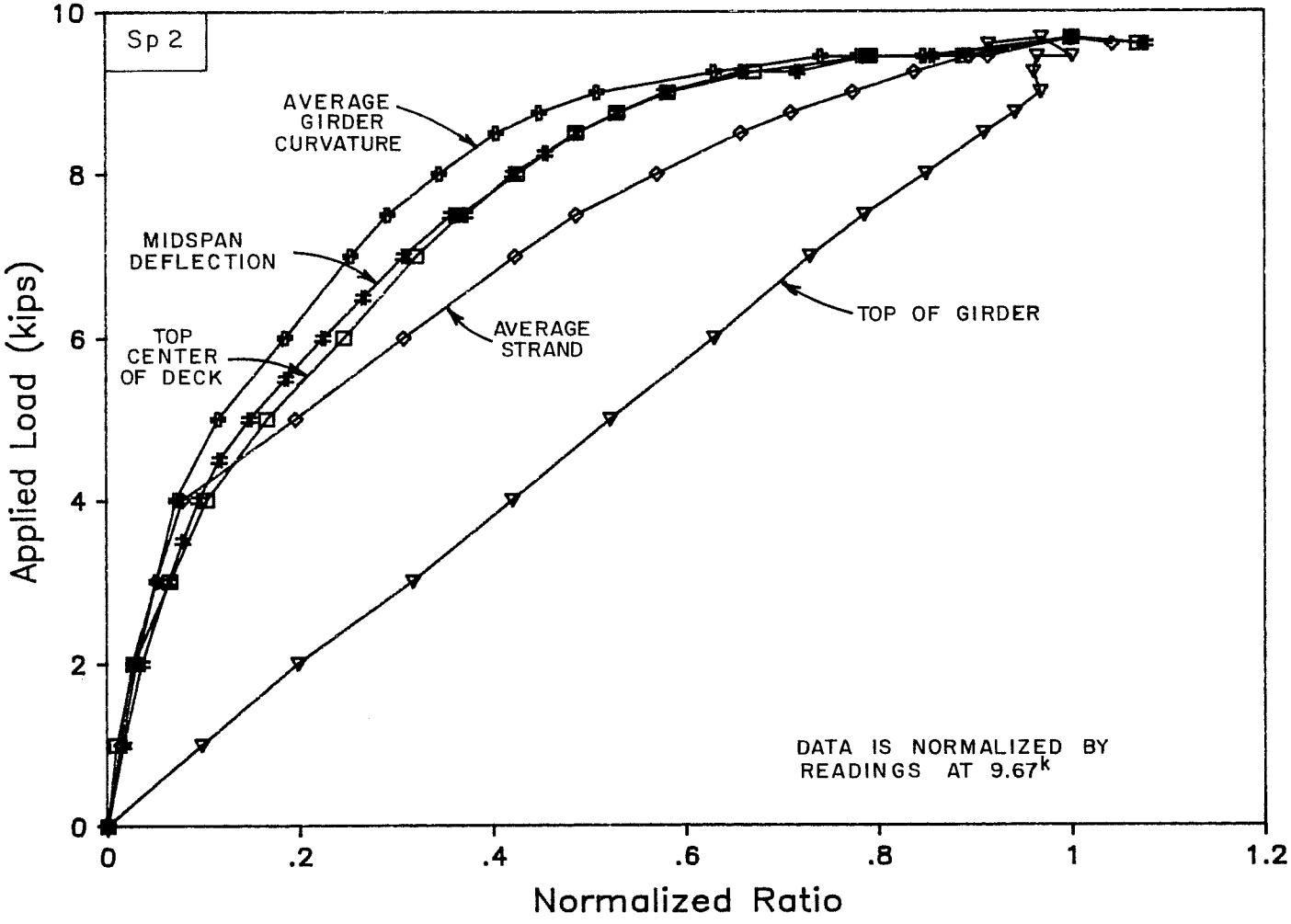

Fig. 6.82 Comparison of different types of data during flexure test

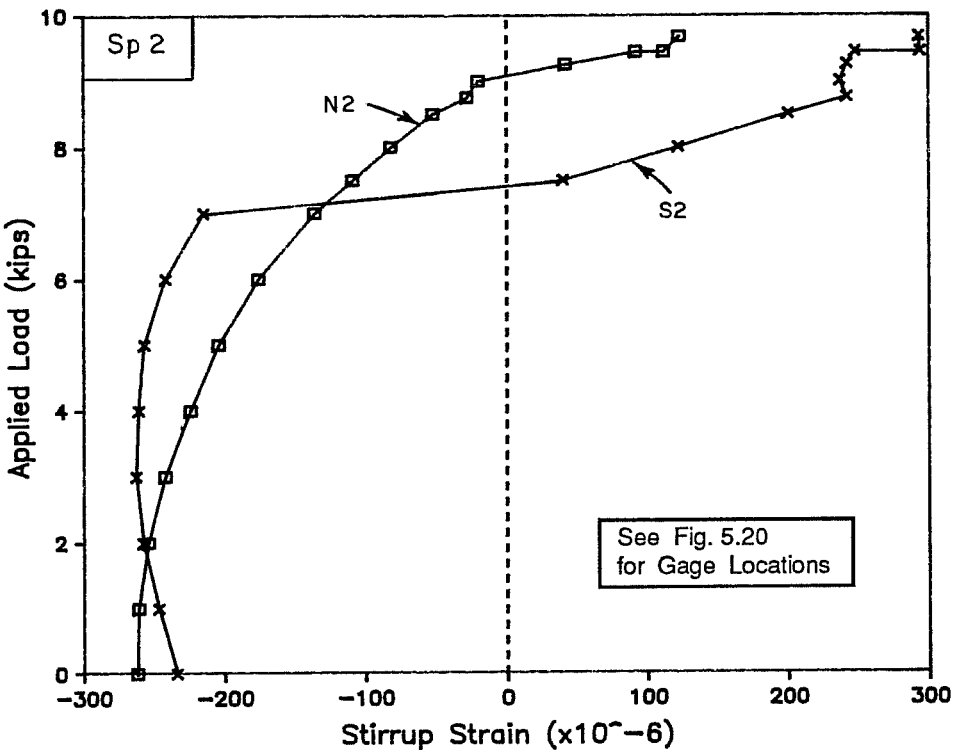

Fig. 6.83 Stirrups strains during flexure test

No strand slip was measured at the ends of the girder during the flexure test.

6.3.3 Shear Test of South End.

6.3.3.1 General Description of Behavior. The shear test consisted only of an ultimate test since the girder was cracked previously due to shrinkage. Additional cracking occurred near the ends of the girder during the latter stages of the flexure test when a few shrinkage cracks were observed to extend.

As mentioned for the tests of Specimen 1, no dead load compensation was used which, combined with a reduced span, produced a state of stress in the web much different from that during the flexure test. Therefore, shear test results cannot be directly applied to the specimen as tested in flexure.

Cracks completely penetrated the deck at many locations outside the shear span due to the effects of the flexural failure and the reduction of dead load moment resulting from the shortening of the span. These cracks had no apparent effect on the shear capacity of the specimen.

Deflection and slip readings were collected at all load stages and strain readings were recorded at most load stages. The maximum applied shear was used to designate load stages.

Load was applied in 4, 2, or 1 kip increments of the maximum shear using a screw-type testing machine. Web shear cracks were observed to extend at a shear of 8.33 kips. These branched from

preexisting shrinkage cracks. These cracks, and a few others which formed at subsequent load stages, continued to grow wider with increasing load. The first crack to move into the bottom flange occurred at a shear of 12 kips. A new flexure crack was observed under the load point at a shear of 38 kips. Few additional flexure cracks formed prior to failure and none grew sufficiently to become inclined. At a shear of 41 kips, a web crack that had extended into the bottom flange was observed to reach nearly to the level of the bottom row of strands. When reloading after reaching 41 kips shear, strand slippage occurred at a shear of 40.9 kips. The load decreased as additional deformation was applied. The shear crack that had nearly reached the bottom of the girder at 41 kips shear completely penetrated the flange when the strands slipped (Fig. 6.84). A second crack, which was located 3 in. farther into the shear span, also completely crossed the bottom flange at strand slip. The wide opening of these two cracks led to the increased deflection observed at failure. Although a reduced load carrying capacity remained, no further loading was attempted.

As for the Specimen 1 tests, failure was not catastrophic, but gradual, as increasing strand slip permitted the failure crack to open (Fig. 6.85). The use of a stiff, deflection controlled loading system prevented a sudden and complete failure.

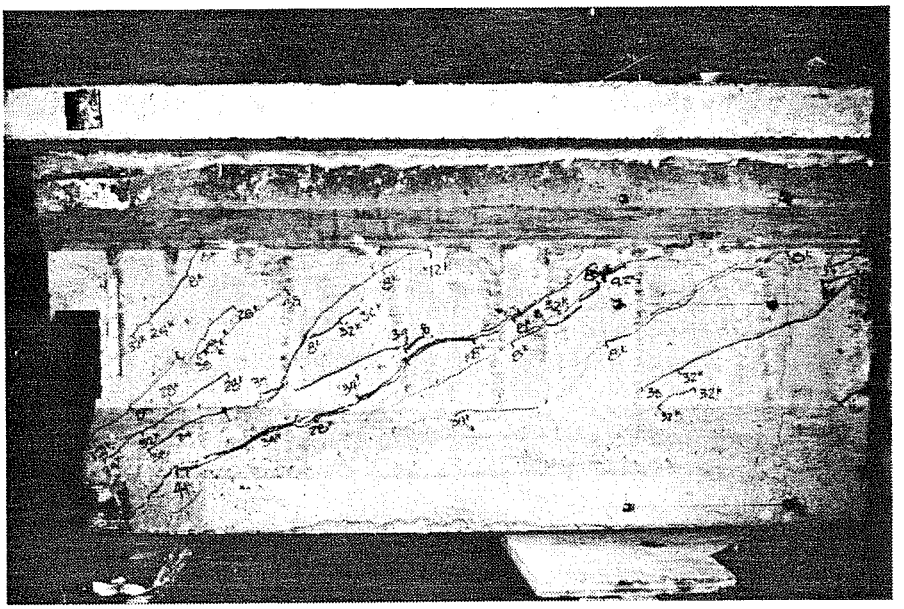

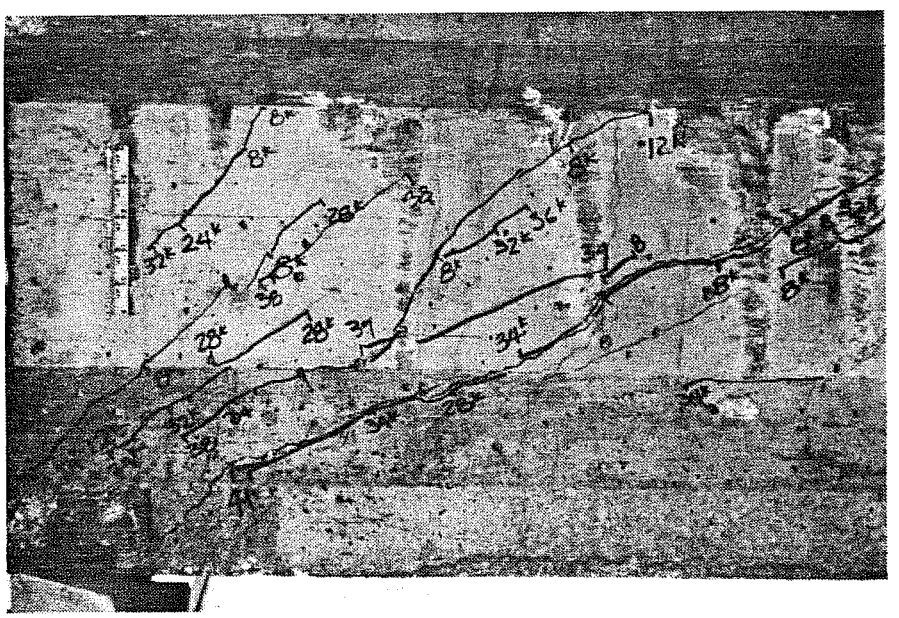

Fig. 6.84 Photographs after shear failure - south end, Specimen 2: a) east side, shear span; b) east side, near support

A longitudinal crack formed on the underside of the girder, extending from the failure crack into the shear span. Cracks also formed across the end of the girder in the bottom flange (Fig. 6.85).

Prior to failure, shear cracks were narrow. Inclination of web cracks ranged from approximately 20 to 50 degrees with most cracks being inclined at approximately 30 degrees. Shear cracks did not close completely upon removal of load.

Flexure cracks were restricted to a region very close to the load point and did not appear to contribute to the loss of bond. The flexure crack nearest the support was located 44 in. from the center of the bearing pad. Shrinkage cracks that crossed the bottom flange were located as close as 13.5 in. from the center of the bearing but did not open during the test. Flexure cracks closed tightly when all load was removed.

Significant events during the shear test are summarized in Table 6.11 which also includes computed and design loads. These loads will be compared with test results later in this chapter and in the following chapter.

6.3.3.2 Deflections. Deflections at midspan and the load point are shown in Fig. 6.86. Deflections were corrected for compression of the bearing pads. Shear cracking had a negligible effect on the stiffness of the structure.

6.3.3.3 Stirrup and Strand Strains. Typical load-strain curves for stirrup gages are shown in Fig. 6.87. Strains for each

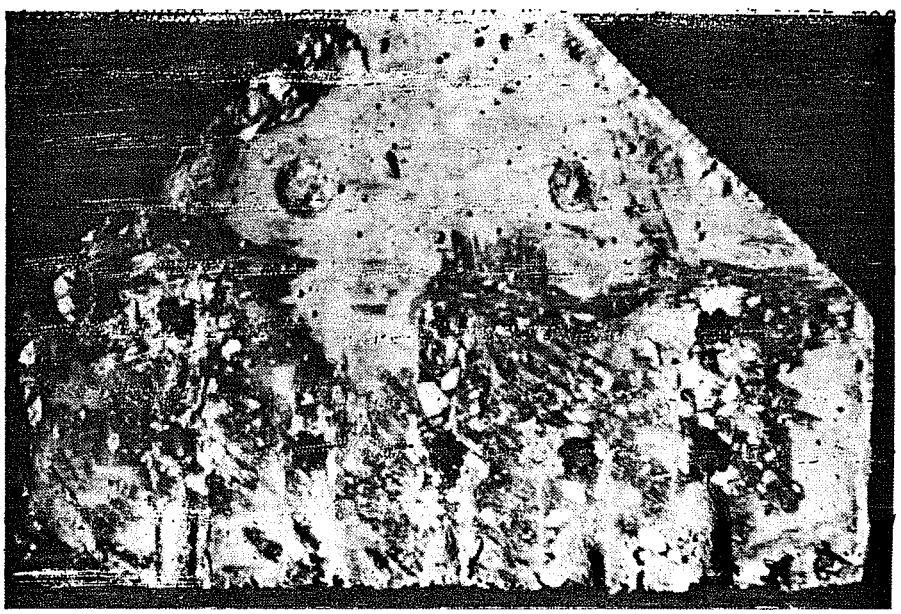

Fig. 6.85 Photograph of strand slip after shear failure - south end, Specimen 2

Table 6.11 Load stages of interest during shear test of south end - Specimen 2

Key (Fig. 6.86)	Description of Load Stage	Load (kips)
Computed and Observed Behavior		
W	Observed Web Cracking	8.33
E	Web Crack Extends into Btm Flg. at End	12.00
CW	Computed Web Cracking at h/2	23.40
CD	Computed Decompression at Load Point ($0\sqrt{f_c'}$)	29.37
CF	Computed Flexural Cracking at Load Point ($7.5\sqrt{f_c'}$)	36.99
F	Observed Flexural Cracking ($10.4\sqrt{f_c'}$)	38.00
U	Ultimate Load	41.00
P	Post-Ultimate Load	40.88
CI	Computed Inclined Flexural Cracking at h/2 from Load Point	47.10
Computed Shear Capacity		
	Web Cracking (Controls):	
NW	Computed Nominal Capacity (ϕ = 1.0)	39.49
	Inclined Flexural Cracking:	
NI	Computed Nominal Capacity (ϕ = 1.0)	63.31

Note: "Shear" is the applied shear in the shear span of interest.

Stirrups were equivalent to $4.25\sqrt{f_c'}b_w d$.

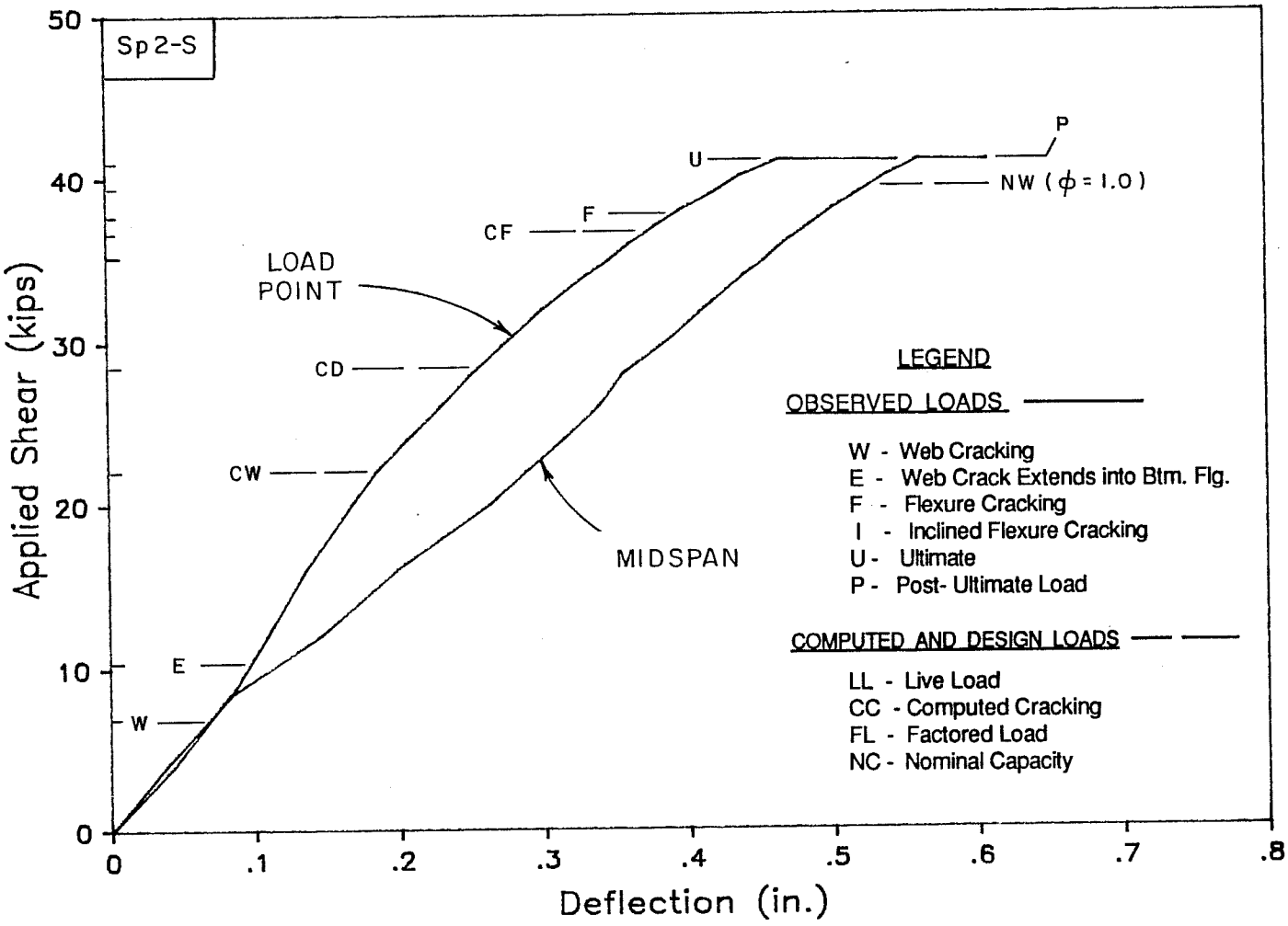

Fig. 6.86 Deflection at midspan and load point

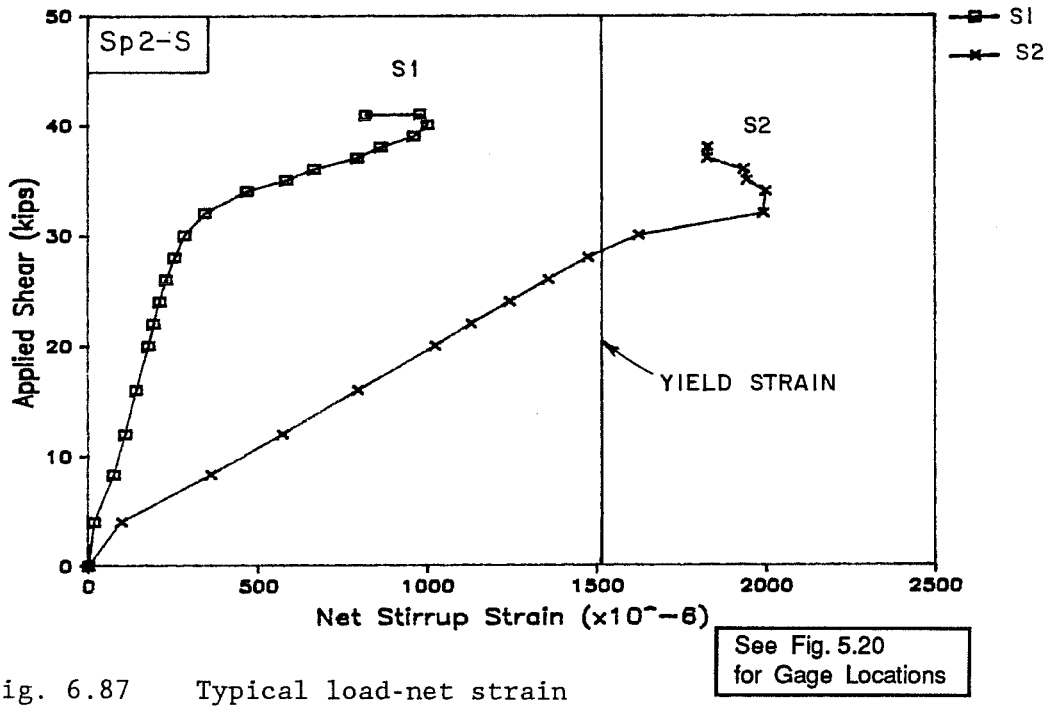

Fig. 6.87 Typical load-net strain curves for stirrups

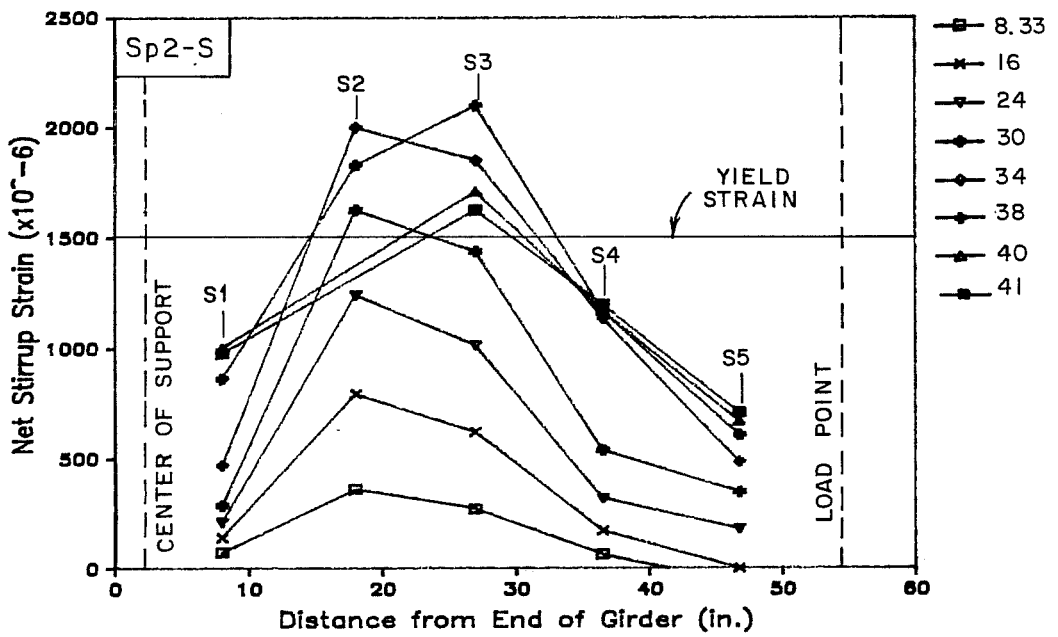

Fig. 6.88 Net stirrup strains along span at selected loads

instrumented stirrup at selected loads are shown in Fig. 6.88 with respect to their location along the span. The data indicate that only stirrups located at approximately 20 and 30 in. from the end of the girder reached yield.

Corrected strand strains are presented in Fig. 6.89. Strains at selected loads are shown with respect to their location in Fig. 6.90. It appears that cracking occurred at slightly above 32 kips shear, as indicated by the softening of the shear-strand strain plot for the gage under the load point (S5). The strand does not appear to be near yield at failure at any location. The increase in strain near the end of the girder at the final load stages is indicative of the increased requirements placed on the strand due to the nearby cracking in the bottom flange.

6.3.3.4 Strand and Deck Slip. Strand and deck slip are shown in Fig. 6.91. Strand slip was small until late in the test when the bottom strand began to slip gradually. At failure, both lower rows of strands pulled in approximately 0.1 in. at failure. The top strand showed only negligible slip up to and following failure. No slip or cracking was visible at the deck/girder interface after failure, although a small slip was measured (Fig. 6.91). The sign of the measured slip indicated that the deck was being pulled toward the span with respect to the girder, which was the expected direction of movement.

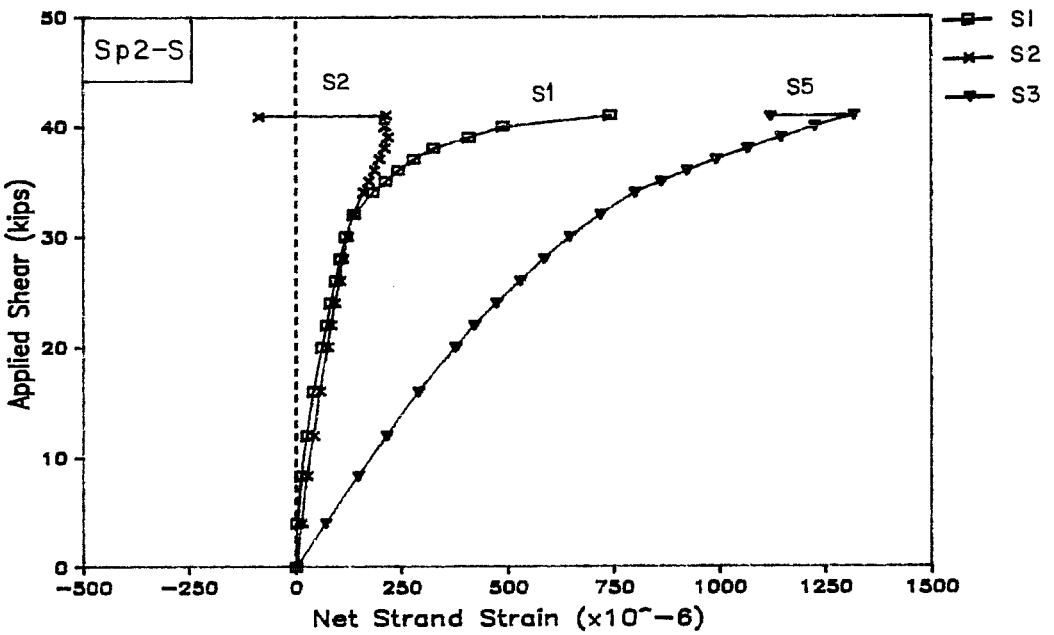

Fig. 6.89 Net strand strains along span at selected loads

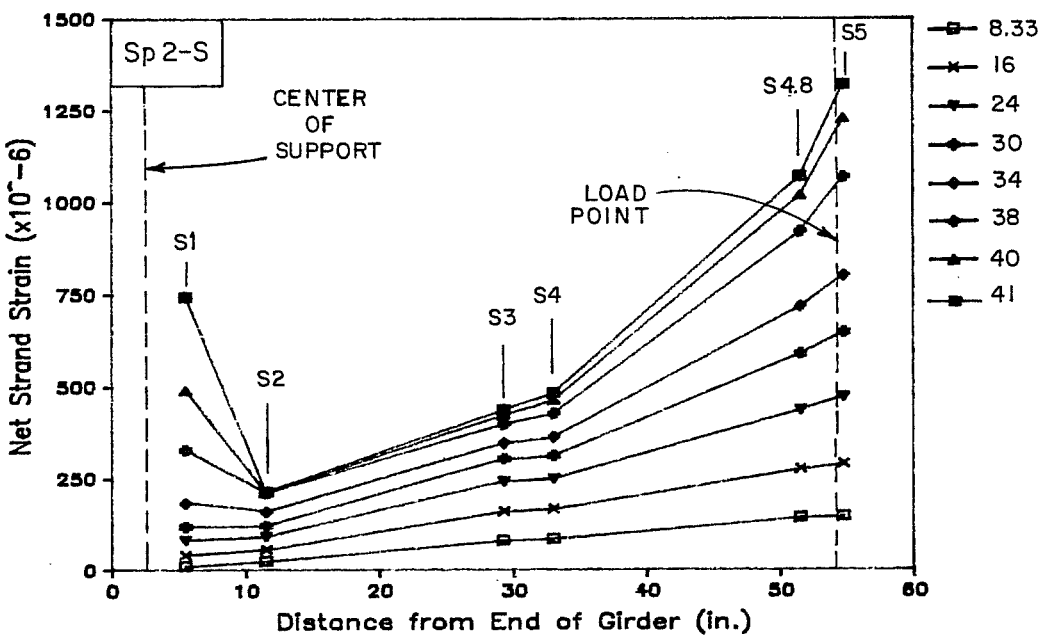

Fig. 6.90 Net strand strains along span at selected loads

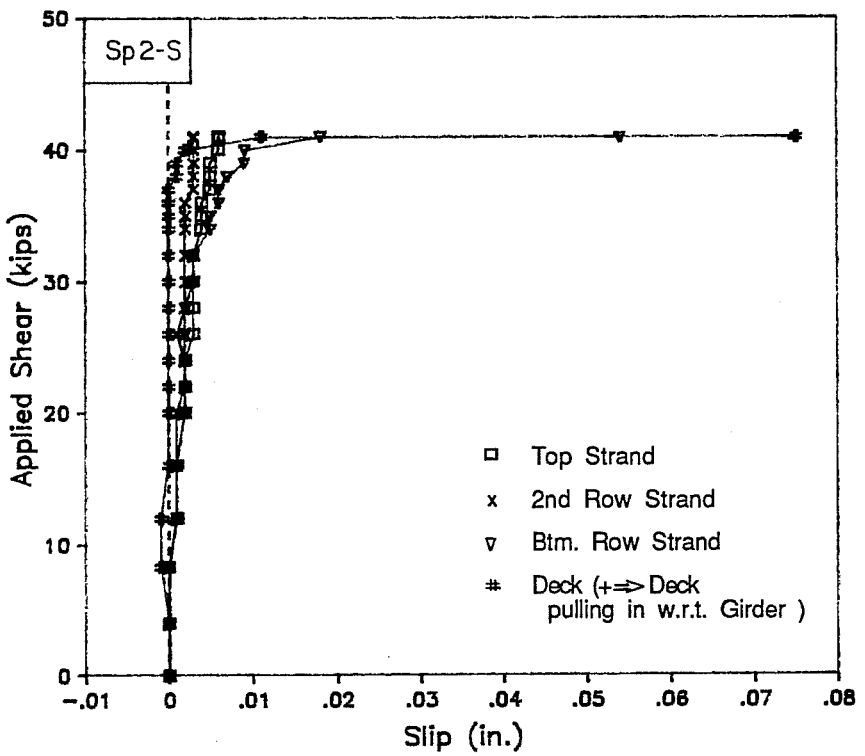

Fig. 6.91 Slip of strands and deck at end of girder during shear test

6.3.4 Shear Test of North End - With Overhang.

6.3.4.1 General Description of Behavior. Condition of the north end prior to testing and procedures for testing were the same as for the south end. The only difference between this end and the south end was the addition of a 6 in. overhang beyond the bearing which was intended to improve bond.

Existing web shrinkage cracks extended and a new web crack formed near the load point at a shear of 8 kips. No web cracking other than extension of these cracks occurred. The first web cracks extended into the bottom flange at a shear of 32 kips. No cracks appeared in the web above the support in the region where a "fan" usually forms. Shrinkage cracks in the bottom flange became visible near the load point at a shear of 34 kips, and new flexure cracks appeared at a shear of 40 kips. Flexure cracks remained very narrow and were confined to the region near the load point. Cracking at a shear of 44 kips is shown in Fig. 6.92. At a shear of 46 kips, a second web crack extended to the level of the bottom strands and began to propagate horizontally, which is typical of anchorage cracking. When the shear reached 47.9 kips, concrete began to crush at the junction of the web and top flange near the middle of the shear span, and the load dropped off with increasing deflection. However, upon reloading, a maximum shear of 48.8 kips was obtained as crushing spread in both directions along the junctions of the web and the top and bottom flanges (Fig. 6.93).

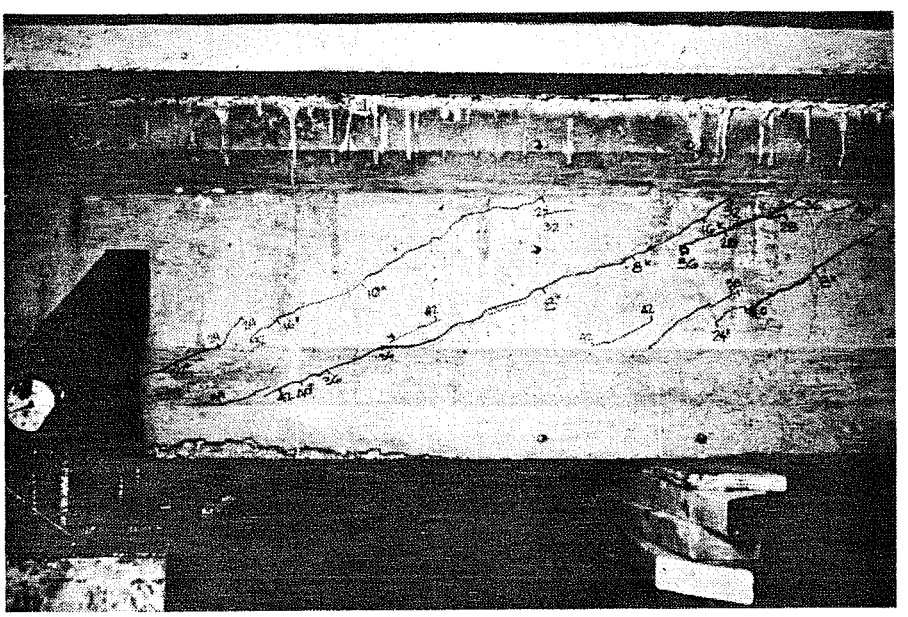

Fig. 6.92 Photograph during shear test at shear of 44 kips - north end, Specimen 2

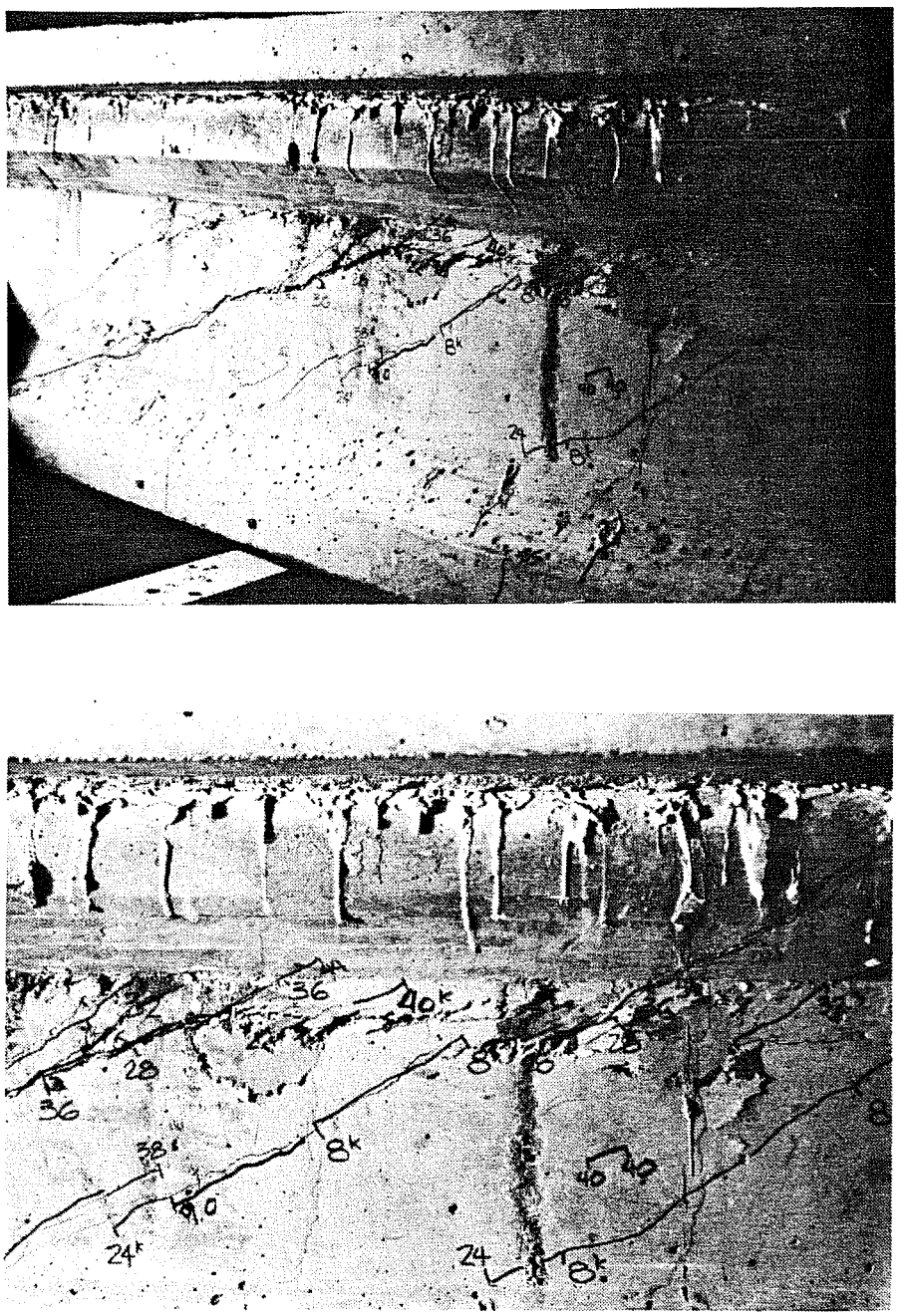

Fig. 6.93 Photographs of web crushing at shear failure - north end, Specimen 2: a) west side, shear span; b) west side top of web

Crushing of the concrete was characterized by slow spalling or flaking and was not explosive. While web cracks opened widely as shear approached the maximum level, they did not extend through the bottom flange, and no new cracks appeared other than those associated with spalling of the concrete. After crushing had begun, a flexure crack was observed to penetrate well into the deck under the load point. After load was removed, this crack was observed to extend completely through the deck, remaining open slightly with all load removed. A crack was also observed in the deck at approximately 12 in. from the support after crushing had commenced. This crack was opening from the top and extended into the top of the girder. Strands never exhibited significant slippage. Loading was halted after crushing was widespread and load began to drop more rapidly with added deflection.

After the specimen was unloaded, the spalled concrete was removed (Fig. 6.94). The crushed concrete followed the draped strand located near the top of the web. In one location, concrete across the entire thickness of the web had crushed.

Shear cracks did not close when the load was removed, but flexure cracks did. Shear cracks were open widely prior to web crushing, and continued to open as web crushing progressed. These cracks extended the full depth of the web but did not extend into either of the flanges, except for the single crack near the end which penetrated the bottom flange. Inclination of web cracks ranged from

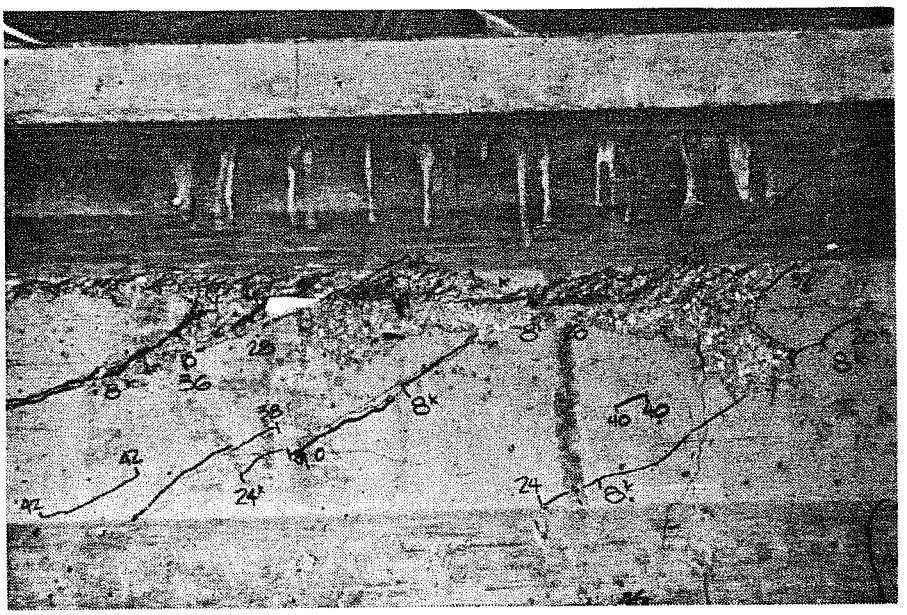

Fig. 6.94 Photograph of west side after removal of crushed concrete - north end, Specimen 2

approximately 20 to 37 degrees with an average of approximately 25 degrees.

The flexure crack nearest the support was located 39 in. from the center of the bearing pad. Only one shrinkage crack crossed the bottom flange between this crack and the support, and it was located 10.5 in. from the bearing. This shrinkage crack did not open during the test.

The difference in failure load and mode indicates that strand bond was significantly improved by the use of the overhang and that capacity of the member was strongly affected by the strand bond. It should be noted that bond in the specimen does not accurately model bond in the prototype due to problems associated with scaling. Therefore, these test results should not be directly construed as indicating the need for a similar extension of prototype girders beyond the bearing.

As for the south end, Table 6.12 is provided as a summary of observed, computed, and design loads.

6.3.4.2 Deflections. Deflections at midspan and load point are shown in Fig. 6.95. The plots indicate a softening of the section even though flexural cracks were not opening. A plateau is evident at the load associated with the onset of web crushing. This was not observed in any of the previous shear tests where the bond failure led to brittle failure. Further comparisons of this test data with the other shear tests appear later in this chapter.

Table 6.12 Load stages of interest during shear test of north end Specimen 2

Key (Fig. 6.95)	Description of Load Stage		Load (kips)
Computed and Observed Behavior			
CW	Computed Web Cracking at h/2		23.13
CD	Computed Decompression at Load Point	($0\sqrt{f_c'}$)	29.11
W	Observed Web Cracking		8.00
CF	Computed Flexural Cracking at Load Point	($7.5\sqrt{f_c'}$)	36.73
F	Observed Flexural Cracking	($10.4\sqrt{f_c'}$)	40.00
CI	Computed Inclined Flexural Cracking at h/2 from Load Point		46.84
WC	Initial Web Cracking		47.93
U	Ultimate Load		48.83
P	Post-Ultimate		44.78
Computed Shear Capacity			
	Web Cracking (Controls):		
NW	Computed Nominal Capacity (ϕ = 1.0)		39.22
	Inclined Flexural Cracking:		
NI	Computed Nominal Capacity (ϕ = 1.0)		63.05

Note: "Shear" is the applied shear in the shear span of interest.

Stirrups were equivalent to 4.25 $\sqrt{f_c'}b_w d$.

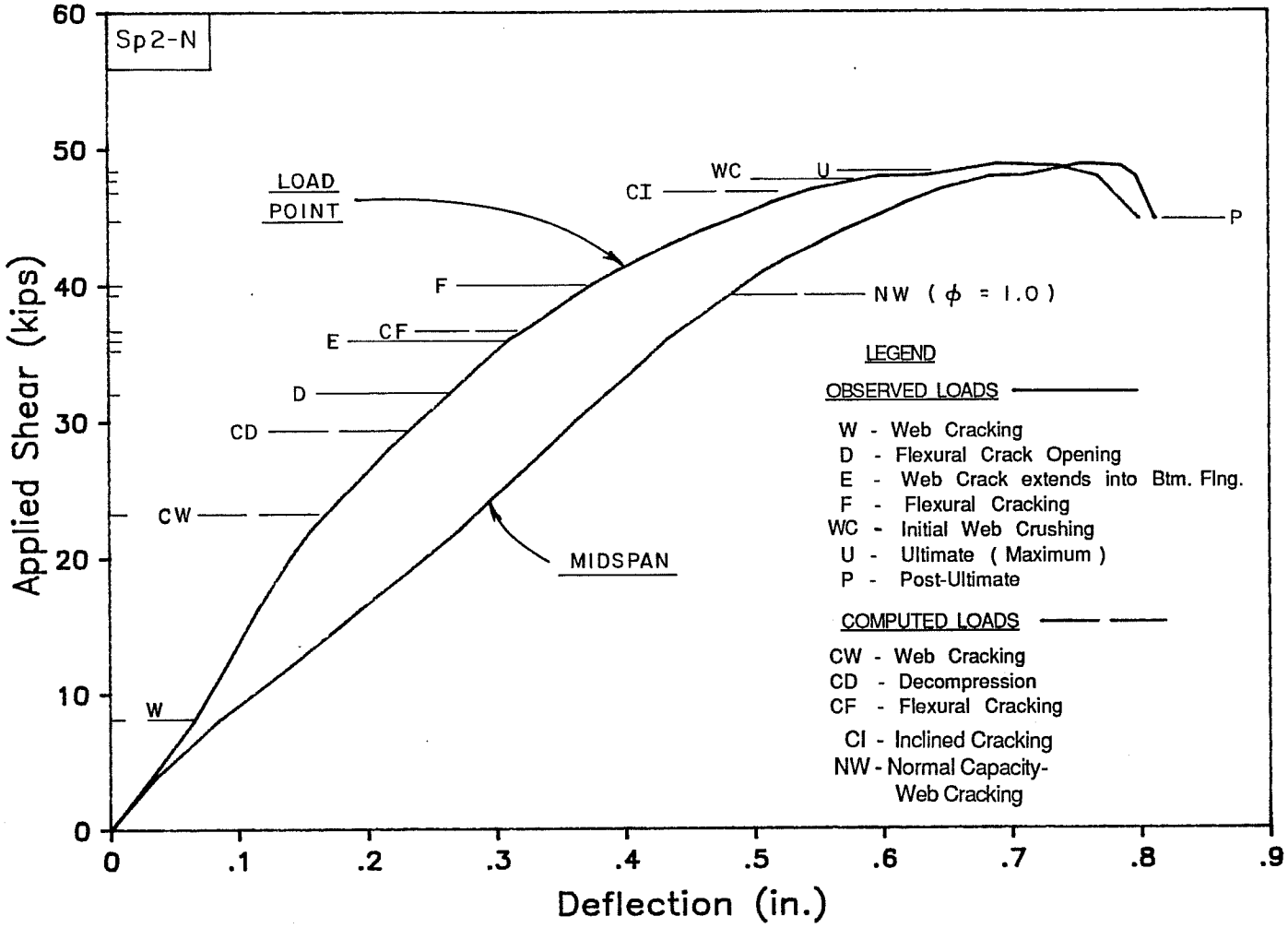

Fig. 6.95 Deflection at midspan and load point

6.3.4.3 Stirrup and Strand Strains. Typical load-strain curves for stirrup gages are given in Fig. 6.96. Strains for stirrups at selected loads are shown with respect to location in Fig. 6.97. The three instrumented stirrups near the center of the shear span appeared to yield. Strain in stirrups near each end of the shear span was increasing as high loads were applied, with the stirrup nearest the support showing a sudden increase as web crushing progressed.

Corrected strand strains at three locations are presented in Fig. 6.98. Strains at selected loads appear with respect to their location in Fig. 6.99. Flexure cracks appeared to open near the load-point gage at a shear of approximately 38 kips as indicated by the departure of the plot from linear behavior. This agrees with visual observations of cracking. Strains near the end did not increase significantly at any time during the test.

6.3.4.4 Strand and Deck Slip. Strand slip data are shown in Fig. 6.100. The observed slip, while measurable, was very small and developed only at the last load stages. After failure, strand slippage could not be detected visually. No significant slip was measured between the deck and girder and no cracking was visible along the interface.

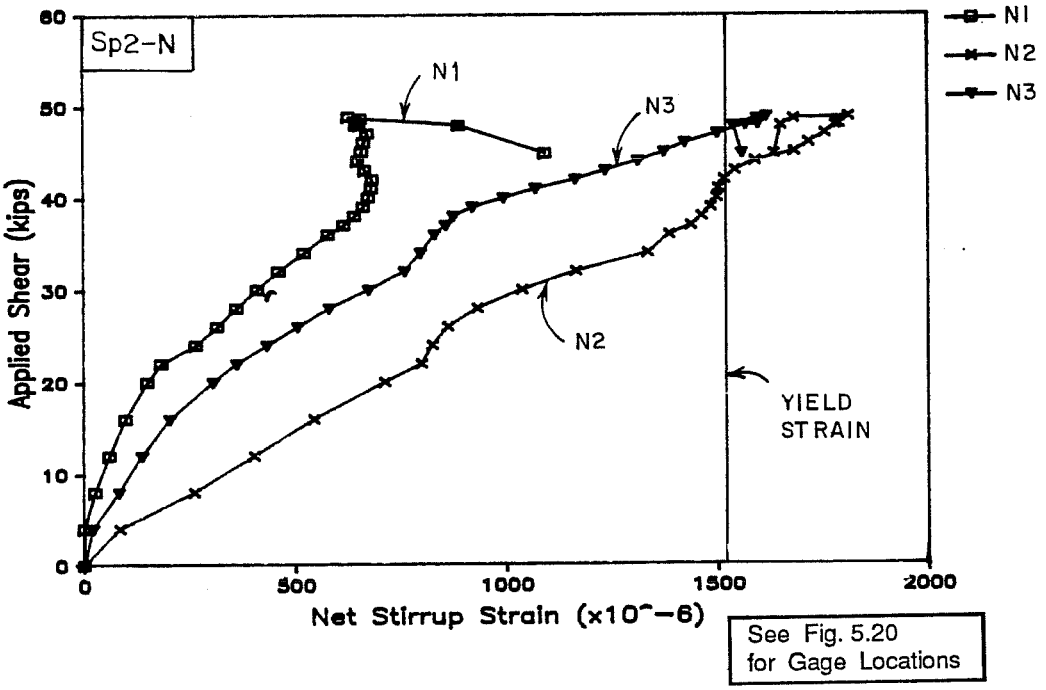

Fig. 6.96 Typical load-net strain curves for stirrups

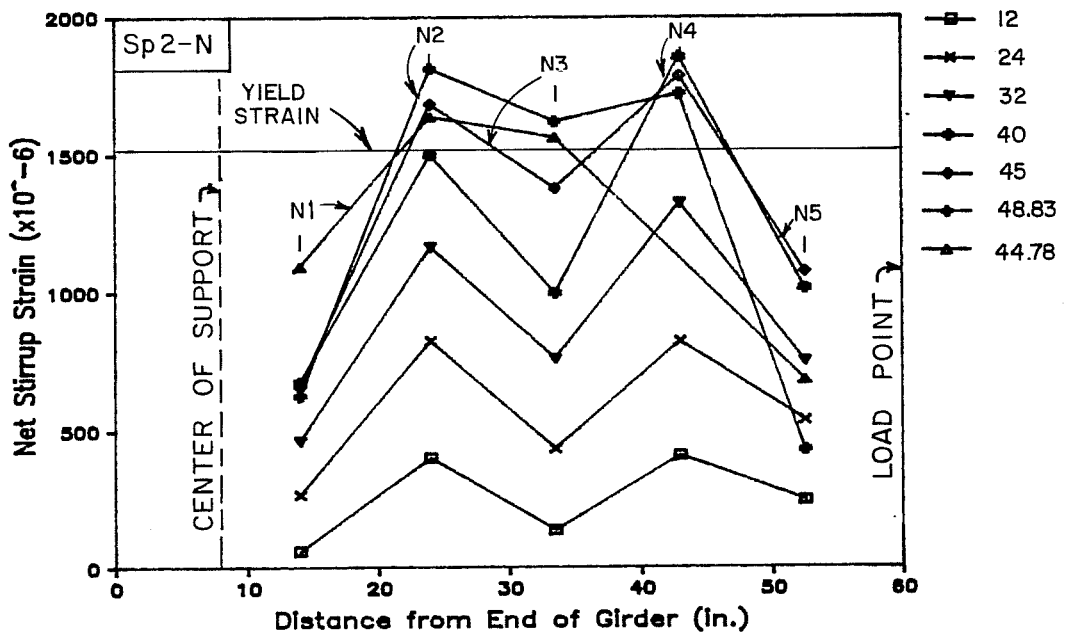

Fig. 6.97 Net stirrup strains along span at selected loads

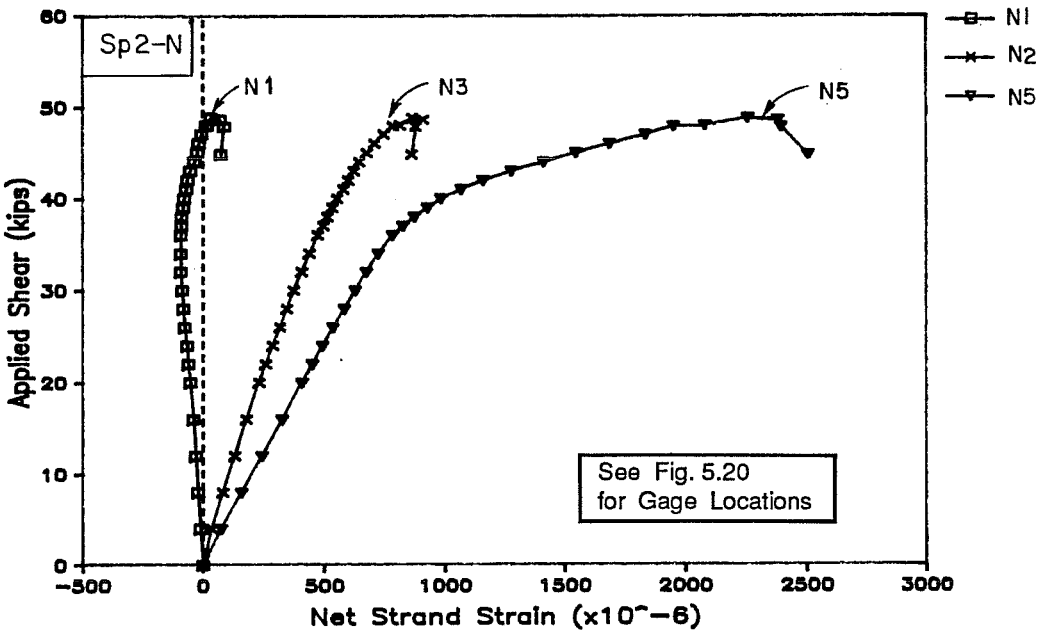

Fig. 6.98 Net strand strains during shear test

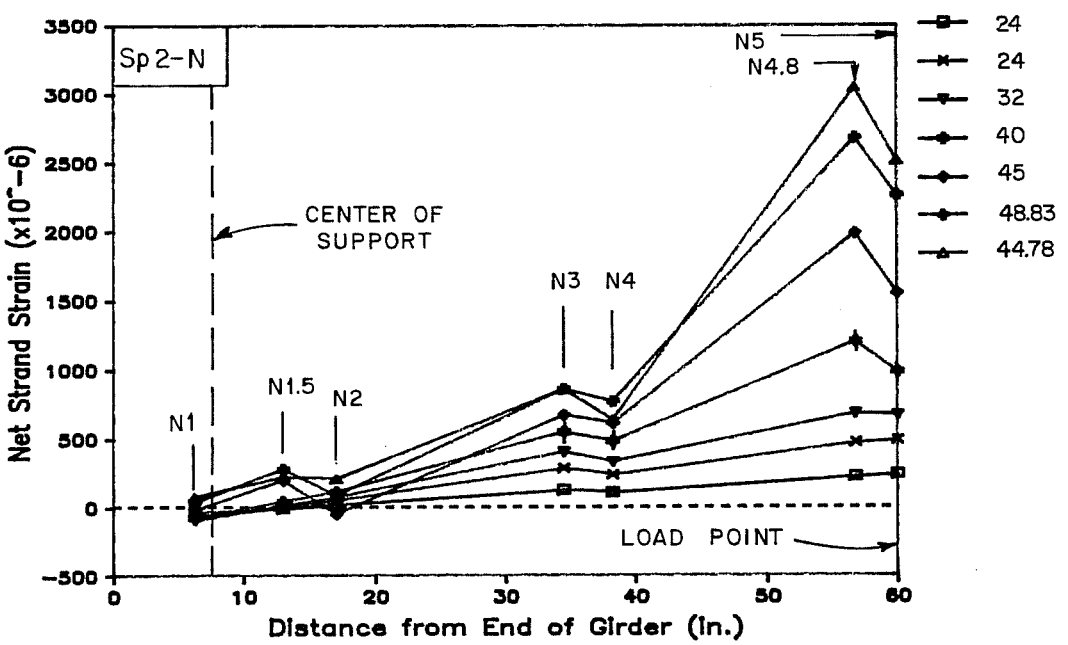

Fig. 6.99 Net strand strains along span at selected loads

6.4 Comparison of Specimens 1 and 2

6.4.1 Prior to Flexure Tests.

6.4.1.1 Concrete Material Properties. Stress-strain curves for both specimens are compared in Fig. 6.101. The girder concrete for Specimen 1 appears to be more brittle than the weaker Specimen 2 concrete because the curve deviated little from linear response at failure and no unloading branch was recorded.

6.4.1.2 Effective Stresses and Creep Strains. Effective stresses and losses are presented in Table 6.13. The effect of shrinkage on Specimen 2 is evident in increased losses prior to release. Losses at release were higher for Specimen 1 because of a higher prestress force. Strand stresses remained at reasonable levels for both specimens.

While the specimens were scale models, some of the factors that affect prestress losses could not be properly scaled. For example, the volume to surface ratio of the modified Type IV prototype girder is 4.19 while the ratio is 1.39 for the scale-model girder. This difference, which approximately corresponds to the scale factor, could result in nearly three times more shrinkage for the model than for the prototype for the time scale involved in the testing schedule according to test data presented in Ref. [51]. The same test data [51] also indicated that creep tends to be greater for sections with smaller volume-to-surface ratios. Therefore, losses of the magnitude

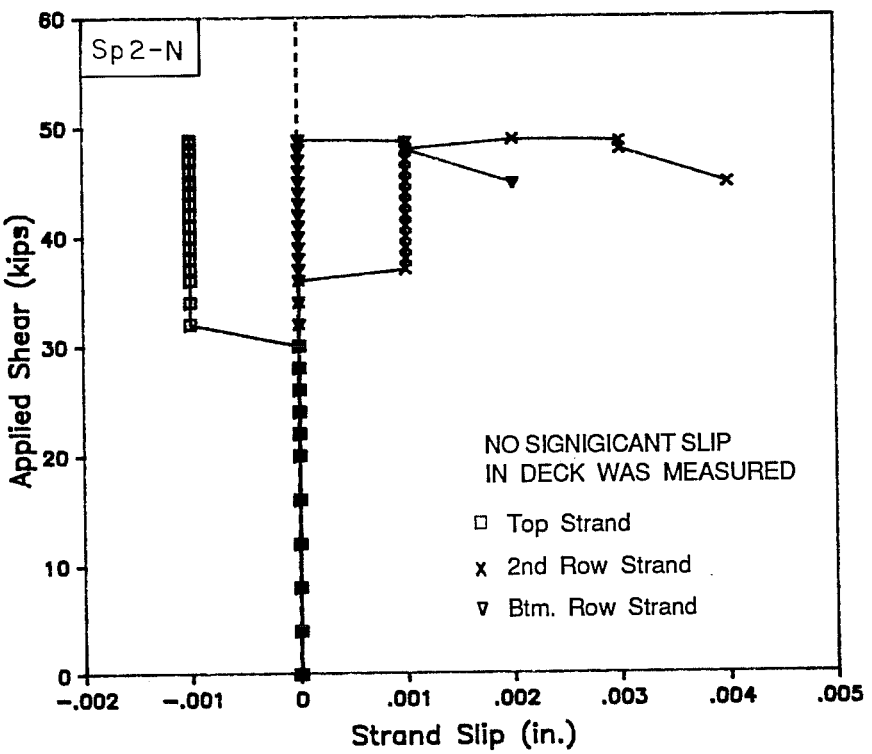

Fig. 6.100 Slip of strands at end of girder during shear test

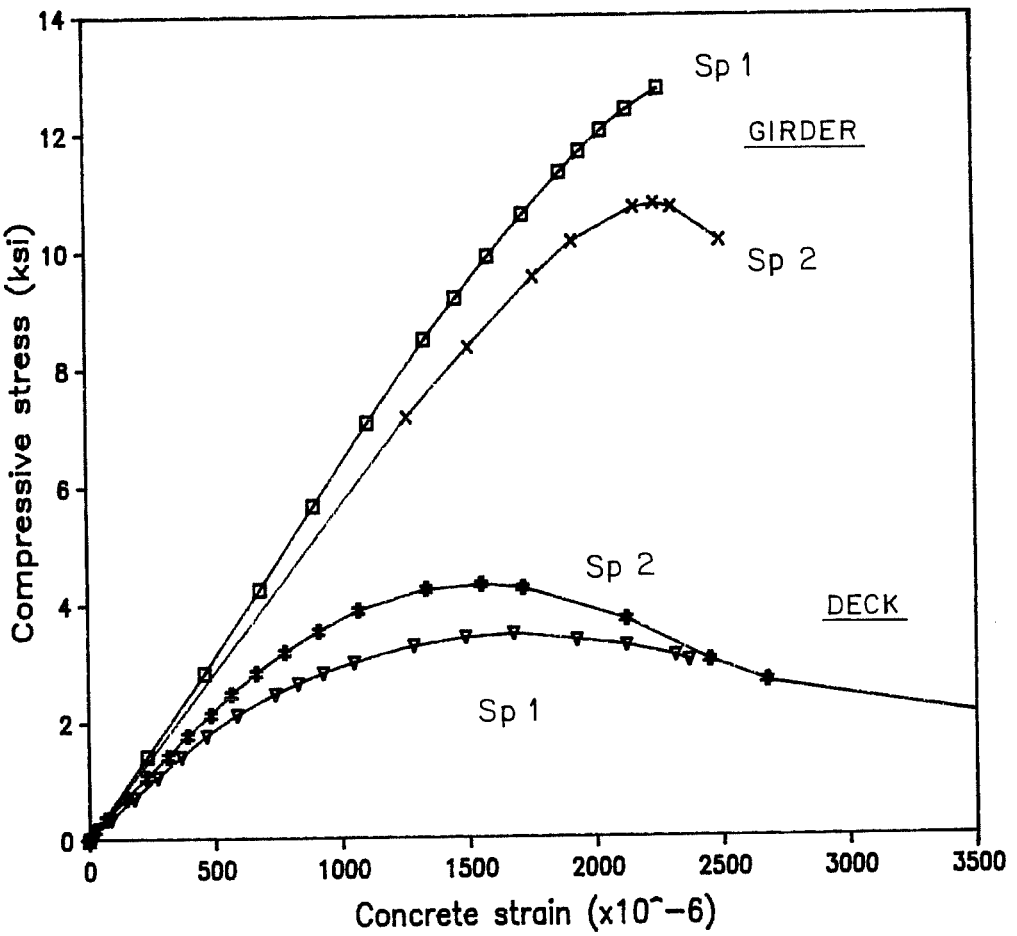

Fig. 6.101 Comparison of concrete stress-strain curves

found in these girders should not be expected in a prototype structure.

Girder creep strains, which are the difference between corrected strains before the flexure tests and after release, are compared in Fig. 6.102. Specimen 1 experienced creep of approximately 600 microstrains which was uniform with depth. Creep experienced by Specimen 2 amounted to about 400 microstrains and increased toward the top of the girder. The lower creep for Specimen 2 was expected because of the lower prestress force.

Deck creep strains are presented in Fig. 6.103. Creep for Specimen 1 was approximately 350 microstrains at the top of the deck and about 300 microstrains at the bottom. Because the deck for Specimen 2 was added only eight days before the flexure test, the creep was much lower, only reaching about 100 microstrains.

6.4.2 Flexure Tests.

6.4.2.1 General Description of Behavior. Behavior of the two specimens was very similar. Cracking progressed similarly with cracking loads being higher for Specimen 1 due to the higher prestress force. The most striking aspect of the behavior of the specimens was that the failures were nearly identical. The failure surfaces were nearly indistinguishable.

Computed and observed cracking loads and ultimate loads are compared in Fig. 6.104 using computed values as the basis for comparison. Observed cracking loads exceed computed loads by a large

Table 6.13 Comparison of effective strand stresses and losses

	Specimen 1 (Table 6.3)		Specimen 2 (Table 6.9)	
	Stress (ksi)	Loss (ksi)	Stress (ksi)	Loss (ksi)
Full Tensioning				
All locations	187.6	---	206.7	---
Prior to Release				
All locations	181.7	5.9	193.6	13.1
After Release				
Midspan	159.6	28.0	177.6	29.1
Midspan *	159.6	28.0	179.4	27.3
North end *	164.2	23.4	173.5	33.2
South end *	164.4	23.2	173.5	33.2
Flexure Test				
Midspan	152.5	35.1	173.1	33.6
North end	147.5	40.1	156.8	49.9
South end	143.6	44.0	156.8	49.9
Shear Tests				
North end	143.1	44.5	156.8	49.9
South end	140.5	47.1	156.8	49.9

* - These values represent computed instantaneous elastic losses plus 25% and were calculated as noted in Tables 6.3 and 6.9.

Note: Losses were computed by subtracting effective stresses from the stress present when strands were fully tensioned.

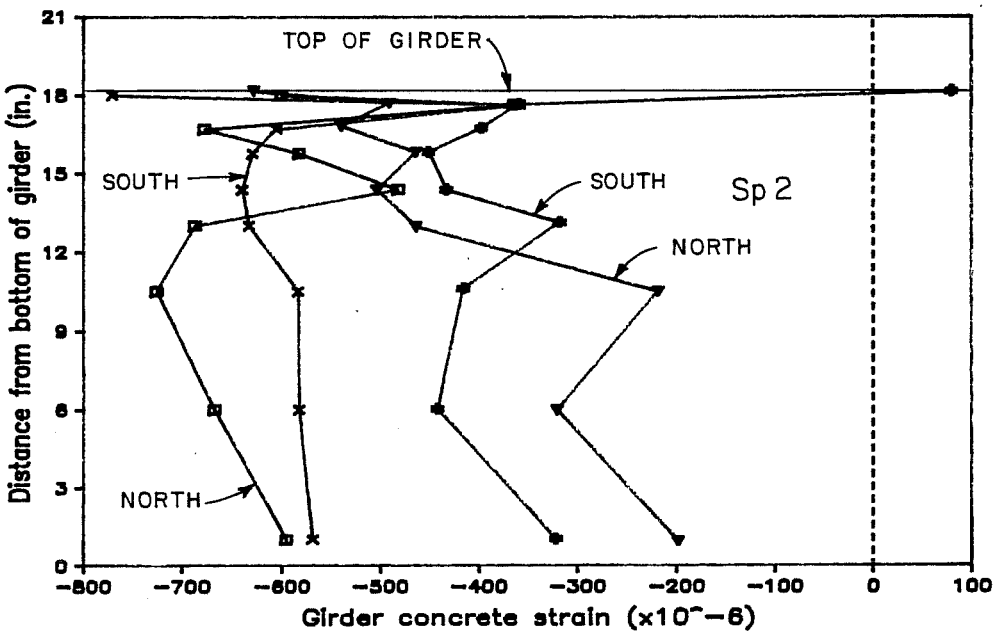

Fig. 6.102 Girder concrete creep strains at midspan at ultimate flexure tests

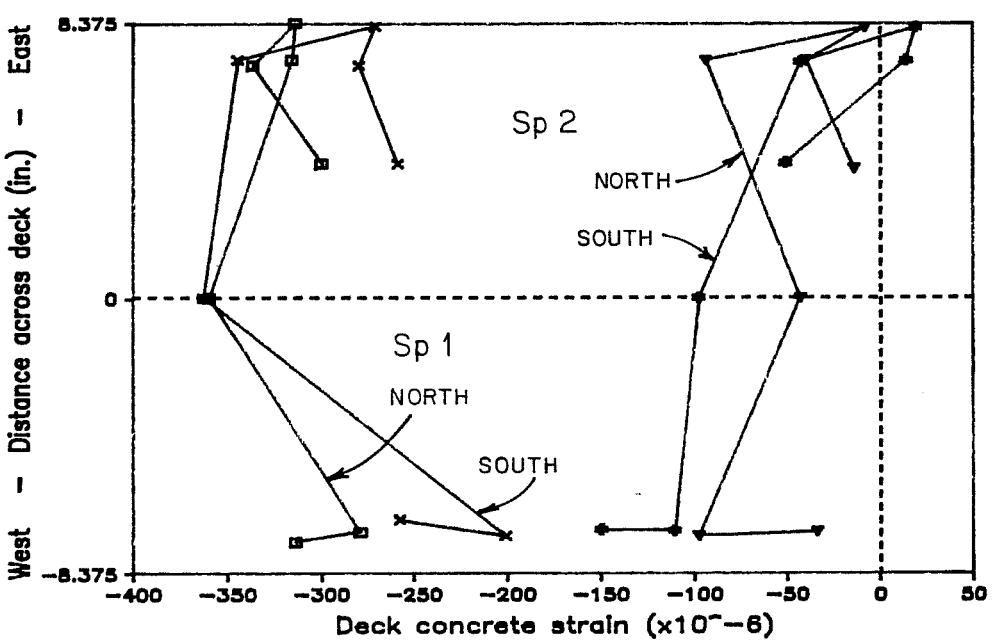

Fig. 6.103 Deck concrete creep strains at midspan at ultimate flexure tests

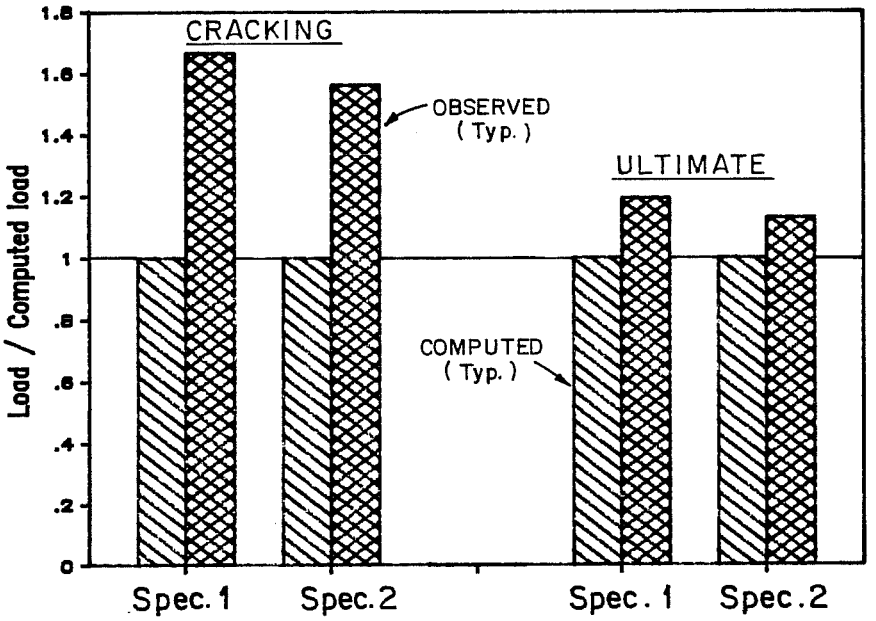

Fig. 6.104 Relative comprisons of computed and observed loads at cracking and ultimate

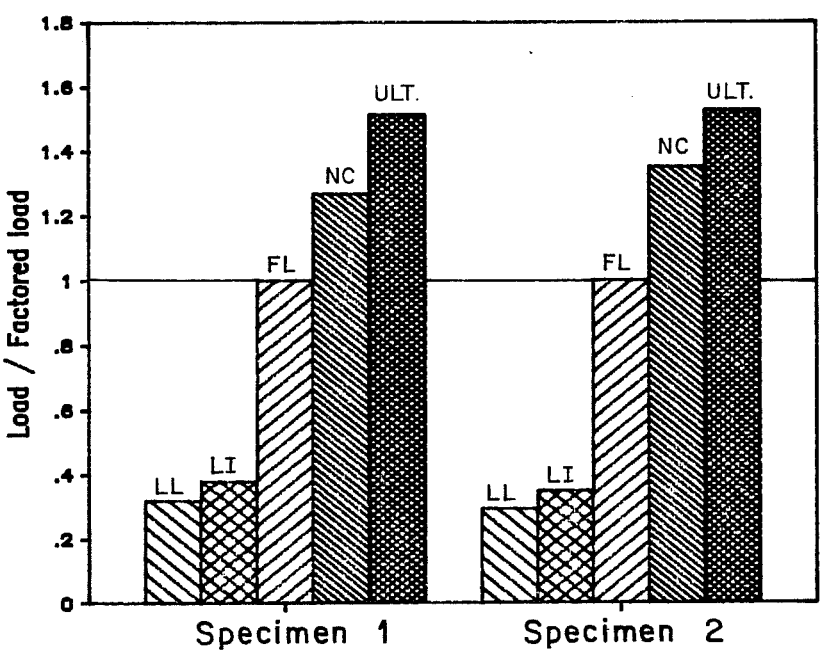

Fig. 6.105 Comparisons of design and ultimate loads

margin for both specimens. This is probably because actual tensile capacity was higher than the assumed value. Any error in estimates of prestress force would also affect cracking loads. Observed ultimate loads exceeded computed values by 20 percent or less which is reasonable.

Design and ultimate loads are compared in Fig. 6.105 using factored load as the basis for comparison. Factored load is nearly three times the live load due to the high dead load to live load ratio. The figure also shows the considerable excess nominal capacity provided because allowable stress criteria control the design. The computed nominal capacity exceeds the factored load by 25 to 35 percent. Where computed and observed capacity should be equal, since $\phi = 1.0$ for laboratory tests, the observed ultimate exceeded the computed value for both specimens.

6.4.2.2 Deflections. Midspan deflections are plotted in Fig. 6.106 which also shows some of the significant loads. At low loads, the stiffnesses are similar because specimens were essentially uncracked. Specimen 2 appears more ductile because it has an apparent yield plateau, although it was rather limited. Deflections at design, ultimate, and failure loads are summarized and compared with the span length as an index of their relative magnitude in Table 6.14.

The area beneath the load-deflection curve, which is an index of ductility, is shown in Fig. 6.107 for the specimens. At ultimate

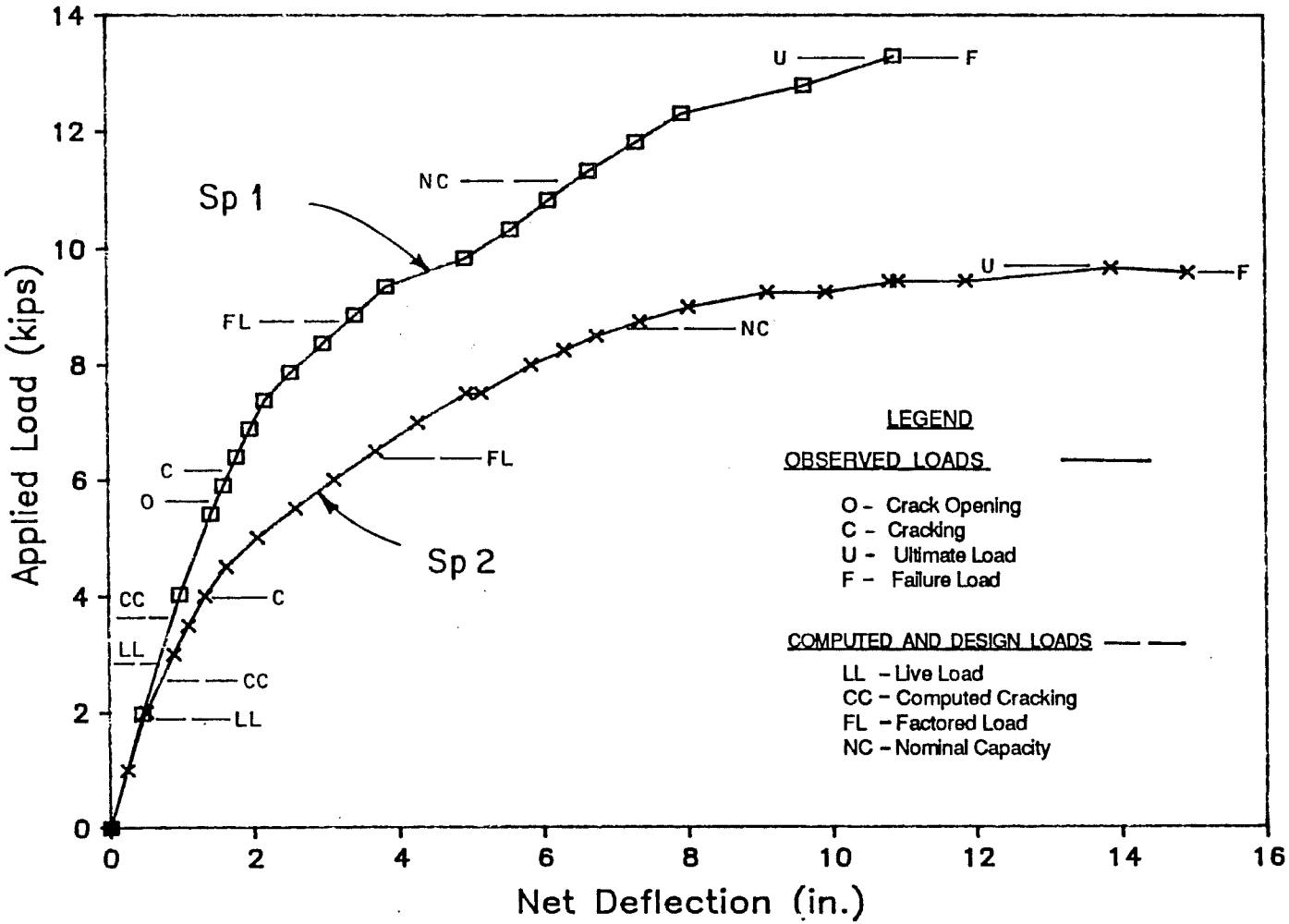

Fig. 6.106 Net deflection at midspan during ultimate flexure tests

Table 6.14 Comparison of deflections to span length during ultimate flexure tests

Load Stage	Load (kips)	Deflection (in.)	% of Span	Span/Defl.
Specimen 1				
Live Load	2.81	0.668	0.11	874.4
Live + Impact	3.33	0.801	0.14	729.2
Factored Load	8.79	3.354	0.57	174.1
Ultimate Load	13.29	10.880	1.86	53.7
Failure Load	13.29	10.880	1.86	53.7
Specimen 2				
Live Load	1.87	0.464	0.08	1258.6
Live + Impact	2.22	0.585	0.10	998.3
Factored Load	6.34	3.501	0.60	166.8
Ultimate Load	9.67	13.863	2.37	42.1
Failure Load	9.59	14.925	2.56	39.1

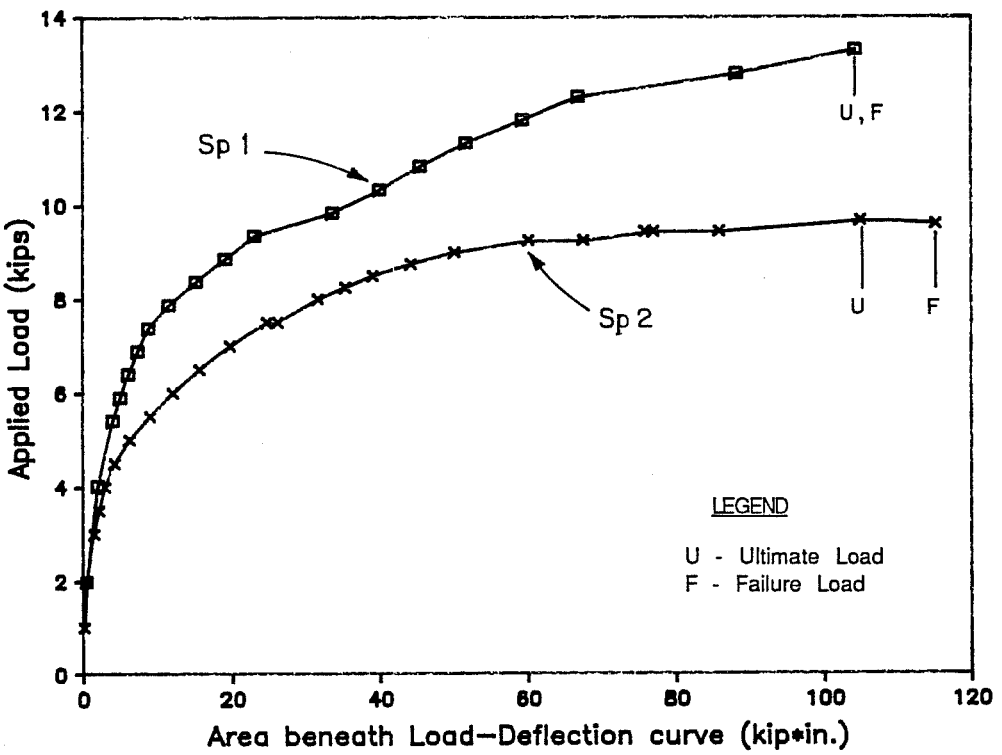

Fig. 6.107 Area beneath load-deflection curves

the areas beneath the load-deflection curves were nearly identical, indicating similar energy absorption capacities.

6.4.2.3 Strand and Concrete Strains. Average and net average strand strains are shown in Fig. 6.108. At failure, strains, and therefore stresses (Fig. 6.109), reached nearly the same level although the change in strain during the test for Specimen 2 was less than for Specimen 1. While it was expected that Specimen 2 would reach higher strains because of its lighter reinforcement, the suspected debonding of the strands limited the strains to values lower than expected when considering overall member behavior (see Fig. 6.81 for comparison of measured and computed strand strains for Specimen 2). Stresses in both specimens reached or exceeded 95 percent of the measured ultimate stress and came very close to or exceeded the specified ultimate stress of 270 ksi.

Corrected concrete strains at the top of the girder, which appear in Fig. 6.110, show that Specimen 1 reached much higher strains than Specimen 2 even though the curves are nearly identical for the range of loads encountered by Specimen 2. This is found to be reasonable if crack height and curvature data are considered.

Typical corrected strains for the top of the deck are shown in Fig. 6.111. Both specimens reached similar levels of strain at failure which were well below the expected ultimate strain capacity of the concrete.

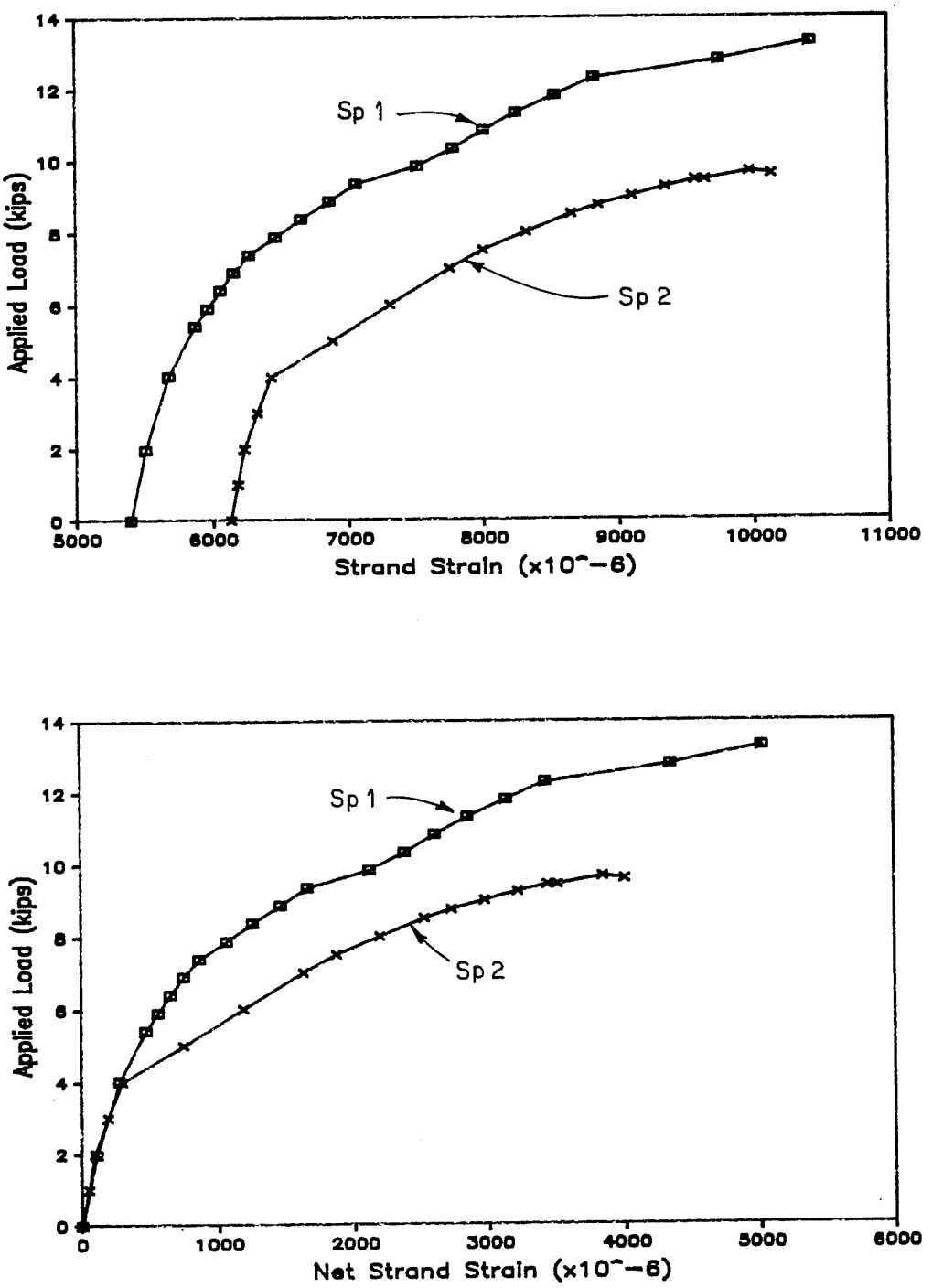

Fig. 6.108 Average strand strains during ultimate flexure tests: a) average strains; b) net average strains

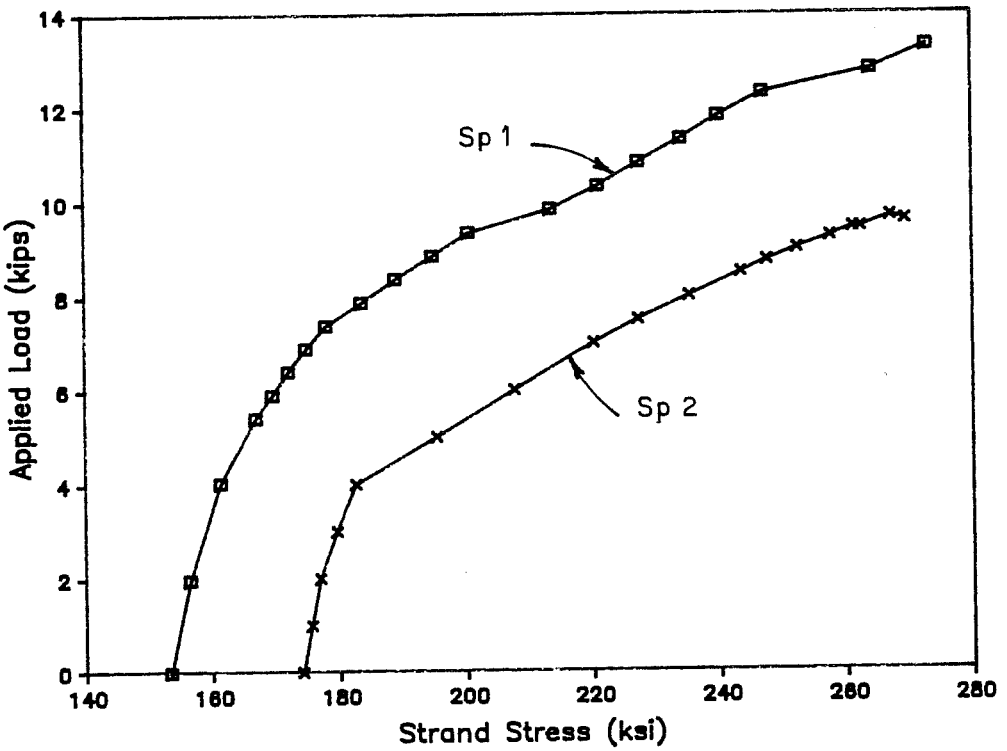

Fig. 6.109 Average strand stresses during ultimate flexure tests

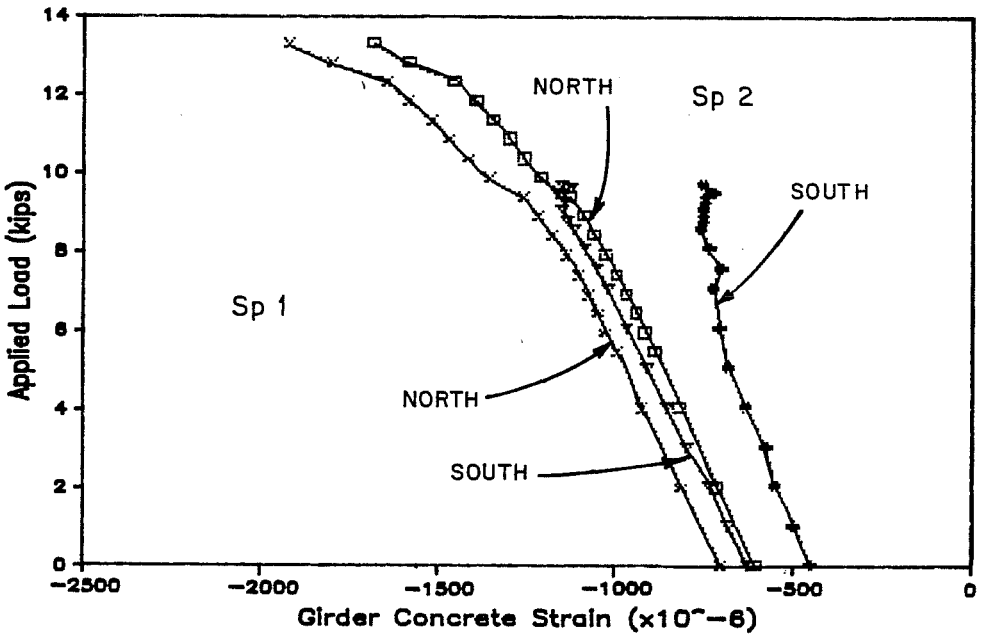

Fig. 6.110 Corrected top of girder concrete strains during ultimate flexure tests

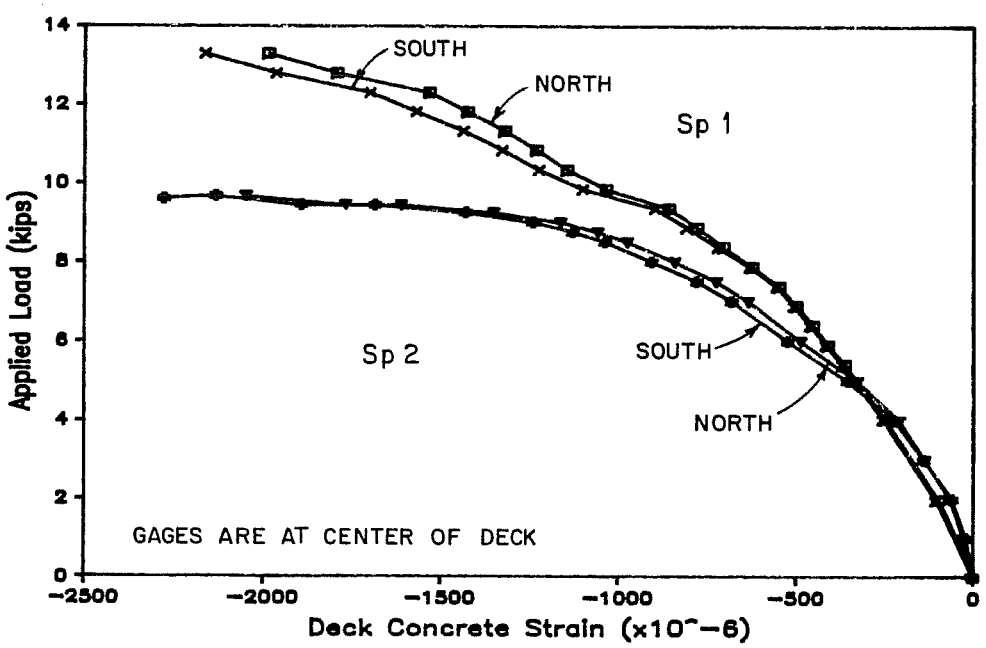

Fig. 6.111 Corrected top of deck concrete strains during ultimate flexure tests

Strain gradients at selected loads are shown for girder and top of deck strains in Fig. 6.112. These plots demonstrate that the strain gradient for the section due to applied load remained linear to failure. Therefore, full composite action was present for both specimens at all levels of load.

Crack heights computed using corrected girder strains are shown in Fig. 6.113. Cracks rose higher in Specimen 2 with less reinforcement. The crack height was rising rapidly as failure was approached for Specimen 2 while the crack height was more stable for Specimen 1 at high loads.

Moment-curvature plots are compared in Fig. 6.114. The curvature at ultimate for Specimen 2 is 22 percent greater than for Specimen 1; at failure, the curvature is 42 percent higher for Specimen 2 than for Specimen 1. This indicates greater ductility in Specimen 2, but it is less of a difference than expected.

All types of data for each specimen are shown in Fig. 6.115. These curves demonstrate some basic differences in behavior between the specimens. For Specimen 1, the strand strain increased most slowly at first and the deflection and curvature were nearly indistiguishable, which is surprising. After a load of about 9.5 kips, the curves all follow the same path as they converge on the load stage prior to failure. Specimen 2 behavior is different with the curvature being the quantity to increase most slowly and the midspan deflection and the top of deck strain being almost

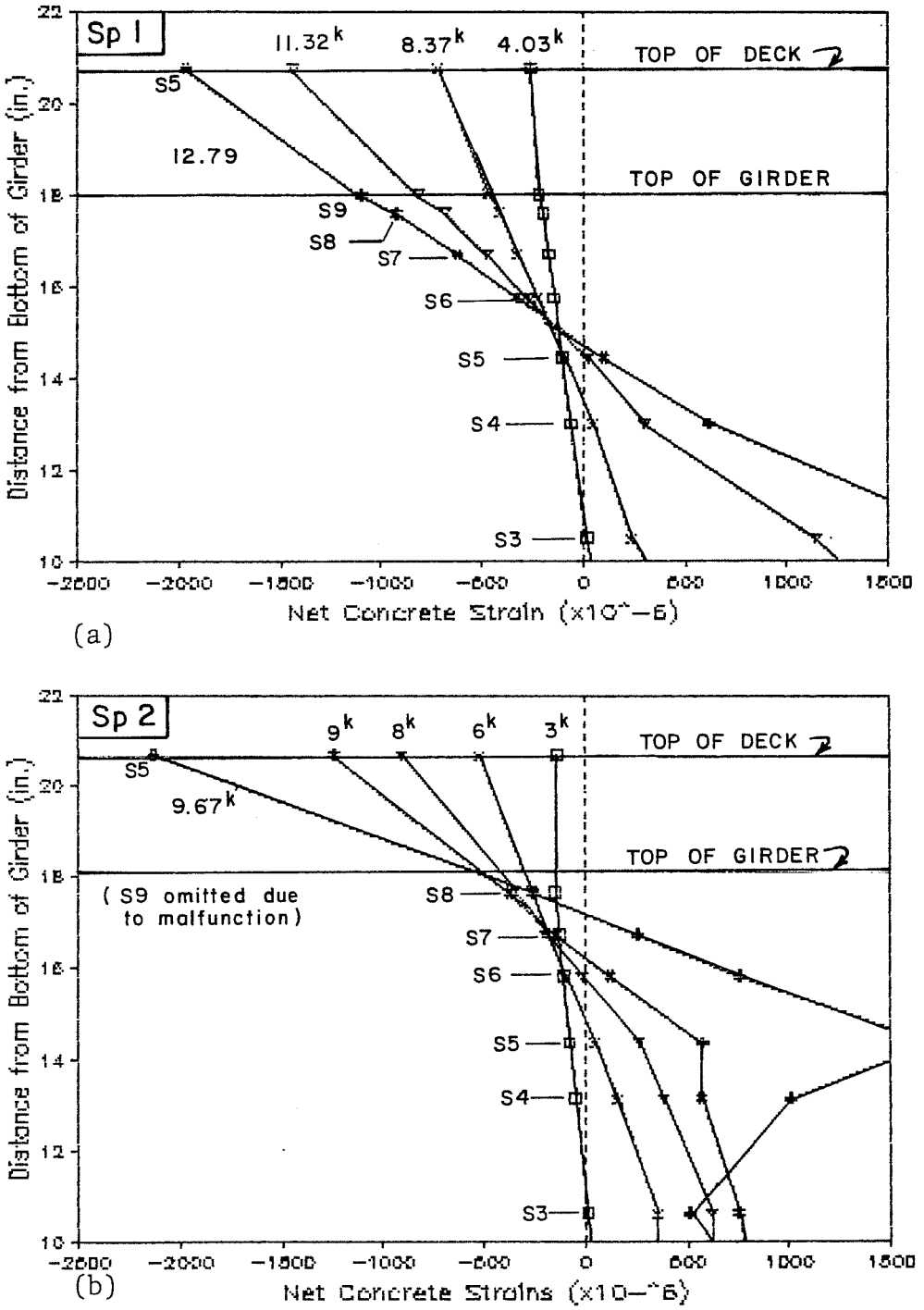

Fig. 6.112 Net girder and deck concrete strains at selected loads during flexure test: a) south gages, Specimen 1 b) south gages, Specimen 2

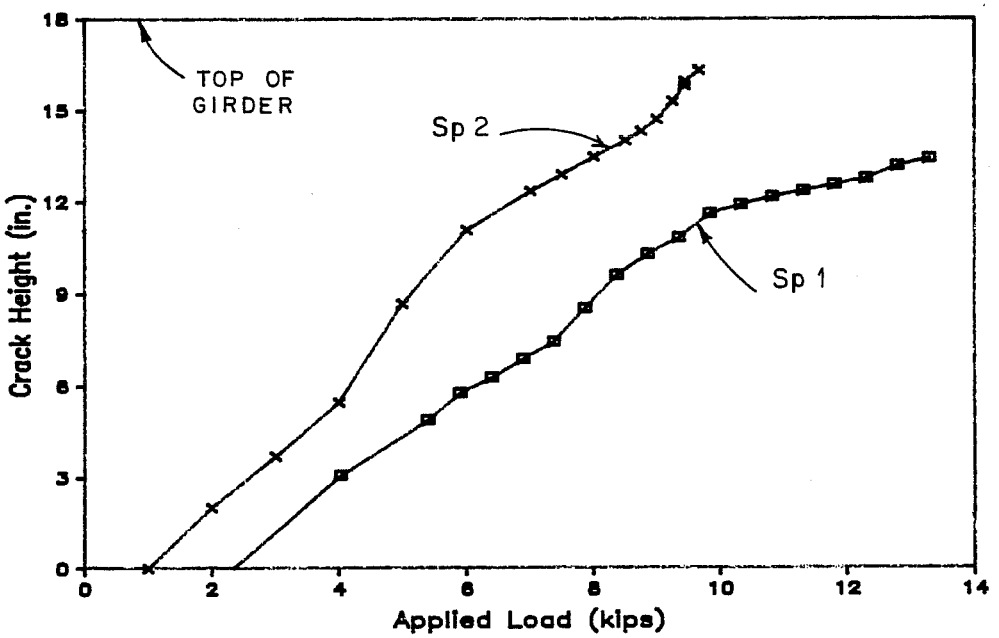

Fig. 6.113 Computed crack height during ultimate flexure tests

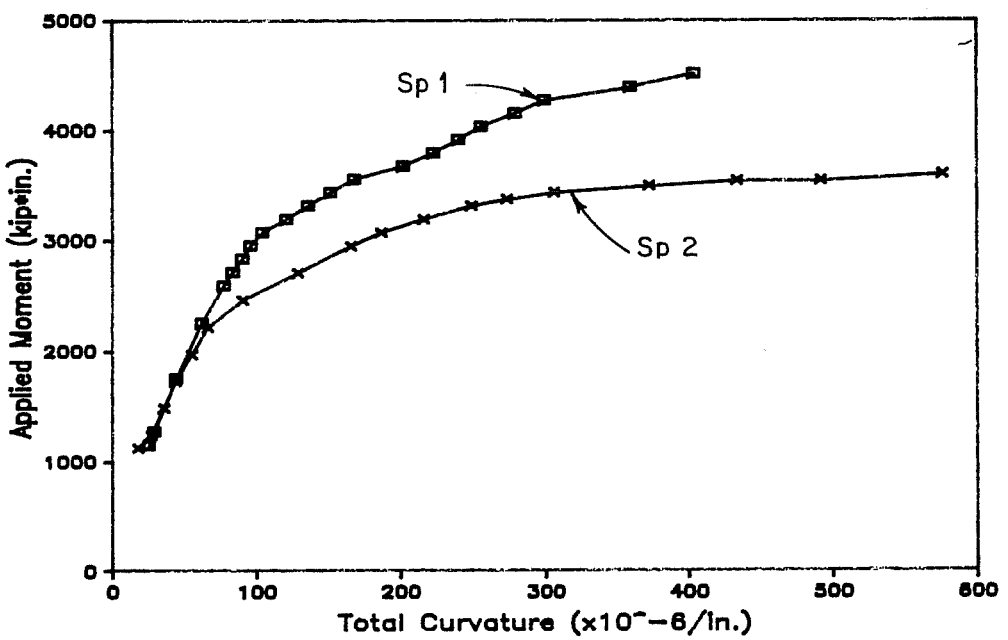

Fig. 6.114 Moment-curvature curves during ultimate flexure tests

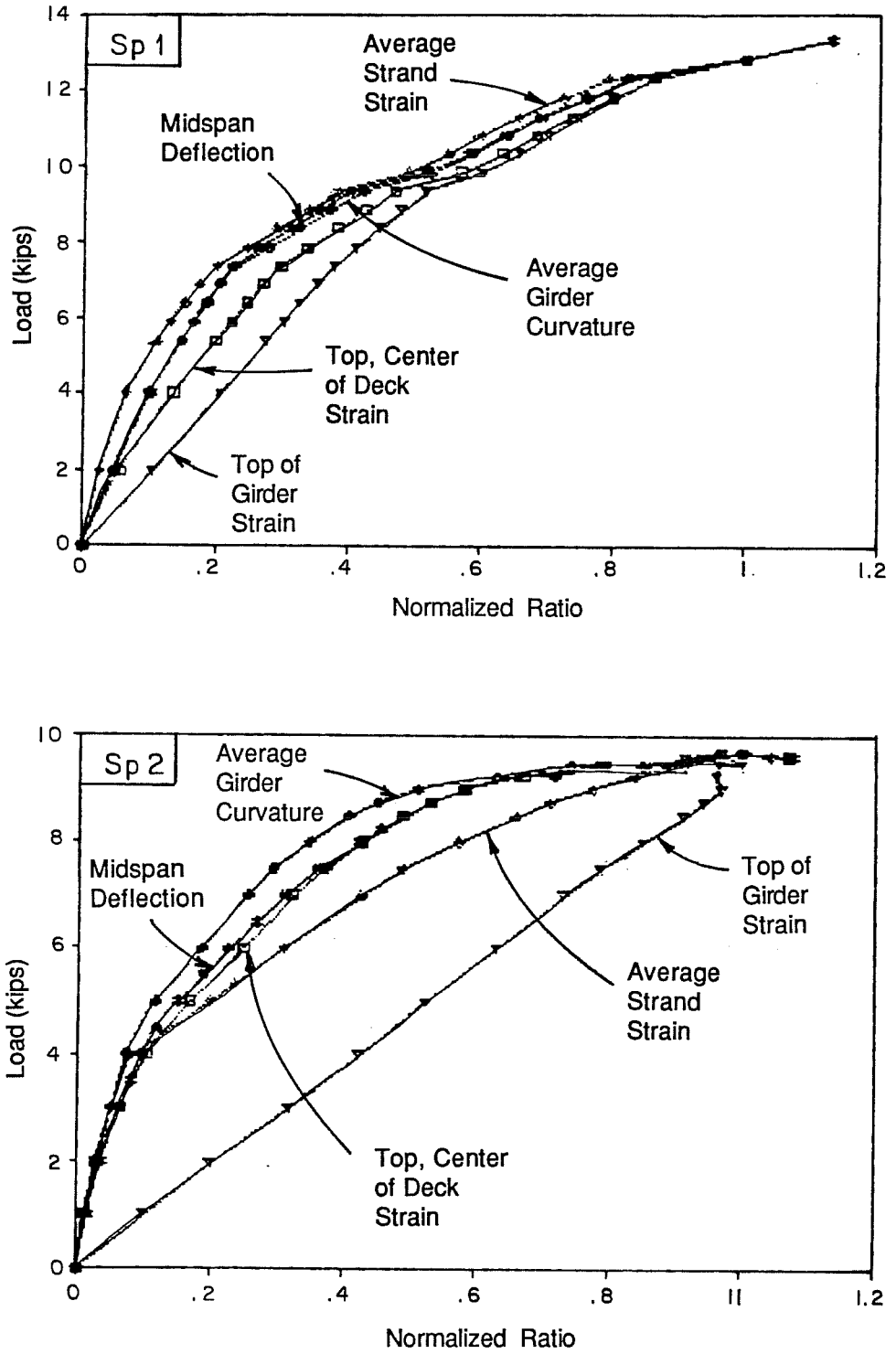

Fig. 6.115 Comparison of different types of data during ultimate flexure tests: a) Specimen 1; b) Specimen 2

indistinguishable. The average strand strain followed the girder curvature up to 4 kips, then departed as it began to change more rapidly. The top of girder strain was striking in that it remained essentially linear up to the ultimate load. Identifying the reasons for the differences in behavior is not simple due to the complex interrelation of the quantities.

6.4.3 Shear Tests. A general discussion of the behavior observed during the four shear tests will be presented in this section. These tests were preliminary in nature and were used to provide background for a more complete study of shear that followed in this overall test program.

Testing the ends of the flexural test specimens proved to be quite successful. While formation of cracks in the shear spans of interest during flexure tests precluded determination of cracking loads in some cases, the total capacity was apparently unaffected. Load-deflection curves obtained during the tests were affected by the presence of cracks in the deck due to insufficient dead load moment as a result of the shortened span. However, the capacity of the member was unaffected. The end of the shear specimen that was near midspan of the complete flexure specimen experienced little additional cracking during shear tests, and existing cracks were unaffected.

Measured and predicted shear capacities of the specimens are compared in Fig. 6.116. Predicted ultimate shears were computed using the ACI equation for web cracking with a capacity reduction factors

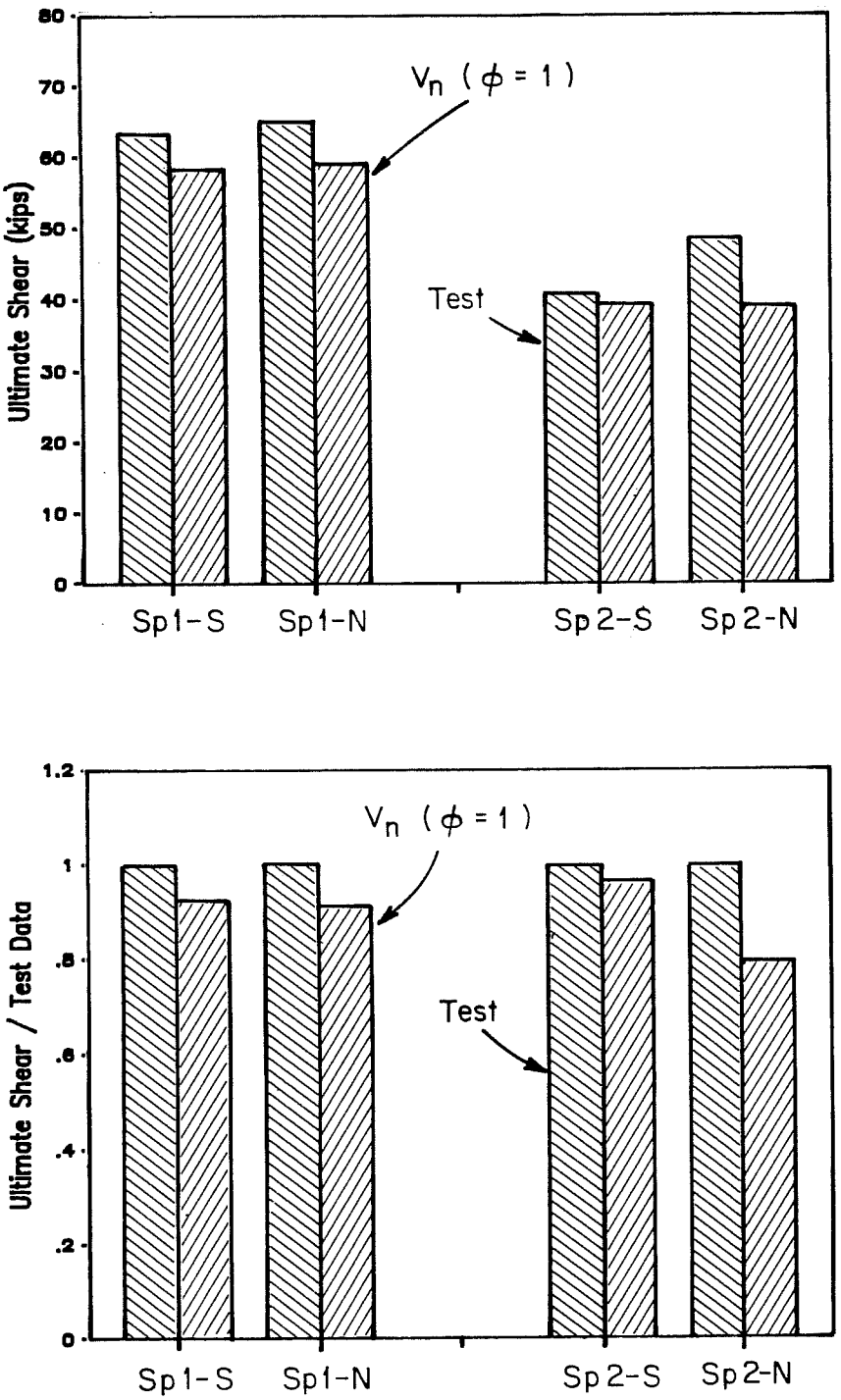

Fig. 6.116 Comparison of measured and predicted capacities for shear tests: a) ultimate shear capacity; b) normalized with respect to test data

(ϕ) of 1.0, as appropriate for laboratory tests. The upper half of the figure compares the actual shear values while the lower half contains data normalized using the test results. In all four tests, the predicted values were reasonably conservative when compared with the test data. The predicted values were most conservative for the north end of Specimen 2 where strand slippage did not occur. It is expected that, if strand slippage had been prevented for the other specimens, the predicted capacities would be more conservative.

A similar comparison was made between observed shears at web cracking and shears at which the ACI equation predicted web cracking (Fig. 6.117). In all cases the computed value greatly exceeded the observed cracking shears. The large discrepancy between observed and computed shears causing web cracking may be partially due to the presence of prior cracking resulting from the violent flexural failures and shrinkage.

Load-deflection behavior of the specimens during the four ultimate shear tests is shown in Fig. 6.118. As mentioned above, the curves include the effect of deck cracks closing as load was added. Flexural cracking played a more significant role in the Specimen 1 tests as indicated by the more clearly bilinear shape of the curves. Both shear tests for Specimen 1 ended in strand slippage which is a brittle failure that led to a sudden departure from the linear behavior of the member. Significant capacity remained after slip occurred, although loading was not continued to complete failure. The

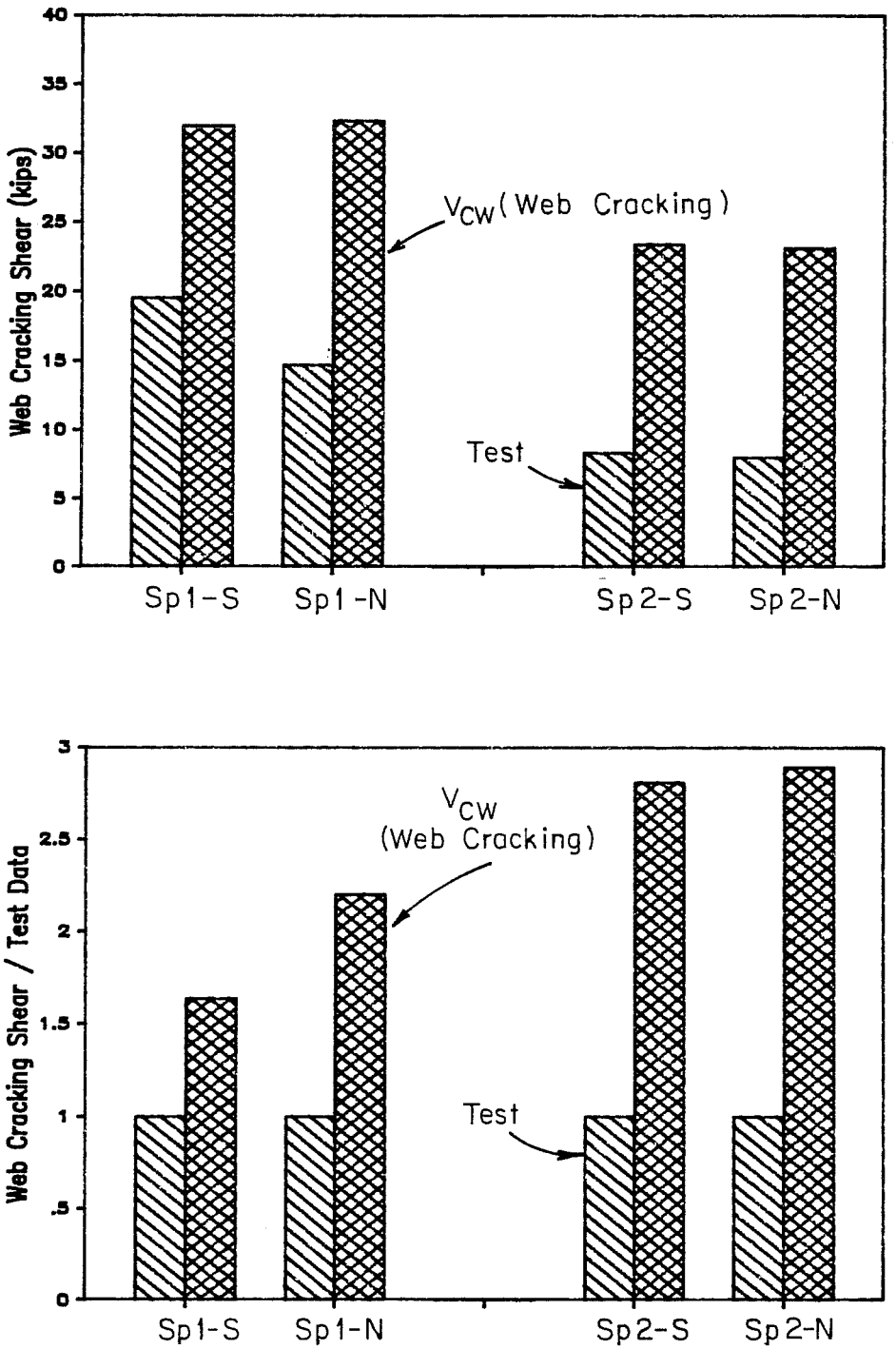

Fig. 6.117 Comparison of measured and predicted web cracking shears for shear tests: a) web cracking shear; b) normalized with respect to test data

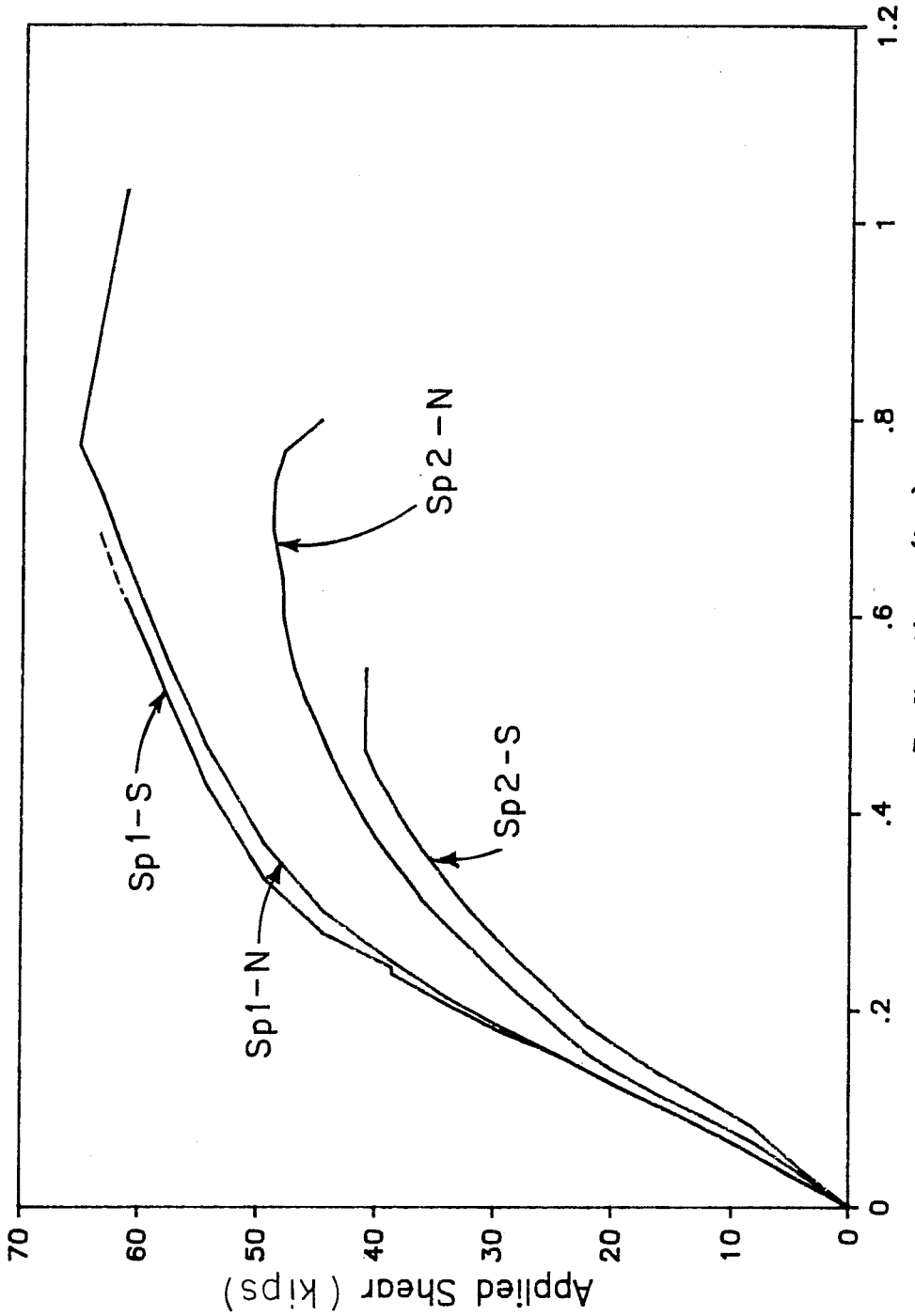

Fig. 6.118 Deflection at load point during ultimate shear tests

south end of Specimen 2 displayed similar behavior with the capacity controlled by strand slippage. While the north end of Specimen 2 failed in web crushing, the capacity continued to increase slightly as crushing began and decreased only gradually as crushing became widespread. This failure mode led to a load-deflection curve (Fig. 6.118) that exhibited a degree of ductility. Flexural cracking was not a significant factor in the behavior of either end of Specimen 2.

Failure modes were basically brittle where strand slippage was involved since shear decreased immediately following the slip, although the shear resisted by the member decreased only slightly. The web crushing failure proved to be more ductile because the shear resisted initially continued to increase slightly as deflection continued.

Other aspects of behavior of the specimens were quite similar. Most instrumented stirrups yielded during the four shear tests, especially those in the central portion of the shear span. Strand strains were also approximately the same for Specimen 1 and the north end of Specimen 2 even though the load applied to Specimen 2 at failure was approximately 75 percent of the maximum load applied during both tests of Specimen 1. The maximum strand strain for the south end of Specimen 2 was lower than for the north end, although it corresponded well with the strains measured at the same load for the test of the north end.

CHAPTER 7

EVALUATION OF TEST RESULTS AND CURRENT DESIGN PRACTICE

7.1 Introduction

In this chapter, results of the literature review of Chapter 3 and data gathered during the test programs are compared and evaluated with emphasis on the effect of high strength concrete on design. The organization parallels that of Chapter 3. Major sections conclude with a summary and recommendations where appropriate.

7.2 Philosophy of Design

The use of allowable stress and ultimate strength criteria as the basis for design of prestressed members is reasonable and has served the industry well. However, other aspects of design must also be considered if a bridge is to give satisfactory performance. Therefore, consideration of other important aspects of member design and behavior should be clearly and directly addressed. This is especially necessary as structures extend customary limits and become increasingly complex. Analysis capabilities have also become more sophisticated, enabling designers to directly determine quantities that have often been entirely neglected or indirectly limited due to a lack of computational methods. The intent of the code must be clear so that designers can correctly apply the code in unusual situations.

The topic of ductility is one such area that must be adequately addressed in a manner that can be understood and correctly applied by the designer. The current indirect approach of limiting the reinforcement index has apparently been sufficient, but the intent of the limit is not clear to the designer and may be misinterpreted. New limits are proposed and it is suggested that the basis or derivation of the limits be included in codes or commentaries. In this way, the intent of the provisions can be understood and applied where the specific limits are not applicable or where a more complete analysis is used, which would permit direct application of limits for which the code provisions are approximations.

Other areas in which the design of highway bridges should take a more direct approach are deflections, stability, and fatigue. In the sections that follow, direct approaches for determining member behavior in these areas will be presented and discussed.

With these considerations, codes would move toward a more complete consideration of member behavior and would therefore produce structures that have been directly examined for all aspects of behavior.

7.3 Basic Properties of High Strength Concrete

This section presents a further review of the data presented in Chapter 3 and compares that information with data and observations collected during construction and testing of the long-span girder specimens.

7.3.1 Compressive Strength. The limited data reported from this study in Appendix A indicates that the mean variation between strengths for the two sizes of cylinders is small (<3.5 percent) with 4 x 8-in. cylinders giving higher strengths than standard cylinders. The magnitude of variation between the two sizes of cylinders is in agreement with data reported in Sec. 3.3.1, although the reported strengths for 4 x 8-in. cylinders are higher instead of lower than strengths for 6 x 12-in. cylinders. Therefore, because available data are limited and inconsistent, it is recommended that a correlation between 4 x 8-in. and 6 x 12-in. cylinder strengths should be determined on a local basis when 4 x 8-in. cylinders will be used. Because of the increased 3 variability in tests of 4 x 8-in. cylinders reported by Malhotra [78], which may contribute to the inconsistency between results reported by investigators, it is also recommended that at least twice as many 4 x 8-in. cylinders should be tested as the number of 6 x 12-in. cylinders currently tested in order to obtain the same level of confidence [78].

Use of a later design age for concrete strengths does not appear to be of great consequence but may be desirable when a mix shows a large increase in strength with time and the design strength is not required until the later date. Proper controls on the strength must be developed in order to determine satisfaction of design criteria at early ages as discussed by Drake [43].

Data presented in Appendix A indicate that curing cylinders in ambient conditions following the application of curing compound after stripping the molds reduced the strength of the concrete by less than 5 percent when compared with cylinders cured in a lime bath. This agrees with data reported by other investigators. Therefore, cylinders cured in a wet or moist environment can be used to estimate the concrete strength in girders cured under ambient conditions, although the cylinders will have a somewhat higher strength than the girder, assuming that cylinders cured with the girder give a good indication of girder strength.

Greater reductions in strength may be possible between ambient and moist- or wet-cured cylinders because of the severe curing conditions to which some girders are subjected. While most girders are removed from forms less than 24 hours after casting and are immediately placed in an open yard for storage, the girders in this study remained in the forms for two or four days after casting, received a liberal coat of curing compound, and were stored and tested

under the shelter of a roof, which prevented direct exposure to sunlight. Further study is needed to determine the effect of severe curing conditions on concrete strength. However, for pretensioned girders, the design strength is generally not critical because concrete strength requirements at release control the mix design. This results in a concrete strength at the design age significantly greater than the strength required in almost all cases.

7.3.2 Modulus of Elasticity and Stress-Strain Curve.

Average modulus of elasticity data for the girder concrete of Specimens 1 and 2 at various ages are summarized in Table 7.1. This data for 6 x 12-in. cylinders, was obtained with a mechanical extensometer (compressometer) with an 8-in. gage length, or for a single case, strain gages attached to the cylinders. Data for Specimen 1 at 66 days were inconsistent, with the compressometer data giving lower modulus values than those determined using strain gages. Strain gage measurements agreed closely with compressometer measurements taken at 44 days. The discrepancy between moduli determined using strain gage and compressometer measurements was unexpected because in previous tests where both strain gage and compressometer readings were made for the same cylinders, agreement was very good.

After adjustment for unit weight, the average data given in the table was added to Fig. 3.4 and appears here as Fig. 7.1. Air

Table 7.1 Average Modulus of Elasticity Data for Girder Concrete - Specimens 1 and 2

Age	Curing	Strength	Average Modulus	$Ec/\sqrt{f'_c}$
(days)		(ksi)	(ksi)	($x10^3$)
Specimen 1 - Steel molds				
44	Air	13.02	6,380	55.9
66	Air	12.91	5,980	52.6
66 *	Air	12.91	6,430	56.5
Specimen 2 - Plastic molds				
7	Air	9.20	5,300	55.3
21	Air	10.12	5,550	55.2
28	Air	10.75	5,720	55.2
28	Wet	10.66	7,000	67.8
56	Air	10.78	5,675	54.7

Note: Unit weight of concrete is approximately 150 pcf.

* - Modulus determined using two electronic strain gages on each cylinder. All other data taken using a compressometer.

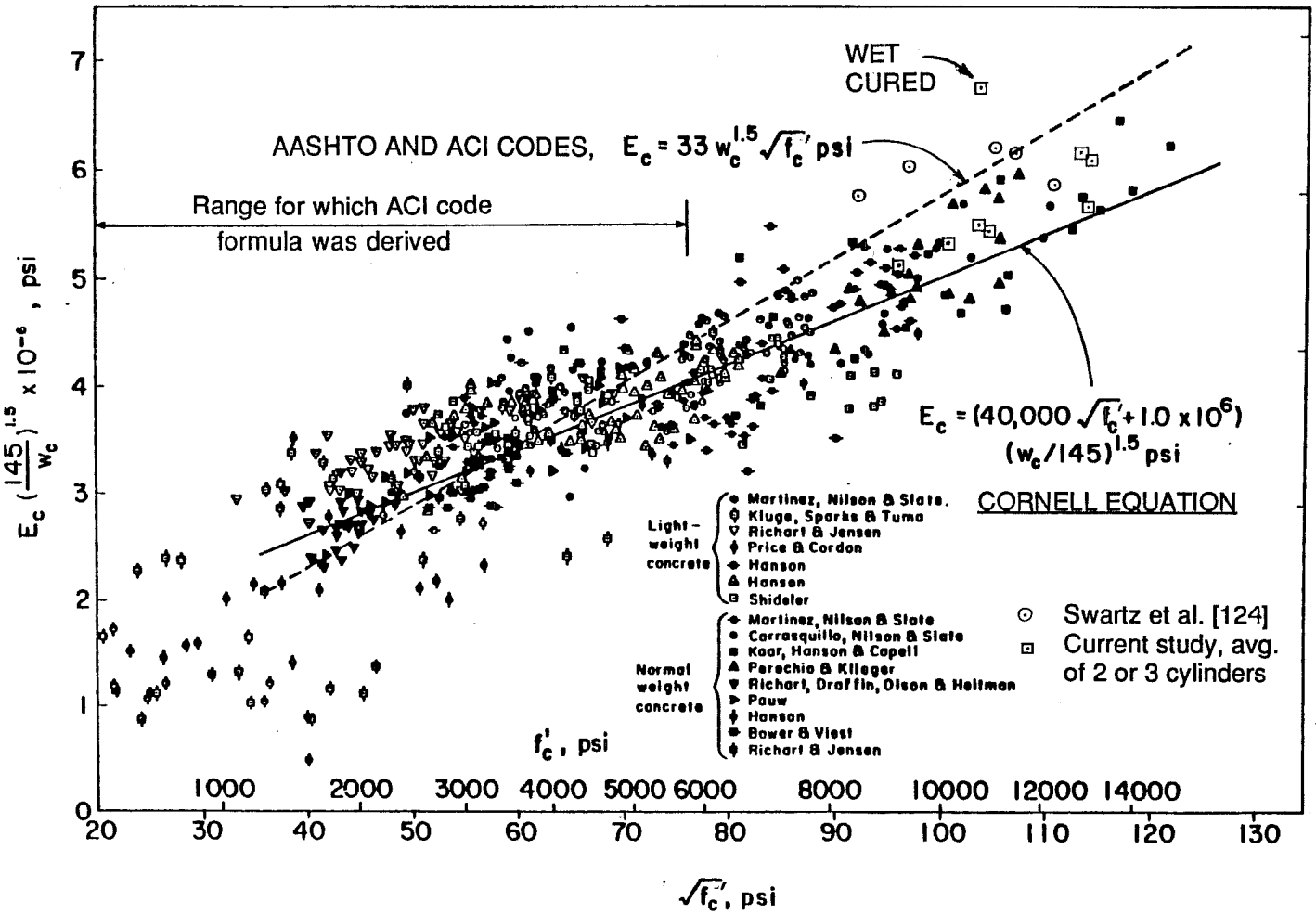

Fig. 7.1 Modulus of elasticity versus concrete strength including data from current study [81, 124]

cured cylinders are positioned between the ACI and Cornell equations while the single wet cured data point is significantly above the ACI equation. In this case, the modulus is much more sensitive to curing conditions than the strength. However, two air cured cylinders from the final trial batch for the girder concrete had moduli of 8,160 and 8,680 ksi for cylinder strengths of 12,410 and 14,000 psi, respectively. These data points are well above the ACI equation but were not included on Fig. 7.1 because they were obtained using strain gages rather than a compressometer. Unit weight for this batch at casting was 153.8 pcf.

The data of Fig. 7.1 and the additional data mentioned above confirm the potential for wide scatter in modulus values due to differences in curing conditions and materials. Also, it should be noted that the data from which the proposed Cornell equation was developed were obtained from a limited variety of aggregate sources. Therefore, it appears prudent, in situations where the modulus is a critical factor in design, to determine the effect of specific materials and conditions by measuring the modulus for high strength concrete. The current AASHTO and ACI expression for modulus of elasticity appears sufficiently accurate for estimating the modulus if data on a specific mix are not available. The effect that using the current modulus equation or the equation proposed by investigators at Cornell has on designs is considered in Sec. 7.4.5.4.

Average stress-strain curves for the girder and slab concrete at the time of the flexure tests are shown in Fig. 7.2. Curves for Specimen 1 were obtained using strain gages attached to manual strain indicators while data for Specimen 2 were obtained using a plotter to record head displacement of the testing machine. The method of measurement was changed to permit determination of the stress-strain curve approaching and beyond the peak stress. This was not possible for Specimen 1 using strain gages because of spalling of the concrete surface to which the gages were attached, and because the data recording device used with the gages did not permit accurate, continuous monitoring of strain. Plots obtained for Specimen 2 cylinders were calibrated using modulus measurements made with a compressometer. While cap deformation was included in strains measured for Specimen 2, the error introduced was estimated to be less than 2 percent. The shapes of the curves are similar to the typical curves shown in Fig. 3.3, although the strains at maximum stress are lower. Curves for high strength concrete end with the sudden destruction of the cylinder while low strength cylinders continue to resist load beyond the strains shown, although the concrete is badly crushed and the usefulness of such data is questionable.

The shape and extent of the descending branch of the stress-strain curves are affected by the stiffness of the testing machine and the testing method. When the stiffness of the descending

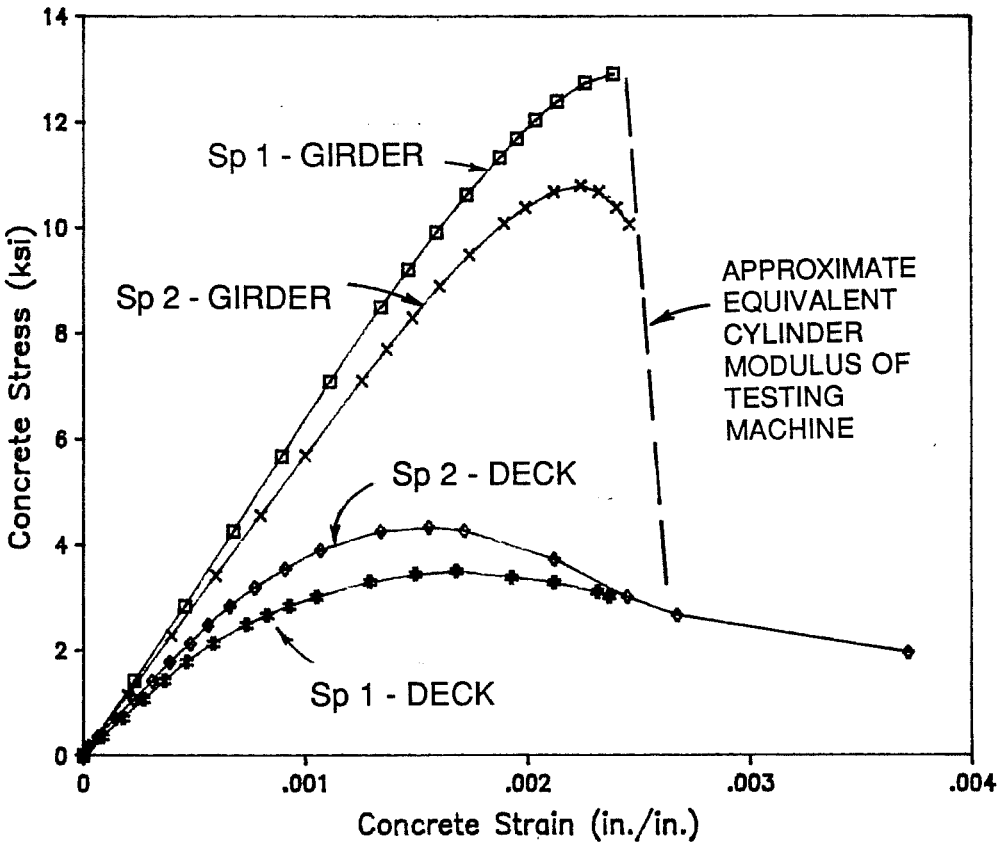

Fig. 7.2 Average stress-strain curves for concrete at time of flexure test for Specimens 1 and 2

branch of the stress-strain curve for a concrete cylinder approaches the stiffness of the testing machine, energy in the testing machine is unloaded on the cylinder resulting in the sudden destruction of the cylinder. An equivalent cylinder modulus of elasticity of 51,000 ksi was computed for the testing machine considering only the axial stiffness of the sidewalls of the machine. A dashed line corresponding to this equivalent modulus is indicated on Fig. 7.2. Since the descending branch for the low strength deck concrete was less stiff, the stress-strain curve was minimally affected by the properties of the testing machine. The descending branch of the stress-strain curves for the high strength girder concrete cylinders, however, was apparently very steep and was therefore strongly influenced by the machine. Use of a stiffer machine may have resulted in a longer descending branch for the high strength concrete.

Measured strains at maximum stress and ultimate strains for the girder concrete of Specimen 2 are summarized for three 4 x 8-in. cylinders in Table 7.2. These values were obtained from measurements of the testing machine head displacement at an age of 56 days. This data is used for the following comparisons because it appears more reliable than the data obtained for Specimen 1 using strain gages. As described earlier, the strain monitoring device could not be expected to give accurate data as the peak of the stress-strain curve was approached or exceeded.

Table 7.2 Strain at Maximum Stress and Ultimate Strain for Girder Concrete - Specimen 2

f'_c	ϵ_0	ϵ_{cu}
(ksi)	(in/in)	(in/in)
10.72	0.002240	0.002500
10.95	0.002290	0.002480
10.73	0.002190	0.002400

Note: Data shown are for 4 x 8-in. cylinders.

Strains at maximum stress from Table 7.2 are compared with compression (cylinder) data and combined flexure and compression data from the literature in Fig. 7.3. The current data are among the highest reported concrete strengths and lowest strains.

Ultimate strains from Table 7.2 are compared with cylinder data and combined data from the literature in Fig. 7.4. The current data are representative of cylinder data for comparable concrete strength and are low for combined data, which is expected because ultimate strains for cylinder data are typically lower than for flexural data.

Estimated and measured values for the deck and girder concrete strains at failure are given for Specimens 1 and 2 in Table 7.3 along with strains at maximum stress and failure for corresponding cylinder tests. These data are presented graphically in Fig. 7.5. The estimated strains at failure for Specimen 1, which represent an average for a number of gages, were computed using measured changes in deflection (see Sec. 6.2.2.3). The strain at the top of the Specimen 2 girder was estimated using data for the single active gage for which readings had been essentially constant for load stages preceding failure. The deck strain at failure of Specimen 2 was measured by manually following the reading for a single gage with a strain indicator as load was being applied. This gage was representative of most other deck gages on the top of Specimen 2,

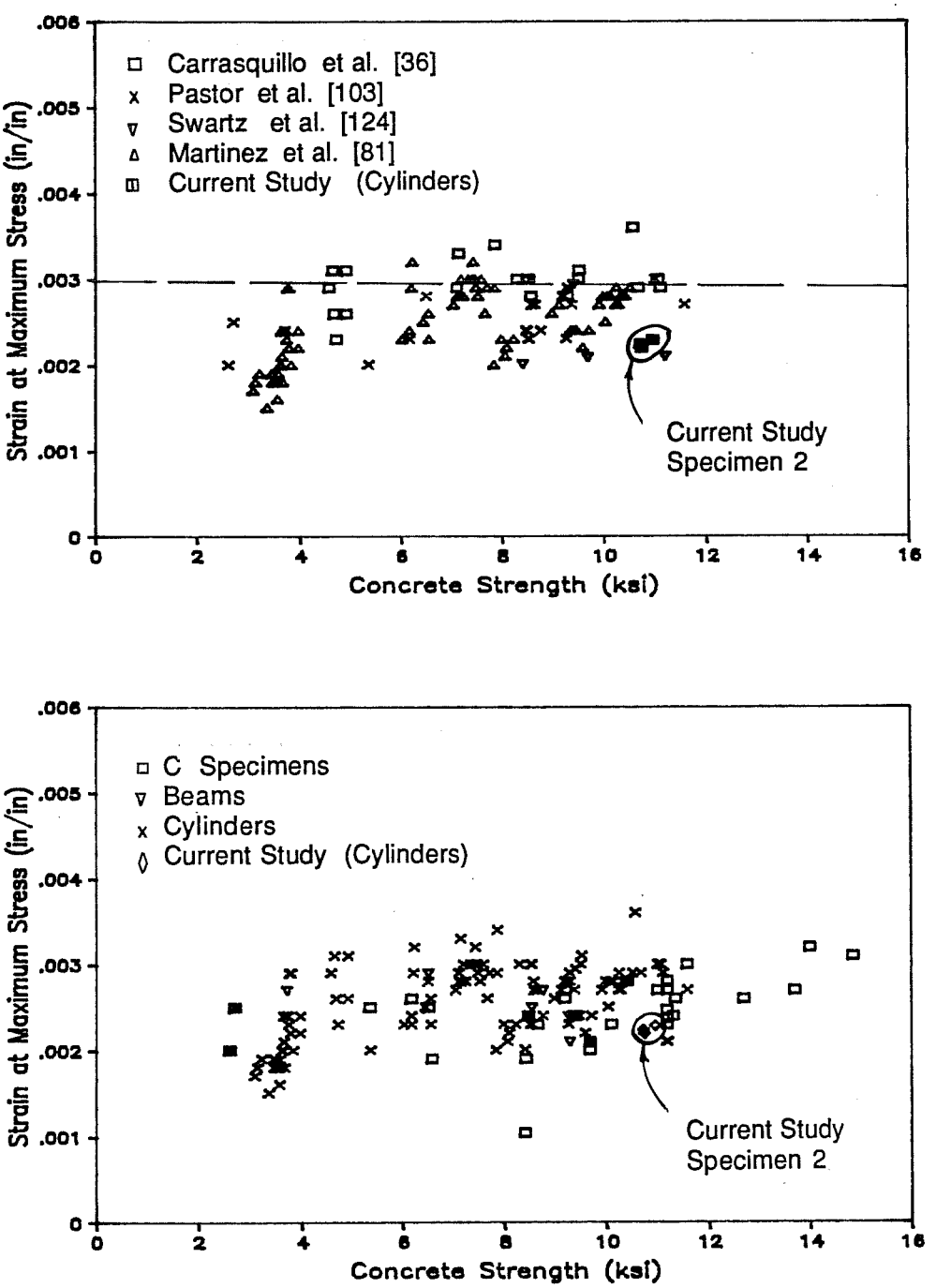

Fig. 7.3 Comparison of Specimen 2 data for strain at maximum stress with other data: a) cylinder data; b) combined data

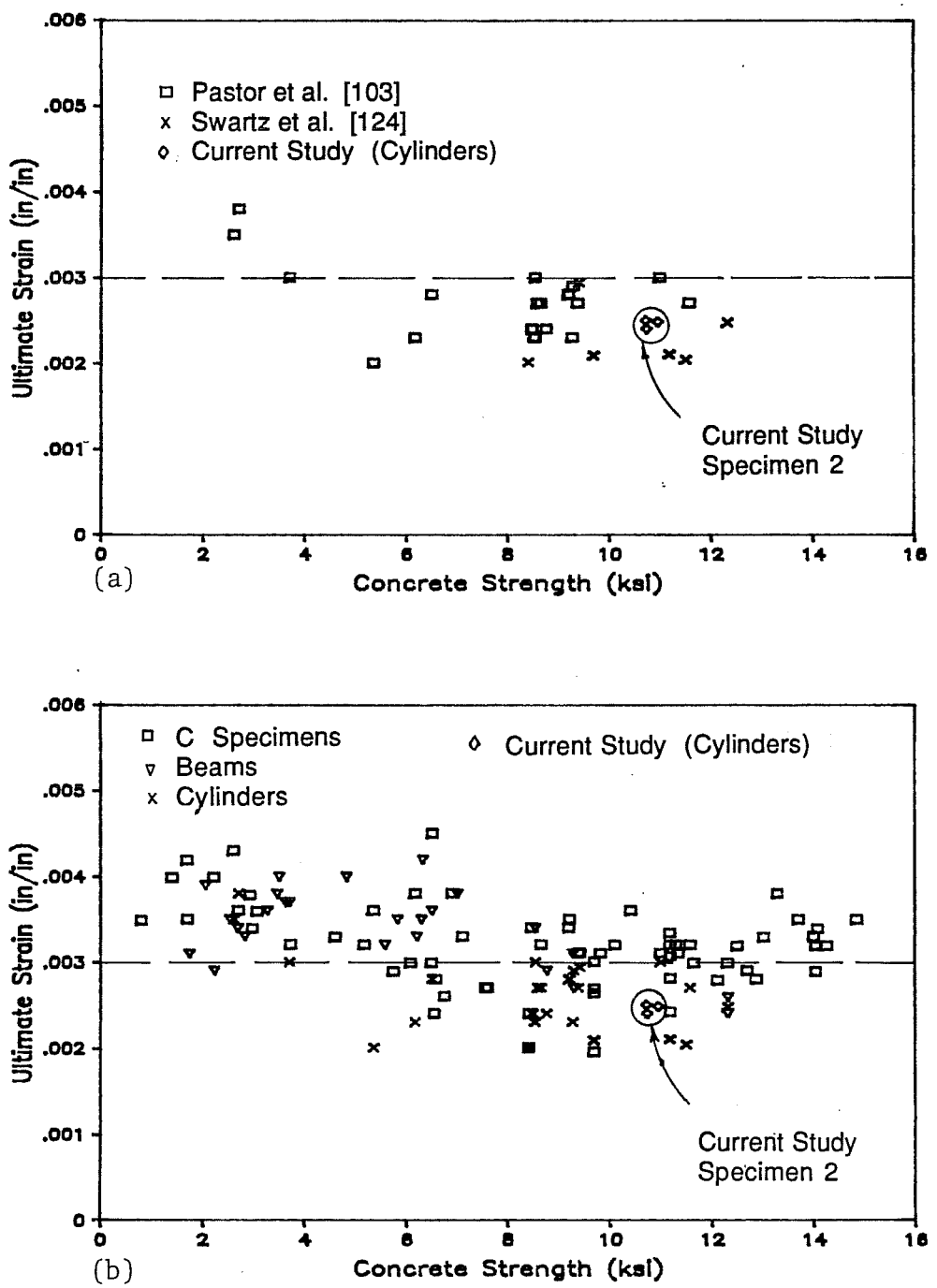

Fig. 7.4 Comparison of Specimen 2 data for ultimate straine with other data: a) cylinder data; b) combined data

Table 7.3 Critical Strains for Specimens and Related Cylinders

		Test Specimens	----- Cylinders -----	
	f'_c	ϵ_{max}	ϵ_0	ϵ_{cu}
	(ksi)	(in./in.)	(in./in.)	(in./in.)
Specimen 1				
Girder	12.90	0.001900 E	0.002400	0.002400
Deck	3.50	0.002080 E	0.001600	0.002370 *
Specimen 2				
Girder	10.80	0.001090 E	0.002240	0.002460
Deck	4.35	0.002240 M	0.001550	0.003710 **

ϵ_{max} = corrected strain at top fiber of element at failure of member.

E = Estimated strain
M = Measured strain

ϵ_0 = strain at maximum stress in cylinder.

ϵ_{cu} = strain at failure of cylinder.

* - strain limited by failure of strain gages rather than failure of cylinder.

** - strains in excess of this value were recorded, but concrete was badly crushed.

failure were 30 and 45 percent (for Specimens 1 and 2, respectively) higher than the strain at maximum stress. Since high levels of load, which corresponded to strains in the deck approaching maximum levels, were maintained for significant periods of time during the tests (see Appendix B), it appears likely that sustained loading effects contributed to the crushing of the deck concrete.

Considering all available data (see also Fig. 3.7), use of the current maximum usable concrete strain of 0.003 for ultimate flexural design in all cases appears questionable for both normal and high strength concrete. Significant variations in both the strain at maximum stress and the ultimate strain result from use of different aggregates and mix designs as demonstrated by the differences in the curves of Fig. 3.3 and 7.1. For composite, pretensioned structures the ultimate strain for high strength concrete will most likely not be critical because a girder will seldom approach even a reduced limiting strain prior to the deck reaching its limiting strain. If the deck concrete crushes at strains below the specified limiting strain, which appears possible in light of the preceding data and discussion, the girder strain would be lower with respect to its limiting strain when the deck concrete crushes. However, in non-composite structures, the maximum usable strain is critical and should be investigated further. Data from other investigators (Fig. 3.7), which indicate that beam specimens have failed at strains below 0.003, support this concern.

High strength concrete with a high modulus of elasticity appears most likely to have reduced strains at maximum stress and failure and should therefore be the object of special concern. The effect of using a reduced maximum usable concrete strain on design is discussed in Sec. 7.4.4 and 7.4.5.

7.3.3 Tensile Strength. Table 7.4 contains a summary of tensile strength measurements made for Specimens 1 and 2. The last column of the table provides a comparison between measured strengths and those predicted using current equations. In all cases the current coefficient of 7.5 for modulus of rupture is conservative. However, the coefficient of 6.7 for the split cylinder tests was unconservative in one case and was only slightly conservative for the remaining cases. Curing conditions greatly affected the beam specimens as demonstrated by the modulus of rupture for wet specimens exceeding those for air cured specimens by an average of about 70 percent. For the single comparison available, split cylinders showed much less sensitivity with a difference of only about 5 percent between air and wet cured tests.

Observed cracking loads during specimen flexure tests were quite high as shown in Tables 6.4 and 6.10. High cracking loads may be due to undetected cracking at lower load stages, cracking occurring early in a load increment, or errors in determining the effective prestress.

Table 7.4 Average Tensile Strength Data for Specimens

	Age	Cure	f_r	f'_c	$f_r/\sqrt{f'_c}$
	(days)		(ksi)	(ksi)	
Beams					
Specimen 1	28	Air	0.908	12.00	8.29
		Wet	1.650	12.42	14.81
	44	Air	1.019	13.02	8.93
		Wet	1.715	13.66	14.67
Specimen 2	7	Air	0.879	9.20	9.16
		Wet	1.598	8.90	16.94
	28	Air	0.965	10.75	9.31
		Wet	1.533	10.66	14.85
	55	Air	1.100	10.78	10.59
Split cylinders					
Specimen 1	114	Air	0.724	13.16	6.31
Specimen 2	29	Air	0.722	10.75	6.96
		Wet	0.756	10.66	7.32

Note: Above tensile data are averages of two tests.

Therefore, the estimate of cracking stress currently used in the Codes, $7.5\sqrt{f'_c}$ is conservative for use with high strength concrete cured under normal conditions encountered in the production of prestressed members.

7.3.4 Creep, Shrinkage, and Thermal Effects. A detailed study of the creep of high strength concrete was not conducted as part of the current study. However, data for the high strength concrete girders indicate that creep strains prior to the flexure test were roughly equal to the elastic strains. This means that the creep coefficient, Ccu, is approximately 2, which is slightly higher than values given in Table 3.1. Since deflection-time plots indicate that most of the creep had occurred by the time of the flexure tests, this estimate for the creep coefficient is a reasonable estimate for the total creep. On the basis of this limited data, it appears that use of a creep coefficient of 2 for high strength concrete is appropriate and probably conservative.

While no direct measurements of shrinkage were made, the formation of widespread shrinkage cracks in the Specimen 2 girder prior to release indicates that this property of high strength concrete should be explored further. It should be noted, however, that the scale-model specimens, because of their thin (2 in.) webs and a volume to surface ratio approximately one-third that of the

prototype girder, could be expected to experience shrinkage up to three times greater than a prototype girder [51]. The cracking did not appear to significantly affect member behavior, as indicated by the fact that prestress losses were not excessive.

No data on thermal properties of high strength concrete were obtained in this study. It is recommended that the same thermal properties used for normal strength concrete be used for high strength concrete [22].

7.3.5 Cover and Durability. Current limits on cover over reinforcement are appropriate for use with high strength concrete because of its improved impermeability and durability. In order to further improve the durability of high strength concrete, use of entrained air is suggested where the accompanying reduction of strength is tolerable.

7.3.6 Unit Weight. The unit weight of the high strength concrete used in this study was 150 pcf. This is similar to the findings of Carrasquillo et al. [36] which are recommended for use (see Sec. 3.3.6).

7.3.7 Placement of Concrete. Concerns have been expressed about the practicality of placement of high strength concrete in girder forms. This project demonstrated that high strength concrete could be placed without difficulty in girder forms with very tight clearances. This success was attributed to the use of

super-plasticizers which produced flowing concrete that did not segregate. Therefore, the use of high strength concrete in the construction of bridge girders appears feasible.

7.4 Flexural Design and Analysis

This section opens with a brief consideration of current allowable stresses for concrete. Two methods of ultimate analysis of composite bridge members are then considered: the simplified approaches of the AASHTO [10] and ACI [15] Codes, and the strain-compatibility method. Details of the application of each method for use with high strength concrete will be presented. The methods will then be compared with the measured behavior of the long-span girder specimens. Finally, various aspects of flexural design will be investigated using a range of bridge designs. Conclusions will be made at the end of the major subsections.

7.4.1 Allowable Concrete Stresses. Limiting concrete stresses to the levels given in the codes is intended to provide good serviceability in structures by limiting cracking and preventing deterioration of the concrete due to fatigue. It has been reported that current stress limits in tension are appropriate for use with concrete that is cured in field conditions [99] and, although data is very limited, fatigue behavior of high strength concrete is expected to be comparable to that for lower strength concretes [22].

Therefore, current allowable concrete stresses appear appropriate for use with high strength concrete and should be used for design.

7.4.2 Simplified Ultimate Analysis Methods. This sub-section begins by considering the application of the current equivalent rectangular stress block (ERSB), as found in the ACI Code and AASHTO Specifications, to high strength concrete. Design of composite members with a normal-strength deck and high-strength girders, where the neutral axis is located below the deck, will then be considered. Finally, AASHTO and ACI equations used to estimate strand stress at ultimate will be evaluated.

7.4.2.1 Stress Block Parameters. From the data presented in Chapter 3 and later in this chapter, the concrete stress block parameters in current use for high strength concrete appear sufficiently accurate and conservative for the prediction of the flexural strength of a section. These parameters include the stress block factor, β_1, the effective compression stress at ultimate, and the maximum usable strain in compression, ϵ_{cu}. The use of these parameters for computations other than the ultimate capacity may be less accurate, however. This is due to the fact that the ultimate strain may be less than the Code specified value of 0.003, as discussed earlier in this chapter. Ductility considerations are especially sensitive to inaccuracies in these parameters and will be discussed in a later section of this chapter.

7.4.2.2 Composite Design. Composite design using the simplified methods is straightforward when the compression zone at ultimate remains in the deck. However, if high strength concrete in the girder is also in compression at ultimate, the application of the analysis becomes unclear because of the different concrete strengths and stress block parameters. A similar situation would exist with light-weight concrete girders because of the different stress block parameters for light-weight and normal-weight concrete.

The analysis of flanged sections in which the neutral axis at ultimate is located below the deck, which will be referred to as "flanged section analysis", deducts the area of steel required to develop the overhanging flange from the total area of tension steel in order to obtain an area of steel for use in strength calculations. This type of analysis is not necessary for flexural strength calculations using the ACI ERSB but is included in the AASHTO equations.

Four possible approaches to representing composite cross-sections for ultimate analysis are illustrated in Fig. 7.6. Case I assumes that all concrete in the composite member has the strength of the deck. In Case II, the assumptions of the ERSB are applied to both the deck and girder concrete which requires the top of the girder as well as the deck to be at the maximum usable strain. While this condition is very unlikely, it could exist for composite

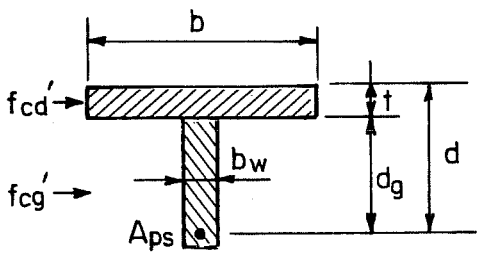

ACTUAL SECTION

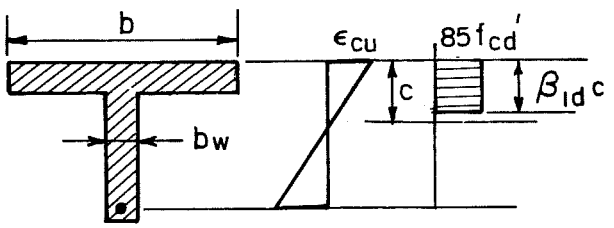

CASE I

- Same dimensions
- Assume uniform $f'_c = f'_{cd}$

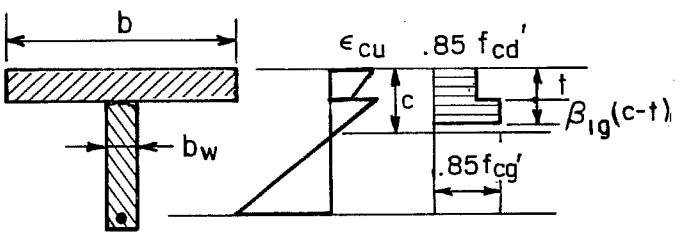

CASE II

- Consider deck and girder individually
- Assume top of girder strain is 0.003

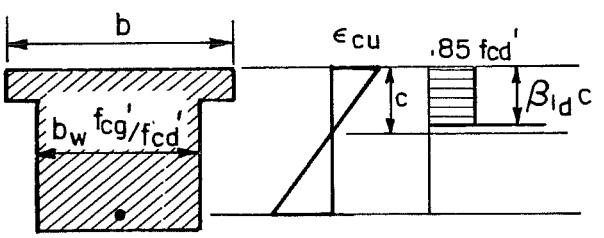

CASE III

- Transform girder to deck concrete

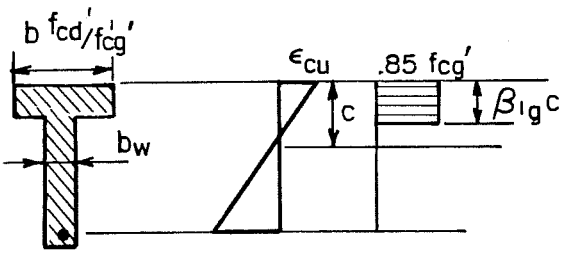

CASE IV

- Transform deck to girder concrete

Fig. 7.6 Possible approaches to ultimate analysis of composite sections

sections in which a large difference in strain exists between the top of girder and bottom of deck, which generally occurs only in pretensioned girders. Therefore, this case is reasonable only for composite sections with pretensioned girders. Cases III and IV transform the section by ratios of concrete strengths to obtain an equivalent section with a uniform concrete strength. Case III transforms the section to an equivalent section with concrete strength equal to the deck concrete strength while Case IV transforms the section to the girder concrete strength. All four approaches neglect actual differences in strain and curvature between the girder and deck.

The approaches represented by Cases I, III, and IV can be used with the flexural strength equations given in the AASHTO Specifications while all cases can be used with the ACI ERSB approach. However, the current code flanged section analysis will give different results for Case II. The flanged section analysis approach is used in both codes to compute the reinforcement index to be compared with the maximum reinforcement limit. The major difference between AASHTO and ACI estimates of the flexural strength for a given case results from different estimates of the strand stress at ultimate. Therefore, only Case I will be shown for AASHTO in the following studies, since the ACI strand stress equation is considered to be superior, as discussed in the following section.

Strand stress at ultimate is not affected by the different cases when computed using either the AASHTO or ACI equations. Therefore, for a given section and steel content, the total compression force is the same for all cases. Expressions for the depth of the equivalent stress block and the depth to the neutral axis are derived in Table 7.5 for each case. These can be reduced to a common form by recognizing a common term, designated a_g^*, which represents the depth of the compression block in the girder. This depth of the compression block in the girder is the same for Cases II, III, and IV and is related to the depth for Case I by the ratio of concrete strengths.

The variation in the total depth to the neutral axis, c, versus the term a_g^* for a composite section with the same deck thickness as used for the specimens is shown in Fig. 7.7. Also shown are data points for the specimens, which were determined using strand stresses corresponding to measured strand strains and the location of the neutral axis computed from girder strains. This demonstrates that the neutral axis depth computed using Cases II, III, and IV are similar while those computed using Case I are similar for small depths of compression but diverge from the other cases with increasing depth of compression and increasing difference between deck and girder concrete strengths. Data for the two specimens fall among the lines representing Cases II, III, and IV with the points being closest to

Table 7.5 Derivations of Stress Block Dimensions for Composite Design

CASE I: Nominal dimensions; deck concrete strength

$$C = A_{ps}f_{ps} = 0.85f'_{cd}[(b-b_w)t + b_w a]$$

$$a = na^*_g + t = [(A_{ps}f_{ps} - bt0.85f'_{cd})/(b_w 0.85f'_{cd})] + t$$

$$c = a/\beta_{1d} = (na^*_g + t)/\beta_{1d}$$

CASE II: Nominal dimensions; deck and girder concrete strengths

$$C = A_{ps}f_{ps} = bt0.85f'_{cd} + b_w a0.85f'_{cg}$$

$$a = a^*_g + t = [(A_{ps}f_{ps} - bt0.85f'_{cd})/(b_w 0.85f'_{cg})] + t$$

$$c = t + (a-t)/\beta_{1g} = a^*_g/\beta_{1g} + t$$

CASE III: Transformed dimensions; deck concrete strength

$$C = A_{ps}f_{ps} = 0.85f_{cd}[(b-nb_w)t + nb_w a]$$

$$a = a^*_g + t = [(A_{ps}f_{ps} - bt0.85f'_{cd})/(b_w 0.85f'_{cg})] + t$$

$$c = a/\beta_{1d} = (a^*_g + t)/\beta_{1d}$$

CASE IV: Transformed dimensions; girder concrete strength

$$C = A_{ps}f_{ps} = 0.85f'_{cd}[(b/n-b_w)t + b_w a]$$

$$a = a^*_g + t = [(A_{ps}f_{ps} - bt0.85f_{cd})/(b_w 0.85f'_{cg})] + t$$

$$c = a/\beta_{1g} = (a^*_g + t)/\beta_{1g}$$

Common terms: $a^*_g = [(A_{ps}f_{ps}-bt0.85f'_{cd})/(b_w 0.85f'_{cg})]$

$n = f'_{cg}/f'_{cd}$

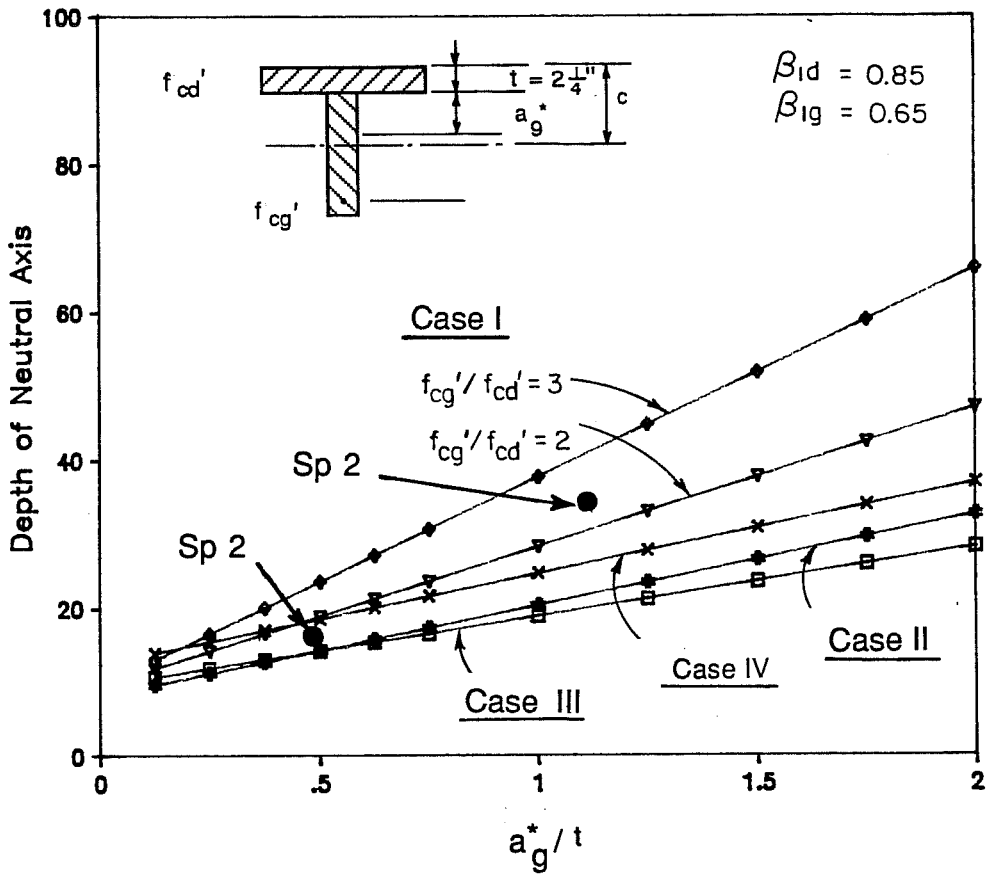

Fig. 7.7 Depth of neutral axis versus depth of compression block for specimens and composite analysis

the line for Case II. This shows that these three cases give reasonable estimates for the location of the neutral axis while Case I overestimates the depth to the neutral axis for the specimen data, especially where the difference between girder and deck concrete strengths is large (Specimen 1). It can also be shown that the ultimate moment computed using the four cases will be identical if the deck is considered separately for Case II rather than using the flanged section analysis found in the current codes. However, as discussed in the section concerning ductility which follows, the cases provide significantly different measures of ductility.

When some combinations of dimensions and concrete strengths are used with Cases III and IV, the deck width of the transformed section will be less than the width of the top of girder. While use of the current flanged section analysis in this situation results in a negative area of steel required to develop the flange, results are consistent and the situation should not be alarming.

7.4.2.3 Strand Stress at Ultimate. The current equation for estimating stress in bonded prestressing strands at ultimate is based on the observation that stress at ultimate is roughly related to the depth of the neutral axis which is proportional to a term similar to the reinforcement index. No derivation for the form of the equation was found in the literature. The equation was apparently calibrated using test data and was intended for use with rectangular sections.

However, as demonstrated by Mattock [84], the original equation and the modified form which now appears in the ACI Code work remarkably well. Mattock also investigated the use of the modified equation for a single series of monolithic T-beams and found that, while the equation becomes unconservative when the neutral axis is located below the bottom of the flange, the maximum reinforcement limit terminates use of the equation before the stress becomes excessively unconservative. However, for the full range of T-beam designs considered, the nominal moment strength computed using the modified equation agreed very well with results of a compatibility analysis. Therefore, he concludes that

> it would be reasonable to use the proposed modified Eq. (18-3) to calculate the stress at nominal moment strength in the prestressed reinforcement of T-beams of normally encountered proportions, providing that the limit of $0.36\beta_1$ on the reinforcement index is observed.

The use of this equation for composite members will be examined further when results of strain compatibility analyses are considered later in this section.

Since the equation includes the concrete strength and, in its modified form, the stress block parameter β_1, its application to a composite section where the compression zone extends below the bottom of the flange is unclear where the concrete strength of the girder and deck differ significantly. Since it appears to be the most reasonable approach, the concrete strength of the deck and its

corresponding β_1 value will be used in the equation. This interpretation will be used in the analyses that follow.

7.4.2.4 Summary. The preceding discussion of the use of the simplified methods given in AASHTO and ACI for computing the flexural strength of composite sections can be summarized as follows.

1. Based on available data, the stress block parameters currently used for high strength concrete in the ACI ERSB flexural strength calculations are appropriate.
2. Four possible approaches for determining flexural strength of composite members using the simplified AASHTO and ACI methods are presented. In predicting the depth of the compression zone, the four methods were similar, although the approaches using transformed dimensions (Cases III and IV) and the ERSB for both girder and deck (Case II) provided best estimates for data collected during the two scale-model girder flexure tests.
3. The major difference in estimates of flexural strength using the AASHTO equation and the ACI ERSB is due to different estimates of strand stress at ultimate.
4. Deck concrete strength and effective width should be used for the computation of strand stress at ultimate using either the AASHTO or ACI equations.

5. The computed negative area of steel that results from a flanged section analysis using transformed sections is not in error and provides correct overall results.

7.4.3 Strain Compatibility Method. Analytical representations of concrete and steel stress-strain curves are compared with measured properties from specimen tests. General stress-strain curves are presented for use in the strain compatibility analysis. Details of the analysis are then presented.

7.4.3.1 Concrete Stress-Strain Relationships. In order to develop a successful strain compatibility model for member behavior, stress-strain behavior of the concrete must be accurately modelled. Figures 7.8 and 7.9 show stress-strain curves from cylinder tests of deck concrete at the time of the flexure test and compare these curves with those predicted by Burns [34] and Carriera and Chu [37] using measured and estimated values for the modulus, and strain at maximum stress. These two analytical stress-strain curves were selected for comparison because they are continuous equations that provide reasonable agreement with the data. Both predictive equations do well when the measured modulus and strain are used (Fig. 7.8a and 7.9a). Agreement is not as good when estimated values are used for the modulus and strain at maximum stress. Burns' equation becomes poor for higher strains but it was not intended to be used in this range. The same type of plots are presented in Fig. 7.10 and 7.11 for the

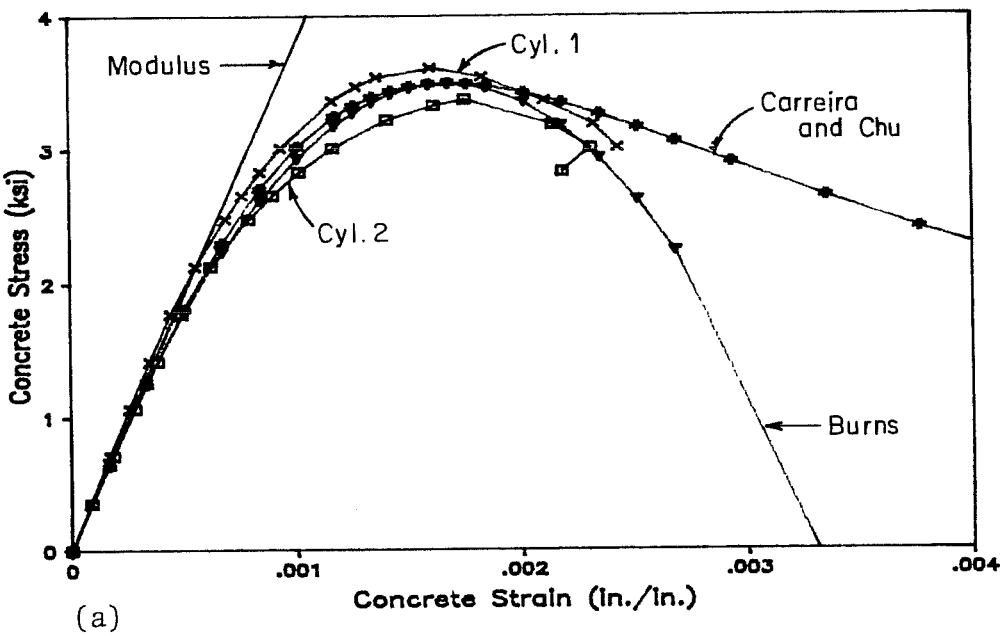

(a)

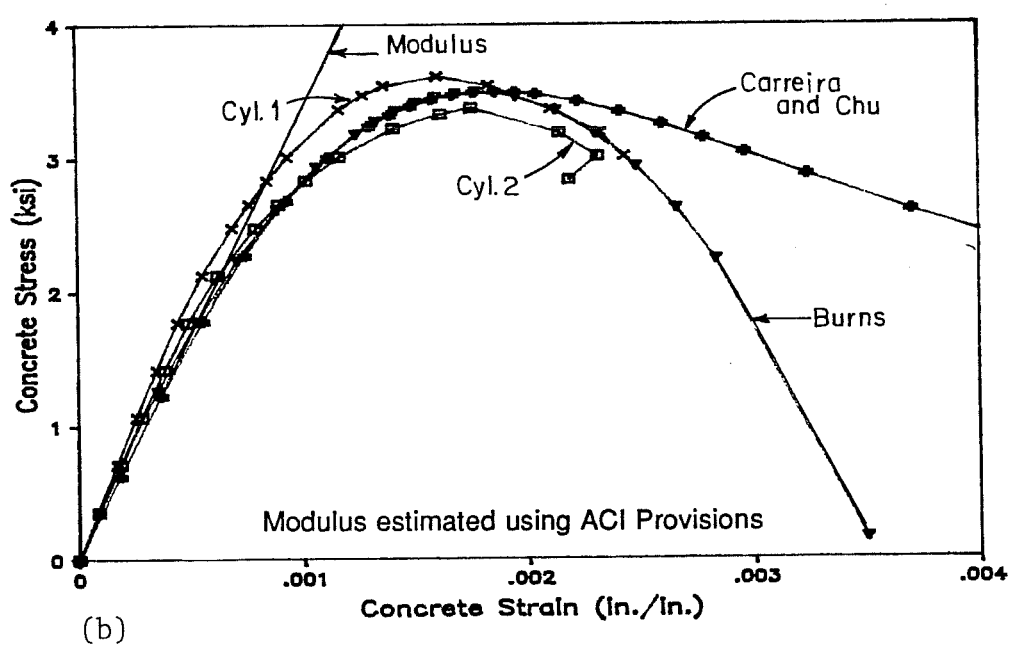

(b)

Fig. 7.8 Measured and analytical stress-strain curves for deck concrete - Specimen 1: a) Using measured E_c and ϵ_0; b) Using estimated E_c and ϵ_0

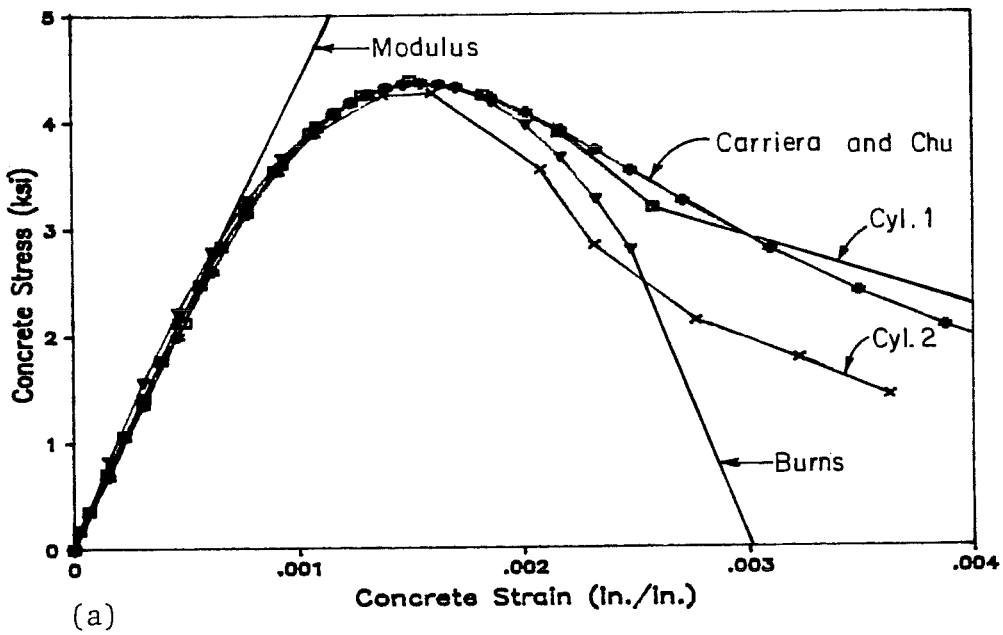

(a)

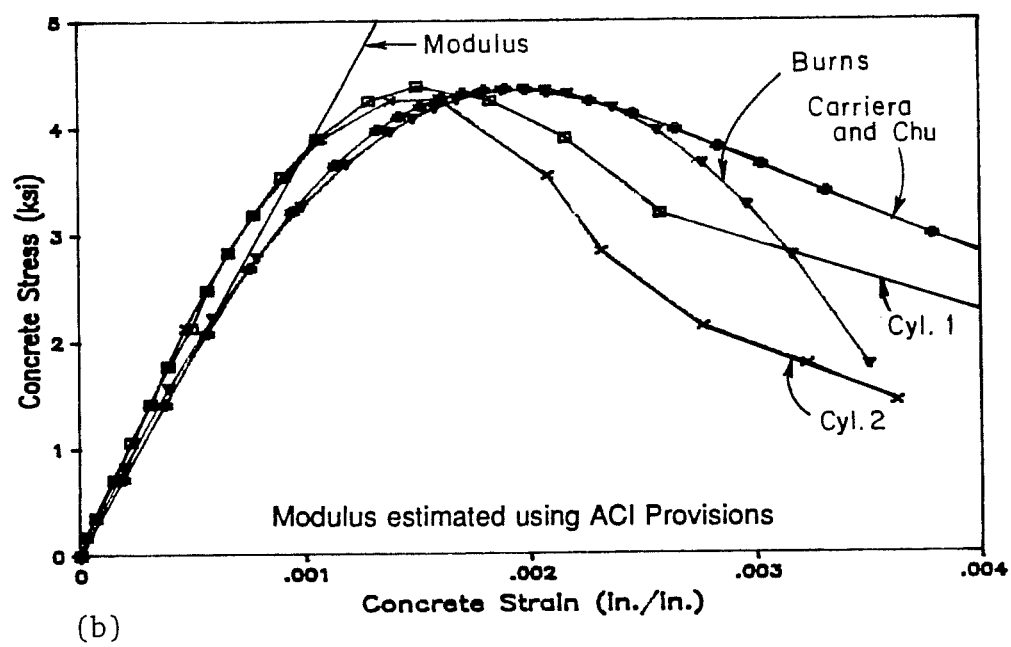

(b)

Fig. 7.9 Measured and analytical stress-strain curves for deck concrete - Specimen 2: a) Using measured E_c and ϵ_c; b) Using estimated E_c and ϵ_c

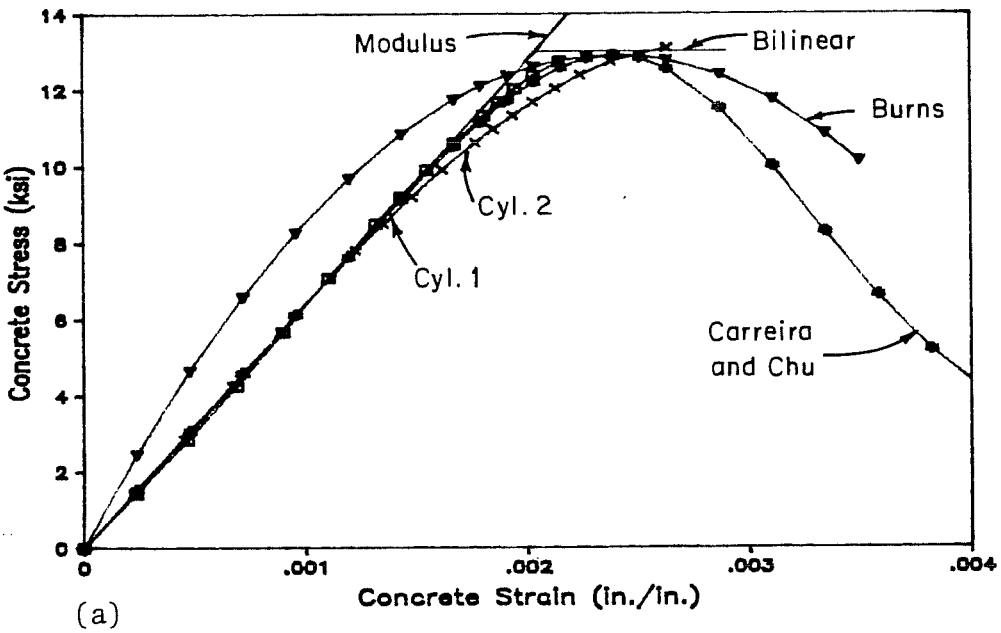

(a)

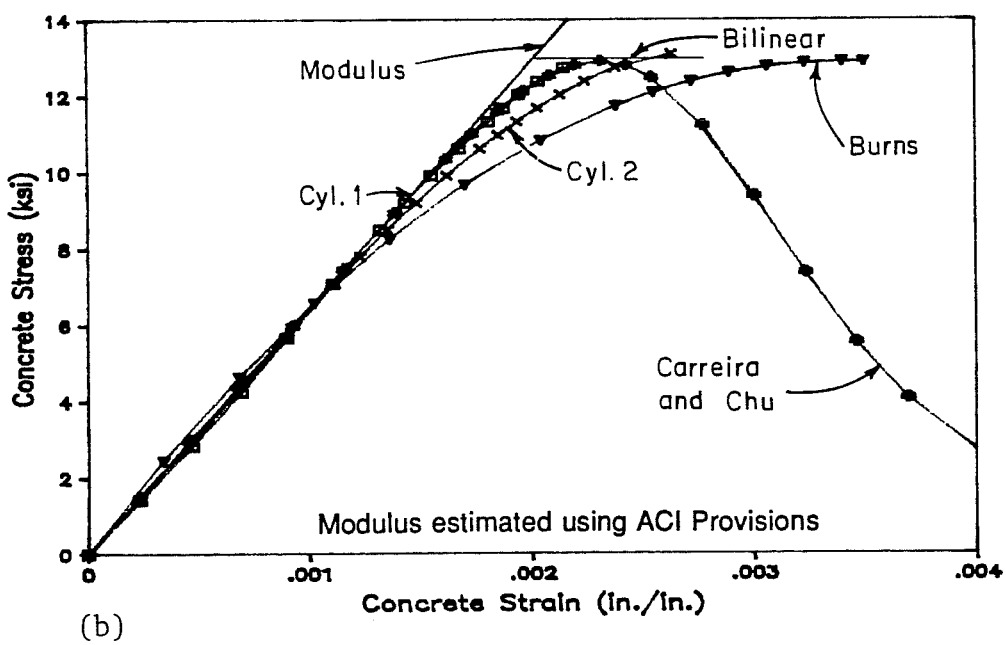

(b)

Fig. 7.10 Measured and analytical stress-strain curves for girder concrete - Specimen 1: a) Using measured E_c and ϵ_c; b) Using estimated E_c and ϵ_c

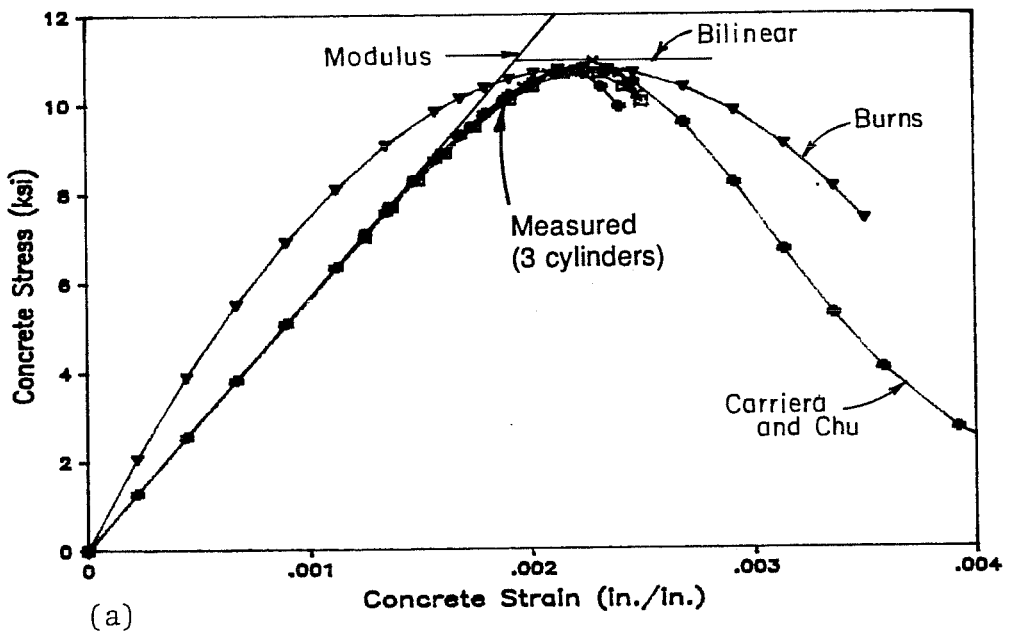

(a)

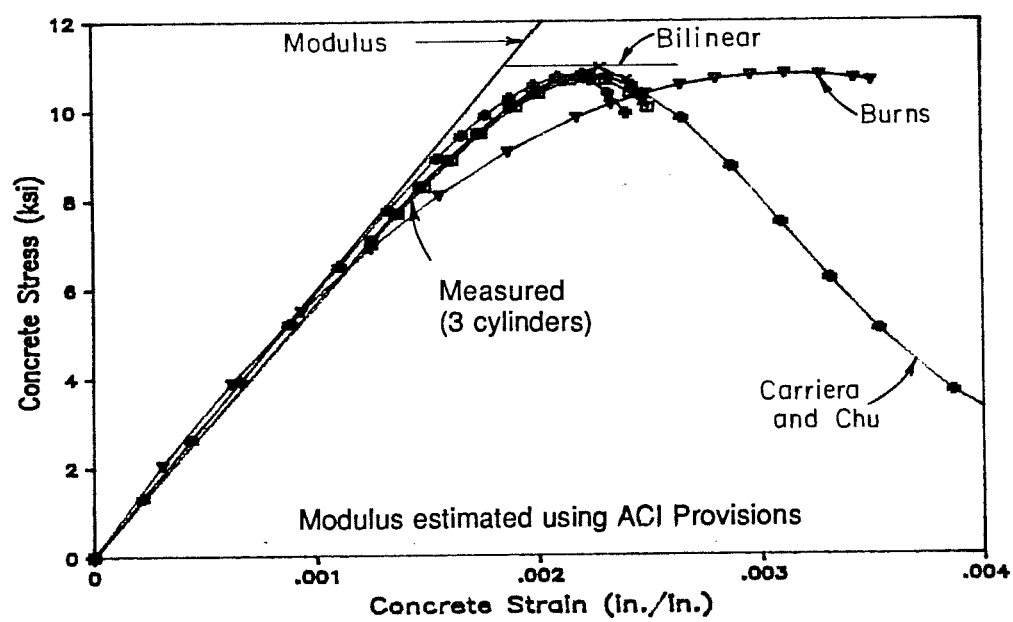

(b)

Fig. 7.11 Measured and analytical stress-strain curves for girder concrete - Specimen 2: a) Using measured E_c and ϵ_c; b) Using estimated E_c and ϵ_c

high strength girder concrete. The equation by Carriera and Chu provides very good agreement for both the ascending and descending branches of the curve when both measured and estimated values are used for the modulus and strain at maximum stress. The equation by Carriera and Chu may be used for both normal and high strength concrete when strains beyond ϵ_0 will be considered in analysis. However, the equation should be used with caution because, if the term $f'_c/(E_c\epsilon_0)$ in the definition of the parameter β closely approaches or exceeds 1, the equation produces unsatisfactory results.

For a simplified analysis where strains are not expected to greatly exceed the strain at maximum stress, a bilinear approximation to the curve as shown will give satisfactory results for high strength concrete. This bilinear relationship is the same as the Jensen stress block without the β factor which is used to determine the ultimate strain.

For the strain compatibility analyses that follow, a modified form of Burns' equation is used for the deck concrete because the analysis is simplified by a closed-form solution for the integral of the area and the location of the centroid of the area. The stress-strain curve is modified by using a linear descending branch that begins at maximum stress and closely matches the measured

descending branch of the curve. A bilinear stress block will be used to approximate the high strength girder concrete stress-strain curve for the specimens. The measured and analytical stress-strain curves for the concrete in the specimens at the time of the flexure tests are shown in Fig. 7.12 and the parameters defining the curves are given in Table 7.6.

For the general analyses discussed later in this chapter, a deck strength of 4 ksi will be used. The same type of modified stress-strain curve will be used for the deck as discussed above with the strain at maximum stress approximately equal to that measured for the specimen concrete, and a descending branch slope equal to the average for the two specimens. For the girder, three concrete strengths will be used and the stress-strain curves will be modelled using the bilinear relationship discussed above. The bilinear approximation will not be as accurate for the lower concrete strengths but will still give a reasonable estimate of section capacity and rotations. Stress-strain curves for the general analyses are shown in Fig. 7.13 with the corresponding parameters given in Table 7.6.

7.4.3.2 Strand Stress-Strain Relationships. Strand stress-strain curves will be defined using the Menegotto and Pinto equation [95] (see Fig. 3.17). Coefficients were developed by trial and error to match the strand used in the specimens and to model

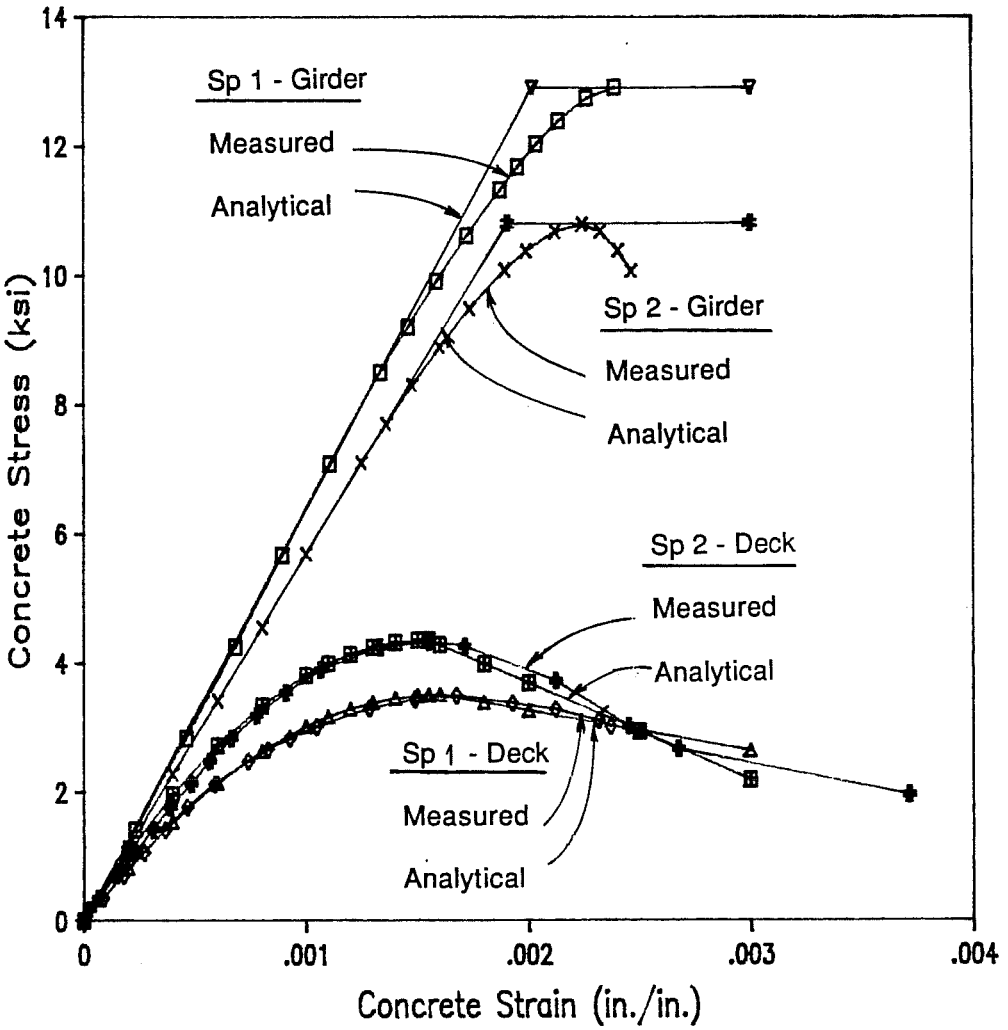

Fig. 7.12 Comparison of average measured and analytical concrete stress-strain curves for Specimens 1 and 2

Table 7.6 Parameters for Analytical Stress-Strain Curves for Concrete

	f_c'	E_c	ϵ_0	Slope
	(ksi)	(ksi)	(in./in.)	(ksi)
Specimen 1				
Girder	12.90	6,400		
Deck	3.50	3,800	0.001600	-625
Specimen 2				
Girder	10.80	5,675		
Deck	4.35	4,370	0.001550	-1,500
General Analyses				
Girder	12.00	6,244		
Girder	9.00	5,407		
Girder	6.00	4,415		
Deck	4.00	3,605	0.001600	-1,060

$E_c = 57{,}000\sqrt{f'_c}$ (psi)

Table 7.7 Parameters for Analytical Stress-Strain Curves for Strand

		Specimens	General Analyses	
		LL Strand	LL Strand	SR Strand
E_c	(ksi)	28,400	28,000	28,000
f_{py}	(ksi)	267.10	243.00	229.50
ϵ_y	(in./in.)	0.0100	0.0100	0.0100
f_{pu}	(ksi)	284.00	270.00	270.00
ϵ_{pu}	(in./in.)	0.0547	0.0350	0.0350
N		16.000	6.440	4.510
K		1.0573	1.0800	1.1150
Q		0.001255	0.010536	0.019483

LL = Low relaxation (Low Lax)
SR = Stress-relieved

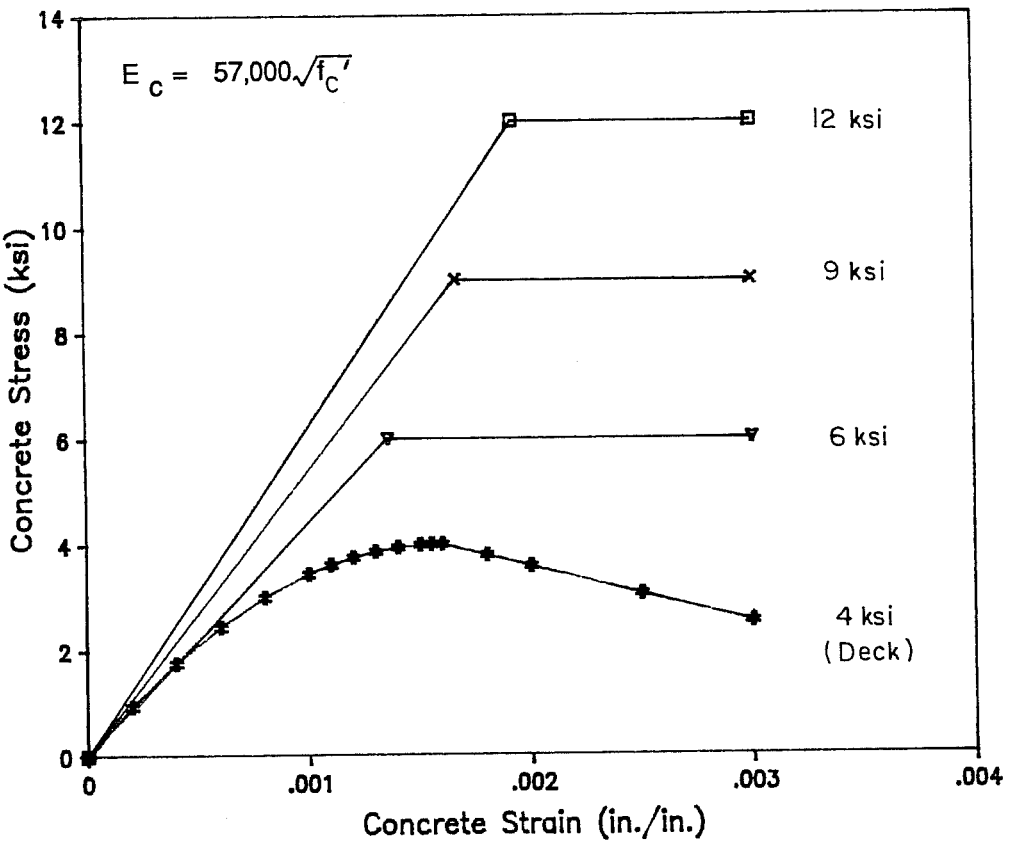

Fig. 7.13 Analytical concrete stress-strain curves for general analyses

strand behavior for stress-relieved and low relaxation strands that satisfy minimum requirements. Figure 7.14 shows the excellent agreement between measured and analytical stress-strain behavior for the strand used in the specimens, and Fig. 7.15 shows stress-strain curves satisfying minimum requirements. The coefficients used to produce the curves are given in Table 7.7.

7.4.3.3 Details of Analysis. A computer program (MOMCURV) was developed to analyze the uncracked, cracked and ultimate behavior of a composite section. The concrete and strand stresses at full dead load conditions serve as the starting point of the analysis. These initial conditions are used to determine differences in strain and curvature between the girder and deck which remain constant throughout the loading of the section. Uncracked behavior is computed using elastic properties and includes the effect of the increase in strand stress that occurs with added load. For cracked section analysis, an iterative technique employing the stress-strain relationships described above is used to establish equilibrium for different levels of strain in the top fiber of the deck. For each value of top fiber strain, the corresponding moment, concrete and strand stresses and strains, curvatures, and location of the neutral axis are determined. The ultimate capacity of the section is defined either by the maximum moment resisted by the section or by the moment reached at a limiting strain in the top of the deck.

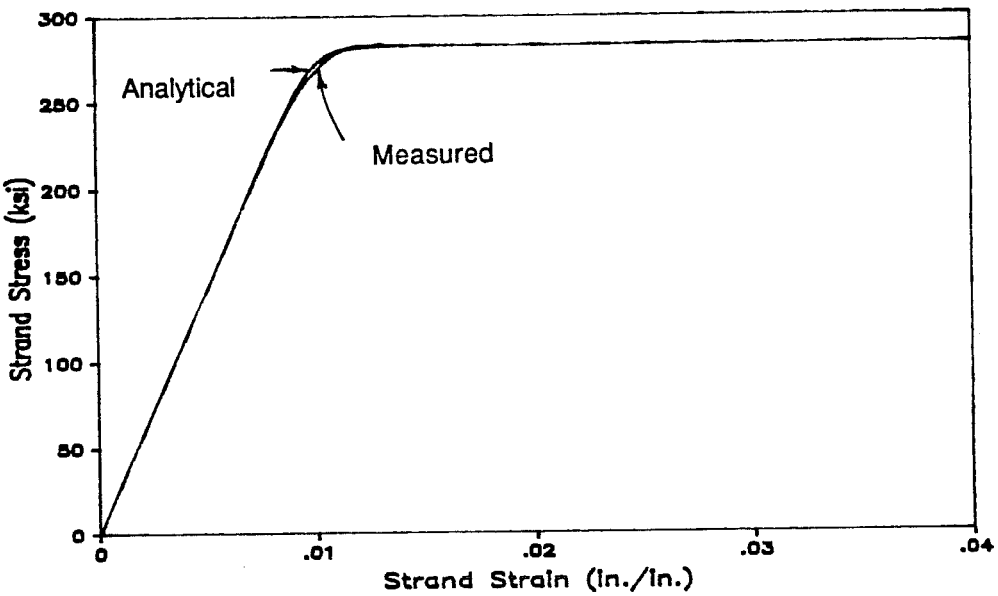

Fig. 7.14 Measured and analytical strand stress-strain curves for Specimens 1 and 2

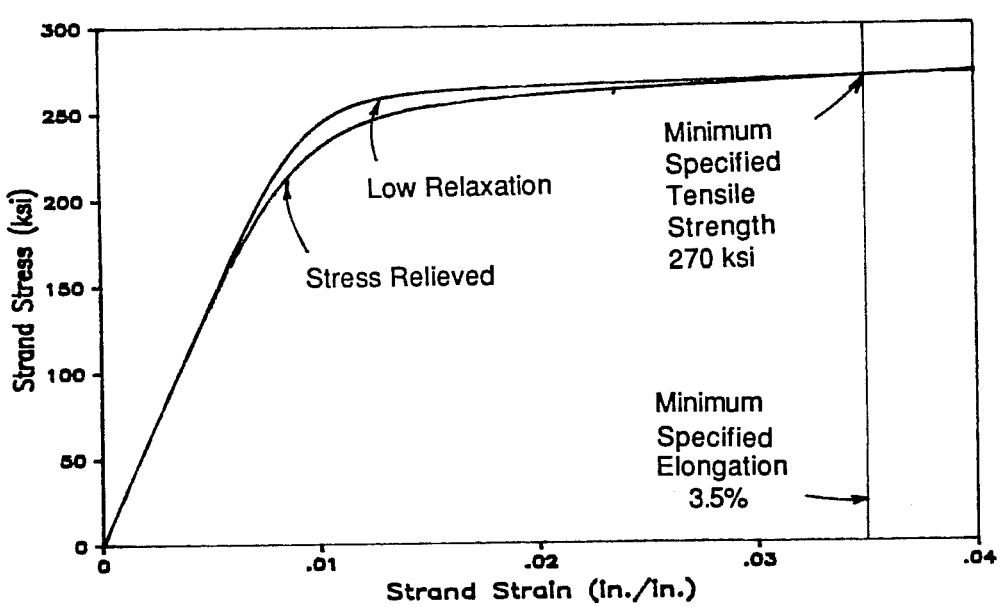

Fig. 7.15 Analytical strand stress-strain curves for general analyses

A more complete discussion of the program MOMCURV, with sample input and output, is given in Appendix C.

Load-deflection behavior was obtained using a semi-manual process. The moment-curvature relationship was obtained at 2-ft intervals along half of the specimen using the strain-compatibility program. The effective prestress was assumed to vary linearly from the drape points to the ends with a constant prestress between drape points. A computer spreadsheet program was then used to compute the moments at selected load stages at the intervals along the span, to interpolate between values input from the moment-curvature relationship, and to determine the deflection at midspan using moment-area principles. For Specimen 1, concrete stresses were allowed to reach $7.5\sqrt{f'_c}$ before cracked section analysis results were used at a given location. Since Specimen 2 had well distributed cracks due to shrinkage, cracked section analysis results were used at a given location when tension developed in the bottom fiber. After the maximum moment was reached at midspan, the entire constant moment region was assumed to be following the descending portion of the moment-curvature curve. This led to slightly larger curvatures at the load point than at midspan for loads beyond maximum, which would result in a very small increase in midspan deflections. A slightly better estimate might have been to

use the curvature computed at midspan for the entire region between load points after maximum moment was reached.

7.4.3.4 Summary. The following is a summary of the preceding discussion regarding aspects of the strain compatibility analysis:

1. The equation by Carriera and Chu appears to be the best mathematical representation of the concrete stress-strain curve for all concrete strengths.
2. The stress-strain curve for high strength concrete can be adequately modelled by a bilinear curve using the modulus and cylinder strength.
3. A modified form of the stress-strain curve used by Burns provides a good approximation of the stress-strain curve for normal strength concrete.
4. Mathematical estimates of stress-strain curves are improved if measured rather than estimated values for the modulus and strain at maximum stress are used.
5. The strand stress-strain curve developed by Menegotto and Pinto provided excellent agreement with the measured strand stress-strain curve. Using a trial and error process, coefficients for the equation were determined for the strand used in the specimens and for strand

meeting the minimum requirements of the ASTM specification.

6. The strain compatibility analysis used in this study is presented. A computer program MOMCURV was developed to perform this analysis.

7. Load-deflection behavior can be determined using MOMCURV results and a semi-manual integration process.

7.4.4 Prediction of Test Results. This section first compares measured specimen behavior as load was applied to that predicted by the strain compatibility analysis. The measured or computed conditions at ultimate are then compared with those predicted by the strain compatibility analysis and the simplified methods of the ACI Code [15] and the AASHTO Specifications [10]. Conclusions regarding the accuracy of the predictive methods as compared with this set of test data close the section.

7.4.4.1 Behavior with Increasing Load. Load-deflection curves for both specimens are shown in Fig. 7.16. The predicted curves are close to the measured curves although the analytical curve for Specimen 1 lies below the measured curve. The difference between curves could indicate that the effective prestress at midspan or along the span was actually higher than assumed in the analysis. By a trial and error process, effective stresses of 185 ksi at midspan and 160 ksi at the ends were found to produce very close agreement between

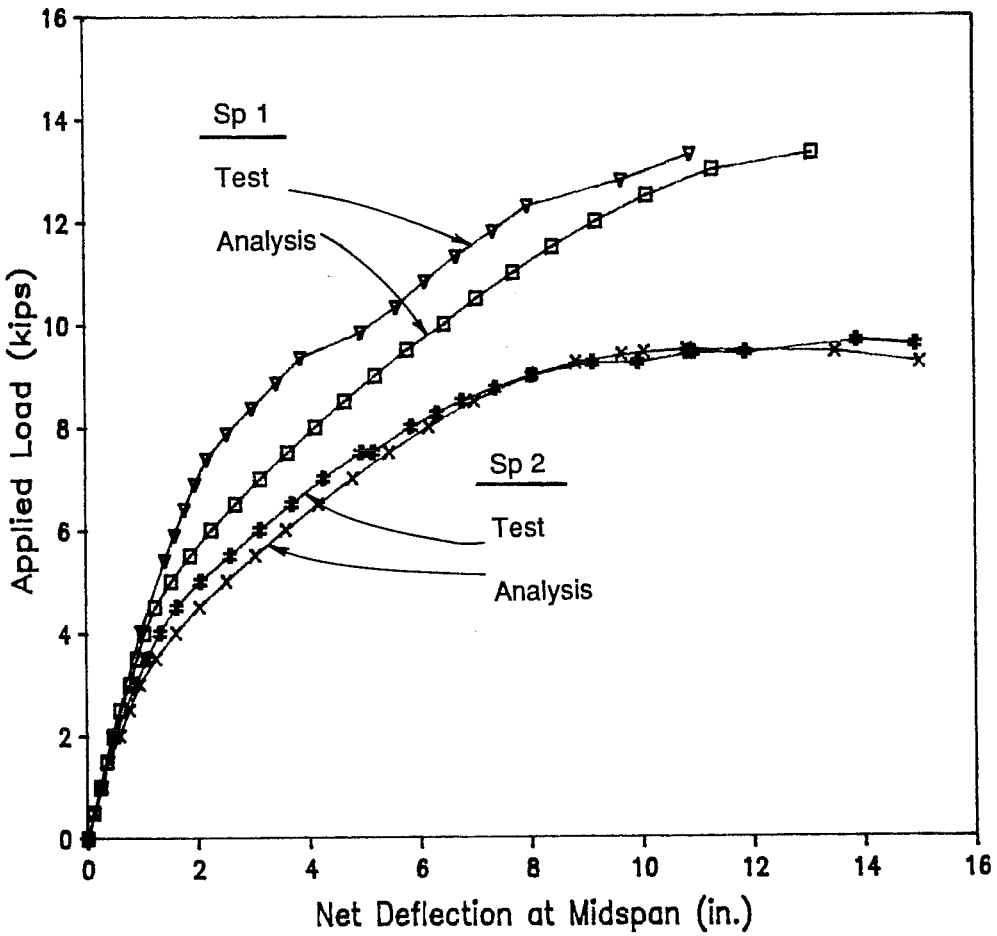

Fig. 7.16 Measured and predicted load-deflection curves during flexure tests.

measured and computed member behavior. Load-deflection curves for the original analysis and the second analysis using increased effective stresses are compared with the measured curve in Fig. 7.17. Agreement for other aspects of behavior was good as well. However, this level of prestress is roughly equivalent to the initial tension placed on the strands in the prestressing bed which would leave no allowance for losses. Therefore, such a high stress appears unreasonable. An increase in the cracking stress, which was measured to be approximately $9\sqrt{f'_c}$ would also tend to extend the linear portion of the load-deflection behavior of the specimen in the analysis. It is possible that other factors could be modified to produce better results as well.

The shape of the calculated load-deflection curves are very similar to those measured in the tests, differing by an offset after cracking that remained fairly constant for the remainder of the test. Aspects of behavior such as stiffness before and after cracking and the extent of the yield plateau prior to failure are quite similar for the predicted and observed response. As considered below in greater detail, the ultimate capacity of the member is also accurately determined. Discontinuities in the test data were a result of reloading the member after maintaining the deflection for long periods during the test, and should not be considered as part of the short-term deflection curve. The short-term deflection of other

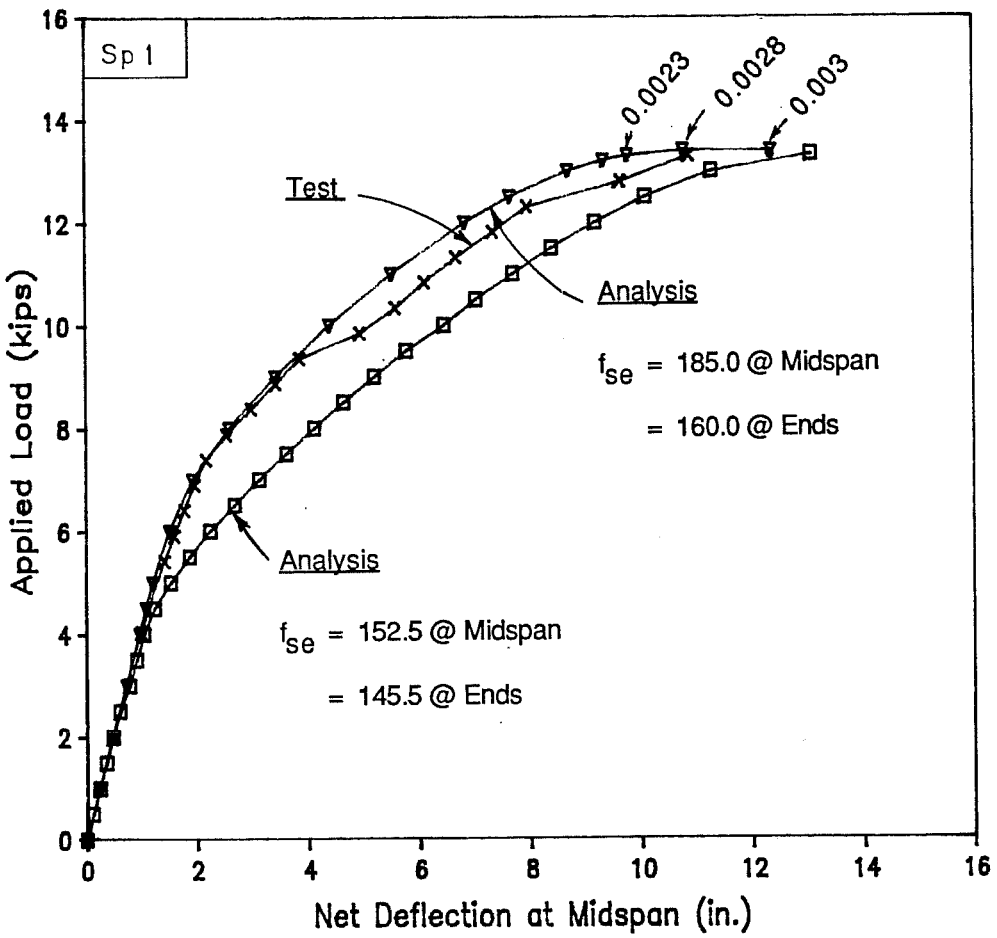

Fig. 7.17 Comparison of measured and predicted load-deflection curves during flexure test for Specimen 1 using revised effective prestress

members should therefore be reasonably estimated using the method, described above with cracking at $7.5\sqrt{f_c'}$ assumed.

Figures 7.18 and 7.19 show the increase in strand strain and stress, respectively, with load during the flexure tests. Agreement is good, although again, it appears that the prestress or cracking stress may be underestimated for both specimens since the analytical curves depart from their initial tangent earlier than the test data. The similarity between member behavior, as indicated in the load-deflection response, and section behavior, as reflected in this and other load-strain relationships, indicate that assumptions regarding member and section properties and behavior appear consistent. Use of analytical curves, which assume cracking to occur at a stress of $7.5\sqrt{f'_c}$, to determine strand stresses during the tests appears reasonable.

The variation in top-of-girder and top-of-deck strains with increasing load are shown in Fig. 7.20 and 7.21, respectively. The predicted curves in Fig. 7.20 are terminated at a strain of 0.003 at the top of the deck. Curves are again similar to experimental curves which are slightly stiffer than predicted curves. It is interesting that the measured and predicted girder strains for Specimen 2 were similar up to nearly the maximum load where the analytical curve began to "yield" while strains measured in the test failed to increase.

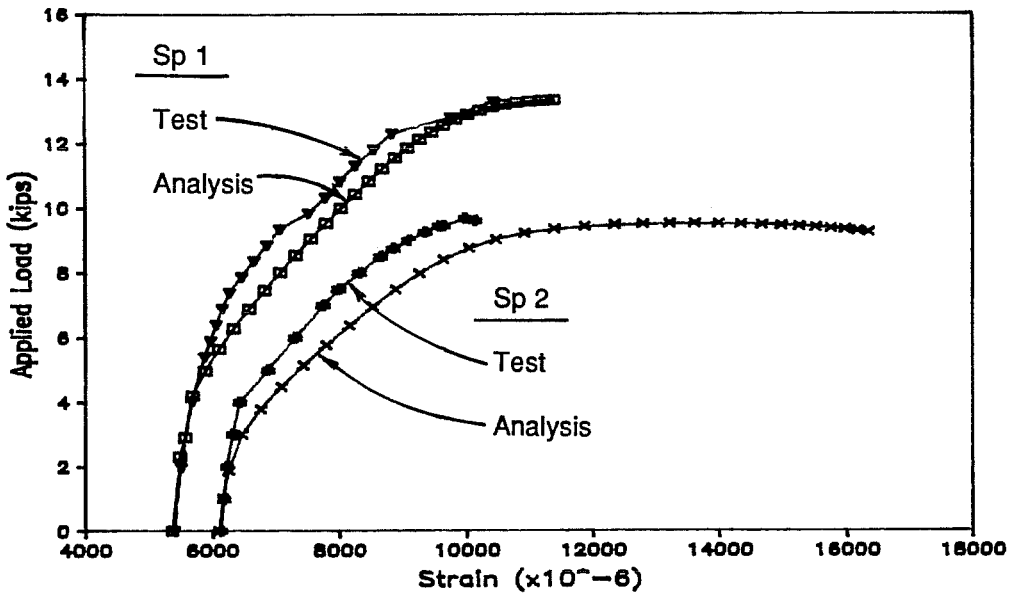

Fig. 7.18 Comparison of measured and predicted strand strains during flexure tests

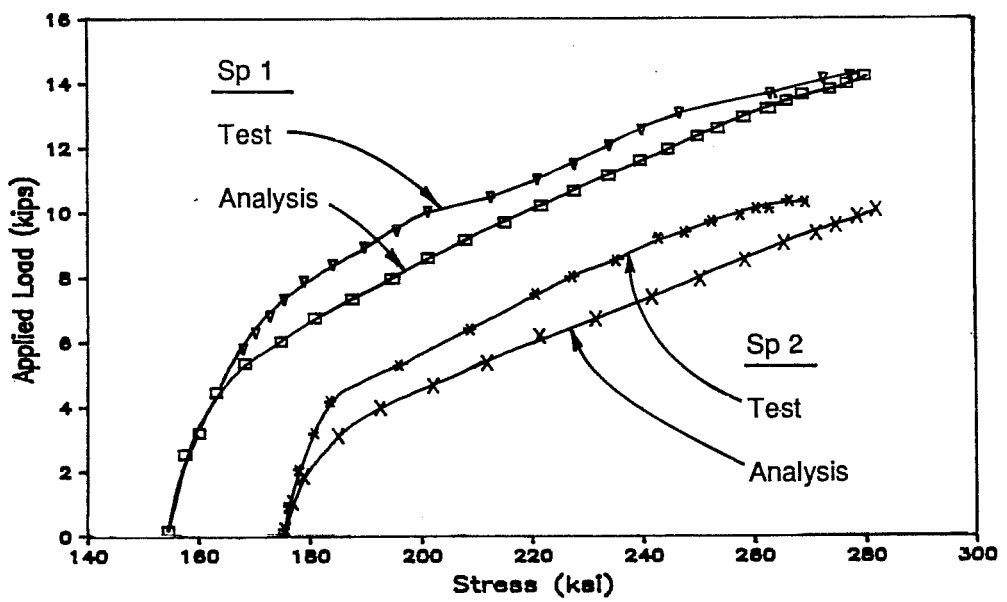

Fig. 7.19 Comparison of measured and predicted strand stress during flexure tests

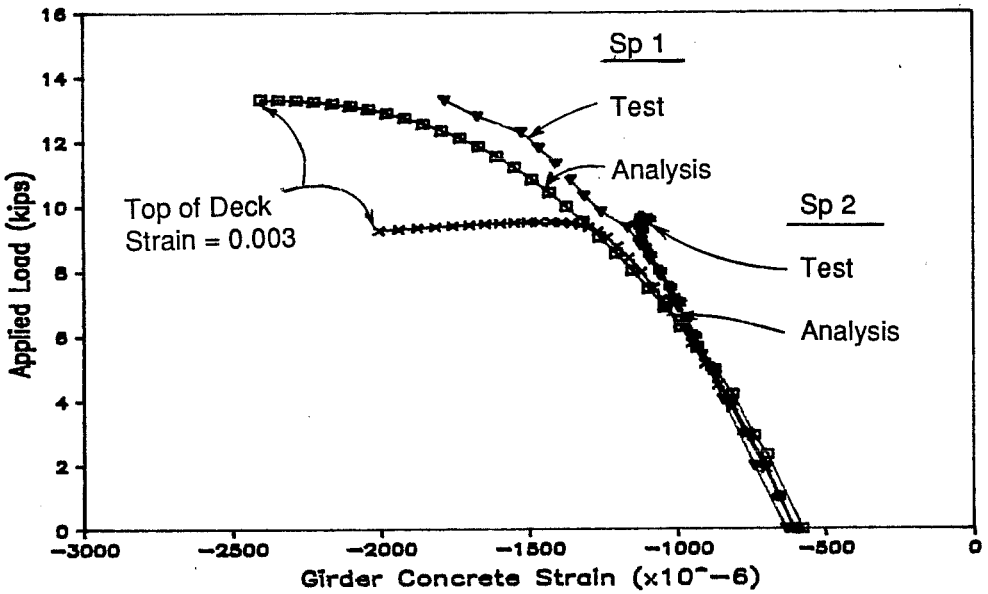

Fig. 7.20 Comparison of measured and predicted top-of-girder concrete strains during flexure tests

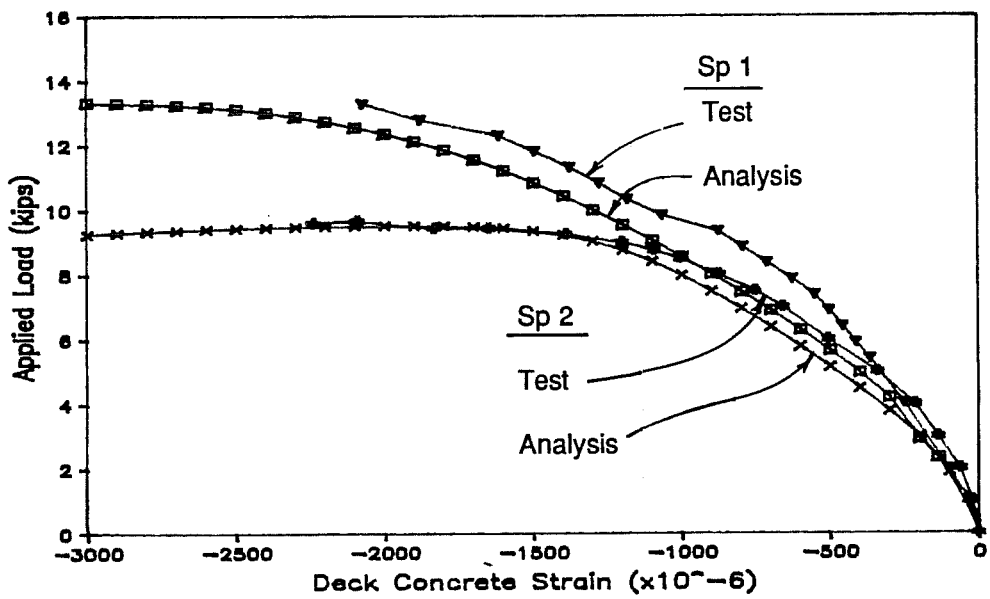

Fig. 7.21 Comparison of measured and predicted top-of-deck concrete strains during flexure tests

The crack height computed using selected strain gage data compares favorably with that from the analysis, especially at loads near failure, as shown in Fig. 7.22. Curvatures computed using the same strain gage data are compared with those from analysis in Fig. 7.23. Slopes of the curvature curves are similar to the test data, although cracking appears early as in other curves. The curves differ significantly at failure with the analytical curves exhibiting a longer yield plateau than the test data. This indicates that failure occurred prior to reaching a top fiber strain of 0.003 in the deck, which determines the final point of the predicted curvature plots.

A final set of curves comparing analytical and test data appear in Fig. 7.24 and 7.25, where the top-of-girder strain and the strand strains, respectively, are plotted versus the top-of-deck strain, which was the independent variable in the analysis. Agreement here is quite good for both quantities for Specimen 1 while divergence is significant for Specimen 2. This indicates that both the strands and the top of girder failed to gain strain as expected as failure approached. For the strands, this could be due to debonding between cracks, but the cause for low strains in the girder is not known. The curves clearly indicate that concrete strains at failure were well below 0.003 and the excellent agreement between the analytical and

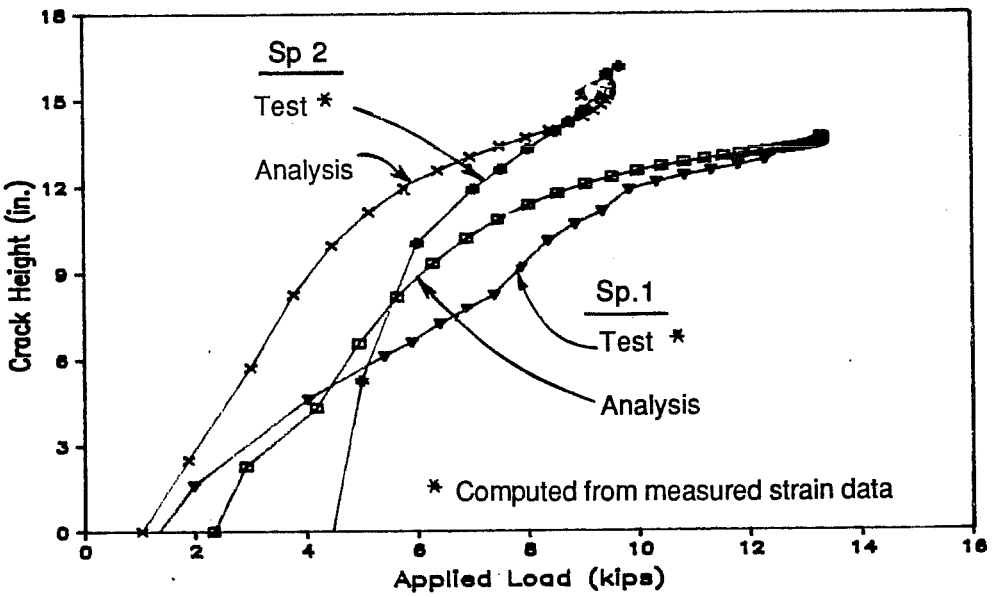

Fig. 7.22 Comparison of computed and predicted crack height during flexure tests

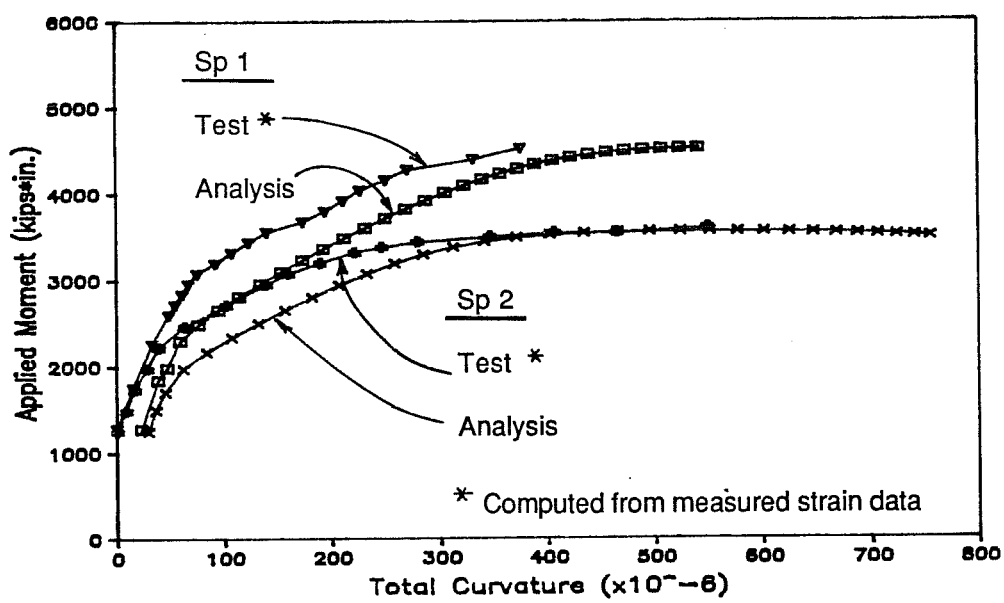

Fig. 7.23 Comparison of computed and predicted total curvature during flexure tests

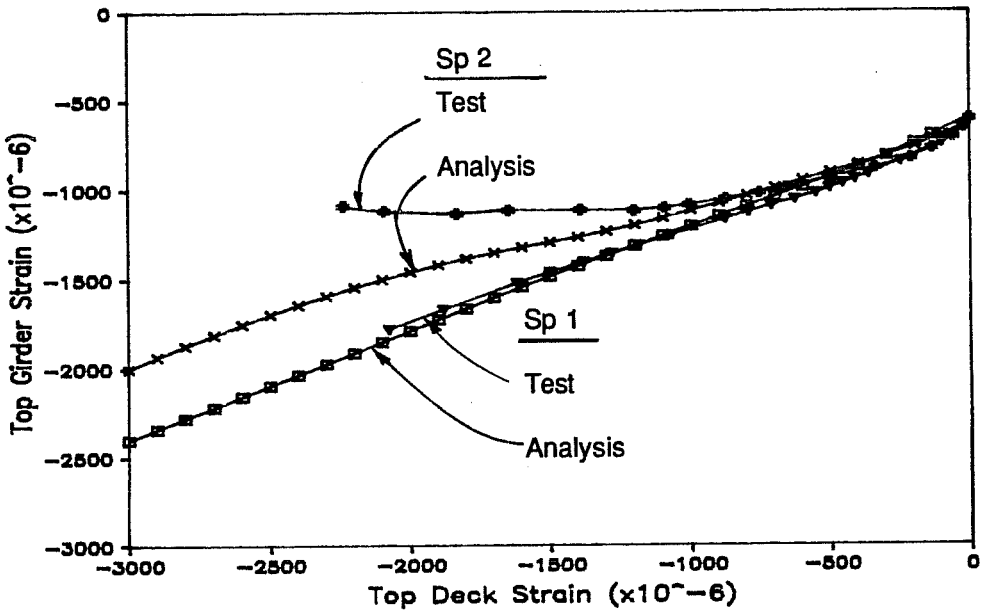

Fig. 7.24 Comparison of measured and predicted concrete strains at top of girder and top of deck during flexure tests

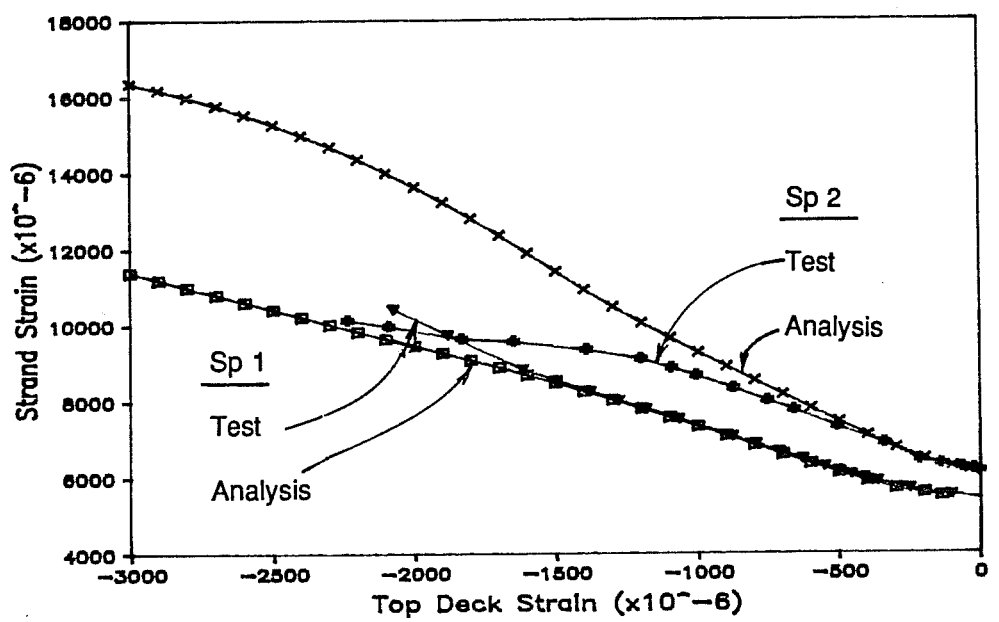

Fig. 7.25 Comparison of measured and predicted strand strains and concrete strains at top of deck during flexure tests

test curves for Specimen 1 as shown in Fig. 7.24 seems to indicate that the measured strains were reasonable.

The excellent agreement when strains are plotted versus strains is puzzling because of the poor agreement for strains plotted versus load. The good agreement between measured and predicted behavior when strains are plotted versus strains may indicate that the analysis is correct, but that somehow the relationship between load and strain is in error. The good agreement between measured and predicted ultimate loads and the fact that loads involved in the test were known with sufficient precision seem to eliminate the possibility that the loads applied during the test or the dead loads were in error.

7.4.4.2 Capacity and Conditions at Failure. Measured and predicted quantities at failure and defined ultimate conditions will now be compared. The current definition for the stress-block parameter β_1 is used in the following analyses because other investigators have found it to be appropriate for use with high strength concrete as discussed in Sec. 3.4.1.

The moment and load at defined ultimate conditions and failure are shown in Fig. 7.26 and 7.27, respectively. Values from the strain compatibility analysis are given for top-of-deck strains equal to the measured strain at failure, the code specified maximum usable concrete strain (0.003), and the maximum moment. Results were computed for

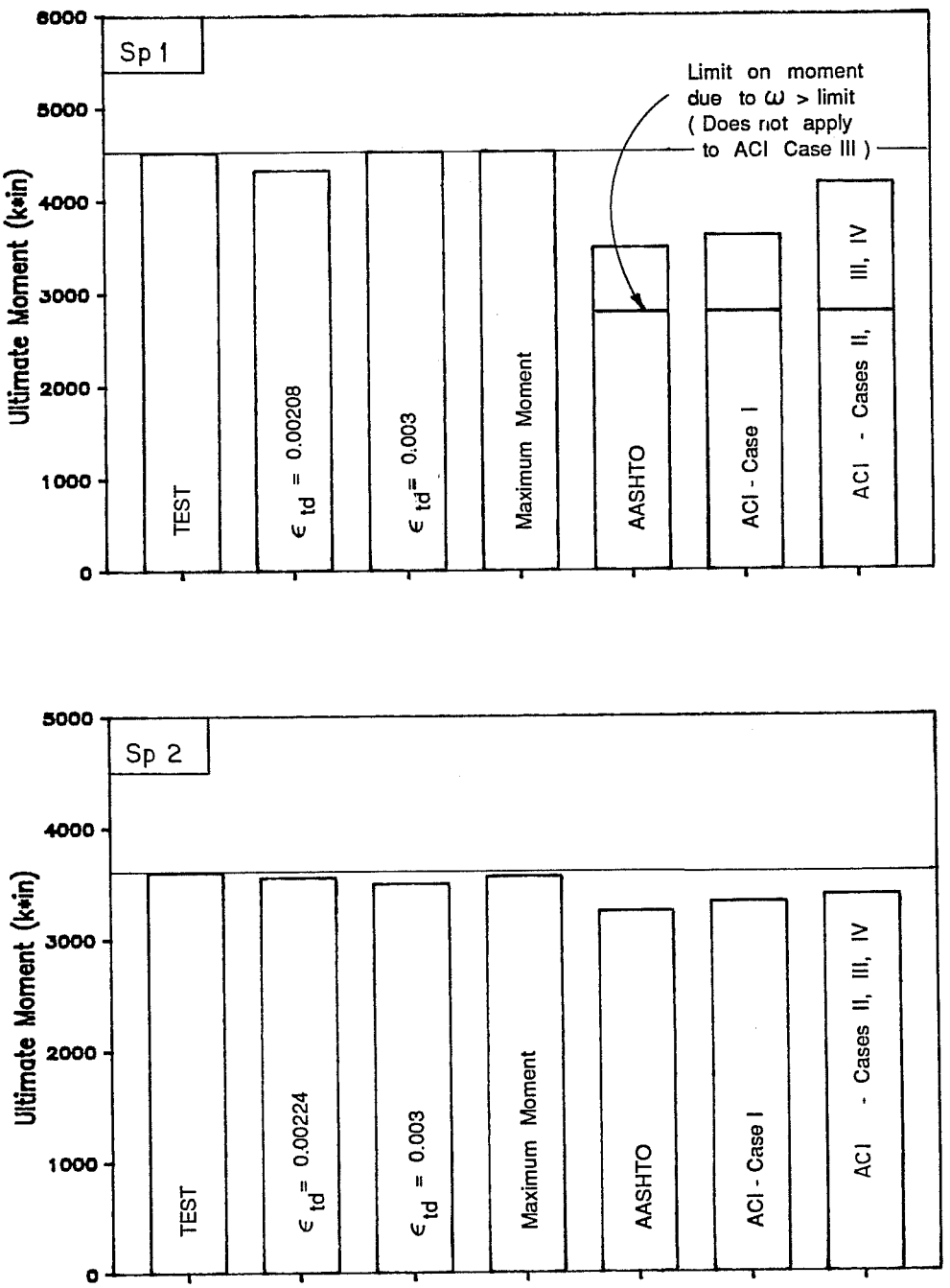

Fig. 7.26 Comparison of measured and predicted ultimate moment capacity for flexure tests

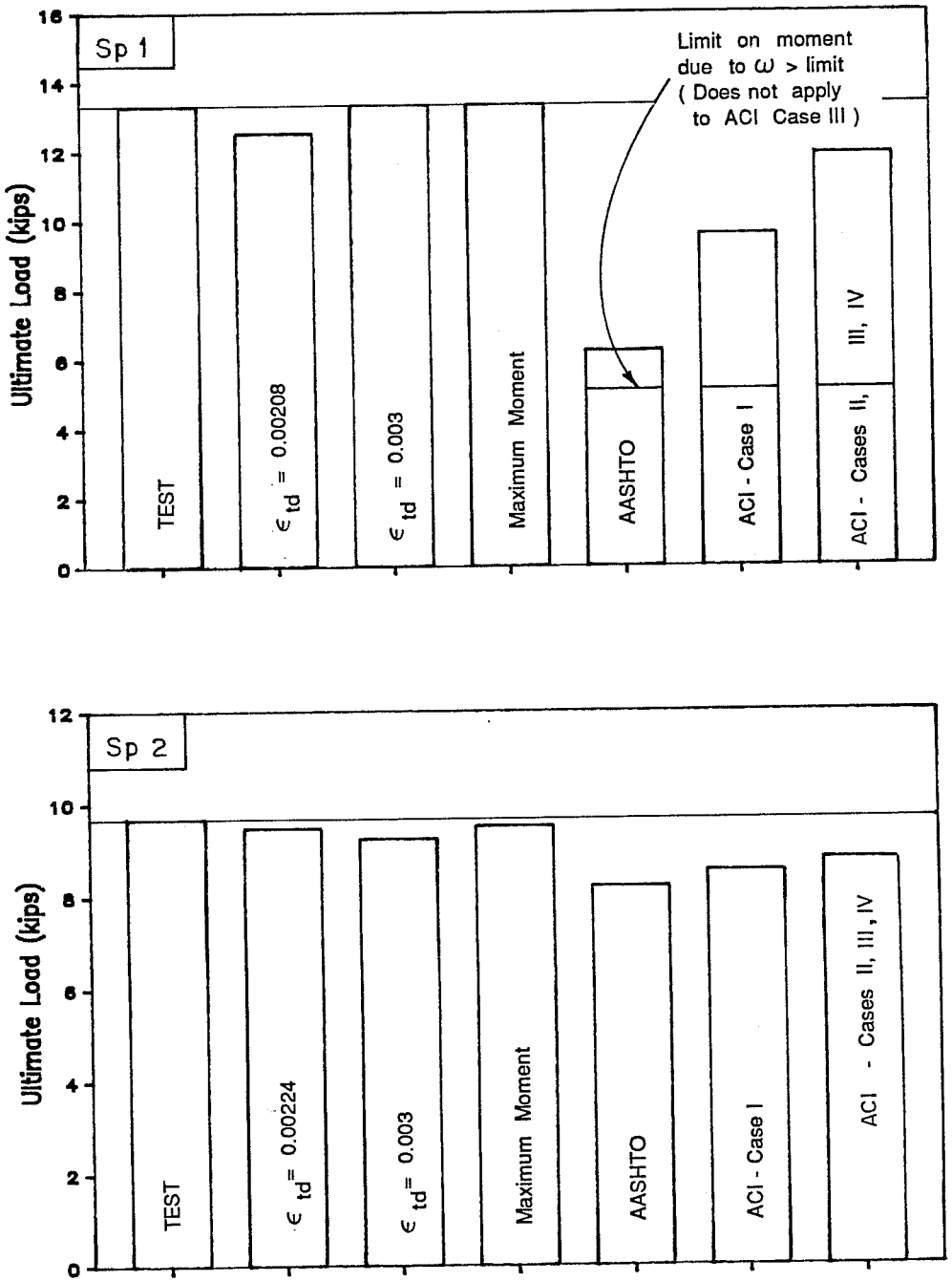

Fig. 7.27 Comparison of measured and predicted ultimate loads for flexure tests

the simplified analysis methods by using the appropriate strand stress equation with the ultimate moment equations in the AASHTO Specifications or the ACI ERSB with the approaches discussed in Section 7.4.2.2. Because the reinforcement index exceeded code specified limits for Specimen 1, computed member capacities were reduced using the equations provided by the AASHTO Specifications and the ACI Code Commentary. Moments and loads predicted by the strain compatibility analysis show very good agreement with test data while the reduced capacities computed using the simplified code methods are significantly below measured values. It is interesting that capacities computed using the simplified methods without the required reduction were conservative for this test data. Agreement is slightly worse for loads because of the conversion from total moment to applied load, which subtracts the dead load moment from the total ultimate moment before the applied load is computed.

Strand stresses at ultimate are compared in Fig. 7.28. Stresses computed by the strain compatibility analysis agree well with measured values, although agreement is better for Specimen 1 where strains increased steadily until failure. Stresses computed using the simplified methods were consistently lower than the values obtained from analysis. No modifications were made in the calculation of ultimate strand stress due to the excessive

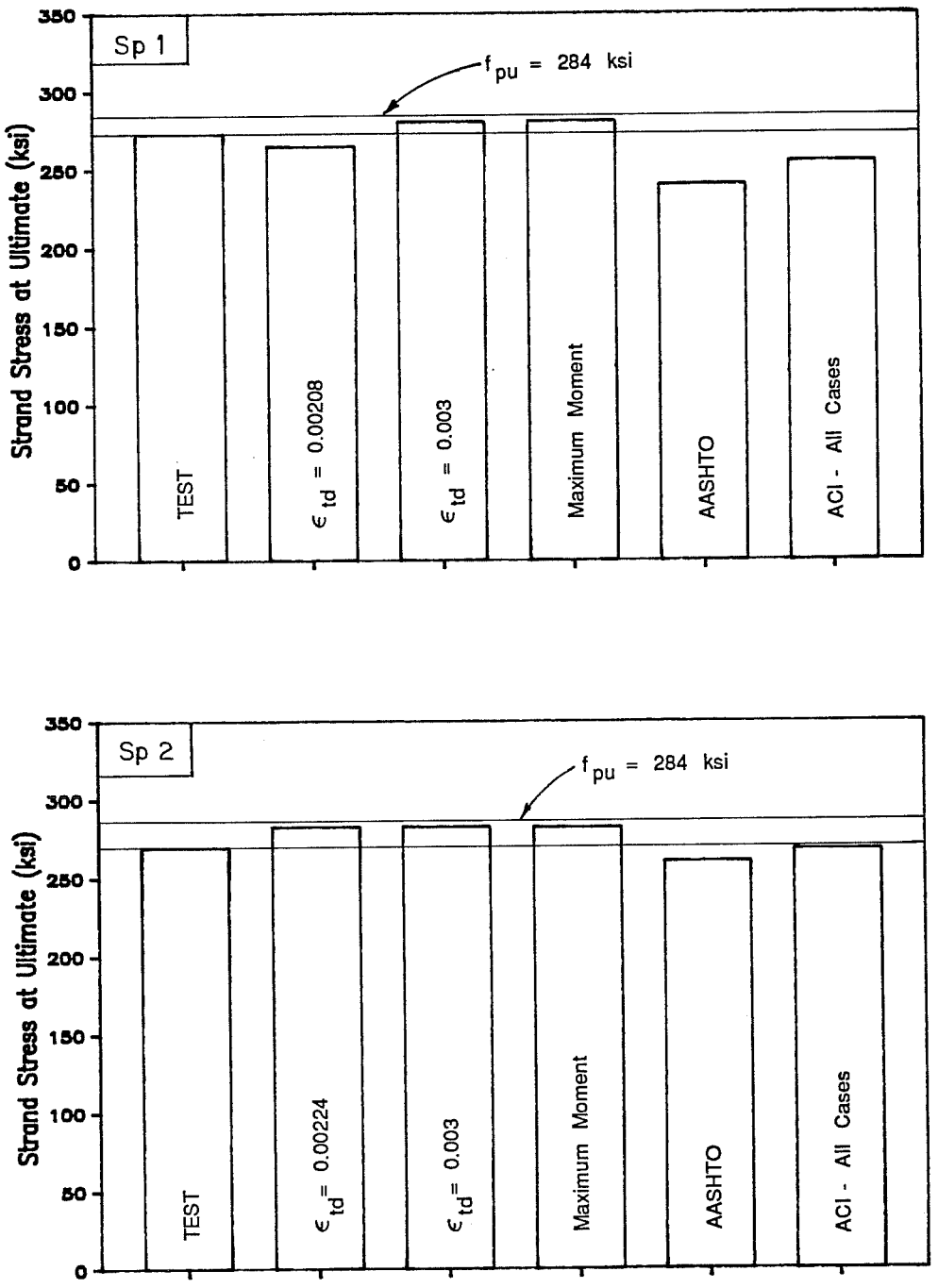

Fig. 7.28 Comparison of measured and predicted strand stress at ultimate for flexure tests

reinforcement index of Specimen 1 because no such guidance is given in the codes.

Measured deck and girder strains at failure are compared with strains corresponding to the defined ultimate conditions in Fig. 7.29 and 7.30, respectively. For the deck, the measured strain at failure was well below both analytical definitions of ultimate for Specimen 1 while for Specimen 2, failure occurred at a strain near the top-of-deck strain corresponding to maximum moment from the analysis, but was well short of the 0.003 that is assumed to correspond to failure. The results are similar for the top-of-girder strain, although the comparison for Specimen 2 is hampered by the previously noted low girder strain at failure. For Specimen 1, the strain in the deck and girder at failure agrees well for the analysis. That is, the measured strain in the top of the girder at failure agrees well with the predicted strain when the top of the deck is at the strain measured at that location at failure.

7.4.4.3 Summary. This section summarizes the preceding examination of test data, analytical results, and estimates based on the simplified methods given in the codes.

1. Use of the current definition for β_1 is appropriate for use with high strength concrete.
2. The strain compatibility analysis used here provided a conservative yet realistic estimate of all aspects of

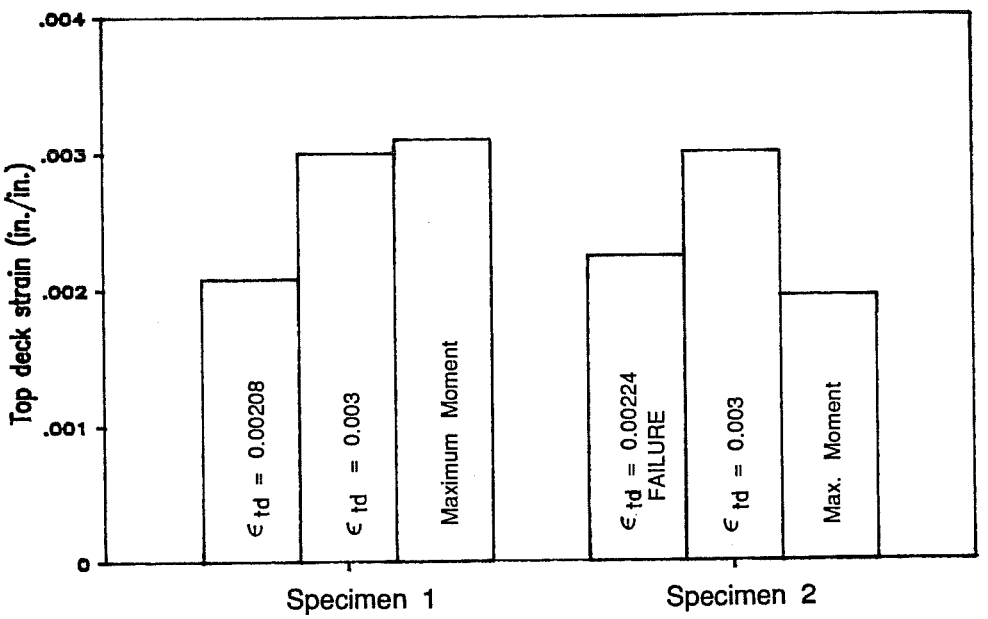

Fig. 7.29 Comparison of top-of-deck concrete strains measured at failure and predicted by analysis at ultimate conditions

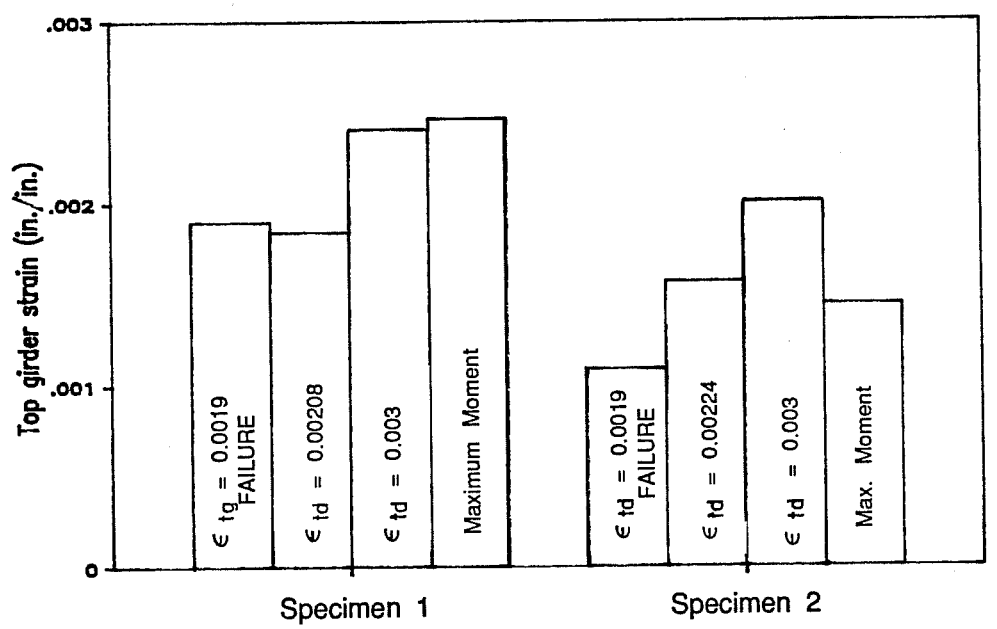

Fig. 7.30 Comparison of top-of-girder strains measured at failure and predicted by analysis at failure and ultimate conditions

flexural behavior, including ultimate capacity, deflections, and strand stresses.

3. The maximum usable concrete strain for sections of this type may be less than the 0.003 specified in the ACI Code, as reflected by strain readings from test specimens. For this data, an average value for the strain at failure for the deck concrete was approximately 0.0022, which was corroborated by results of the strain compatibility analysis. While it is not possible to be dogmatic about an exact value for the ultimate concrete strains measured in the tests because of various limitations in the data (see Sec. 7.3.2), it appears certain that the strains at failure were less than the specified maximum usable strain.
4. The simplified analysis methods provided conservative estimates of the ultimate capacity of the specimens tested.
5. The strain compatibility analysis gave a better estimate of flexural strength than the simplified methods.
6. For Specimen 1, the calculated capacity was reduced because the reinforcement index exceeded specified limits. The reduced capacity greatly underestimated

the failure load while the uncorrected capacity provided a reasonable, conservative estimate of the failure load.

7. The strain compatibility analysis provided a good, although slightly high, estimate of the measured strand strains and stresses at failure.

8. Strand stress at ultimate was conservatively and reasonably estimated using the equations from the codes. The recently revised ACI equation provided the better estimate.

9. Agreement between test data and the strain compatibility analysis was better when the information was plotted versus top-of-deck strains than when plotted versus load.

7.4.5 Predicted Behavior for Typical Designs. In this section, designs for a range of span and girder spacings will be compared. An AASHTO-PCI Type IV girder (see Fig. 2.1) is used with three concrete strengths: 6, 9, and 12 ksi. Two girder spacings (GS) will be used, 4 and 10 ft, which represent practical extremes in the range of girder spacings. The deck was assumed to be applied to an unshored girder and had a concrete strength of 4 ksi. Two categories of designs are considered: (1) a design for a given span of 75 ft (GS = 10 ft) or 120 ft (GS = 4 ft), which are extremes for the design using this girder section with 6 ksi concrete, and (2) a design for

the maximum span possible for a given girder spacing and concrete strength. The maximum span designs represent extremes of behavior and could be used for actual designs. The typical span designs using the higher strength concrete would not likely be used since the same design could be achieved using normal strength concrete. These typical designs were included to give a direct comparison between behavior of normal and high strength concrete members. Concrete strengths at release are 75 percent of the 28 day strength, except for a series of designs in which the release strength was varied to determine the minimum release strength required for a given span and girder spacing. Low relaxation strands with a 0.5-in. diameter are used for all designs. The recommendations by Zia et al. [137] are used for computing prestress losses.

Actual, practical designs were used for this study to ensure that combinations of variables were reasonable, rather than performing a sensitivity analysis on a few parameters without restraining their relationship by the constraints of practical design. Therefore, the conclusions of this study can be construed as being representative of a range of designs that could be encountered in actual design situations.

Designs were executed using the computer program BRIDGE (see Appendix C.2) which was written for this study. Results of the design were used as input for the strain compatibility analysis program

(MOMCURV) to determine the behavior of the designs at ultimate conditions.

The "ultimate condition" is defined as the state of the member or section when the maximum capacity is attained. Other definitions, however, are provided to permit estimation of this maximum capacity. In the following study, three definitions for the ultimate condition will be considered in all cases: (1) the strain at the top of the deck equal to the maximum usable strain of 0.003, (2) the maximum moment resisted by the section, and (3) the top of the deck reaching a strain of 0.0022, which is an approximate average of top fiber strains at failure for the specimens tested. An additional case will be considered where the strand strain reaches the minimum specified elongation of 0.035 prior to the top of the deck reaching a strain of 0.003.

The spans used and number of strands required for the 12 designs considered in this and following sections are summarized in Fig. 7.31 and 7.32, respectively. Figure 7.31 indicates the increase in span with increasing concrete strength for the maximum span designs. The maximum span designs for 9 and 12 ksi concrete with GS = 4 ft exceed the maximum lifting spans corresponding to the girder concrete strength at release, and would therefore require special consideration in design and handling (see Sec. 7.7). Figure 7.32 shows that the use of high strength concrete provides only a slight,

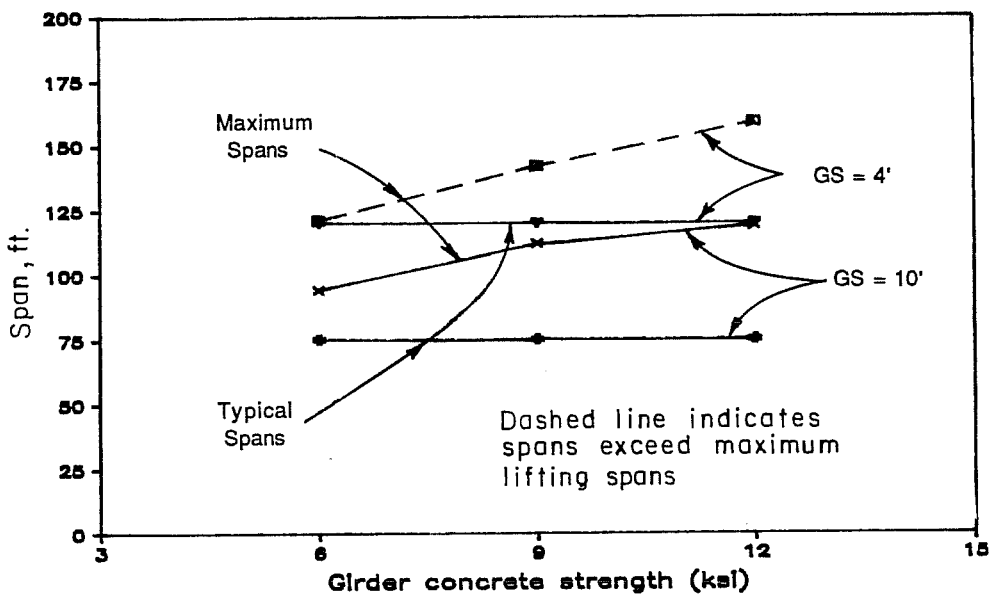

Fig. 7.31 Span length versus girder concrete strength for maximum and typical span designs

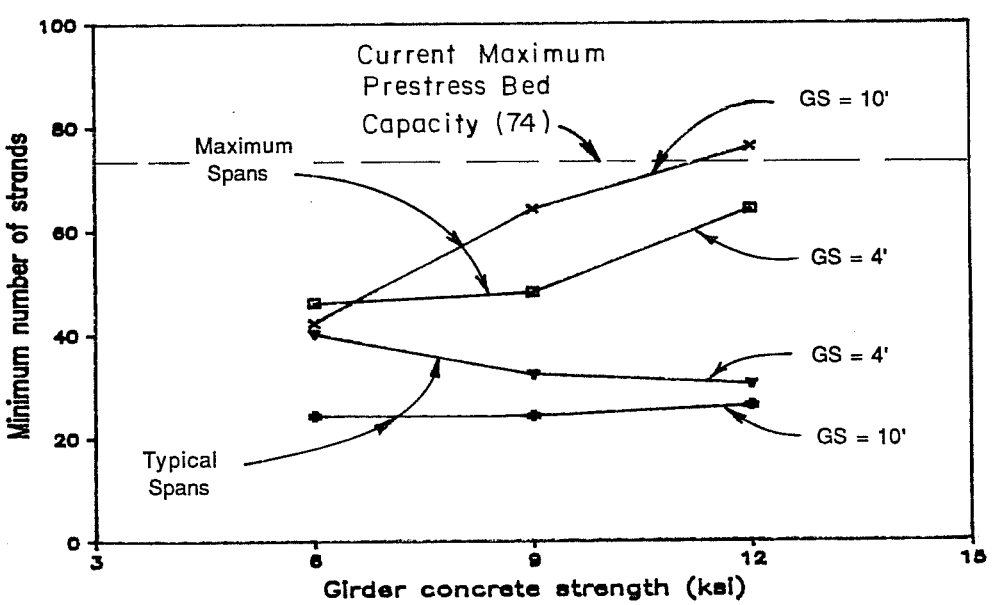

Fig. 7.32 Minimum number of strands versus girder concrete strength for maximum and typical span designs

if any, decrease in the required number of strands for the typical span designs. A large number of strands is required for the maximum span designs, especially where high strength concrete is used. For the case where f'_c = 12 ksi and GS = 10 ft, the strand limit of 74 was exceeded. This leads to the need for suitable ductility limits in order to control over-reinforcement.

Results from these designs will be considered in this section as they relate to ultimate capacity, strand stress at ultimate, the effect of the girder concrete modulus on the design and ultimate capacity, and the required strength at release. Other results from these designs will be considered in the sections that follow.

The data from the designs are generally presented in bar-chart form with bars grouped for the concrete strengths and separate plots given for the two girder spacings used. Plots for the typical span designs and the maximum span designs will generally appear on separate pages. The bars are labelled for the first group of bars only, with unlabelled bars appearing in the same order as those that are labelled.

7.4.5.1 Ultimate Design Moment. The ultimate capacity of a highway bridge designed by the AASHTO Specification must exceed both the ultimate moment, M_u, which is a combination of factored service loads, and 1.2 times the cracking moment, M_{cr}, computed using a

modulus of rupture of $7.5\sqrt{f'_c}$. The ultimate moment is determined using the following equation for the typical load combination of dead and live loads:

$$M_u = 1.3*(M_{DL} + 1.67*M_{L+I}) \quad (7.1)$$

where I = impact fraction (maximum 30 percent)

$$= 50/(L+125) \quad (7.2)$$

L = span in feet

M_{DL} = dead load moment

M_{LL} = live load moment

$M_{L+I} = M_{LL}(1+I)$

The variation of the impact factor with span length is shown in Fig. 7.33 along with tabulated values for selected spans. For spans greater than 125 ft, the impact factor is less than 20 percent.

Ultimate strength design includes the use of a strength reduction factor, ϕ. The AASHTO Specifications use $\phi = 1.0$ for flexural analysis of factory produced precast prestressed concrete members. This factor is usually used for composite bridges with pretensioned girders, although deck concrete placed in the field would generally require use of a lower factor. The use of a m factor of 1 for flexural analysis of the entire structure appears appropriate since the use of the precast element provides good control over the quantities of greatest importance in the flexural analysis.

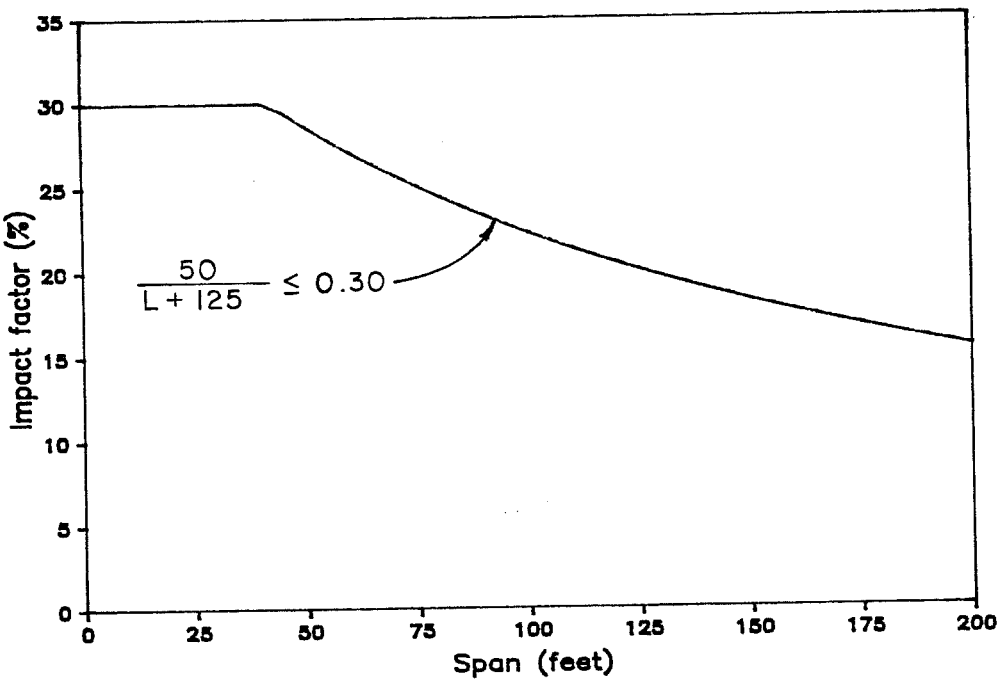

Fig. 7.33 AASHTO live load impact factor

Span	Impact Factor	Span	Impact Factor
0	30.00	120	20.41
40	30.00	125	20.00
45	29.41	130	19.61
50	28.57	135	19.23
55	27.78	140	18.87
60	27.03	145	18.52
65	26.32	150	18.18
70	25.64	155	17.86
75	25.00	160	17.54
80	24.39	165	17.24
85	23.81	170	16.95
90	23.26	175	16.67
95	22.73	180	16.39
100	22.22	185	16.13
105	21.74	190	15.87
110	21.28	195	15.63
115	20.83	200	15.38

Errors in dimensions or strength of the deck will have only a small effect on the capacity of the member. The analysis has also been shown to be conservative and realistic, as was demonstrated earlier in this chapter.

The second limit on ultimate capacity is intended to prevent failure shortly after initial cracking due to a lack of reinforcement, and is actually considered a minimum reinforcement requirement. The cracking moment, M_{cr}, which is the total moment producing cracking, can be expressed as a sum of the dead load moment and some fraction greater than 1 times the live load moment including impact factor, i.e.,

$$M_{cr} = X*M_{L+I} + M_{DL} \tag{7.3}$$

With the cracking moment defined in this way, the 1.2 times M_{cr} limit can be compared with the ultimate moment limit by expressing both limits in terms of the ratio M_{SL}/M_{DL} (where M_{SL} = service load moment = $M_{L+I} + M_{DL}$) or M_{L+I}/M_{DL} as shown in Fig. 7.34. This plot demonstrates that the ultimate load criteria will control for most situations, since X is usually less than 2. Values for the live load plus impact-to-dead load ratio for some of the span/girder spacing combinations are shown on the figure, indicating that most designs

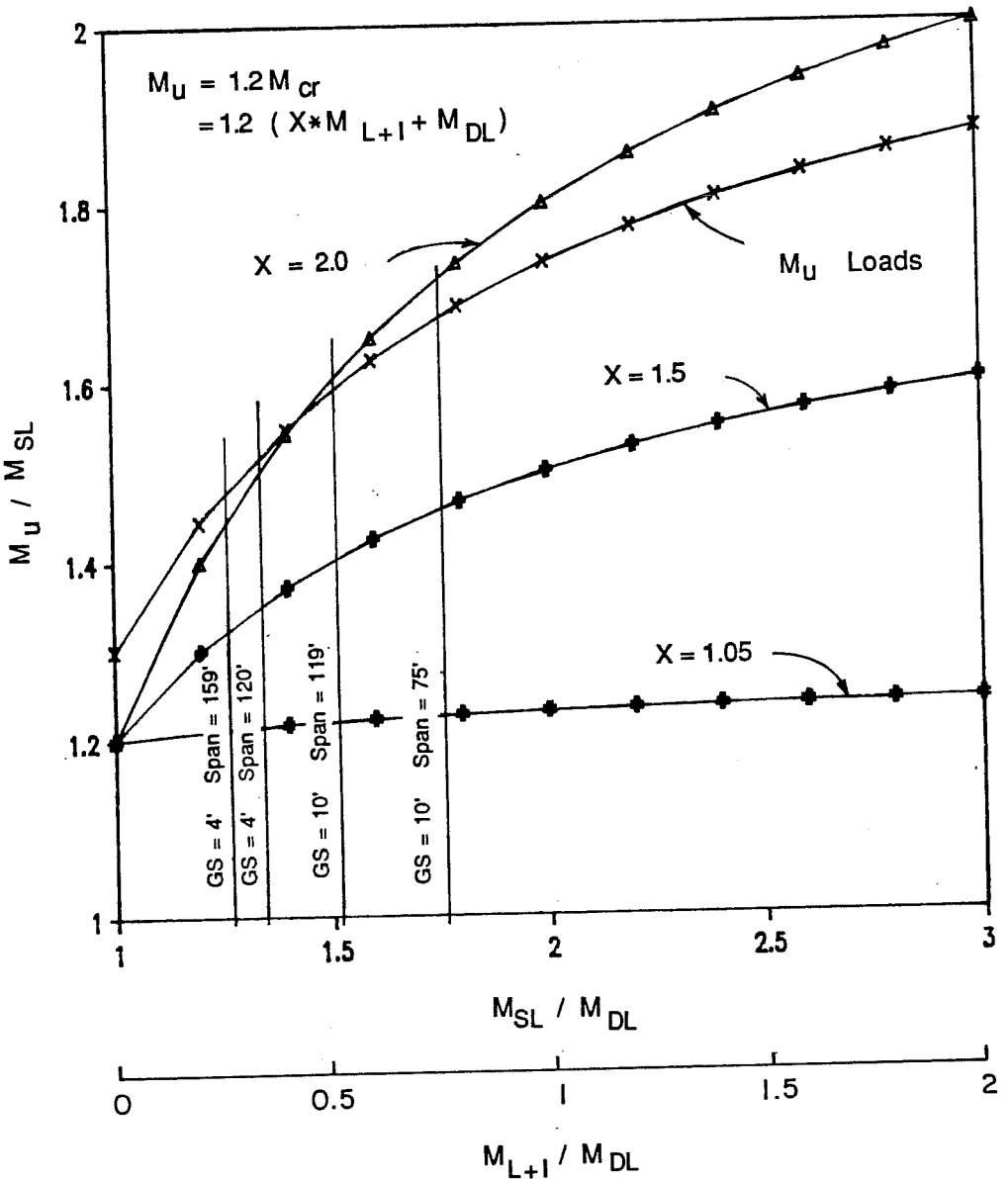

Fig. 7.34 Relative magnitude of ultimate moment limits

will be at values of M_{SL}/M_{DL} near or less than 1.5. A further manipulation of the equations gives the multiple of the live load including impact required to reach the ultimate moment or 1.2 M_{cr} as shown in Fig. 7.35. This figure indicates that an overload of 2.5 to 3 times the live load including impact factor must be applied to bridge members considered in this section in order to reach the ultimate load. While it appears unlikely that such an overload could occur, a comparison of actual and potential highway loadings with AASHTO specified loadings would provide a basis for evaluating the significance of the magnitude of overload required.

This analysis indicates that for most designs, M_u should control. This will not be the case if the cracking moment M_{cr} is computed using a simplified equation in which the effects of dead load are neglected. This simplification is appropriate for shear analysis of noncomposite uniformly loaded beams but has apparently been used for flexural analysis of composite members as well. Using a concrete tensile strength of $7.5\sqrt{f'_c}$, cracking moments computed using the simplified approach overestimated the actual cracking moment by as much as 25 percent. Therefore, full consideration should be given to all loads applied on the appropriate section in the computation of the cracking moment.

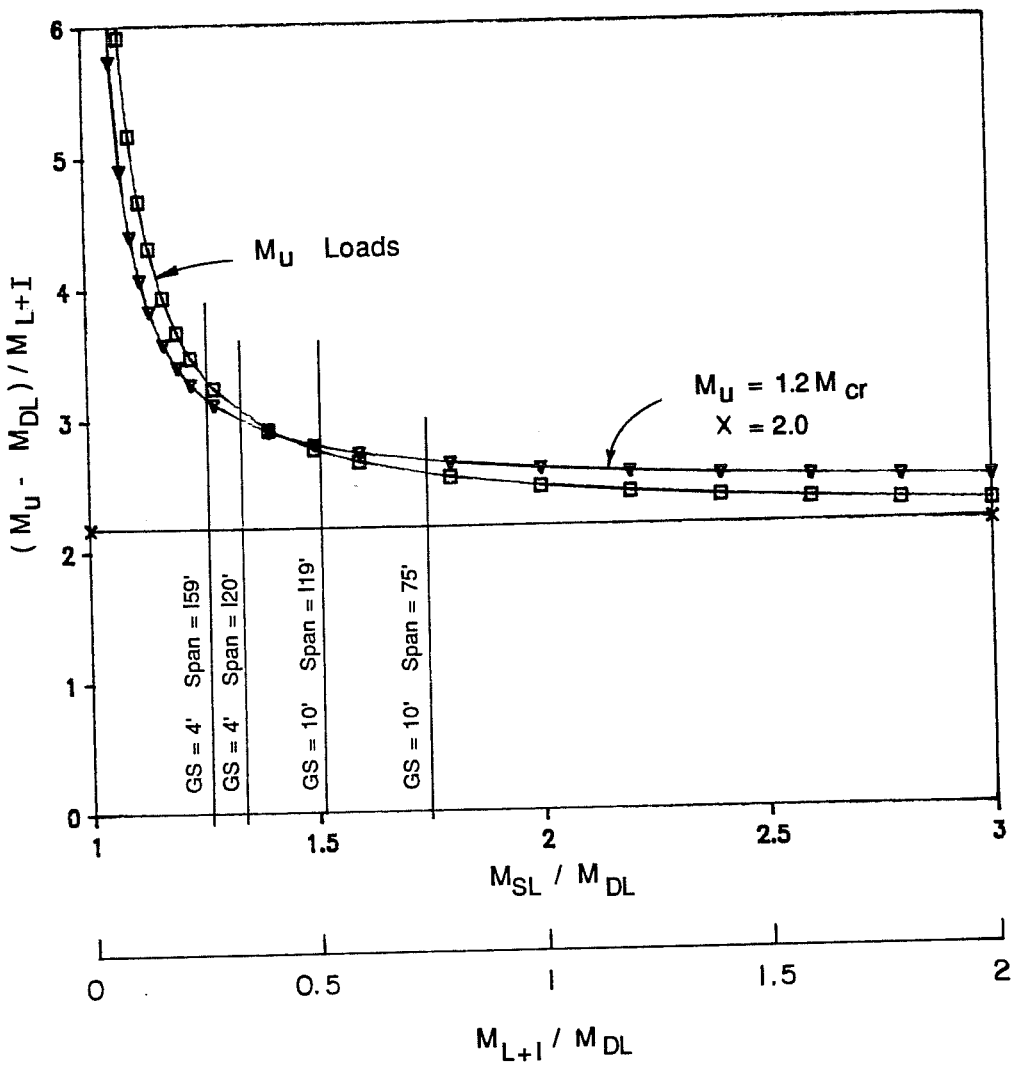

Fig. 7.35 Relative overload required to reach ultimate load

7.4.5.2 Ultimate Moment Capacity. Ultimate moment capacities computed using the strain compatibility analysis and the simplified approaches are shown in Fig. 7.36 and 7.37 for maximum and typical span designs, respectively. Spans, girder spacings, and girder concrete strengths are shown on the figures.

Agreement is very good between capacities computed using the strain compatibility analysis for the different ultimate conditions. This indicates that the capacity is very close to the maximum when the top-of-deck strain reaches 0.0022 and that it remains near the maximum up to a strain of 0.003. For the maximum span case of GS = 10 ft and f'_{cg} = 6 ksi, the strand reached the minimum elongation at the ultimate capacity. However, for all typical span designs with GS = 10 ft, the strand reached the minimum elongation at the required ultimate capacity, which was slightly below the capacity predicted using the other measures of the ultimate condition and very close to the capacities computed using the simplified methods. This is a cause for concern and will be considered further in the section that follows.

The simplified methods showed good agreement with the strain compatibility analysis. Only in the case where the reinforcement index exceeded the specified limits and the capacities were reduced (max. spans, GS = 4 ft, f'_{cg} = 12 ksi) were the simplified methods overly conservative.

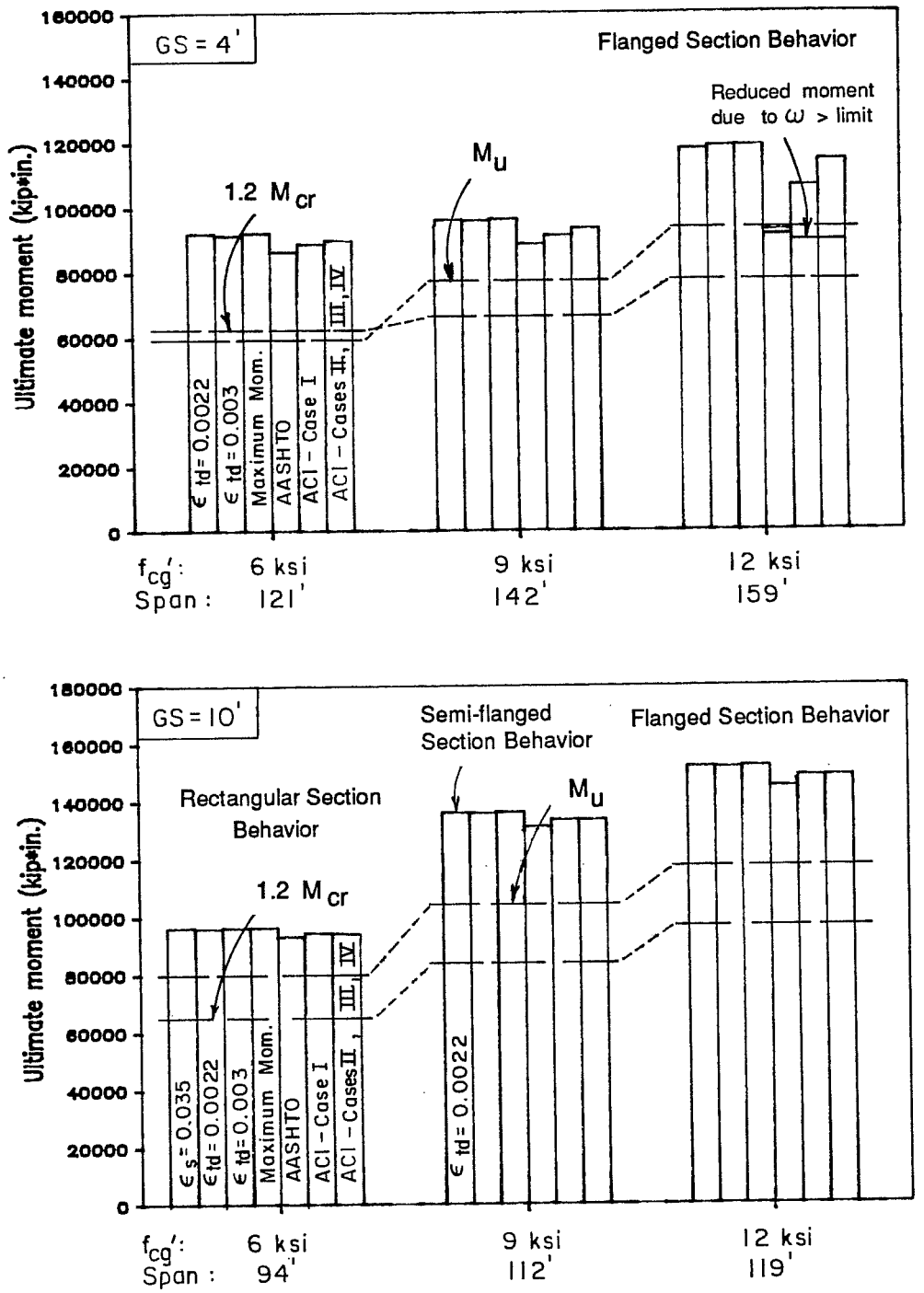

Fig. 7.36 Ultimate moment capacity for maximum span designs

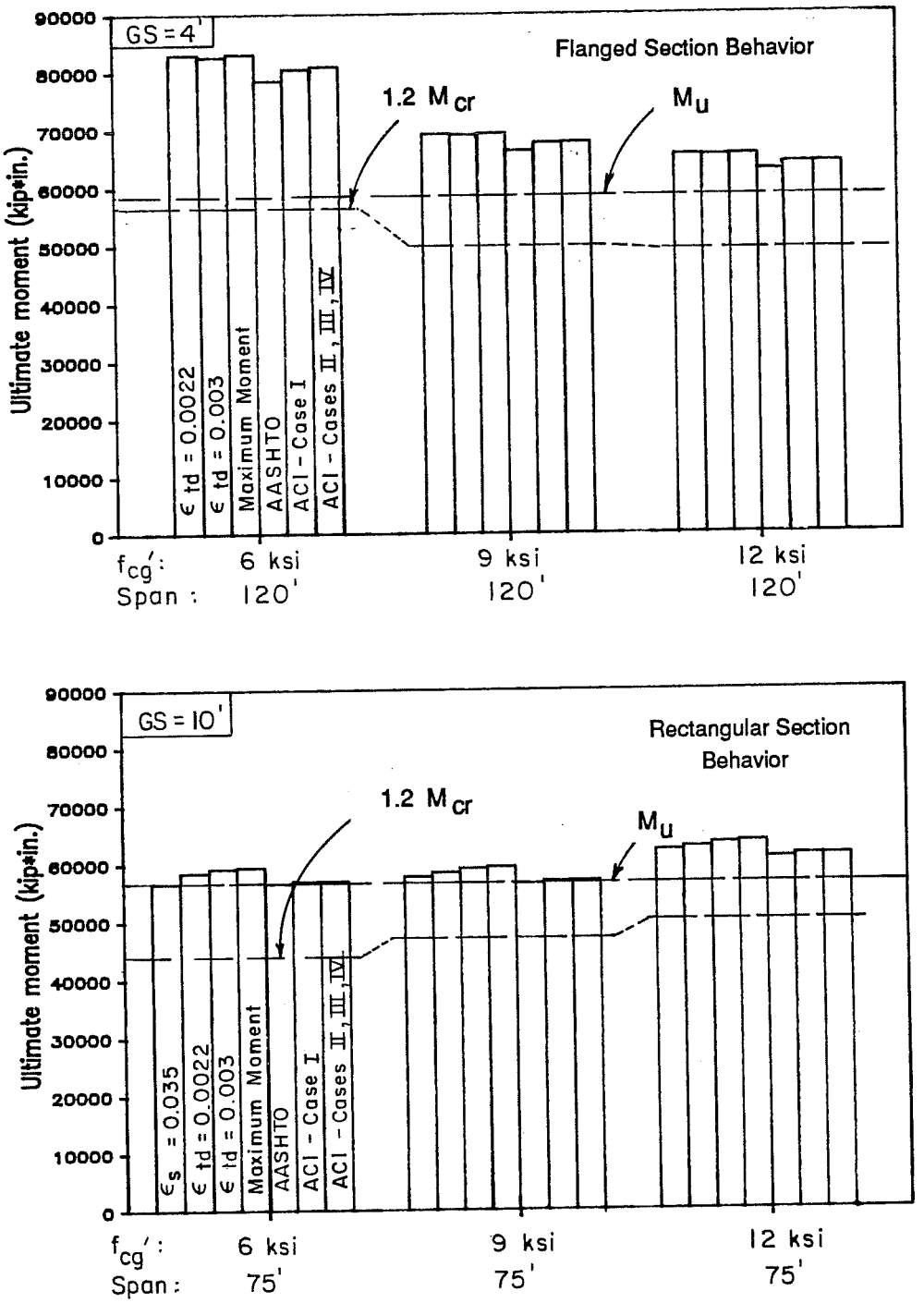

Fig. 7.37 Ultimate moment capacity for typical span designs

The factored ultimate load and the 1.2 M_{cr} limit are also shown on these figures. The 1.2 M_{cr} value plotted is based on a full cracking analysis including dead loads. However, the design program used the approximate relationship to check ultimate capacities during the design process. The larger value obtained using this incomplete analysis controlled the typical span design for GS = 10 ft and f'_{cg} = 12 ksi. If the correct cracking moment had been used, the 12 ksi design would have been essentially the same as for the other concrete strengths considered.

For all but one design, the factored load was larger than the cracking criteria. There was generally a large margin between the controlling ultimate load and the ultimate capacity. This was not the case for the short typical span with a wide girder spacing where ultimate capacity controlled design or came very close to controlling the design. Only in the single case where the reinforcement index exceeded the specified limit and the capacity was reduced did the capacity predicted by the simplified methods fall below the required ultimate capacity. This would have necessitated the addition of more reinforcement in a final design for the member, or a slight reduction in the span.

Flanged section analysis was required for designs where GS = 4 ft. For Cases III and IV, where section dimensions were transformed by the ratio of concrete strengths, a negative value was obtained for

the area of steel required to develop the flange as shown in Fig. 7.38. This occurred because the deck of the transformed section was narrower than the top of the girder. While this appears to indicate a flaw in the analysis, the results are reasonable and results of analyses of these sections with transformed dimensions are consistent with other designs.

The maximum span design with GS = 10 ft and $f_{cg}' = 9$ ksi exhibited "semi-flanged" behavior as noted on Fig. 7.36. This meant that the strain compatibility analysis revealed that the top of the girder remained in compression after the deck cracked. This condition was stable and persisted throughout the range of top-of-deck strains corresponding with all three conditions of ultimate considered for this design. While this condition is not of great importance for ultimate design, it would be significant if ductility limits were expressed in terms 36 of the depth of compression at ultimate, as has been proposed by some.

Figure 7.39 indicates the levels of reinforcement present in the designs. The reinforcement ratios are computed using the full girder width (for GS = 10 ft, the effective width was 110 in.) and full area of prestressing steel. It is clear from this figure that the minimum specified elongation of the strand was exceeded for typical span designs with GS = 10 ft because of very low reinforcement ratios in these designs.

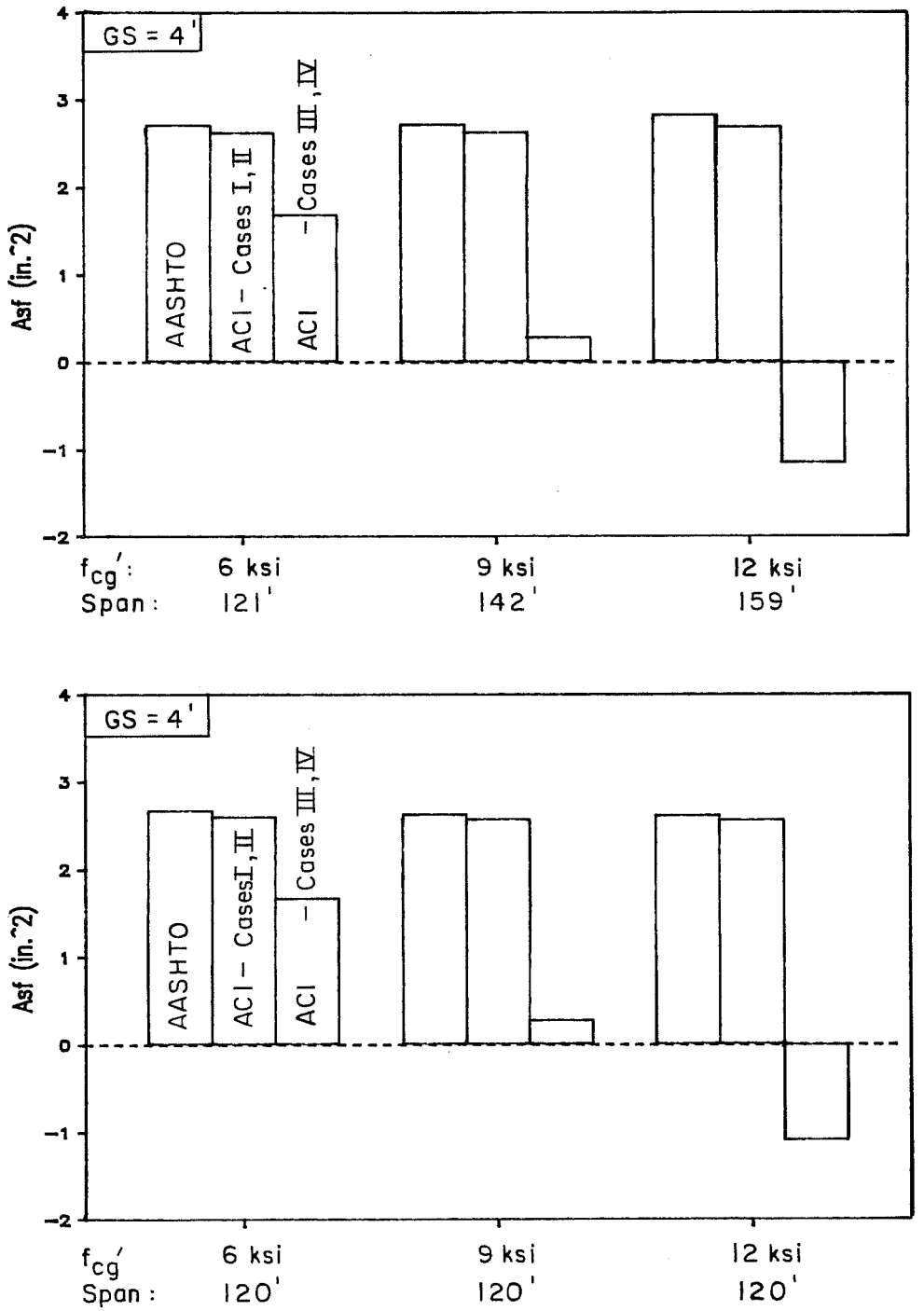

Fig. 7.38 Area of steel required to develop flange for maximum and typical span designs with GS = 4 ft

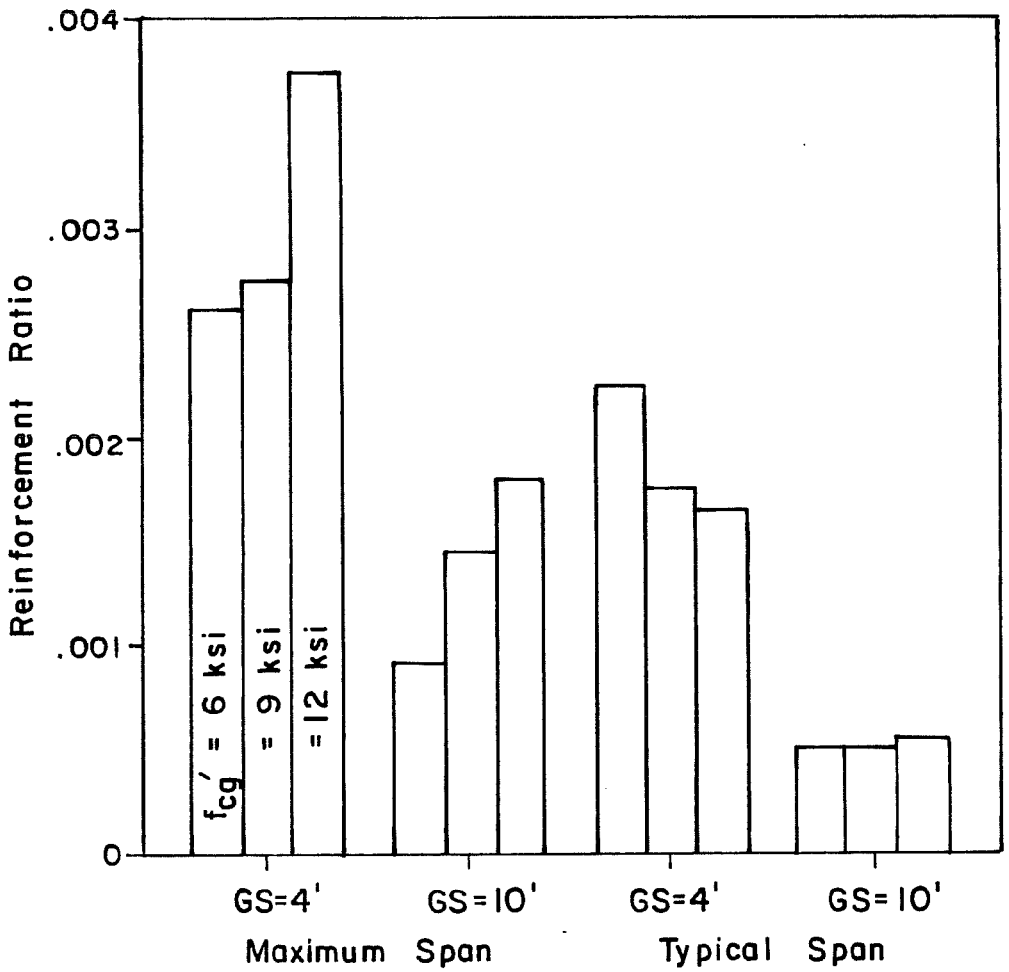

Fig. 7.39 Reinforcement ratio for maximum and typical span designs

The top-of-deck strains corresponding to the four conditions of ultimate for the strain compatibility analyses are shown in Fig. 7.40 and 7.41 for maximum and typical span designs, respectively.

These figures show that the maximum moment frequently occurs at top-of-deck strains below the maximum usable strain of 0.003 but always greater than the estimated failure strain of 0.0022. For the typical span designs with GS = 10 ft, the moment was still increasing, although only slightly, when the analysis was terminated at a top-of-deck strain of 0.0035. For the same design situation, the strand strain exceeded the minimum elongation well before the top-of-deck strain reached 0.0022, and the strand strains were approximately 6 percent when the top-of-deck strain reached 0.003.

Earlier, Fig. 7.36 and 7.37 indicated that the moment corresponding to a top fiber strain of 0.003 was very close to the maximum capacity of the section and therefore provided a good estimate of the ultimate capacity. However, Fig. 7.40 and 7.41 show that a large difference may exist between the top-of-deck strain at the maximum moment and the maximum usable strain. This difference is an indication that other quantities at ultimate, such as curvature, deflection, depth of compression, and strand strain, may be overestimated when the maximum usable strain of 0.003 is used to determine these other conditions at ultimate.

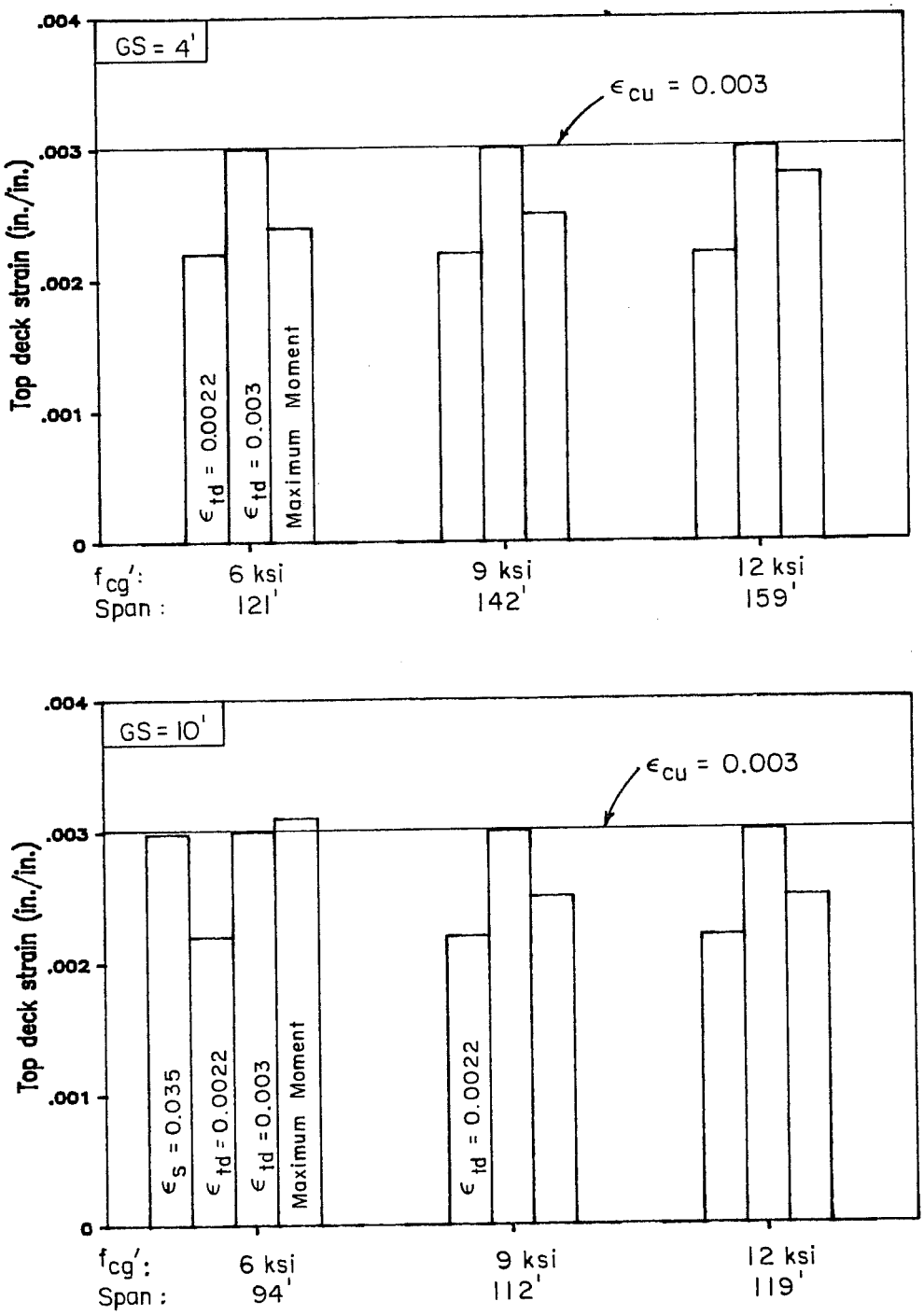

Fig. 7.40 Concrete strains at top of deck for maximum span designs

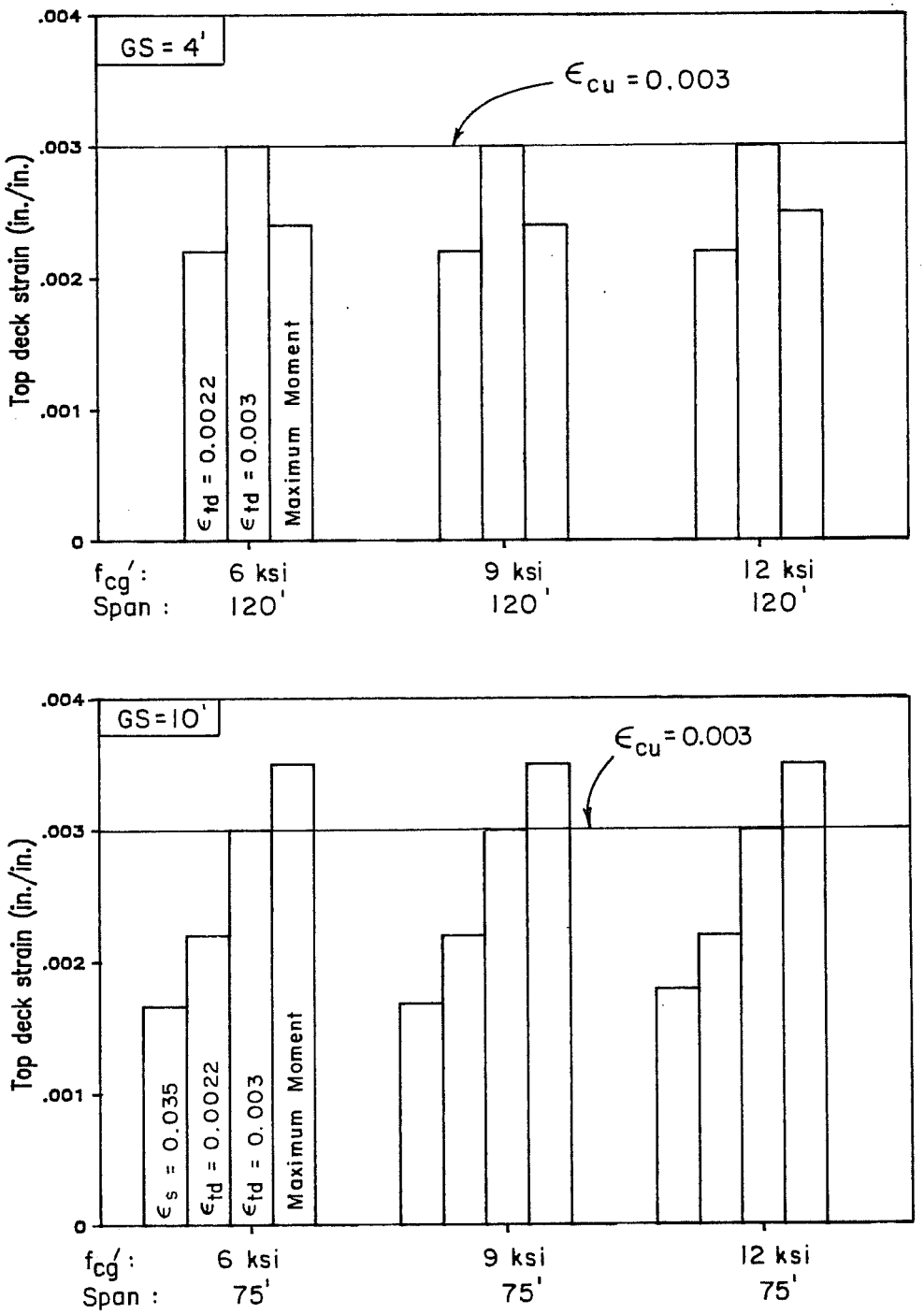

Fig. 7.41 Concrete strains at top of deck for typical span designs

Figures 7.42 and 7.43 show the top-of-girder strains when the top-of-deck strains reach 0.003 for maximum and typical span designs, respectively. The girder strains are shown to be less than or just over 0.002 when the top-of-deck strain reaches 0.003. This indicates that failure in the girder is unlikely, especially since failure of the deck could occur at a strain less than 0.003, which would also result in a lower girder strain.

7.4.5.3 Strand Stresses and Strains at Ultimate. Strand stresses at ultimate computed using the strain compatibility analysis and the simplified approaches are shown in Fig. 7.44 and 7.45 for maximum and typical span designs, respectively. The four conditions at ultimate used in the strain compatibility analyses given in the preceding section are also used here. The ultimate strand stress, f_{pu}, which occurs at a strain of 0.035, and the yield stress, f_{py}, which occurs at a strain of 0.01, are indicated on the figures. These stresses and corresponding strains are minimum values specified in ASTM A416 [25] and are typically exceeded by a significant margin for actual strands. The strain 0.035 is specified as the minimum permitted elongation at the ultimate strength of the strand. This strain therefore serves as a maximum strain limit for strands and will be referred to as the "limiting strain" in the following discussion.

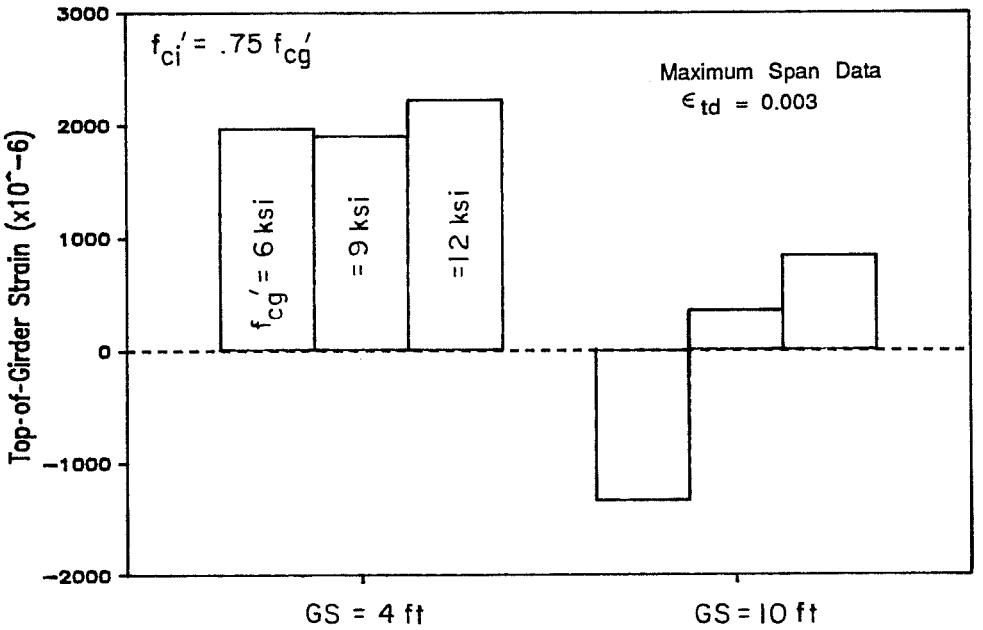

Fig. 7.42 Concrete strains at top of girder for maximum span designs

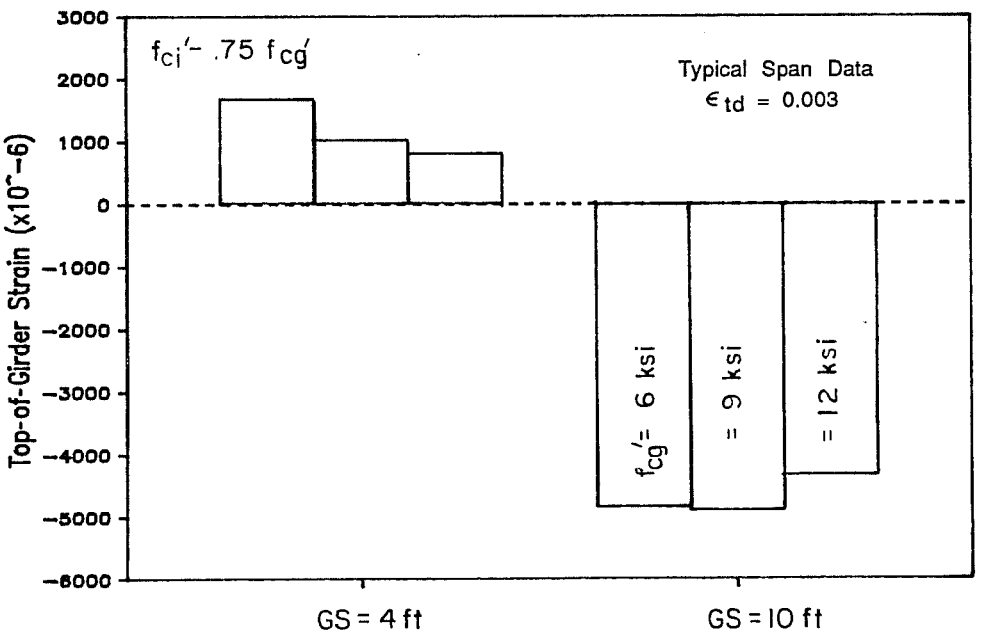

Fig. 7.43 Concrete strains at top of girder for typical span designs

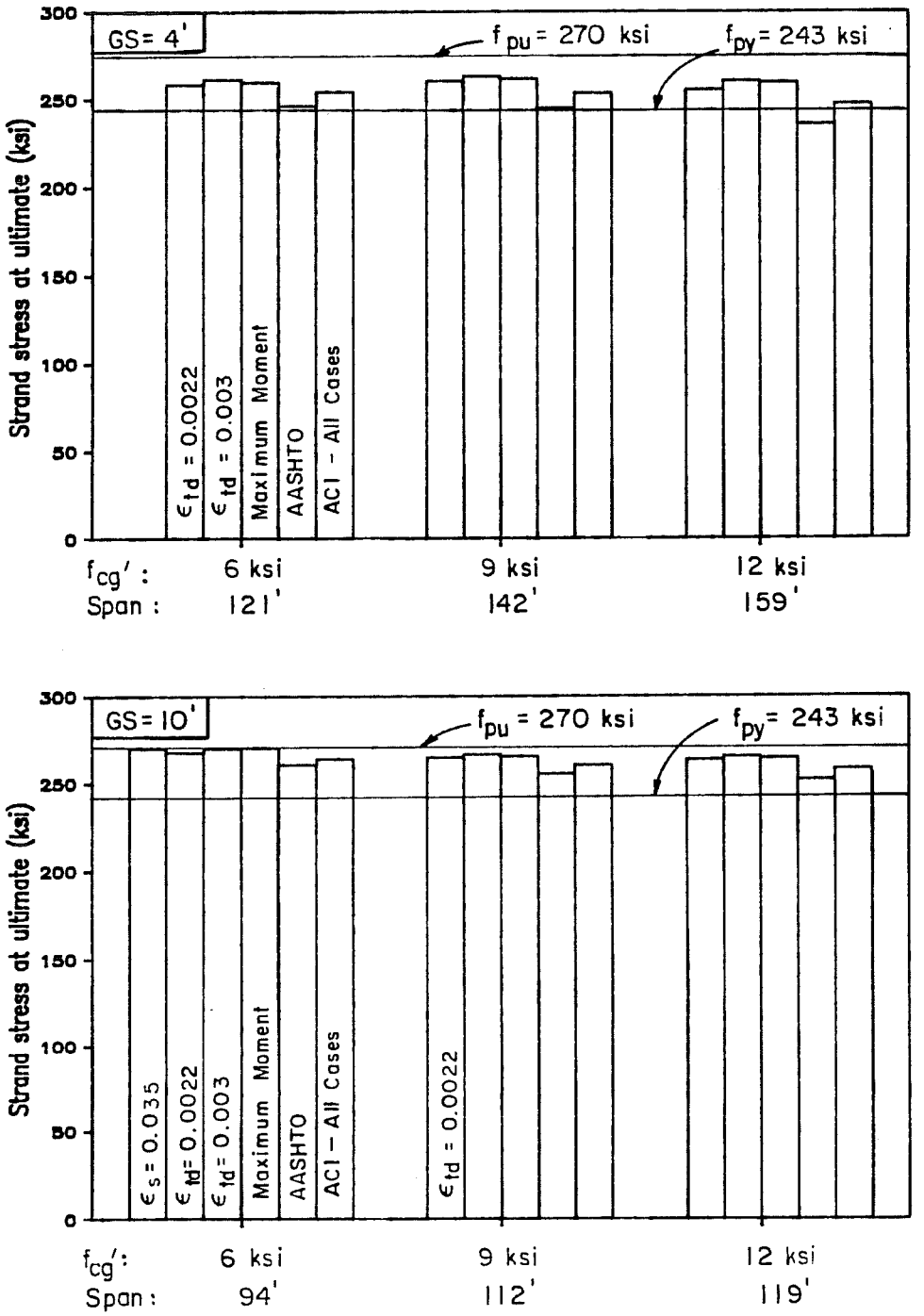

Fig. 7.44 Strand stress at ultimate for maximum span designs

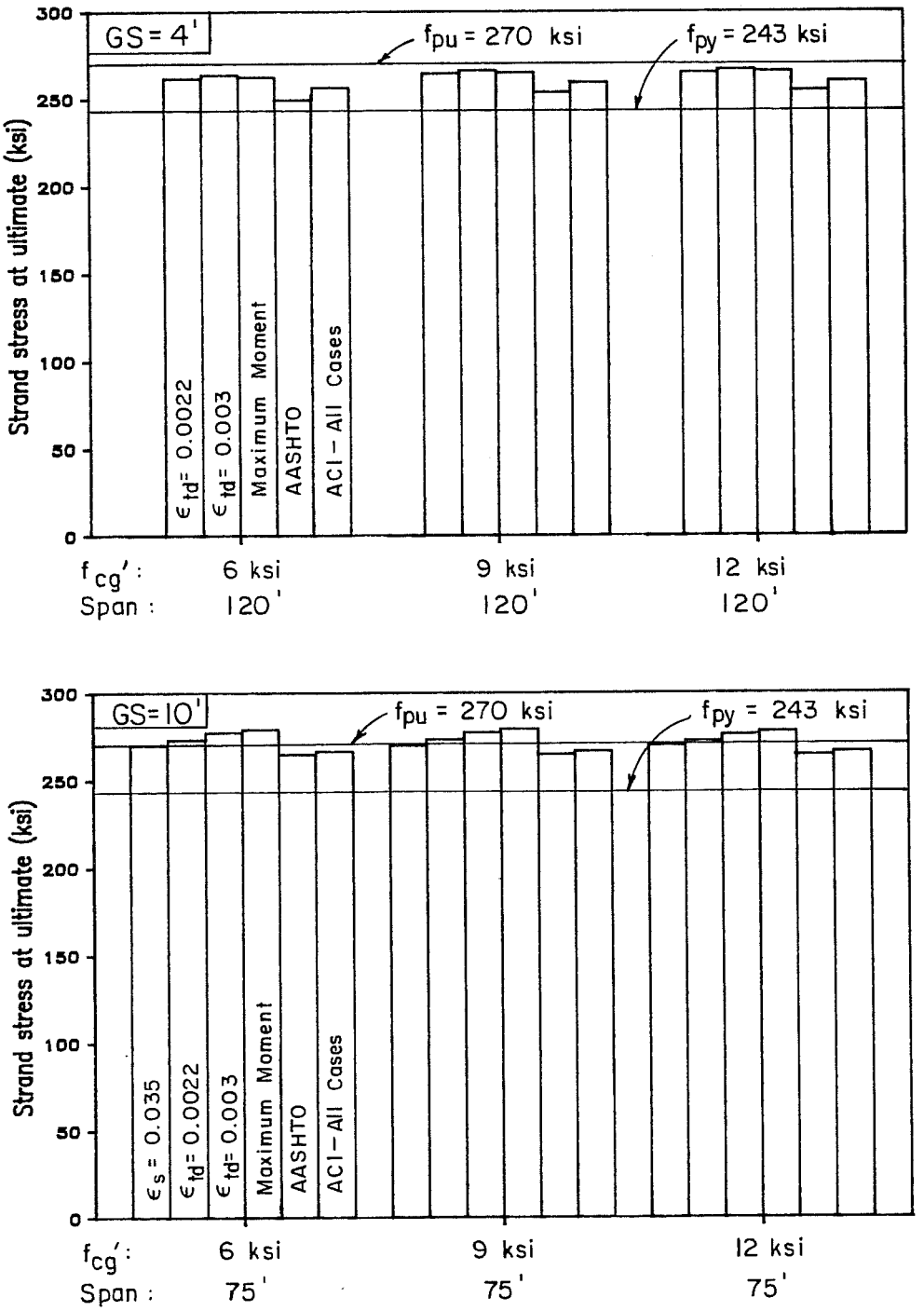

Fig. 7.45 Strand stress at ultimate for typical span designs

For both maximum and typical span designs, the strand stresses at ultimate are very similar at the different ultimate limits used in the strain compatibility analysis. All values exceed the yield stress, which is considered desirable and indicates that the sections are under-reinforced. Where the strand strain exceeds the limiting strain early in the load history of the member (typical spans, GS = 10 ft), the strand stress exceeds the ultimate value. This occurs because the strand stress-strain curve equation does not terminate at the specified ultimate stress, but simply passes through the point and continues to higher stresses.

The simplified analysis methods showed reasonable agreement with the stresses obtained from the strain compatibility analysis. The AASHTO equation gave the lowest estimate for strand stresses, especially for high reinforcement ratios where the modifications that appear in the ACI equation for low relaxation strand have the greatest effect. The modification for concrete strength had no effect on the ACI ultimate stress values in these designs because the deck concrete strength was used in the equation and it remained constant. The simplified methods can give no indication that the strand stresses are excessive at ultimate because the equations are constructed so that the computed ultimate strand stress will approach but never exceed the ultimate strand stress.

While the moment capacity of the maximum span design for GS = 4 ft and f'_{cg} = 12 ksi was reduced for both AASHTO and ACI designs because reinforcement index limits were exceeded, this appears to be overly conservative considering the results of the strain compatibility analysis in which strand stresses were well above yield for this design. This question will be addressed further in a later section on ductility.

From this discussion and that in preceding sections regarding excessive strand stresses at ultimate, it appears that a minimum reinforcement limit needs to be developed. The current limit of 1.2 M_{cr} which is intended as a minimum limit was not effective in the case considered here, because it was not the controlling ultimate load criteria (see Fig. 7.37). While the actual design considered here may not be frequently encountered in practice, the design of brittle structures must be prevented.

The limiting strain of 0.035 was obtained from ASTM A416 [25] and applies to both stress-relieved and low relaxation strands. Preston [107], however, states that strand can generally sustain an elongation of 0.045 or more before failure. However, even this elongation is well below the 0.060 strain indicated by analysis to occur at a deck strain of 0.003 for the typical span designs with GS = 10 ft. The top-of-deck strains could be expected to reach 0.003 in these cases because a large strain gradient would be present in the

deck near ultimate since the neutral axis is located within the deck. It is helpful to put the limiting strain for strands in perspective by noting that the minimum elongation (limiting strain) for new billet Grade 60 deformed bars varies from 0.07 to 0.09 (ASTM A615, [25]) and that deformed bars made of rail steel need an elongation of only 0.045 to 0.06 to meet the specification (ASTM A616, [25]). While these values are minimums, the high strength steel in strands is generally accepted to be more brittle than mild steel reinforcement.

Further consideration of the problem of an effective minimum reinforcement ratio in the context of overall member behavior will be given later in the section on ductility.

7.4.5.4 Effect of Concrete Modulus. In this section, the effect of the concrete modulus on the design and ultimate capacity of selected girder designs will be considered. The equation for estimating the modulus currently found in the codes [10,15]

$$E_c = 33 w_c^{1.5} \sqrt{f'_c} \text{ psi} \tag{7.4a}$$

$$= 57{,}000 \sqrt{f'_c} \text{ psi (for normal wt. conc.)} \tag{7.4b}$$

where w_c = unit weight of concrete, lb per cu ft

will be compared with the equation for normal weight concrete proposed by investigators at Cornell [82]

$$E_c = 40{,}000 \sqrt{f'_c} + 1{,}000{,}000 \text{ psi} \tag{7.5}$$

The two equations are plotted in Fig. 7.1.

The effect of the modulus on the design of a composite member is related to the ratio of deck to girder moduli since this is the ratio used to transform the deck concrete. This ratio is plotted versus the girder concrete strength for the two modulus equations in Fig. 7.46 using a constant deck concrete strength of 4 ksi. The percentage difference between these ratios, and the percentage difference between moduli for the two equations for a given concrete strength are shown in Fig. 7.47. These quantities vary less than 15 percent for concrete strengths considered in this study. The effect of using the different moduli on transformed section properties for different girder spacings and for different concrete strengths is shown in Fig. 7.48 and 7.49, respectively. These figures show that the moment of inertia is affected by less than 5 percent in both comparisons and that the section modulus for the bottom of the girder changes less than 2 percent. The top-of-girder section modulus, which is the most affected of all section properties, changes by as much as 12 percent.

When a design was performed using the two modulus equations, it was found that the difference was negligible. Using girder spacings of 4 and 10 ft with f'_{cg} = 12 ksi, the maximum spans differed by only one foot. The ultimate behavior was also compared using the strain compatibility analysis and the results were nearly indistinguishable, with ultimate moment capacities varying by at most

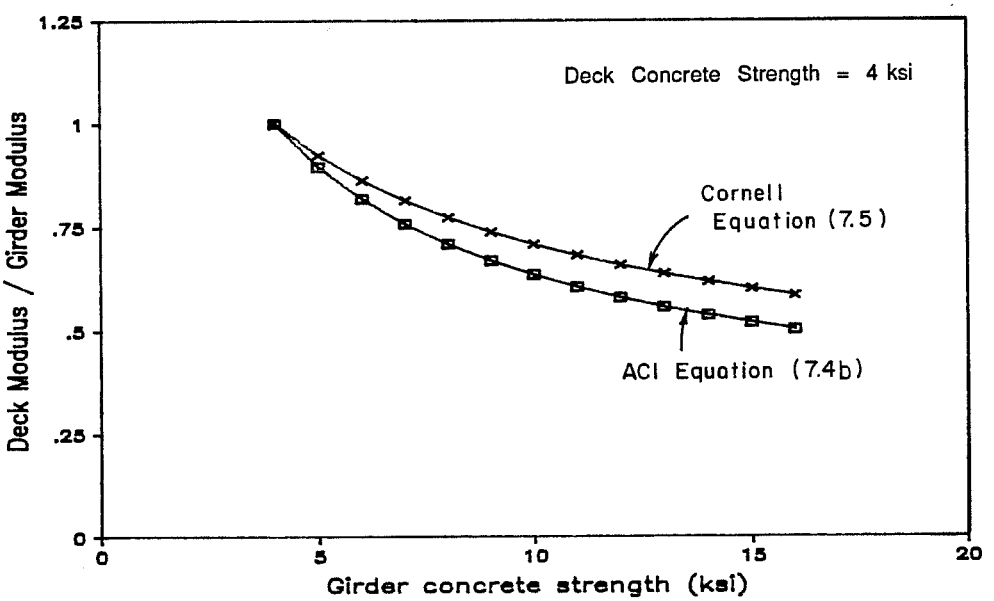

Fig. 7.46 Ratio of deck modulus to girder modulus for increasing concrete strength

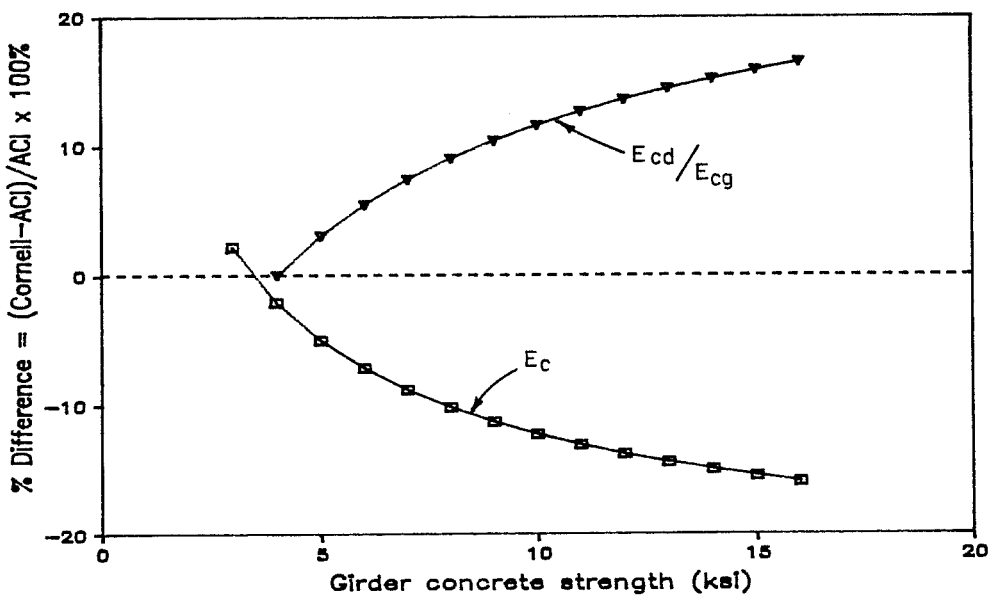

Fig. 7.47 Percentage difference between modulus equations for modulus and ratio of deck to girder moduli

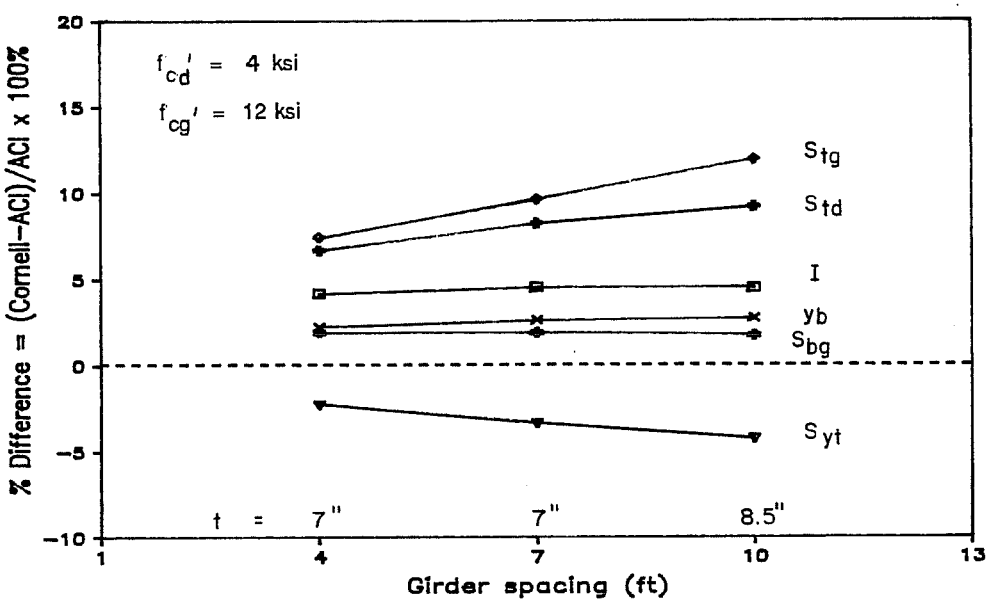

Fig. 7.48 Effect of modulus equations on section properties for different girder spacings

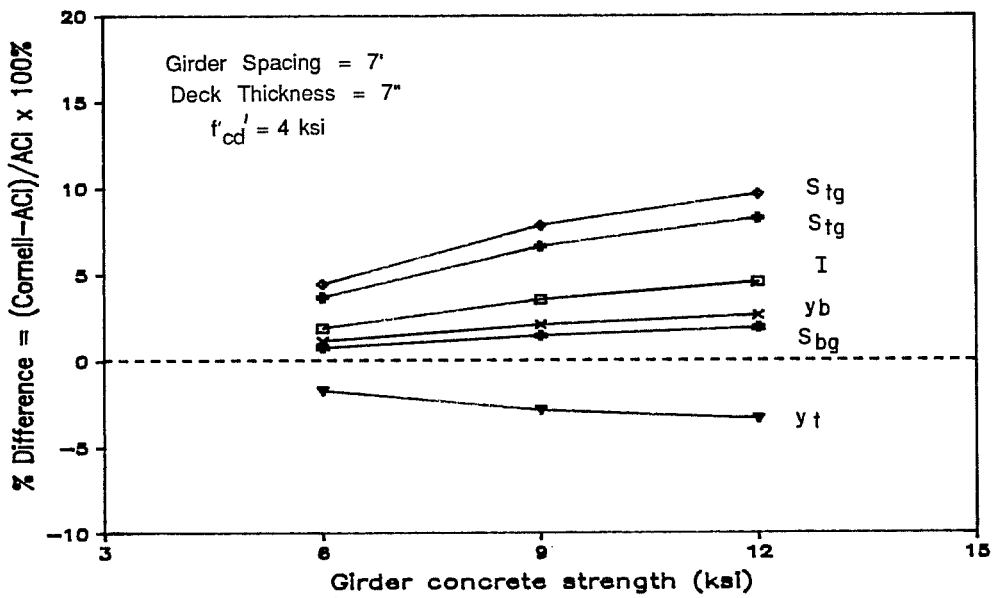

Fig. 7.49 Effect of modulus equations on section properties for different girder concrete strengths

0.5 percent and the strand stress at ultimate differing by at most 0.25 percent. The depth to the neutral axis varied most with a 10.8 percent difference between the designs using the different modulus equations. The modulus does not affect ultimate capacities computed using the simplified methods.

A comparison of deflections was made for the same designs. For a beam constructed only of high strength concrete, the computed deflections would be 16 percent greater using the Cornell equation. However, for a composite, pretensioned bridge, the comparison is not as straightforward because the modulus affects losses and the effect of the deck in the composite structure differs according to the modulus of the girder. For the 120 ft spans with GS = 10 ft, the initial camber was 12.3 percent greater and the live load deflection was 9.8 percent greater for the Cornell equation. The comparison for the 159 ft span, which was not as clear because two fewer strands could be used for the design using the Cornell equation, indicated a 4.2 percent increase in the live load deflection but the initial camber decreased by 1.1 percent when the Cornell equation was used. These comparisons indicate deflections are more sensitive to changes in the modulus than the allowable stress design and ultimate capacity and that the effect of the modulus on deflections decreases as the span increases.

This analysis shows that the differences between designs using the two equations for concrete modulus of elasticity are minor. Therefore, a decision on which equation should be used is not critical and should be postponed until more data becomes available to determine whether the Cornell equation or some other expression will provide a better estimate of the modulus than the formula in current use.

7.4.5.5 Concrete Strength Required at Release. A study of the minimum release strength required to satisfy design criteria was conducted for both maximum and typical span designs. The results are presented in Fig. 7.50. The first part of the figure shows the minimum concrete strengths required at release for the 12 designs considered. In all cases, the span length and number of strands used for the initial design, which used $f'_{ci} = 0.75\ f'_{cg}$ except where this was inadequate for some of the 6 ksi designs, were maintained. In the case of the maximum span design with GS = 4 ft and f'_{cg} = 12 ksi, two designs were considered when it was found that the release strength could be reduced further by the addition of strands beyond the number required for the initial design. For the typical span designs, the minimum release strength actually decreased or remained constant as the design strength was increased, while the required minimum release strength for maximum span designs was found to increase with increases in the design strength.

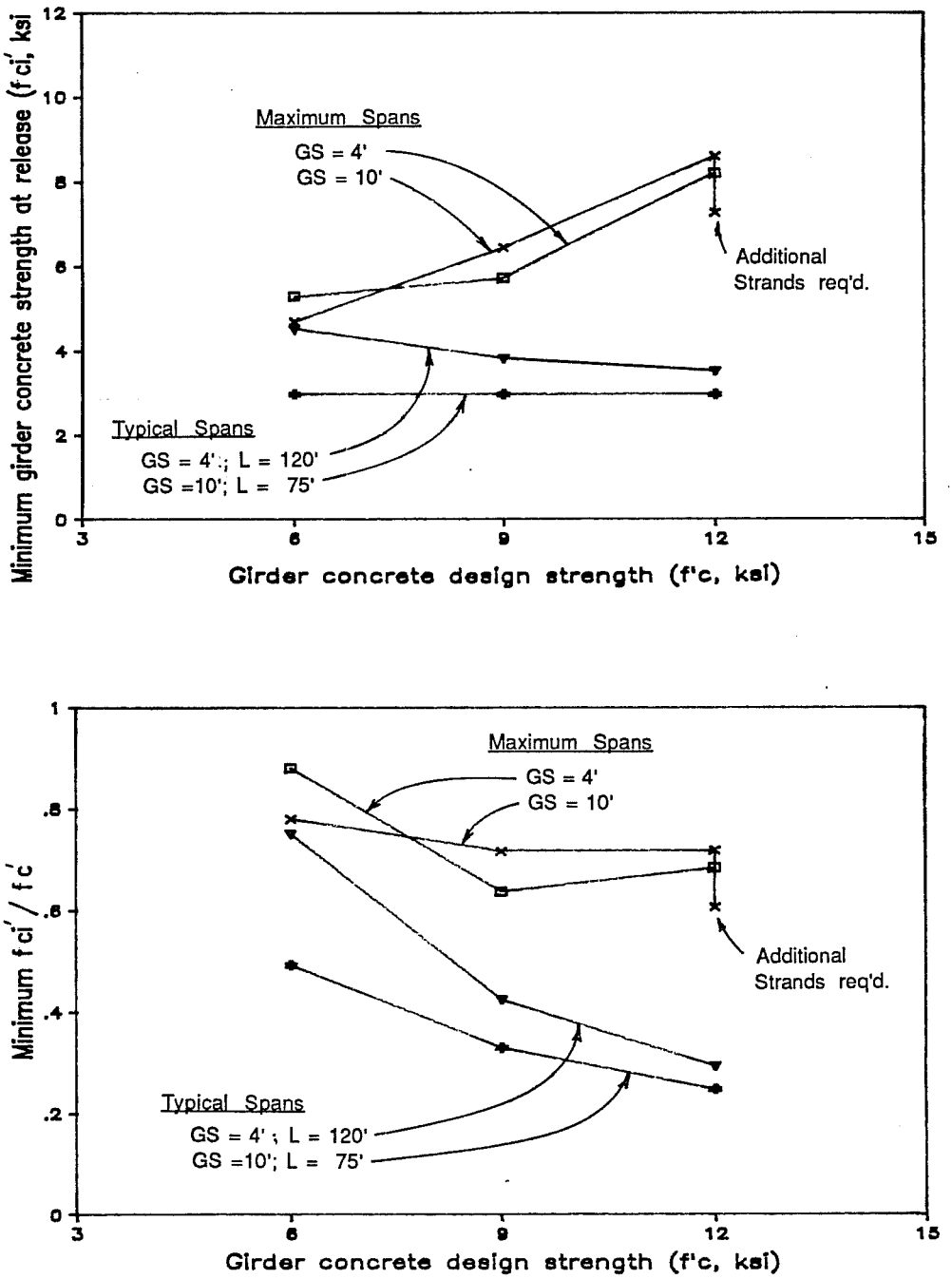

Fig. 7.50 Relationship between minimum concrete strength at release and design concrete strength for maximum and typical span designs: a) Minimum required concrete strength at release; b) Minimum release strength as fraction of design strength

The second portion of Fig. 7.50 shows the minimum release strengths as a fraction of the design strength. The higher design strength concrete generally requires a smaller portion of its strength to be available at release, although the reduction is small for the maximum span designs which are more typical of actual practice. For the typical span designs, the release strength could be as low as 25 percent of the 28 day strength. This would be of great benefit to the precast producers.

7.4.5.6 Summary. The following observations are made to summarize the discussion in the preceding sections.

1. Ultimate load criteria will govern most designs rather than the 1.2 M_{cr} limit.
2. An overload of 2.5 to 3 times the live load including impact is required to reach the factored load capacity for the range of designs considered if the dead load is held constant.
3. The cracking moment should be calculated considering all dead load effects rather than using an approximate form which neglects dead load.
4. The capacity for the range of designs considered remains nearly constant for a wide range of top-of-deck strains including 0.0022 to 0.003.

5. Analysis shows that strand may reach the minimum ASTM specified elongation (limiting strain) prior to the top of deck reaching the maximum usable concrete strain.
6. The simplified analysis methods using current assumptions for the ERSB agreed well with ultimate capacities computed using the strain compatibility analysis for a range of concrete strengths including high strength concrete.
7. The computed nominal capacity for the range of designs considered was generally significantly larger than the controlling ultimate load. In cases of short spans, however, the ultimate load controlled design.
8. Analysis indicates that it is possible to obtain a stable "semi-flanged" behavior condition in which, for a wide range of top-of-deck strains, the top of the girder remains in compression after the bottom of the deck has cracked.
9. The maximum moment frequently occurs at a top-of-deck strain less than the maximum usable concrete strain (0.003), but always greater than 0.0022 for the designs studied here.
10. The use of a maximum usable strain of 0.003, while sufficiently accurate for ultimate capacity

may lead to unconservative estimates for quantities such as curvature, depth of compression, and strand strain.

11. It is unlikely that the girder concrete would crush prior to the deck concrete in the designs considered here.
12. The strand stress remained fairly constant for the range of top-of-deck strains considered (0.0022 to 0.003).
13. In all designs, the strand stress computed using the strain compatibility analysis exceeded the specified yield stress at ultimate.
14. The simplified methods provided conservative, yet reasonable estimates of the strand stress at ultimate when compared with the strain compatibility analysis results. The current ACI ultimate strand stress equation provided a better estimate of strand stress at ultimate than the AASHTO equation, especially for high reinforcement ratios.
15. The reduction of the ultimate capacity when the reinforcement index exceeds specified limits appears to be over-conservative.
16. The current minimum reinforcement limit involving the cracking moment is not sufficient to prevent rupture of

strands before the top of the deck has reached the maximum usable concrete strain. This situation occurred in very lightly reinforced girders which may not be considered typical designs.

17. The effect of using the concrete modulus equation given in the codes or proposed by investigators at Cornell is small for both allowable stress design and strength analysis using the strain compatibility method. Deflections were affected more strongly, but the difference became small at the maximum span length. Therefore, a change in equation does not appear warranted until further study can be made.

18. The minimum concrete strength required at release may be as low as 25 percent of the design strength for high strength concrete and is typically less than that required using normal strength concrete. However, the minimum release strength remains a fairly constant fraction of the design strength for designs at or near the maximum span for a given concrete strength, which are more typical of current design practice. Any reduction in the release strength relative to the design strength would be an advantage in the manufacture of pretensioned members.

While not directly studied in this section, it is recommended that a maximum usable concrete strain of 0.003 be used for composite sections where the neutral axis is within the deck at ultimate, and a maximum usable concrete strain of 0.0022 46 to 0.0025 be used where the neutral axis is located within the girder at ultimate. The difference is a result of the strain gradient present at failure, which would be great for the first situation in which the concrete near the extreme fiber, which is not as highly stressed, would offer confinement to the extreme fiber concrete. However, when the girder is in compression at failure, the compression in the deck is more uniform and the confining effect would not be as great. Further study of this problem is needed.

7.5 Ductility

While ductility can be defined in many ways, the historic approach taken for prestressed and reinforced concrete members to ensure a ductile failure is the limitation of the quantity of reinforcement. Limits based on the reinforcement ratio have apparently worked well and they avoid the difficulties encountered when curvatures or deflections are used as a measure of ductility for a prestressed section or member.

This section opens by investigating the accuracy of the reinforcement index computed using the simplified methods when

compared with results of strain compatibility analyses. Proposals are then made for both maximum and minimum reinforcement limits that are based on the same reasoning as the original maximum reinforcement limits. The limits will be compared with test and analytical data to determine the adequacy of the limits.

7.5.1 Accuracy of Reinforcement Index for Simplified Methods. Since reinforcement limits for prestressed members are based on the reinforcement index, the accuracy of this quantity was investigated. Because values of the reinforcement index computed using the AASHTO and ACI simplified methods differ only by the estimate for the ultimate strand stress, the ACI equation 47 will be used since it is more accurate. Flanged section analysis is used in both codes to compute the reinforcement index when the neutral axis is located below the deck at ultimate.

The reinforcement index, ω_p, computed using the equation

$$\omega_p = \rho_p f_{ps} / f'_c$$

was determined for each maximum and typical span design using the ACI simplified method and results of the strain compatibility analysis. The two values are compared graphically in Fig. 7.51 for both gross section (Cases I and II) and transformed section (Cases III and IV) approaches. The plots include data from Naaman et al. [97] for monolithic rectangular and T-beam sections for a range of concrete strengths. The data is closely clustered about the line of equality

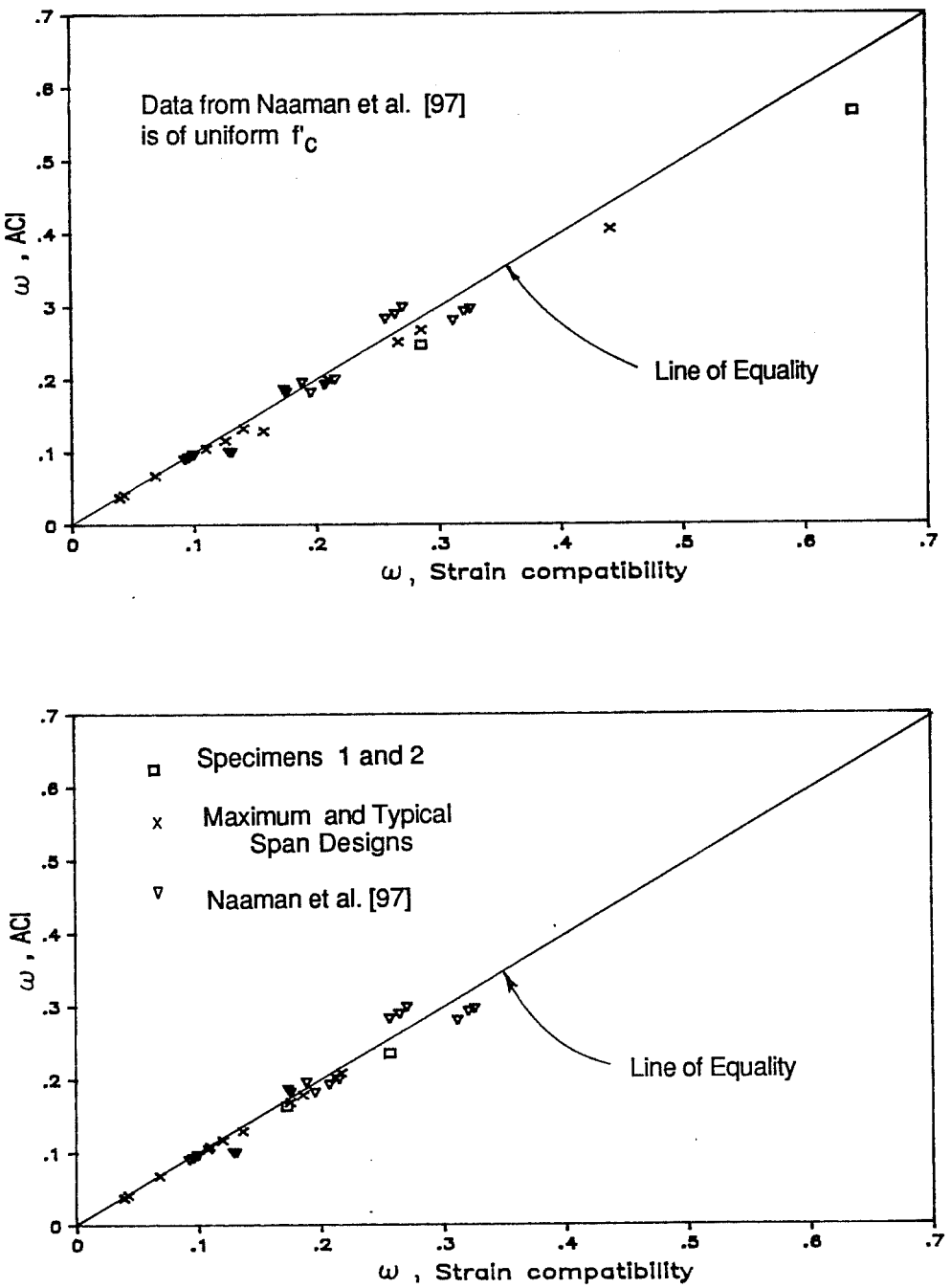

Fig. 7.51 Comparison of w computed using simplified ACI approach and strain compatibility analysis: a) Gross section dimensions - Cases I and II; b) Transformed section dimensions - Cases III and IV

for data from both the current study and Naaman et al. [97]. Agreement is similar for the different cases of gross and transformed section dimensions. This demonstrates that the simplified methods give good estimates of the actual reinforcement ratio and will therefore provide reasonable estimates for use with limits. Use of the AASHTO equation will, however, give unconservative estimates since the AASHTO estimate of ultimate strand stress is low. The comparison with Naaman's data indicates that agreement between the simplified method and strain compatibility analysis is consistent for monolithic and composite members.

The effect of nonprestressed tension reinforcement and compression reinforcement can be included in the reinforcement index. The expression proposed by Naaman et al. [97]

$$\omega = \left[A_{ps}f_{ps} + A_s f_s - A_s' f_s' - 0.85\beta_1 f_c' h_f (b-b_w) \right]/(b_w d f_c') \qquad (7.6)$$

appears to be suitable, although it was derived using a slightly different definition of the effective depth.

7.5.2 Maximum Reinforcement Limit. Current and proposed limits on the reinforcement index are discussed and are then compared with test and analytical data to determine the adequacy of the limits.

7.5.2.1 Current and Proposed Limits. For reinforced concrete sections, a maximum allowable reinforcement ratio is set by limiting

the percentage of steel to three-quarters of that required to produce a balanced failure, i.e.,

$$\rho = A_s/bd \leq 0.75\ \rho_b$$

where ρ_b = reinforcement ratio corresponding to a balanced failure.

By definition, a balanced failure occurs when the strain in the extreme compression fiber reaches the maximum usable concrete strain as first yielding of the steel occurs. The reinforcement ratio corresponding to balanced failure can be computed for rectangular sections using the following equation

$$\rho_b = \beta_1 0.85 f'_c/f_y[87/(87+f_y)] \tag{7.7}$$

where stresses are expressed in ksi units, which is given in the Commentary of the ACI Code [17].

For prestressed concrete members, a slightly different approach is taken in which the reinforcement index,

$$w_p = \rho_p f_{ps}/f'_c$$

where ρ_p = ratio of prestressed reinforcement

$= A_{ps}/bd_p$

must be less than a limiting value which is intended to correspond to the balanced failure condition. For prestressed members, the definition of a balanced failure is not as clear as for reinforced members because the yield point for prestressing steel is not as well defined as that for reinforcing bars. The motivation for the

different approach for prestressed sections was discussed in Sec. 3.5.1 and appears to be reasonable.

The assumptions used to derive the current maximum reinforcement limits are summarized in Fig. 7.52, which also includes an early proposal by Warwaruk et al. [133] which never appeared in the codes. As shown in the figure, the maximum reinforcement limits for both AASHTO and ACI are based on an approximate strain compatibility analysis of a section at ultimate. The top fiber strain was assumed to be 0.004 which is inconsistent with the maximum usable strain specified elsewhere in the codes and significantly exceeds the strains measured in the scale-model tests. The limits also assume a yield strain of 0.01 and an average of typical values for the effective prestress which were based on the use of Grade 250 strand.

The new proposal, which follows the same reasoning as the current limits, is also shown in Fig. 7.52. A more complete development of the limit is given in Appendix D.1. The equation expressing the new limit is

$$\omega_p \leq 0.85\beta_1[84/(114 + f_{pu} - f_{se})] \tag{7.8}$$

where f_{pu} and f_{se} are expressed in ksi. This equation, while more complex than current limits, considers important parameters that are neglected in the current limits and corrects assumptions that are

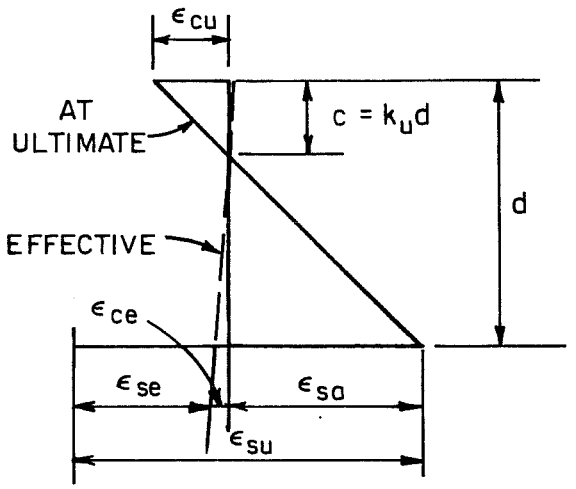

$$k_u = \frac{F\epsilon_{cu}}{F\epsilon_{cu} + \epsilon_{sa}}$$

$$= \frac{F\epsilon_{cu}}{F\epsilon_{cu} + \epsilon_{su} - \epsilon_{se} - \epsilon_{ce}}$$

$$= \rho \frac{f_{su}}{f_{cu}}$$

$$= c/d$$

	Warwaruk et al. 1962	ACI Comm 323 (current AASHTO) 1958	ACI 318-83 1983	Proposal
Reference	[133]	[10, 19]	[15]	Appendix D
F	1	1	1	1
ϵ_{cu}	0.003	0.004	0.004	0.003
ϵ_{su}min.	0.01*	0.01*	0.01*	$0.01+(f_{pu}-250)/28000$
ϵ_{se}	0.0045**	0.0045**	0.0045**	$f_{se}/28000$
ϵ_{ce}	0	0	0	0
$k_u$limit	≤ 0.353	≤ 0.421	≤ 0.421	$\leq 84/[114+f_{pu}-f_{se}]$
f_{cu}	$0.7f'_c$	$0.7f'_c$	$0.85\beta_1 f'_c$	$0.85\beta_1 f'_c$
ω	0.25	0.30	$0.36\beta_1$	$0.85\beta_1[84/(114+f_{pu}-f_{se})]$

* - Based on Grade 250 material.

**- An average of the expected range from 0.004 to 0.005.

Modules of strand is assumed to be 28000 ksi. Stress units in ksi.

Fig. 7.52 Summary of maximum reinforcement limit assumptions

inconsistent with the remainder of the current codes. The maximum usable concrete strain of 0.003 used in the derivation of the proposed limit agrees with the requirements of the ERSB. While this strain may be larger than the actual strain in some cases as mentioned in preceding sections, use of 0.003 is an improvement over the current limit and this value can be modified as needed by the designer or code writers if the derivation of the limit is made available in code documents. Since Grade 270 strand is now in general use and further increases in strength are possible, the yield strain was expressed as a function of the ultimate strength of the strand in order to reflect the changing shape of the stress-strain curve. Although current limits assume a fixed value for the effective prestress, variation in the effective prestress was found to have a significant effect on the limit and is therefore included in the expression. Since the effective prestress is known in design, its inclusion in the equation is not a large complication. The proposed equation appears in a form that is very similar to the equation used to determine the limiting reinforcement ratio for reinforced concrete sections (Eq. 7.7) and should therefore be easily understood and accepted by the profession. The derivation of the limit is based on a monolithic section and is therefore an estimate of the behavior for a composite section, since the difference in curvature between the

girder and deck is not included in the analysis. However, this error is small.

It was found that the current limits can be unconservative when compared with the more accurate and consistent proposed limit. This is because existing limits use a high limiting concrete strain and neglect variation in the effective prestress. The existing AASHTO and ACI limits are compared with the proposed limit for low and high strength concrete and three grades of strand in Fig. 7.53. The unconservatism of the current limits for some values of effective prestress and the substantial effect of variation in the effective prestress and grade of strand is evident. The effect of the concrete strength on the limits is removed to facilitate comparison with the ACI limit in Fig. 7.54, and the ratio of the proposed limit to the ACI limit is shown in Fig. 7.55. In Fig. 7.55, it can be seen that for lower effective prestress levels and for increasing strand strength current limits become more unconservative. For the effective prestress encountered in the designs considered in this chapter, which varied from 156 ksi to 182 ksi, the proposed limit for Grade 270 strand is from 87 to 98 percent of the current ACI limit. Therefore, the unconservatism of the current limit is not great and conversely, the proposed limit does not vary greatly from the current limit.

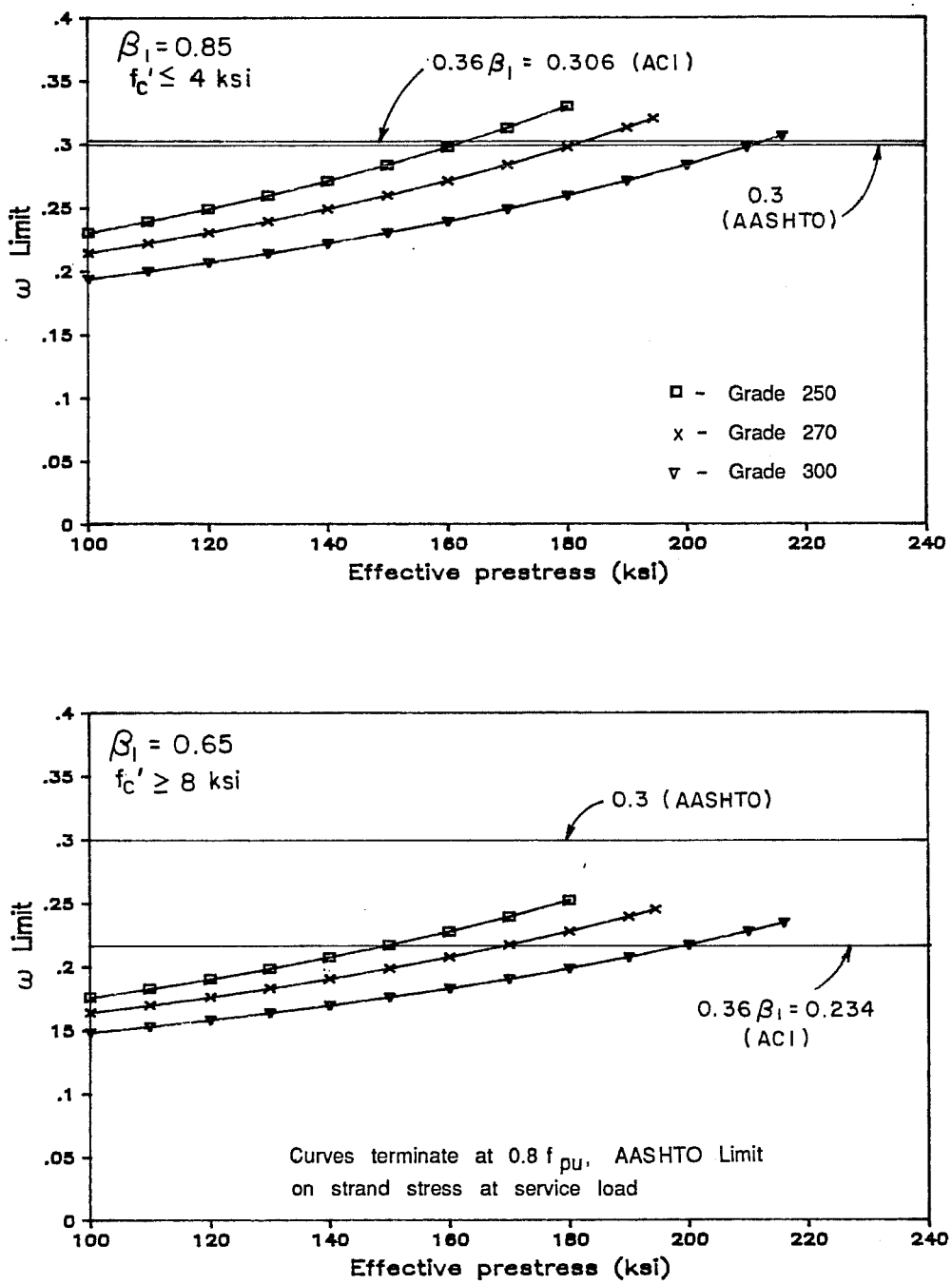

Fig. 7.53 Maximum reinforcement limits versus effective prestress: a) Low strength concrete - $f'_c \leq 4$ ksi; b) High strength concrete - $f'_c \geq 8$ ksi

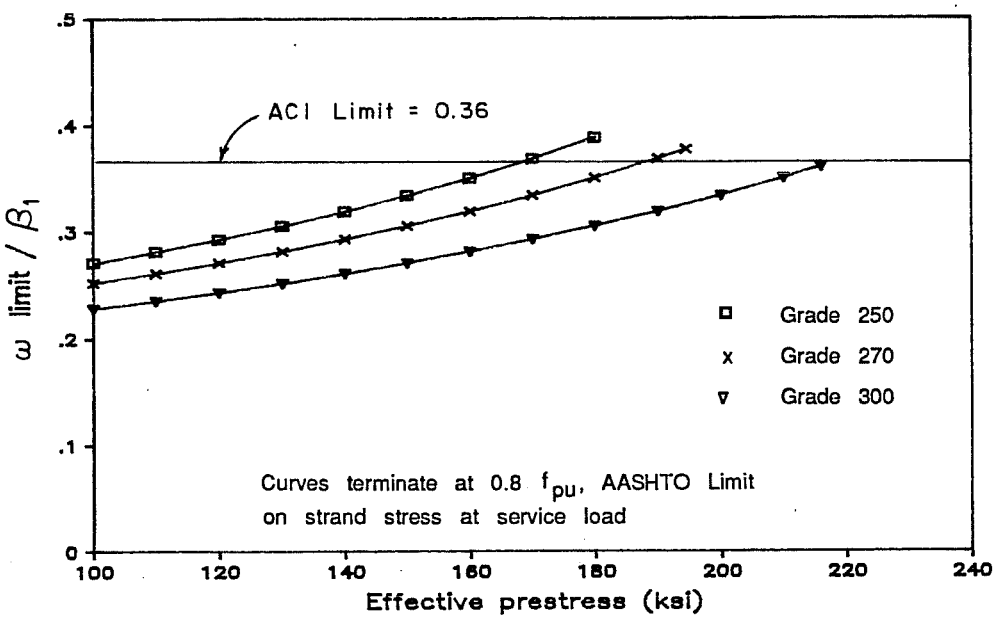

Fig. 7.54 Ratio of maximum reinforcement limit to β_1 versus effective prestress

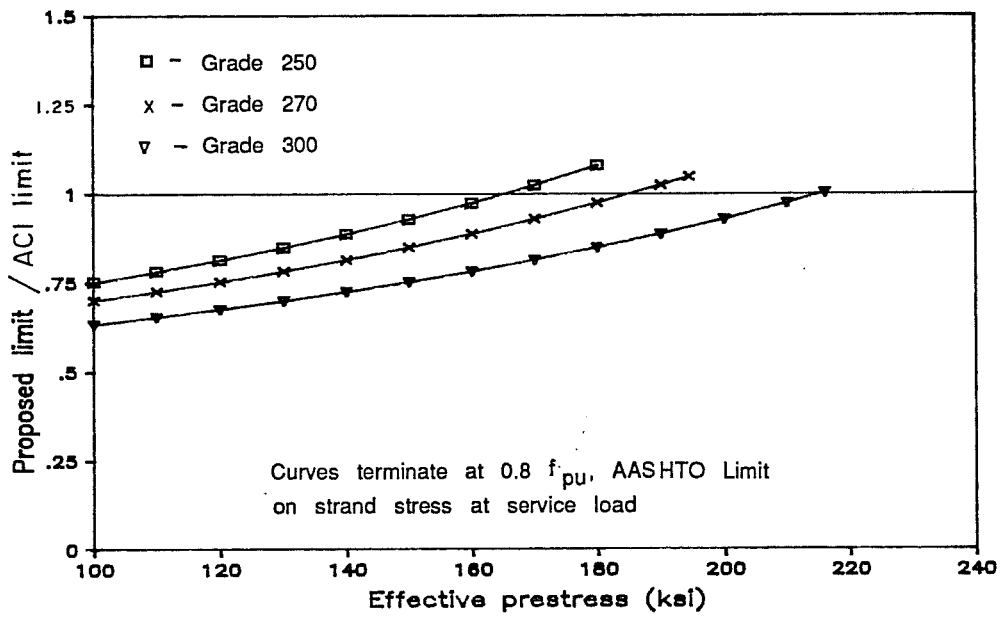

Fig. 7.55 Ratio of proposed maximum reinforcement limit to ACI limit versus effective prestress

7.5.2.2 Accuracy of Maximum Reinforcement Limit. Two factors are of interest in exploring the accuracy of the maximum reinforcement limit: determination of the best method to use for computing the reinforcement index, ω and whether the limit accurately or conservatively predicts yielding of the strand.

The need for the determination of appropriate assumptions to be used to compute ω is clear from the variety of values and their relationship to the limits displayed in Fig. 7.56 for the test specimens and maximum span designs with GS = 4 ft. The designs shown in the figure were the only designs where ductility limits were of concern. The confusion is greatest for Specimen 1 and for the 12 ksi maximum span design. In these cases, the limits were exceeded by a large margin for the untransformed cases (AASHTO and ACI Cases I and II) which indicated that failure would be expected well before yielding of the strand.

Examination of Fig. 7.57, which gives the increase in strand strain for the specimens during flexure tests, indicates that failure occurred just after reaching the yield strain. Similar curves for the 12 ksi maximum span designs, which include the case with GS = 4 ft mentioned above, appear in Fig. 7.58 and indicate definite straining of the strand past yield prior to failure. Therefore, the untransformed values of ω are over-conservative. The transformed cases (ACI Cases III and IV) appear to be more reasonable

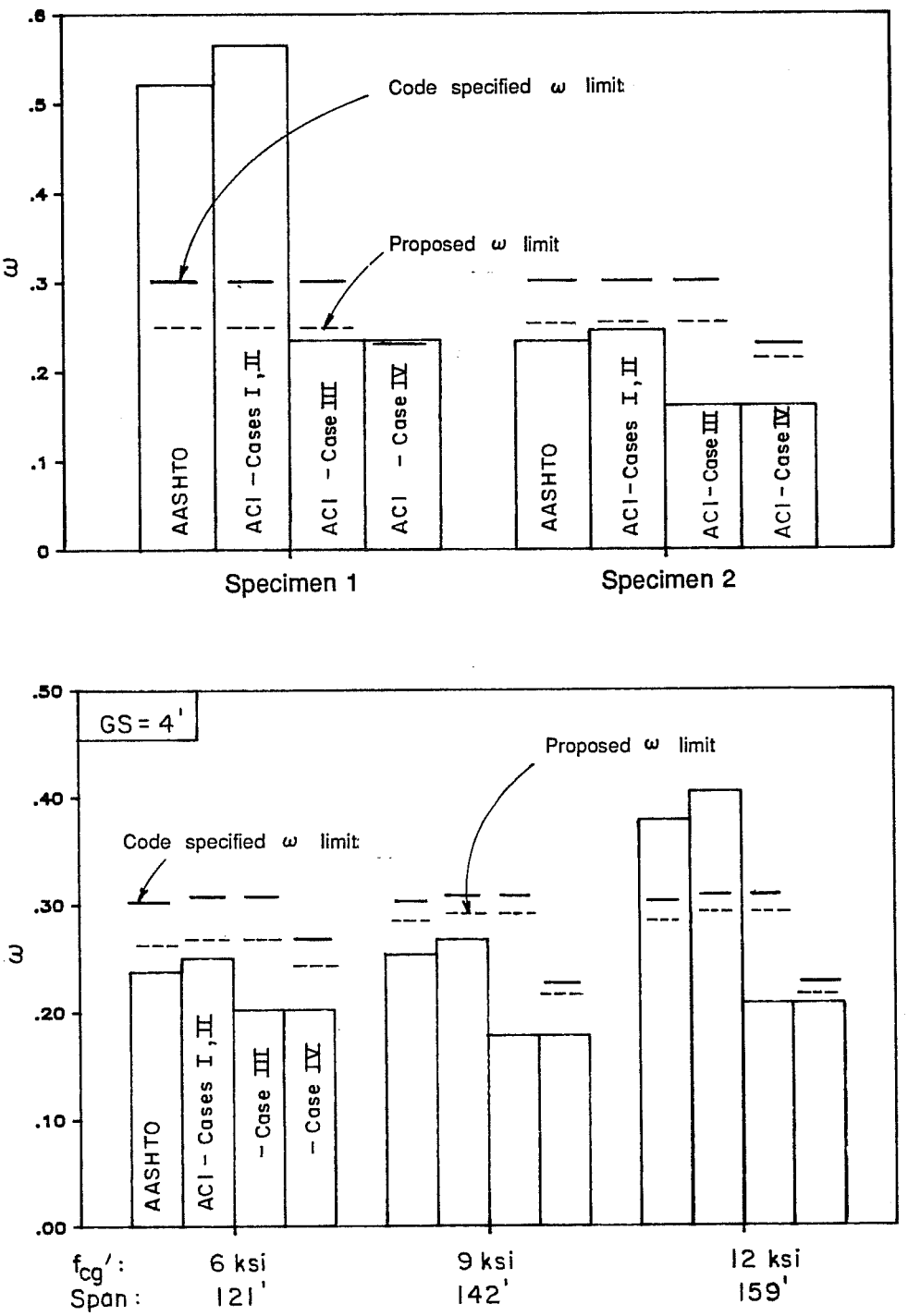

Fig. 7.56 Comparison of values and maximum limits for w for specimens and maximum span designs with GS = 4 ft

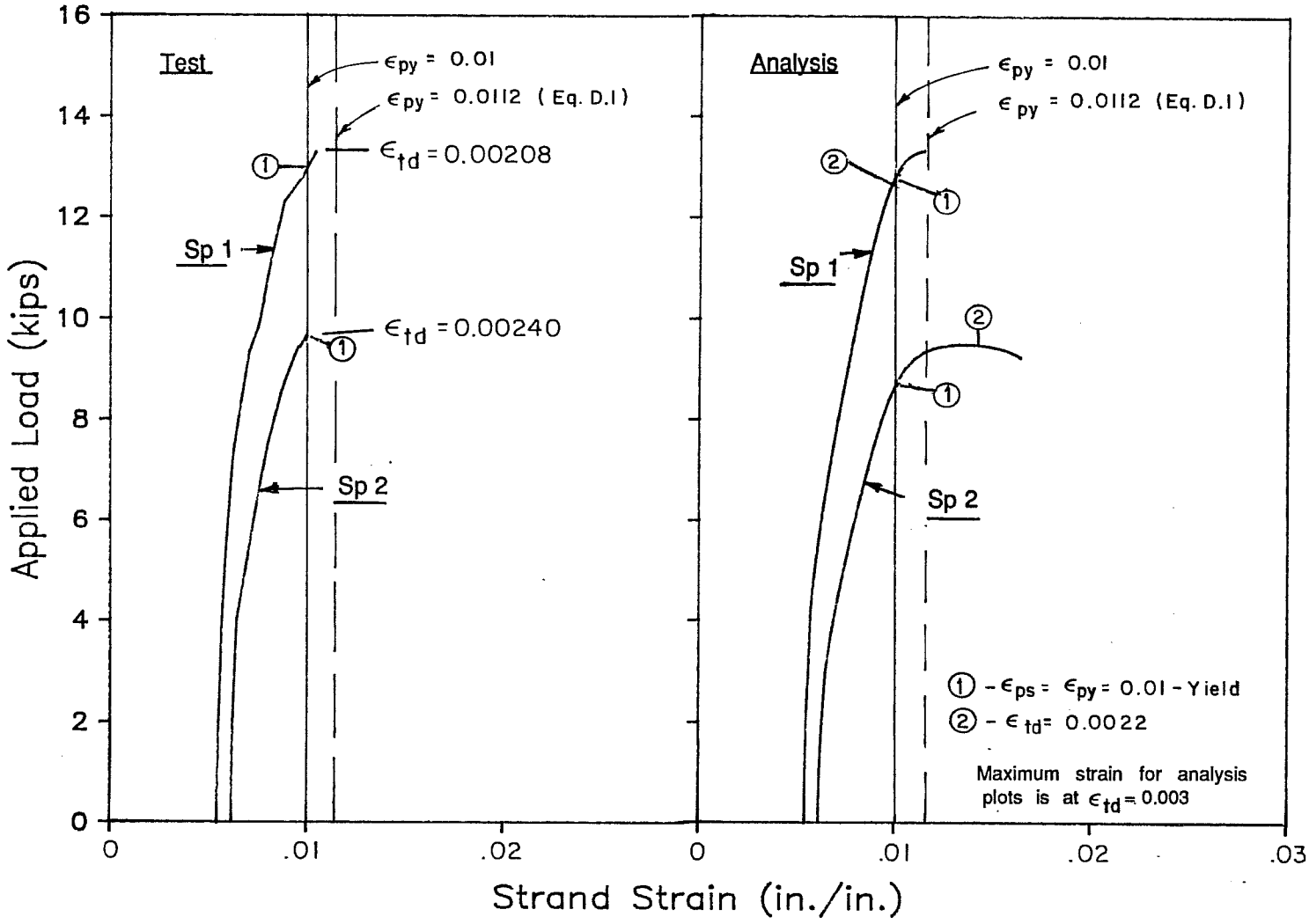

Fig. 7.57 Strand strain versus applied load for specimens

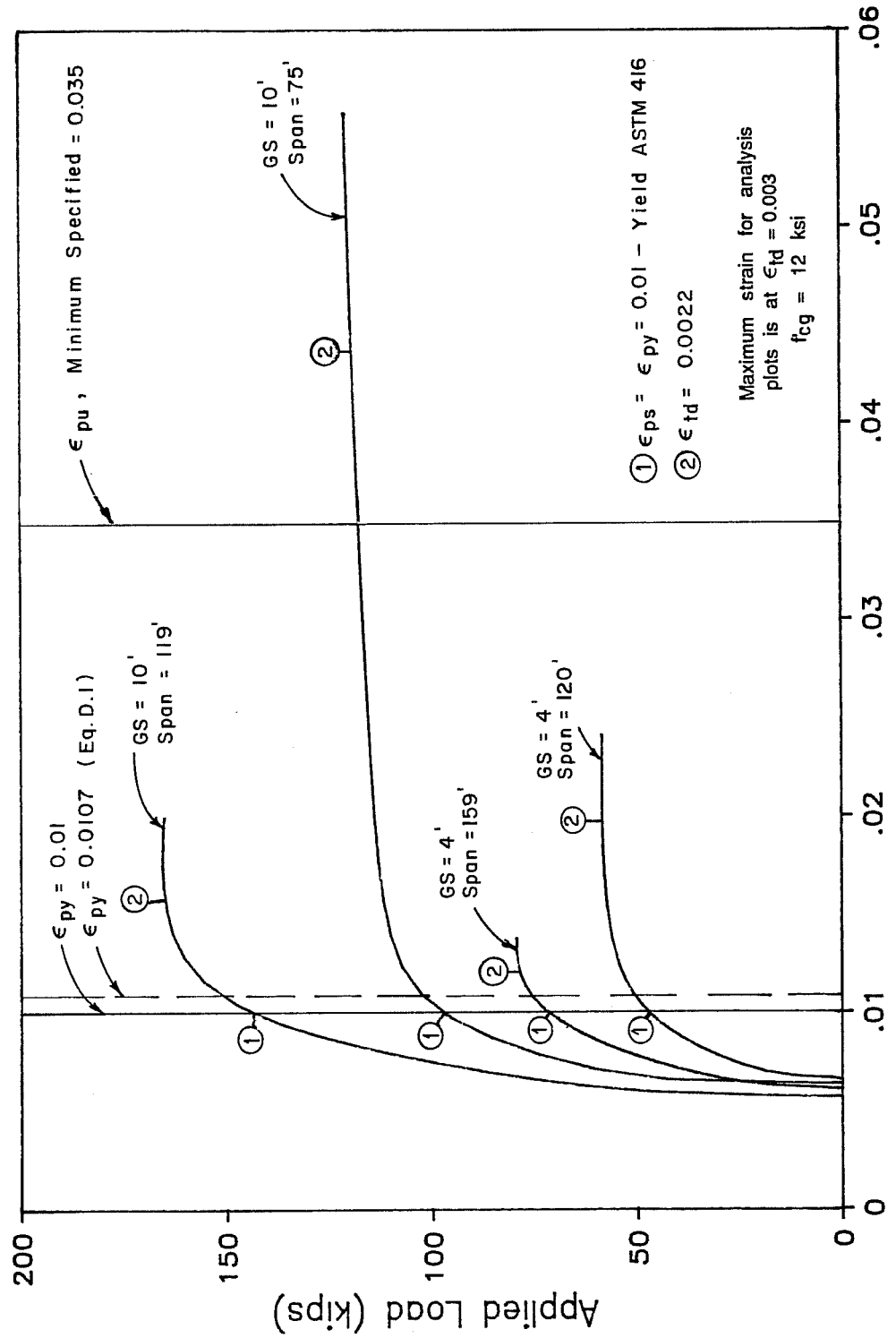

Fig. 7.58 Strand strain versus applied load for maximum and typical span designs with f'_c = 12 ksi

representations of behavior, indicating that yield was still reached or was very close to being attained. Of the two transformed cases, Case III appears to be the more accurate because it correctly predicts that yielding, although limited, would occur in both Specimen 1 and the 12 ksi maximum span design. It is also clear from this comparison that the proposed limit is a better approximation of behavior for Case III, since, for Specimen 1, ω is very close to the limit as is the case based on the test and analytical data.

Another comparison which demonstrates that the transformed methods are more accurate is shown in Fig. 7.59. This comparison is based on findings by Naaman et al. [96,97] that, for a wide variety of monolithic rectangular and T-beam sections with a range of concrete strengths and prestressed and nonprestressed reinforcement, the ratio of the depth of the compression zone at ultimate to the effective depth is linearly related to the reinforcement index. The regression equation they developed is shown in the figure. When values for the specimens and designs used in this chapter are added to these plots, it can be seen that data points with ω computed using gross section dimensions do not conform to the trend observed by Naaman, while points using transformed dimensions conform very well. Therefore, it is recommended that ω be computed using section dimensions transformed by the ratio of the concrete strengths of the deck and

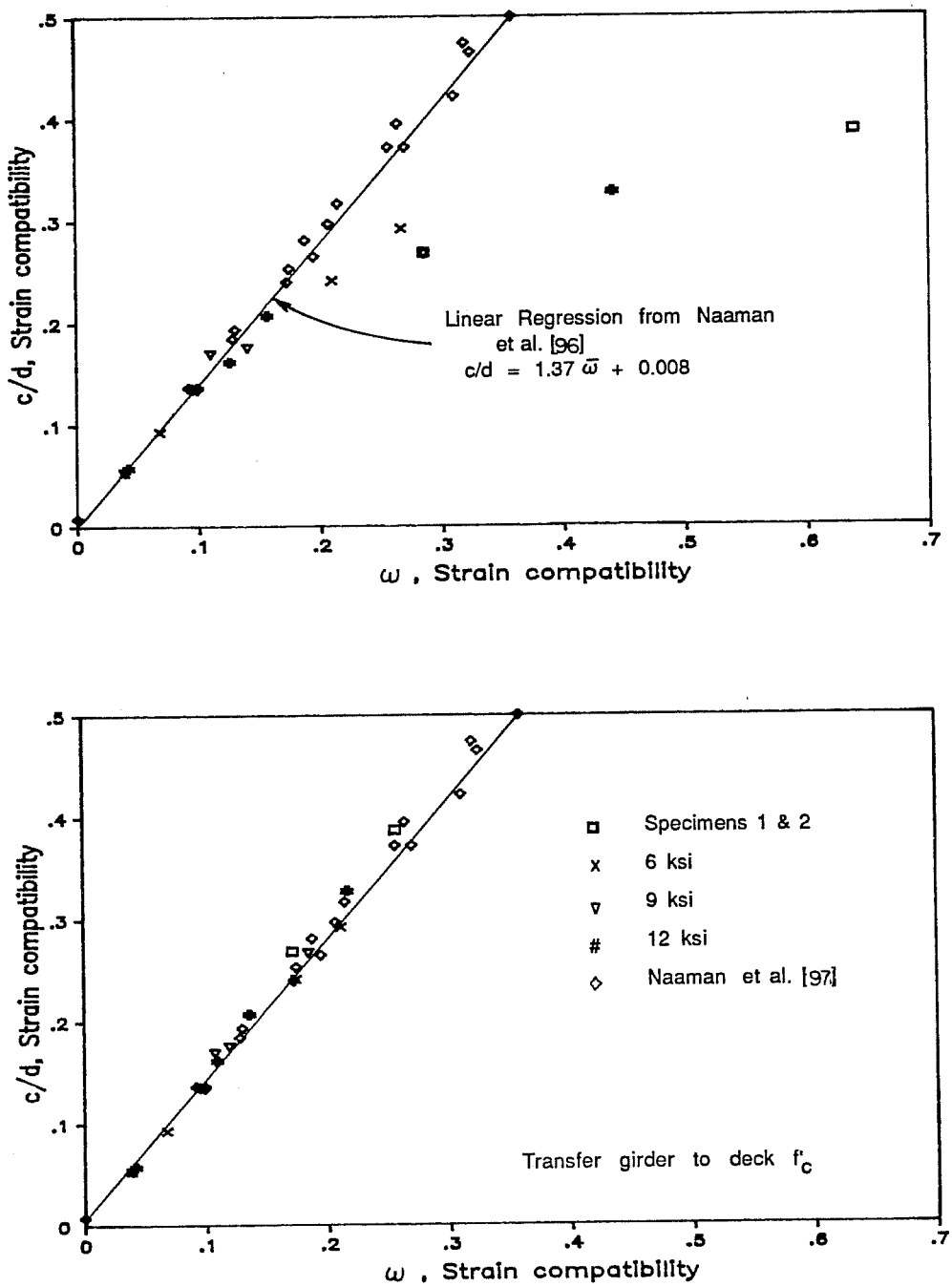

Fig. 7.59 Variation of c/d with ω from of strain compatibility analysis: a) ω computed using gross section dimensions; b) ω computed using transformed section dimensions

girder so that predicted behavior for composite sections will conform to behavior of monolithic sections.

A final series of comparisons is made using Fig. 7.60, 7.61 and 7.62, which show the ratio of the ultimate strand strain to the yield strain versus the corresponding ratio of ω to the ω limit for Cases I and II, Case III, and Case IV, respectively. The yield strain is defined by the function of the ultimate strength of the strand as used in the proposed limit (Eq. 7.8) and discussed in Appendix D.1. Points plotted in the figures represent the test specimens and all maximum and typical span designs. Data for the maximum and typical span designs are connected with a curve to indicate the trend of the data. The strain ratio should approach unity as the ω ratio approaches unity if the limit is accurate. The ω limit is conservative if the strain ratio is greater than unity when the ω ratio is one, because this indicates that the strand is actually yielding even though the ω limit has been reached. Data for Cases I and II (Fig. 7.60) demonstrate the conservatism of the use of gross section dimensions. Data for Case IV in Fig. 7.62 is also conservative. The data shown in Fig. 7.61 for Case III appears to best fit the desired behavior.

The maximum reinforcement ratio for prestressed members appears to represent the balanced failure condition ($\rho/\rho_{bal}=1$)

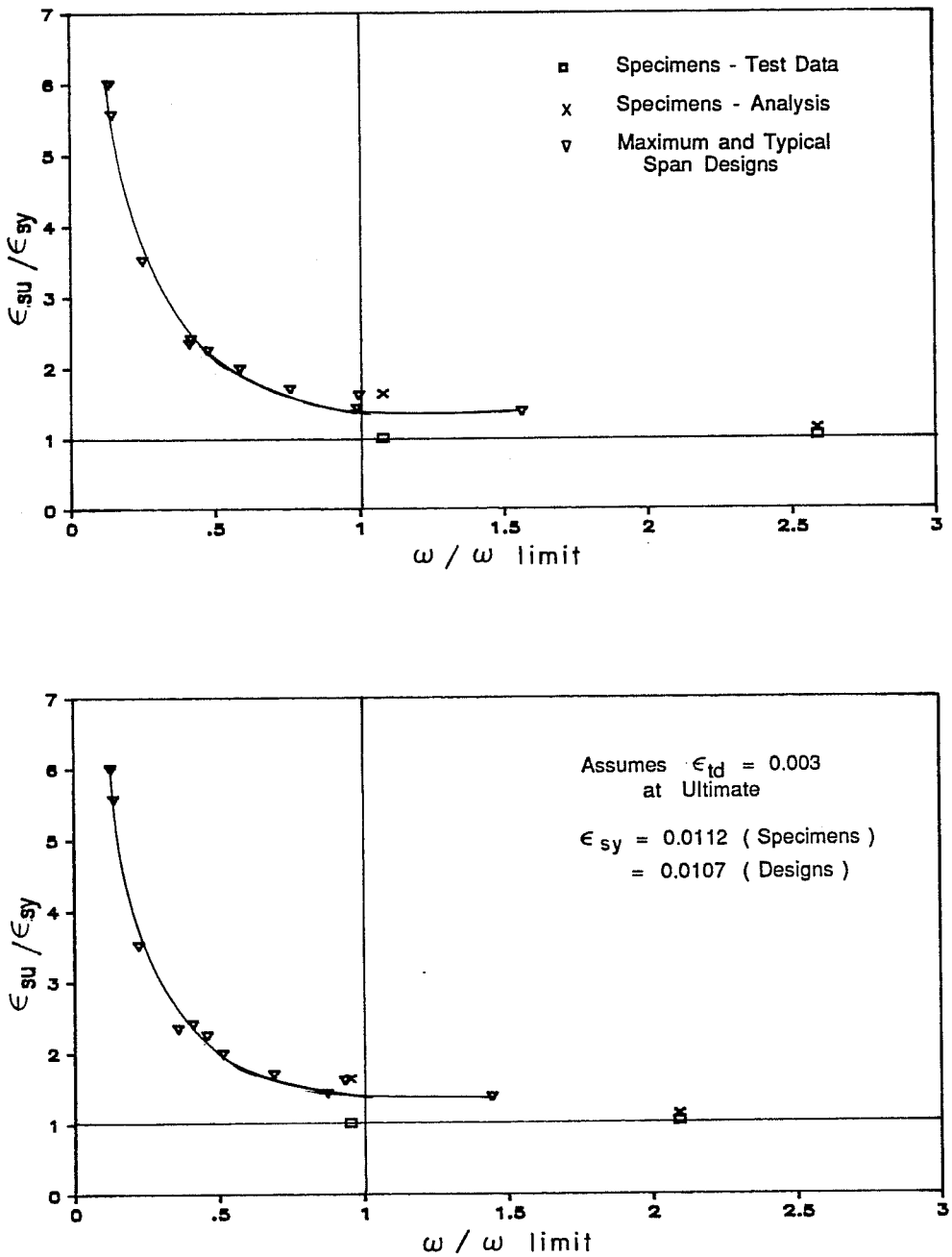

Fig. 7.60 Strand strain ratio at ultimate ($\epsilon_{su}/\epsilon_{sy}$) versus ω ratio (ω/ω maximum limit) - Cases I and II: a) Proposed limit; b) Current ACI limit

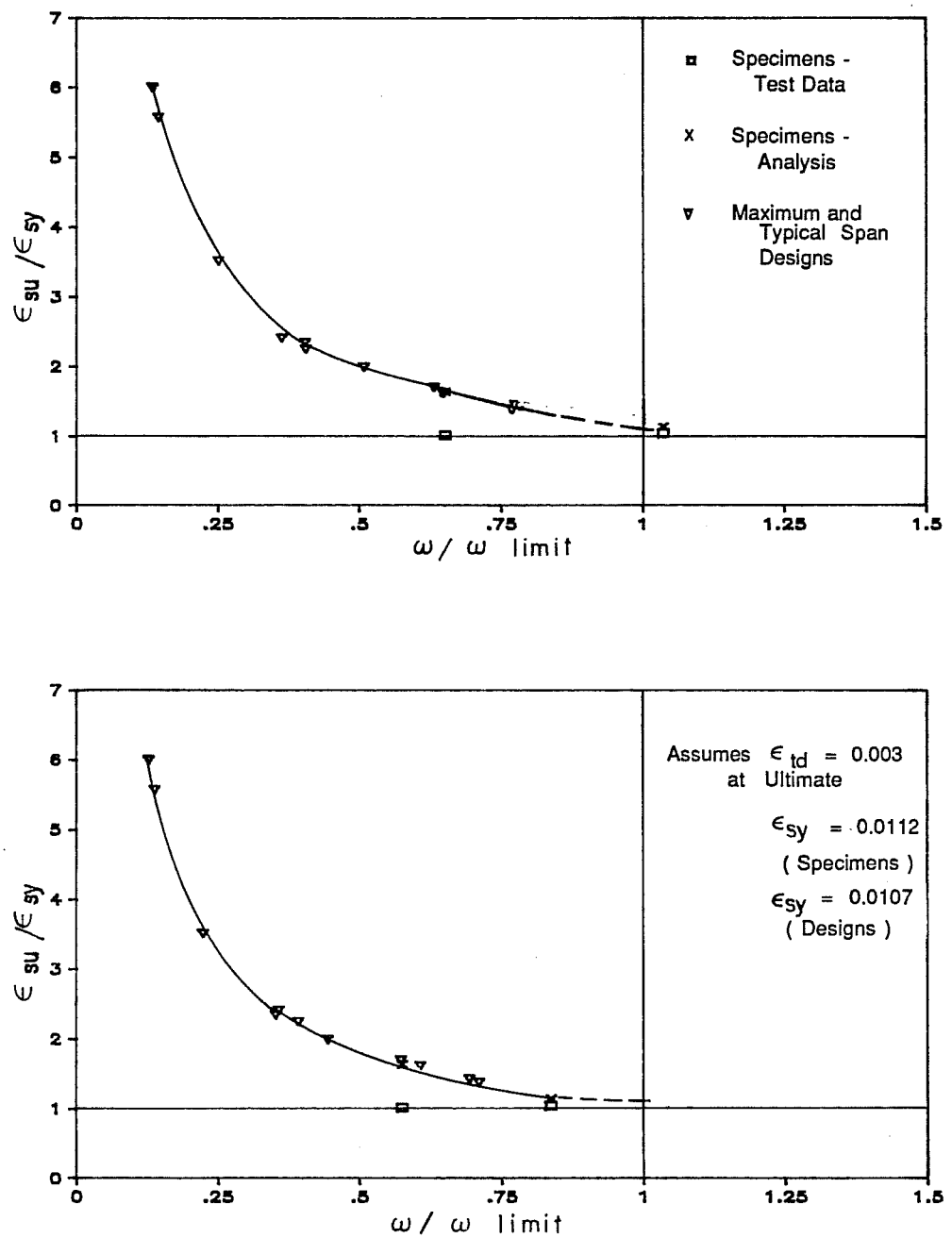

Fig. 7.61 Strand strain ratio at ultimate ($\epsilon_{su}/\epsilon_{sy}$) versus ω ratio (ω/ω maximum limit) - Case III: a) Proposed limit; b) Current ACI limit

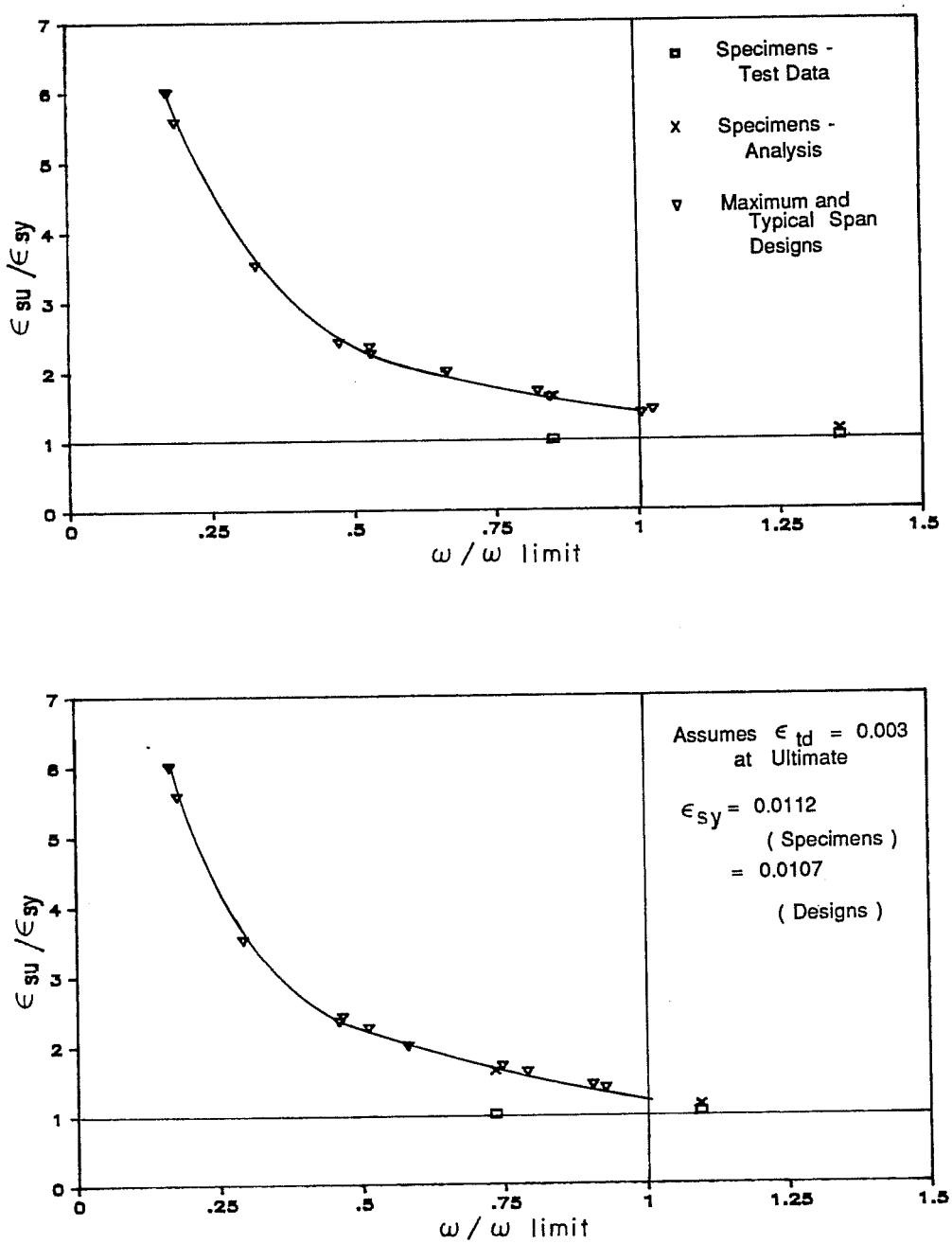

Fig. 7.62 Strand strain ratio at ultimate ($\epsilon_{su}/\epsilon_{sy}$) versus ω ratio (ω/ω maximum limit) - Case IV:
a) Proposed limit; b) Current ACI limit

because the strand strain that forms the basis for the limit is the yield strain. This yield strain, however, does not have the same meaning as the yield strain for conventionally reinforced concrete members where the stress-strain behavior of the reinforcement is essentially bilinear. For conventional reinforcement, the yield strain represents the strain at which inelastic behavior begins. Strands, however, experience significant inelastic deformation before reaching the defined yield strain. This aspect of strand behavior is demonstrated dramatically by Specimen 1 in which the strand strain just reached the yield strain prior to crushing of the concrete, yet the deflection was large, providing sufficient warning of impending collapse.

7.5.3 Minimum Reinforcement Limit. The current minimum reinforcement limit insists that the ultimate capacity of the member must exceed the cracking load by a 20 percent margin. However, this limit is not sufficient to prevent designs in which strands rupture before the extreme concrete fiber reaches the maximum usable strain, which has been indicated to be a possibility by the 75 ft span designs studied in this chapter. The load-strain plot for this span in Fig. 7.58 shows that strands could rupture (exceed the limiting strain equal to the ASTM minimum elongation of 0.035) prior to developing even a strain of 0.0022 in the top fiber of the deck.

To address this deficiency in the Codes, a minimum reinforcement limit was developed using the same reasoning as used for the maximum limit. Appendix D.2 contains the derivation of this limit which is based on the limiting strain of 0.035. The complete form of the limit is

$$\omega \geq 0.85\beta_1[84/(1064 - f_{se})] \tag{7.9}$$

with a simplified form being

$$\omega \geq 0.08\beta_1 \tag{7.10}$$

where f_{se} is expressed in ksi. The simplified form is acceptable for the minimum limit because it is less sensitive to variation in the effective prestress than the maximum limit. This limit is also quite accurate for composite members because the large strand strain involved minimizes the effect of the strain and curvature differences between the deck and girder.

Accuracy of this limit is demonstrated for maximum and typical span designs in Fig. 7.63 where the ratio of strand strain at ultimate to the limiting strain is plotted versus the ratio of ω to both forms of the minimum reinforcement limit. The data are connected with a curve to indicate the trend of the data. The strain ratio should be unity when the ω ratio is unity to satisfy the intent of the limit. This plot indicates excellent agreement between both forms of the limit and data, which is demonstrated by the trend of the data

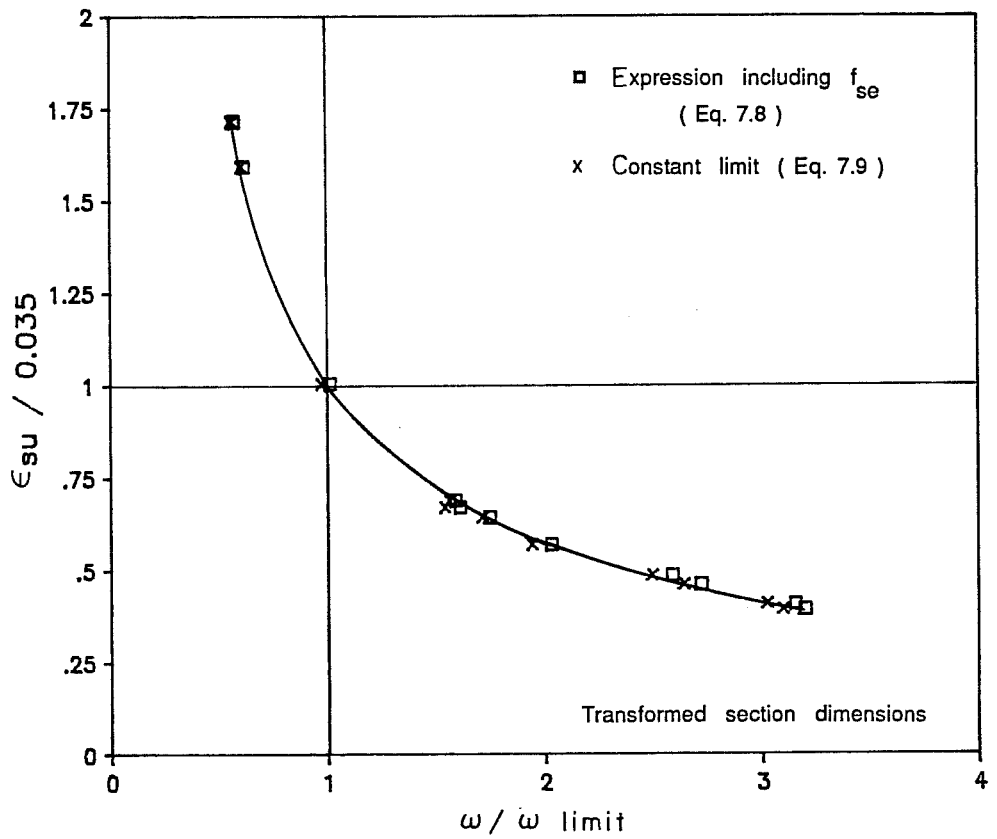

Fig. 7.63 Strand strain ratio at ultimate (ϵ_{su}/0.035) versus ω ratio (ω/ω minimum limit)

passing through the intersection of the lines representing unity on the two axes.

7.5.4 Summary. The following observations can be made regarding ductility and reinforcement limits for composite prestressed members:

1. The reinforcement index, ω correlates well with aspects of behavior related to ductility.
2. Proper use of ω for comparison with certain limits can ensure adequate ductility. It also avoids problems of definition and computation that are associated with use of other quantities, such as the depth of the compression zone at ultimate and ductility ratios based on yield and ultimate curvatures or deflections.
3. Reinforcement indices computed using the simplified design assumptions of the AASHTO and ACI codes are accurate estimates of reinforcement indices computed using a strain compatibility analysis.
4. The effect of nonprestressed tension reinforcement and compression reinforcement can be included in the reinforcement index by using an expression such as proposed by Naaman et al. [97].

5. Use of a proposed maximum reinforcement limit, which is derived using assumptions consistent with current codes and practice, is recommended.
6. To obtain the same behavior for different grades of strand, the limiting strand strain for use in the maximum reinforcement limit should be a function of the ultimate strength of the strand. A function is proposed and included in the proposed limit.
7. The proposed limit maximum reinforcement limit is more restrictive in most cases than current limits.
8. The effective prestress was shown to be a significant factor in determining the maximum reinforcement limit, although it is neglected in the current limit. It is, however, included in the proposed limit.
9. In computing the reinforcement index, section dimensions for composite sections should be transformed by the ratio of the deck and girder concrete strengths to provide the most accurate comparison with reinforcement limits and to be consistent with results from analysis of monolithic construction. A transformation to a section using the deck concrete strength is recommended.
10. A proposed minimum reinforcement limit, which would be used in addition to the current minimum requirement, is

intended to prevent rupture of strands prior to the strain at the top fiber reaching the maximum usable strain. The proposed minimum reinforcement limit is based on a limiting strand strain of 0.035.

11. The simplified form of the proposed limit is as effective as the more complete form in establishing an accurate minimum reinforcement limit.

Furthermore, it is recommended that strand strain limits equivalent to both the maximum and minimum reinforcement limits be provided in the code or commentary. These equivalent limits could be used with more detailed analyses that compute strand strains and stresses and therefore do not require an indirect approach. This would be appropriate since the intent of the current and proposed limits is to ensure a specified level of strain in the strand at ultimate.

Derivations for the reinforcement limits should also be provided in the commentary to the codes so that they may be understood and properly applied by designers. Such an explanation is currently included in the ACI Code Commentary for the maximum reinforcement limit for reinforced concrete sections, but no information is given on the limit for prestressed members.

7.6 Deflections

This section contains discussions regarding the evaluation of both long- and short-term deflections. Limits for these deflections are also considered.

7.6.1 Long-Term Deflections. Long-term deflections were computed using the computer program CAMBER [72] for the maximum and typical span designs using 12 ksi concrete. The construction schedule, creep factors and humidity assumed by Kelly [72] for his examples and actual, rather than estimated, quantities for section properties were used as input. Elastic deflections computed by the girder design program BRIDGE were also input.

The results of the analysis are shown in Fig. 7.64. While the typical span designs (GS = 4 ft, span = 120 ft; GS = 10 ft, span = 75 ft) produced deflections that were very stable with time, the maximum span designs exhibited large cambers and significant continuing sag with time. The longest span design experienced a sag of approximately 3.5 in. after the deck was added. This could be an unacceptably large value. The long-term behavior indicated in the figure generally agrees with PBEAM [119] analyses performed during the preliminary design of the specimens.

As part of a related study, Kelly [72] performed a sensitivity analysis of the girders he was considering to determine the effect of variations in significant parameters on the time-

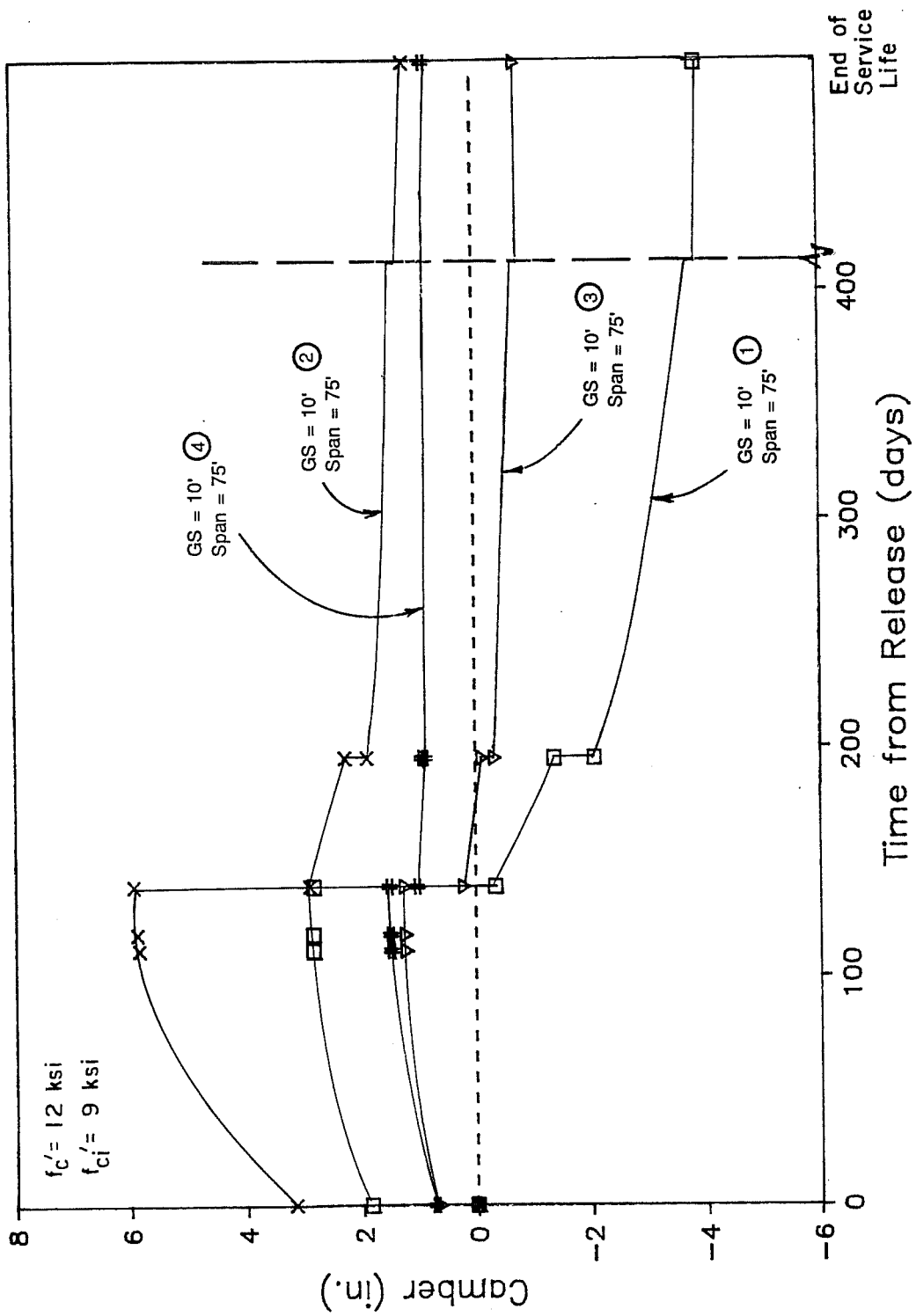

Fig. 7.64 Time dependent deflections for maximum and typical span designs

dependent deflections of girders. Such a study should be performed for high strength girders to determine the possible range in camber due to different age at release, curing conditions, age at erection, and other effects. The use of very long spans with high strength concrete may result in greater sensitivity to variations in parameters which would result in unacceptably large differential camber between girders. When significant parameters are known to be different for girders within the same span, steps can be taken, as suggested by Kelly, while girders are in storage to reduce the final differences in camber.

The program CAMBER could also be used to study the effect of release strength and strand profile on the long-term deformation of the member. Since designs using high strength concrete can be achieved with different combinations of strengths at release and strand profiles, the designer could select a combination which would provide the best performance considering both initial and final conditions.

As observed in the instrumented girders reported by Kelly [72] and from discussions with Texas SDHPT field personnel, there is generally no long-term deflection problem after the deck has been placed. This was also confirmed by the early PBEAM analyses. This is reasonable because the deck will resist any time-dependent movement of the girder, causing a small amount of load redistribution.

However, long-term deflections for very long members should be investigated due to the lack of field experience with such members.

An attempt was made to relate the curvature at release and the curvature under full dead load to the long-term deflections experienced under these conditions as shown in Fig. 7.65. This approach seemed reasonable because a large curvature would generally indicate a tendency for camber or sag with time. However, the data in the figure do not indicate a close correlation. This is probably due to the fact that deflection depends on the strain conditions all along the member and therefore, span length and other considerations are also significant factors in determining the final deflection of a member.

In the absence of a correlation between curvature and long-term deflections, it is recommended that any designs which approach the maximum span for a given girder spacing should be investigated for possibly excessive long-term deflections. An indication of a possible problem may be a large curvature, but this needs to be investigated further. Use of the program CAMBER is recommended for estimation of long-term deflections.

7.6.2 Deflections Due to Applied Loads. Deflections with applied load have been discussed in preceding sections. Calculation of deflections for uncracked members is straightforward and can be performed using elastic analysis

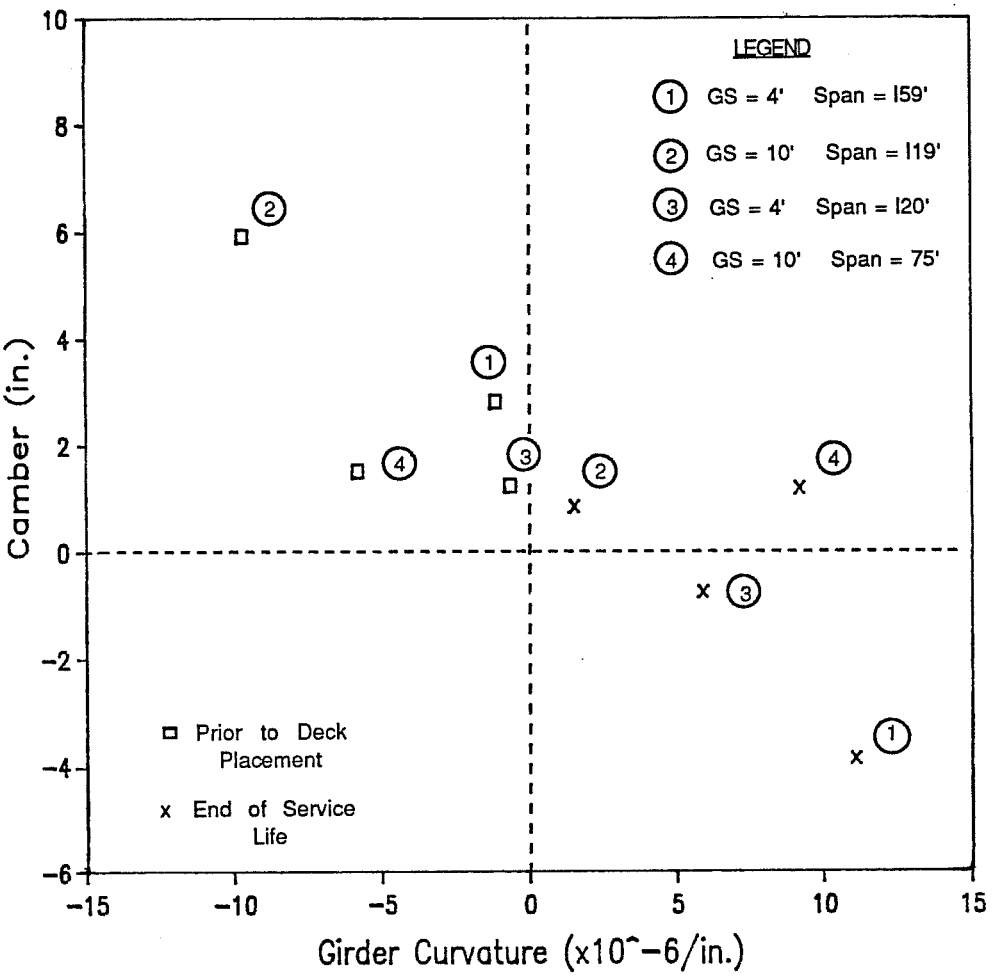

Fig. 7.65 Camber versus girder curvature prior to deck placement and at end of service life for maximum and typical span designs with f'_c = 12 ksi

techniques. For loadings beyond cracking, computation of deflections is a lengthy and tedious process unless a computer program is used. Programs such as PBEAM [119] are available to perform the calculations, or the partially automated approach used in this study can be employed. These methods, which employ some form of strain compatibility analysis, provide sufficient accuracy in the prediction of deflections all the way to failure. Since the criteria used to define failure will affect the computed deflection, it is recommended that a careful assessment of the conditions at ultimate be made to determine the level of concrete strain that may correspond to failure or maximum capacity. It appears that a value of 0.003 will be appropriate if the compression region is confined to the deck, resulting in a significant strain gradient across the deck. If the girder remains in compression at failure, a value of 0.0022 to 0.0025 may be more appropriate, since the deck is in more uniform compression and lacks the confining effect associated with a strain gradient.

7.6.3 Deflection Limits. As mentioned in Chapter 3, there are no limits on deflection for prestressed members in the current AASHTO Specifications. However, the live load deflection limit of the span divided by 800, which applies to steel members in the AASHTO Specifications [10], is often used for prestressed bridge members. This limit is compared to deflection-to-span ratios in Fig. 7.66 for the sample designs used in this chapter. An additional limit

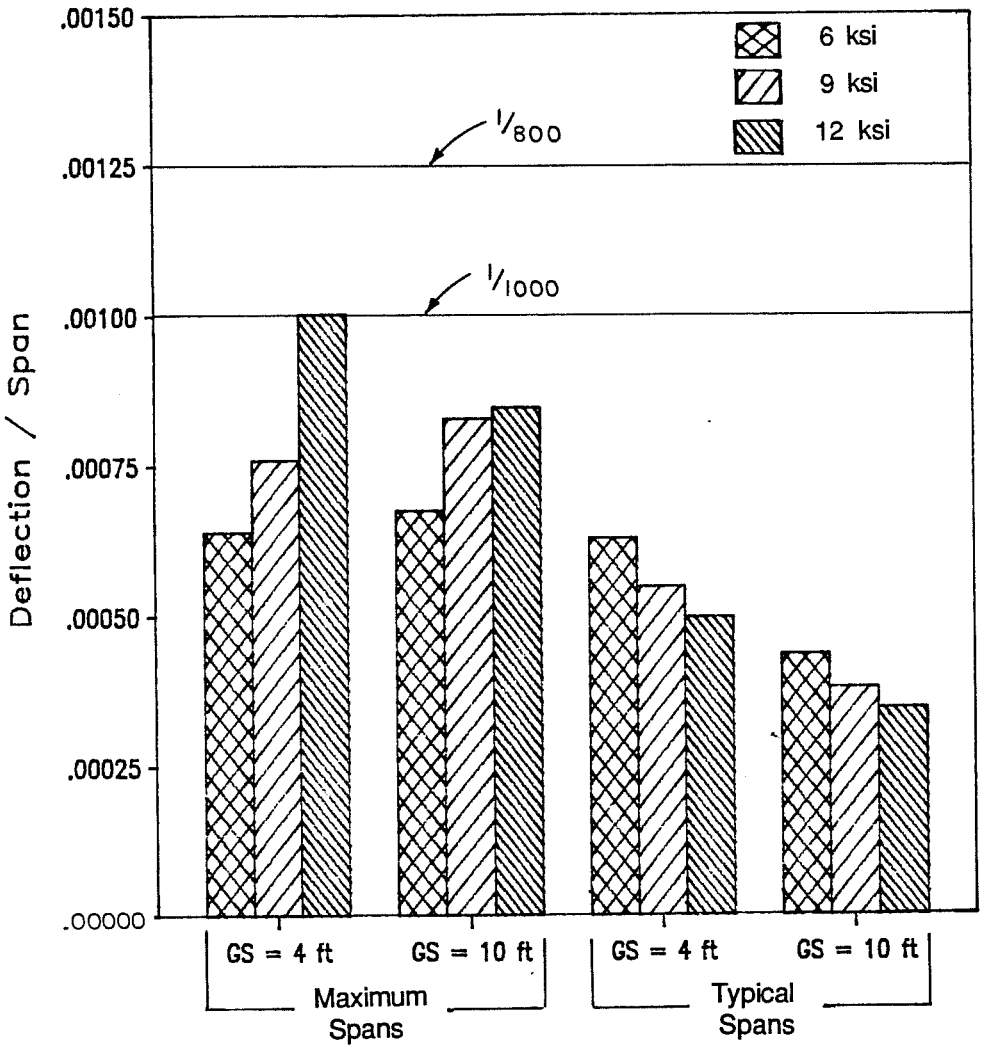

Fig. 7.66 Comparison of live load deflections to limits for maximum and typical span designs

of the span divided by 1000, which is specified for steel bridges with pedestrian traffic, is also shown on the figure. The deflections are well below the span/800 limit for all cases and only for the longest span is the more strict limit encountered. The data also shows the expected decrease in deflection with use of high strength concrete for a given span. The decrease is not sizable and would not be sufficient motivation to use high strength concrete in most cases. However, where member depths are restricted, the use of high strength concrete may be warranted in order to control deflections.

No limits for final long-term deflections are known to exist. As means to compute long-term deflections become more practical, it appears prudent that such limits be developed, especially where very long spans are used. These limits should be correlated to the level of deformation in a bridge that creates an unacceptable ride or results in maintenance or other problems.

7.7 Girder Stability

In this section, the methods of stability analysis discussed in Chapters 2 and 3 will be developed further. The analysis will then be used to study the lateral stability of the girder cross-sections considered in Chapter 2. Methods for improving the lateral stability of girders are also discussed. Experience related to lateral

stability during the fabrication and testing of the long-span scale-model specimens is then discussed.

7.7.1 Analysis. The approach and associated equations presented in Chapter 3 for determining the factor of safety against lateral buckling can be solved for the maximum span. Where lifting points are located at a distance, a, from the ends of the girder, the weak axis deflection at midspan can be written as

$$\Delta_y = \frac{\omega_g}{16E_cI_y}\,(l\text{-}2a)^2\,((5/24)(\partial 1\text{-}2a)^2 - a^2) \tag{7.11}$$

Using this equation with the definition for the factor of safety against lateral buckling, FS,

$$FS = y_T/0.64\,\Delta_y \tag{7.12}$$

the maximum lifting span for a girder, l_{max}, can be computed using the following equation:

$$l_{max} = \sqrt[4]{\frac{(y_T/.64FS)(16E_cI_y/\omega_g)}{(1\text{-}2\ (a/l))^2((5/24)(1\text{-}2(a/l)))^2\text{-}(a/l)^2)}} \tag{7.13}$$

The quantity (a/l), which is the ratio of the distance from the lifting point to end of the girder to the full span length, is assumed to be a constant. The equation assumes all quantities to have consistent units. This equation was used to compute spans given in Table 2.5.

As indicated by Swann [122], y_T is the vertical distance between a line through the two lifting points and the center of gravity of the whole beam, and represents the distance from the center of mass of the girder to its center of rotation. This definition can therefore be expressed as

$$y_T = y_t + y_L - y_C \tag{7.14}$$

where y_t = distance from centroid of section to top of girder

y_L = vertical distance from top of girder to lifting eye

y_C = vertical distance from centroid of section at lifting points to centroid of whole member due to camber of girder

$$= (0.67 - 4\,(a/l)^2)\,\Delta_c \tag{7.15}$$

Δ_c = camber of member at midspan.

Because most lifting loops are not rigid enough to prevent rotation about a point lower than their full height, use of a reduced height or zero is recommended. However, the full height may be used for rigid lifting yokes that are rigidly attached to the girder. The definition for y_C (Eq. 7.15) assumes that a girder with camber has a parabolic shape.

The equation by Swann [122] can be used to determine the lateral bending moment, M_y, caused by imperfections in the member. The lateral bending moment, which is the potential cause of failure, is related to the moment due to member self-weight about the x-axis,

M_x, the tilt due to imperfections, θ_o, and the factor of safety against lateral buckling, FS. The equation is:

$$M_y = M_x\theta_o(FS/(FS-1)) \tag{7.16}$$

where FS is defined using Eq. 7.12 and the correction for lifting point location that is applied to Δ_c in Eq. 7.15 is also applied to θ_o, resulting in the expression

$$lqf_o = (d_o + (.67 - 4\ (a/l)^2)b_o)/y_T \tag{7.17}$$

where d_o = transverse distance from the minor axis of the section to where the lifting points have been inadvertently fixed

b_o = lateral bow or sweep of the beam at midspan.

The proposed definition for y_T (Eq. 7.14) should be used in these equations. When using Eq. 7.17 to examine the condition of an actual member, the direction of sweep and lifting point eccentricity should be considered because they may act in opposite directions. For design purposes, realistic maximum values for d_o and b_o acting in the same direction should be used.

If cracking occurs due to the lateral moment, transverse section properties are reduced which can lead to increasing instability (Δ_y increases, resulting in a decrease in FS, which leads to a further increase in M_y and the cycle repeats) and sudden collapse [122]. Therefore, to avoid cracking and failure, the total stress at the extreme fiber due to lateral moment, prestress, and

self-weight should be limited to a value less than the cracking stress. It is recommended that an allowable stress of $6\sqrt{f'_c}$ be used. The extreme fiber stress can be computed using the equation

$$\begin{aligned} f_{ytop} &= \text{total stress in top fiber of the girder including effect of lateral moment } M_y \\ &= f_{top} - M_y/S_{ytop} \\ &\geq -6\sqrt{f'_c} \end{aligned} \tag{7.18}$$

where f_{top} = stress in the top fiber of the girder due to prestress and self-weight, with compression positive.

S_{ytop} = section modulus about the weak axis for the top flange of the section

$= I_y/(b1/2)$

$b1$ = width of top flange.

This equation assumes that cracking due to the lateral moment occurs in the top flange, which is generally the case because the greater precompression of the bottom flange delays cracking. However, stresses in the bottom flange should also be checked because in some cases (see data for the Specimen 2 prototype in Table 7.9), cracking may initiate at this location. The critical stress for the bottom flange will typically occur at the top corner of the bottom flange.

These equations can be used to determine the factor of safety against lateral buckling for perfect girders, and to estimate the extreme fiber stress due to the lateral moment caused by initial imperfections (sweep, b_o, and eccentricity of lifting points, d_o) Using these equations, the factor of safety (FS) and the top fiber stress (in terms of $\sqrt{f_c'}$) were determined over a range of span lengths for the sections considered in Chapter 2. The results are shown in Fig. 7.67 for the 54-in. sections and in Fig. 7.68 for both the 40-in. and 72-in. sections. A sweep of 2 in. and a lifting point eccentricity of 0.5 in. were used in the calculations as reasonable estimates of the quantities, although larger values could occur. The net stress at the top fiber prior to consideration of lateral effects was assumed to be zero in order to simplify the comparison. However, if f_{top} were a tensile stress, the spans shown would be reduced, while presence of a compressive stress would lengthen the spans. Camber was neglected and the height of lifting points above the top of the girder was assumed to be zero. Other assumptions are indicated on the figures. Spans greater than maximum lifting span lengths computed using Eq. 7.13, which are repeated in Table 7.8, are shown on the figure as dashed lines.

The comparisons shown in Fig. 7.67 and 7.68 indicate that the factor of safety against buckling gradually approaches 2 as the span

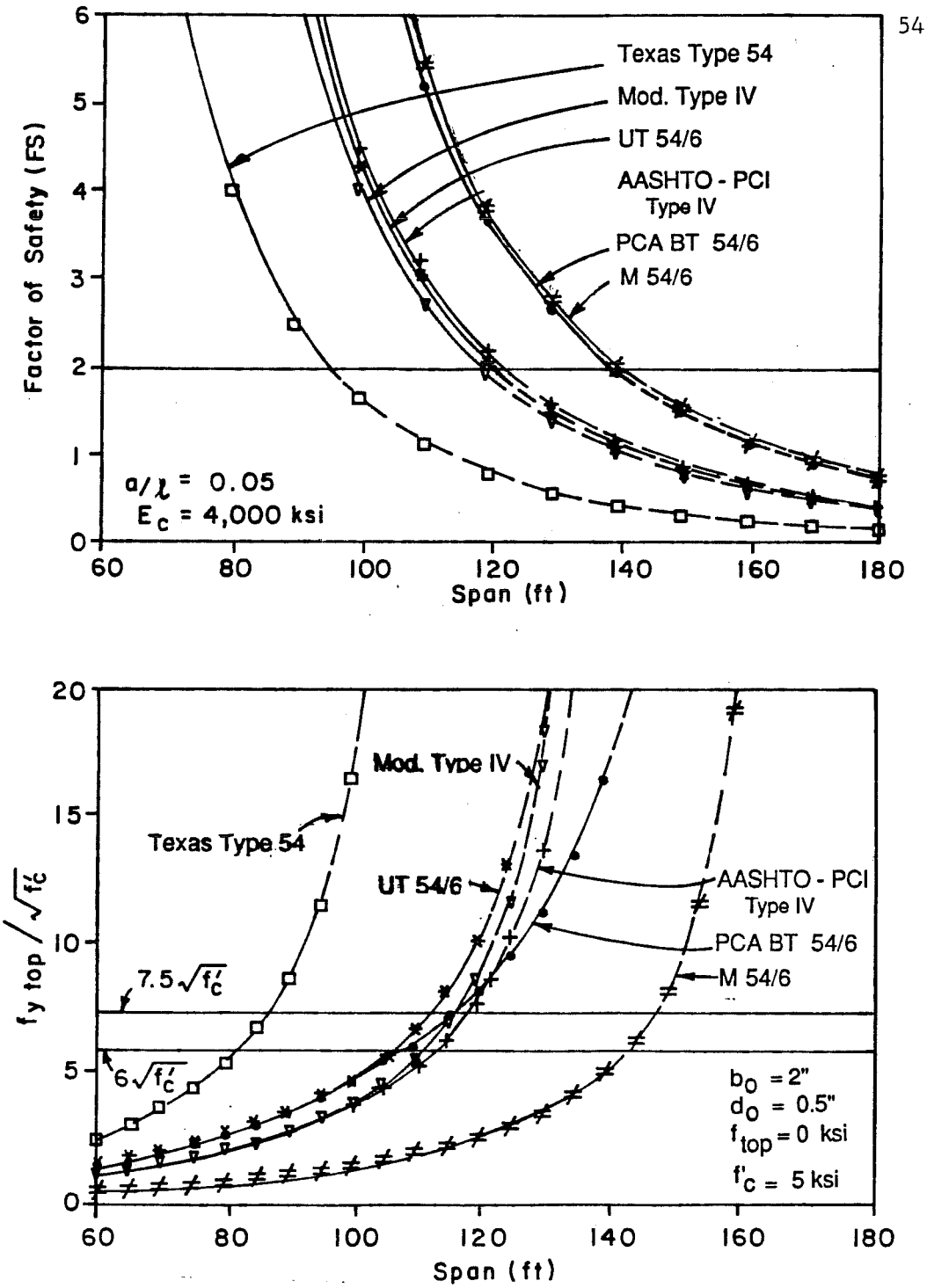

Fig. 7.67 Factor of safety and top fiber stress versus span length for 54-in. sections: a) Factor of safety (FS); b) Top fiber stress

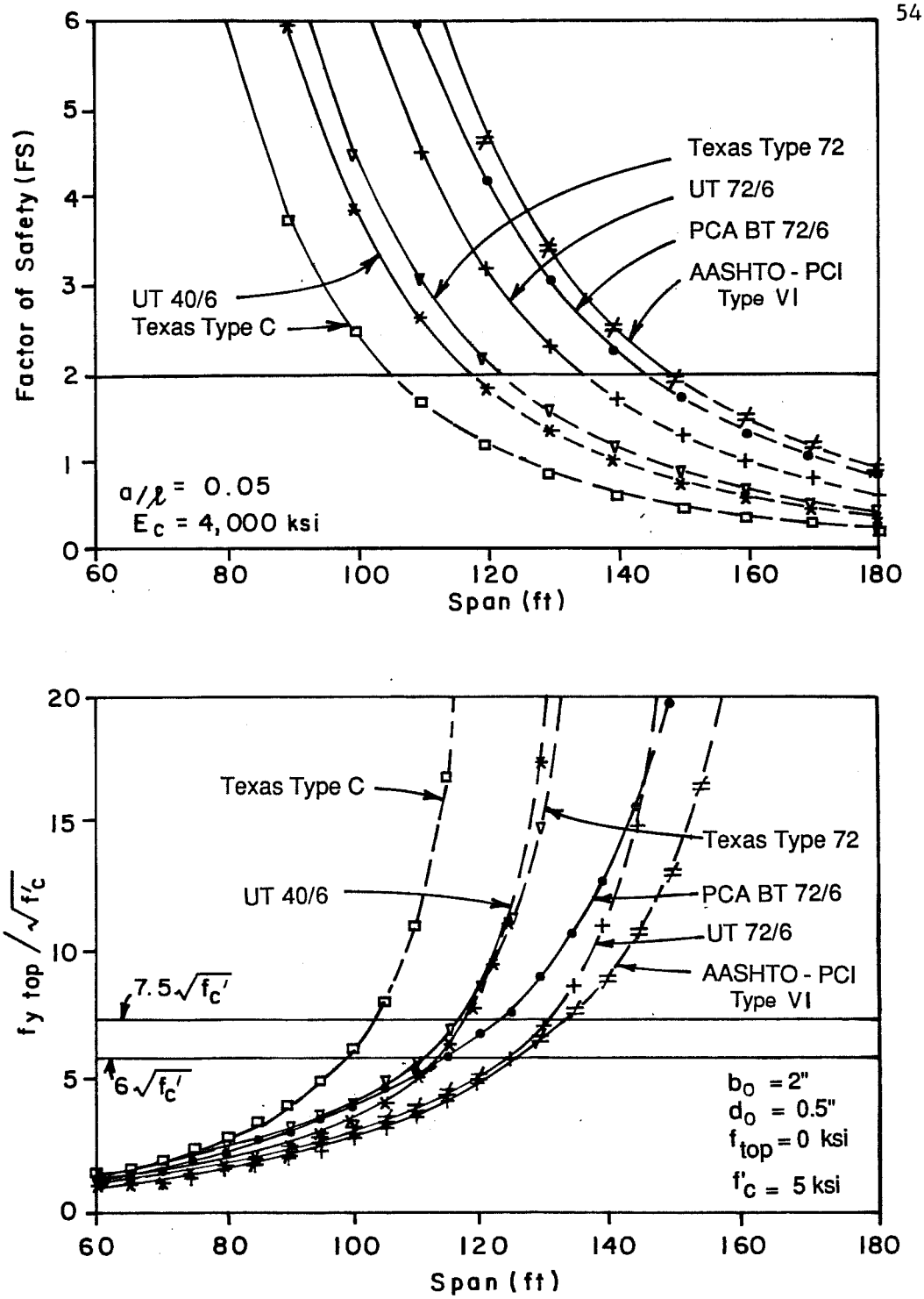

Fig. 7.68 Factor of safety and top fiber stress versus span length for 40- and 72-in. sections: a) Factor of safety (FS) b) Top fiber stress

approaches l_{max}. The maximum lifting span, l_{max}, occurs at the intersection of the curves and the line representing FS = 2. An additional increase in span of approximately 20 ft is required to obtain FS = 1. The second half of the figures shows that the total top fiber stress, f_{ytop}, caused by the lateral moment resulting from the specified imperfections, increases rapidly as the span is increased. Stresses approach infinity as FS approaches one. These plots indicate that, at the maximum lifting span (the span at which the dashed line begins), f_{ytop} exceeds the allowable stress ($6\sqrt{f'_c}$) and even the cracking stress ($7.5\sqrt{f'_c}$) for all sections except the MOT/C&CA inverted-tee section (M 54/6). Values for $f_{ytop}/\sqrt{f'_c}$ at the maximum lifting spans are tabulated in Table 7.8. The fact that stresses at l_{max} exceed the cracking stress for most sections indicates that the presence of initial imperfections of moderate size could lead to a lateral stability failure at spans less than l_{max}.

For most sections the span at which f_{ytop} equals the allowable stress is approximately 15 ft less than the maximum lifting span (for the specified values of b_o and d_o). For the PCA bulb-tee sections and the AASHTO-PCI Type VI, the difference is from

Table 7.8 Additional Section Properties Influencing Girder Stability

	y_T * (in.)	I_y ($in.^4$)	ω_g (plf)	$\sqrt[4]{y_T I_y}/\omega_g$ ($in.^{1.5}/lb^{0.25}$)	l_{max} ** (ft)	S_{ytop} ($in.^3$)	f_{ytop}/f'_c ***
40-in. sections							
Texas Type C	22.91	13,020	516	51.3	106	1,860	-8.34
UT 40/6	23.40	18,486	477	57.4	118	2,311	-7.61
54-in. sections							
Texas Type 54	28.47	6,927	514	46.3	95	866	-11.69
AASHTO-PCI Type IV	29.27	29,513	822	59.6	123	2,951	-8.83
Modified Type IV	29.63	22,550	709	58.0	119	2,506	-8.39
MOT/C&CA M 54/6	32.45	37,410	654	68.7	141	4,676	-5.32
PCA BT 54/6	26.56	41,310	617	68.0	140	1,721	-16.30
UT 54/6	27.72	23,578	649	59.0	121	1,965	-10.83
72-in. sections							
Texas Type 72	38.27	24,707	899	59.6	123	2,246	-9.71
AASHTO-PCI Type VI	35.62	72,776	1,130	72.4	149	3,466	-12.55
PCA BT 72/6	35.64	41,634	730	70.3	145	1,735	-15.24
UT 72/6	38.55	32,560	808	65.7	135	2,713	-8.72

* - $y_T = y_t$

** - Maximum lifting spans, l_{max}, computed using Eq. 7.13, assuming lifting point located at 0.051 from ends of girder, factor of safety against buckling (FS) = 2.0, and E_c = 4,000 ksi.

*** - $f_{ytop} = M_y/S_{ytop}$ for l_{max} using Eqs. 7.16 and 7.18, and assuming d_o = 0.5 in., b_o = 2 in., f_{top} = 0 ksi, and f'_c = 5 ksi.

25 to 30 ft. Therefore, Eq. 7.16, 7.17, and 7.18 should be used even when spans are less than l_{max} to estimate expected behavior for anticipated or actual imperfections in members to determine whether special steps need to be taken to ensure safe handling of girders.

Plots similar to those in Fig. 7.67 are shown in Fig. 7.69 for 54-in. sections with high strength concrete. Maximum lifting spans increase only 8 percent for an 80 percent increase in f_c' and a corresponding 35 percent increase in the modulus. Top fiber stresses were reduced only slightly at l_{max} and the M 54/6 remained the only 54-in. section for which f_{ytop} at l_{max} was less than the allowable stress. However, for a given span (especially those approaching lmax), increasing the concrete strength leads to a significant reduction in the stress at the extreme fiber. For example, the extreme fiber stress for an AASHTO-PCI Type IV with a 120 ft span is $7.8\sqrt{f_c'}$ with normal strength concrete (Fig. 7.67) while for high strength concrete at the same span (Fig. 7.69), the stress is $4.8\sqrt{f_c'}$, which is below the allowable limit. Therefore, high strength concrete can be more effectively used to reduce stresses due to lateral moments for a given span rather than to increase the maximum lifting span.

These figures also reveal that the maximum lifting spans are similar for sections of different depths. To illustrate, maximum

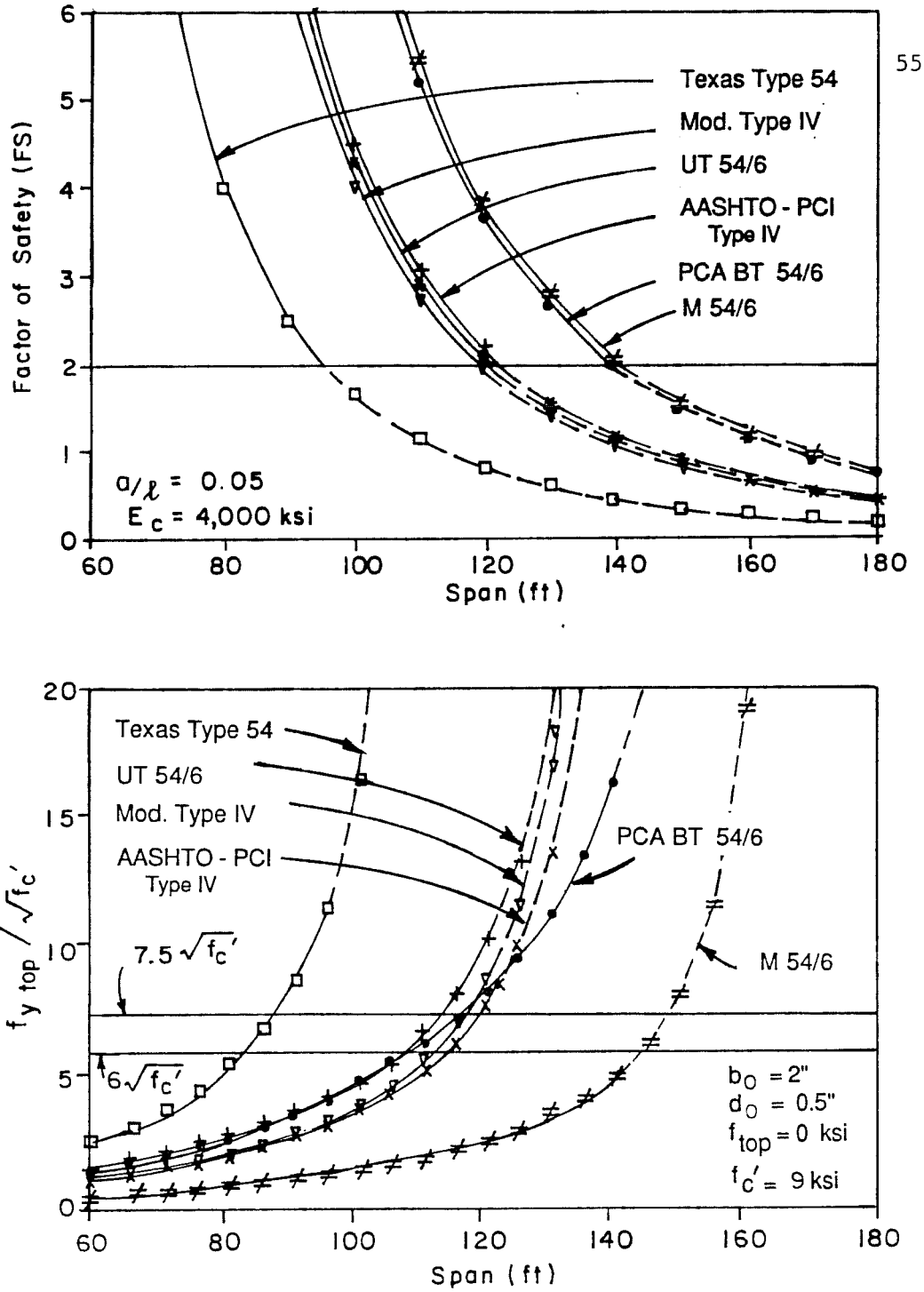

Fig. 7.69 Factor of safety and top fiber stress versus span length for 54-in. sections using high strength concrete: a) factor of safety (FS); b) Top fiber stress

lifting spans for the UT 40/6, the modified Type IV (54 in. deep) and the Texas Type 72 are 118, 119, and 123 ft, respectively. This occurs because transverse section dimensions for deeper sections are the same or only slightly larger than those for shallower sections. Therefore, the change in weak axis properties is small for sections of different depths. This leads to an increasing disparity between the strong and weak axis moments of inertia which means that maximum span designs, which are based on strong axis properties, will increase more than the maximum lifting span, which is strongly influenced by weak axis properties. Therefore, if both the span length and lateral stability are to be improved, the weak axis section properties must be increased significantly for deeper members.

A lateral stability factor was developed relating section properties to the maximum lifting span for a given a/l ratio. The factor is taken from Eq. 7.13 and appears in the fourth column of Table 7.8, which contains the quantities that are used in the factor. This factor is linearly related to l_{max} as demonstrated in Fig. 7.70 for different values of a/l. The figure demonstrates that the AASHTO-PCI Type IV and the Texas Type 72, which have the same value for the lateral stability factor, will have the same maximum lifting span when lifting points are located at a given distance from the ends of the girder. This factor is therefore an indicator of the lateral stability of a section, with larger values indicating that a

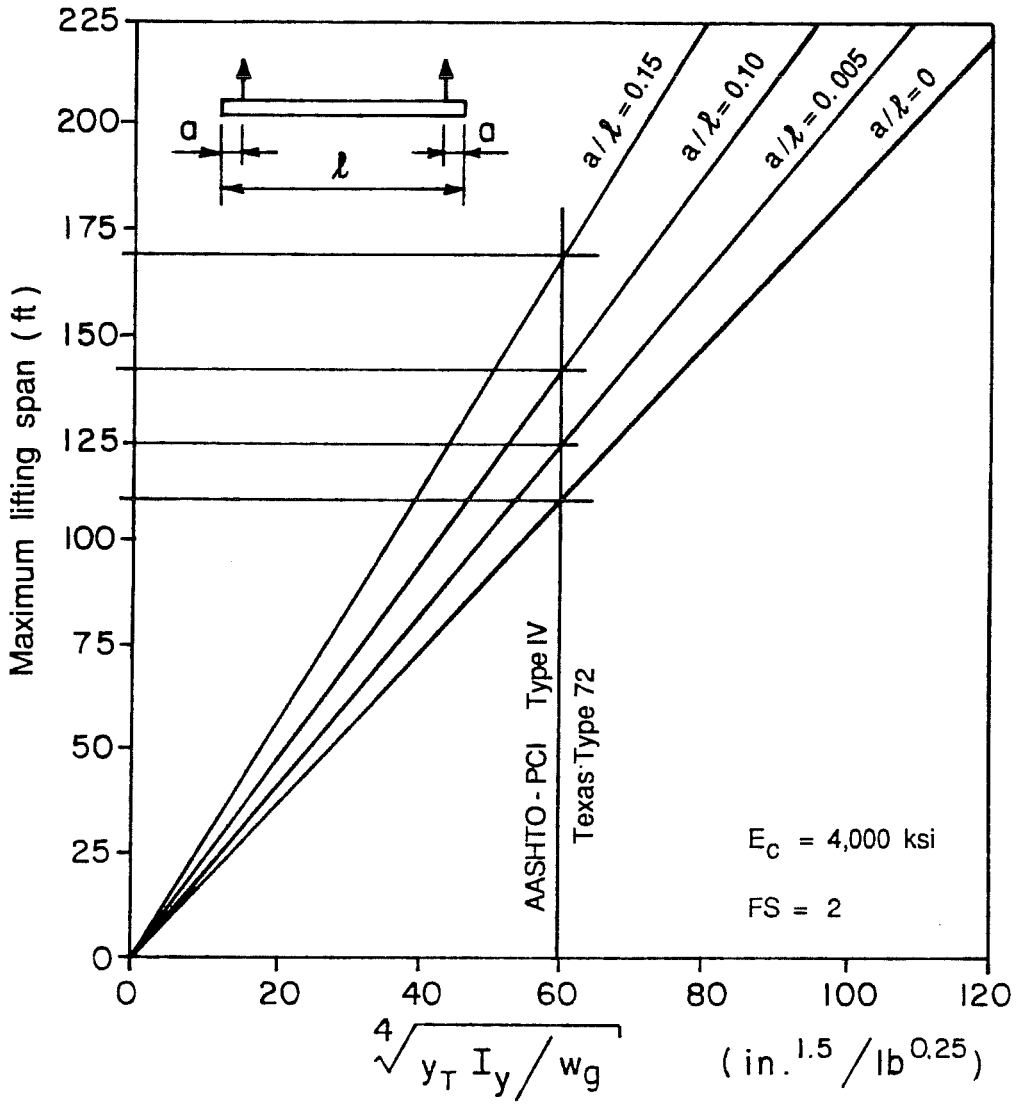

Fig. 7.70 Maximum lifting span versus lateral stability factor

longer maximum lifting span would be possible. However, stresses caused by lateral moments must also be investigated for a complete understanding of the stability of a member, as illustrated by the fact that the bulb-tee sections have among the highest (best) values for the lateral stability factor, yet have the highest (worst) stresses due to lateral moment at the maximum lifting span.

A simple relationship was also sought for stress at the top fiber (last column in Table 7.8), but the relationship was too complex. The weak axis section modulus for the top flange is included in the table for use in computing the stress. Because the inverted-tee M 54/6 had the smallest stress and was the only section for which the stress was below the allowable value ($6\sqrt{f'_c}$), this section could be used at l_{max} without cracking for the values of b_o and d_o considered. Stresses at l_{max} for the bulb-tee sections were the highest and exceeded twice the cracking stress. Increased initial imperfections and large cambers would increase stresses further, thus increasing the potential for failure. Because stresses at lmax for the bulb-tees and AASHTO-PCI Type VI exceed the stress for the Texas Type 54, which was reported as having stability problems in use, it is possible that problems may also occur with these sections when spans near the maximum lifting span are used.

Considering the lateral stability factor and the above findings with respect to stresses caused by lateral moments resulting

from sweep and lifting point eccentricity, the MOT/C&CA M 54/6 inverted-tee section or one like it appears to provide the best combination of potential maximum span lengths with increasing concrete strength (Chapter 2) and satisfaction of stability criteria. This occurs because the section has a large weak axis moment of inertia, a fairly low weight per foot, and the largest value of y_t for any 54-in. section considered.

The complete stability analysis presented here should be used to compare sections in order to obtain the most complete understanding of the stability of a section instead of relying on the partial perspective given by the lateral stability factor and the maximum lifting span. Girder designs should also be checked to determine whether initial cracking due to the lateral moment could occur at the bottom flange rather than the top flange as assumed for the analyses in this section.

As mentioned in Sec. 3.7, a number of means are available to improve the lateral stability of members with spans greater than the maximum lifting span or where extreme fiber stresses due to lateral moment caused by imperfections exceeds the allowable stress. A very effective method for increasing the maximum lifting span is to locate lifting points farther from the ends of the girder. The plots shown in Fig. 7.70 indicate that, by locating lifting points at 15 percent of the span from the ends of the girder rather than 5 percent, the

maximum lifting span is increased by approximately 35 percent. This improvement in l_{max} is related to the ratio a/l and is independent of section shape or span. The member must be capable of resisting the stresses produced by lifting the member at these locations.

The use of external bracing or "hog rods" can also be used to stiffen members during handling and transportation. The Texas State Department of Highways and Public Transportation specifies their use when span lengths exceed limits given in Chapter 3. Another externally applied means for increasing the stability of members during lifting, which is relatively simple and effective, is the use of a rigidly attached lifting yoke. This increases y_T by introducing a value for y_L which results in a significant improvement in stability, especially for members where y_t is small, such as for the bulb-tee sections. If a yoke is provided with a height sufficient to double y_T, the maximum lifting span is increased 19 percent. A rigid lifting yoke is any device which maintains the lifting eye, to which the hook of the crane is attached, in the plane of the y-axis of the member.

The effect of using higher strength concrete was discussed earlier (see Fig. 7.69). Since the stability of a section improves only slightly when high strength concrete is used, it is recommended that other means be used as primary methods for improving stability.

More study of the lateral stability of long, slender pretensioned girders during fabrication and erection is needed. A survey of the experience of state and federal highway departments, fabricators, and erectors with long, slender members should be taken, since such data certainly exists but has not been collected and published. A range of expected values for sweep and lifting point eccentricity should also be obtained. The analysis presented and discussed above should then be compared to actual experience to determine whether it is appropriate and whether the limiting factor of safety and allowable stresses are sufficient.

7.7.2 Experience with Scale-Model Specimens. The specimens were lifted using nearly vertical cables. No difficulties were encountered during handling although sweep was present in both girders. The cause of the observed increase in camber of both specimens following placement of the deck is uncertain. It is possible that irregularities in the deck forms could have forced the girder out of alignment or the added load above the girder could have aggravated the stability problem. The deck forms, however, were sufficiently rigid to stiffen the top flange and prevent buckling. The fact that an increase in sweep following release of approximately 0.6 in. for Specimen 1 and 0.4 in. for Specimen 2 indicates the lateral behavior of these members is sensitive to added load and manipulation during the construction process.

Table 7.9 gives information concerning the lateral stability of the specimens and corresponding prototypes. The specimen data reflects conditions at the time at which the girder was lifted from the prestressing bed, which was immediately following release for Specimen 1 but was approximately 6 weeks after release for Specimen 2. Specimen 1 had no added dead load when moved while Specimen 2 had full dead load compensation present when moved. The added dead load for Specimen 2 was hung from spreader beams which crossed over the top of the girder. Because the height of the centroids of the hanging masses were located close to the height of the centroid of the girder, the height of the centroid of the girder was used for the centroid of the combined masses of the girder and added dead load. Data for prototypes is assumed to be at release which occurs within one or two days after casting.

The data in Table 7.9 indicate that Specimen 2 was close to the maximum lifting span and had a low value for factor of safety against buckling, but because of the small initial imperfections and the presence of compression in the top flange due to prestress and self-weight, both the top and bottom of the girder were in compression after lateral bending had been considered. The maximum lifting span and factor of safety for Specimen 1 were greater than for Specimen 2 because no dead load compensation was used. The total stress at the top of Specimen 1 was slightly greater than half the

Table 7.9 Lateral Stability Data for Specimens and Prototypes

Quantity	Units	Test Specimens		Prototypes	
		Sp 1	Sp 2	Sp 1	Sp 2
I_y	$in.^4$	276	276	22,550	22,550
ω_g	plf	78.4	235.2	709	709
S_{ytop}	$in.^3$	92	92	2,506	2,506
S_{ybot}	$in.^3$	69	69	1,880	1,880
f'_c	ksi	10.2	10.75	10.2	10.75
E_c	ksi	5,750	5,700	5,750	5,700
l	ft	49	49	147	147
a	ft	5	5.5	15	15
Net camber	in.	1.6	0.1	2.95	1.63
d_o	in.	0	0	0.5	0.5
b_o	in.	0.5	0.03	2.0	2.0
l_{max}	ft	64.1	51.4	147.8	148.6
y_T	in.	8.87	9.81	27.8	28.6
Δ_y	in.	2.37	6.31	21.2	21.4
FS		5.85	2.43	2.04	2.09
θ_o	rad.	0.0354	0.0019	0.0632	0.0614
M_x	k in.	167	467	13,601	13,601
M_y	k in.	7.14	1.50	1,684	1,604
f_{top}	ksi	-0.279	0.534	1.840	1.690
$f_{bot\ flng}$*	ksi	3.781	2.495	3.110	2.022
f_{ytop}	ksi	-0.357	0.518	1.168	1.050
f_{ybot}	ksi	3.677	2.473	2.213	1.169
$f_{lim}=6\ f'_c$	ksi	-0.606	-0.622	-0.606	-0.622
$f_{ymin}/\ f'_c$	**	-3.53	4.99	11.6	10.1

* - At top corner of bottom flange.
** - Minimum of total stress at top or bottom.

$y_L = 0$ for all analyses.

allowable stress due to the effect of larger initial imperfections and tension in the top flange.

Prototype designs corresponding to the specimens are included in Table 7.9 to obtain an indication of whether the behavior of scale-model girders could be expected to be indicative of the stability of the prototype girders and to illustrate the application of the preceding equations to actual designs. Specimen 1 does not compare well to the prototype designs because the full dead load compensation was not in place when the girder was lifted. The same values for concrete strength and modulus are used for companion specimens and prototypes to assist in comparisons regarding the scale effect. Stresses at the top and bottom of the prototype girders after release were taken from the design calculations in which losses were computed. The length of the prototype girders was very slightly less than l_{max} for both designs while the difference between girder length and l_{max} was greater for both specimens. Therefore, the factor of safety for each of the prototype girders was approximately to 2, which was less than the FS values for the specimens. The smaller values of FS and the larger values of θ_o (due to larger assumed sweep and lifting point eccentricities) resulted in moderately large lateral moments. However, since the stresses at the top of girder were larger, total stresses were larger than in the specimens. It was determined that if the lateral moment

had been sufficiently large, the prototype corresponding to Specimen 2 would crack in the bottom flange prior to the top flange.

7.8 Fatigue

While little data is available on the fatigue characteristics of high strength concrete, it is expected that the fatigue strength of high strength concrete is the same as that for concretes of lower strengths [22]. However, it appears that the fatigue characteristics of strands actually control the fatigue behavior of composite pretensioned girder bridges. Therefore, the fatigue of strands will be the focus of this section.

This section includes a discussion of the recommended approach for considering fatigue in the design of pretensioned members. Methods for computing strand stress ranges are then compared. Finally, strand stress ranges for various designs are considered.

While not considered in this section, it has been found that the fatigue behavior of pretensioned girder bridges is extremely sensitive to the actual prestress. This fact should be taken into consideration when the following analysis approach is used to evaluate the fatigue performance of pretensioned girders.

7.8.1 Design Approach. Recommendations made by Overman et al. [101] provide a direct approach to the consideration of fatigue in the design of pretensioned girders. The approach

recognizes strand fatigue as the limiting factor in the fatigue of pretensioned girders. While they conclude that use of a nominal bottom fiber concrete stress of $3\sqrt{f_c'}$ may be adequate to provide acceptable fatigue behavior, the limiting of strand stress ranges to ensure good fatigue resistance is recommended. Where strand stress ranges are used, the fatigue life of the girder would be determined using either the strand fatigue model

$$\text{Log } N = 11.0 - 3.5 \text{ Log } S_r \qquad (7.19)$$

where N = the fatigue life in number of cycles

S_r = the strand stress range

= maximum stress - minimum stress (ksi)

or the more conservative AASHTO Category B fatigue model for redundant structural steel members [10]. Where service life criteria are not satisfied, the design would have to be altered by reducing girder spacing or by increasing bottom flange reinforcement as recommended in the report.

An effective endurance limit of 16 ksi, which corresponds to a fatigue life of 6 million cycles, is recommended for use with either fatigue model. However, no fatigue endurance limit greater than 10 ksi was found in the tests he reported and some of the tests were loaded to 10 million cycles.

For bridge members, the strand stress range is the difference between strand stresses computed at full dead load and service load

conditions. The effect of an overload equal to 10 percent of the live load will also be considered.

7.8.2 Estimation of Strand Stress Range. Overman et al. [101] proposed a simplified approach for estimating the strand stress range in a cracked section that can be performed by hand. The method requires the strand stress and moment for three conditions: (1) at full dead load (effective prestress), (2) when a crack extends to the bottom of the web, and (3) at ultimate capacity. A bilinear relationship between applied moment and strand stress is defined by these three points from which the strand stress range may be computed.

The strand stress at full dead load and at ultimate capacity will normally be computed as part of the design process. The strand stress and moment corresponding to the remaining condition are determined by developing expressions for the steel tension and concrete compression forces in terms of the curvature across the section and elastic material properties. The curvature is then determined by equating the two expressions. The deck is transformed by the ratio of moduli of elasticity as in standard uncracked analyses. A stress offset between the girder and deck is used and the curvature is assumed to be the same for girder and deck. The shape of the section is approximated by rectangles by neglecting the triangular transition from web to top flange.

A computerized method for computing the strand stress range in a cracked section was developed for use in the program BRIDGE. This method uses an iterative strain compatibility analysis with elastic material properties to determine the stress directly for a given moment. Full section properties are used. This routine differs from the strain compatibility analysis used elsewhere in this chapter only in the use of elastic material properties and its capability to solve for conditions at a given moment rather than at a given top-of-deck strain.

The two methods are similar, since both are based on strain compatibility, but the BRIDGE analysis is more accurate than Overman's method because it directly computes the strand stress for a given moment and considers the full girder cross-section. It provides, however, a slightly less accurate estimate than would be obtained from the other strain compatibility analysis since elastic properties are used. The error, however, is very small due to the low stress levels involved in service load analysis. Overman's analysis is also dependent on the accuracy of the estimate of ultimate conditions made by the AASHTO equations. Since the simplified code approaches underestimate the ultimate capacity, the resulting estimate of stress range is greater than the value predicted by strain compatibility analysis.

Stress ranges computed by the two methods for live load and a 10 percent overload are compared in Fig. 7.71 for maximum and typical span designs using 12 ksi concrete. A third value was computed using a modification of Overman's method in which the initial difference between deck and girder curvatures is preserved in the analysis. Both forms of Overman's method used AASHTO equations for ultimate strand stress and moment. A computer spreadsheet program was used to perform calculations for both forms of Overman's analysis. In all but one case, both types of Overman's analysis gave slightly larger values of the stress range compared with values from the BRIDGE analysis. No specific reason could be found for the one exception for which the difference was small. The difference between the two forms of Overman's analysis is negligible which demonstrates that, for the accuracy intended for the original analysis, the complication added by considering the difference in deck and girder curvatures outweighs the increase in accuracy gained.

The accuracy of the strain compatibility analysis using inelastic section properties (MOMCURV) is compared with strand stresses determined from the tests of Specimens 1 and 2 in Fig. 7.72. Computed design loads are indicated on the curves. Agreement between the analysis and test data was excellent for Specimen 1 to loads exceeding a 10 percent overload. Behavior of Specimen 2 was accurately modelled to a load equal to the live load, at which point

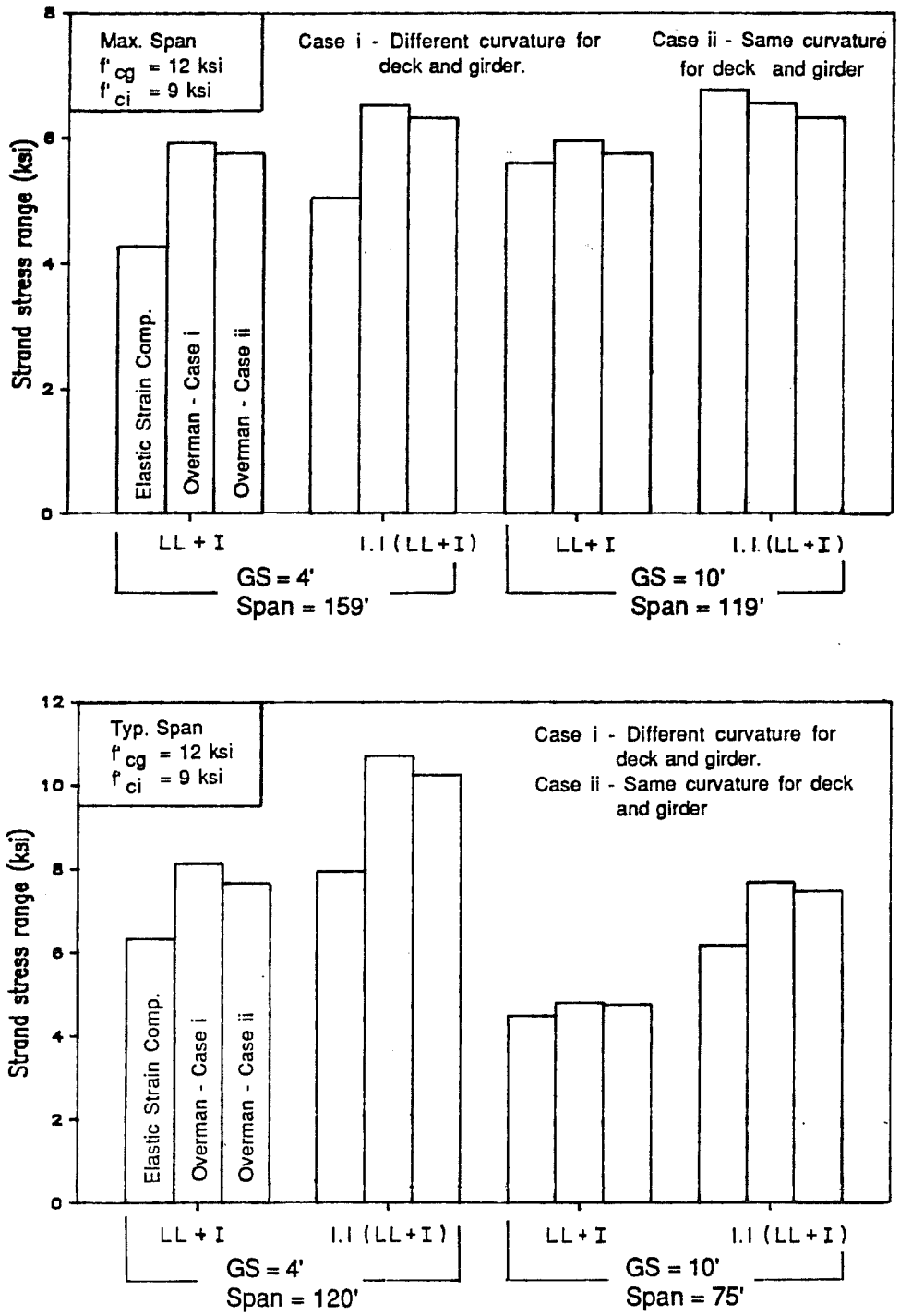

Fig. 7.71 Comparison of methods for computing strand stress range

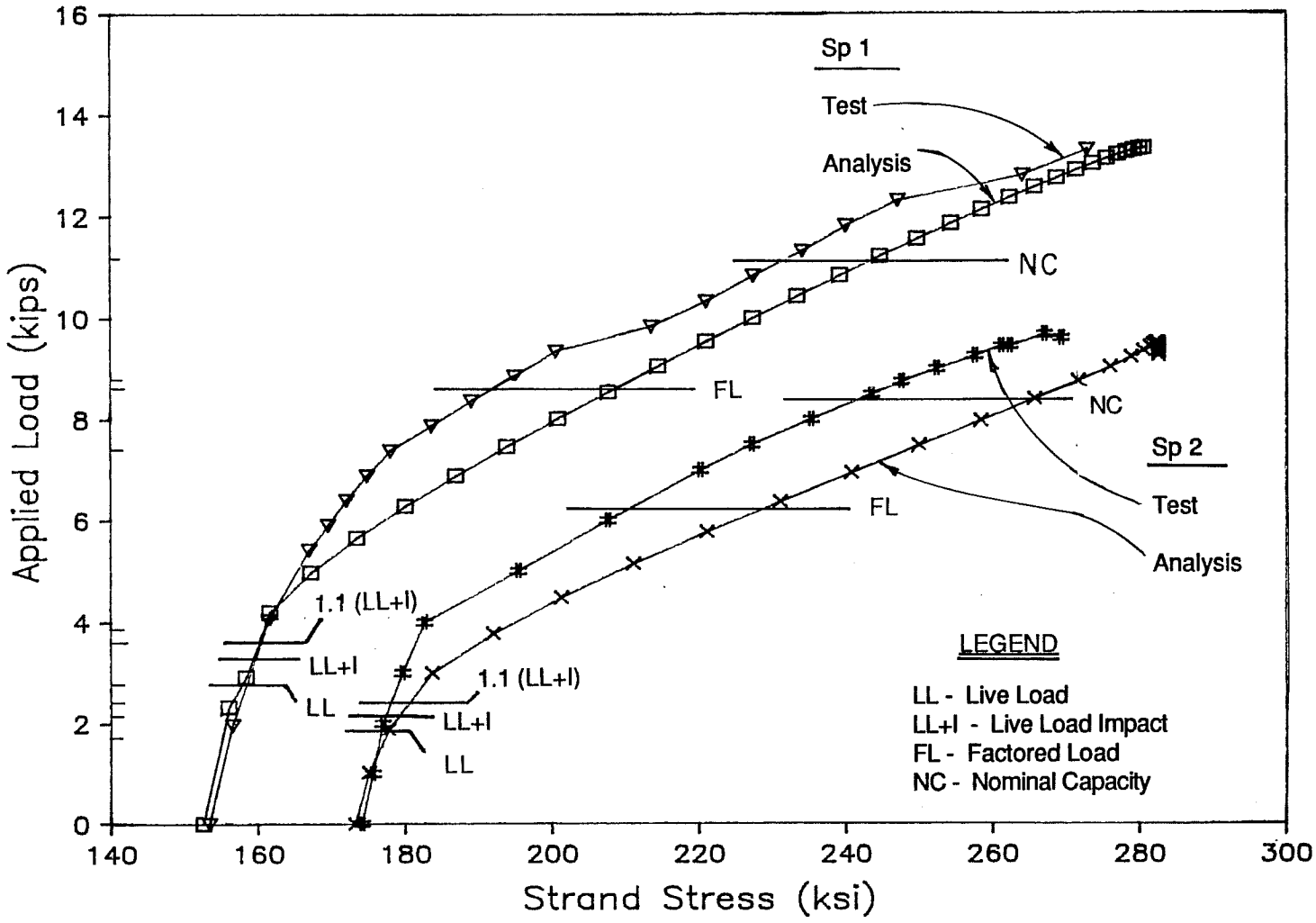

Fig. 7.72 Measured and predicted load-strand stress curves for Specimens 1 and 2

the curves began to diverge. While the approximation became worse with increasing load, the error, which was conservative, remained small for loads up to a 10 percent overload. It can therefore be expected, on the basis of this limited data, that strand stress ranges computed using strain compatibility methods should be reasonable estimates of actual stress ranges.

7.8.3 Investigation of Strand Stress Ranges. Strand stress ranges were computed for all maximum and typical span designs considered in this chapter using the routine included in BRIDGE. Data for the initial analysis using a concrete strength at release of 0.75 times the design strength and the subsequent analysis in which the minimum release strength was determined are shown in Fig. 7.73 and 7.74 for maximum and typical span designs, respectively. Where data is not given for designs with normal strength concrete, either a design using a release strength of 0.75 times the design strength was not possible or the girder was not in tension at service load or overload. The maximum stress range for a cracked section with live load was about 11 ksi, and the overload condition produced a maximum stress range of just over 14 ksi. The stress ranges at service load differed by as much as 6 ksi for uncracked and cracked sections, and the overload caused stress ranges up to 4 ksi greater than those at the service load level with a cracked section. The change in concrete strength at release had little effect on the stress range. It is

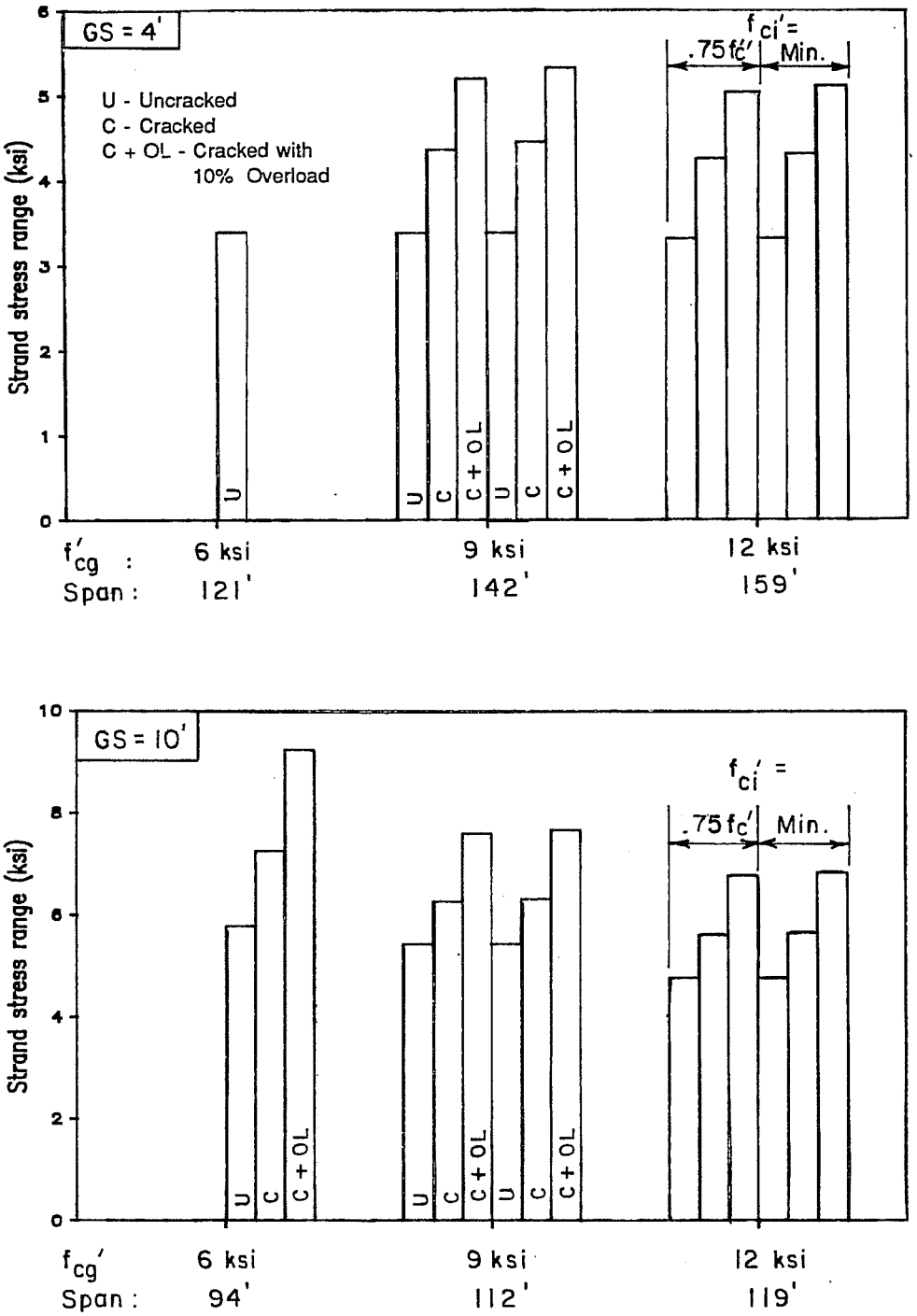

Fig. 7.73 Strand stress ranges for maximum span designs

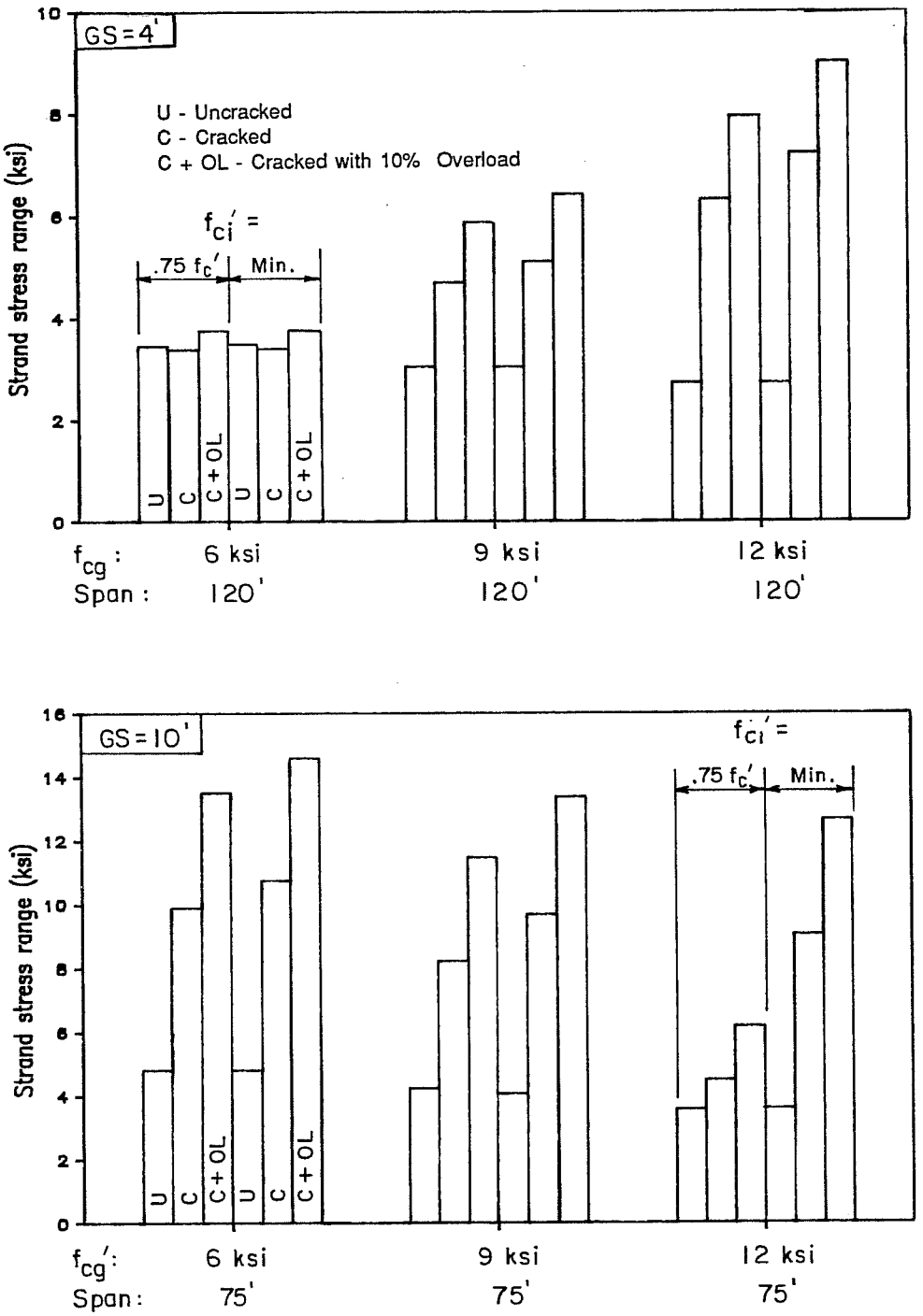

Fig. 7.74 Strand stress ranges for typical span designs

interesting that for the typical span design with GS = 4 ft, increasing the concrete strength caused a significant increase in the strand stress range. This was due to the fact that the girders were lightly reinforced and that cracking extended higher in the stronger concrete since less area of the cross section was required to provide the compression force. The marked decrease in the cracked section stress ranges for the 12 ksi design with a 75 ft span was due to the addition of 2 strands (from 24 to 26) to the lower strength designs. This dramatically demonstrates the sensitivity of stress range to quantity of reinforcement.

Due to the sensitivity of the stress range to the cracked or uncracked condition of the section, the ratio of the applied load that causes cracking to the live load (including impact) was computed for the maximum and typical span designs. The results are summarized in Fig. 7.75. This data reveals that some designs are very susceptible to cracking with only a small overload. The maximum span designs are especially sensitive with some cracking at overloads as low as 12 percent. Use of a lower release strength lowered these values only a very small amount.

The difference between strand stress ranges at the centroid of the strands and for the bottom row of strands was considered. It was found that the difference was negligible because where the stress range was large, the girder was lightly reinforced and the distance

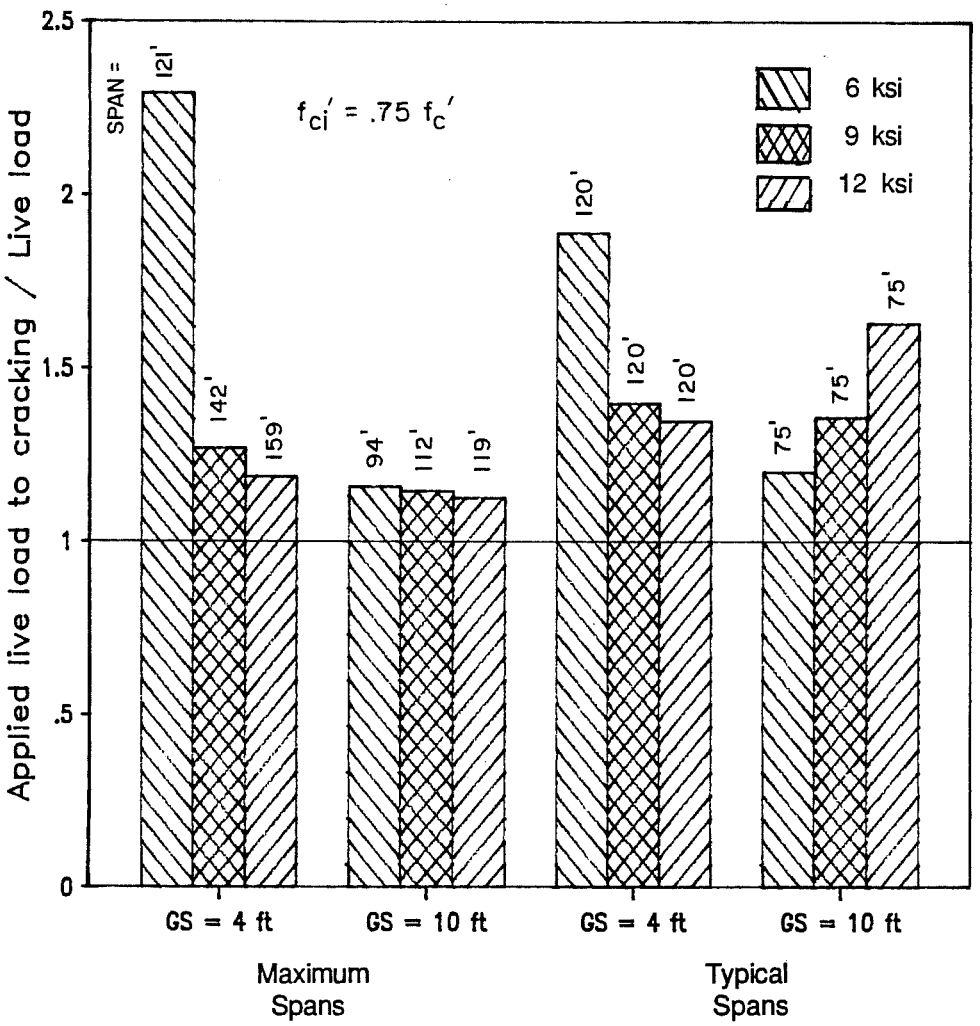

Fig. 7.75 Applied load to cracking as a fraction of live load for maximum and typical span designs

from the centroid of the strands to the bottom strand was small. However, if strand patterns are used that distribute strands in the bottom flange rather than filling each row from the bottom, the difference could be significant and should be investigated.

Due to the sensitivity of strand stress ranges to cracking and the potential for some girders to crack with small overloads, it is recommended that cracked section analysis be used to determine strand stress ranges. This is not a prohibitive limit on design since the likelihood that the endurance limit will be exceeded is small. However, an accurate assessment of the actual loads experienced by bridge girders should be made and the elevated stress ranges caused by overloads should be considered in design. Overman's method of computing stress ranges should be sufficient to provide conservative estimates of strand stress ranges. However, a more sophisticated strain compatibility analysis should be used if more accurate results are desired.

7.9 Prestress Losses

The method for computing prestress losses proposed by Zia et al. [137] was used for the design of the beams used in the comparisons in this chapter. However, Kelly [72] recommends that the method provided in the AASHTO Specifications [10] or a slight modification of that method be used. He points out that the current

AASHTO procedure gives losses that are probably a few percent greater than the actual losses, but closer to reality than the method by Zia et al. [137] which underestimates losses.

The losses computed for maximum and typical span designs used in this chapter are presented in Fig. 7.76 and 7.77, respectively. The AASHTO losses shown are computed using the procedure currently appearing in the AASHTO Specifications. While a direct comparison is difficult for the maximum span data because the span length affects the losses, the losses do appear to be of similar magnitude. For the typical span designs with GS = 4 ft, losses decreased markedly as the concrete strength increased. However, the trend reversed slightly for the typical span designs with GS = 10 ft. Therefore, it appears that no definitive statement can be made with respect to prestress losses and high strength concrete, although losses are generally of the same magnitude as computed for normal strength girders.

7.10 Bond of Prestressing Steel

Data from the transfer tests reported in Chapter 4 are shown graphically in Fig. 7.78. It is clear from the tests that high strength concrete had shorter transfer lengths than normal strength concrete. The AASHTO equation for transfer length is quite conservative for the high strength concrete data shown. This behavior is comparable to the data reported by Mayfield et al. [89]. It

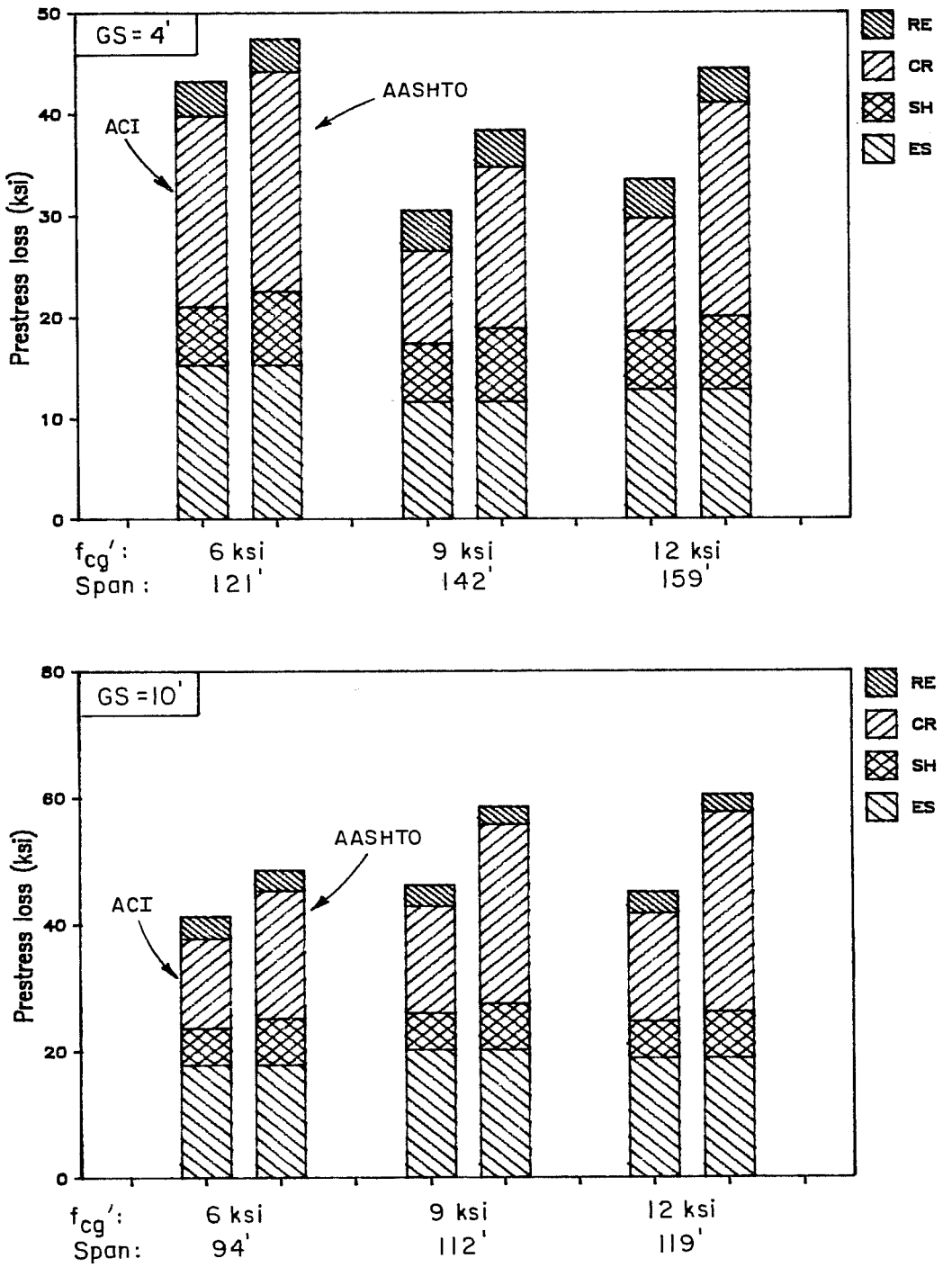

Fig. 7.76 Prestress losses for maximum span designs

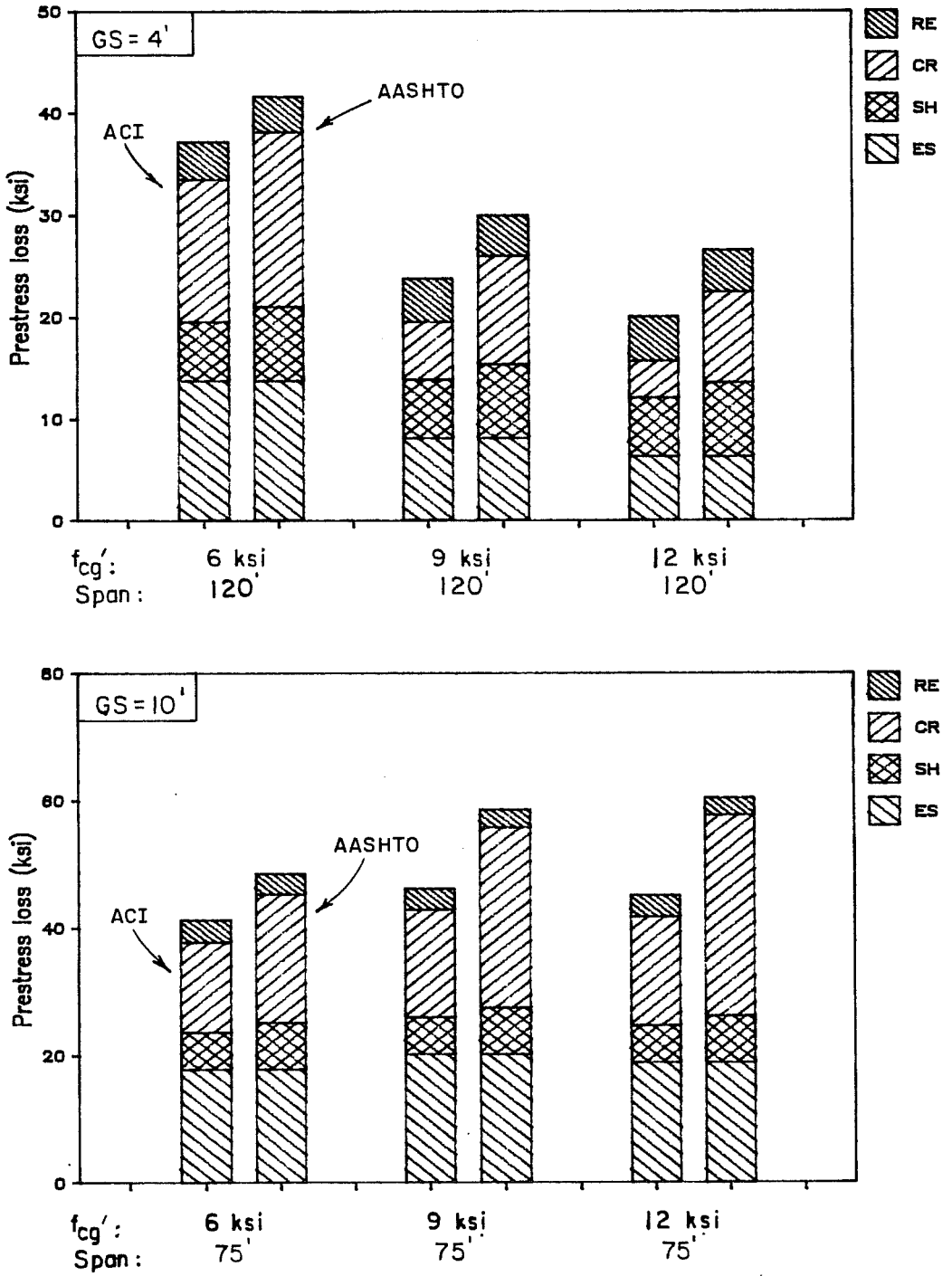

Fig. 7.77 Prestress losses for typical span designs

should be noted that the strand was cut using a torch between only two of the specimens for each strength, giving a "cut end" condition for only those specimens. The specimens with the longest transfer lengths (for normal strength concrete) were released by detensioning the ram. Figure 7.79 shows data from Kaar et al. [70], Hanson [53], Mayfield et al. [89] and data from this test. No distinction is made between cut end or dead end conditions. The AASHTO transfer equation is also plotted on the figure. It appears that transfer lengths tend to decrease with increasing concrete strength and the AASHTO equation becomes more conservative with higher concrete strength. Therefore, the current equation should be used with confidence for high strength concrete because it works at least as well if not better for high strength concrete than for normal strength concrete.

More work needs to be done on the development length of strand in high strength concrete.

7.11 Ultimate Shear Strength

This section contains discussion of preliminary shear tests of portions of the long-span girder specimens. Comment is also made on design for horizontal shear in composite members with high strength concrete girders.

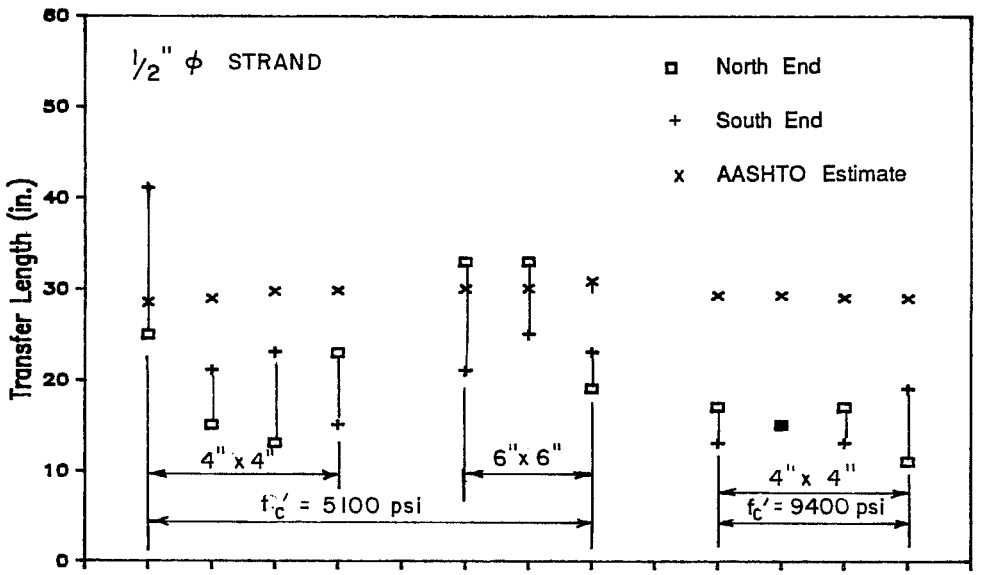

Fig. 7.78 Transfer length data from this study

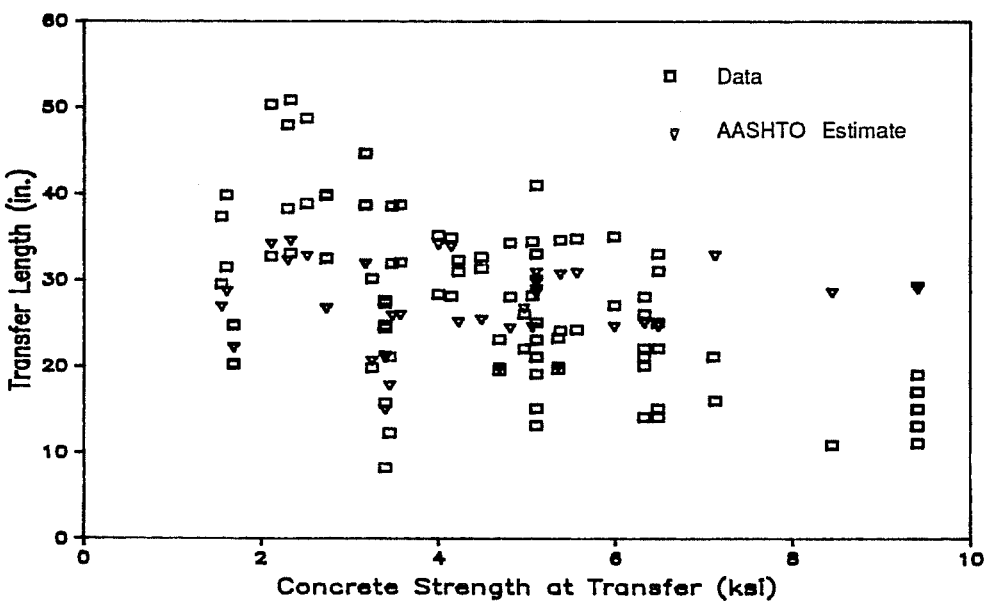

Fig. 7.79 Comparison of measured and computed transfer lengths

7.11.1 Vertical Shear. Data obtained from shear tests of ends of the long-span scale-model girders is very limited but does give preliminary indications of the behavior of high strength concrete in shear for composite members with pretensioned I-section girders.

The current AASHTO equations conservatively predicted the capacity of the specimens for all tests. Predictions for shear at web cracking, however, were in error by a large margin, although this may have been due in part to the prior cracking of the section. Although the AASHTO method is acceptably accurate in predicting the ultimate shear, because the model does not appear accurate in predicting web cracking, it is not clear whether the AASHTO method will be appropriate for use with high strength concrete. Other methods should be investigated to determine whether they are more appropriate for shear design than current methods.

Bond of the strands at the ends of the girder figured prominently in the failure of three of the four tests. These failures were sudden, with a reduction in capacity when strand pull-in occurred. It must be recalled, however, that bond in the strands was not accurately modelled due to restrictions on available materials for use in the scale model. A prototype would be expected to have better bond and therefore increased capacity prior to strand slip. The fourth test, in which the bearing was placed 6 in. farther from the

end of the girder, demonstrated dramatically the effect of bond by increasing the capacity of the member by nearly 20 percent and preventing loss of bond.

The fourth test was most interesting because failure occurred by crushing of the web. The failure, however, was ductile with the load remaining nearly constant while crushing and deflection continued. After the test, it was found that the top of the web was crushed completely through the web over a significant portion of the shear span. It is suggested that the concrete did not crush explosively because the web in shear is a highly redundant structure capable of redistributing the load as crushing proceeded. The concrete was simply not able to "blow out" because it was restrained by adjacent concrete which was also able to absorb the redistributed load. This was evident by the progression of crushing to different locations as additional deformation was applied to the member.

Considering the basic form of the truss model as presented in Ref. [38,110,111], the stress in the compression diagonal, f_d, can be computed using the equation

$$f_d = V/(b_w z \sin\alpha \cos\alpha) \tag{7.20}$$

where z = the moment arm between compression and tension resultants

α = inclination of the compression struts or field.

The derivation of this equation assumes a uniform concrete compression field and a yielding tension chord. Using 20 and 30 degrees as

extreme values for α at failure in the test of the north end of Specimen 2, the computed stress (using Eq. 7.20) in the diagonal compression field at maximum shear ranges between 3.5 and 4.8 ksi, which corresponds to 30 and 40 percent of the girder concrete strength at test. This level of stress is much lower than would normally be expected to cause web crushing, although it exceeds the limit on web stresses of $30\sqrt{f_c'}$, which equals 3.2 ksi in this case, proposed by Ramirez and Breen [110]. Crushing at such apparently low stresses may be due to a number of causes among which are the following: (1) the web was not behaving as a field but rather as discrete struts which were therefore overloaded, or (2) the lack of cracking in the bottom flange of the girder near the support so confined the web that the assumptions made in deriving the truss or compression field theory were no longer valid. Both points cannot be developed from this limited data and require further experimental results.

It was clear that the presence of a bottom flange on the section has a significant effect on the shear capacity of the section. The flange served as a crack arrestor, not permitting web cracks to propagate through the bottom flange and develop the open cracks that are the basis of the classical truss model. The inclusion of the effect of the bottom-flange geometry would be difficult, however, in a general approach to shear design.

On the basis of these tests, the concern voiced by a number of investigators regarding shear cracks in high strength concrete being too smooth to permit adequate shear transfer across cracks by aggregate interlock does not appear to be critical. Shear cracks were not as smooth as some which had been observed in material tests, and appeared sufficiently rough to permit shear transfer if necessary.

7.11.2 Horizontal Shear. From a study of the references mentioned in Chapter 3, it appears that current provisions for horizontal shear can be used with confidence with high strength concrete. This is based on the observation of an increase in shear capacity with increased concrete strength and that concrete strength appears to serve only to limit the effectiveness of the reinforcement. Therefore, the lower strength deck concrete will limit the capacity of the horizontal shear connection. Properties of the deck concrete should be used where the shear friction design procedure is used. No changes in the AASHTO provisions appear necessary.

7.12 Notation

The differences in notation between AASHTO and ACI codes are confusing and unnecessary. Notation found in both codes gives the impression of being assembled in a piecemeal, haphazard manner rather than in a way to provide order and meaning.

The simple proposal made here is that the first letter subscript to any quantity be indicative of the material to which the quantity applies. Specifically, these letters when appearing as a first subscript would have the following meaning:

p: prestressing steel

s: nonprestressed steel

c: concrete.

A single quotation mark used as a superscript would differentiate between the quantity in the compression zone, where the same quantity without the mark would apply to the tension zone, e.q., d_p applies to tension zone prestressed reinforcement and d_p' refers to compression zone prestressed reinforcement. These subscripts would be applied to stresses, strains, areas of steel, and effective depths to the centroid of the area of steel.

A set of letters used as the second subscript would also have unique meanings:

0: initial value, at tensioning

i: initial value, after release

e: effective value, at full dead load

y: value at yield

n: value at computed nominal capacity

u: specified ultimate value for material.

Other letters may also appear as second subscripts with unique meanings.

The letter w may be used as either the only or the second subscript to indicate the web dimension or a quantity determined using web dimensions for flanged analysis, such as the reinforcement ratio.

This system of notation would permit use of variables without subscripts to represent a total or resultant value. Examples of this would be the use ω to indicate the total reinforcement index or the use of d to represent the distance from the extreme fiber to the resultant tension force of all reinforcement.

Table 7.10 presents a sample of the proposed notation system and compares it with the current equivalent notation used in the AASHTO and ACI codes. Definitions are given only as an indication of the meaning of the entries in the table and are not intended to be new or proposed definitions. Notation for both codes would be changed in some instances to conform with the proposed notation. Changes in other notation would be necessary to create complete uniformity among the codes.

While the proposed change in notation to provide uniformity among codes is desirable, it is recognized that there may be considerable resistance to such a change. It would also be a change of convenience and is not necessary to improve the safety or accuracy of designs using the codes.

Table 7.10 Proposed and Current Notation

Proposed	AASHTO	ACI	Brief definition
f_{p0}	-	-	stress in prestressed reinforcement immediately after tensioning
f_{pi}	-	-	stress in prestressed reinforcement immediately after release
f_{pe}	f_{se}	f_{se}	effective stress in prestressed reinforcement after losses
f_{py}	f^*_y	f_{py}	specified yield stress of prestressed reinforcement
f_{pu}	f'_s	f_{pu}	specified ultimate tensile stress of prestressed reinforcement
f_{pn}	f^*_{su}	f_{ps}	stress in prestressed reinforcement at nominal strength
f_{sy}	f_{sy}	f_y	specified yield stress of non-prestressed reinforcement in tension
f_{sn}	-	-	stress in nonprestressed reinforcement in tension at nominal strength
f'_{sy}	f'_y	f_y	specified yield stress of non-prestressed reinforcement in compression
f'_{sn}	-	-	stress in nonprestressed reinforcement in compression at nominal strength
A_p	A^*_s	A_{ps}	area of prestressed reinforcement
A_{pf}	A_{sf}	-	area of prestressed reinforcement required to develop overhanging portion of flange
A_{pw}	A_{sr}	-	area of prestressed reinforcement required to develop web of a flanged section
A_s	A_s	A_s	area of nonprestressed tension reinforcement
A'_s	A'_s	A'_s	area of nonprestressed compression reinforcement

Table 7.10 Proposed and current notation (continued)

Proposed	AASHTO	ACI	Brief definition
ρ_p	p*	ρ_p	ratio of prestressed reinforcement
ρ_s	p	ρ	ratio of nonprestressed tension reinforcement
ρ'_s	p'	ρ'	ratio of nonprestressed compression reinforcement
ω_p	-	ω_p	reinforcement index for prestressed reinforcement
ω_{pw}	-	ω_{pw}	reinforcement index for prestressed reinforcement for flanged section
ω_s	-	ω	reinforcement index for prestressed tension reinforcement
ω_{sw}	-	ω_w	reinforcement index for nonprestressed tension reinforcement for flanged sections
d_p	d	d_p	distance from extreme fiber to centroid of prestressed reinforcement
d_s	-	d	distance from extreme fiber to centroid of nonprestressed tension reinforcement
d'_s	-	d'	distance from extreme fiber to centroid of nonprestressed compression reinforcement
E_p	E_s	E_s	modulus of elasticity for prestressed reinforcement
E_s	E_s	E_s	modulus of elasticity for nonprestressed reinforcement
E_c	E_c	E_c	modulus of elasticity for concrete at 28 days
E_{ci}	E_{ci}	-	modulus of elasticity for concrete at release

CHAPTER 8

SUMMARY AND CONCLUSIONS

8.1 Summary

Recently, it has been demonstrated that high strength concrete can be produced using conventional materials and appropriate admixtures. For purposes of this study, high strength concrete is defined as concrete with a design compressive strength from 6,000 psi to 12,000 psi, which is the current range of strengths for readily attained field-produced concrete. For some analytical investigations in this study, concrete with strengths up to 15,000 psi was considered in order to identify trends.

Use of high strength concrete is expected to produce more economical bridge designs by allowing fewer girders for a given span, or increased span lengths. However, there are uncertainties about use of current design codes for high strength concrete because of differences in behavior between high and normal strength concrete and the lack of test data for structures constructed with high strength concrete. Current codes are also largely empirical and are based on tests utilizing concrete with compressive strengths rarely greater than 6 ksi. Realization of the full potential of high strength concrete may also be limited by outdated design and construction practices.

Therefore, this study was conceived for the purpose of investigating the use of high strength concrete in design of pretensioned girders with a normal strength composite deck. The scope of the study was limited to the consideration of simple span, non-skew pretensioned girder highway bridges where a composite deck is placed with the girder unshored.

A selection of pretensioned girder sections was compared to determine how well given sections utilize high strength concrete. It was demonstrated that a significant increase in span or girder spacing was possible with use of high strength concrete. The lateral stability of girders during handling was found to restrict the span capability of many sections although some means are available to improve girder stability. Three new girder cross-sections were developed and shown to have span capabilities similar to or better than sections of the same depth that are currently used in Texas.

A review of the literature was conducted to determine the state-of-the-art in design using high strength concrete, and to determine the intent of pertinent code provisions. A wide range of topics were considered because the observed brittle behavior of high strength concrete and the potential of extending sections and materials to their limits necessitated the examination of nearly all aspects of design.

Due to the lack of data for composite bridge construction with high strength concrete pretensioned girders, two test programs were developed and completed.

The first set of tests compared transfer characteristics of 0.5-in. diameter seven-wire strand in normal and high strength concrete. Two strengths of concrete were used to cast two sizes of specimens with square cross section which were pretensioned with a single concentric strand. The strands were pretensioned to levels common in practice. Concrete strains measured mechanically before and after release were used to determine transfer lengths. The data collected allowed evaluation of current code transfer length provisions with respect to use with high strength concrete.

Two scale-model high strength concrete pretensioned girders with normal strength composite decks, which were representative of possible long-span bridge designs, were tested in the second phase of the project. The specimens were one-third scale models of prototype modified Type IV girders spanning 146 ft and spaced 4 ft apart. The span-to-total depth ratio was 28.8. Specimen 2 contained close to the minimum number of strands permitted using current allowable stress and ultimate strength design criteria. Specimen 1 contained additional strands and still satisfied the allowable stress criteria but exceeded the maximum reinforcement limit.

High strength concrete was easily placed in the girders even where reinforcement was very congested. No problems in consolidation

were encountered. Widespread shrinkage cracking occurred prior to release of Specimen 2. Although sweep was measured in both specimens at release, no difficulties were encountered handling the girders. Prior to testing, however, both specimens were found to have significant sweep that necessitated lateral restraint of the specimens during testing to prevent further lateral movement.

The specimens were tested in flexure by applying equal loads at equal distances from midspan. Data were collected throughout the tests for strand strains, concrete strains, and deflections. A sudden and violent compression failure occurred for both specimens. At failure, the top portion of the girder was still in compression. It was not possible to determine conclusively whether crushing of the girder or deck concrete initiated failure.

Shear tests were conducted on the ends of each specimen. Specimens were loaded at the quarter point nearest the end of the half girder in order to force failure to occur in a region where cracking from the flexure test was limited. The shear span-to-effective depth ratio was approximately 3.5 for Specimen 1 and 2.9 for Specimen 2. Of the four shear tests conducted, all failures occurred in the desired shear span with three failing as a result of slip in strands at the end of the girder. For the fourth test, the support was located 6 in. further from the end of the girder to provide improved bond. Failure was caused by web crushing in this case.

The literature review and test data were then used as the basis for evaluation of current design practice. The test data were used to verify a basic strain compatibility analysis program as a simple yet effective and accurate tool for analysis of composite pretensioned girder bridges. Representative bridge designs were used to determine the accuracy and appropriateness of current design procedures, and to study the sensitivity of design aspects to different parameters. Recommendations were made where changes to current code provisions and practice appeared necessary.

8.2 Conclusions

In this section, major conclusions from the study are presented. Each conclusion or group of related conclusions is numbered and followed by a reference to the section from which the conclusion is taken. More complete and detailed conclusions were given as specific topics were considered in the body of the text.

1. The use of high strength concrete in pretensioned bridge girders results in significant increases in span length or girder spacing. (2.4.1)
2. Increasing the concrete strength for a given span and spacing will not generally affect the minimum number of strands required to satisfy design criteria. (2.4.2)
3. The lateral stability requirements for handling severely limit the above mentioned increase in maximum span

capacity for some sections, especially 54- and 72-in. sections. (2.3.3, 2.4.1)

4. Sweep and eccentricity of lifting points have a significant effect on the lateral stability of girders and must be considered in design. (7.7.1)
5. The use of high strength concrete to improve the stability of a girder is most effective when used for a given span rather than to increase the maximum lifting span. (7.7.1)
6. The lateral stability of a girder may also be improved by moving lifting points in from the ends of a girder, using external bracing ("hog-rods"), or using rigidly attached lifting yokes. (7.7.1)
7. Sections with greater weak-axis moments of inertia generally have the greatest lateral stability when lifted. The MOT/C&CA M 54/6 section, which has a large bottom flange, had the best overall performance with respect to stability. (2.3.3, 2.4.1, 7.7.1)
8. In some cases, use of high strength concrete will permit a reduction in the fraction of design strength required at release as compared to that required for normal strength designs. (7.4.5.5)

9. Three proposed sections provide good alternatives to currently used sections considering span capabilities, section size, and lateral stability. (2.4.1)
10. A comparison of actual designs provides the best indication of relative performance of different sections. (2.3.1, 2.4.3)
11. On the basis of limited test data, the transfer length of strand in high strength concrete is slightly shorter than for normal strength concrete. (4.6)
12. The AASHTO expression for estimating transfer length is conservative for high strength concrete. (4.6)
13. Because the modulus of elasticity can vary widely due to a number of factors, it is recommended that the modulus be determined experimentally when an accurate value is needed. (7.3.2)
14. Current code expressions for the modulus of elasticity are sufficiently accurate if data for a specific mix is not available. (7.3.2)
15. The effect of using the modulus equation proposed by investigators at Cornell rather than current modulus equations is small. (7.4.5.4)
16. In this study, the maximum usable concrete strain was found to be lower for high strength concrete than for

normal strength concrete, which agrees with the trend of data reported by other investigators. (7.3.2, 7.4.3.2)

17. In composite members, the normal strength deck concrete will generally reach the maximum usable strain before the girder concrete reaches its limiting strain. (7.4.4.2, 7.4.5.2)

18. In this study, compression failures occurred while measured compressive strains in both the deck and girder concrete were below the current code specified value of 0.003. (7.3.2)

19. The use of a reduced maximum usable concrete strain in design and analysis does not generally affect the capacity but would result in reduced deflections, section ductility, and other strain related quantities at failure. (7.4.5.2)

20. Placement of high strength concrete in narrow, congested sections is possible through the use of high range water reducers (superplasticizers). (7.3.7)

21. The AASHTO and ACI simplified ultimate flexural design approaches provide good, conservative estimates of the capacity of composite sections when compared with test data and results of strain compatibility analyses. (7.4.4.2, 7.4.5.2)

22. Horizontal girder dimensions should be transformed by the ratio of girder-to-deck concrete strengths when using the simplified ultimate analysis methods in order to obtain the best agreement with results of strain compatibility analyses. (7.4.2.2, 7.5.2.2)
23. Current expressions for determining strand stress at ultimate are adequate. The revised equation in the ACI Code gives better estimates than the AASHTO expression when compared to test data and results of strain compatibility analyses. (7.4.4.2)
24. The strain compatibility analysis program MOMCURV gave conservative yet realistic estimates of measured flexural behavior for specimens. The capacity of the section was very closely predicted and provided a better estimate of capacity than the simplified methods. (7.4.3)
25. Suitably accurate analytical relationships for defining concrete and steel stress-strain curves are available and should be used to obtain the best estimate for all aspects of section behavior when using a strain compatibility analysis. (7.4.3.1, 7.4.3.2)
26. The current practice of limiting the reinforcement index ω to ensure a section has sufficient ductility is appropriate and accurate. (7.5.1, 7.5.2.2)

27. The current maximum reinforcement limit is based on assumptions that are inconsistent with other code provisions and current practice. (7.5.2.1)
28. A maximum reinforcement limit that is consistent with code provisions and current practice, and similar to the current limit is proposed. This limit includes the effect of strand strength and effective prestress. The limit is slightly more restrictive than the current limit in most cases. Because the proposed limit appears in a form similar to the maximum reinforcement limit for reinforced concrete members, it should be readily understood and accepted for use by designers. (7.5.2.1)
29. A minimum reinforcement limit is proposed which would prevent rupture of strands prior to the extreme concrete compression fiber reaching the maximum usable strain. The proposed limit has the same form as the maximum reinforcement limit but can also be expressed in a simplified form without significant loss of accuracy. (7.5.3).
30. Deflections due to applied loads can be accurately estimated using a strain compatibility analysis. (7.6.2)
31. Live load deflections should be limited to the levels currently specified for steel bridges in the AASHTO Specification. (7.6.3)

32. Long-term deflections should be estimated for girders to ensure good serviceability, especially for long-span members. Limits for long-term deflections of pretensioned concrete highway bridges should be developed. The possibility for differential camber should be investigated where significant differences in age or curing conditions exist between girders within a span. (7.6.1)

33. Strand stress ranges should be used for determining the fatigue resistance of pretensioned girder bridges. Suitably accurate estimates of strand stress ranges in cracked sections can be made using a strain compatibility analysis. (7.8)

34. Current code provisions for estimating shear strength are conservative compared with data collected in this study, although web cracking occurred at shears well below those predicted by code provisions. (7.11.1)

35. Bond of longitudinal reinforcement at the ends of a girder is an important factor in determining the shear capacity of a pretensioned member. Lack of sufficient bond results in premature failure. (7.11.1)

36. Where sufficient bond was available at the end of the girder, web crushing occurred at shears below that expected to produce this failure condition. The

assumptions of the classic truss model were not satisfied when web crushing occurred because the bottom flange was not cracked and the tension chord was not yielding. (7.11.1)

8.3 Recommendations

The following recommendations are made for further study or for changes in current codes of practice. The same format will be used as for the conclusions.

1. Further study should be performed to determine the strain in the top fiber that leads to crushing in a member, especially for T-shaped members. The development of a correlation between maximum usable concrete strain and depth of the neutral axis at failure should be explored.
2. Derivations and intent of the proposed maximum and minimum reinforcement limits should be published as part of the codes or in associated commentaries in order to help designers understand the reinforcement limits.
3. Further study should be conducted on the lateral stability of girders during lifting and transportation operations. A survey of state and federal highway departments, fabricators, and erectors is recommended to determine their experience with different sections and to obtain data which can be used to verify stability

analyses. A range of typical imperfections should also be obtained for use in the design process. (7.7.1)

4. Shear tests should be conducted on full-scale girders or on scale-model girders with provision for adequate bond to determine the effect of bond on shear capacity in girders. The effect of debonding strands at the ends of girders should be included in the study. Further work must be performed to continue development of comprehensive design and analysis methods for shear, including the effect of size and shape of the web and bottom flange. (7.11.1)
5. Further study should be conducted on typical bridge designs for various sections. In these studies, the effect of various parameters, including concrete strength, should be studied to determine how they affect all aspects of design, including lateral stability, fatigue, cracking, and deflections.
6. Use of an approximate equation to compute the cracking moment for the current minimum reinforcement limit should be discontinued since it leads to excessively high ultimate strength requirements in some cases.
7. AASHTO and ACI notation should be revised to be consistent in order to minimize confusion. The notation

proposed in Chapter 7 is consistent and could serve as a starting point for the standardization process.

A P P E N D I X A

MIX AND STRENGTH DATA FOR HIGH STRENGTH CONCRETE

This Appendix presents the mix and strength data for the high strength concrete used in the girders of Specimens 1 and 2. Data pertaining to materials and admixtures used in the concrete are given in Tables A.1 and A.2. Mix proportions and properties are given in Table A.3. Strength test data for compression and tension are given for the two specimens in Tables A.4 and A.5. Modulus data for both specimens appear in Table A.6. Values appearing in the tables are averages for the indicated number of tests performed. Plots of compressive and tensile strength data with age appear in Fig. A.1 and A.2 for the two specimens.

Concrete used in Specimen 1 was reported in Ref. [35] as mix number 22-110-34. The trial batch on which this mix design is based appeared in the same report as mix number 21-112-34.

Table A.1 Properties of Materials Used in Mix

MATERIAL	MATERIAL PROPERTIES
Cement	ASTM C150 Type I
Fly Ash	ASTM C618 Class C TSDHPT Type B BSG = 2.64 La Grange Type C Trinity Pozzolanic Admixture General Portland
Coarse Aggregate	Crushed dolomite ASTM C33 No. 8, 3/8-in. to #8 DRUW = 100 pcf BSG_{ssd} = 2.79 AC_{ssd} = 0.5%
Fine Aggregate	Natural river sand BSG_{ssd} = 2.62 AC_{ssd} = 1.0%

Table A.2 Properties of Chemical Admixtures Used in Mix

ADMIXTURE TYPE	ADMIXTURE PROPERTIES
Water reducing and retarding admixture (R-Plus - Gifford Hill)	ASTM C494 Type D Polymer-based S.G. = 1.24 % solids = 42% Dosage rates: 2-4 oz./cwt
High-range water reducing admixture (PSI Super-Gifford Hill)	ASTM C494 Type F Naphthalene-based S.G. = 1.21 % solids = 42% Dosage rates: Flowing concrete: 6-12 oz./cwt High-range water reduction: 12-16 oz./cwt

Table A.3 Final Mix Design and Properties

Design Strength	12,000 psi
Mix Design (Quantites in lbs. per cu. yard)	
Cement	698
Fly Ash	298
Coarse aggregate	1821
Fine aggregate	1039
Water	282
Water reducing and retarding admixture	20 oz.
High-range water reducing admixture	80 oz. at batch plant 100 oz. at laboratory
Quantity delivered (c.y.)	4
Cost per yard delivered	$65
Mix Properties	
Slump	1 in. at batch plant before adding HRWR
	10 in. at laboratory after second dose of HRWR
Unit weight	150 pcf
Air content	1.3 %
Water/Cement ratio	0.29
Cementitious content (sacks/cy)	10.5
% Cementitious as fly ash	30 %
% DRUW (Dry Rodded Unit Weight)	66 %

Table A.4 Results of Cylinder and Beam Tests - Specimen 1

	Age (Days)	Curing	Mold	Cap	No.	f'_c (ksi)
Compression Strength Tests						
6 x 12-in. cylinders	2	---	Plastic	S	2	7.58
	7	Air	Plastic	S	2	10.21
	14	Air	Plastic	S	2	10.84
	21	Air	Plastic	S	2	12.53
	28	Air	Steel	S	2	12.00
		Wet	Steel	S	2	12.42
	44	Air	Steel	S	2	13.02
		Wet	Steel	S	2	13.66
	66	Air	Steel	S	2	12.91
		Air	Plastic	S	3	12.49
	94	Air	Plastic	S	2	12.99
	114	Air	Plastic	S	2	13.16
		Air	Plastic	P	2	13.29
	135	Wet	Steel	P	2	14.69

Tensile Strength Tests

			No.	f'_t	$f'_t/\sqrt{f'_c}$
Beam Tests					
6 x 6 x 21-in.	28	Air	2	0.908	8.29
Third point loading		Wet	2	1.650	14.81
	44	Air	2	1.019	8.93
		Wet	2	1.715	14.67
Split Cylinder Tests - Plastic molds					
6 x 12-in. cylinders	114	Air	2	0.724	6.31

Notes:

Curing: Air - Curing compound applied after form removal. Cylinders and beams cured with girder
Wet - Cylinders and beams cured in lime bath

Cap type: S - High-strength sulfur capping compound
P - Pad caps

Table A.5 Results of Cylinder and Beam Tests - Specimen 2

	Age (Days)	Curing	Mold	Cap	No.	f'_c (ksi)
Compression Strength Tests						
6 x 12-in. cylinders	4	---	Plastic	S	2	8.62
	7	Air	Plastic	S	2	9.20
		Wet	Plastic	S	2	8.90
	14	Air	Plastic	S	2	10.10
	21	Air	Plastic	S	2	10.12
	28	Air	Plastic	S	3	10.75
		Wet	Plastic	S	3	10.66
	48	Air	Plastic	S	2	10.12
	55	Air	Plastic	S	3	10.78
		Wet	Plastic	S	3	11.14
	265	Air	Plastic	S	3	11.34
		Air	Steel	S	3	11.49
4 x 8-in. cylinders	28	Air	Steel	S	2	11.11
	55	Air	Steel	S	3	10.80
3 x 6-in. cylinders	29	Air	Steel	S	3	10.30
	55	Air	Steel	S	3	9.97

Tensile Strength Tests

			No.	f'_t	$f'_t/\sqrt{f'_c}$
Beam Tests					
6 x 6 x 21-in.	7	Air	2	0.879	9.16
Third point loading		Wet	2	1.598	16.94
	28	Air	2	0.965	9.31
		Wet	2	1.533	14.85
	55	Air	2	1.100	10.59
	265	Air	2	1.275	11.89
Split Cylinder Tests - Plastic molds					
6 x 12-in. cylinder	29	Air	2	0.722	6.96
		Wet	2	0.756	7.32

See Table A.4 for Notes

Table A.6 Modulus of Elasticity Data for Girder Concrete

Age (days)	Curing	Individual Cylinders Strength (ksi)	Individual Cylinders Modulus (ksi)	Average Strength (ksi)	Average Modulus (ksi)	$E_c/\sqrt{f'_c}$ ($\times 10^3$)
Specimen 1 - Steel molds						
44	Air	12.82	6410	13.02	6380	55.9
		13.22	6350			
66	Air	12.73	5900	12.91	5980	52.6
		13.09	6060			
66 *	Air	12.73	6360	12.91	6430	56.5
		13.09	6490			
Specimen 2 - Plastic molds						
7	Air	9.34	5260	9.20	5300	55.3
		9.06	5340			
21	Air	10.07	5550	10.12	5550	55.2
		10.17	5550			
28	Air	10.93	5850	10.75	5720	55.2
		10.62	5640			
		10.17	5680			
28	Wet	10.63	7760	10.66	7000	67.8
		10.79	6660			
		10.56	6690			
56	Air	10.78	5590	10.78	5675	54.7
		10.69	5710			
		10.87	5730			

Note: Unit weight of concrete is approximately 150 pcf

* Modulus determined using two electronic strain gages on each cylinder. All other data taken using a compressometer.

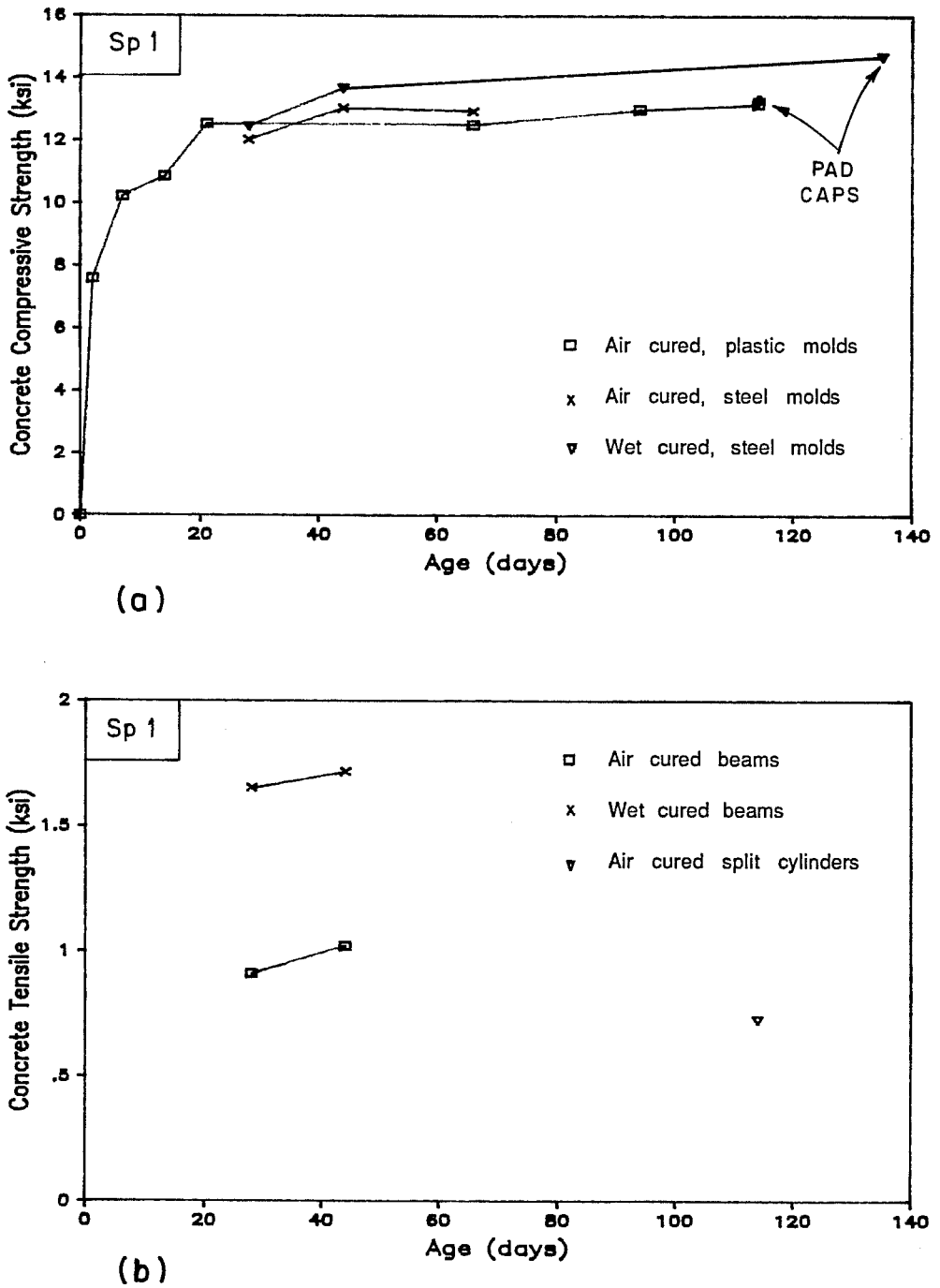

Fig. A.1 Strength gain with age for Specimen 1: a) compressive strength; b) tensile strength

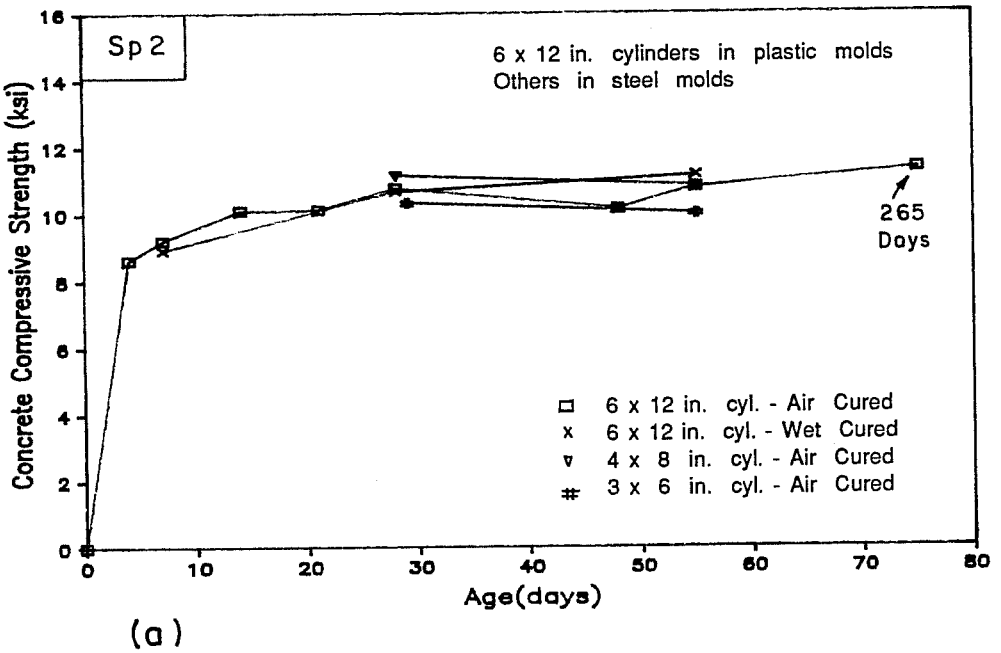

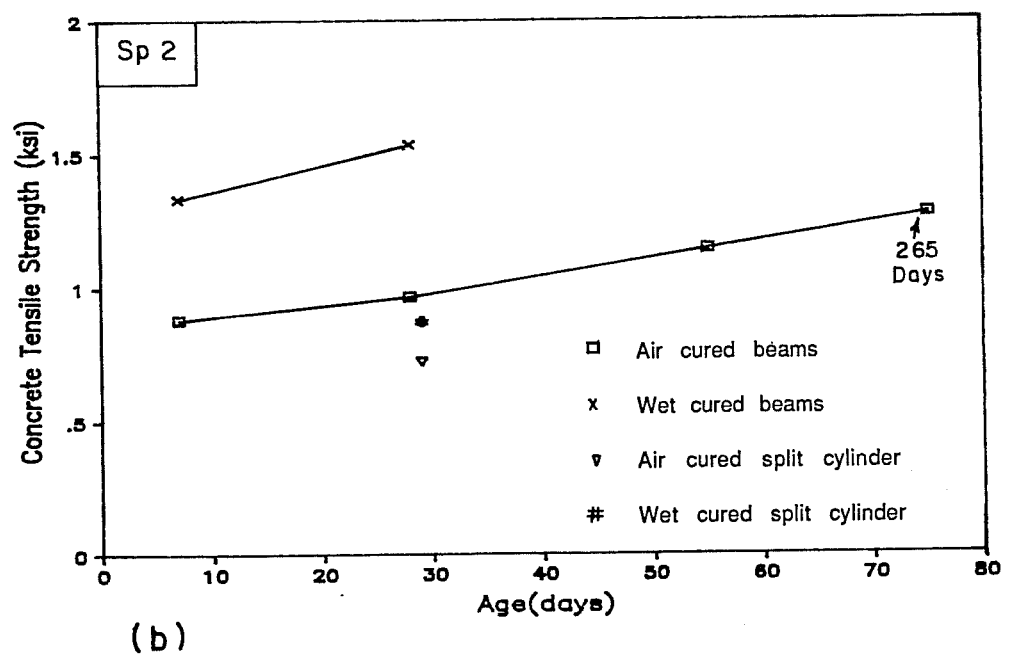

Fig. A.2 Strength gain with age for Specimen 2: a) compressive strength; b) tensile strength

A P P E N D I X B

HISTORY OF LONG-SPAN GIRDER SPECIMENS

B.1 Specimen 1 (13 strands)

Cast dates and significant changes in load are highlighted.

A detailed account of the ultimate flexure test is given because high strains were sustained for significant periods of time during the tests and such long-term load effects may have affected the response of the specimen. Only brief summaries are given for shear tests because long term effects were not as significant.

Date	Time	Net Time (hours)	Comments
1/ 8/86	16.5	-44.7	Connect 4 midspan strand gages to strain indicator
1/10/86	13.2	.0	ZERO HOUR FOR HISTORY - Zero readings for midspan strand gages
1/10/86	13.3	.1	Tension gaged strands to 17 kips each
1/10/86	13.4	.2	Tension gaged strands to 10 kips each
1/10/86	13.5	.3	Gaged strands seated
1/10/86	14.0	.8	All strands tensioned and seated
----------			STRANDS FULLY TENSIONED
1/16/86	13.3	144.1	Prior to fully tensioning all strands with large ram
1/16/86	16.4	147.2	All strands tensioned to approx 17 kips
1/21/86	10.1	260.9	Just prior to arrival of truck with girder concrete
1/21/86	12.4	263.3	Just prior to casting girder - truck arrived at 12:15
**********			CAST GIRDER
1/21/86	13.7	264.6	Finishing of concrete surface complete
1/21/86	15.3	266.1	Curing burlap and plastic in place
1/23/86	14.5	313.3	Remove girder forms
1/23/86	15.0	313.8	Apply curing compound by rag
1/27/86	17.0	411.8	Connect remaining strand, girder concrete and 4 stirrup ... ... gages to strain indicators; take initial readings.
1/28/86	14.4	433.3	Begin release procedure - hold downs released
1/28/86	14.6	433.4	NOTE: NO LOAD PLACED ON GIRDER DURING OR AFTER RELEASE
----------			RELEASE
1/28/86	15.0	433.8	Full release by detensioning with ram
1/28/86	16.3	435.1	Cut strands
1/29/86	10.5	453.3	Begin to move girder to pedestal
1/29/86	14.8	457.6	Girder in final location
----------			ADD 20 PLF DECK FORM LOAD
1/31/86	10.1	500.9	Slab forms placed; fully supported by girder
1/31/86	15.8	506.6	Just prior to placing dead load blocks

			Note: Dead load compensation blocks weigh approx. 470 lb. ea.
----------			ADD 156 PLF GIRDER DEAD LOAD COMPENSATION
1/31/86	17.0	507.8	16 dead load blocks placed to compensate for girder dead load
----------			ADD 78 PLF DECK DEAD LOAD COMPENSATION
2/ 4/86	8.3	595.2	24 blocks in pairs at 4 feet
----------			SUBTRACT 78 PLF DECK DEAD LOAD COMPENSATION
2/ 5/86	10.6	621.4	8 blocks removed since cast is delayed - 16 remain
----------			ADD 78 PLF DECK DEAD LOAD COMPENSATION
2/ 6/86	9.5	644.4	24 blocks again in place for full d.l. compensation
**********			CAST DECK
2/ 6/86	12.0	646.8	Deck concrete in place
2/ 6/86	13.3	648.1	Excess concrete removed
2/ 6/86	15.8	650.6	Curing burlap and plastic in place
2/11/86	11.5	766.3	Burlap and plastic removed
----------			SUBTRACT 20 PLF DECK FORM LOAD
2/11/86	15.2	770.1	Forms removed; 23 dead load blocks replaced on specimen ...
			... spaced at 2 feet with one at midspan
2/14/86	17.2	844.0	Connect deck concrete gages to strain indicators ...
			... take initial readings
2/18/86	8.3	931.1	1 block removed at each load point for loading head
2/18/86	14.3	937.2	Large cross head in place at each load point ...
			... no significant change in load
2/20/86	11.0	981.8	Rams and load cells in place
3/ 4/86	14.6	1273.5	Preliminary loading to to 2 kips to check setup
----------			FIRST ATTEMPT TO LOAD TO CRACKING
3/ 6/86	13.1	1319.9	Begin test
3/ 6/86	15.5	1322.3	7.14 kips - maximum load; increasing sweep halts test
3/ 6/86	16.8	1323.6	Unload
3/11/86	12.0	1438.8	Cross heads removed for modification
3/24/86	9.1	1747.9	New tied lower cross heads in place; dead load blocks ...
			... rearranged but load remains essentially unchanged
3/25/86	14.9	1777.7	Push and hold specimen to east to reduce sweep
----------			SECOND ATTEMPT TO LOAD TO CRACKING - SIDE SWAY PREVENTED
3/26/86	10.2	1797.0	-0.59 kips - No applied load
3/26/86	10.4	1797.2	0.00 kips - upper cross heads lifted by rams
3/26/86	10.6	1797.4	0.98 kips
3/26/86	10.8	1797.6	1.97 kips
3/26/86	10.8	1797.7	2.95 kips
3/26/86	11.0	1797.8	3.94 kips
3/26/86	11.0	1797.9	4.92 kips
3/26/86	11.2	1798.0	5.41 kips
3/26/86	11.3	1798.2	5.66 kips
3/26/86	11.4	1798.3	5.90 kips
3/26/86	11.6	1798.4	6.15 kips
3/26/86	12.0	1798.8	6.40 kips
3/26/86	12.3	1799.1	6.65 kips
3/26/86	12.4	1799.2	6.89 kips
3/26/86	12.6	1799.5	7.14 kips
3/26/86	12.8	1799.7	7.38 kips - Maximum load
3/26/86	13.2	1800.0	6.01 kips - load remaining after delay

3/26/86	13.3	1800.1	4.92 kips
3/26/86	13.5	1800.3	3.43 kips
3/26/86	13.6	1800.5	1.98 kips
3/26/86	13.8	1800.6	-0.73 kips - upper cross heads supported on nuts
----------			ULTIMATE FLEXURAL TEST
3/26/86	14.4	1801.3	-0.52 kips - No applied load
3/26/86	15.1	1802.0	1.97 kips
3/26/86	15.3	1802.1	4.03 kips
3/26/86	15.4	1802.3	5.41 kips
3/26/86	15.6	1802.4	5.90 kips
3/26/86	15.7	1802.5	6.40 kips
3/26/86	15.8	1802.7	6.89 kips
3/26/86	16.0	1802.8	7.38 kips
3/26/86	16.2	1803.0	7.87 kips
3/26/86	16.5	1803.3	8.37 kips
3/26/86	16.7	1803.5	8.86 kips
3/26/86	16.9	1803.8	9.35 kips - Reset load heads
3/26/86	17.6	1804.4	9.84 kips
3/26/86	17.8	1804.7	10.33 kips
3/26/86	18.0	1804.9	10.83 kips
3/26/86	18.2	1805.0	11.32 kips
3/26/86	18.3	1805.2	11.81 kips
3/26/86	18.5	1805.3	12.30 kips
3/26/86	18.8	1805.6	12.79 kips - Reset load heads
3/26/86	19.1	1806.0	13.29 kips - Failure occurred as load stage attained
----------			PREPARE SOUTH END FOR SHEAR TEST - STD STIRRUP DETAIL
			Note: No dead load blocks used during shear tests of south end
4/15/86	13.3	2280.2	Begin initial shear test
4/15/86	14.9	2281.8	Load system problems, stop test at approx. load of 24.34 kips
4/15/86	15.5	2282.3	Unload from initial test
4/23/86	14.1	2472.9	Begin preliminary loading to test load system
4/23/86	14.9	2473.7	Maximum load of preliminary loading - 24.34 kips
4/23/86	15.3	2474.1	Unload from preliminary test
----------			CRACKING SHEAR TEST - SOUTH END
4/24/86	9.1	2491.9	Begin test
4/24/86	10.8	2493.6	Maximum load - 34.83 kips
4/24/86	11.5	2494.4	Unload
----------			ULTIMATE SHEAR TEST - SOUTH END
4/24/86	13.3	2496.1	Begin test
4/24/86	16.2	2499.0	Failure occurred when shear of 63.24 kips achieved
4/24/86	17.1	2499.9	Partial unload
4/24/86	17.5	2500.4	Unload
----------			PREPARE NORTH END FOR SHEAR TEST - MODIFIED STIRRUP DETAIL
			Note: No dead load blocks used during shear tests of north end
5/ 8/86		2818.8	Place North end in testing frame
5/ 9/86		2842.8	Position specimen; set bearings and load head
----------			CRACKING SHEAR TEST - NORTH END
5/13/86	14.0	2952.8	Begin test
5/13/86	16.6	2955.4	Maximum load of 33.88 kips shear
5/13/86	17.3	2956.1	Unload

----------			ULTIMATE SHEAR TEST - NORTH END
5/14/86	13.5	2976.3	Begin test
5/14/86	16.6	2979.4	Failure occurred at shear of 65.22 kips
5/14/86	16.7	2979.6	Specimen supported a shear of 61.27 kips upon reloading
5/14/86	17.0	2979.8	Unload

B.2 Specimen 2 (9 strands)

Cast dates and significant changes in load are highlighted.

A detailed account of the ultimate flexure test is given because high strains were sustained for significant periods of time during the tests and such long-term load effects may have affected the response of the specimen. Only brief summaries are given for shear tests because long term effects were not as significant.

Date	Time	Net Time (hours)	Comments
6/27/86	14.3	.0	Connect strand gages to boxes; initial readings
6/30/86	9.1	66.8	Strands lying slack in bed
6/30/86	9.3	67.0	17 kips applied to strand 1 (center bottom row)
6/30/86	9.5	67.2	10 kips reapplied to strand 1
6/30/86	9.6	67.3	Strand 1 is seated
6/30/86	9.7	67.5	17 kips applied to strand 2 (draped strand row 3 at midspan)
6/30/86	9.8	67.6	10 kips reapplied to strand 2
6/30/86	12.3	70.0	All 9 strands are seated with approx 10 kips in each
7/ 1/86	11.2	92.9	Adjust height of north draped strand hold-up; tie stirrups
7/22/86	9.2	595.0	Begin tying end detail steel and preparing for casting
7/23/86	10.9	620.7	Just prior to full tensioning
----------			STRANDS FULLY TENSIONED
7/23/86	11.6	621.4	Full pretension force applied
7/23/86	18.3	628.1	Girder forms in place
7/24/86	12.6	646.3	Prior to casting
**********			CAST GIRDER
7/24/86	14.1	647.9	Concrete in place in girder forms
7/24/86	16.9	650.7	Curing burlap,towels and plastic sheeting in place
7/28/86	10.1	739.9	Forms removed; water and curing compound applied
7/31/86	14.7	816.4	8 dead load blocks in place near midspan
7/31/86	15.4	817.2	Zero readings taken on girder surface gages
7/31/86	15.8	817.6	Begin to pressurize ram for release
----------			RELEASE
			8 DEAD LOAD COMPENSATION BLOCKS PLACED IN PAIRS AT 3' AND 8.5' EACH SIDE OF MIDSPAN
			Note: Dead load blocks weigh approx. 470 lb. each
7/31/86	16.1	817.8	Release is complete; chucks are loose at both ends

8/ 1/86	9.2	834.9	Cut strands at each end
----------			ADD 8 DEAD LOAD BLOCKS; 16 TOTAL IN PAIRS AT 6 FT SPCG.
			FULL GIRDER DEAD LOAD COMPENSATION - 156 PLF
8/ 1/86	14.0	839.8	8 dead load blocks added; girder placed on bearing pads
9/ 9/86	11.7	1773.4	Girder moved from prestress bed and placed on pedestals
9/ 9/86	12.3	1774.0	Instrumentation boxes removed from girder - placed on table
			Central 8 blocks removed for placement of forms
			Center 3 form sections in place; place 8 blocks on these
			Remove 12 dead load blocks to place remaining forms
----------			ADD DECK FORM LOAD - 20 PLF - PLUS 8 DEAD LOAD BLOCKS
9/ 9/86	18.2	1780.0	All forms in place; 8 dead load blocks placed in pairs ...
			... at 4 ft spacing symm about midspan
9/10/86	7.4	1793.1	No change in loading
----------			ADD DEAD LOAD COMPENSATION FOR DECK - 235 PLF TOTAL
9/10/86	14.6	1800.3	All 24 blocks in place, spaced in prs at 4 ft
9/10/86	15.0	1800.8	Ready mix concrete truck arrives
**********			CAST DECK
9/10/86	15.6	1801.4	Concrete in place
9/10/86	17.0	1802.8	Deck finishing completed
9/10/86	17.7	1803.4	Burlap and plastic in place for curing
9/12/86	12.7	1846.5	Curing materials removed; curing cmpd applied to top surface
9/12/86	14.0	1847.8	Apply demecs and 3 gages ea location to deck at midspan
9/13/86	11.8	1869.6	Connect top deck gages to boxes; initial readings
9/15/86	8.0	1913.8	Ready to begin block removal and form stripping
----------			SUBTRACT DECK FORM LOAD - 20 PLF
9/15/86	13.8	1919.5	Deck forms removed; 18 dead load blocks and lower cross- ...
			... head in place for full dead load compensation
9/15/86	17.3	1923.1	Apply and connect remaining deck gages; initial readings
9/16/86	14.7	1944.4	Specimen pushed and held about .33 in. to west
9/16/86	17.0	1946.8	Deflection readings taken using optical level
9/17/86	8.0	1961.8	Initial readings taken for all instrumentation for test
----------			FLEXURE TEST
9/18/86	8.7	1986.5	Initial readings for flexure test
9/18/86	9.1	1986.9	0.00 kips - lift upper cross heads; rezero pressure transducers
9/18/86	9.4	1987.1	1.00 kip
9/18/86	9.6	1987.4	2.00 kips
9/18/86	9.8	1987.5	3.00 kips
9/18/86	9.9	1987.6	3.50 kips
9/18/86	10.0	1987.7	4.00 kips
9/18/86	10.3	1988.0	4.50 kips
9/18/86	10.3	1988.1	5.00 kips
9/18/86	10.6	1988.4	5.50 kips
9/18/86	10.7	1988.5	6.00 kips
9/18/86	11.1	1988.9	6.50 kips
9/18/86	11.2	1988.9	7.00 kips
9/18/86	11.4	1989.1	7.50 kips - lock deflection; retract rams; reset upper heads
9/18/86	11.6	1989.4	7.50 kips - reload
9/18/86	11.7	1989.4	8.00 kips
9/18/86	11.9	1989.7	8.25 kips

9/18/86	12.0	1989.7	8.50 kips
9/18/86	12.2	1990.0	8.75 kips
9/18/86	12.4	1990.2	9.00 kips
9/18/86	12.7	1990.4	9.25 kips - lock deflection; reset rams; reset upper heads
9/18/86	13.0	1990.7	9.25 kips - reload
9/18/86	13.1	1990.8	9.44 kips - lock deflection to replace leaking hose
9/18/86	13.5	1991.2	9.44 kips - reload
9/18/86	13.6	1991.4	9.67 kips - lock deflection; reset rams; reset upper heads
9/18/86	13.9	1991.7	9.59 kips - Failure during reload
9/18/86	17.0	1994.7	Unload
----------			PREPARE SOUTH END FOR SHEAR TEST - STD END DETAIL
			Note: No dead load blocks used during shear test of south end
4/14/87			Place specimen in 600 kip testing machine
----------			SHEAR TEST OF SOUTH END
4/15/87	10.5	7004.2	Begin shear test - no cracking test because girder previously cracked by shrinkage
4/15/87	13.9	7007.6	Maximum shear of 41 kips reached
4/15/87	14.1	7007.8	Specimen fails while reloading at 40.9 kips due to loss of strand bond. Application of additional displacement causes slow reduction of capacity.
4/15/87			Remove specimen from testing machine
----------			PREPARE NORTH END FOR SHEAR TEST - 6 INCH EXTENSION OF GIRDER BEYOND BEARING
			Note: No dead load blocks used during shear test of north end
4/15/87			Place specimen in 600 kip testing machine
----------			SHEAR TEST OF NORTH END
4/16/87	11.0	7028.7	Begin shear test - no cracking test because girder previously cracked by shrinkage
4/16/87	14.8	7032.5	Web crushing begins - load drops as deformation added
4/16/87	15.1	7032.8	Shear increases again when additional deformation applied
4/16/87	15.2	7032.9	Maximum shear of 48.8 kips reached
4/16/87	15.9	7033.6	Final load stage - web crushing is extensive and load is dropping with additional deformation

A P P E N D I X C

DESCRIPTIONS OF COMPUTER PROGRAMS USED IN THIS STUDY

C.1 Program BRIDGE

This interactive program performs flexural design for composite pretensioned girder highway bridges. The program was written in BASICA for an IBM PC-compatible microcomputer. It is similar to a program of the same name that appears in Ref. [109], but has a number of extensions and improvements, including computation of losses rather than using lump sum losses. The program also computes a number of quantities that are not required for the design of members by current allowable stress or ultimate strength design criteria. These features were included so that all information to be used in this study related to a particular design could be obtained by running a single program.

For a given set of input data, the program determines the minimum number of strands required to satisfy flexural design requirements for a typical interior girder. Using data retrieved from a file that defines the eccentricity for a given number of strands, strands are added to the initial number until all criteria are satisfied. Additional computations are then executed for the successful design before output is sent to the printer. The program

will then compute the maximum number of strands that will satisfy the design criteria before returning for another design.

Input required for the program includes the following:

A file that contains eccentricities for a given number of strands. This file also contains a reference to another file which contains dimensions and properties for the cross-section.

Strand type, which may be either stress-relieved, low relaxation, or the strand used in the specimens.

Girder spacing. The program determines the deck thickness from this input using Table C.1 [109]. The effective deck span is defined in Fig. C.1.

Girder design concrete strength and strength at release.

Deck design concrete strength.

Additional loads, including non-composite uniform load, midspan diaphragm load, and composite uniform load. Default values were computed for the diaphragm load and composite uniform loads using standard concrete diaphragm details and an asphalt topping load of 32 psf.

Span length.

Initial guess for number of strands. A number of strands greater than the minimum may also be entered to determine conditions for that number of strands.

Table C.1 Deck Thickness [109]

Effective Deck Span (ft)	Deck Thickness (in.)	Deck Reinforcement* Bar Size	Deck Reinforcement* Spacing (in.)
1 to 3 inclusive	7	No. 5	10.0
3 to 4 inclusive	7	No. 5	8.5
4 to 5 inclusive	7	No. 5	7.5
5 to 6 inclusive	7	No. 5	6.5
6 to 7 inclusive	7	No. 6	8.0
7 to 8 inclusive	7.5	No. 6	8.0
8 to 9 inclusive	8	No. 6	8.0
9 to 10 inclusive	8.5	No. 6	8.0

* Reinforcement shown is for each of top and bottom layers.

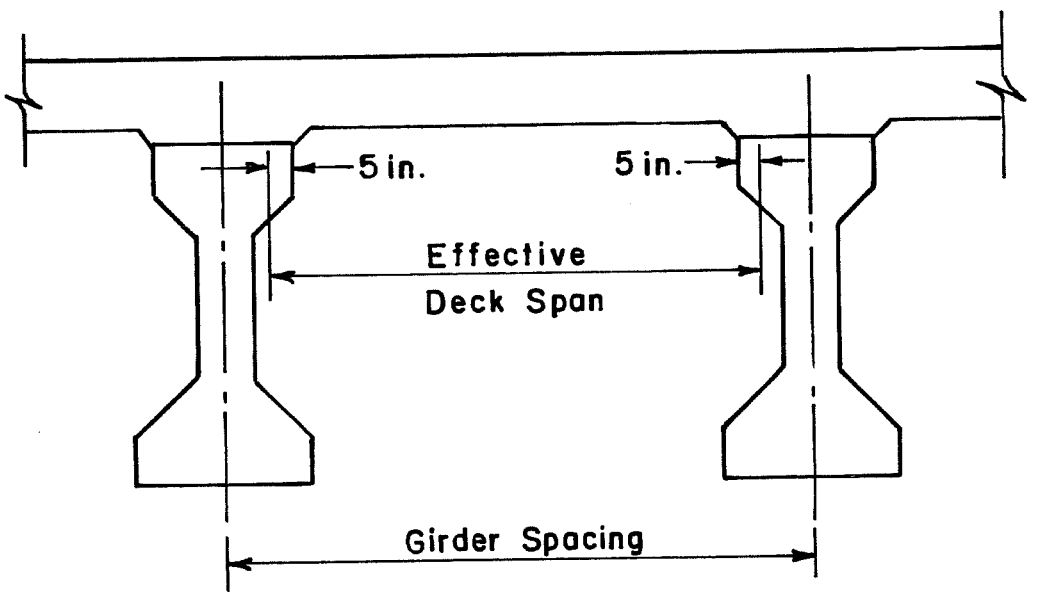

Fig. C.1 Effective deck span [109]

For the analyses presented in this study, the following assumptions were made:

Modulus for all concrete was computed using 57,000 $\sqrt{f_c'}$

Girder concrete strength at release was 75 percent of the design strength unless noted otherwise.

Deck concrete strength was 4 ksi.

Low relaxation strands were used, except for analyses of test specimens.

A 2 by 2-in. grid was used for strands with 2 rows centered in the web and 2 in. from center of strand to surface of concrete. Strands were added to the lowest unfilled row.

Strands were draped at locations 0.1 times the span on each side of midspan.

Strands were raised as necessary at ends to satisfy stresses. Where stresses could not be satisfied with strands raised as high as possible, end stresses controlled the design.

Losses were computed using the proposal of Zia et al. [137].

An approximate equation was used to compute the cracking moment for comparison with the nominal capacity of the section. Use of this equation is not correct and affected one

design as noted in Chapter 7. Consideration of all loads in the determination of the cracking moment is recommended.

Nominal capacity was computed using assumptions of the ACI ERSB for both deck and girder concrete. While the capacity computed in this way compares favorably with values computed using the strain compatibility analysis, it is not recommended for use in maximum reinforcement considerations, as discussed in Chapter 7.

The effective width of the deck was computed using the criteria of the AASHTO Specifications.

Stresses were computed using gross section properties but adjusted to account for the increase in strand stress and force that accompanies added loads.

The standard HS 20-44 and lane load were used as live loads as specified in the AASHTO Specifications. The alternate military loading does not govern designs for spans considered in this study. The specified impact factor was applied to the controlling live load, which was distributed according to the factor provided in the Specification, assuming a bridge designed for two or more lanes of traffic.

Elastic deflections at midspan were computed for all changes in loading. The live load deflection at midspan was estimated for the truck loading but an exact calculation was made when the lane loading

governed. The AASHTO live load deflection limit for steel bridges without pedestrian traffic, L/800, where L = span, was computed, but no action was taken if the live load deflection exceeded this limit. Long-term deflections were estimated using the PCI multipliers, but this method is not recommended. The program CAMBER, discussed briefly in the third section of this appendix, provides better estimates of long-term deflections.

The correct elastic analysis is performed to determine the cracking moment. The approximate cracking moment is also computed. The ratio of the applied cracking moment to the live load is computed to determine the magnitude of overload required to produce cracking, assuming a modulus of rupture of $7.5\sqrt{f_c'}$.

Losses and corresponding concrete stresses at critical stages of construction are computed and displayed using both the AASHTO method and the method proposed by Zia, et al. [137].

The ultimate capacity is computed and printed for three methods of calculation: Case II, using the ACI ERSB assumptions; Case III, using transformed dimensions; and the AASHTO equation (see Chapter 7). The reinforcement index is also computed for each approach, taking into account flanged section analysis when necessary.

The program computes the stress range at the centroid of the strands from full dead load to service load conditions and also to a 10 percent overload. Stress ranges are computed for both an uncracked

and cracked section. For cracked sections, a strain compatibility analysis was used that assumed elastic material properties.

Where tension occurs in the bottom flange at service load, the equivalent tension force is computed and an area of mild reinforcement is given to resist this tension force at a working stress of 24 ksi. A similar calculation is performed for the top flange at release and an area of steel to resist the equivalent tension force is also given.

An index of cost is computed by the program based on the quantities of material used and relative cost factors.

A sample of the output from the program is given in Table C.2. Input data is echoed in the output.

C.2 Program MOMCURV

This interactive program models the behavior of a section throughout the load history using the strain compatibility analysis with non-linear material properties which was described in Sec. 7.4.2. This discussion provides further detail about the program, which was written in BASICA for an IBM PC-compatible microcomputer.

MOMCURV requires the following input, which was taken from output from the program BRIDGE or computed by hand:

Top and bottom fiber stresses for girder and deck at the full dead load condition.

Full dead load moment.

```
BRIDGE.BAS     Version 2.2    DETAILED DESIGN                  04-11-1987    15:19:16              PAGE 1

ECCTYPIV.DAT      Record no.  41      AASHTO-PCI Type IV - computed properties

                  SPAN = 159   SPCG = 4   DT = 7   f'cg = 12   f'cgi = 9   f'cd =  4   ft = -.6572671

MATERIAL PROPERTIES     ************************************

CONCRETE PROPERTIES                 Transfer - Girder - Service          Deck
                  Strength          9                 12                 4
                  Unit Weight       150               150                150
                  Modulus           5407.495          6244.037           3604.997
                  Allow. Tension    -.7115125         -.6572671
                  Allow. Compression 5.4              4.8                1.6
                  Beta 1                              .65                .85
                  Ultimate strain                     .003               .003

PRESTRESSING STRAND PROPERTIES - Low Relaxation strand
                  Area =  .153      Modulus =  28000    Unit weight =  490  fp0 =  202.5
                  MENEGOTTO-PINTO STRESS-STRAIN CURVE PARAMETERS
                       fpu =  270         epu =  .035        fpy =  243         epy =  .01
                       N =  6.44          K =  1.08          Q =  .0105357

PASSIVE REINFORCEMENT PROPERTIES      Working stress =  24      Yield stress =  60

SECTION PROPERTIES     ************************************

GIRDER PROPERTIES - Neglects any reinforcement
                  Area =  789       I =  260740.6      Depth =  54        Lb per ft =  821.875
                  yt =  29.26616    yb =  24.73384     St =  8909.286     Sb =  10541.86
                  Rho =  .4565354   Alpha =  .856096   Perim =  166.4264  V/S =  4.740834
                  rstrong =  18.17883 Tilt =  62.27379                    Web =  8

DECK PROPERTIES   DEPTH =  7       Washington Standards were used to determine the deck thickness.
                  Width =  48       Eff.width =  48    Trans.width =  27.71281
                  Area =  336       Eff. area =  336   Trans. area =  193.9897
                  Lb per ft =  350
```

Table C.2 Typical output from program BRIDGE

```
COMPOSITE SECTION PROPERTIES - Transformed deck included
                Area =  973.1977    I =  422789.9       Depth =  61         N   =  .5773503
                yt =  29.55386      yb =  31.44614      Stg =  18745.79     Sbg =  13444.89
                Rho =  .4674573     Alpha =  .7836145   Std =  14305.74     Sbd =  18745.79
                Lb per ft =  1171.875         Gross area =  1125            Ag/Agross =  .7013334

STRAND PATTERN
                H spcg =  2         V spcg =  2         No. in web =  2     Center of strand to cover =  2
                No. of strand below NA =  74            Max no. of strands possible with this grid =  102

SPAN =  159     GIRDER SPACING =  4      Holddown located at 15.900 feet each side of midspan - General standards

LOADS, MOMENTS AND REACTIONS     **************************

LOADS (k/ft,k)    Girder =  .821875  Deck =  .35        N-comp =  0         Compos =  .128      Diaph @ CL =  .8048611
MOMENTS (k*in)    Girder =  31166.73  Deck =  13272.53  N-comp =  0         Compos =  4853.952  Diaph @ CL =  383.9188
                  Total noncomposite dead load moment =  44823.17         Total dead load moment =  49677.13
                  Live load moment =  14050.99 , produced by Lane loading.  Impact =  1.176056  LL Dist =  .3636364
                  Total =  63728.12  Live/Total =  .2204834               Ultimate moment  =  95024.08
REACTIONS (kips)  Dead =  103.7425   Live =  32.87826   Total =  136.6208  Live/Total =  .2406535
                  Ultimate =  206.1016
                  Weight of girder =  130.6781
```

Table C.2 Typical output from program BRIDGE (continued)

ECCTYPIV.DAT Record no. 41 AASHTO-PCI Type IV - computed properties

SPAN = 159 SPCG = 4 DT = 7 f'cg = 12 f'cgi = 9 f'cd = 4 ft = -.6572671

RESULTS OF DESIGN No. strands = 64 Area = 9.792 CL ecc = 17.98384 CL g = 6.75 Top row CL = 7
Rho p = 0.003760 Max top row = 26 End ecc = 14.48384 End g = 10.25 Top row end = 15

PRESTRESS LOSSES BY AASHTO AND ACI METHODS - ACI Recommendations used for design

	ES	SH	CR	RE	Init	%fp0	Totl	%fp0	fsi	%fpu	fse	%fpu
AASHTO	12.781	7.250	21.041	3.357	14.459	7.140	44.429	21.940	188.041	69.645	158.071	58.545
ACI	12.781	5.750	11.146	3.813	14.687	7.253	33.490	16.538	187.813	69.560	169.010	62.596

ELASTIC SECTION ANALYSIS - Change in strand stress is included in analysis

	AASHTO				ACI				Both	
	Top G	Btm G	CGS	Strands	Top G	Btm G	CGS	Strands	Top D	Btm D
TRANSF	-0.7115	+5.4000			-0.7115	+5.4000				
Transf	+2.1152	+2.5184	+2.4680	+188.041	+2.1169	+2.5118	+2.4624	+187.813		
MATURE	+4.8000	-0.6573			+4.8000	-0.6573			+1.6000	+1.6000
Erectn	+3.8684	+0.3504	+0.7901	+156.800	+3.7880	+0.6689	+1.0587	+167.739		
Full DL	+4.1274	-0.0107	+0.5066	+158.071	+4.0469	+0.3078	+0.7752	+169.010	+0.1959	+0.1495
Service	+4.8675	-0.9626	-0.2337	+161.391	+4.7871	-0.6442	+0.0349	+172.330	+0.7499	+0.5768

Deflections PS init = 10.23116 G init = -8.38247 Camber = 1.848693 Pre Er = 2.908524 Post Erec = -0.254484
PS erec = 18.41609 G erec = -15.50757 NC tot = -3.163008 C Totl = -0.697254 Full Dead = -0.951738
PS finl = 22.50856 G finl = -20.11793 NC fin = -7.274918 C finl = -2.091762 Final Dead = -6.976051
Approximate Live Load = -1.912888 L/800 = -2.385 + Full = -2.864626 LL+Final = -8.888939

ULTIMATE STRENGTH DESIGN	ACI - Case II	ACI - Case III	AASHTO
fps	247.4245	247.4245	235.7336
Tension force	2422.781	2422.781	2308.304
Ultimate moment (K*in)	114456.7	114456.7	102674.2
Depth of compression	13.27638	13.27638	

Table C.2 Typical output from program BRIDGE (continued)

```
Top fiber to neut.axis    16.65596          15.61927
Rotation, phi (rad/in)    7.353584E-04      2.658415E-04
.36*Beta1                 .306              .306
Omega p, gross            .2326018          .2326018          .2216113
Omega p, flanged          .404696           .208017           .3783188
Area steel for flange     2.693347          -1.154292         2.82692
.85*a/dp                  9.833952E-02      .208017

Ultimate moment requirement =  95024.08    Mu loads =  95024.08    1.2*Mcr =  92646.48   1.2*Mcr =  79616.28
Shear stresses using ultimate reaction     Nom stress =  .4748885  /fpc^.5 =  4.335119   Hor stress = 0.12319

TENSION IN BOTTOM FLANGE @ S.L.   Force = -53.63179   NA to btm = 6.404532   Req'd area =  2.234658   fs =  24

CRACKED SECTION ANALYSIS USING STRAIN COMPATIBILITY        S.L. Crk Ht = 8.405079   Remaining depth = 52.59492
                                  Top girder  Btm girder  Top deck   Btm deck   Centr stl   Strand
Stresses at zero tension            +4.2863     +0.0000    +0.3750    +0.2877    +0.5358   +170.0836
Add'l stresses to S.L.              +0.5433     -0.8903    +0.4210    +0.3137    -0.7111     +3.1890
Final stresses at S.L.              +4.8296     -0.8903    +0.7960    +0.6014    -0.1753   +173.2725
Stresses w/10% Over Load            +4.9202     -1.1021    +0.8710    +0.6537    -0.3493   +174.0529

Moments      Live =  14050.99   0 tens =  4543.423  Excess =  9507.568  Crackg =  16669.76  Crack/Live =  1.186376

Strand stress range at centroid strands    Uncracked section =  3.319687      Cracked section =  4.262406
Section rotation, phi (rad/in)             Uncracked section =  1.610789E-05  Cracked section =  1.696393E-05

COST INDICES:  STEEL (LB/SF)    Strand =  8.33      Deck =  2.977431   Top flg =  0          Btm flg =  1.901011
                 Relative cost         =  66.64         =  35.72917          =  0                  =  17.1091
               CONC. (LB/SF)    Girder =  205.4688  Deck =  87.5
                 Relative cost         =  205.4688      =  87.5
                 Total Costs    Girder =  272.1088  Deck =  123.2292  Total  =  395.3379
                                Girder =  289.2178  Deck =  123.2292  Total  =  412.447

Maximum number of strands satisfying allowable stresses =  64
```

Table C.2 Typical output from program BRIDGE (continued)

Effective strand stress, after losses, which corresponds to full dead load condition.

Strand type. Three types were available: stress-relieved and low relaxation strand, based on minimum properties; or strand conforming to measured properties of material used in specimens.

Effective deck width.

Thickness of deck.

Girder concrete strength and modulus at 28 days.

Deck concrete strength and modulus at 28 days.

Strain at maximum stress for deck concrete. A value of 1,600 microstrains was used as a default, which was representative of data from specimen tests.

Slope of descending branch of deck stress-strain curve. A value of 1,060 ksi was used, which was an average value for the data from specimen tests.

Distance to centroid of strand from bottom of girder.

Number of strands.

Area of single strand.

Modulus of elasticity of strand. A value of 28,000 ksi was assumed in accordance with the AASHTO Specifications.

Uncracked section behavior was computed using elastic material properties and gross girder section properties with a transformed

deck. The section was analyzed at the load causing zero stress in the bottom fiber (zero tension load) and at the cracking load, where the bottom fiber stress is $7.5\sqrt{f_c'}$. Computations were adjusted to account for the increase in strand stress and force that accompanies added load. The results of the analysis at these two loads could be used to compute conditions at other loads since all quantities were linearly proportional while the section remained uncracked.

The cracked section analysis used non-linear concrete and prestress steel properties and actual section dimensions. The analysis was performed for values of strain in the top fiber of the deck, which were increased in small increments up to a strain of 0.0035. The number of data points for which the cracked section analysis was performed depended upon the top of deck strain increment chosen. The section was also analyzed using the cracked section analysis for the condition of no stress in the bottom fiber to determine the consistency between cracked and uncracked analyses. Agreement between the types of analyses was not exact, apparently due to differences in assumptions regarding material properties.

The output, a sample of which is given in Table C.3, begins with an echo of input data. More complete output is given for the cracked section analysis and included concrete strains as well as stresses. The option was also provided for writing the results of

```
MOMCURV.BAS                    04-11-1987   15:24:02                    PAGE 1

Cracked section analysis using strain compatibility

SECTDIM.DAT Record no. 41     AASHTO-PCI Type IV - computed properties

INPUT DATA

   Full dead load moment =  49677.13      Strand stress =  169.01
   Deck stresses                Top =  .1959    Bottom =  .1495
   Girder stresses              Top =  4.0469   Bottom =  .3078

   Deck thickness  =  7          Deck width =  48
   Modular ratio   = 0.5774      Effective deck width =  0.0000
   Girder strength = 12.0000     Girder modulus   =  6244.04
   Deck strength   =  4.0000     Deck modulus     =  3605.00
   e0 (strain at maximum stress in deck concrete) =   1600
   Slope of Descending branch (ksi/(in/in))       =   1060

   Strand g    =  6.75       No. strands    =  64
   Area strand =  .153       Strand modulus =  28000

   Menegotto and Pinto stress-strain curve for low relaxation strand

        fpy       fpu        esu          N         K          Q
     243.00    270.00   0.035000     6.4400    1.0800    0.010536

UNCRACKED SECTION ANALYSIS

   Strand is not transformed in section properties
   Effect of increasing strand stress is included in uncracked analysis
   Uncracked section moments and stresses are linearly related above full dead load
```

Table C.3 Typical output fromprogram MOMCURV

Moment	fs	Tension	Strain	Btm G	Top G	Top D	Btm D	Phi
Moment and stresses at zero tension in bottom fiber:								
54220.32	170.084	1665.458	0.00607	0.000	4.286	0.375	0.288	1.271D-05
66347.06	172.949	1693.519	0.00618	-0.822	4.925	0.853	0.656	1.704D-05

CRACKED SECTION ANALYSIS

Strain offset at interface = 607 Difference in curvature = -9.251D-06

Moment	Tens	Comp	Crk Ht	fs	Strain	Top G	Strain	Phi G	Top D	Strain	Phi D	Btm D	Strain
54838.93	1665.0	1665.0	-0.00	170.0	6132	4.233	678	1.255D-05	0.458	94	3.302D-06	0.348	71
55435.30	1666.3	1666.3	0.49	170.2	6137	4.259	682	1.275D-05	0.484	100	3.498D-06	0.369	76
64472.31	1694.8	1694.8	8.70	173.1	6249	4.713	755	1.666D-05	0.938	200	7.412D-06	0.706	148
70953.80	1739.2	1739.2	16.37	177.6	6426	5.114	819	2.177D-05	1.359	300	1.252D-05	0.991	212
76176.53	1793.6	1793.6	22.29	183.2	6647	5.480	878	2.768D-05	1.750	400	1.843D-05	1.240	271
80821.39	1852.6	1852.6	26.60	189.2	6893	5.826	933	3.405D-05	2.109	500	2.480D-05	1.465	326
85082.57	1913.9	1913.9	29.81	195.5	7156	6.157	986	4.076D-05	2.438	600	3.151D-05	1.672	379
89046.53	1975.6	1975.6	32.26	201.8	7434	6.478	1037	4.771D-05	2.734	700	3.846D-05	1.864	431
92746.83	2036.3	2036.3	34.17	208.0	7720	6.790	1088	5.484D-05	3.000	800	4.559D-05	2.043	481

Table C.3 Typical output fromprogram MOMCURV (continued)

CRACKSC.BAS 04-11-1987 15:26:05 PAGE 2

Cracked section analysis using strain compatibility

SECTDIM.DAT Record no. 41 AASHTO-PCI Type IV - computed properties

CRACKED SECTION ANALYSIS - Continued

Moment	Tens	Comp	Crk Ht	fs	Strain	Top G	Strain	Phi G	Top D	Strain	Phi D	Btm D	Strain
96192.32	2094.8	2094.8	35.70	213.9	8014	7.098	1137	6.210D-05	3.234	900	5.285D-05	2.211	530
99381.17	2150.3	2150.3	36.94	219.6	8314	7.400	1185	6.947D-05	3.438	1000	6.021D-05	2.370	578
102308.28	2202.0	2202.0	37.97	224.9	8617	7.699	1233	7.691D-05	3.609	1100	6.766D-05	2.519	626
104969.24	2249.5	2249.5	38.83	229.7	8925	7.996	1281	8.441D-05	3.750	1200	7.516D-05	2.660	674
107362.54	2292.6	2292.6	39.56	234.1	9234	8.290	1328	9.197D-05	3.859	1300	8.272D-05	2.793	721
109490.55	2331.2	2331.2	40.19	238.1	9546	8.583	1375	9.955D-05	3.937	1400	9.030D-05	2.918	768
111359.98	2365.3	2365.3	40.73	241.6	9858	8.875	1421	1.071D-04	3.984	1500	9.790D-05	3.036	815
112981.35	2395.2	2395.2	41.20	244.6	10170	9.167	1468	1.147D-04	4.000	1600	1.055D-04	3.148	862
114327.55	2420.7	2420.7	41.60	247.2	10476	9.465	1516	1.222D-04	3.894	1700	1.130D-04	3.254	909
115406.29	2442.3	2442.3	41.92	249.4	10773	9.770	1565	1.295D-04	3.788	1800	1.203D-04	3.356	958
116270.22	2460.5	2460.5	42.19	251.3	11060	10.082	1615	1.367D-04	3.682	1900	1.274D-04	3.452	1008
116960.27	2476.0	2476.0	42.41	252.9	11340	10.400	1666	1.437D-04	3.576	2000	1.344D-04	3.543	1059

Table C.3 Typical output fromprogram MOMCURV (continued)

117940.05	2500.6	2500.6	42.75	255.4	11880	11.053	1770	1.573D-04	3.364	2200	1.481D-04	3.702	1164
118275.70	2510.4	2510.4	42.88	256.4	12141	11.387	1824	1.640D-04	3.258	2300	1.547D-04	3.771	1217
118531.96	2518.9	2518.9	42.99	257.2	12396	11.725	1878	1.705D-04	3.152	2400	1.613D-04	3.831	1271
118721.96	2526.3	2526.3	43.08	258.0	12647	12.000	1932	1.770D-04	3.046	2500	1.677D-04	3.883	1326
118843.53	2532.7	2532.7	43.15	258.6	12889	12.000	1988	1.833D-04	2.940	2600	1.741D-04	3.925	1382
118901.11	2538.2	2538.2	43.20	259.2	13121	12.000	2046	1.894D-04	2.834	2700	1.802D-04	3.959	1439
118904.29	2542.9	2542.9	43.23	259.7	13342	12.000	2104	1.953D-04	2.728	2800	1.861D-04	3.984	1497
118861.01	2547.0	2547.0	43.24	260.1	13553	12.000	2164	2.011D-04	2.622	2900	1.918D-04	3.997	1557
118778.32	2550.6	2550.6	43.23	260.5	13755	12.000	2225	2.066D-04	2.516	3000	1.974D-04	3.981	1618
118668.04	2553.8	2553.8	43.22	260.8	13949	12.000	2287	2.121D-04	2.410	3100	2.028D-04	3.915	1680
118535.30	2556.7	2556.7	43.19	261.1	14139	12.000	2350	2.174D-04	2.304	3200	2.081D-04	3.848	1743
118382.36	2559.3	2559.3	43.16	261.4	14323	12.000	2413	2.226D-04	2.198	3300	2.134D-04	3.781	1806
118211.11	2561.7	2561.7	43.12	261.6	14501	12.000	2477	2.278D-04	2.092	3400	2.185D-04	3.713	1870
118023.05	2563.8	2563.8	43.08	261.8	14674	12.000	2542	2.328D-04	1.986	3500	2.235D-04	3.645	1935

Table C.3 Typical output fromprogram MOMCURV (continued)

both the uncracked and cracked analyses to a disk file in comma separated value format for use in other programs.

C.3 Program CAMBER

This program was written as part of the work by Kelly reported in Ref. [72]. The program calculates long-time camber and deflection multipliers for composite highway bridges constructed with pretensioned girders. The program also computes the long-time camber or deflection at important construction events and at the end of the service life of the bridge.

A description, user's guide, and listing of CAMBER may be found in the original reference. The program was written in FORTRAN 77 and runs on an IBM AT microcomputer with a math coprocessor chip.

Input files used to generate data for Fig. 7.63 and 7.65 are listed here as Tables C.4 and C.7. Elastic deflections for when loads changed on the structure were computed by BRIDGE and were used as input here. Therefore, the option of having the program estimate all deflections, elastic and long-term, was not used.

A typical output file is given in Table C.8. This output corresponds with the input file shown in Table C.4.

Table C.4 CAMBER Input File for Maximum Span Design with GS = 4 ft

```
.8,112,119,140,196
2.35,4.74,65,0.617
14.8
0
1
-8.382,10.231,0,0,0,-3.163,-0.697
```

Table C.5 CAMBER Input File for Maximum Span Design with GS = 10 ft

```
.8,112,119,140,196
2.35,4.74,65,0.425
19.8
0
1
-2.630,5.795,0,0,0,-3.032,-0.377
```

Table C.6 CAMBER Input File for Typical Span Design with GS = 4 ft

```
.8,112,119,140,196
2.35,4.74,65,0.617
5.7
0
1
-2.720,3.362,0,0,0,-1.034,-0.225
```

Table C.7 CAMBER Input File for Typical Span Design with GS = 10 ft

```
.8,112,119,140,196
2.35,4.74,65,0.425
7.4
0
1
-0.415,1.149,0,0,0,-0.487,-0.059
```

Table C.8 CAMBER Output File for Maximum Span Design with GS = 4 ft

Long-Time Deflection and Camber Multipliers

The age of the beam during significant events (days)

1.	Release of prestress force	0.80
2.	Placed in the bridge (erection)	112.
3.	Super-imposed load is added to the noncomposite beam (ex. the weight of deck panels)	119.
4.	The composite slab is cast	140.
5.	Super-imposed load is added to the composite beam (ex. the weight of an asphalt overlay)	196.

The uncorrected ultimate creep coefficient is 2.35
The volume-to-surface ratio is 4.74 inches
The average percent relative humidity is 65.%
The ratio of noncomposite-to-composite moment of inertia is 0.62
The total time dependent percent prestress loss (not including the initial loss due to elastic shortening) is 14.8 %

The beam is moist cured
The elastic cambers and deflections are :
(Camber is positive, values are in inches)

a.	Deflection at release due to the weight of the beam	-8.38
b.	Camber due to prestress force at release	10.23
c.	Camber due to the reduced span when placed in storage	0.00
d.	Deflection due to an increased span length when placed in the bridge	0.00
e.	Deflection due to a super-imposed load added to the noncomposite beam (ex. the weight of deck panels)	0.00
f.	Deflection due to the weight of the cast-in-place slab	-3.16
g.	Deflection due to a super-imposed load added to the composite beam (ex. the weight of an ACP overlay)	-0.70

Table C.8 CAMBER Output File for Maximum Span Design with GS = 4 ft (continued)

Event listed above	Time from release (days)	Camber (inches) before	Camber (inches) after	Time to next event (days)	Camber just before the next event (inches)
1	0.00	0.00	1.85	0	1.85
Placed in storage	0.00	1.85	1.85	111	2.83
2	111	2.83	2.83	7	2.83
3	118	2.83	2.83	21	2.82
4	139	2.82	-0.34	56	-1.37
5	195	-1.37	-2.07		-3.88
End of design life			-3.88		

A P P E N D I X D

DEVELOPMENT OF REINFORCEMENT LIMITS

D.1 Maximum Reinforcement Limit

The development of this limit will be presented in outline form, explaining the assumptions made for each quantity listed in Fig. 7.52 which is repeated here as Fig. D.1.

F — This is a factor which indicates the efficiency or effectiveness of the bond between concrete and steel. The value of 1 used indicates that the bond is full and that strains computed in the concrete at the level of the steel will also apply to the steel. This is a reasonable assumption for bonded prestressed construction.

ϵ_{cu} — This is the maximum usable concrete strain at ultimate. As the summary in Fig. D.1 indicates, the early and current forms of the limit used a value of 0.004 for the limiting concrete strain in the derivation of the maximum reinforcement limit. This is inconsistent with other provisions in current codes. Therefore, to correct this inconsistency, a value of 0.003 is used for the proposed limit.

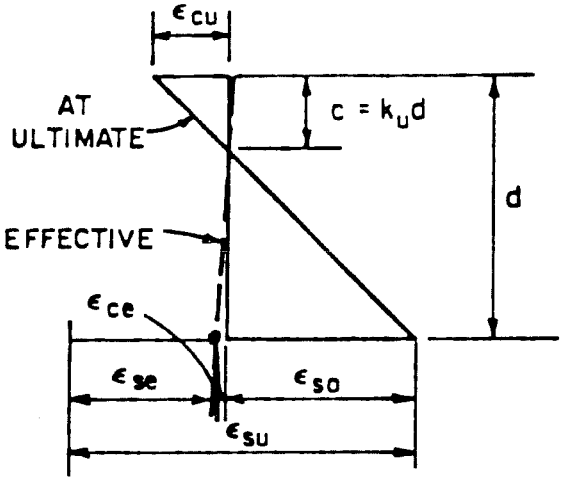

$$k_u = \frac{F\epsilon_{cu}}{F\epsilon_{cu} + \epsilon_{sa}}$$

$$= \frac{F\epsilon_{cu}}{F\epsilon_{cu} + \epsilon_{su} - \epsilon_{se} - \epsilon_{ce}}$$

$$= \rho \frac{f_{su}}{f_{cu}}$$

$$= c/d$$

	Warwaruk et al. 1962	ACI Comm 323 (current AASHTO) 1958	ACI 318-83 1983	Proposal
Reference	[133]	[10, 19]	[15]	Appendix D
F	1	1	1	1
ϵ_{cu}	0.003	0.004	0.004	0.003
ϵ_{su}min.	0.01*	0.01*	0.01*	$0.01+(f_{pu}-250)/28000$
ϵ_{se}	0.0045**	0.0045**	0.0045**	$f_{se}/28000$
ϵ_{ce}	0	0	0	0
$k_u$limit	≤ 0.353	≤ 0.421	≤ 0.421	$\leq 84/[114+f_{pu}-f_{se}]$
f_{cu}	$0.7f'_c$	$0.7f'_c$	$0.85\beta_1 f'_c$	$0.85\beta_1 f'_c$
ω	0.25	0.30	$0.36\beta_1$	$0.85\beta_1[84/(114+f_{pu}-f_{se})]$

* - Based on Grade 250 material.

**- An average of the expected range from 0.004 to 0.005.

Modules of strand is assumed to be 28000 ksi. Stress units in ksi.

Fig. D.1 Assumptions for maximum reinforcement limits

ϵ_{su} This strain is the limit which represents yield in the strand. The intent of the limit is for this strain to be reached or exceeded at ultimate conditions. The full development of the reason for this limit is given in Chapter 3 but can be summarized as follows:

> The capacity of the section is very sensitive to material or dimensional variations when the strand strain at ultimate is in the linear portion or initial part of the knee of the stress-strain curve. Therefore, it is desirable for the strain at ultimate to be greater than that corresponding to the latter part of the knee in the stress-strain curve.

The value of 0.01 which was used for the derivation of prior limits was based on the use of Grade 250 material. However, Grade 270 material is now the standard and higher grades of material are being developed. Therefore, it appears appropriate to increase this limit to provide the same behavior as was intended with the original limit. This can be accomplished by assuming stress-strain curves for different grades of steel differ only in the extent of the initial linear portion of the curve. The limiting strain could then be determined for other grades of steel by adding an increment of strain to the original

limit (0.01) which is assumed equal to the difference in ultimate strand stresses divided by the modulus of the strand. This is illustrated in Fig. D.2. The following expression is then used to compute the limiting strain:

$$\epsilon_{su} = 0.01 + \left(f_{pu} - 250\right)/ E_p \qquad (D.1)$$

where E_p = modulus of prestressed reinforcement

= 28,000 ksi (from AASHTO)

and f_{pu} is expressed in ksi. As the strains shown in Fig. D.2 indicate, the difference between the proposed expression for ϵ_{su} and the current limit of 0.01 is only 7 percent for Grade 270 strand. The difference would become greater for either higher or lower grades of steel. For lower grade prestressing reinforcement, the current limit would be overly conservative.

It should also be noted that this approach to limiting the strain in the prestressing steel is based on balanced failure as the limit. While this is consistent with the practice of allowing over-reinforced prestressed after an appropriate reduction in ultimate capacity, it does not agree with the

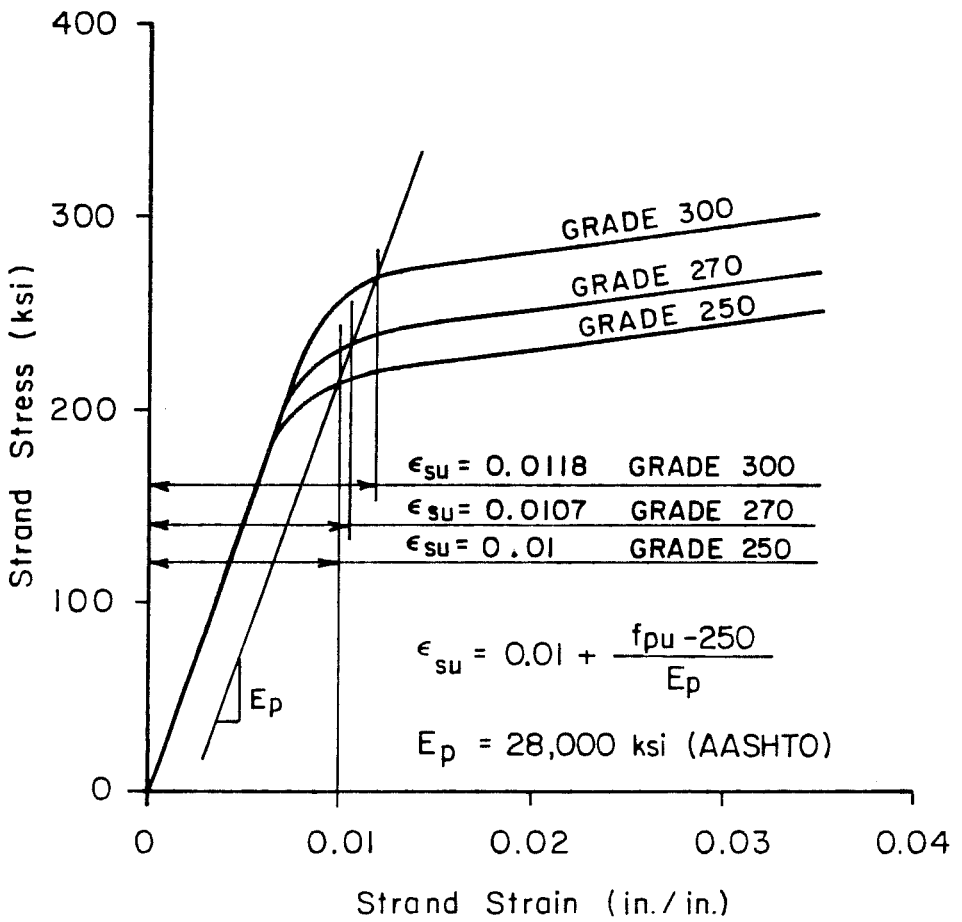

Fig. D.2 Limiting prestressed reinforcement strain for maximum reinforcement limit

concept employed for reinforced concrete sections where the strain in the reinforcement is forced to be nearly twice the yield strain at ultimate. Therefore, this limit could not be extended for use with reinforced members without modification.

ϵ_{se} This is the effective strain in the steel after losses which corresponds to the stress f_{se}. In the current limits, a value of 0.0045 is assumed which represents and average of the expected range of strains (0.004 to 0.005). However, as was demonstrated in Sec. 7.5.2.1, the limit is sensitive to the value of ϵ_{se} used. These strains, however, also represent the practice for Grade 250 steel and correspond to stresses of 112 to 140 ksi, which are very low for current practice. The use of such low strains would result in excess conservatism in the limit. It is therefore proposed that the effective prestress be used in the limiting equation. This would not be an undue hardship on the designer since this value must be computed for use in the allowable stress design of the member.

The sensitivity of the new limit to variation in effective strand stress is demonstrated for Grade 270

steel in Table D.1. The limit varies approximately ±8 percent for stresses ranging 20 ksi below and 15 ksi above the 170 ksi value which is a rough estimate for current practice using Grade 270 steel.

The use of higher grades of steel would lead to higher effective stresses, resulting in a conservative error if an average value for Grade 270 steel were used. However, where lower grades of prestressed reinforcement are used, use of the average effective prestress for Grade 270 strand would lead to unconservative results.

It appears that this error introduced by using grades of steel other than the one with which the limit was derived would tend to offset the error introduced by using a constant value for the limiting strain as mentioned above. However, even though this may be the case, a direct approach where all variables are considered individually is preferred over an approximate method that remains reasonable by the chance interaction of variables. Such limits cannot be applied to unusual situations. The inclusion of both the ultimate stress of the strand and the effective stress is therefore strongly recommended to maintain

Table D.1 Variation of proposed maximum reinforcement limit with effective prestress

f_{se} (ksi)	Eq. D.2 $\beta_1 = 0.85$	Eq. D.2 $\beta_1 = 0.65$	% diff. *
150	0.2594	0.1983	9.33
170	0.2836	0.2169	0
185	0.3050	0.2332	-7.02

* The percentage difference (% diff.) is between the 170 ksi and the other values of f_{se} (150 or 185 ksi) and is computed using the other values as the basis of the comparison. The percentages apply to both values of β_1.

validity and clarity for future situations which are not reflected in current practice.

ϵ_{ce} The effective strain in the concrete at the level of the prestressed reinforcement is small compared with the other stresss involved in the analysis. Neglecting this component of total strand strain is unconservative, but the magnitude of the error is very small.

ϵ_{sa} This strain (the notation is taken from Warwaruk et al. [133]) is the produce of the curvature across the section at ultimate and the distance from the neutral axis to the centroid of the prestressed reinforcement. This quantity appears in the derivation and is replaced by the difference between the limiting strain, ϵ_{su}, and the effective strain, ϵ_{se}.

f_{cu} This is the average stress in the compression zone. It was used in the Warwaruk et al. report [133] to describe the stress block rather than the equivalent rectangular stress block. However, this quantity can be expressed in terms of the stress block parameter β_1 as shown in Fig. D.1. This was the basis for the change in the limit that appeared in ACI 318-83.

The inclusion of the β_1 factor is appropriate and will be used in the proposed limit.

The derivation of the limit is shown in Fig. D.1. It is based on the determination of the factor k_u which represents the ratio of the depth of compression at ultimate, c, to the effective depth, d. This limit has been shown to be related to the reinforcement ratio and in this way, using the relationship between f_{cu} and f_c', the following limit for the reinforcement index can be developed:

$$\omega \leq 0.85\beta_1\left[84/\left(114 + f_{pu} - f_{se}\right)\right] \qquad (D.2)$$

where f_{pu} and f_{se} are expressed in ksi.

This approach is identical to that used for developing the reinforcement ratio corresponding to balanced failure, with the addition of the effective prestress term. The resulting equation appears very similar to that used for rectangular reinforced concrete sections. Therefore, it is anticipated that such an expression would gain rapid acceptance among designers since it is not an unfamiliar concept and because it adds reason to a limit which at the present time is misunderstood as a result of the total lack of information on its intent and derivation.

D.2 Minimum Reinforcement Limit

The derivation of the minimum reinforcement limit follows the same approach as discussed for the maximum limit. The only difference is that the limiting strand ϵ_{su} is changed to 0.035, which is the ASTM minimum specified elongation for seven wire stress-relieved and low-relaxation prestressing strand. This limit will be assumed to be constant for all grades of strained, although it could be different for prestressing materials other than seven wire strands. Therefore, the only variable related to strand stress that appears in the expression for the limit is the effective prestress. The minimum reinforcement limit is

$$\omega \geq 0.85\beta_1\left[84/(1064 - f_{se})\right] \tag{D.3}$$

where f_{se} is expressed in ksi. However, since the constant in the denominator is fairly large compared with the effective prestress, the use of a constant value for f_{se} is appropriate for Grade 270 strand. The resulting limit, where f_{se} is approximately 170 ksi, is

$$\omega \geq 0.08\beta_1 \tag{D.4}$$

A comparison of the limits from Eq. D.3 and D.4 is made in Table D.2 for Grade 270 strand and $\beta_1 = 0.85$. A single value is considered for β_1 because the ratios between limits computed with the two equations will be identical for any value of the constant.

Table D.2 Variation of proposed minimum reinforcement limit with effective prestress

f_{se} (ksi)	Eq. D.3 $\beta_1 = 0.85$	% diff. *	Eq. D.4 $\beta_1 = 0.85$	% diff. **
150	0.0664	2.24	0.0680	2.41
170	0.0679	0	0.0680	0.16
185	0.0690	-1.67	0.0680	-1.51

* The percentage difference (% diff.) is between the 170 ksi and the other values of f_{se} (150 or 185 ksi) and is computed using the other values as the basis of the comparison. These percentages apply to all values of β_1.

** The percentage difference is between values of the minimum limit calculated using Eq. D.4. and D.3 and is computed using Eq. D.3 values as the basis for the comparison. These percentages apply to all values of β_1.

The data in the table indicates that the error in using the constant limit would be no more than 2.5 percent for Grade 270 steel, which is an acceptable level of error for this limit.

While a constant limit may be used, it is essential that the derivation and intent of the limit be made available to engineers at large so that modifications to the limit can be made where necessary for other grades of steel or where it can be shown that the elongation of the strand is greater than the 0.035 value assumed in this limit.

REFERENCES

1. Ahmad, S.H., and Shah, S.P., "Stress-Strain Curves of Concrete Confined by Spiral Reinforcement," ACI Journal, Proceedings Vol. 79, No. 6, Nov.-Dec. 1982, pp. 484-490.

2. Ahmad, S.H., and Shah, S.P., "Structural Properties of High Strength Concrete and Its Implications for Precast Prestressed Concrete" PCI Journal, Vol. 30, No. 6, Nov.-Dec. 1985, pp. 92-119.

3. Ahmad, S.H., Khalo, A.R., and Poveda, A., "Shear Capacity of Reinforced High-Strength Concrete Beams," ACI Journal, Proceedings Vol. 83, No. 2, Mar.-Apr. 1986, pp. 297-305.

4. Aitcin, Pierre-Claude, Laplante, Pierre, and Bedard, Claude, "Development and Experimental Use of a 90 MPa (13,000 psi) Field Concrete", High Strength Concrete, SP-87, American Concrete Institute, Detroit, 1985, pp. 51-70.

5. Ali, I. Discussion of "Researches Toward a General Flexural Theory for Structural Concrete," by Hubert Rusch, ACI Journal, Proceedings Vol. 32, No. 9, Mar. 1961, pp. 1147-1149.

6. Anderson, Arthur R., "Lateral Stability of Long Prestressed Concrete Beams", PCI Journal Vol. 16, No. 3, May-June 1971, pp. 7-9.

7. Anderson, Arthur R., Author's closure to discussion of "Lateral stability of Long Prestressed Concrete Beams," PCI Journal, Vol. 16, No. 6, Nov.-Dec. 1971, pp. 86-87.

8. American Association of State Highway Officials, Standard Specification for Highway Bridges, Seventh Edition, Washington, D.C., 1957.

9. American Association of State Highway Officials, Standard Specification for Highway Bridges, Eighth Edition, Washington, D.C., 1961.

10. American Association of State Highway and Transportation Officials, Standard Specification for Highway Bridges, Thirteenth Edition, Washington, D.C., 1983.

11. American Concrete Institute, "Building Code Requirements for Reinforced Concrete (ACI 318-56)", ACI Journal, Proceedings, Vol. 52, No. 9, May 1956, pp. 913-986.

12. American Concrete Institute, Building Code Requirements for Reinforced Concrete (ACI318-63), Detroit, 144 pp.

13. American Concrete Institute, Building Code Requirements for Reinforced Concrete (ACI 318-71), Detroit, 78 pp.

14. American Concrete Institute, Building Code Requirements for Reinforced Concrete (ACI 318-77), Detroit, 102 pp.

15. American Concrete Institute, Building Code Requirements for Reinforced Concrete (ACI 318-83), Detroit, 111 pp.

16. American Concrete Institute, Commentary on Building Code Requirements for Reinforced Concrete (ACI 318-63), SP-10, American Concrete Institute, Detroit, 1965.

17. American Concrete Institute, Commentary on Building Code Requirements for Reinforced Concrete (ACI 318-83), Detroit, 1983.

18. American Concrete Institute, 318 Change Submittal, No. CE11, "Shear Strength of High Strength Concrete", Nov. 19, 1986.

19. American Concrete Institute - American Society of Civil Engineers, Committee 323, "Tentative Recommendations for Prestressed Concrete," ACI Journal, Proceedings Vol. 54, No. 7, Jan. 1958, pp. 545-578.

20. American Concrete Institute - American Society of Civil Engineers, Committee 327, Ultimate Load Design, "Ultimate Strength Design", ACI Journal, Proceedings Vol. 52, No. 5, Jan. 1956, pp. 505-524. Also, "Report of ASCE-ACI Joint Committee on Ultimate Strength Design," Proceedings, ASCE, Vol. 81, Oct. 1955, 68 pp.

21. American Concrete Institute Committee 343, "Analysis and Design of Reinforced Concrete Bridge Structures," ACI Manual of Concrete Practice, Part 4, American Concrete Institute, Detroit, 1981, 118 pp.

22. American Concrete Institute Committee 363, "State-of-the Art Report on High-Strength Concrete," ACI Journal, Proceedings Vol. 81, No. 4, July-Aug. 1984, pp. 363-411.

23. American Concrete Institute Committee 435, "Deflections of Prestressed Concrete Members," (ACI 435.1R-63)(Reaffirmed 1979), ACI Journal, Proceedings Vol. 60, No. 12, Dec. 1963, pp. 1697-1728. Also, ACI Manual of Concrete Practice, Part 4, American Concrete Institute, Detroit, 1981.

24. American Concrete Institute Committee 435, Subcommittee 5, "Deflections of Prestressed Concrete Members," ACI Journal, Proceedings Vol. 60, No. 12, Dec. 1963, pp. 1697-1728.

25. ASTM Standards in ACI 301, 318 and 349, SP-71, American Concrete Institute, Detroit.

26. Aswad, A. and Hester, W.T. "Impact of High-Strength Concrete on Design and Service Behavior of Prestressed Precast Concrete Members," High Strength concrete, SP-87, American Concrete Institute, Detroit, 1985, pp. 9-20.

27. Base, G.D., "An Investigation of Transmission Length in Pre-Tensioned Concrete," Session III, Paper No. 9, Third Congress of the Federation Internationale de la Preconstrainte, Berlin, 1958, Papers, pp. 603-623.

28. Base, G.D., "An Investigation of Transmission Length in Pretensioned Concrete," Research Report No. 5, Aug., 1958, Cement and Concrete Association, London, 24 pp.

29. Base, G.D., "An Investigation of the Use of Strand in Pretensioned Prestressed Concrete Beams," Research Report No. 11, Jan. 1961, Cement and Concrete Association, London, 12 pp.

30. Billet, D.F., and Appleton, J.H., "Flexural Strength of Prestressed Concrete Beams", ACI Journal, Proceedings, Vol. 50, No. 10, June 1954, pp. 837-854.

31. Blume, J.A., Newmark N.M., and Corning, L.H., "Design of Multistory Reinforced Concrete Buildings for Earthquake Motions," Portland Cement Association, Chicago, 1961, 318 pp.

32. Bradberry, T.E., "Time Dependent Deformation of Long Span Prestressed Concrete Beams Having Low Relaxation Strands," Unpublished M.S. Report, The University of Texas at Austin, May 1986.

33. Bureau of Public Roads, Strength and Serviceability Criteria - Reinforced Concrete Bridge Members - Ultimate Design, U.S. Department of Commerce, U.S. Government Printing Office, Washington, D.C., Aug. 1966, 81 pp.

34. Burns, Ned H., "Moment Curvature Relationships for Partially Prestressed Concrete Beams," PCI Journal, Vol. 9, No. 1, Feb. 1964, pp. 52-63.

35. Carrasquillo, P.M. and Carrasquillo, R.L., "Guidelines for Use of High Strength Concrete in Texas Highways," Research Report 367-1F, Center for Transportation Research, The University of Texas at Austin, Aug. 1986, 227 pp.

36. Carrasquillo, R.L., Nilson, A.H., and Slate, F.O., "Properties of High Strength Concrete Subject to Short-Term Loads", ACI Journal, Proceedings Vol. 78, No. 3, May-June 1981, pp. 171-178.

37. Carreira, Domingo J., and Chu, Kuang-Han, "Stress-Strain Relationship for Plain Concrete in Compression," ACI Journal, Proceedings, Vol. 82, No. 6, Nov.-Dec. 1985, pp. 797-804.

38. Castrodale, R.W., "The Shear Design of Prestressed Concrete Members Using the Truss Model," Unpublished M.S. Thesis, University of Texas at Austin, Dec. 1983, 348 pp.

39. Colaco, J.P., "75-Story Texas Commerce Plaza, Houston - The Use of High-Strength Concrete," High Strength Concrete, SP-87, American Concrete Institute, Detroit, 1985, pp. 1-8.

40. Collins, M.P., and Mitchell, D., "Shear and Torsion Design of Prestressed and Non-Prestressed Concrete Beams," PCI Journal, Vol. 25, No. 5, Sept. - Oct. 1980, pp. 32-100.

41. Comite Euro-International du Beton, Recommendations for an International Code of Practice for Reinforced Concrete, Translation by American Concrete Institute and Cement and Concrete Association, 156 pp.

42. Csagoly, P., "Bridge Girder Test," Engineering News-Record, Mar. 13, 1986, p. 9.

43. Drake, Kingsley D., "High-Strength Concrete in Seattle," High Strength Concrete, SP-87, American Concrete Institute, Detroit, MI, 1985, pp. 21-34.

44. Elzanaty, A.H., Nilson, A.H. and Slate, F.O., "Shear-Critical High-Strength Concrete Beams," Research Report No. 85-1, Department of Structural Engineering, Cornell University, Feb. 1985, 216 pp.

45. Elzanaty, A.H., Nilson, A.H., and Slate, F.O., "Shear Capacity of Reinforced Concrete Beams Using High-Strength Concrete," ACI Journal, Proceedings Vol. 83, No. 2, Mar.-Apr. 1986, pp. 290-296.

46. Elzanaty, A.H., Nilson, A.H., and Slate, F.O., "Shear Capacity of Prestressed Concrete Beams Using High-Strength Concrete," ACI Journal, Proceedings Vol. 83, No. 3, May-June 1986, pp. 359-368.

47. Fafitis, A., and Shah, S.P., "Lateral Reinforcement for High-strength Concrete Columns," High Strength Concrete, SP-87, American Concrete Institute, Detroit, 1985, pp. 213-232.

48. Furlong, R.W., "Design of Concrete Frames by Assigned Limit Moments," ACI Journal, Proceedings Vol. 67, No. 4, Apr. 1970, pp. 341-353.

49. Ghosh, S.K., and Chandrasekhar, C.S., Discussion of "Flexural Behavior of High-Strength Concrete Beams" by Leslie, Rajagopalan and Everard, ACI Journal, Proceedings Vol. 74, No. 3, Mar. 1977, pp. 140-142.

50. Grossfield, B., and Birnstiel C., "Tests of T-Beams with Precast Webs and Cast-in-Place Flanges," ACI Journal, Proceedings Vol. 59, No. 6, June 1962, pp. 843-851.

51. Hansen, T.C., and Mattock, A.H., "Influence of Size and Shape of Member on the Shrinkage and Creep of Concrete," ACI Journal, Proceedings Vol. 63, Feb. 1966, pp. 267-290. Also PCA Bulletin D103 which contains an added appendix.

52. Hanson, Norman W., "Precast-Prestressed Concrete Bridges - 2. Horizontal Shear Connections," Journal of the PCA Research and Development Laboratories, Vol. 2, No. 2, 1960, pp. 38-58.

53. Hanson, Norman W., "Influence of Surface Roughness of Prestressing Strand on Bond Performance," PCI Journal, Vol. 14, No. 1, Feb. 1969, pp. 32-45.

54. Hanson, N.W., and Kaar, P.H., "Flexural Bond Tests of Pre-Tensioned Prestressed Beams," ACI Journal, Proceedings Vol. 55, Jan. 1959, pp. 783-802.

55. Harajli, M.H., and Naaman, A.E., "Deformation and Cracking of Partially Prestressed Concrete Beams under Static and Cyclic Fatigue Loading," Research Report No. UMEE 84R1, Department of Civil Engineering, The University of Michigan, Ann Arbor, Aug. 1984, 179 pp.

56. Harajli, M.H., and Naaman, A.E., "Static and Fatigue Tests on Partially Prestressed Beams," Proceedings, ASCE, Vol. 111, ST7, July 1985, pp. 1602-1618.

57. Harajli, M.H., Naaman, A.E., and Wight, J.K., "Analysis of Ductility in Partially Prestressed Concrete Flexural Members", PCI Journal, V. 32, No. 3, May-June 1986, pp. 64-87.

58. Hognestad, Eivind, "A Study of Combined Bending and Axial Load in Reinforced Concrete Members," Bulletin No. 399, University of Illinois Engineering Experiment Station, Nov. 1951, 128 pp.

59. Hognestad, Eivind, "Confirmation of Inelastic Stress Distribution in Concrete," Proceedings, ASCE, Vol. 83, ST2, Mar. 1957, pp. 1-17. Also PCA Bulletin D31.

60. Hognestad, E., Hanson, N.W., and McHenry, D., "Concrete Stress Distribution in Ultimate Strength Design," ACI Journal, Proceedings Vol. 52, Dec. 1955, pp. 455-479. Also PCA Bulletin D6.

61. Hognestad, E., Hanson, N.W., and McHenry, D., Authors' closure to discuss of "Concrete Stress Distribution in Ultimate Strength Design," ACI Journal, Proceedings Vol. 52, Part 2, Dec. 1956, pp. 1305-1330. Also, PCA Bulletin D6A.

62. Horn, D.G., and Preston, H.K., "Use of Debonded Strands in Pretensioned Bridge Members", PCI Journal, Vol. 26, No. 4, July-Aug. 1981, pp. 42-58.

63. Huang, T., "Loss Estimation for Multistage Prestressed Concrete Members," Advances in Structural Concrete Design, Proceedings of NJIT-ASCE-ACI Structural Concrete Design Conference, Newark, 1983, pp. 187-203.

64. Hunt, F.F., and Preston, H.K., "Performance of a New Corrosion Resistant Prestressing Strand", Presentation at "Advances in Prestressed Concrete" Session at ASCE Fall Convention and Structures Congress, Houston, Texas, Oct. 17-21, 1983.

65. Janney, Jack R., "Nature of Bond in Pretensioned Prestressed Concrete," ACI Journal, Proceedings, Vol. 50, May 1954, pp. 717-736. Also, PCA Bulletin D2.

66. Janney, J.R., Hognestad, E., and McHenry D., "Ultimate Flexural Strength of Prestressed and Conventionally Reinforced Concrete Beams", ACI Journal, Proceedings Vol. 52, Feb. 1956, pp. 602-620. Also, PCA Bulletin D7.

67. Janney, Jack R., "Report of Stress Transfer Length Studies on 270k Prestressing Strand", PCI Journal, Vol. 8, No. 1, Feb. 1963, pp. 41-45.

68. Jensen, V.P., "The Plasticity Ratio of Concrete and Its Effect on the Ultimate Strength of Beams," ACI Journal, Journal Vol. 39, No. 6, June 1943, pp. 565-582.

69. Jobse, H.J., "Applications of High Strength Concrete for Highway Bridges,", Report No. FHWA/RD-82/097, Oct. 1981, Federal Highway Administration, 228 pp.

70. Karr, P.H., LaFraugh, R.W., and Mass, M.A. "Influence of Concrete Strength on Strand Transfer Length," PCI Journal Vol. 8, No. 5, Oct. 1963, pp. 47-67. Also, PCA Bulletin D71.

71. Kaar, P.H., Hanson, N.W., and Capell, H.T., "Stress-Strain Characteristics of High-Strength Concrete," Douglas McHenry International Symposium on Concrete and Concrete Structures, SP-55, American Concrete Institute, Detroit, 1978, pp. 161-185.

72. Kelly, D.J., "Time Dependent Deflections of Pretensioned Beams," Unpublished M.S. Thesis, The University of Texas at Austin, Aug. 1986, 307 pp.

73. Kent, D.C., and Park R., "Flexural Members with Confined Concrete," Proceedings, ASCE, Vol. 97, ST7, July 1971, pp. 1969-1990.

74. Khachaturian, Marbey, and Gurfinkel, German, Prestressed Concrete, McGraw-Hill, New York, 1969, 460 pp.

75. Kriz, L.B. and Lee, S.L., "Ultimate Strength of Over-Reinforced Beams," Proceedings, ASCE, Vol. 86, EM3, June 1960. Also, PCA Bulletin D36.

76. Leslie, Keith E., Rajagopalan, K.S., and Everard, Noel J., "Flexural Behavior of High-Strength Concrete Beams," ACI Journal, Proceedings Vol. 73, No. 9, Sept. 1976, pp. 517-521.

77. MacGregor, J.G., "Ductility of Structural Elements," Handbook of Concrete Engineering, 1st Ed., M. Fintel (Editor), Prentice Hall, 1974, pp. 229-248.

78. Malhotra, V.M., "Are 4 X 8 Inch Concrete Cylinders as Good as 6 X 12 Inch Cylinders for Quality Control of Concrete?", ACI Journal, Proceedings Vol. 73, No. 1, Jan. 1976, pp. 33-36.

79. Martin, L.D. and Scott, N.L., "Development of Prestressing Strand in Pretenioned Members," ACI Journal, Proceedings Vol. 73, No. 8, Aug. 1976, pp. 453-456.

80. Martin, L.D., "A Rational Method for Estimating Camber and Deflection of Precast Prestressed Members," PCI Journal, Vol. 22, No. 1, Jan.-Feb. 1977, pp. 100-108.

81. Martinez, S., Nilson, A.H., and Slate, F.O., "Short-Term Mechanical Properties of High-Strength Light-Weight Concrete," Research Report No. 82-9, Dept. of Structural Engineering, Cornell University, Aug. 1982, 98 pp.

82. Martinez, S., Nilson, A.H., and Slate, F.O., "Spirally Reinforced High-Strength Concrete Columns," ACI Journal, Proceedings Vol. 81, No. 5, Sept.-Oct. 1984, pp. 431-442.

83. Mast, R.F., "Auxiliary Reinforcement in Concrete Connections," Proceedings, ASCE, Vol. 94, ST6, June 1968, pp. 1485-1504.

84. Mattock, Alan, H., "Modification of ACI Code Equation for Stress in Bonded Prestressed Reinforcement at Flexural Ultimate," ACI Journal, Proceedings Vol. 81, No. 4, July-

85. Mattock, A.H., Kaar, P.H., "Precast-Prestressed Concrete Bridges - 4. Shear Tests of Continuous Girders," Journal of the PCA Research and Development Laboratories, Vol. 3, No. 1, Jan. 1961, pp. 19-46.

86. Mattock, Alan, H., and Kriz, Ladislav, B., "Ultimate Strength of Nonrectangular Concrete Members," ACI Journal, Proceedings Vol. 57, No. 7, Jan. 1961, pp. 737-766.

87. Mattock, Alan H., Kriz, Ladislav, B., and Hognestad, Eivind, "Rectangular Concrete Stress Distribution in Ultimate Strength Design", ACI Journal, Proceedings Vol. 57, Feb. 1961, pp. 875-928. Also PCA Bulletin D49.

88. Mattock, A.H., and Hawkins, N.M., "Shear Transfer in Reinforced Concrete - Recent Research," PCI Journal, Vol. 17, No. 2, Mar.-Apr. 1972, pp. 55-75.

89. Mayfield, B., Davies, G., and Kong, F.K., "Some tests on the transmission length and ultimate strength of pretensioned concrete beams incorporating Dyform strand:", Magazine of Concrete Research, Vol. 22, No. 73, Dec. 1970, pp. 219-226.

90. Mphonde, Andrew G., and Frantz, Gregory C., "Shear Tests of High- and Low-Strength Concrete Beams Without Stirrups," ACI Journal, Proceedings Vol. 81, No. 4, July-Aug. 1984, pp. 350-357.

91. Mphonde, A.G., and Frantz, G.C., "Shear Tests of High- and Low-Strength Concrete Beams with Stirrups," High Strength Concrete, SP-87, American Concrete Institute, Detroit, 1985, pp. 179-196.

92. Muller, Jean, "Lateral Stability of Precast Members During Handling and Placing," PCI Journal, Vol. 7, No. 1, Feb. 1962, pp. 20-31.

93. Naaman, A.E., "Ultimate Analysis of Prestressed and Partially Prestressed Sections by Strain Compatibility," PCI Journal, Vol. 22, No. 1, Jan.-Feb. 1977, pp. 32-51.

94. Naaman, A.E., "A Proposal to Extend Some Code Provisions on Reinforcement to Partial Prestressing," PCI Journal, Vol. 26, No. 2, Mar.-Apr. 1981, pp. 74-91.

95. Naaman, A.E., "Partially Prestressed Concrete: Review and Recommendations," PCI Journal, Vol. 30, No. 6, Nov.-Dec. 1985, pp. 30-71.

96. Naaman, A.E., Harajli, M.H., and Wight, J.K., "Analysis of Ductility in Partially Prestressed Flexural Members," PCI Journal, Vol. 31, No. 3, May-June 1986, pp. 64-87.

97. Naaman, A.E., Harajli, M.H., and Wight, J.K., Authors' Closure to discussion of "Analysis of Ductility in Partially Prestressed Flexural Members," PCI Journal, Vol. 32, No. 1, Jan.-Feb., 1987, pp. 142-145.

98. Ngab, Ali S., Nilson, Arthur H., and Slate, Floyd O., "Shrinkage and Creep of High Strength Concrete," ACI Journal, Proceedings Vol. 78, No. 4, July-Aug. 1981, pp. 255-261.

99. Nilson, Arthur H., "Design Implications of Current Research of High-Strength Concrete," High Strength Concrete, SP-87, American Concrete Institute, Detroit, 1985, p. 85-118.

100. Over, R.S., and Au, Tung, "Prestress Transfer Bond of Pretensioned Strands in Concrete," ACI Journal, Proceedings Vol. 62, No. 11, Nov. 1965, pp. 1451-1460.

101. Overman, T.R., Breen, J.E., and Frank, K.H., "Fatigue Behavior of Pretensioned Concrete Girders," Research Report 300-2F, Center for Transportation Research, The University of Texas at Austin, Nov. 1984, 354 pp.

102. Park, R., and Paulay, T. Reinforced Concrete Structures, John Wiley and Sons, New York, 1975, 769 pp.

103. Pastor, J.A., Nilson, A.H., and Slate, F.O., "Behavior of High-Strength Concrete Beams," Research Report No. 84-3, Department of Structural Engineering, Cornell University, Feb. 1984, 311 pp.

104. Peterman, M.B. and Carrasquillo, R.L., "Production of High Strength Concrete," Research Report 315-1F, Center for Transportation Research, The University of Texas at Austin, Oct. 1983, 286 pp.

105. PCI Committee on Allowable Stresses in Prestressed Concrete Design, "Allowable Tensile Stresses for Prestressed Concrete," PCI Journal, Vol. 15, No. 1, Feb. 1970, pp. 37-42.

106. PCI Committee on Prestress Losses, "Recommendations for Estimating Prestress Losses", PCI Journal, Vol. 20, No. 40, July-Aug. 1975, pp. 43-75.

107. Preston, H.K., "Testing 7-Wire Strand for Prestressed Concrete - The State of the Art", PCI Journal, Vol. 30, No. 3, May-June 1985.

108. Rabbat, B.G., and Russell, H.G., "Optimized Sections for Precast, Prestressed bridge Girders," (RD080.01E), Portland Cement Association, 1982.

109. Rabbat, B.G., Takayanagi, T., Russell, H.G., "Optimized Sections for Major Prestressed Concrete Bridge Girders," Report No. FHWA/RD-82/005, Feb. 1982, Federal Highway Administration, 172 pp.

110. Ramirez, J.A., and Breen, J.E., "Proposed Design Procedures for Shear and Torsion in Reinforced and Prestressed Concrete," Research Report 248-4F, Center for Transportation Research, The University of Texas at Austin, Nov. 1983, 254 pp.

111. Ramirez, J.A., and Breen, J.E., "Review of Design Procedures for Shear and Torsion in Reinforced and Prestressed Concrete," Research Report 248-2, Center for Transportation Research, The University of Texas at Austin, Nov. 1983, 186 pp.

112. RILEM, Final REcommendations, Reinforcements for Reinforced and Prestressed Concrete: II. Recommendations for Prestressing Steels. Materials and Structures, Research and Testing (RILEM, Paris), Vol. 12, No. 68, Mar.-Apr. 1979, pp. 75-127.

113. Rowe, R.E., "Trends and Needs in Concrete Bridge Design," Seventh Annual Henry M. Shaw Lecture Series in Civil Engineering, Department of Civil Engineering, North Carolina State University, Raleigh, Mar. 1972, 36 pp.

114. Rusch, Hubert, "Researches Toward a General Flexural Theory for Structural Concrete," ACI Journal, Proceedings Vol. 57, No. 1, July 1960, pp. 1-28.

115. Saemann, J.C., and Washa, G.W., "Horizontal Shear Connections Between Precast Beams and Cast-in-Place Slabs," ACI Journal, Proceedings, Vol. 61, No. 11, Nov. 1964, pp. 1383-1409.

116. Shaikh, A.F., and Branson, D.E., "Non-Tensioned Steel in Prestressed Concrete Beams," PCI Journal, Vol. 15, No. 1, Feb. 1970, p. 14-36.

117. Smadi, M.M., Slate, F.O., and Nilson, A.H., "High-, Medium-, and Low-Strength Concretes Subject to Sustained Overloads - Strains, Strengths, and Failure Mechanisms," ACI Journal, Proceedings Vol. 82, No. 5, Sept.-Oct. 1985, pp. 657-664.

118. Smith, R.G., Discussion of "Researches Toward a General Flexural Theory for Structural Concrete," by Hubert Rusch Reference, ACI Journal, Proceedings Vol. 32, No. 9, Mar. 1961, pp. 1160-1163.

119. Suttikan, C., "A Generalized Solution for Time Dependent Response and Strength of Non-Composite and Composite Prestressed Concrete Beams," Unpublished Ph.D. Dissertation, The University of Texas at Austin, Aug. 1978.

120. Swamy, R.N., "High-Strength Concrete - Material Properties and Structural Behavior," High Strength Concrete, SP-87, American Concrete Institute, Detroit, 1985, pp. 119-146.

121. Swamy, R.N., and Anand, K.L., "Transmission Length and Prestress Losses in High Strength Concrete," Paper presented at the Seventh International Congress of the Federation Internationale de la Preconstrainte, New York, May 26 - June, 1974.

122. Swann, R.A., Discussion of "Lateral Stability of Long Prestressed Concrete Beams," by Arthur R. Anderson, PCI Journal, Vol. 16, No. 6, Nov.-Dec. 1971, p. 85-86.

123. Swann, R.A., and Godden, W.G., "The Lateral Buckling of Concrete Beams Lifted by Calbes," The Structural Engineer, Vol. 44, No. 1, Jan. 1966, London, pp. 21-23.

124. Swartz, S.E., Nikaeen, A., Harayan Babu, H.D., Periyakaruppan, N., and Refai, T.M.E. "Structural Bending Properties of Higher Strength Concrete," High Strength Concrete, SP-87, American Concrete Institute, Detroit, 1985, pp. 147-178.

125. Tadros, M.K., and Peterson, D.N., "Code Consideration of Flexural Design with Partial Prestressing," Vol. 3, Hyperstatic Structures: Nonlinear Design, Codes and Practice, International Symposium - Nonlinearity and Continuity in Prestressed Concrete, University of Waterloo, 1983, pp. 125-156.

126. Thoman, William, H., and Raeder, Warren, "Ultimate Strength and Modulus of Elasticity of High Strength Portland Cement Concrete," ACI Journal, Proceedings Vol. 30, No. 3, Jan. - Feb., 1934, pp. 231-=238.

127. Thompson, K.J., and Park R., "Ductility of Prestressed and Partially Prestressed Concrete Beam Sections," PCI Journal, Vol. 25, No. 2, Mar.-Apr. 1980, pp. 46-70.

128. Tognon, G., Ursella, P., and Copetti, G., "Design and Properties of Concretes with Strength over 1500 kgf/cm^2," ACI Journal, Proceedings Vol. 77, No. 3, May-June 1980, pp. 171-178.

129. Towles, Thomas T., "Advantages in the Use of High Strength Concretes," ACI Journal, Proceedings, Vol. 28, No. 9, May 1932, pp. 607-612.

130. Wang, F., Shah, S.P., and Naaman, A.E., Discussion of "Flexural Behavior of High-Strength Concrete Beams," ACI Journal, Proceedings Vol. 74, No. 3, Mar, 1977, pp. 143, 144.

131. Wang, Pao-Tsan, Shah, Surendra P., and Naaman, Antoine E., "High-Strength Concrete in Ultimate Strength Design", Proceedings, ASCE, Vol. 104, ST11, Nov. 1978, pp. 1761-1773.

132. Wang, P.T., Shah, S.P., and Naaman, A.E., "Stress-Strain Curves of Normal and Lightweight Concrete in Compression," ACI Journal, Proceedings, Vol. 75, No. 11, Nov. 1978, pp. 603-611.

133. Warwaruk, J., Sozen, M.A., and Siess, C.P., "Investigation of Prestressed Reinforced Concrete for Highway Bridges, Part III - Strength and Behavior in Flexure of Prestressed Concrete Beams," Bulletin No. 464, Engineering Experiment Station, University of Illinois, Urbana, 1962, 105 pp.

134. Whitney, Charles S., "Plastic Theory of Reinforced Concrete Design," Proceedings ASCE, Dec. 1940; Transactions ASCE, Vol. 107, 1942, pp. 251-326.

135. Zia, Paul, "Review of ACI Code for Design with High Strength Concrete," Concrete International: Design and Construction, Vol. 5, No. 8, Aug. 1983, pp. 16-20.

136. Zia, P., and Mostafa, T., "Development Length of Prestressing Strands," PCI Journal, Vol. 22, No. 5, Sept. - Oct. 1977, pp. 54-65.

137. Zia, P., Preston, H.K., Scott, N.L., and Workman, E.B., Estimating Prestress Losses," Concrete International: Design and Construction, Vol. 1, No. 6, June 1979, pp. 32-38.

V I T A

Reid Wilson Castrodale was born in Perry, Oklahoma, on September 11, 1956, the son of Emily Martenis Castrodale and Milford Walter Castrodale, Jr. Upon graduation from Jessie O. Sanderson High School in Raleigh, North Carolina, in 1974, he entered the Georgia Institute of Technology in Atlanta, Georgia. While at Georgia Tech he worked for the Southern Railway System as a co-op student. After recieving the degree of Bachelor of Civil Engineering, Cooperative Plan, With Highest Honor, in June, 1979, he was employed as a structural engineer with Burns and McDonnell Engineers-Architects-Consultants in Kansas City, Missouri. Shortly thereafter he married the former Miss Jessica Milo Dixon of Atlanta, Georgia. In June 1981 he entered the Graduate School of The University of Texas at Austin. He received a Masters of Science in Engineering degree in December, 1983. He is presently employed as a structural engineer with Ralph Whitehead and Associates, a bridge design consulting firm, in Charlotte, North Carolina.

Permanent Address: 833 Ingraham Place
Matthews, North Carolina 28105

This dissertation was typed by Reid W. Castrodale with assistance in preparation of the final copy from Sharon Cunningham.